

**BASIN ANALYSIS OF TERTIARY STRATA
IN THE PATTANI BASIN
GULF OF THAILAND**

by

ANUN CHONCHAWALIT

M.Sc., Engineering Geology, Asian Institute of Technology, 1985

**A THESIS SUBMITTED IN PARTIAL FULFILLMENT OF
THE REQUIREMENTS FOR THE DEGREE OF
DOCTOR OF PHILOSOPHY**

in

**THE FACULTY OF GRADUATE STUDIES
Department of Geological Sciences**

We accept this thesis as conforming
to the required standard

THE UNIVERSITY OF BRITISH COLUMBIA

JANUARY, 1993

© ANUN CHONCHAWALIT

In presenting this thesis in partial fulfilment of the requirements for an advanced degree at the University of British Columbia, I agree that the Library shall make it freely available for reference and study. I further agree that permission for extensive copying of this thesis for scholarly purposes may be granted by the head of my department or by his or her representatives. It is understood that copying or publication of this thesis for financial gain shall not be allowed without my written permission.

(Signature)

Department of Geological Sciences

The University of British Columbia
Vancouver, Canada

Date 18-3-1993

ABSTRACT

The stratigraphic and structural evolution of the Pattani Basin, the most prolific petroleum basin in Thailand, reflects the extensional tectonic regime of the Continental Southeast Asia. East-west extension, a product of the northward collision of India with Eurasia since the Early Tertiary, resulted in the formation of a series of N-S trending sedimentary basins including the Pattani Basin. Subsidence and thermal histories of the basin can generally be accounted for by nonuniform lithospheric stretching. The validity of nonuniform lithospheric stretching as a mechanism for the formation of the Pattani Basin is confirmed by a reasonably good agreement between the modeled and observed vitrinite reflectance at various depths and locations. The amount of stretching as well as surface heat flow generally increases from the margin to the basin center. Crustal stretching factor (β) varies from 1.3 at the basin margin to 2.8 in the center. Subcrustal stretching factor (δ) ranges from 1.3 at the basin margin to more than 3.0 in the basin center. The stretching of the lithosphere may have extended the basement rocks as much as 45 to 90 km and have caused the upwelling of asthenosphere resulting in high heat flow.

The sedimentary succession in the Pattani Basin is divisible into synrift and post-rift sequences. The synrift sequence comprises three stratigraphic units: 1) Late Eocene to Early Oligocene alluvial fan, braided river and floodplain deposits; 2) Late Oligocene to Early Miocene floodplain and channel deposits; and 3) an Early Miocene regressive package comprises marine to nonmarine sediments. Deposition of the synrift sequences corresponded to rifting and extension which included episodic block faulting and rapid subsidence. Post-rift succession comprises: 1) an Early to Middle Miocene regressive package of shallow marine sediments through floodplain and channel deposits; 2) a late Early Miocene transgressive package; and

3) a Late Miocene to Pleistocene transgressive succession. The post-rift phase is characterized by slower subsidence and decreased sediment influx. The present-day shallow marine condition in the Gulf of Thailand is the continuation of this latest transgressive phase.

The dispersed organic matter in Tertiary strata is composed mainly of Type III and Type IV kerogen with minor amounts of Type II kerogen. The organic matter is predominantly detrital and continental in origin as evident from low HI and high OI values, and maceral composition (mainly vitrinite). The variation in abundance of organic matter occurs both within the stratigraphic units and across the units; the lowest TOC and HI occur in the high energy nonmarine deposits such as alluvial fan and braided stream deposits, whereas higher TOC and HI generally occur in low energy deposits.

Prospective petroleum source rocks generally have low TOC and very low hydrocarbon potential as defined by pyrolysis. The presence of numerous commercial gas fields suggests either that the source rocks here, despite very low genetic potentials, are very effective in producing, migrating, and accumulating hydrocarbon or higher quality source rocks occur within the basin but have not yet been reached by drilling. Mean activation energies (E_0) of the perspective source rocks range from 46.1 to 60.6 kcal/mol which agree well with the activation energies required to break down carbon-oxygen and carbon-carbon bonds (40-70 kcal/mol). The dispersion of activation energies (σ_E) varies from 0.26 to 9.30% of the mean values (E_0). Analyses of hydrocarbon generation history, using a chemical kinetic model based on the Arrhenius equation, indicates, except for the youngest unit (unit 1), the strata are either mature or overmature with respect to the oil window. The main phase of hydrocarbon generation started at about 33-35 Ma.

TABLE OF CONTENTS

ABSTRACT	ii
TABLE OF CONTENTS	iv
LIST OF TABLES	viii
LIST OF FIGURES	ix
ACKNOWLEDGEMENT	xvii
1. INTRODUCTION	1
1.1 General Overview	1
1.2 Location of the study area	3
1.3 Data sources	3
1.4 Exploration history in the Gulf of Thailand	5
1.5 Purpose of study	5
2. REGIONAL GEOLOGY	7
2.1 Introduction	7
2.2 Present-day geologic setting	7
2.3 Tectonic elements	9
3. STRATIGRAPHY AND SEDIMENTOLOGY	12
3.1 Abstract	12
3.2 Introduction	14
3.3 Methods of study	14
3.4 Stratigraphic subdivision	19
3.4.1 Unit 6	20
3.4.2 Unit 5	30
3.4.3 Unit 4	35
3.4.4 Unit 3	44
3.4.5 Unit 2	53
3.4.6 Unit 1	60
3.5 Discussion	65
3.5.1 Synrift sedimentation	66
a. Late Eocene to Early Oligocene (40-30 Ma)	66
b. Late Oligocene to Early Miocene (30-24 Ma)	67
c. Early Miocene (24-20 Ma)	68
3.5.2 Post-rift sedimentation	70

a. Late Early to Middle Miocene (20-15 Ma)	70
b. Middle Miocene (15-12 Ma)	72
c. Late Miocene to Pleistocene (12-0 Ma)	72
3.6 Summary and conclusions	76
 4. TECTONIC EVOLUTION AND BASIN MODELLING OF THE PATTANI BASIN, THE GULF OF THAILAND	 79
4.1 Abstract	79
4.2 Introduction	80
4.3 Methods of study	82
4.3.1 Geohistory analysis	82
a. Decompaction	83
b. Backstripping	87
c. Eustatic correction	88
4.3.2 Basin forming modelling	88
4.4 Basin forming mechanism in the Pattani Basin	95
4.5 Timing of basin formation	95
4.6 Subsidence history	96
4.6.1 Total subsidence and burial history	100
4.6.2 Tectonic subsidence	102
4.6.3 Lithospheric stretching factors	118
4.7 Thermal history	123
4.7.1 Heat flow history	123
4.7.2 Thermal history and present-day geothermal gradients	124
4.7.3 Vitrinite reflectance	126
4.8 Discussion	132
4.9 Summary and conclusions	139
 5. ORGANIC CHARACTERISTICS AND PETROLEUM SOURCE ROCK POTENTIAL OF TERTIARY STRATA IN THE PATTANI BASIN	 142
5.1 Abstract	142
5.2 Introduction	143
5.3 Methods of study	144
5.4 Summary of Tertiary stratigraphy in the Pattani Basin	149
5.5 General characteristics of organic matter	158
5.5.1 Unit 6	189
5.5.2 Unit 5	236
5.5.3 Unit 4	237
5.5.4 Unit 3	239
5.5.5 Unit 2	240

5.5.6 Unit 1	242
5.6 Discussion	243
5.6.1 Origin of variation in organic matter	243
a. Origin of organic matter	244
b. Organic characteristics and depositional environments	245
c. Organic characteristics and maturation	247
d. Organic abundance and sedimentation rate	248
e. Organic abundance and age	254
f. Discussion	258
5.6.2 Source rock considerations	259
5.7 Summary and conclusions	262
 6. ORGANIC MATURATION AND HYDROCARBON GENERATION	266
6.1 Abstract	266
6.2 Introduction	268
6.3 Methods of study	273
6.3.1 Kinetics and organic maturation modelling	273
6.3.2 Determination of kinetic parameters	277
6.4 Summary of Tertiary stratigraphy and organic characteristics in the Pattani Basin	282
6.5 Kinetic parameters of the potential source rocks	286
6.5.1 Unit 6	287
6.5.2 Unit 5	287
6.5.3 Unit 4	290
6.5.4 Unit 3	290
6.5.5 Unit 2	291
6.5.6 Unit 1	291
6.6 Hydrocarbon generation modelling	292
6.7 Discussion	320
6.7.1 Variation of kinetic parameters	320
a. Sample preparation vs. kinetic determinations	320
b. Type of organic matter vs. kinetic variation	322
c. Depositional environment vs. kinetic variation	323
d. Degree of thermal maturation vs. kinetic variation	324
6.7.2 Hydrocarbon generation history	324
6.7.3 Hydrocarbon potential considerations	326

6.7.4 Other considerations	327
6.8 Summary and conclusions	328
7. SUMMARY AND CONCLUSIONS	331
REFERENCES	339
APPENDIX A: BASIN FORMATION MODELLING	348
APPENDIX B: ORGANIC MATURATION MODELLING	356
APPENDIX C: DETERMINATION OF KINETIC PARAMETERS OF SOURCE ROCKS	363

LIST OF TABLES

Table 3.1 Stratigraphy and depositional environments of Tertiary strata in the Pattani Basin	21
Table 4.1 Thermo-physical parameters used in the lithospheric stretching model	101
Table 4.2 Summary of crustal and subcrustal stretching factors, geothermal gradients, organic maturation gradients, and present-day heat flow in the Pattani Basin	119
Table 4.3 Kinetic parameters used to model vitrinite maturation	130
Table 5.1 Measured and calculated parameters derived from Rock-Eval/TOC analysis	146
Table 5.2 Generalized characteristics of organic facies A-D	150
Table 5.3 Stratigraphy and depositional environments of Tertiary strata in the Pattani Basin	155
Table 5.4 Summary of organic geochemical characteristics of Tertiary stratigraphic units in the Pattani Basin	207
Table 5.5 Summary of organic geochemical characteristics of Tertiary stratigraphic subunits in the Pattani Basin	207
Table 6.1 Kinetic parameters of potential source rocks of Tertiary stratigraphic units in the Pattani Basin	288

LIST OF FIGURES

Figure 1.1 Tertiary basins in the Gulf of Thailand	2
Figure 1.2 Location of well data used in this study	4
Figure 2.1 Tectonic map of Southeast Asia	8
Figure 2.2 Generalized W-E cross section of the Pattani Basin	10
Figure 3.1 Location map of the Pattani Basin	15
Figure 3.2 Four characteristic gamma log motifs	17
Figure 3.3 Diagram showing three common grain-size motifs	17
Figure 3.4 Cenozoic palynological zones	18
Figure 3.5 W-E stratigraphic section-1	23
Figure 3.6 W-E stratigraphic section-2	23
Figure 3.7 W-E stratigraphic section-3	24
Figure 3.8 W-E stratigraphic section-4	24
Figure 3.9 N-S stratigraphic section-5	25
Figure 3.10 N-S stratigraphic section-6	25
Figure 3.11 Typical log profiles of unit 6	27
Figure 3.12 Isopach map of the stratigraphic unit 6	28
Figure 3.13 Typical log profiles of unit 5	31
Figure 3.14 Isopach map of the stratigraphic unit 5	32
Figure 3.15 Typical log profiles of unit 4	36
Figure 3.16 Isopach map of the stratigraphic unit 4	37
Figure 3.17 Isopach map of unit 4's lower subunit	39
Figure 3.18 Isopach map of unit 4's middle subunit	41
Figure 3.19 Isopach map of unit 4's upper subunit	43
Figure 3.20 Typical log profiles of unit 3	46
Figure 3.21 Isopach map of the stratigraphic unit 4	47
Figure 3.22 Isopach map of unit 3's lower subunit	48
Figure 3.23 Isopach map of unit 3's middle subunit	50
Figure 3.24 Isopach map of unit 3's upper subunit	52
Figure 3.25 Typical log profiles of unit 2	55
Figure 3.26 Isopach map of the stratigraphic unit 2	56
Figure 3.27 Isopach map of unit 2's lower subunit	57
Figure 3.28 Isopach map of unit 2's upper subunit	59
Figure 3.29 Typical log profiles of unit 1	61
Figure 3.30 Isopach map of the stratigraphic unit 4	62
Figure 3.31 The regressive cycle of unit 4	69
Figure 3.32 The regressive cycle of unit 3	71
Figure 3.33 The transgressive cycle of unit 2	73
Figure 3.34 Tectonic subsidence and sedimentation of Tertiary strata in the Pattani Basin	74
Figure 3.35 Schematic evolution of sedimentary environments in the Pattani Basin	75
Figure 4.1 Location of well data used in this study	81

Figure 4.2 W-E stratigraphic section-1	97
Figure 4.3 W-E stratigraphic section-2	97
Figure 4.4 W-E stratigraphic section-3	98
Figure 4.5 W-E stratigraphic section-4	98
Figure 4.6 N-S stratigraphic section-5	99
Figure 4.7 N-S stratigraphic section-6	99
Figure 4.8 Basin subsidence, heat flow history, and vitrinite reflectance at Ranong-1 well	103
Figure 4.9 Basin subsidence, heat flow history, and vitrinite reflectance at Kung-1 well	103
Figure 4.10 Basin subsidence, heat flow history, and vitrinite reflectance at Surat-1 well	104
Figure 4.11 Basin subsidence, heat flow history, and vitrinite reflectance at Platong-8 well	104
Figure 4.12 Basin subsidence, heat flow history, and vitrinite reflectance at Platong-1 well	105
Figure 4.13 Basin subsidence, heat flow history, and vitrinite reflectance at Insea-1 well	105
Figure 4.14 Basin subsidence, heat flow history, and vitrinite reflectance at Pakarang-1 well	106
Figure 4.15 Basin subsidence, heat flow history, and vitrinite reflectance at Pladang-3 well	106
Figure 4.16 Basin subsidence, heat flow history, and vitrinite reflectance at South Platong-2 well	107
Figure 4.17 Basin subsidence, heat flow history, and vitrinite reflectance at Trat-1 well	107
Figure 4.18 Basin subsidence, heat flow history, and vitrinite reflectance at Dara-1 well	108
Figure 4.19 Basin subsidence, heat flow history, and vitrinite reflectance at Erawan-12-1 well	108
Figure 4.20 Basin subsidence, heat flow history, and vitrinite reflectance at Erawan-12-8 well	109
Figure 4.21 Basin subsidence, heat flow history, and vitrinite reflectance at Satun-3 well	109
Figure 4.22 Basin subsidence, heat flow history, and vitrinite reflectance at Jakrawan-2 well	110
Figure 4.23 Basin subsidence, heat flow history, and vitrinite reflectance at Krut-1 well	110
Figure 4.24 Basin subsidence, heat flow history, and vitrinite reflectance at Erawan-K-1 well	111
Figure 4.25 Basin subsidence, heat flow history, and vitrinite reflectance at Baanpot-1 well	111
Figure 4.26 Basin subsidence, heat flow history, and vitrinite reflectance at Baanpot-B-1 well	112

Figure 4.27 Basin subsidence, heat flow history, and vitrinite reflectance at Jakrawan-1 well	112
Figure 4.28 Basin subsidence, heat flow history, and vitrinite reflectance at Funan-1 well	113
Figure 4.29 Basin subsidence, heat flow history, and vitrinite reflectance at Yala-2 well	113
Figure 4.30 Basin subsidence, heat flow history, and vitrinite reflectance at Kaphong-3 well	114
Figure 4.31 Basin subsidence, heat flow history, and vitrinite reflectance at Kaphong-1 well	114
Figure 4.32 Basin subsidence, heat flow history, and vitrinite reflectance at Platong-5 well	115
Figure 4.33 Basin subsidence, heat flow history, and vitrinite reflectance at South Platong-1 well	115
Figure 4.34 Basin subsidence, heat flow history, and vitrinite reflectance at Satun-2 well	116
Figure 4.35 Basin subsidence, heat flow history, and vitrinite reflectance at Satun-1 well	116
Figure 4.36 Basin subsidence, heat flow history, and vitrinite reflectance at Erawan-12-9 well	117
Figure 4.37 Basin subsidence, heat flow history, and vitrinite reflectance at Erawan-12-7 well	117
Figure 4.38 Lateral variation of crustal lithospheric stretching (β)	120
Figure 4.39 Lateral variation of subcrustal lithospheric stretching (δ)	121
Figure 4.40 Lateral variation of total lithospheric stretching (ϵ)	122
Figure 4.41 Present-day surface heat flow (HFU)	125
Figure 4.42 Calculated present-day geothermal gradients ($^{\circ}\text{C}/\text{km}$)	127
Figure 4.43 Observed present-day organic maturation gradients ($\%R_o/\text{km}$)	131
Figure 4.44 Tectonic map of Southeast Asia and South China showing the main fault patterns	134
Figure 4.45 Structural map of the Gulf of Thailand	135
Figure 5.1 Location of well data used in this study	151
Figure 5.2 W-E stratigraphic section-1	152
Figure 5.3 W-E stratigraphic section-2	152
Figure 5.4 W-E stratigraphic section-3	153
Figure 5.5 W-E stratigraphic section-4	153
Figure 5.6 N-S stratigraphic section-5	154
Figure 5.7 N-S stratigraphic section-6	154
Figure 5.8 Rock-Eval pyrolysis result of Ranong-1 well	159

Figure 5.9 Rock-Eval pyrolysis result of Kung-1 well	160
Figure 5.10 Rock-Eval pyrolysis result of Surat-1 well	161
Figure 5.11 Rock-Eval pyrolysis result of Platong-8 well	162
Figure 5.12 Rock-Eval pyrolysis result of Platong-1 well	163
Figure 5.13 Rock-Eval pyrolysis result of Insea-1 well	164
Figure 5.14 Rock-Eval pyrolysis result of Pakarang-1 well	165
Figure 5.15 Rock-Eval pyrolysis result of Pladang-3 well	166
Figure 5.16 Rock-Eval pyrolysis result of South Platong-2 well	167
Figure 5.17 Rock-Eval pyrolysis result of Trat-1 well	168
Figure 5.18 Rock-Eval pyrolysis result of Dara-1 well	169
Figure 5.19 Rock-Eval pyrolysis result of Erawan-12-1 well	170
Figure 5.20 Rock-Eval pyrolysis result of Erawan-12-8 well	171
Figure 5.21 Rock-Eval pyrolysis result of Satun-3 well	172
Figure 5.22 Rock-Eval pyrolysis result of Jakrawan-2 well	173
Figure 5.23 Rock-Eval pyrolysis result of Krut-1 well	174
Figure 5.24 Rock-Eval pyrolysis result of Erawan-K-1 well	175
Figure 5.25 Rock-Eval pyrolysis result of Baanpot-1 well	176
Figure 5.26 Rock-Eval pyrolysis result of Baanpot-B-1 well	177
Figure 5.27 Rock-Eval pyrolysis result of Jakrawan-1 well	178
Figure 5.28 Rock-Eval pyrolysis result of Funan-1 well	179
Figure 5.29 Rock-Eval pyrolysis result of Yala-2 well	180
Figure 5.30 Rock-Eval pyrolysis result of Kaphong-3 well	181
Figure 5.31 Rock-Eval pyrolysis result of Kaphong-1 well	182
Figure 5.32 Rock-Eval pyrolysis result of Platong-5 well	183
Figure 5.33 Rock-Eval pyrolysis result of South Platong-1 well	184
Figure 5.34 Rock-Eval pyrolysis result of Satun-2 well	185
Figure 5.35 Rock-Eval pyrolysis result of Satun-1 well	186
Figure 5.36 Rock-Eval pyrolysis result of Erawan-12-9 well	187
Figure 5.37 Rock-Eval pyrolysis result of Erawan-12-7 well	188
Figure 5.38 Modified Van Krevelen diagram for samples from unit 6's lower subunit	190
Figure 5.39 Modified Van Krevelen diagram for samples from unit 6's upper subunit	190
Figure 5.40 Modified Van Krevelen diagram for samples from unit 5's lower subunit	191
Figure 5.41 Modified Van Krevelen diagram for samples from unit 5's upper subunit	192
Figure 5.42 Modified Van Krevelen diagram for samples from unit 4's lower subunit	193
Figure 5.43 Modified Van Krevelen diagram for samples from unit 4's middle subunit	194
Figure 5.44 Modified Van Krevelen diagram for samples from unit 4's upper subunit	195

Figure 5.45 Modified Van Krevelen diagram for samples from unit 3's lower subunit	197
Figure 5.46 Modified Van Krevelen diagram for samples from unit 3's middle subunit	198
Figure 5.47 Modified Van Krevelen diagram for samples from unit 3's upper subunit	200
Figure 5.48 Modified Van Krevelen diagram for samples from unit 2's lower subunit	202
Figure 5.49 Modified Van Krevelen diagram for samples from unit 2's upper subunit	204
Figure 5.50 Modified Van Krevelen diagram for samples from unit 1's lower subunit	206
Figure 5.51 Modified Van Krevelen diagram for samples from unit 1's upper subunit	206
Figure 5.52 Lateral distribution of TOC (%) of unit 5	208
Figure 5.53 Lateral distribution of TOC (%) of unit 4	209
Figure 5.54 Lateral distribution of TOC (%) of unit 3	210
Figure 5.55 Lateral distribution of TOC (%) of unit 2	211
Figure 5.56 Lateral distribution of TOC (%) of unit 5's lower subunit	212
Figure 5.57 Lateral distribution of TOC (%) of unit 5's upper subunit	213
Figure 5.58 Lateral distribution of TOC (%) of unit 4's lower subunit	214
Figure 5.59 Lateral distribution of TOC (%) of unit 4's middle subunit	215
Figure 5.60 Lateral distribution of TOC (%) of unit 4's upper subunit	216
Figure 5.61 Lateral distribution of TOC (%) of unit 3's lower subunit	217
Figure 5.62 Lateral distribution of TOC (%) of unit 3's middle subunit	218
Figure 5.63 Lateral distribution of TOC (%) of unit 3's upper subunit	219
Figure 5.64 Lateral distribution of TOC (%) of unit 2's lower subunit	220
Figure 5.65 Lateral distribution of TOC (%) of unit 2's upper subunit	221
Figure 5.66 Lateral distribution of QOM (mg HC/g TOC) of unit 5	222
Figure 5.67 Lateral distribution of QOM (mg HC/g TOC) of unit 4	223
Figure 5.68 Lateral distribution of QOM (mg HC/g TOC) of unit 3	224

Figure 5.69 Lateral distribution of QOM (mg HC/g TOC) of unit 2	225
Figure 5.70 Lateral distribution of QOM (mg HC/g TOC) of unit 5's lower subunit	226
Figure 5.71 Lateral distribution of QOM (mg HC/g TOC) of unit 5's upper subunit	227
Figure 5.72 Lateral distribution of QOM (mg HC/g TOC) of unit 4's lower subunit	228
Figure 5.73 Lateral distribution of QOM (mg HC/g TOC) of unit 4's middle subunit	229
Figure 5.74 Lateral distribution of QOM (mg HC/g TOC) of unit 4's upper subunit	230
Figure 5.75 Lateral distribution of QOM (mg HC/g TOC) of unit 3's lower subunit	231
Figure 5.76 Lateral distribution of QOM (mg HC/g TOC) of unit 3's middle subunit	232
Figure 5.77 Lateral distribution of QOM (mg HC/g TOC) of unit 3's upper subunit	233
Figure 5.78 Lateral distribution of QOM (mg HC/g TOC) of unit 2's lower subunit	234
Figure 5.79 Lateral distribution of QOM (mg HC/g TOC) of unit 2's upper subunit	235
Figure 5.80 Variation of TOC and HI with depositional environments	246
Figure 5.81 Variation of TOC and HI with organic maturation	249
Figure 5.82 Variation of TOC and HI with sedimentation rate	251
Figure 5.83 Variation of TOC and HI with age	255
Figure 5.84 Variation of mean sedimentation rate and TOC with age	256
Figure 5.85 Variation of genetic potential and QOM with age	260
Figure 6.1 Location of well data used in this study	269
Figure 6.2 W-E stratigraphic section-1	270
Figure 6.3 W-E stratigraphic section-2	270
Figure 6.4 W-E stratigraphic section-3	271
Figure 6.5 W-E stratigraphic section-4	271
Figure 6.6 N-S stratigraphic section-5	272
Figure 6.7 N-S stratigraphic section-6	272
Figure 6.8 Shift of Tmax with heating rate	279
Figure 6.9 Reaction rate profiles using different values of distribution of activation energies	279
Figure 6.10 Activation energy of each stratigraphic unit	289
Figure 6.11 The extent and rate of hydrocarbon generation at Ranong-1 well	293
Figure 6.12 The extent and rate of hydrocarbon generation at Kung-1 well	293

Figure 6.13 The extent and rate of hydrocarbon generation at Surat-1 well	294
Figure 6.14 The extent and rate of hydrocarbon generation at Platong-8 well	294
Figure 6.15 The extent and rate of hydrocarbon generation at Platong-1 well	295
Figure 6.16 The extent and rate of hydrocarbon generation at Insea-1 well	295
Figure 6.17 The extent and rate of hydrocarbon generation at Pakarang-1 well	296
Figure 6.18 The extent and rate of hydrocarbon generation at Pladang-3 well	296
Figure 6.19 The extent and rate of hydrocarbon generation at South Platong-2 well	297
Figure 6.20 The extent and rate of hydrocarbon generation at Trat-1 well	297
Figure 6.21 The extent and rate of hydrocarbon generation at Dara-1 well	298
Figure 6.22 The extent and rate of hydrocarbon generation at Erawan-12-1 well	298
Figure 6.23 The extent and rate of hydrocarbon generation at Erawan-12-8 well	299
Figure 6.24 The extent and rate of hydrocarbon generation at Satun-3 well	299
Figure 6.25 The extent and rate of hydrocarbon generation at Jakrawan-2 well	300
Figure 6.26 The extent and rate of hydrocarbon generation at Krut-1 well	300
Figure 6.27 The extent and rate of hydrocarbon generation at Erawan-K-1 well	301
Figure 6.28 The extent and rate of hydrocarbon generation at Baanpot-1 well	301
Figure 6.29 The extent and rate of hydrocarbon generation at Baanpot-B-1 well	302
Figure 6.30 The extent and rate of hydrocarbon generation at Jakrawan-1 well	302
Figure 6.31 The extent and rate of hydrocarbon generation at Funan-1 well	303
Figure 6.32 The extent and rate of hydrocarbon generation at Yala-2 well	303
Figure 6.33 The extent and rate of hydrocarbon generation at Kaphong-3 well	304
Figure 6.34 The extent and rate of hydrocarbon generation at Kaphong-1 well	304

Figure 6.35 The extent and rate of hydrocarbon generation at Platong-5 well	305
Figure 6.36 The extent and rate of hydrocarbon generation at South Platong-1 well	305
Figure 6.37 The extent and rate of hydrocarbon generation at Satun-2 well	306
Figure 6.38 The extent and rate of hydrocarbon generation at Satun-1 well	306
Figure 6.39 The extent and rate of hydrocarbon generation at Erawan-12-9 well	307
Figure 6.40 The extent and rate of hydrocarbon generation at Erawan-12-7 well	307
Figure 6.41 Calculated present-day reaction extent of unit 6's hydrocarbon generation	308
Figure 6.42 Calculated present-day reaction extent of unit 5's hydrocarbon generation	309
Figure 6.43 Calculated present-day reaction extent of unit 4's hydrocarbon generation	310
Figure 6.44 Calculated present-day reaction extent of unit 3's hydrocarbon generation	311
Figure 6.45 Calculated present-day reaction extent of unit 2's hydrocarbon generation	312
Figure 6.46 Timing of main hydrocarbon generation phase of unit 6	313
Figure 6.47 Timing of main hydrocarbon generation phase of unit 5	314
Figure 6.48 Timing of main hydrocarbon generation phase of unit 4	315
Figure 6.49 Timing of main hydrocarbon generation phase of unit 3	316
Figure 6.50 Timing of main hydrocarbon generation phase of unit 2	317
Figure 6.51 The effect of sample preparation on kinetic parameters	321
Figure 6.52 Variation of kinetic parameters with depositional environments	321
Figure 6.53 Variation of kinetic parameters with organic maturation	325

ACKNOWLEDGEMENT

The author is grateful to his thesis supervisor Dr. R.M. Bustin for direction, advice, support and patience throughout this study. The author gratefully acknowledges the financial support of the Canadian International Development Agency. The author is grateful to Unocal Thailand Company for providing all the logistical data. Thanks are also due to Dr. M.A. Barnes, Dr. W.C. Barnes, Dr. J.W. Murray, Dr. R.L. Chase, and Dr. G.E. Rouse of the University of British Columbia for their expertise and consultation. Thanks are also extended to Dr. R.L. Braun of the Lawrence Livermore National Laboratory, California, for his consultation in kinetic modelling. Finally, I am grateful to my wife Kwanjai Chonchawalit, without whose patience and moral support, this work would not have been possible.

1. INTRODUCTION

1.1 GENERAL OVERVIEW

The Pattani Basin is a Tertiary depocenter located in the central part of the Gulf of Thailand (Figure 1.1) covering approximately 10,000 square kilometres. The basin is an intracratonic basin containing a succession of more than ten kilometres of Tertiary sedimentary rocks. The sequence is dominated by nonmarine and marginal marine clastics, predominantly sandstone and shale. The origin of the Pattani Basin and other Tertiary basins in Thailand is related to the extensional tectonic regime developed after the collision of the Indian and Eurasian plates.

Tertiary basins, including the Pattani Basin, are the prime target for hydrocarbon exploration in Southeast Asia. Numerous oil and gas discoveries in these basins have stimulated extensive exploration programs in the 1980's and 1990's, the most active of which is centered in the Pattani Basin. Although exploration and production activities in the Pattani Basin have been carried out for more than ten years, there is very limited previous information available on source rocks and organic maturation history (Achalabhuti and Oudom-Ugsorn, 1978; Chinbunchorn et al., 1989). The present investigation attempts to study tectonic evolution, sedimentary history, and hydrocarbon potential of the Tertiary strata in the Pattani Basin. Tectonic evolution of this basin is studied in terms of possible mechanisms of basin formation, burial and thermal histories of the stratigraphic units. The evaluation of hydrocarbon potential includes analysis of source rock properties and potential, organic maturation and hydrocarbon generation histories.

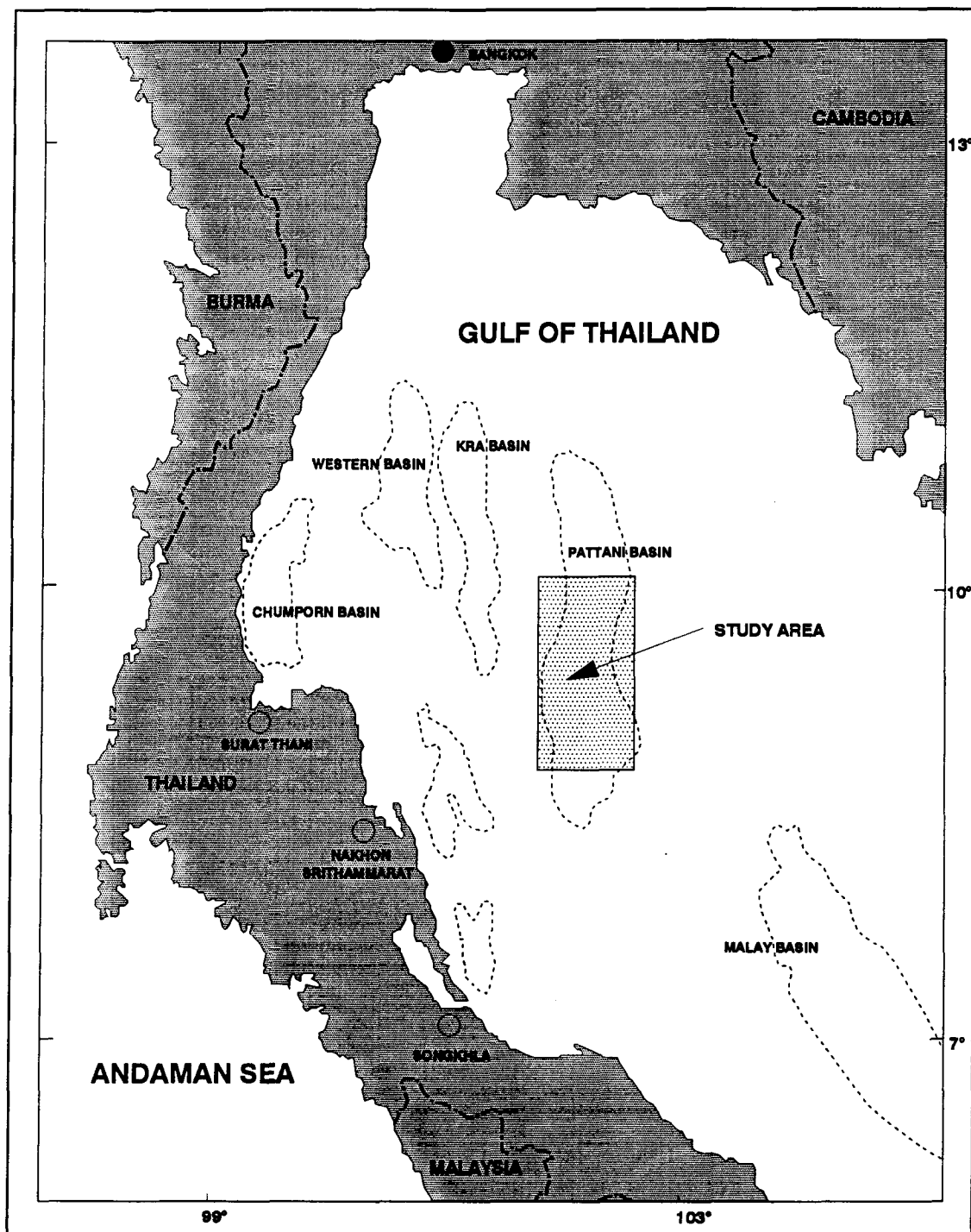


Figure 1.1: Tertiary basins in the Gulf of Thailand. The basins show general N-S trending alignment.

Various analytical techniques have been used in this study. Wireline log analysis, well cutting sample examination and paleontological data are used to interpret stratigraphy and depositional environments in the study area. Backstripping and geohistory analyses are employed to restore the subsidence history of the basin. Models of basin formation and lithospheric stretching are used to predict the thermal history of the basin. Organic petrography is used to establish the degree of organic maturation and the maturity framework of the strata. Rock-Eval pyrolysis and organic petrography are used to identify and characterize potential hydrocarbon source rocks. Modelling of chemical kinetics is used to determine the timing and extent of hydrocarbon generation.

1.2 LOCATION OF THE STUDY AREA

The study area encompasses the western flank of the Pattani Basin, Gulf of Thailand, between latitudes 8° 50'N and 10° 05'N and longitudes 101° 05'E and 101° 45'E (Figure 1.2). The area covers approximately 5,000 square kilometres and lies in water 60-80 m deep. This area was chosen for study in order to enhance our knowledge of geological evolution and hydrocarbon potential of economically important Tertiary strata in the Pattani Basin. The Pattani Basin is the most prolific basin in Thailand, accounting for more than 80% of present-day hydrocarbon production in the country.

1.3 DATA SOURCES

The data and samples used in this study were provided by Unocal Thailand Company. The data includes 2D seismic sections, rotary cutting samples, wireline logs, paleontological reports and other general geological information.

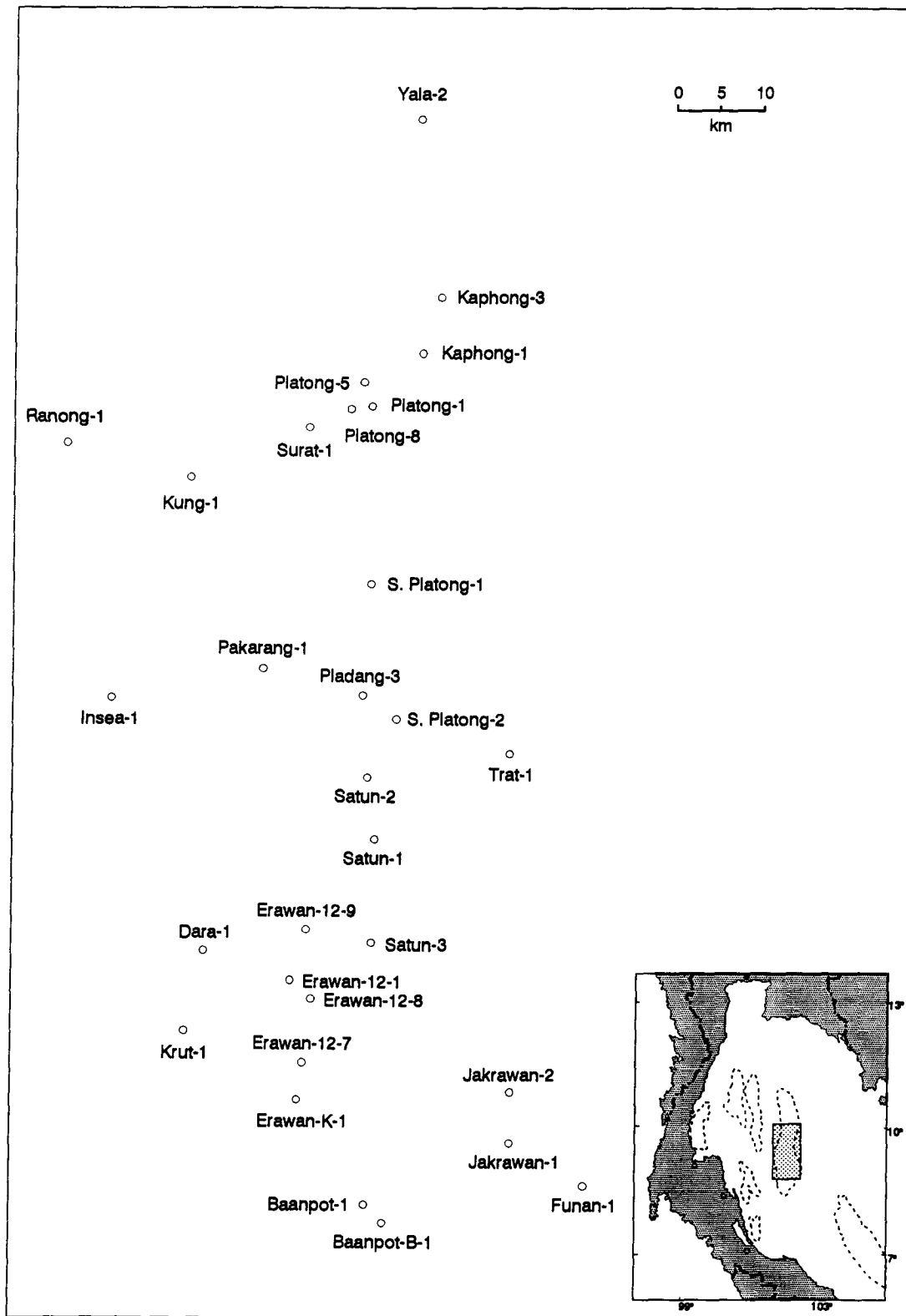


Figure 1.2: Location of well data used in this study

1.4 EXPLORATION HISTORY IN THE GULF OF THAILAND

Petroleum exploration in the Pattani Basin, the largest Tertiary basin in the Gulf of Thailand, began in the early 1970's (Nakanart, 1978). The first well, drilled in 1971 by Continental Oil Company of Thailand, did not encounter hydrocarbons. The first discovery well was completed in 1972 by the Union Oil Company of Thailand. The discovery well encountered natural gas and condensate. Additional drilling and other exploration activities have been carried out since. The first natural gas production began in August, 1981, from Erawan field by Unocal Thailand Company (Lian and Bradley, 1986). There have been more than 10 natural gas and condensate fields found to date. Current production rates from 4 fields, all located in the western flank of the Pattani Basin and operated by Unocal Thailand, are approximately 3200 m³/day of condensate and 15.6 million m³/day of gas (Chinbunchorn et al., 1989). Other fields are being prepared for further production.

1.5 PURPOSE OF STUDY

The main purpose of this investigation is to establish the tectonic evolution, sedimentary history, and hydrocarbon generation of Tertiary strata in the Pattani Basin, Gulf of Thailand. In order to achieve the goals described above, this thesis is divided into four parts. The first part describes the stratigraphy and sedimentological evolution of Tertiary strata. The second part describes the tectonic evolution, subsidence and thermal histories, and possible formation mechanisms of the basin. A computer program, based on geohistory analysis (Van Hinte, 1978; Angevine et al., 1990) and a nonuniform lithospheric stretching model (McKenzie, 1978; Hellinger and Sclater, 1983; Friedinger, 1988), is developed to

calculate decompacted burial and tectonic subsidence histories and to determine the history of heat flow of the basin. The third part evaluates the hydrocarbon source rock potential of the Tertiary strata. The fourth part deals with kinetic properties and organic maturation and histories of hydrocarbon generation of the stratigraphic units. Two computer programs, based on the Arrhenius equation and the distribution of the activation energies (Braun and Sweeney, 1987; Sweeney and Burnham, 1990) were developed to calculate kinetic parameters of the kerogen and to predict timing and extent of hydrocarbon generation respectively.

Results from this integrated study may greatly improve our understanding of the geological evolution of the Pattani Basin and provide a more accurate assessment of hydrocarbon potential of the Tertiary strata in the Pattani Basin, as well as other basins of similar tectonic setting.

2. REGIONAL GEOLOGY

2.1 INTRODUCTION

The regional geology of the Pattani Basin has been summarized by Achalabhuti and Oudom-Ugsorn (1978) and Lian and Bradley (1986). The stratigraphy and history of sedimentation have been studied by Woollands and Haw (1976), ASCOPE (1981), and Bunopas and Vella (1983). Tectonic elements and structural evolution of the study area have been the subject of discussion by various authors (Molnar and Tapponnier, 1975; Bunopas and Vella, 1983; Hellinger and Sclater, 1983; Peltzer and Tapponnier, 1988; Ohnstad, 1989; Polachan and Sattayarak, 1989). This chapter summarizes current ideas on the regional geology and tectonic elements of Tertiary strata in the Gulf of Thailand.

2.2 PRESENT-DAY GEOLOGIC SETTING

The Gulf of Thailand basin is a northwest-trending reentrant into Sundaland, the southwestern most part of the Eurasian plate. It lies near the intersection of two major transcurrent fault systems (Figure 2.1). The first fault system, the NW-SE trending Three Pagoda fault, runs along from the Burmese border through the Three Pagoda Pass and may extend along the northeastern part of the Gulf of Thailand. The second fault system, comprising the NNE-SSW trending Phang Nga-Surat Thani and Ranong faults, cuts across the southern Thai Peninsula and extends into the western part of the Gulf. The displacement direction along both fault systems has been described as left-lateral by some authors (Wilcox et al., 1973; Tapponnier et al., 1986) but as right-lateral by others (O'Leary and Hill, 1989; Polachan and Sattayarak, 1989). The geological structures seen in Tertiary

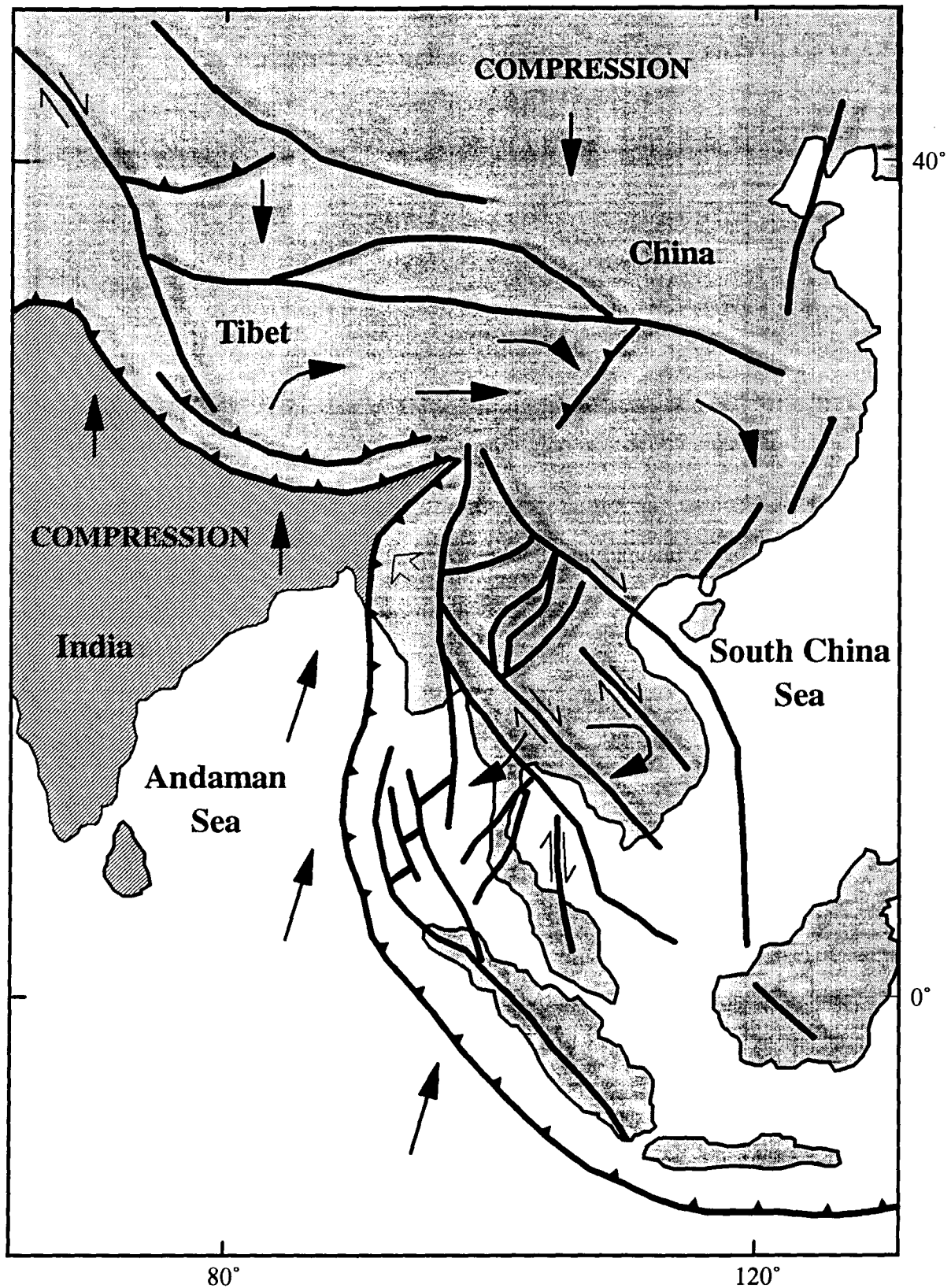


Figure 2.1 Tectonic map of S.E. Asia and South China Sea showing the main fault patterns and the relative movement of crustal blocks in response to the collision of India with Eurasia

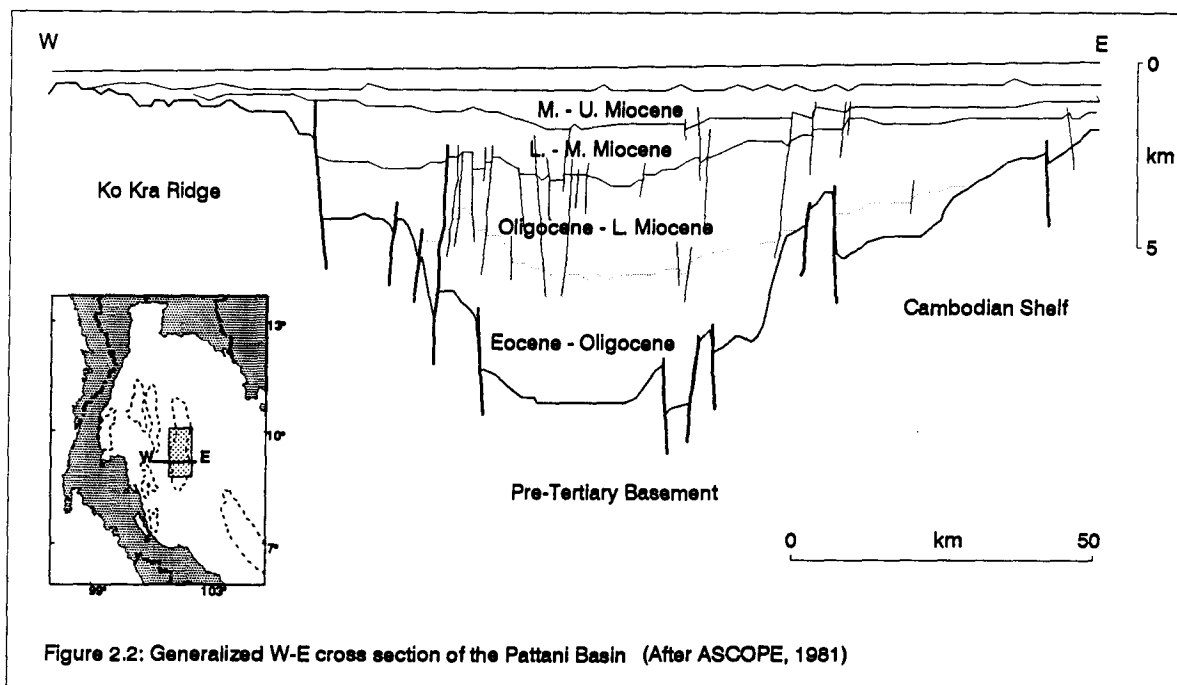
sections in the Pattani Basin and adjacent areas comprise a series of N-S trending elongate grabens, half-grabens, and horsts. Further south, in the Malay basin, grabens and half grabens show a NW-SE trending (Figure 1.1).

2.3 TECTONIC ELEMENTS

Geological structures within the Pattani Basin, the largest basin in the Gulf of Thailand, and adjacent basins indicate a multitude of closely spaced N-S trending normal faults. Many of these normal faults transect Pre-Tertiary basement suggesting a basement-involved extension. An idealized cross section demonstrating a basement-involved extension is illustrated in Figure 2.2.

The Pattani Basin is approximately 300 kilometres long and 50 to 80 kilometres wide. It is bounded to the west by the Ko Kra Ridge, to the east by the shallow Cambodian Shelf, and to the southeast by the Narathiwat Ridge (Figure 1.1 and Figure 2.2). It is filled with Tertiary nonmarine fluvio-deltaic clastic sediments up to ten kilometres thick in the grabens and in places less than one kilometre thick on the horsts. Drilling efforts have not reached basement in the deepest part of the basin due to high temperature resulting from high geothermal gradients. The oldest sediments penetrated by drilling within the basin are Oligocene in age. The stratigraphy in the basin can be broadly subdivided into 3 sequences: (1) prerift sequence: basement rocks that predate the formation of Tertiary basins; (2) synrift sequence: a sequence deposited during active rifting; and (3) post-rift sequence: a sequence deposited after the cessation of rifting (Chinbunchorn et al., 1989).

Geophysical surveys and drilling results show that the Pre-Tertiary basement comprises diverse rocks of different ages including upper Paleozoic metamorphic,



clastic, and carbonate rocks, Mesozoic clastic rocks, and upper Paleozoic and Mesozoic granites (Lian and Bradley, 1986).

The dominant period of rifting of Pre-Tertiary basement lasted about 20 m.y. from Late Eocene to Early Miocene (Hellinger and Sclater, 1983; Chinbunchorn et al., 1989). The synrift sequence consists predominantly of low-energy alluvial plain and lacustrine deposits with high-energy alluvial fan and braided stream deposits in the lower part. The upper part of synrift sequence comprises mainly fluvial deposits, delta-front deposits, and some ephemeral lacustrine deposits in the central part of the basin.

The post-rift sequence, deposited during late Early Miocene to Quaternary time, comprises a transgressive succession beginning with mangrove swamp at the base with minor nonmarine deposits and extends into the present-day shallow marine environment.

3. STRATIGRAPHY AND SEDIMENTOLOGY

3.1 ABSTRACT

The Pattani Basin is a N-S elongate rift basin which comprises part of the Tertiary rift system in the Gulf of Thailand. The basin is of significant economic importance as a major hydrocarbon province in Thailand. The sedimentary evolution in this area is a response to rifting process which began in Late Eocene. The sedimentary succession is divided into synrift and post-rift sequences. Deposition of synrift sequences corresponds to rifting and extension of Continental Southeast Asia which included episodic block faulting and rapid subsidence. The main controlling factors of the sedimentary records of synrift sequences are high subsidence rate and large sediment influx which are the direct result of rifting. Deposition of post-rift sequences, on the other hand, corresponds to a period of relatively slower subsidence and less sediment influx. Hence eustatic sea-level fluctuation played a more important role in the resulting sedimentary records.

The synrift sequence comprises three stratigraphic units. The basal unit represents Late Eocene to Early Oligocene nonmarine, alluvial fan and braided stream deposits in the lower part and floodplain-channel deposits in the upper part. The middle synrift unit represents Late Oligocene to Early Miocene nonmarine, floodplain and channel deposits in the lower part and mainly channel deposits in the upper part. The upper synrift unit comprises an Early Miocene regressive sequence in which basal prodelta to shallow marine sediments are overlain by distributary mouth bar deposits and beach ridge complexes which, in turn, are overlain by nonmarine floodplain and meandering channel deposits. The first marine transgression in the Pattani Basin occurred in the Early Miocene and may have been the result of rapid

subsidence due to an episode of block faulting and/or eustatic sea-level rise. The following regressive succession in the upper part of synrift sequence resulted when the deposition rate exceeded the rate of relative sea-level rise. Although not reached by drilling, a thick succession of synrift lacustrine deposits are believed to have been deposited in the vicinity of the basin center throughout the early part of the rifting period.

The post-rift succession comprises three stratigraphic units. The lower post-rift unit represents an Early to Middle Miocene regressive sequence similar to that of the upper synrift unit. The late Early Miocene transgression, which was probably the result of a rapid eustatic sea-level rise, created a brief period of nondeposition during which the rate of relative sea-level rise exceeded the rate of deposition. As the deposition rate slowly exceeded the rate of relative sea-level rise, a regressive succession resulted. The middle post-rift unit represents a Middle Miocene transgressive succession which was probably the result of slow rise of relative sea-level and a decreasing amount of sediment supply. A rapid fall of relative sea-level which resulted in subaerial exposure, intense oxidation, and possibly erosion of the Middle Miocene sediments was probably the effect of eustatic sea-level fall at the end of the Middle Miocene. The upper post-rift unit represents a Late Miocene to Pleistocene transgressive succession indicating a slow rise of eustatic sea-level, slow subsidence, and decreasing amount of sediment influx. The present-day shallow marine condition in the Pattani Basin is the continuation of the latest transgression.

3.2 INTRODUCTION

The Pattani Trough is the largest of a series of N-S trending rift basins in the Gulf of Thailand (Figure 3.1) containing more than ten kilometres of Tertiary sediments. The Tertiary basins in Thailand have striking geological similarities in origin and tectonic setting. The evolution of the Pattani Basin, thus, provides a general model for other basins in the area. Although the stratigraphy of the Pattani Basin has been studied by Woollands and Haw (1976); Achalabhuti and Oudom-Ugsorn (1978) and Lian and Bradley (1986), these studies generally have considered regional stratigraphy. The present investigation provides a somewhat more detailed description and interpretation of the sedimentary and stratigraphic development of the Tertiary strata in the Pattani Basin. This section describes and interprets the stratigraphic successions in terms of typical log profiles, thickness, facies distribution, and depositional environments. Data are from well logs, cutting samples, 2D seismic sections, and unpublished paleontology reports provided by the Unocal Thailand Company. The study area is located on the west flank of the Pattani Basin which has been most extensively explored.

3.3 METHODS OF STUDY

The stratigraphic correlation and sedimentological analysis in this study are based mainly on wireline logs, cutting samples, and palynological data.

The gamma-ray log patterns can be used to identify vertical sequence and log facies because gamma-ray logs reflect clay content and grain-size profiles in clastic sequences. As vertical profiles of sediment grain-size are often environmentally diagnostic in clastic rocks. Log signatures, combined with knowledge of the

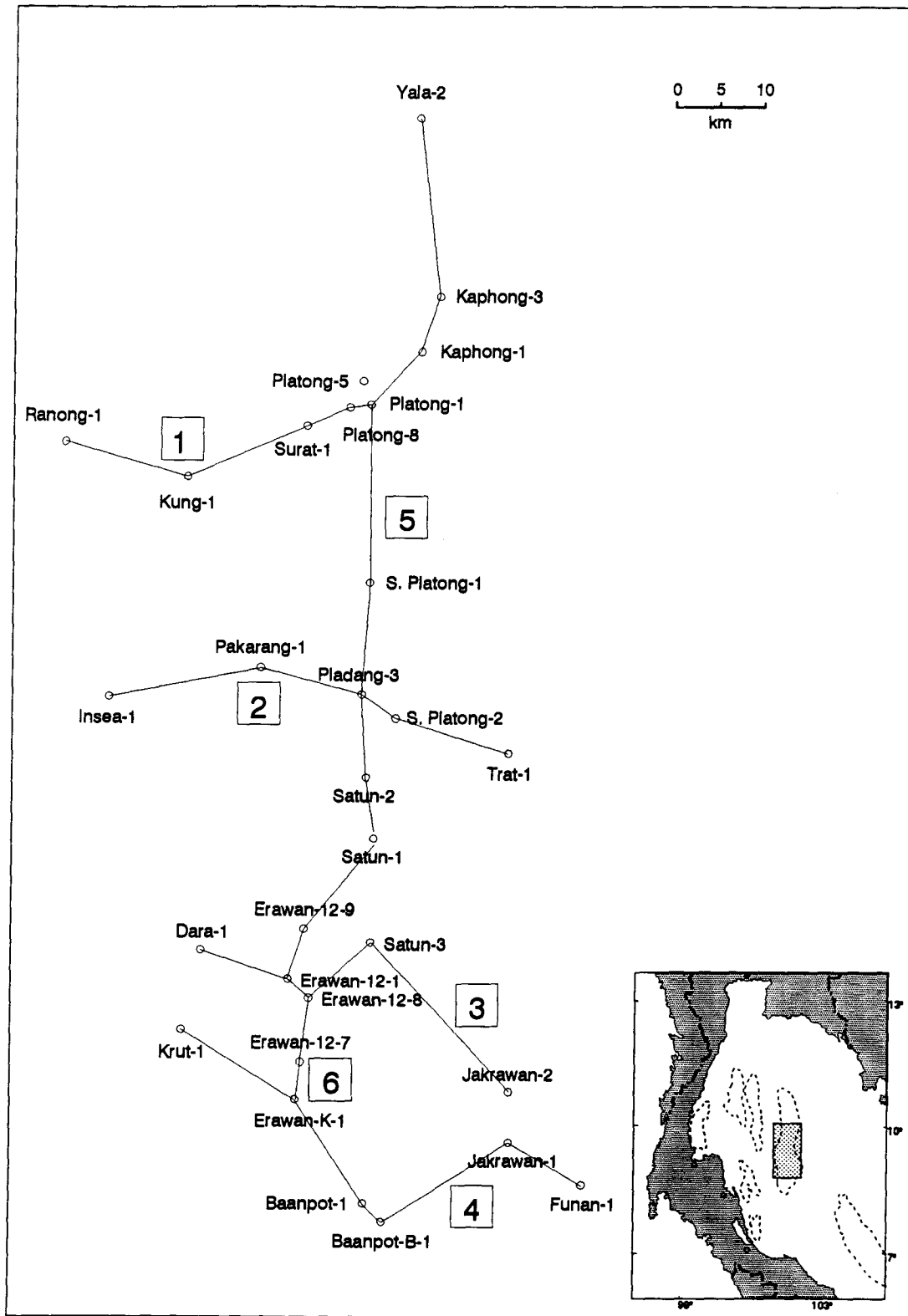


Figure 3.1: Location of well data used in this study. Numbers in the box indicate the cross sections shown in Figures 3.5 through 3.10

general depositional setting, the vertical distribution of glauconite (marine indicator) and carbonaceous detritus (winnowing index), are a powerful tool in diagnosing clastic environments (Selley, 1979). Figures 3.2, and 3.3 show typical log signatures and their various combinations and interpretation. Environmental interpretation from wireline logs utilized in this study is based on Fisher (1969), Selley (1979), Galloway and Hobday (1983), Cant (1984) and Walker (1984).

Drill-cutting samples were used to obtain the lithology of the strata. Micropaleontological data, where available, were used as a framework for age determination and, together with log signatures, for interpretation of depositional environment. Because no core samples were available, lithologies and depositional environments interpreted from wireline logs had to be calibrated with drill-cutting samples. Electric logs were also used as a secondary tool for correlation. Stratigraphic correlation in the deeper part of the basin, which is not reached by drilling, utilized 2D seismic sections.

Due to the laterally discontinuous sedimentation and close spacing of faults, correlation of individual marker horizons between wells is difficult. Sequence correlation was thus used in this study. The technique involves the recognition and matching of distinctive patterns of sedimentary succession in logs rather than single marker beds (Cant, 1984).

The predominance of nonmarine or marginal marine sediments rules out the use of foraminifera for age correlation and dating. Stratigraphic subdivision was thus made by means of lithological association and palynomorph assemblages (Woollands and Haw, 1976; Ratanasthien, 1988; Scrutton and Tidey, 1974). Figure 3.4 shows the Cenozoic palynological subdivision of various geographic

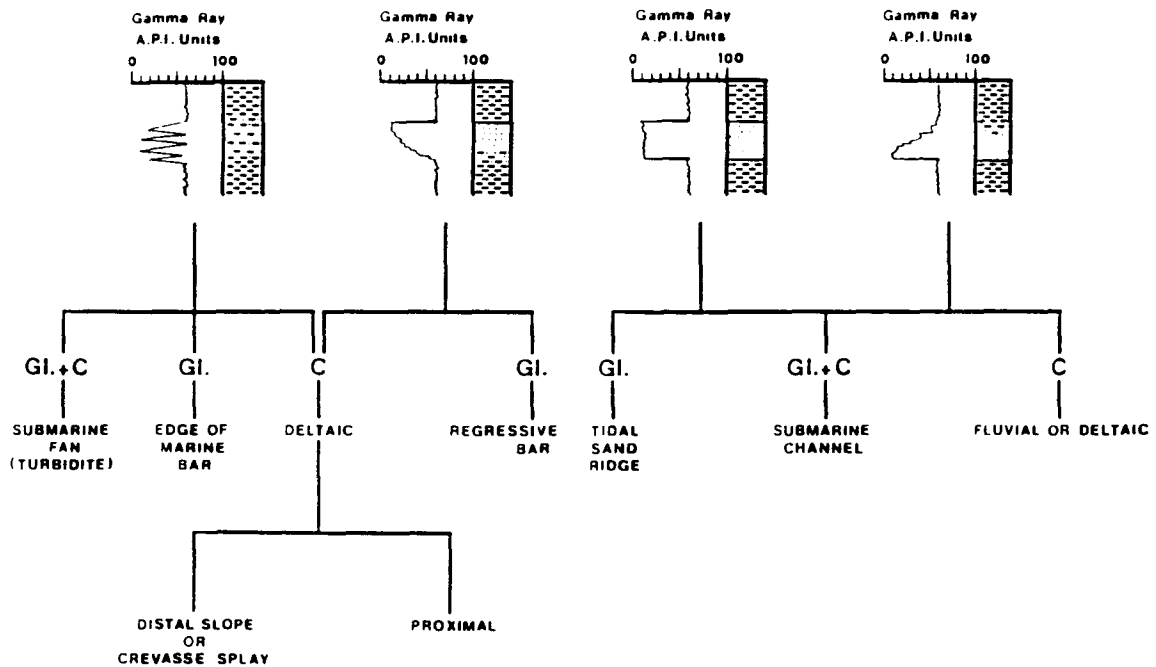


Figure 3.2: Four characteristic gamma ray log motifs. From left to right: thinly interbedded sand and shale; an upward coarsening profile with an abrupt upper sand-shale contact; a uniform sand with abrupt upper and lower contacts; and, furthest right, an upward fining sand-shale sequence with an abrupt base. None of these is environmentally diagnostic on its own. Coupled with data on their glauconite and carbonaceous detritus content, however, they define the origin of many sand bodies. (After Selley, 1979)

Log motif			
Glauconite and shell debris (high-energy marine)	Tidal channel	Tidal sand wave	Regressive barrier bar
Glauconite, shell debris, carbonaceous detritus, and mica (dumped marine)	Submarine channel		Prograding submarine fan
	Turbidite fill	Grain flow fill	
Carbonaceous detritus and mica (dumped)	Fluvial or deltaic channel	Delta distributary channel	Prograding delta or crevasse splay

Figure 3.3: Diagram showing the three common grainsize motifs seen on S.P. and gamma ray logs and how, by combining these with the analysis of well samples, environmental interpretations of sand bodies can be made. (After Selley, 1979)

GEOLOGICAL SUBDIVISION		PALYNOLOGICAL SUBDIVISION					
	AGE IN MILLION YEARS AFTER Funnel (1964)	PANTROPICAL ZONE	ATLANTIC ZONE	CARIBBEAN ZONE	BORNEO ZONE		
PLEISTOCENE	3	Echitricolporites Spinosus		Alnipollenites Verus	Podocarpus		
	7			Echitricolporites McNeillyi	Dacrydium		
MIOCENE	UPPER			Crassorettriletes Vanraadshooveni	Verrutricolporites Rotundiporis	Pachydermites Diederixi	Florschuetzia Meridionalis
	MIDDLE					Grimsdalea Magnaclavata	Florschuetzia Levipoll
	LOWER	Multimaginites Vanderhammeni	Psiladiporites Minimus				
		26	Jandufouria Seamrogiformis				
OLIGOCENE	38	Magnastriatites Howardi	Cicatricosisporites Dorogensis		Florschuetzia Trilobata		
EOCENE	UPPER	Verrucatosporites Usmensis			?		
	45	Monoporites Annulatus		Retitricolporites Gularensis			
	MIDDLE			Psilatricolporites Operculatus			
49	Psilatricolporites Crassus						

Fig 3.4: Cenozoic palynological zones (Modified from Germeraad et al., 1968 and Ratanasthien, 1988)

zones (Germeraad et al., 1968). Based on the palynomorph assemblages of conifer and mangrove pollen present in Borneo and Pantropical zones, palynological subdivisions are the *Podocarpus* floral zone (Quaternary), the *Dacrydium* floral zone (Pliocene), the *Florschuetzia meridionalis* floral zone (Middle to Upper Miocene), and the *Florschuetzia levipoli* floral zone (Lower to Middle Miocene). The Oligocene epoch is represented by the occurrence of the *Florschuetzia trilobata* floral zone in Borneo and the *Magnastriatites howardi* in the Pantropical area. The Upper Eocene epoch is marked by the occurrence of *Verrucatosporites usmensis* in the Pantropical area.

It is important to note that the palynology described above provides only approximate dating and allows only broad correlations. A more detailed chronology is difficult to achieve because palynomorphs suitable for dating are few and the index palynomorphs are facies-controlled to some extent, e.g. *Florschuetzia* pollen is dispersed mainly by water (Woollands and Haw, 1976). The abundance of unfossiliferous red beds further restricts dating and correlation to limited intervals. Benthic foraminifera are present in some intervals, but are not age-diagnostic, and their use is therefore restricted to an indication of marginal marine environments.

3.4 STRATIGRAPHIC SUBDIVISION

Due to rapid lateral variation of individual beds, detailed lithostratigraphic correlations based on electric logs are impossible. Correlation in this study is therefore based on the recognition and matching of distinctive log patterns of sedimentary successions, which reflect broader and more widespread geological events, rather than a single marker bed. Although 2D seismic sections exist, their

use is limited to confirming lateral continuity of stratigraphic sequences between wells and extrapolating stratigraphic units laterally from wells to non-penetrated areas in the deeper part of the basin. No interpretation of sequence stratigraphy has been made in this study for the following reasons: first, the seismic sections available are of relatively poor quality; second, because the successions under study are mainly nonmarine deposits with only minor marine influence; thus, the sequence boundary which is defined by the basinward shift of the sedimentary facies is very difficult to identify especially from the widely-spaced well data (Van Wagoner, 1991).

Six stratigraphic subdivisions can be recognized from subsurface data in the Pattani Basin. They are referred to here, from younger to older ages, as unit 1 through unit 6. Units 6, 5, and 4 are interpreted to be synrift sediments, whereas units 3, 2, and 1 are regarded as post-rift. Figures 3.5 to 3.8 summarize stratigraphic correlation in four E-W sections in the study area whereas Figures 3.9 and 3.10 summarize the stratigraphic correlation in two parts of a continuous north-south section. Table 3.1 summarizes the stratigraphy and depositional environments of Tertiary strata in the study area.

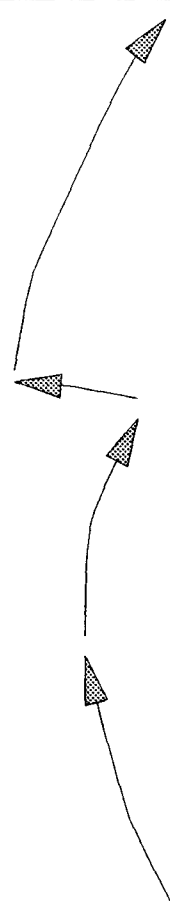
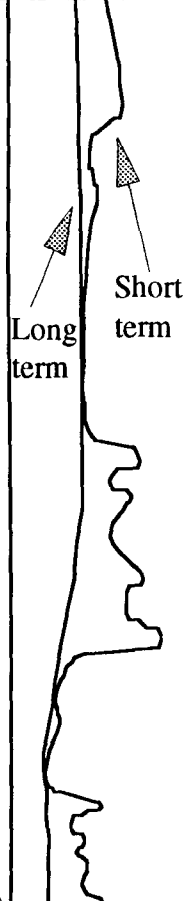
3.4.1 Unit 6

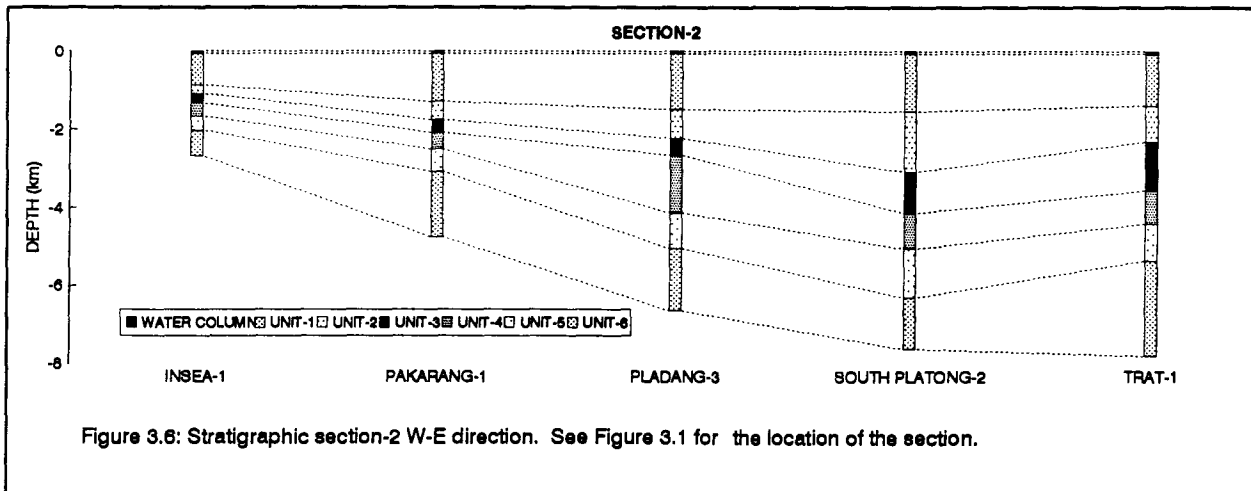
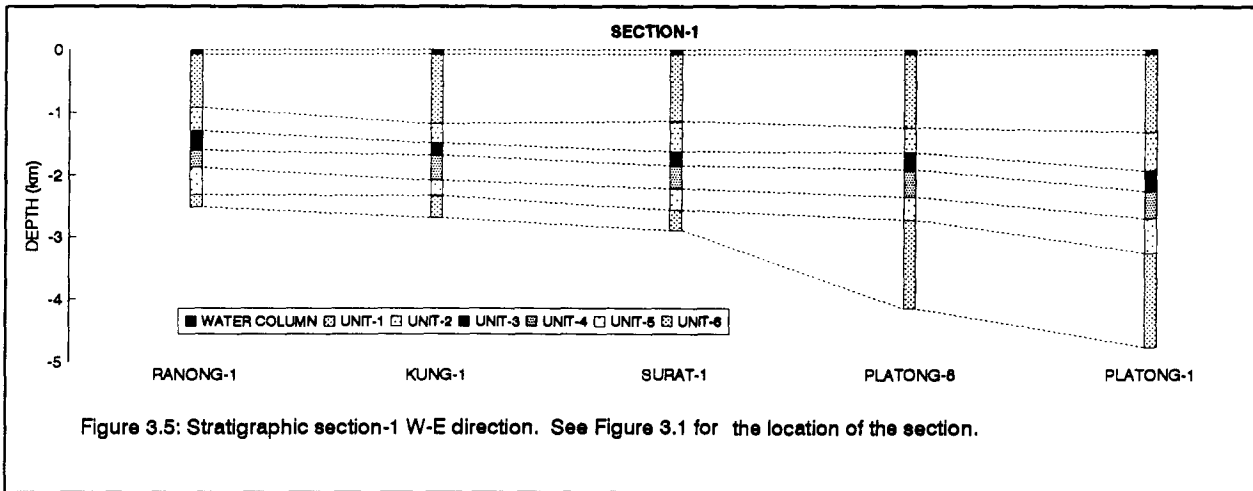
Unit 6 is the oldest Tertiary sediment package encountered in this study. Only three wells located in the northwest corner of the basin completely penetrate this unit. Its lower boundary, where penetrated, is marked by Pre-Tertiary basement rocks such as Cretaceous granite or Paleozoic and Mesozoic sediments. This boundary is clearly seen as a strong and continuous reflector in seismic sections. The upper boundary is marked by the sudden change from low gamma radiation in

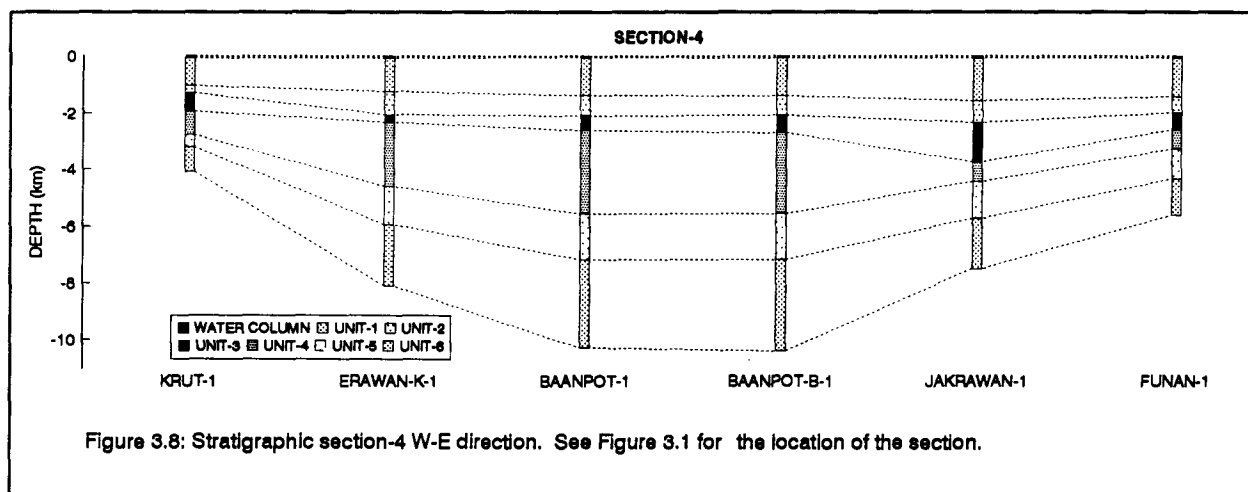
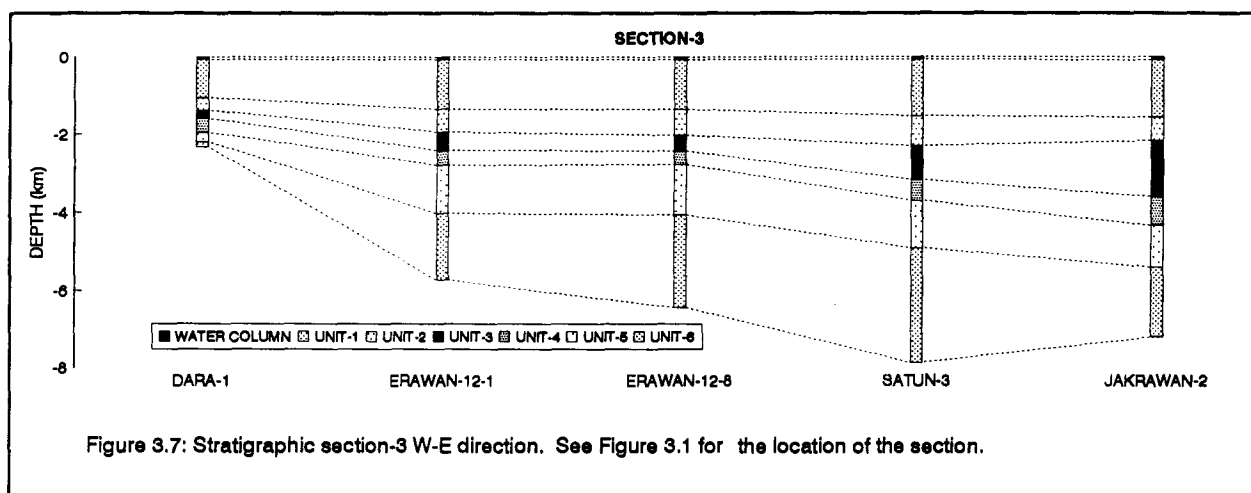
Table 3.1: Stratigraphy and depositional environments of the Tertiary post-rift strata in the Pattani Basin

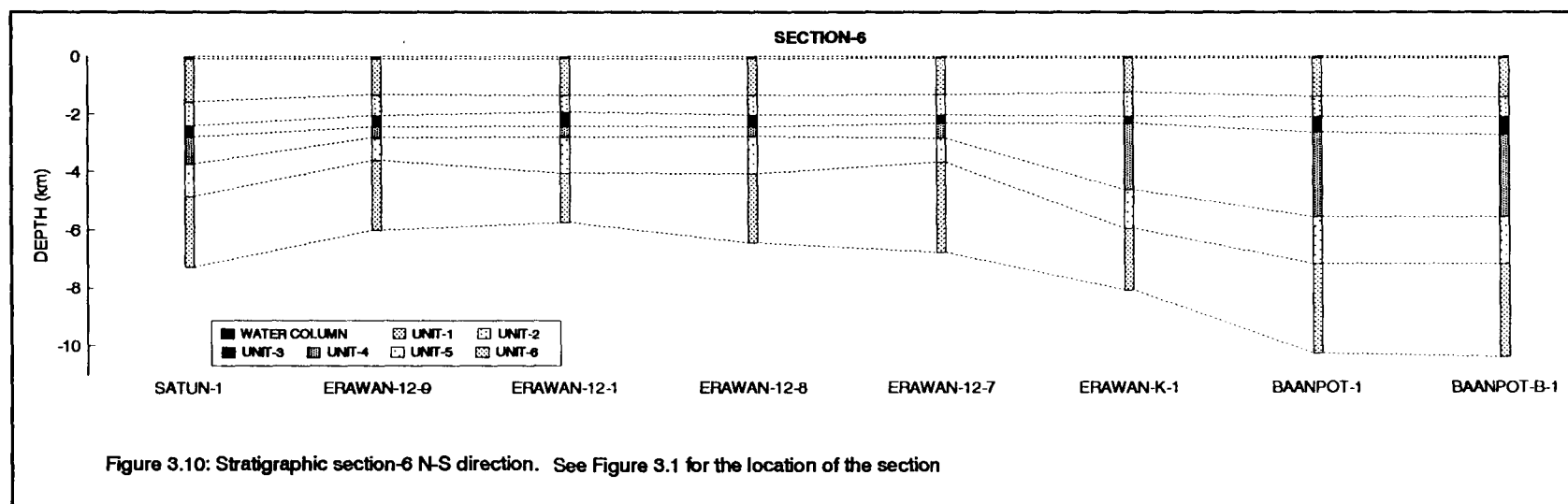
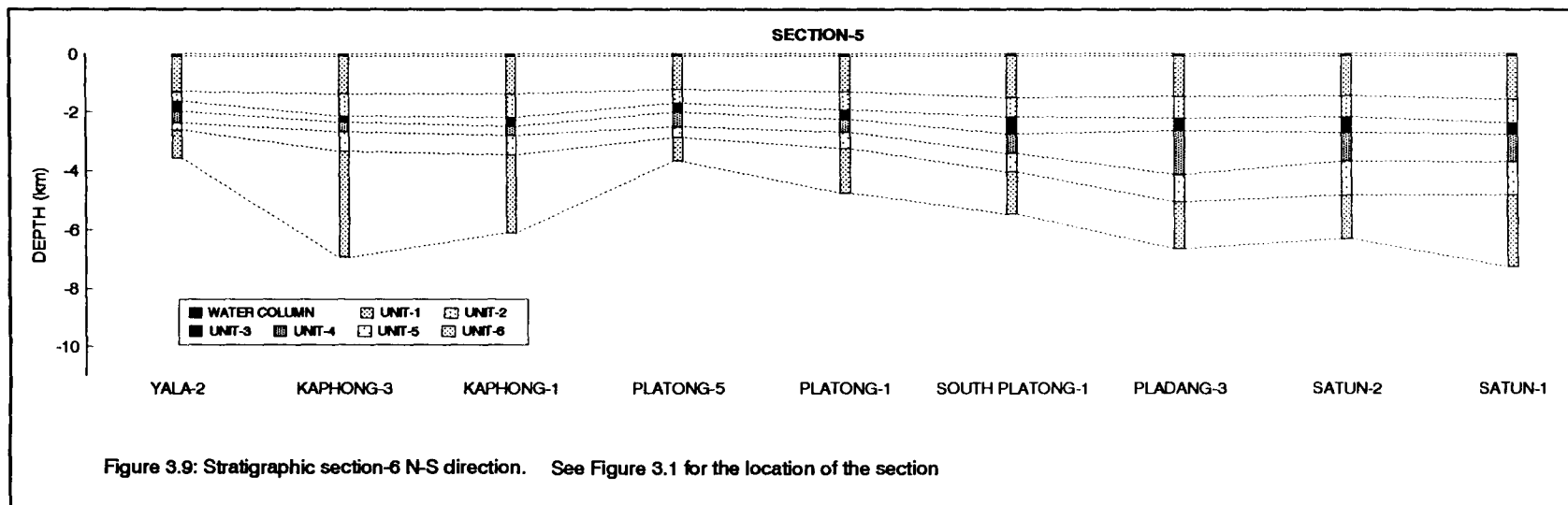
UNIT	SUBUNIT	DEPOSITIONAL ENVIRONMENTS	SEDIMENTARY STRUCTURES	LITHOLOGY	RELATIVE SEA-LEVEL		EUSTATIC SEA-LEVEL	
					+	-	rise	fall
1	Upper	Shallow marine	Fine-grained	Not available				
	Middle	Interdistributary bay and/or crevasse splay	Generally fine-grained	Dark grey claystone				
	Lower	Distributary channel in the Coastal plain	Fining-upward sequences	Reddish brown claystone and sandstone				
2	Upper	Brackish swamp and marginal marine	Generally fine-grained with some fining-upward sequences	Brownish grey claystone and sandstone				
	Lower	Distributary channels and floodplain	Generally fine-grained with fining-upward sequences	claystone and sandstone				
3	Upper	Meandering channel	Fine-grained and fining-upward sequences	Sandstone and minor claystone				
	Middle	Distributary mouth-bar and beach-ridge complex	Coarsening-upward sequences	Sandstone and claystone				
	Lower	Prodelta and shallow marine	Generally fine-grained	Claystone and minor sandstone				

Table 3.1: (continued): Stratigraphy and depositional environments of the Tertiary synrift strata in the Pattani Basin

UNIT	SUBUNIT	DEPOSITIONAL ENVIRONMENTS	SEDIMENTARY STRUCTURES	LITHOLOGY	RELATIVE SEA-LEVEL	EUSTATIC SEA-LEVEL
					+ -	rise fall
4	Upper	Upper delta plain and floodplain	Generally fine-grained with fining-upward sequences	Claystone and sandstone		
	Middle	Distributary mouth-bar and beach-ridge complex	Coarsening-upward sequences	White sandstone and minor claystone		
	Lower	Prodelta and shallow marine	Generally fine-grained	brownish claystone with coal partings		
5	Upper	Nonmarine meandering channel	Fining-upward sequences	Brownish sandstone		
	Lower	Meandering channel and floodplain	Generally fine-grained with fining-upward sequences	Red claystone and sandstone		
6	Upper	Floodplain and channel	Fine-grained and fining-upward sequences	Sandstone and greyish brown claystone		
	Lower	Alluvial fan and braided stream	Coarse-grained and poorly sorted	Conglomerate and coarse-sand		





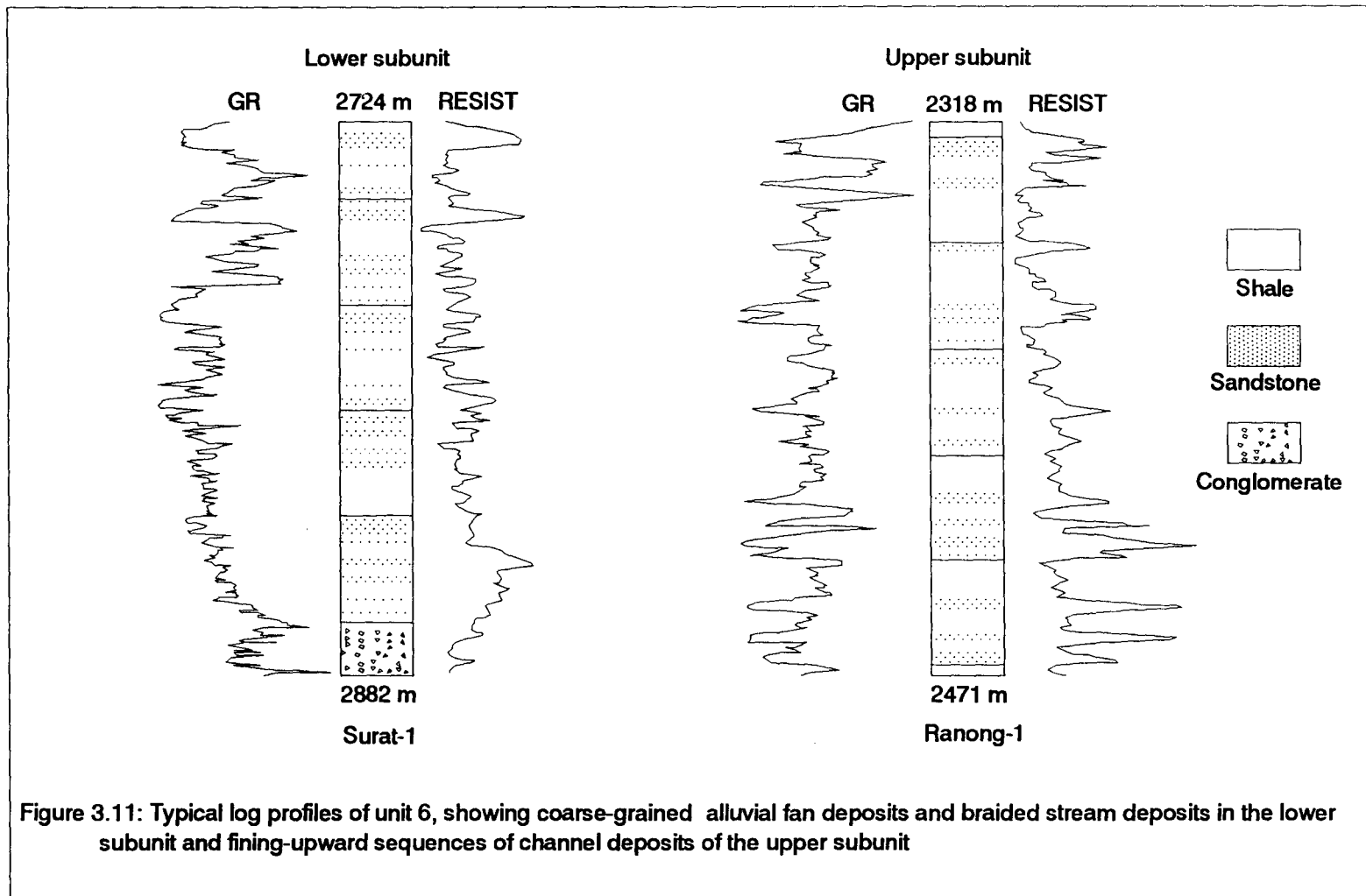


the upper part of unit 6 to high gamma radiation in the lower part of unit 5. This sudden increase of gamma radiation marks the change in lithological association from coarse-grained sediments of unit 6 to fine-grained sediments of unit 5.

A typical composite log profile of unit 6 is shown in Figure 3.11. Surat-1 and Ranong-1 wells encountered Cretaceous granite basement whereas Dara-1 encountered Cretaceous sediments. The presence of Cretaceous sediments is evident from the distinct change in lithology from interbedded grey sandstone and shale of unit 6 to the underlying red shale of the basement and the sharp increase in sonic velocity across this contact. The thickness of this unit varies from 150-350 m in the western margin of the basin to as thick as 3000 m in the basin center (Figure 3.12). Lithologically, unit 6 can be subdivided into lower and upper subunits.

The lower subunit is laterally highly discontinuous. Its thickness varies from 60 m at Surat-1 well to less than 20 m thick at Ranong-1 well to nil at Dara-1 well. A typical log profile of this subunit occurs in Surat-1 well between the depths of 2715-2900 m (Figure 3.11). The subunit consists mainly of conglomerate at the base and grades upward to very coarse- to coarse-grained, angular to subangular sandstone, minor siltstone and claystone. The basal conglomerate comprises quartz pebbles and clasts of quartzose and feldspathic granite. The subunit is barren of any fossils.

The presence of a fining-upward sequence of conglomerate and very coarse-grained, angular to subangular sandstone suggests the lower subunit was deposited in the alluvial fan and braided plain environments. The alluvial fan environment is believed to have developed in a restricted area during the initial phase of basin formation. Block faulting created a high relief topography which, in turn, induced



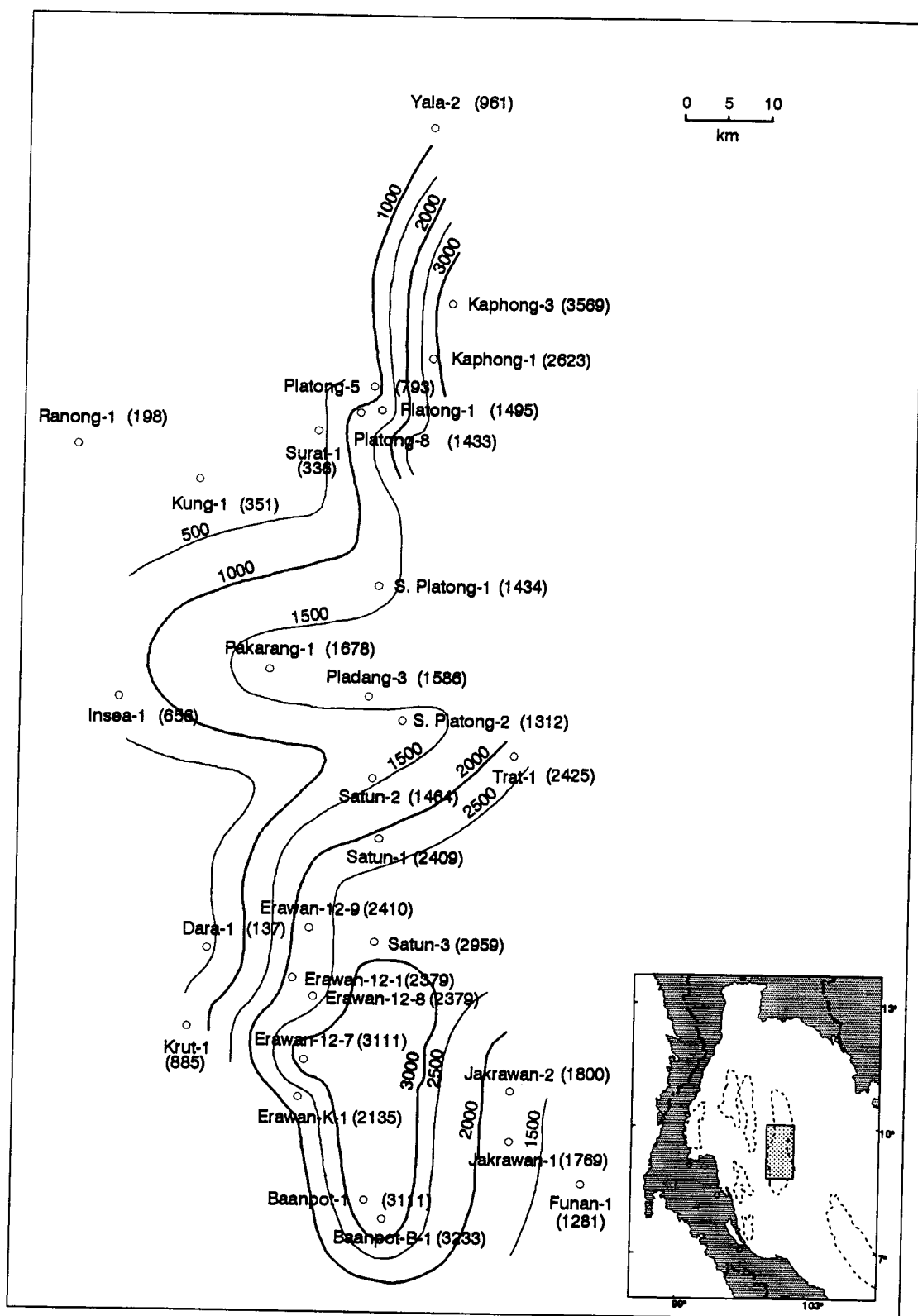


Figure 3.12: Isopach map of the stratigraphic unit 6 (contour interval = 500 m)

mass movement and rapid sedimentation (Nilsen, 1982). Because of limited data, the geometry and extent of the alluvial fan deposits are not known. Away from the marginal faults, the lower subunit was deposited in a braided alluvial plain environment. The occurrence of interbedded sandstone, siltstone and claystone in the upper part of this subunit possibly indicates the transition from braided river environment to that of meandering river with overbank and floodplain deposits (Cant, 1982).

The upper subunit of unit 6 is approximately 80-300 m thick and thickens toward the basin center. Typical successions of this subunit occur in Ranong-1 well between the depths of 2320-2470 m which are shown in Figure 3.11. Log profile shows a series of fining-upward sequences with sharp contacts at the base and gradational contacts at the top. Each sequence is approximately 6-12 m thick. Sandstone beds at the base of the sequences are approximately 2-7 m thick. The subunit consists mainly of white to grey, fine- to medium-grained sandstone and reddish brown to grey brown claystone. Coal seams occur locally interbedding with fine-grained sediments. The palynological assemblages include only rare pollen and lack key fossils. The only microflora present in this interval is the fern spore, *Verrucatosporites usmensis*.

The stacked fining-upward sequences, the presence of a fresh water fern spore, *Verrucatosporites usmensis*, and the oxidation of the sediments (evident by the reddish brown color) suggests the upper subunit was deposited in a fluvial floodplain environment consisting of coarse-grained channel sediments and fine-grained overbank sediments. Uniformly fine-grained sediment intervals in this subunit may indicate an ephemeral lacustrine environment further downslope from the alluvial fans.

The depositional history of unit 6 can be summarized as follows. At the initial stage of basin formation in this area, block faulting and rapid subsidence created a high-relief topography which led to the development of alluvial fan and alluvial plain environments. As the source areas were substantially eroded together with decreasing subsidence rate, floodplain and ephemeral lacustrine environments prevailed.

The presence of *Verrucatosporites usmensis*, a diagnostic species of the Pantropical zone (Figure 3.4) suggests that the age of unit 6 is approximately Late Eocene (Germaraad et al., 1968; Ratanasathien, 1988).

3.4.2 Unit 5

Unit 5 directly overlies unit 6. Its lower boundary is marked by the change in lithological association from a series of fining-upward sequences in the upper part of unit 6 to uniformly fine-grained claystone that characterizes the lower part of unit 5. The upper boundary of this unit is marked by the change in lithological association from coarse-grained sandstone interbedded with claystone in the upper part of unit 5 to generally fine-grained claystone in the lower part of unit 4.

The typical composite log profile of unit 5 is shown in Figure 3.13. Unit 5 was completely penetrated by four wells located in the northwestern and western margin of the basin. Seismic sections were used for correlation in areas where the unit was not penetrated by wells. Generally, the unit thickens toward the center of the basin and thins toward the eastern margin of the basin (Figure 3.14). A prominent depocenter of this unit is located in the southern part of the study area. The

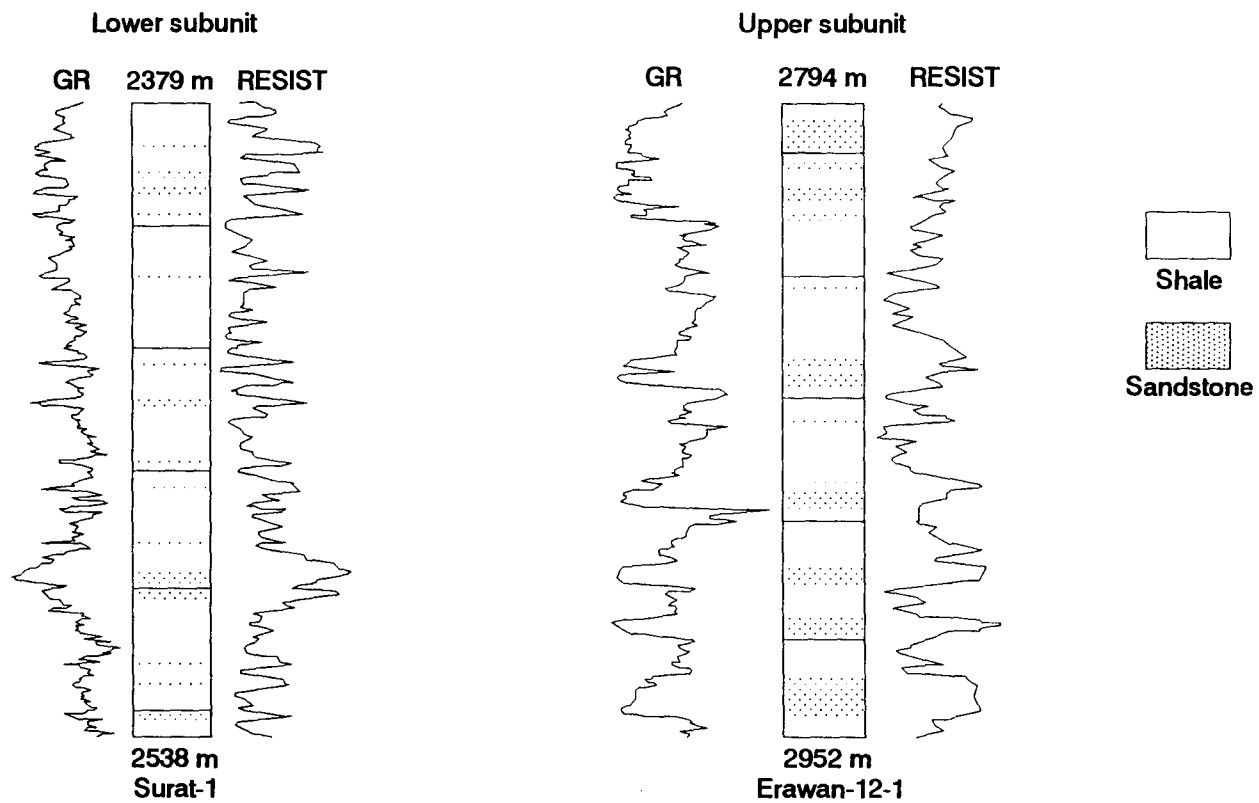


Figure 3.13: Typical log profiles of unit 5, showing general fine-grained floodplain and channel deposits in the lower subunit and fining-upward sequences of channel deposits in the upper subunit

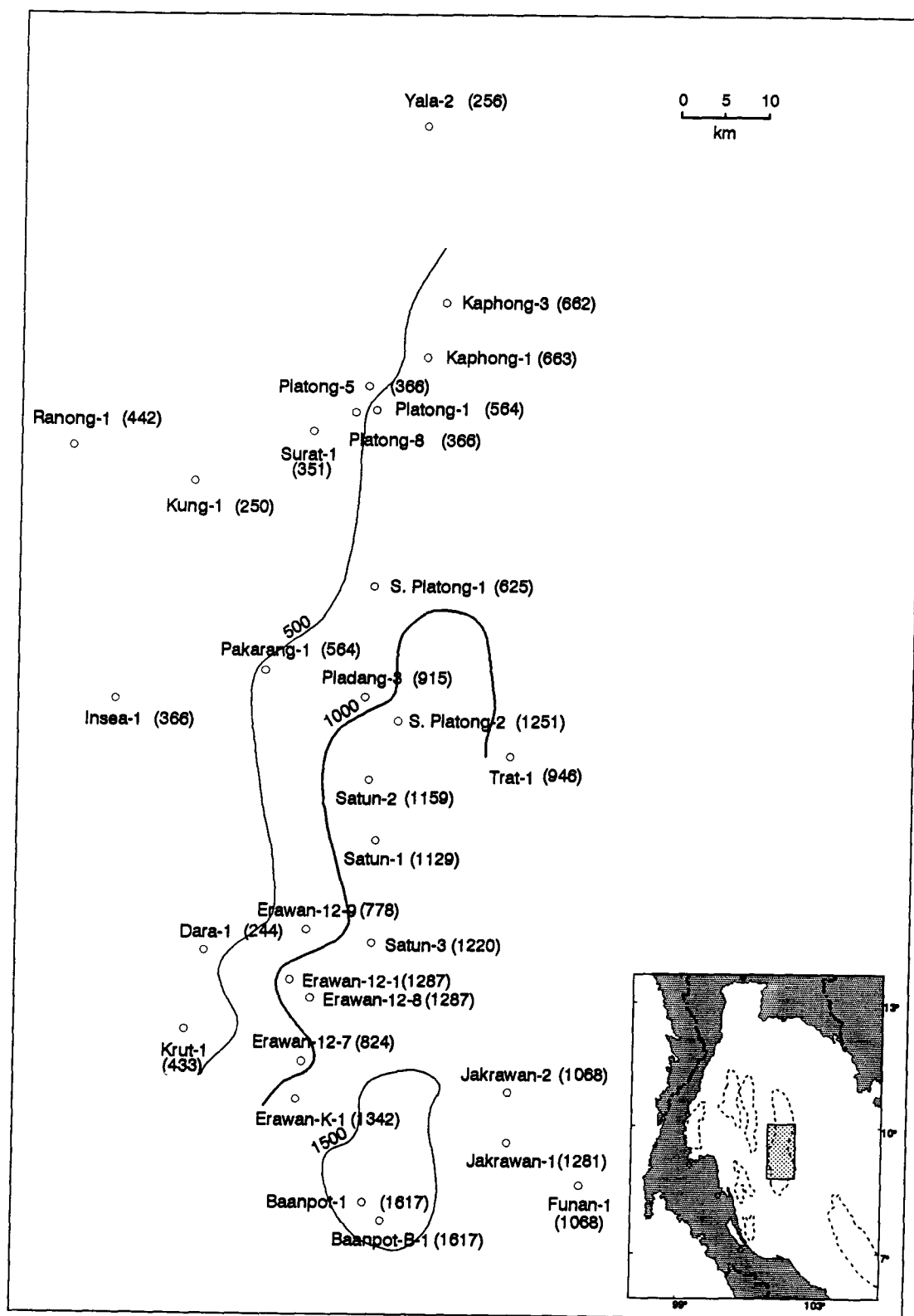


Figure 3.14: Isopach map of the stratigraphic unit 5 (contour interval = 500 m)

thickness varies from approximately 250-450 m in the northern and western margin of the basin to approximately 1300-1600 m in the depocenter in the south. Based on lithological associations, unit 5 can be subdivided into lower and upper subunits.

The lower subunit is approximately 90-200 m thick based on well data. The thickness in the area not penetrated by wells is thought to increase toward the depocenter in the central part of the basin. The typical log profile of this subunit occurs in Surat-1 well between the depths of 2380-2560 m (Figure 3.13). A log profile shows generally high gamma radiation with a few widely-spaced low gamma-ray intervals in between. This log signature reflects mainly fine-grained sediments and minor coarse-grained sediment interbeds. Coarse-grained sediment interbeds show a series of fining-upward sequences. These fining-upward sequences, where present, are approximately 3-9 m thick. The subunit consists mainly of red, reddish brown to brownish grey, noncalcareous claystone and red to brown, mottled argillaceous siltstone. Sandstones are generally grey to brown in color and fine- to medium-grained. The lower subunit contains very sparse pollen and lacks foraminifera. The only palynomorph encountered in this subunit is *Magnastriatites howardi*, fresh water palynomorph.

The generally fine-grained nature of the lower subunit of unit 5, the absence of marine and brackish water indicators, and the presence of the fresh water palynomorph, *Magnastriatites howardi* suggest that this subunit was deposited in a low energy, fresh water floodplain environment. The presence of red beds may possibly have been a result of the subsequent aerial exposure of the sediments, or rapid aerobic decomposition of plant materials which led to oxidation of sediments. A series of thin, fining-upward sandstone sequences represents small-scale meandering channel deposits.

The upper subunit is approximately 90-300 m thick. A typical log profile of this subunit occurs in the Erawan-12-1 well between the depths of 2790-3000 m (Figure 3.13). The profile defines a stacked series of fining-upward sequences with sharp basal and gradational upper contacts. The thickness of each of these sequences varies from 6 m to 12-15 m. Sandstone at the base of the sequences is 3 to 9 m thick. The subunit consists mainly of white to brown, fine- to medium-grained sandstone. Siltstone and claystone are generally brown to red or yellow and noncalcareous. The subunit contains very low palynomorph abundance.

The series of well developed fining-upward sequences and the highly oxidized nature of the sediments, evident from their reddish color, suggest that the upper subunit of unit 5 was deposited in a nonmarine meandering channel environment.

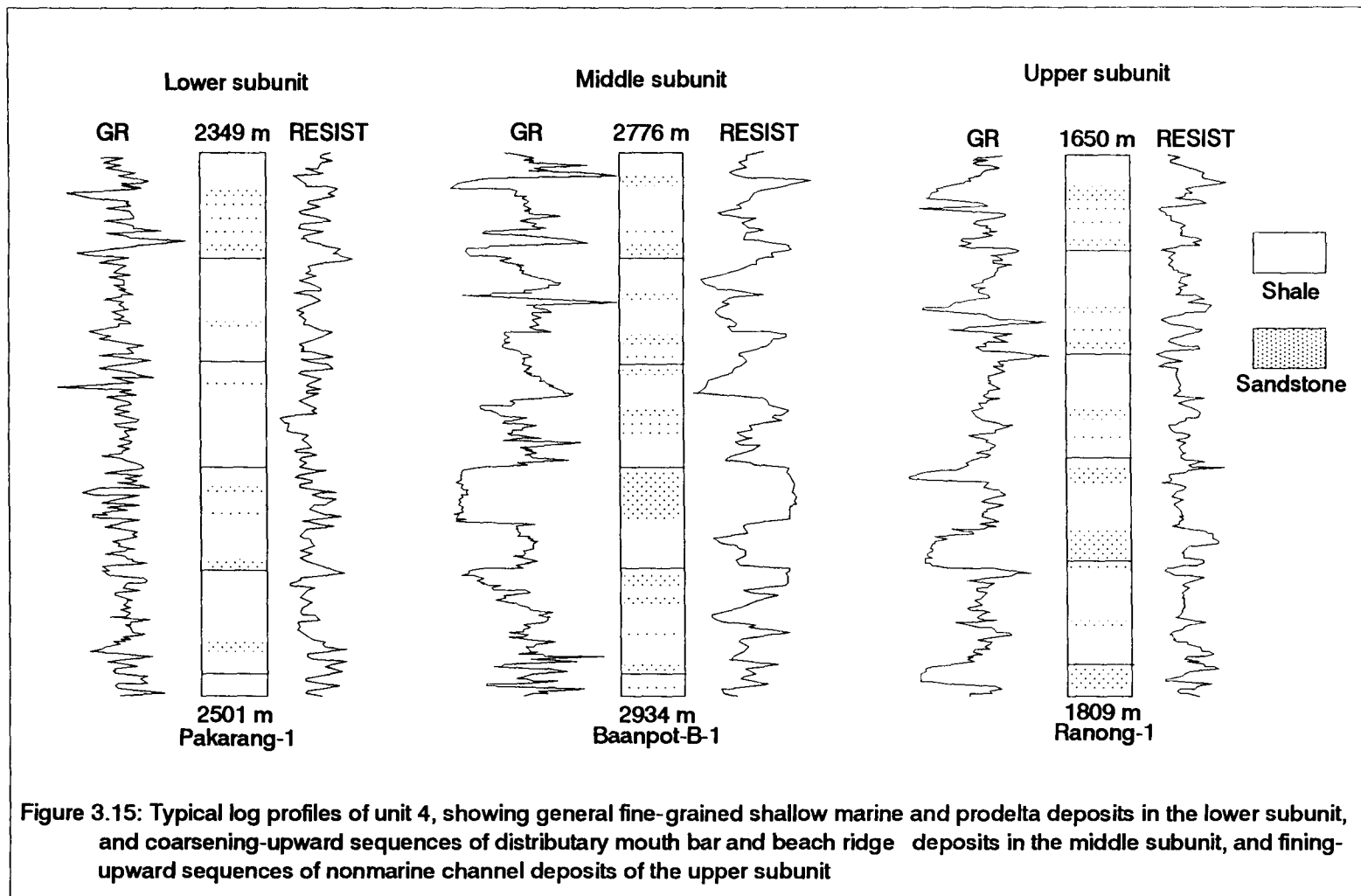
The overall depositional environment of unit 5 is interpreted to be entirely nonmarine and can be summarized as follows. The base of unit 5 represents nonmarine floodplain deposits characterized by generally fine-grained overbank sediments. Small-scale meandering channel deposits are also present and are characterized by a series of widely-spaced, small-scale fining-upward sequences in the fine-grained overbank deposits. These sediments were subsequently subaerially exposed and oxidized as evident from the occurrence of red beds. The upper part of unit 5 represents a change from low energy floodplain deposits into high energy channel-fill and point bar deposits. These high energy deposits are characterized by a predominance of thick, fining-upward sequences with minor interbeds of finer-grained sediments.

No age diagnostic fossil assemblages occur in this interval. The age of unit 5 is interpreted to be Late Oligocene to Early Miocene because this unit directly overlies unit 6 of Late Eocene to Early Oligocene age and underlies unit 4 of Early Miocene age.

3.4.3 UNIT 4

Unit 4 is a coarsening-upward regressive sequence. Its lower boundary is marked by an abrupt change in lithological association from a series of fining-upward sequences in the upper part of unit 5 to generally fine-grained sediments in the lower part of unit 4. This boundary is a surface of nondeposition representing a rapid rise of the relative sea-level (transgression). As the rate of deposition exceeded the rate of sea-level rise, a regressive sedimentary succession resulted. The surface of nondeposition is characterized by the sudden change from nonmarine channel deposits of unit 5 to low energy shallow marine sediments of the lower subunit of unit 4 in the vicinity of the basin center. Westward toward the basin margin, this boundary is marked by a change from high energy channel deposits to low energy floodplain deposits. The upper boundary of unit 4 is marked by a sudden increase in gamma radiation which reflects a change in lithology from coarse-grained sandstone of upper unit 4 to relatively fine-grained claystone of unit 3.

A typical composite log profile of unit 4 is shown in Figure 3.15. This unit generally thickens from about 300 to 400 m in the north and west to about 1400 to 2800 m in the depocenters (Figure 3.16). Two depocenters are recognized (Figure 3.16). The smaller depocenter, located around the Pladang-3 well location, contains sediments up to 1400 m thick. The main depocenter of unit 4 is located



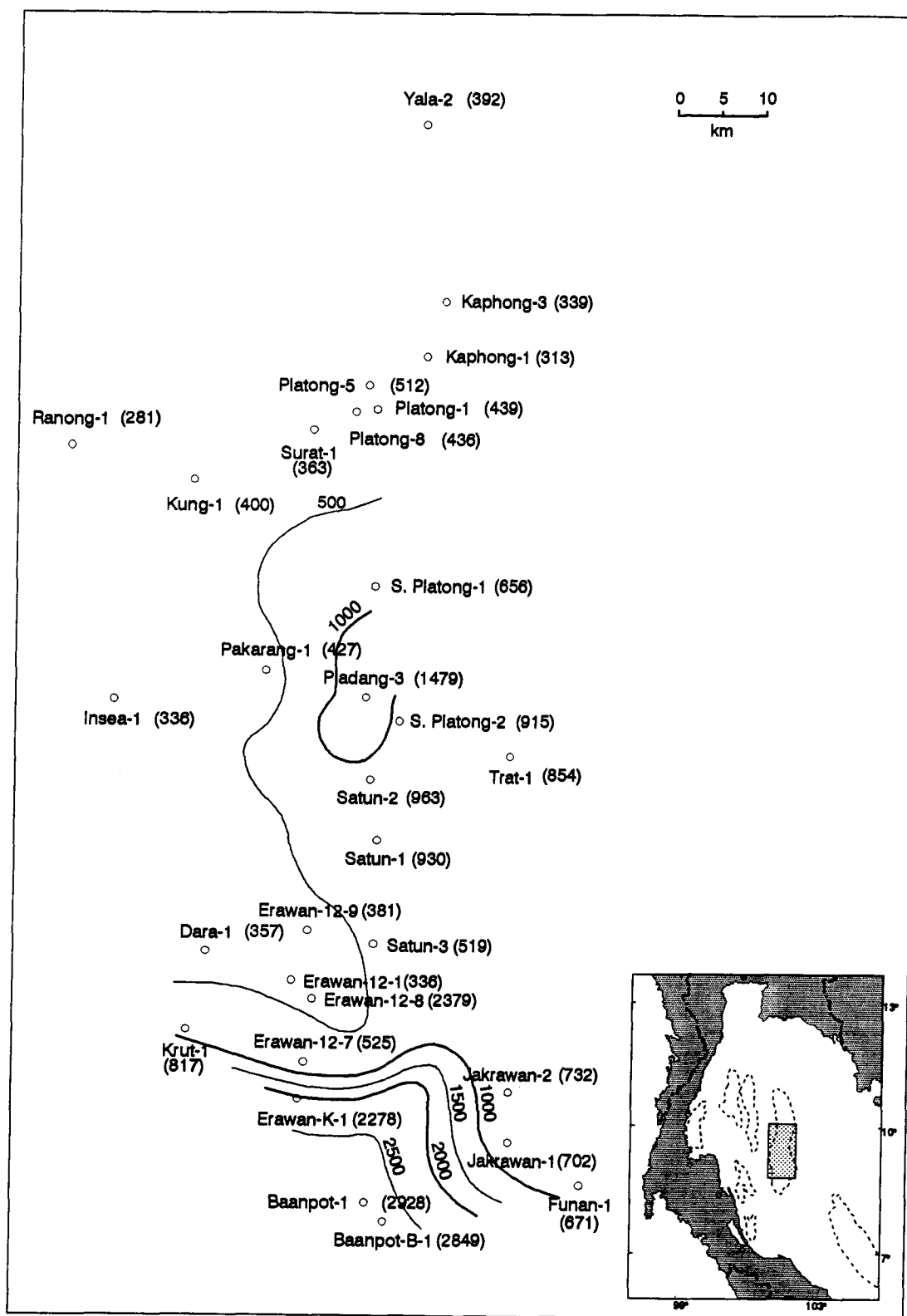


Figure 3.16: Isopach map of the stratigraphic unit 4 (contour interval = 500 m)

further south around the Erawan-K-1, Baanpot-1, and Baanpot-B-1 well locations. This southern depocenter contains sediments greater than 2800 m thick. Based on lithological associations, unit 4 can be subdivided into lower, middle, and upper subunits.

A typical log profile of the lower subunit occurs in Pakarang-1 well between the depths of 2350-2500 m (Figure 3.15). The serrated, generally high-intensity gamma ray signature reflects the generally fine-grained sediments interbedded with thin, coarse-grained sediments. The thickness of this subunit varies from zero in the western margin of the basin to more than 150 m toward the basin center (Figure 3.17). The subunit consists mainly of brown grey to grey, noncalcareous to slightly calcareous claystone and argillaceous siltstone and thin (generally less than 3 m thick) but closely-spaced white to light grey, fine- to medium-grained sandstone. Thin, widely-spaced carbonaceous partings are present throughout the interval. A calcareous benthic foraminiferal assemblage is common in this interval. The predominant species are *Ammonia nipponica* and *A. beccarii*. Microflora and plant debris are rare in this subunit. Where present, the palynomorph assemblages include *Florschuetzia semilobata*, *F. trilobata*, *F. levipoli*, *Crassoretitriletes vanraadshooveni*, and *Magnastriatites howardi*.

The lower subunit of unit 4 consists of shallow marine, prodelta sediments deposited in a littoral to very shallow marine inner sublittoral environment. Such an interpretation is based on the fine-grained nature of the sediments, the presence of shallow marine foraminifera (*Ammonia nipponica* and *A. beccarii*), and the occurrence of mixed fresh water palynomorphs (*Magnastriatites howardi* and *Crassoretitriletes vanraadshooveni*) and brackish water palynomorphs (*Florschuetzia Trilobata* and *F. levipoli*).

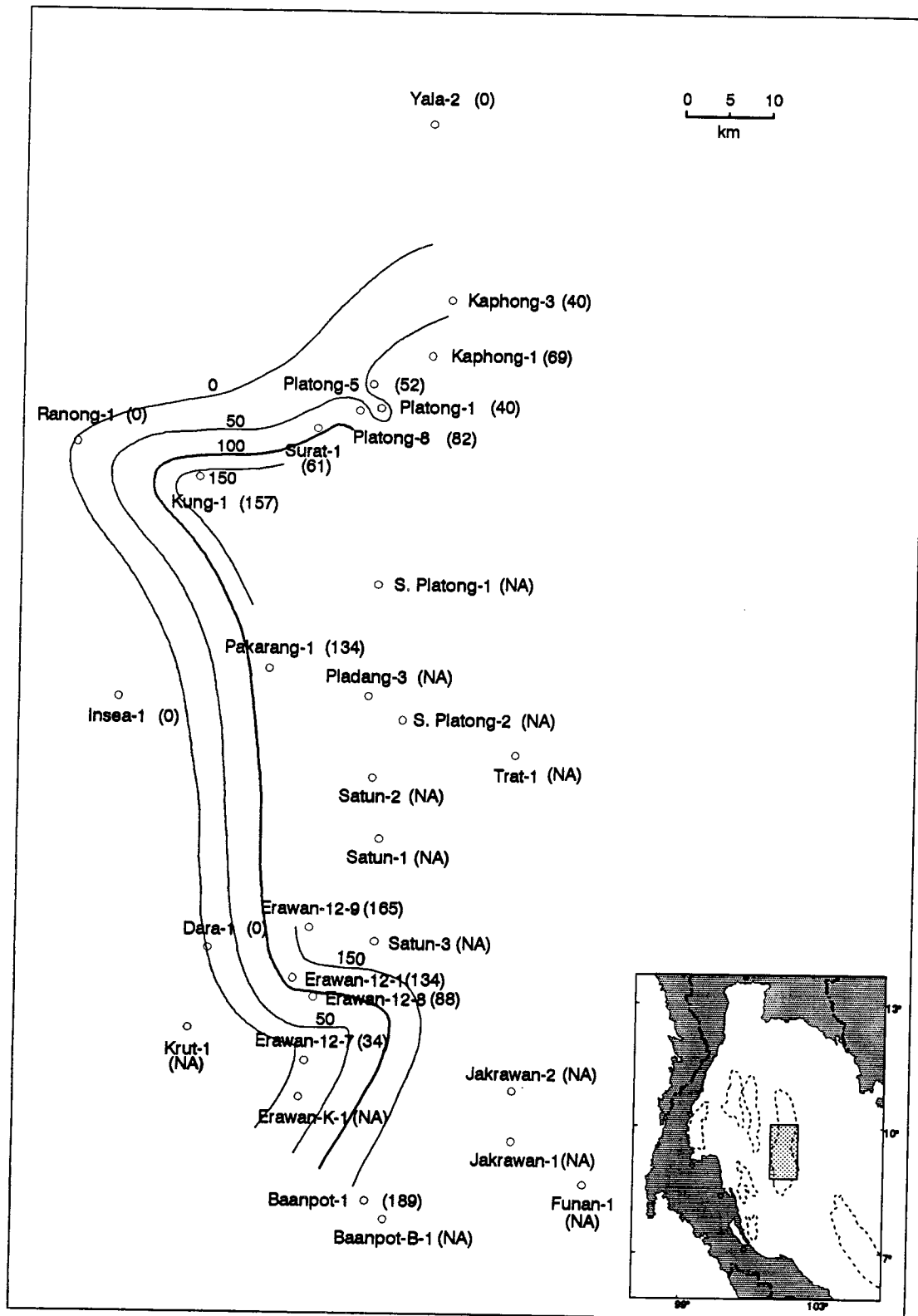


Figure 3.17: Isopach map of unit 4's lower subunit (contour interval = 50 m)

A typical log profile of the middle subunit occurs in Baanpot-B-1 well between the depths of 2800-3000 m (Figure 3.15). The subunit consists mainly of white to light grey, fine- to medium-grained sandstone and grey to light grey and brown claystone, siltstone interbeds and minor carbonaceous partings. The thickness of this subunit varies from zero in the western basin margin to more than 300 m toward the depocenter in the south central part of the basin (Figure 3.18). The log profile depicts a series of coarsening-upward sequences with gradational contacts at the base and sharp contacts at the top. These sequences vary in thickness from more than 30 m in the lower part of the section to approximately 10 m in the upper part. The thickness of clean sandstone beds at the top of each sequence also decreases upward, ranging from as thick as 20 m in the lower part to about 2-7 m in the upper part of the section. The subunit is characterized by the lack of foraminifera and the near absence of palynomorph and other plant debris.

The middle subunit of unit 4 was deposited in a delta-front environment. This interpretation is based on the very low palynomorph abundance and barren intervals in this subunit, together with a series of coarsening-upward sequences and the lithological association of the underlying fine-grained prodelta deposits of the lower subunit and the overlying nonmarine delta plain deposits of the upper subunit. The delta-front sediments of this subunit include both distributary mouth bar deposits and also, where the marine reworking process dominates, beach-ridge complexes (*cf.* Coleman and Prior, 1982; Miall, 1984).

A typical log profile of the upper subunit of unit 4 occurs in Ranong-1 well between the depths of 1620-1830 m (Figure 3.15). The log profile depicts a series of fining-

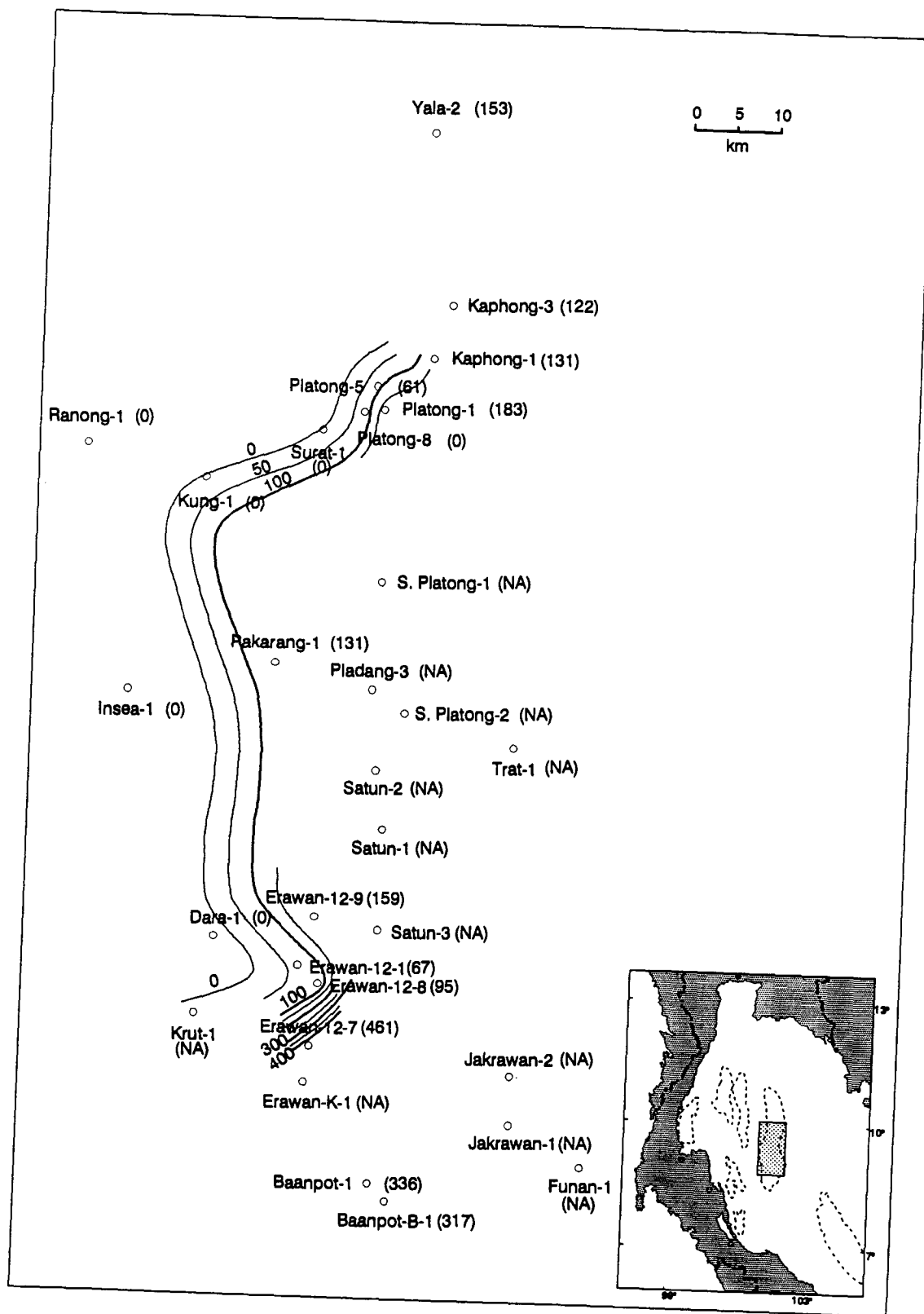


Figure 3.18: Isopach map of unit 4's middle subunit (contour interval = 50 m)

upward sequences with sharp basal contacts and gradational upper contacts. These sequences vary in thickness from less than 3 m to as thick as 20 m. The thickness of sandstone layers at the base of the sequences varies from less than 2 m to approximately 15 m. This subunit consists mainly of interbedded light brown to white sandstone and reddish brown to grey brown claystone. This subunit is thickest (more than 300 m thick) in the western margin of the basin and thins (less than 30 m thick) toward the basin center (Figure 3.19). This subunit contains very low fresh water palynomorph abundance. It lacks both foraminifera and brackish water palynomorphs. The only abundant palynomorph present is the fresh water fern spore *Magnastriatites howardi*.

The upper subunit of unit 4 was deposited in the supratidal floodplain environment. This interpretation is evident from the absence of marine foraminifera and brackish water palynomorphs, the presence of the fresh water fern spore, *Magnastriatites howardi*, a series of fining-upward sequences and the presence of red beds. The series of sand-rich fining-upward sequences may be meandering channel deposits.

The overall depositional environment of unit 4 is a coarsening-upward regressive sequence in which the coastline prograded gradually basinward, resulting in nonmarine deposits superimposed upon the earlier shallow marine or marginal marine deposits. The depositional history of this unit can be summarized as follows. A rapid rise of relative sea-level at the end of unit 5 resulted in a surface of nondeposition (transgressive surface) on which unit 4 was deposited. The base of the unit represents prodelta to shallow marine, inner sublittoral deposits characterized by generally fine-grained sediments and minor sandstone interbeds, shallow marine foraminifera, and a mixture of both brackish and fresh water palynomorphs. Overlying these prodelta to shallow marine deposits are coarse-

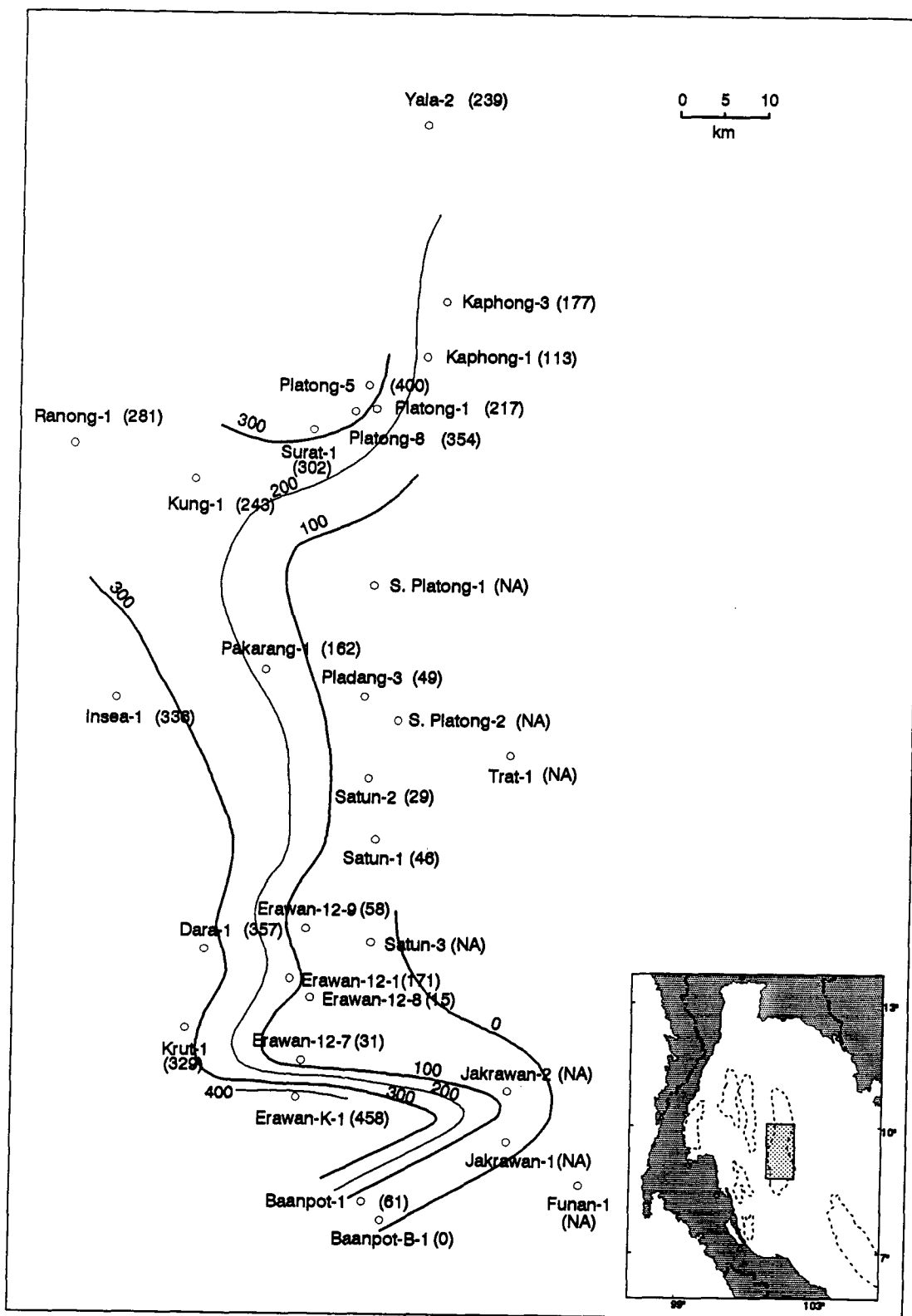


Figure 3.19: Isopach map of unit 4's upper subunit (contour interval = 100 m)

grained, high-energy distributary-mouth bar deposits and beach-ridge complexes, characterized by a series of coarsening-upward sequences and the absence of fossils. The upper part of the unit is nonmarine floodplain and meandering channel deposits, as evident from the absence of foraminifera and brackish water palynomorphs, the occurrence of fresh water fern spores and red beds, together with a series of fining-upward sequences within the generally fine-grained sediments.

Unit 4 correlates positively to the *Florschuetzia levipoli* zone from Borneo (Germeraad et al., 1968; Figure 15, p. 230-232). This is based on the occurrence of *F. levipoli* and *F. semilobata*, which have first occurrence in the *F. levipoli* zone, and the absence of *F. meridionalis* and *Echitricolporites spinosus*, with first occurrence in the *F. meridionalis* zone immediately above the *F. levipoli* zone. The age of unit 4 is, therefore, identified precisely as Early Miocene.

3.4.4 Unit 3

Unit 3 is characterized by a generally coarsening-upward regressive sequence similar to unit 4. In unit 3, nonmarine deposits of the upper subunit lie on top of distributary mouth bar and beach ridge deposits of the middle subunit which, in turn, lie on top of prodelta and shallow marine deposits of the lower subunit. The lower boundary of unit 3 is a surface of nondeposition, a result of rapid rise of relative sea-level. The upper boundary of unit 3 in the vicinity of the basin center is marked by a change in lithological association, from a series of coarsening-upward sequences of a distributary mouth bar or beach ridge deposit of the middle subunit of unit 3 into a series of fining-upward sequences of a floodplain-meandering channel deposit of unit 2. Near the basin margin, this boundary is

marked by a change from a series of fining-upward sequences of a meandering channel deposit of the upper subunit of unit 3 to generally fine-grained floodplain deposits of unit 2.

A typical composite log profile of unit 3 is shown in Figure 3.20. This unit generally thickens from 200-300 m in the northern and western margin to approximately 1200-1400 m in the basin center (Figure 3.21). The likely depocenter occurs at the south-central part of the basin (Figure 3.21). Based on the lithological associations, unit 3 can be subdivided into lower, middle, and upper subunits.

A typical log profile of the lower subunit occurs in Pladang-3 well between the depths of 2380-2535 m (Figure 3.20). The serrated, generally high gamma ray log signature reflects the generally fine-grained sediments interbedded with thin, coarse-grained sediments. This subunit's thickness varies from zero in the western part of the basin to more than 200 m toward the basin center (Figure 3.22). The subunit consists mainly of light grey to grey, calcareous claystone and siltstone interbedded with minor occurrences of coarsening-upward sandstone and carbonaceous shales. Small calcareous benthic foraminifera are common. The main species are *Ammonia cf. beccarii* and *Pseudorotalia cf. yabei*. The palynomorph assemblage encountered in this subunit includes *Florschuetzia semilobata*, *F. levipoli*, *Crassoretitriletes vanraadshooveni*, *Verrumonoletes usmensis*, and *Discoidites boneensis*. Other plant fragments are rare in this subunit.

The lower subunit of unit 3 is interpreted as shelf to prodelta sediments which were deposited in a littoral to shallow marine inner sublittoral environment. This interpretation is based on the fine-grained nature of sediments, the occurrence of

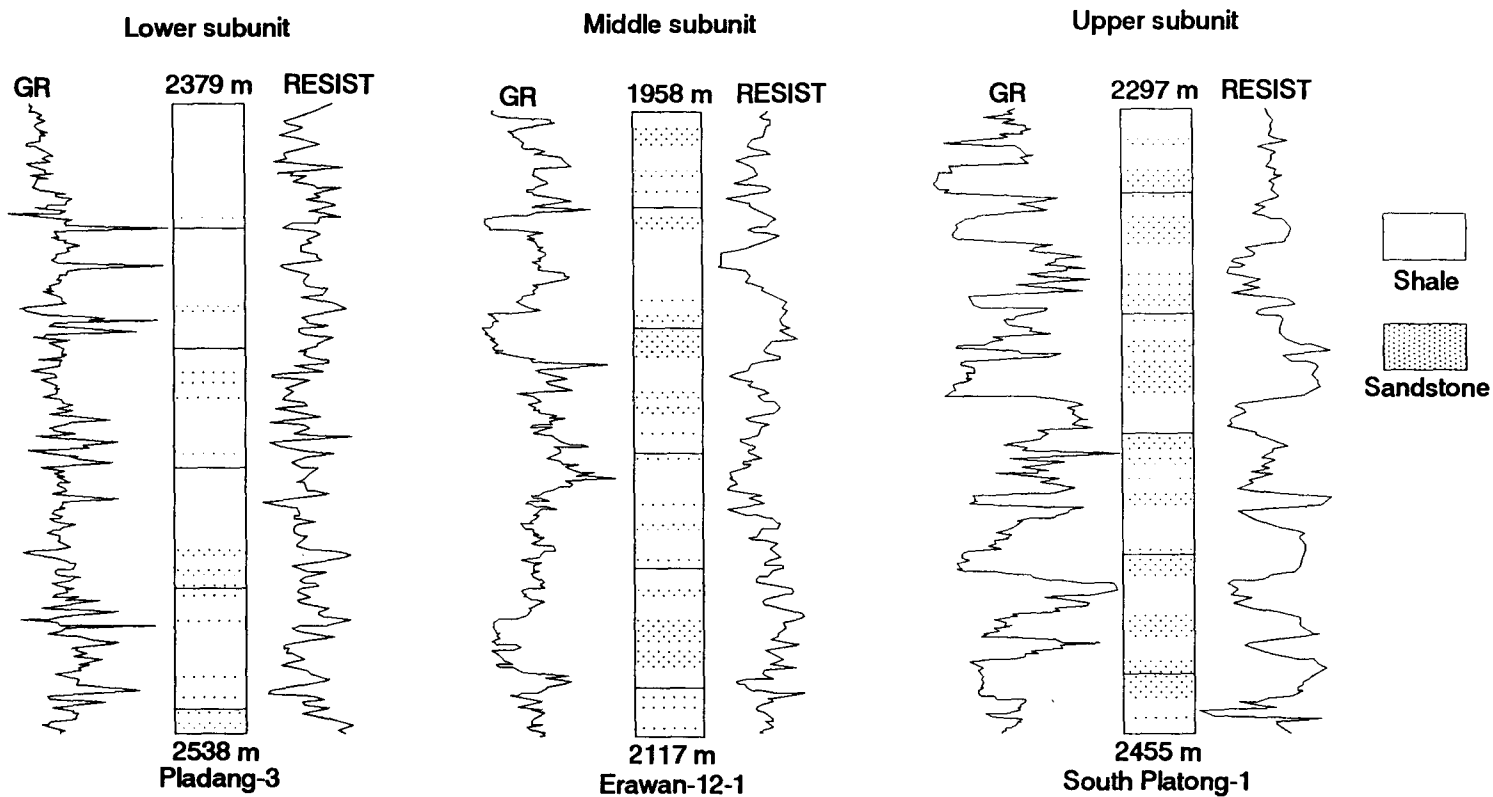


Figure 3.20: Typical log profiles of unit 3, showing general fine-grained shallow marine and prodelta deposits in the lower subunit, and coarsening-upward sequences of distributary mouth bar and beach ridge deposits in the middle subunit, and fining-upward sequences of nonmarine channel deposits of the upper subunit

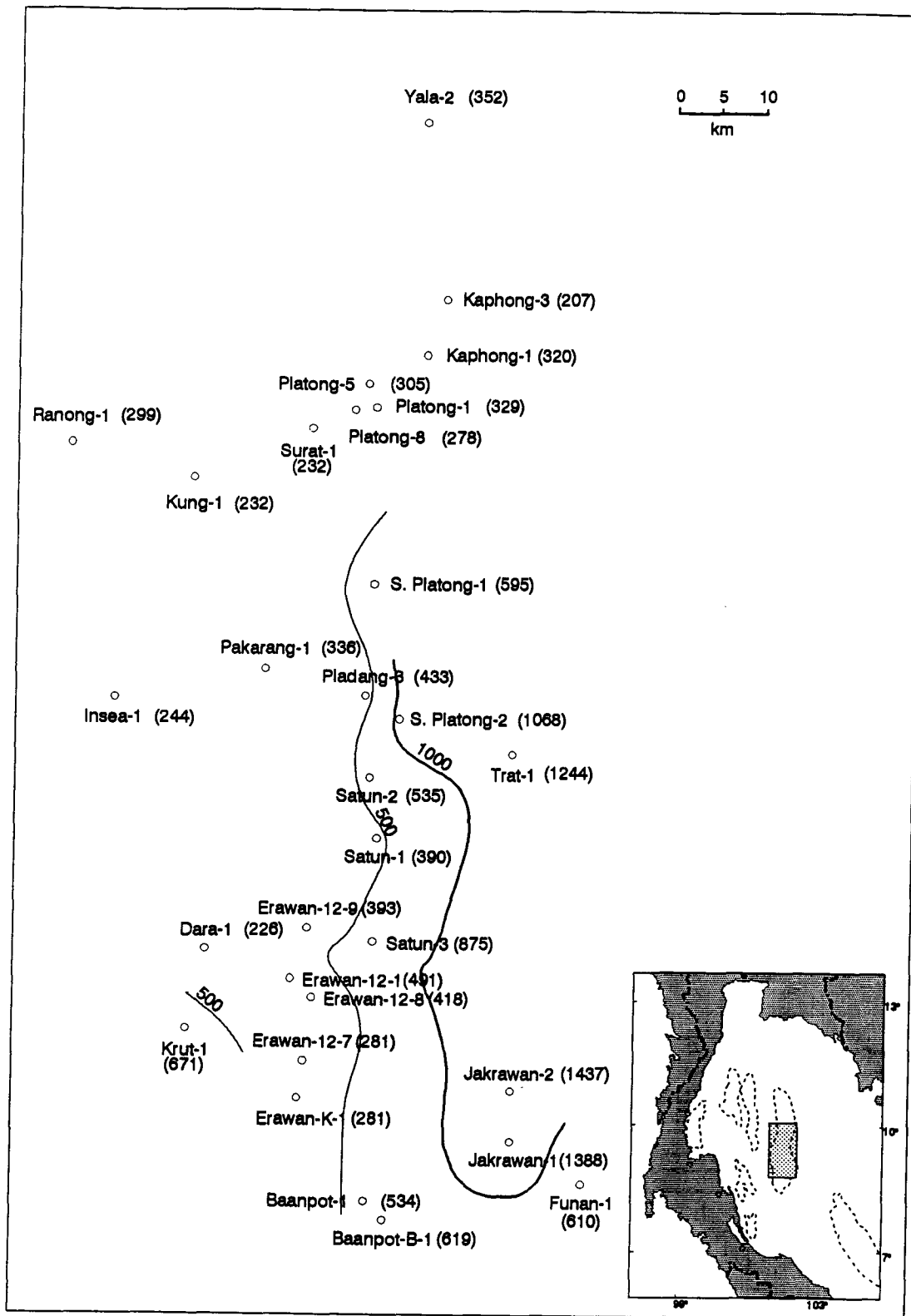


Figure 3.21: Isopach map of the stratigraphic unit 3 (contour interval = 500 m)

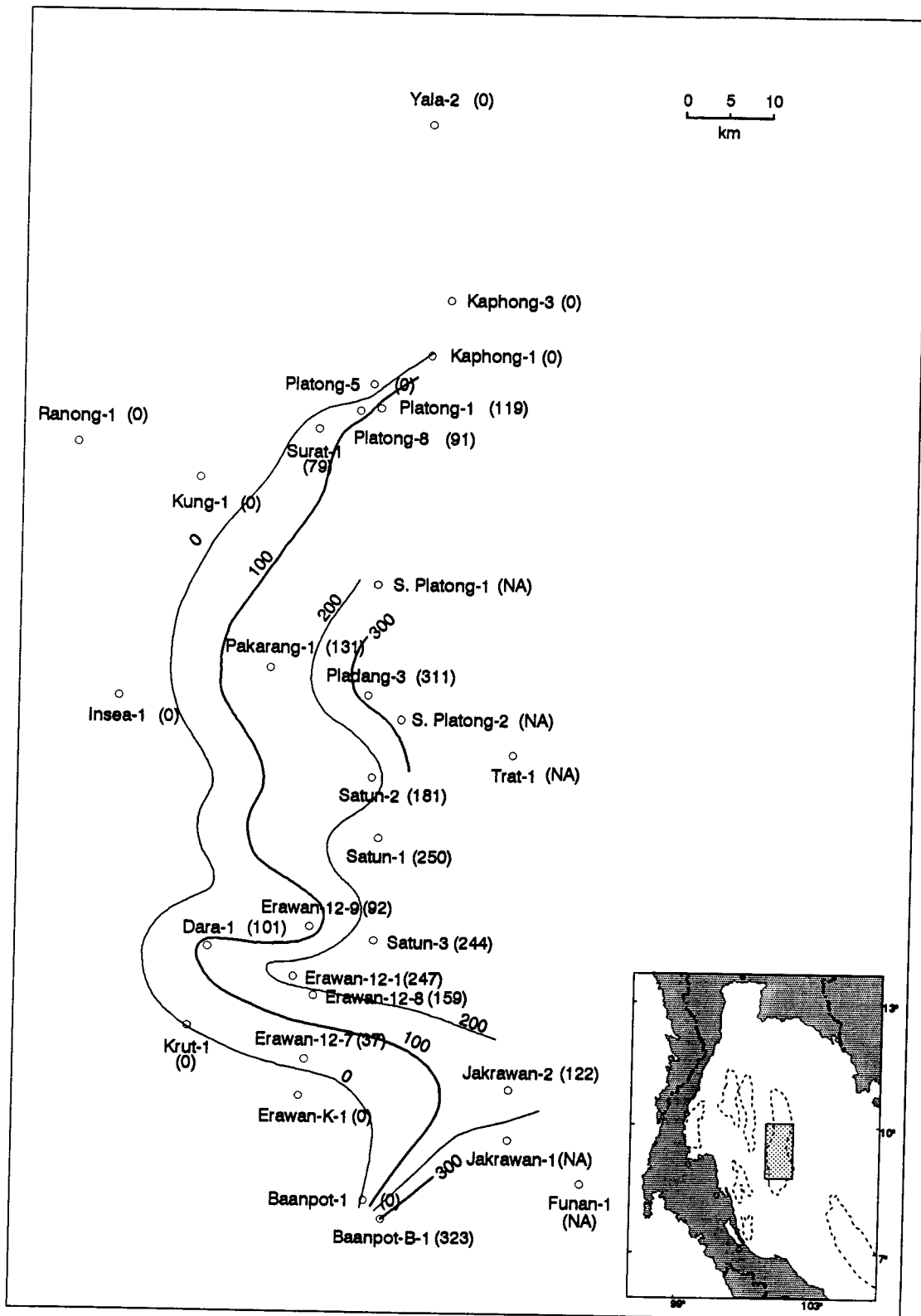


Figure 3.22: Isopach map of unit 3's lower subunit (contour interval = 100 m)

shallow water foraminifera (*Ammonia cf. beccarii* and *Pseudorotalia cf. yabei*), together with the presence of mixed fresh water palynomorphs (*Crassoretitriletes vanraadshooveni*, *Verrumonoletes usmensis*, and *Discoidites boneensis*). The rare coarsening-upward sequences (3-10 m thick) may represent offshore bar deposits.

A typical log profile of the middle subunit of unit 3 occurs in the Erawan-12-1 well between the depths of 1950-2160 m (Figure 3.20). The log profile represents a series of coarsening-upward sequences with gradational basal contacts and sharp upper contacts. Each of these coarsening-upward sequences is approximately 10-40 m thick. Clean sandstone layers at the top of these sequences range from 3-12 m thick. The subunit consists mainly of fine- to coarse-grained, white sandstone and calcareous claystone and siltstone interbeds and minor carbonaceous partings. The thickness of this middle subunit varies from zero in the northwestern margin of the basin to more than 200-300 m in the southern part of the basin (Figure 3.23). Two minor depocenters trending ENE-WSW are recognized in the southern part of the basin (Figure 3.23). The palynomorph assemblage encountered in this subunit includes *Florschuetzia semilobata*, *Florschuetzia levipoli*, *Crassoretitriletes vanraadshooveni*, *Pinus* sp., *Dicolpopollis malesianus*, and *Magnastriatites howardi*. Calcareous foraminifera encountered are *Ammonia cf. beccarii* and *Pseudorotalia cf. yabei*.

The middle subunit was deposited in the distributary mouth bar and beach ridge environments. Evidences for such an interpretation include a series of sand-rich, coarsening-upward sequences; the presence of shallow marine calcareous foraminifera; the mixed occurrences of fresh and brackish water palynomorphs; together with the lithological association of the underlying fine-grained shelf to prodelta deposits of the lower subunit and the overlying nonmarine coastal plain

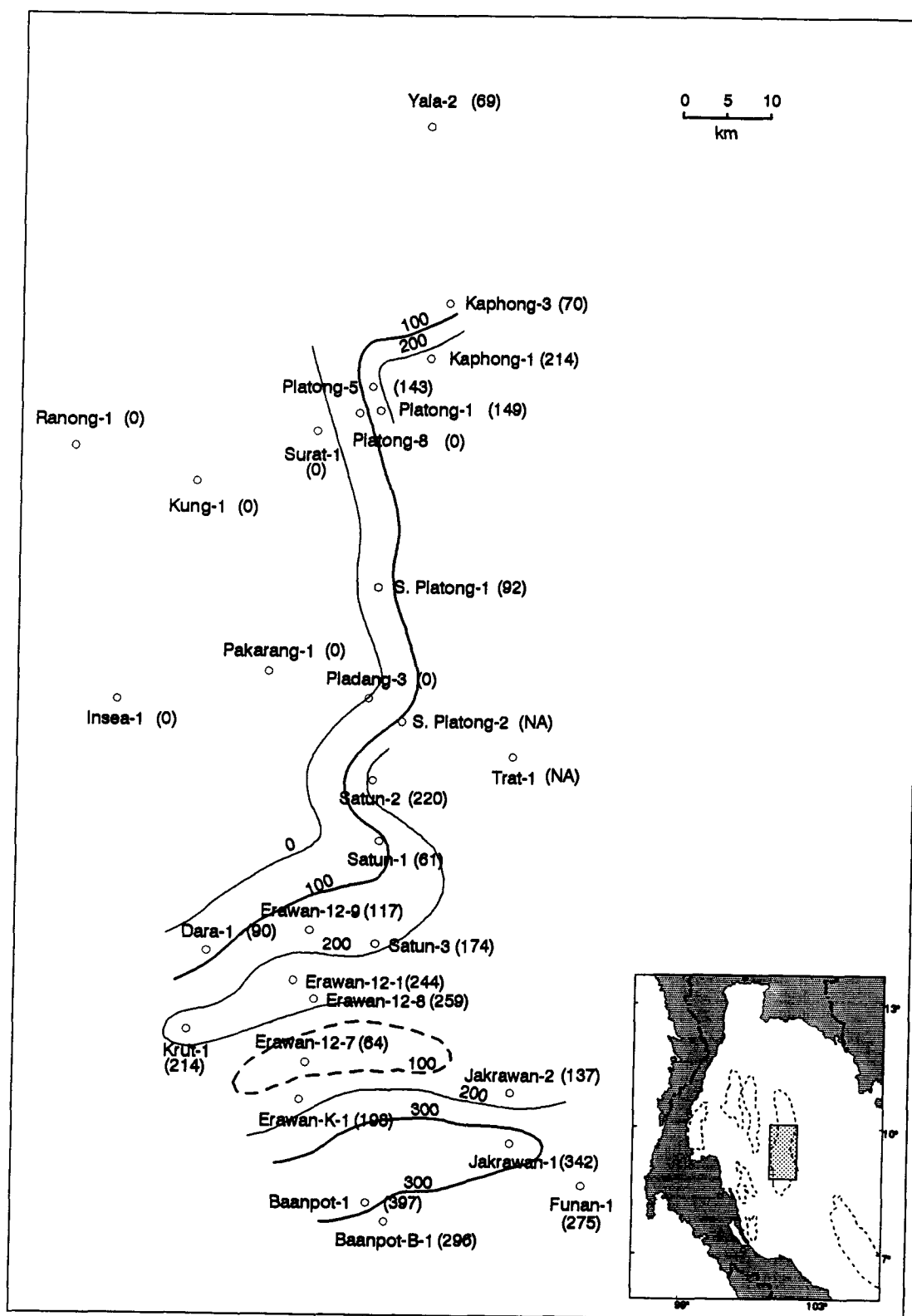


Figure 3.23: Isopach map of unit 3's middle subunit (contour interval = 100 m)

deposits of the upper subunit similar to that of unit 4 (cf. Coleman and Prior, 1984; Miall, 1984).

A typical log profile of the upper subunit of unit 3 occurs in South Platong-1 well between the depths of 2290-2500 m (Figure 3.20). The log profile characterizes a series of fining-upward sequences with sharp basal contacts and gradational upper contacts. These sequences vary in thickness from less than 5 m to as thick as 20 m. The thickness of sandstone layers at the base of the sequences varies from 2 m to approximately 13 m. The subunit consists mainly of interbedded light grey to light brown sandstone, siltstone, and brown grey claystone. The thickness of this subunit varies from zero in the south central part of the basin center to as thick as 250-300 m the western and southeastern basin margins (Figure 3.24). The subunit is barren of any foraminifera and brackish water palynomorphs, but does include a few specimens of the fern spores *Crassoretitriletes vanraadshooveni* and *Magnastriatites howardi*.

The upper subunit of unit 3 was deposited in a nonmarine, meandering channel and floodplain environment. This interpretation is supported by the presence of a series of fining-upward sequences, the absence of marine foraminifera and brackish water palynomorphs, and the occurrence of fresh water fern spores, *Crassoretitriletes vanraadshooveni* and *Magnastriatites howardi*.

The overall depositional environment of unit 3 displays a generally coarsening-upward regressive succession similar to unit 4, and can be summarized as follows. At the end of unit 4 deposition, rapid relative sea-level rise resulted in a surface of nondeposition, at least in the central basin area. This surface marks the boundary between the stratigraphic unit 4 and unit 3. As the rate of deposition exceeded the

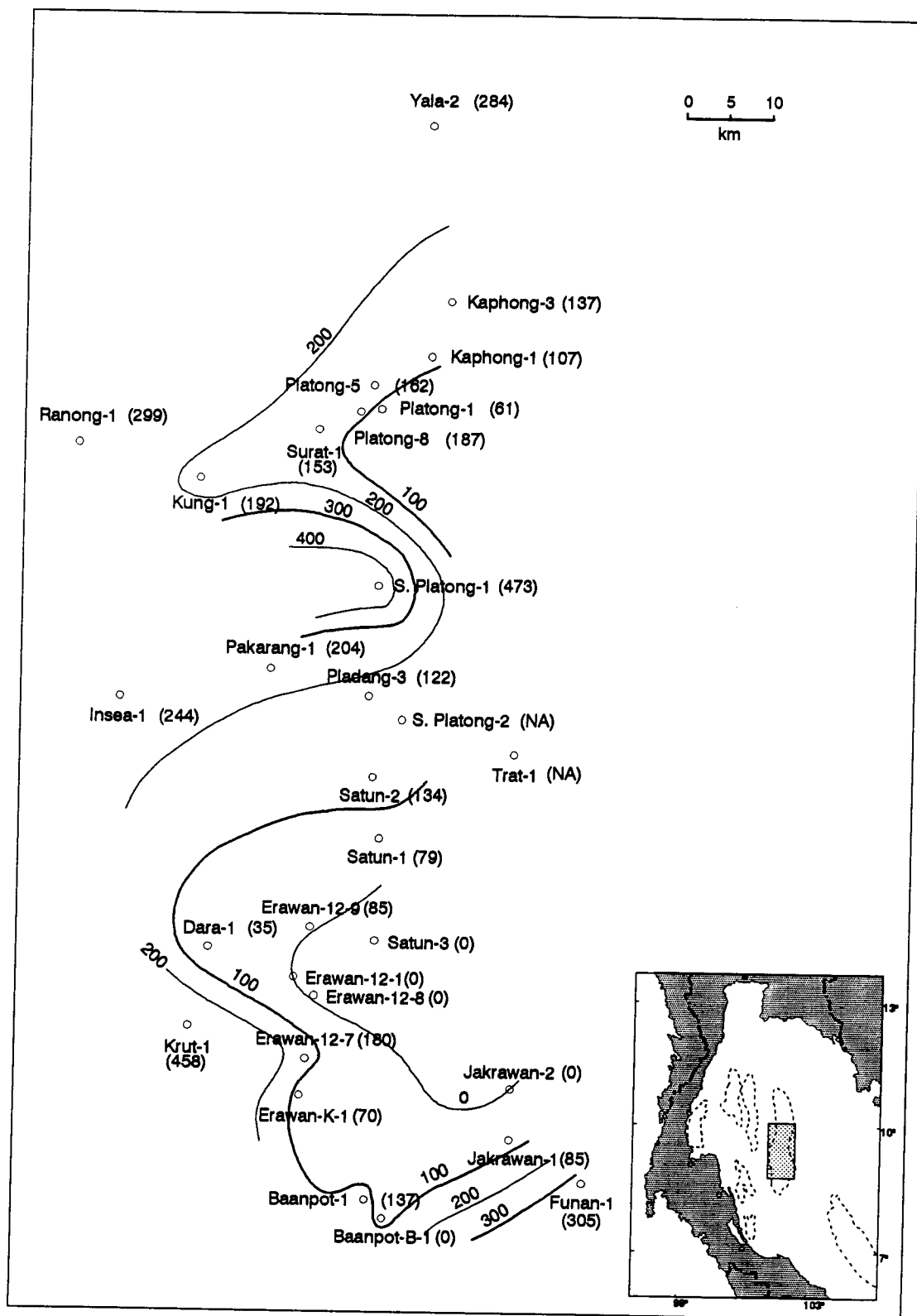


Figure 3.24: Isopach map of unit 3's upper subunit (contour interval = 100 m)

rate of relative sea-level rise, a regressive sedimentary package prograded. At the base of unit 3 are prodelta to shallow-marine to inner sublittoral deposits characterized by fine-grained sediments and minor sandstone interbeds, shallow marine foraminifera and brackish water microfloral assemblages. Higher in the section are coarse-grained, high energy distributary mouth bar and beach ridge deposits. The deposits are characterized by a well developed series of sand-rich, coarsening-upward sequences, shallow marine foraminifera and mixed fresh and brackish water microfloral assemblages. The upper portion of unit 3 represents nonmarine meandering channel and floodplain deposits characterized by the absence of any marine and brackish water indicators, the presence of fresh water microflora and a well developed series of fining-upward sequences.

The presence of *Florschuetzia semilobata*, *F. levipoli*, *Magnastriatites howardi*, and *Crassoretitriletes vanraadshooveni* indicate that unit 3 is in the *Florschuetzia levipoli* Borneo zone which is equivalent to the *Crassoretitriletes vanraadshooveni* Pantropical zone of Late Early-Middle Miocene (Germeraad et al., 1968; Scrutton and Tidey, 1974).

3.4.5 Unit 2

The lower boundary of unit 2 is marked by change from coarse-grained sandstone of the upper part of unit 3 to fine-grained claystone of the lower part of unit 2. Unit 2 is bounded above by the Mid-Miocene unconformity. This unconformity is recognized in the well logs by a sharp increase in sonic velocity downward across the unconformity surface and by a change in color of cuttings from grey above the unconformity to brown or red below indicating oxidizing conditions prevailed

below the unconformity. In seismic sections, however, no angular relationship is evident across this surface.

The typical composite log profile of unit 2 is shown in Figure 3.25. The unit thickens from 250-450 m in the western basin margin to more than 1000 m in the basin (Figure 3.26). A small depocenter occurs in the vicinity of South Platong-2 well in the central part of the basin which contains more than 1500 m of sediments (Figure 3.26). Based on lithological association, unit 2 can be subdivided into lower and upper subunits.

A typical log profile of the lower subunit occurs in Surat-1 well between the depths of 1310-1520 m (Figure 3.25). The log profile depicts a well developed series of fining-upward sequences with sharp basal contacts and gradational upper contacts. The thickness of these sequences varies from 6 m to approximately 20 m. Sandstones at the top of the sequences are approximately 2-10 m thick. This subunit thickens toward the south (Figure 3.27). A prominent depocenter occurs in the southwestern part of the study area which contains a sequence of sandstones and shales more than 800 m thick (Figure 3.27). The subunit consists mainly of intercalations of white to light grey sandstone and mottled red, yellow to brown siltstone and claystone. The subunit is barren of foraminifera and plant debris is scarce. Few palynomorphs consist of fresh water and locally, mixed fresh and brackish water species.

The lower subunit was deposited in a meandering channel-floodplain environment. This interpretation is based on the absence of marine foraminifera, rare occurrence of plant debris and fresh water palynomorphs, the oxidation of the sediments, indicated by the mottled red to yellow siltstone and claystone, and the well

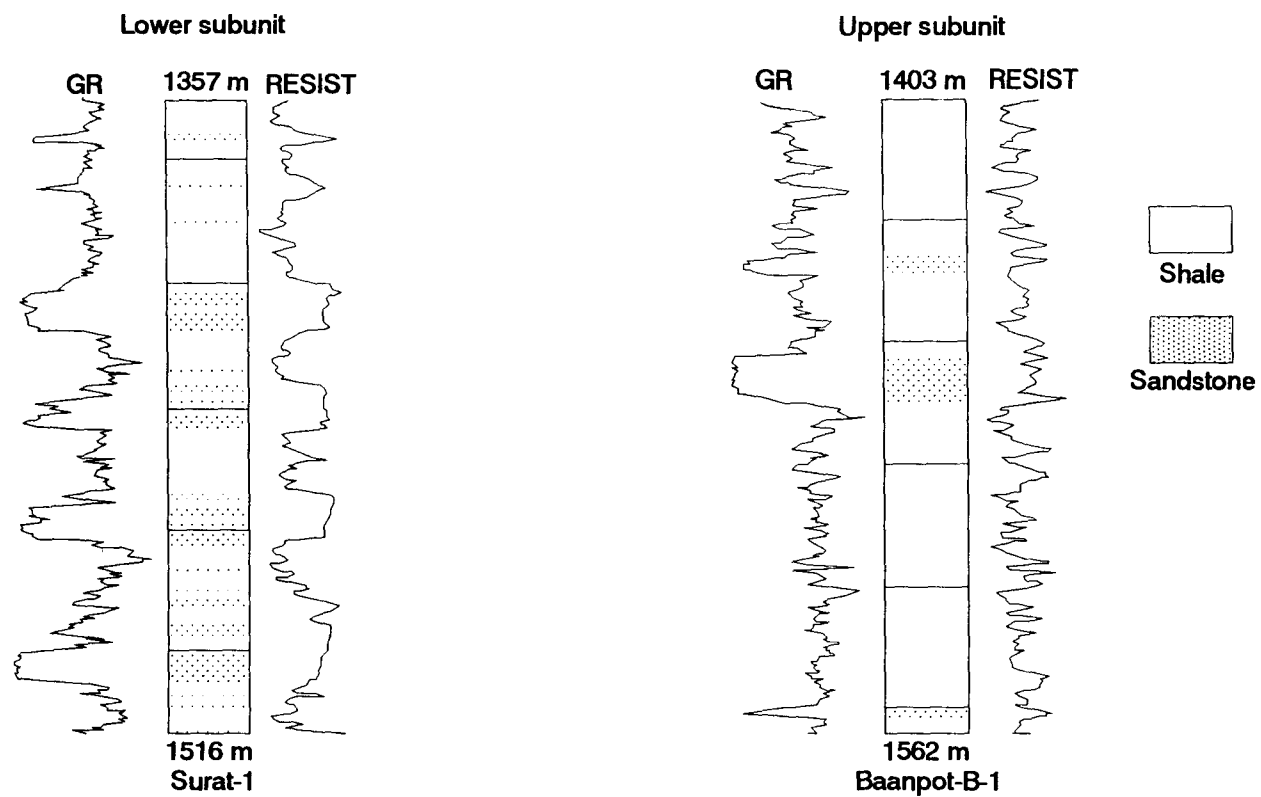


Figure 3.25: Typical log profiles of unit 2, showing general fining-upward sequences of nonmarine channel deposits in the lower subunit and generally fine-grained marginal marine deposits and marsh complexes in the upper subunit

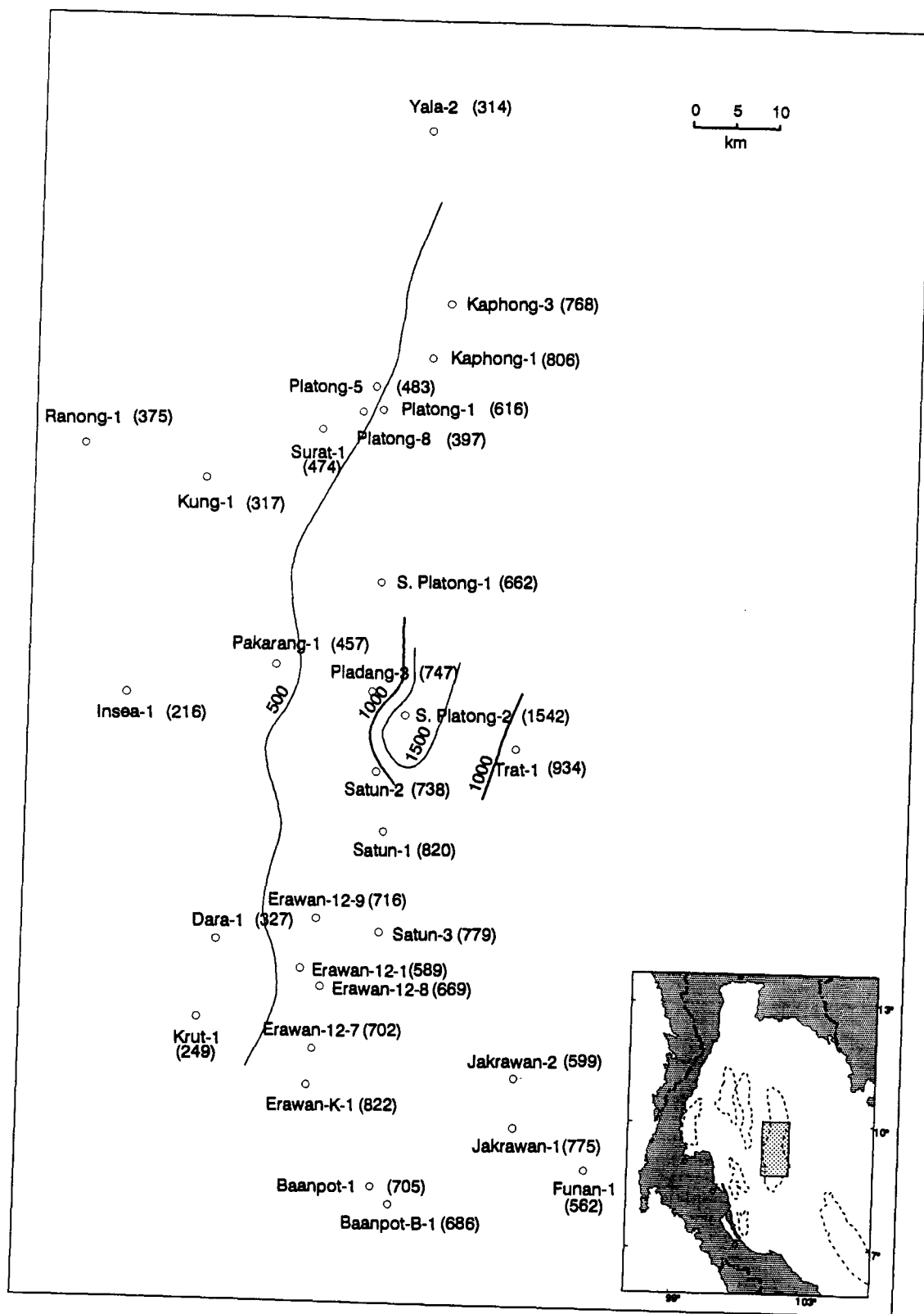


Figure 3.26: Isopach map of the stratigraphic unit 2 (contour interval = 500 m)

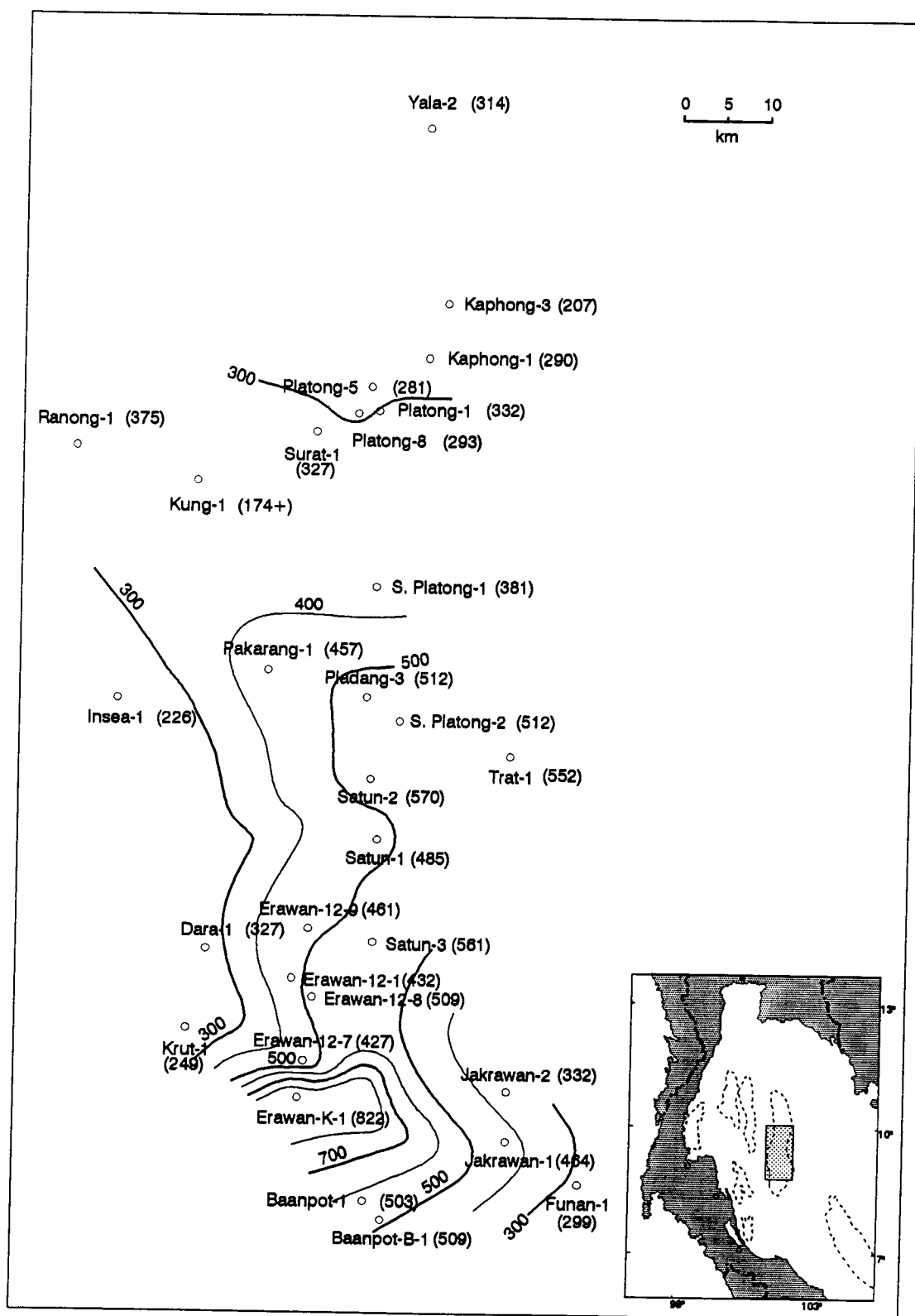


Figure 3.27: Isopach map of unit 2's lower subunit (contour interval = 100 m)

developed fining-upward sequences. Minor influence of brackish water is evident from the local occurrence of brackish water palynomorphs. The oxidation of the sediments suggests that this subunit might have been periodically subaerially exposed.

A typical log of the upper subunit of unit 2 occurs in Baanpot-B-1 well between the depths of 1400-1590 m (Figure 3.25). The profile is characterized by a generally high gamma ray count with minor intercalations of small fining-upward sequences. The subunit consists mainly of reddish brown to grey brown claystone and siltstone with minor light brown sandstone interbeds. This subunit thickens from zero in the western margin of the basin to more than 300 m at the basin center (Figure 3.28). A probable depocenter of this subunit was recognized in the north central part of the basin in the vicinity of the Kaphong-3 and Kaphong-1 wells where up to 500 m thick succession of sediments occurs (Figure 3.28). The subunit is barren of foraminifera and contains abundant plant debris and palynomorphs. Dominant brackish water palynomorphs include *Florschuetzia meridionalis*, *F. levipoli*, and *Zonocostites ramonae* (*Rhizophora* sp.).

The upper subunit of unit 2 was deposited in a brackish water swamp environment. This interpretation is supported by the presence of fine-grained sediments, abundant plant debris and brackish water palynomorphs. The reddish color of the sediments indicates subaerial exposure leading to intense oxidation of exposed sediments.

The overall depositional environment of unit 2 was a transgressive phase in which nonmarine sediments were initially deposited, followed by brackish water, marginal marine deposits. The depositional history of unit 2 can be summarized as follows. At the base of unit 2 are nonmarine meandering channel-floodplain deposits

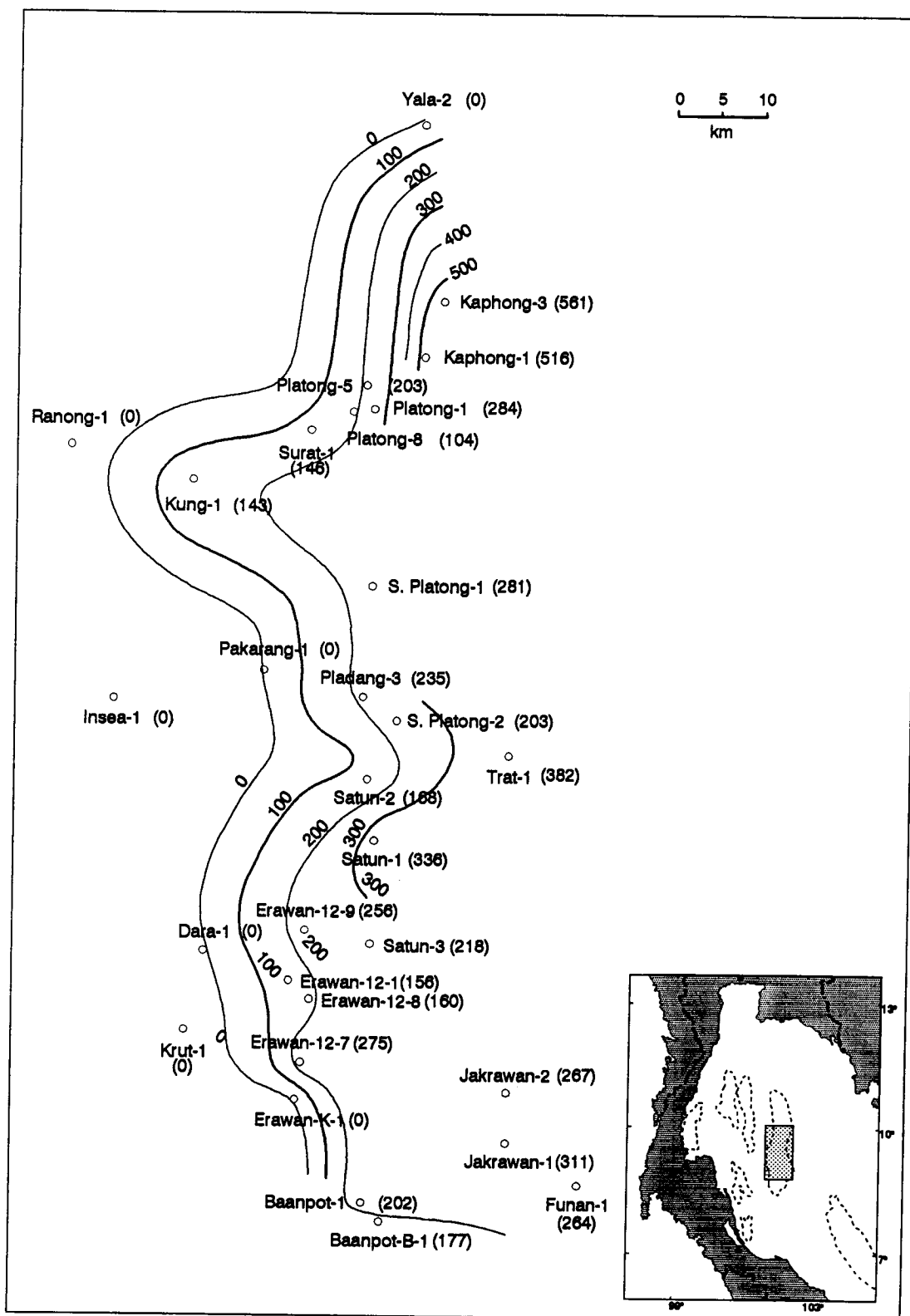


Figure 3.28: Isopach map of unit 2's upper subunit (contour interval = 100 m)

characterized by a series of strongly oxidized, fining-upward sequences, the presence of fresh water palynomorphs, and the absence of marine indicators. Local brackish water deposits contain brackish water palynomorphs. In the upper part of unit 2 are the marginal marine deposits characterized by fine-grained sediments, abundant plant debris and brackish water microflora. Subaerial exposure of the sediments of unit 2 led to intense oxidation resulting in the marked reddish color.

The presence of *Florschuetzia meridionalis*, *F. levipoli*, and *Zonocostites ramonae* (*Rhizophora* sp.), along with the absence of Pliocene palynomorphs, indicate that unit 2 is in the *Florschuetzia meridionalis* Borneo zone of Middle to Late Miocene age (Germaraad et al., 1968).

3.4.6 Unit 1

Unit 1 encompasses the interval from the Mid-Miocene unconformity to the present-day sea bed (approximately 60-80 m subsea elevation). Due to the lack of cutting samples and well log data at shallower depths, only the lowermost part of the unit is discussed here.

A typical composite log profile of unit 1 is shown in Figure 3.29. The thickness of this unit varies from about 800-850 m in the western basin margin to as thick as 1300-1400 m in the basin center (Figure 3.30). No prominent depocenter is recognized. Lithologically, the lower part of unit 1 can be subdivided into 2 subunits.

A typical log profile of the lower subunit occurs in Baanpot-1 well between the depths of 1220-1370 m (Figure 3.29). The profile is characterized by a series of

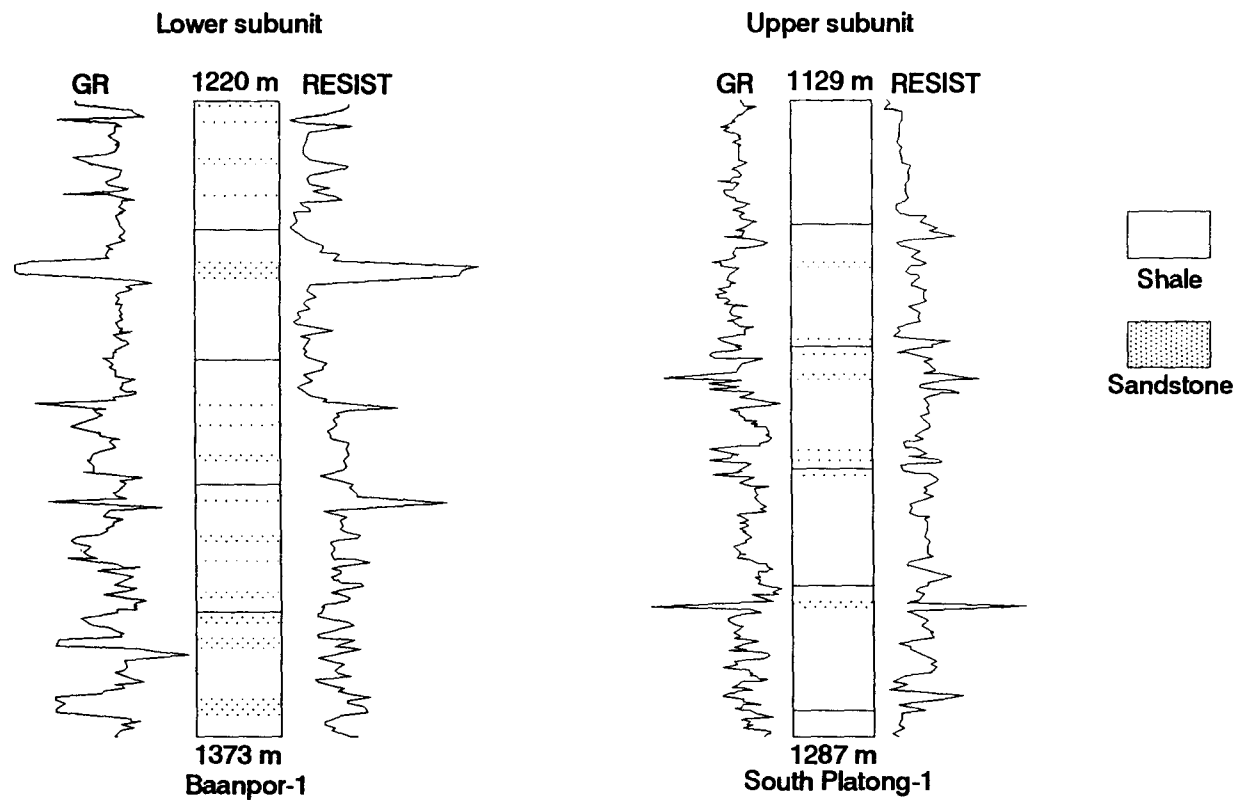


Figure 3.29: Typical log profiles of unit 1, showing general fining-upward sequences of nonmarine channel deposits at the base and generally fine-grained marginal marine deposits at the top of lower subunit and fine-grained shallow marine deposits in the upper subunit

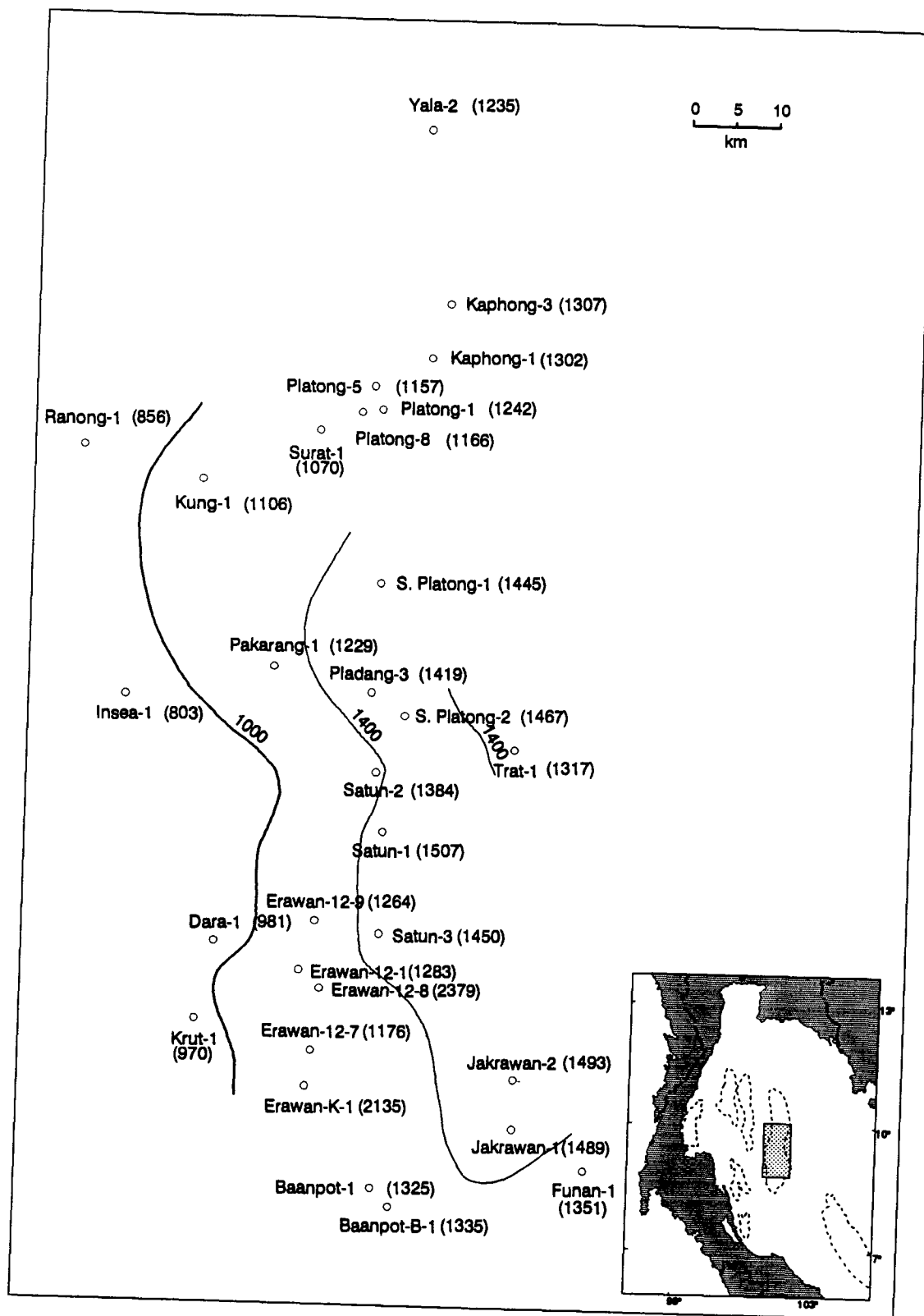


Figure 3.30: Isopach map of the stratigraphic unit 1 (contour interval = 400 m)

interbedded coarsening- and fining-upward sequences in the lower part and more fine-grained intervals in the upper part. Due to the lack of data in the upper part of this subunit, no isopach map was made. This subunit consists mainly of interbedded fine- to very fine-grained sandstone and grey to grey brown claystone and siltstone. Carbonaceous partings are common. The subunit contains abundant plant debris and palynomorphs. The predominant brackish water assemblage includes *Florschuetzia meridionalis*, *Zonocostites ramonae* (*Rhyzophora* sp.), and *Spinizonocolpites echinatus* (*Nypa* sp.). The subunit also contains arenaceous foraminifera such as *Miliammina telemaquensis*.

The lower subunit was probably deposited in distributary channel environments in a coastal plain based on a series of fining- and coarsening-upward sequences, brackish water palynomorphs and foraminifera. The upper part of this subunit was probably deposited in a lower delta plain or interdistributary bay where there was more influence of brackish water and marine processes. This interpretation is based on a series of fining-upward sequences which are overlain by fine-grained sediments, and the presence of brackish water palynomorphs and foraminifera.

A typical log profile of the middle subunit of unit 1 occurs in South Platong-1 well between the depths of 1100-1340 m (Figure 3.29). The serrated, generally high gamma ray log signature reflects fine-grained sediments interbedded with thin, coarse-grained sediments. Small-scale coarsening- and fining-upward sequences locally occur. No isopach map was constructed for this subunit because of the lack of constraint in the upper boundary. The subunit consists mainly of grey to dark grey claystone, siltstone and minor coarsening-upward sandstone and coal. Fragments of limestone also occur. The subunit contains abundant arenaceous foraminifera and palynomorph assemblages. Arenaceous foraminifera encountered

include *Miliammina cf. telemaquensis* and *M. sp.* These are the typical brackish water foraminifera. The palynomorph assemblage, also typical of brackish water, includes *Zononcostites ramonae*, *Florschuetzia meridionalis*, *Avicennia sp.*, and *Spinizonocolpites echinatus* (*Nypa sp.*).

The middle subunit was deposited in interdistributary bay environments. This interpretation is supported by the abundance of brackish water foraminifera and palynomorphs, the generally fine-grained sediments, and the presence of coal interbeds. Locally high concentrations of plant debris and palynomorphs may indicate proximity to distributary systems. The presence of small-scale coarsening- and fining-upward sequences may indicate crevasse splay and channel deposits which built into interdistributary bays.

Based on mud log data, the interval stratigraphically higher than the section described above, consists mainly of dark-grey to black clay and claystone with minor coal and sandstone interbeds. These lithologies together with the fact that the area is now approximately 60-80 m below sea-level suggest that the uppermost part of unit 1 was deposited in a lower delta plain and prodelta to shallow marine environments. This unit may, however, possibly have been exposed during the Pleistocene glaciation.

Arenaceous foraminifera such as *Miliammina cf. telemaquensis* and *M. sp.*, and palynomorphs *Florschuetzia meridionalis*, *Zononcostites ramonae*, and *Spinizonocolpites echinatus* suggest that the lower part of unit 1 is in the *Miliammina* paleontological zone and in the *Florschuetzia meridionalis* floral zone. The presence of fossils described above and the absence of Pliocene floral elements suggest that the lower part of unit 1 is of Late Miocene age.

The overall depositional environment of unit 1 shows a transgressive phase in which shallow marine sediments prograded onto nonmarine or marginal marine deposits. The depositional history of unit 1 is summarized as follows. The base was deposited in a distributary channel environment in a coastal plain characterized by a series of interbedded coarsening- and fining-upward sequences. Brackish water, interdistributary bay deposits subsequently overlaid the coastal plain deposit, evident by the abundance of brackish water foraminifera and palynomorph assemblage. The upper part of unit 1 is a shallow marine deposition characterized by dark-grey to black clay and claystone.

3.5 DISCUSSION

The stratigraphy of the Tertiary succession in the Pattani Basin is a response to the tectonic evolution of the Gulf of Thailand. Figure 3.34 shows temporal variation of the average rates of tectonic basement subsidence and decompacted sedimentation. The rate of tectonic subsidence and decompacted sedimentation rates were calculated using decompaction and backstripping analyses (*cf.* Van Hinte, 1978; Friedinger, 1988; Angevine et al., 1990). The subsidence was at a maximum during the Late Eocene to Early Oligocene interval and has generally decreased with time. The maximum rate of sedimentation occurred during the Early Miocene and Middle Miocene. The dominant period of rifting in the Pattani Basin lasted about 20 m.y. from Late Eocene (40 Ma) to Early Miocene (20 Ma) time and was characterized by episodic normal faulting, rapid subsidence, and high topographic relief (Chinbunchorn et al., 1989). After the rifting, a period of tectonic quiescence ensued and is characterized by relatively slow thermal subsidence. Based on tectonic characteristics of the study area, the Tertiary stratigraphy in the

Pattani Basin comprises two phases of sedimentation: synrift and post-rift. The synrift phase is characterized mainly by nonmarine sediments of unit 6 and unit 5, and a broad regressive sedimentary package of unit 4. The post-rift phase is characterized by a regressive (unit 3) and two transgressive sedimentary units (unit 2 and unit 1). The stratigraphy of Tertiary strata of this area is summarized in Table 3.1. The schematic sedimentary evolution of the Pattani Basin is summarized in Figure 3.35 and is discussed below.

3.5.1 Synrift Sedimentation

a. Late Eocene to Early Oligocene (40-30 Ma)

In the Earliest Tertiary, the Gulf of Thailand probably was elevated above sea level (Achalabhuti and Oudom-Ugsorn, 1978). The shoreline of the ancestral Gulf Basin was several hundred kilometres south of its present position. The initial phase of basin formation probably began in Late Eocene (Hellinger and Sclater, 1983; Chinbunchorn et al., 1989) when the area was subjected to an extensional tectonic regime of block faulting (Figure 3.35A) and rapid subsidence which created high topographic relief and high sediment influx into the basin (Figure 3.34). Rapid subsidence and high sediment supply led to the development of alluvial fan and alluvial plain deposits (Figure 3.35A). Due to limited available data, the distribution of the alluvial fan deposits cannot be documented here. However, it is most likely that the fan deposits, especially the coarse-grained proximal facies, were concentrated along the edge of the basin margin, whereas relatively finer-grained, braided stream deposits of the distal facies were concentrated farther toward the basin center. A narrow restricted depocenter in the south of the study area, and probably another in the north, (Figure 3.12) may have been the site of lacustrine

deposition. Similar conditions also existed in the narrow grabens of the Phitsanulok Basin, northern Thailand where approximately 2000 m of Oligocene to Miocene synrift lacustrine sediments occur (Burri, 1989; Chinbunchorn et al., 1989). Alluvial fan environments may have predominated until the end of the Eocene after which the source areas were substantially eroded, and depositional environments of the Pattani Basin changed from alluvial fans and braided streams to floodplains. Hence, Early Oligocene sediments are predominantly floodplain deposits characterized by generally fine-grained sediments with an occasional series of fining-upward sandstone representing meandering channel deposits. Lacustrine deposition, characterized by uniformly fine-grained sediments and coal interbeds, occurred locally mainly in the areas away from the basin edges. It is believed that thick lacustrine sediments were being deposited in the restricted narrow area in the basin center (Burri, 1989; Chinbunchorn et al., 1989).

b. Late Oligocene to Early Miocene (30-24 Ma)

In the Late Oligocene, the Pattani Basin subsided at a lower rate and consequently had a lower sedimentation rate than during Early Oligocene (Figure 3.34). Rifting and block faulting continued but with less intensity. A depocenter in the southern part of the basin suggests higher subsidence and sedimentation rates in that area. Sedimentation in the Pattani Basin was purely nonmarine (Figure 3.35B). Fluvial sandstone and claystone interbeds characterize a series of fining-upward sequences and the occurrence of fresh water palynomorphs suggest that channel deposition was typical of this synrift phase of basin in-filling. The change from fine-grained sediments in the lower subunit to coarser-grained sediments in the upper subunit probably reflects greater sediment influx which possibly resulted from more active faulting at the end of this time interval. Such episodic block faulting is common

during the rifting stage of basin formation (Allen and Allen, 1990). During this interval, the contemporary shoreline was tens of kilometres southeast of the Pattani Basin.

c. Early Miocene (24-20 Ma)

A rapid marine transgression from the end of the Late Oligocene to the Early Miocene (end of unit 5) is indicated by a sudden change from nonmarine floodplain deposits in the upper part of unit 5 to prodelta and shallow marine deposits in the lower part of unit 4. This transgression was caused by a rapid rise of relative sea-level during the early part of Early Miocene which, in turn, was the result of episodic block faulting and graben formation. Episodic block faulting is evident from an increase in subsidence rate during this time interval (Figure 3.34). The rapid increase in water depth temporarily created a surface of nondeposition, at least in the vicinity of the basin center, which marks the boundary between stratigraphic units 5 and 4. This transgression marks the first marine influence in the Pattani Basin. Following this, the rate of deposition exceeded the rate of water-depth increase, creating a broad regressive sedimentary succession. The regressive succession is characterized by fine-grained, prodelta to shallow marine sediments at the base overlain by a series of coarsening-upward distributary mouth bar and beach ridge deposits which, in turn, are overlain by a series of fining-upward sequences and red beds of floodplain-channel deposits. The updip limit of littoral to shallow marine sediments of the lower subunit of unit 4 (Figure 3.31) approximates the position of the shoreline in the early part of the Early Miocene. Marine influence in this area probably originated from the South China Sea to the east. As regression proceeded, nonmarine sediments progressively prograded over early shallow marine sediments, and the shoreline progressed toward the southeast.

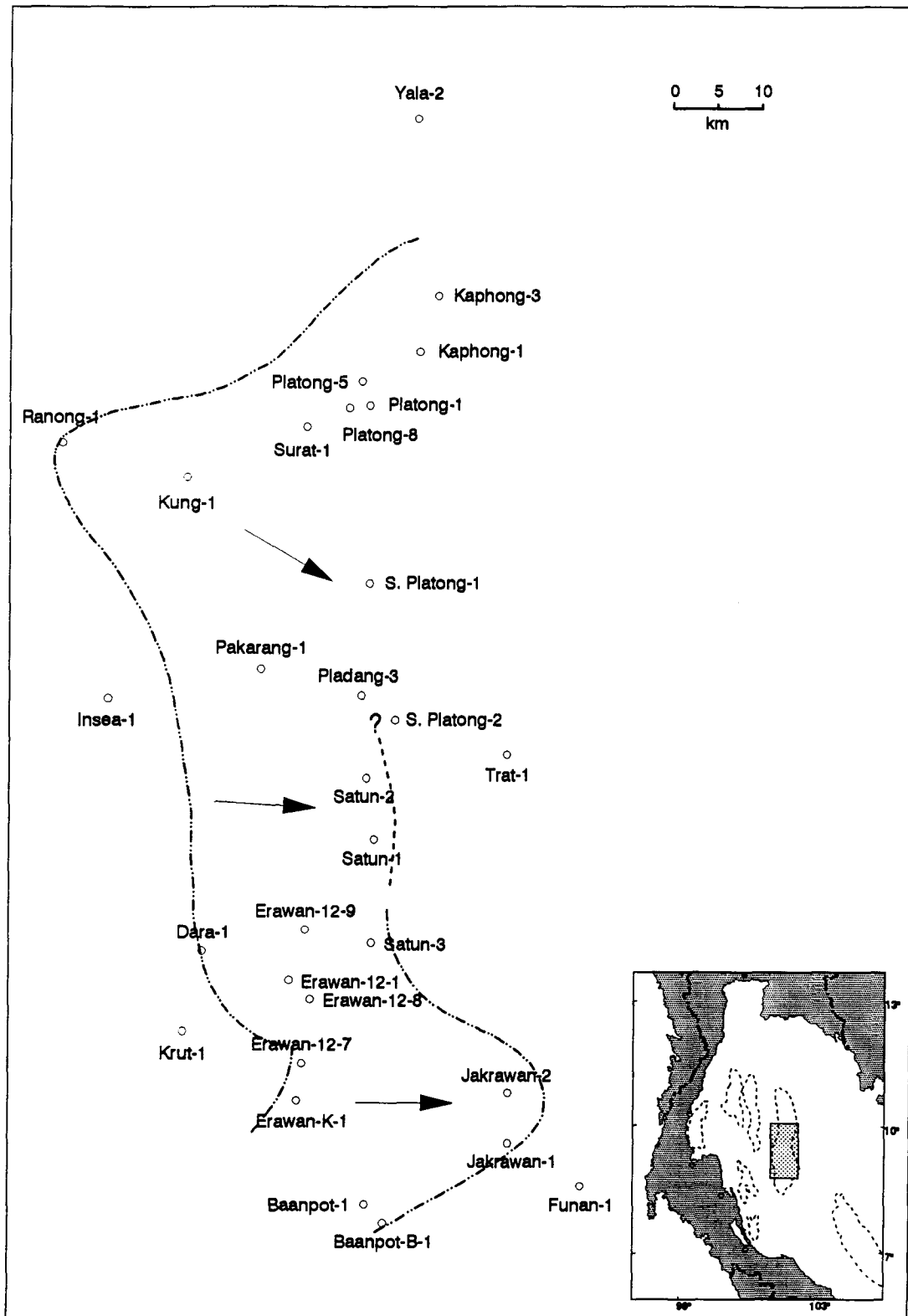


Figure 3.31: The regressive cycle of unit 4. Arrows indicate direction of advancing shoreline.

The distance between the updip limit of the littoral to shallow marine sediments of the lower subunit of unit 4 and the downdip limit of nonmarine deposits of the upper subunit of unit 4 (Figure 3.31) approximates the amount of regression within the Early Miocene interval.

3.5.2 Post-rift Sedimentation

By the end of unit 4 sedimentation, the Pattani Basin became tectonically quiescent. Subsequent evolution of the basin was essentially governed by relatively slow, post-rift thermal subsidence and sediment loading. Although faulting still occurred locally, fault density decreased substantially.

a. Late Early to Middle Miocene (20-15 Ma)

After the Early Miocene (the end of unit 4, about 20 Ma), another rapid transgression occurred in the Pattani Basin (Figure 3.35C). This transgression is recorded by a sudden change from nonmarine floodplain deposits in the upper part of unit 4 to prodelta and shallow marine deposits in the lower part of unit 3. The surface of nondeposition which marks the boundary between stratigraphic units 4 and 3 is the result of rapid rise in relative sea-level. This rapid rise may have been due more to a rapid rise of global eustatic sea-level (Haq et al., 1988) and low sedimentation rate rather than tectonic subsidence, because post-rift subsidence is relatively slow and continuous (Figure 3.34). As the rate of deposition exceeded the rate of relative sea-level rise, a coarsening-upward regressive sedimentary package resulted (Figure 3.32). The updip limit of the prodelta and shallow marine deposits of the lower subunit of unit 3 indicates that late Early Miocene transgression was less extensive in the northwestern part of the basin. The downdip

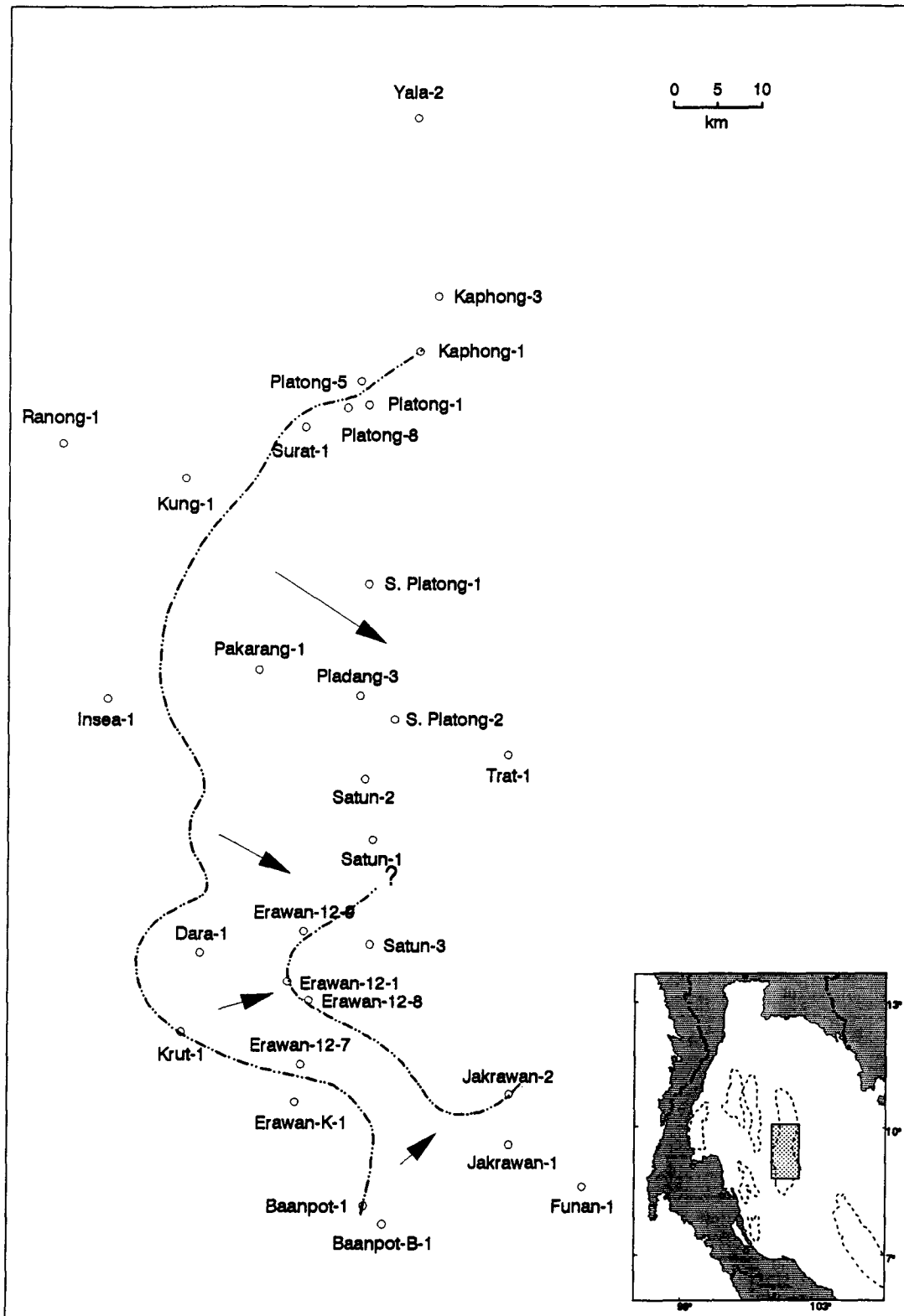


Figure 3.32: The regressive cycle of unit 3. Arrows indicate direction of advancing shoreline.

limit of nonmarine deposits of the upper subunit of unit 3 suggests that during the Middle Miocene (about 15 Ma) marine influence was restricted to a small area in the south-central part of the basin (Figure 3.32).

b. Middle Miocene (15-12 Ma)

During the Middle Miocene, minor basin-margin faulting continued, but with much less intensity. Continued fault movement, although local, is evident from relatively high tectonic subsidence rate (Figure 3.34). A progressive decrease in subsidence and sedimentation rates toward the end of this time interval led to a progressive increase in relative sea-level, i.e. transgression. This Middle Miocene transgression involved brackish water with marginal marine sediments slowly prograding over early nonmarine sediments. As a result, the contemporary shoreline advanced landward toward the northwest of the Gulf of Thailand. The amount of transgression can be approximated from the distance between the downdip limit of nonmarine sediments of the upper subunit of unit 3 and the updip limit of brackish water, marginal marine sediments of the upper subunit of unit 2 (Figure 3.33). Subsequently, a Late Middle Miocene transgression extended further to the north, but less to the west, than the earlier transgression (Figure 3.32 and 3.33). A rapid eustatic sea-level fall at the end of Middle Miocene (Haq et al., 1988) led to rapid regression and subaerial exposure, intense oxidation, and possibly erosion of Middle Miocene sediments (unit 2) in the study area. The shoreline at the end of unit 3 sedimentation was probably located further to the east of the study area.

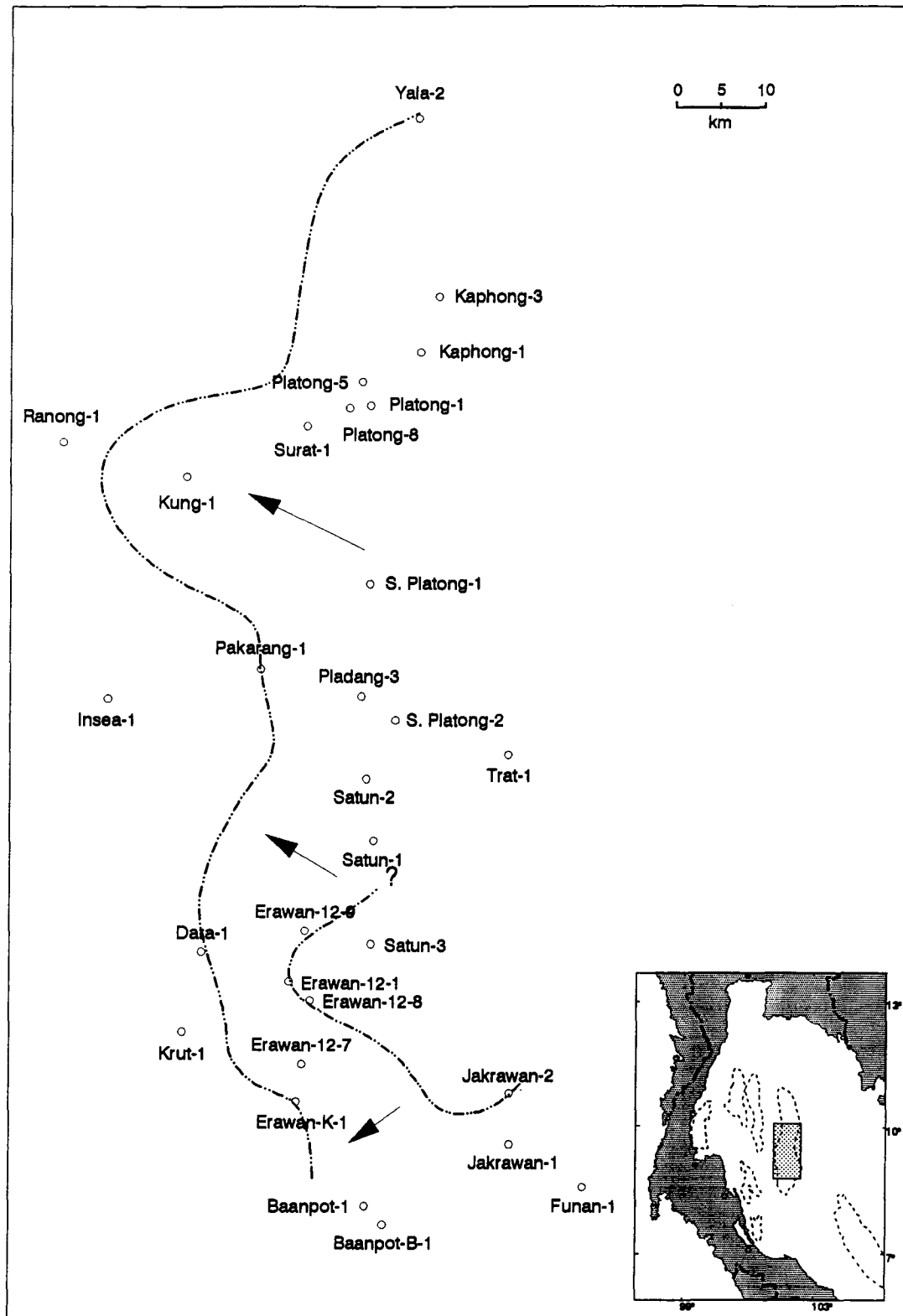


Figure 3.33: The transgressive cycle of unit 2. Arrows indicate direction of advancing shoreline.

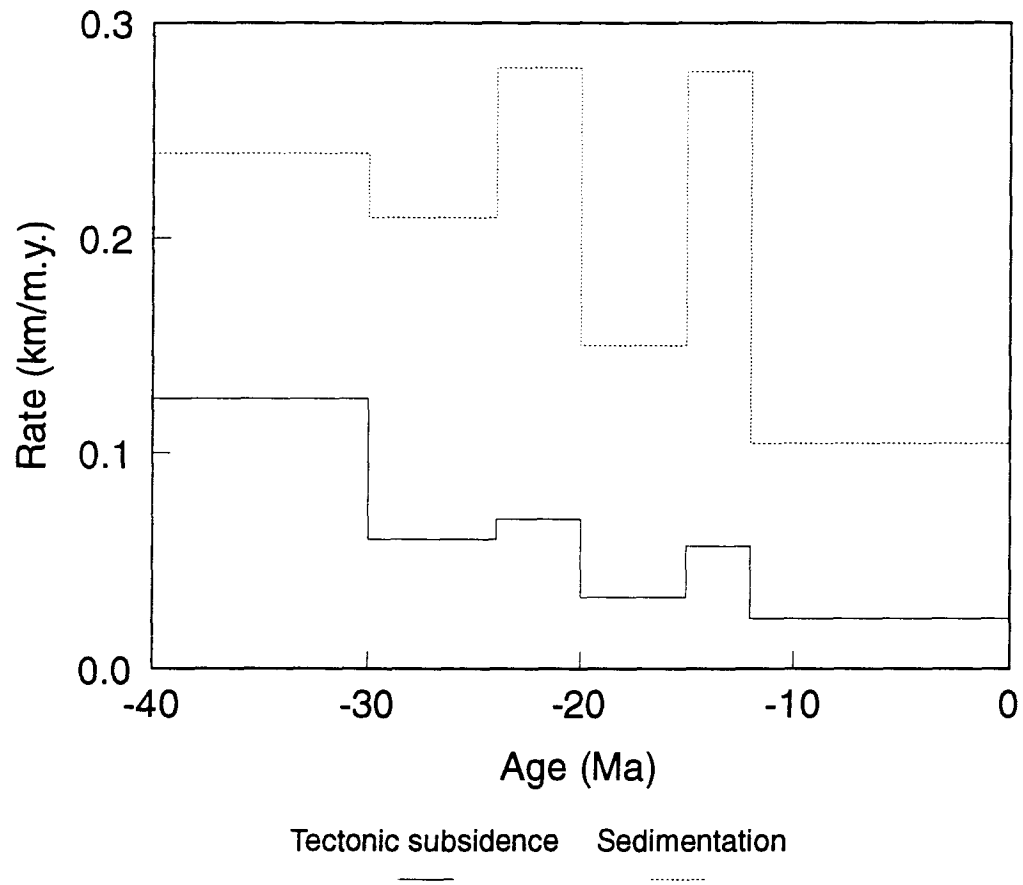


Figure 3.34: Tectonic subsidence (solid line) and decompacted sedimentation (dashed line) rates

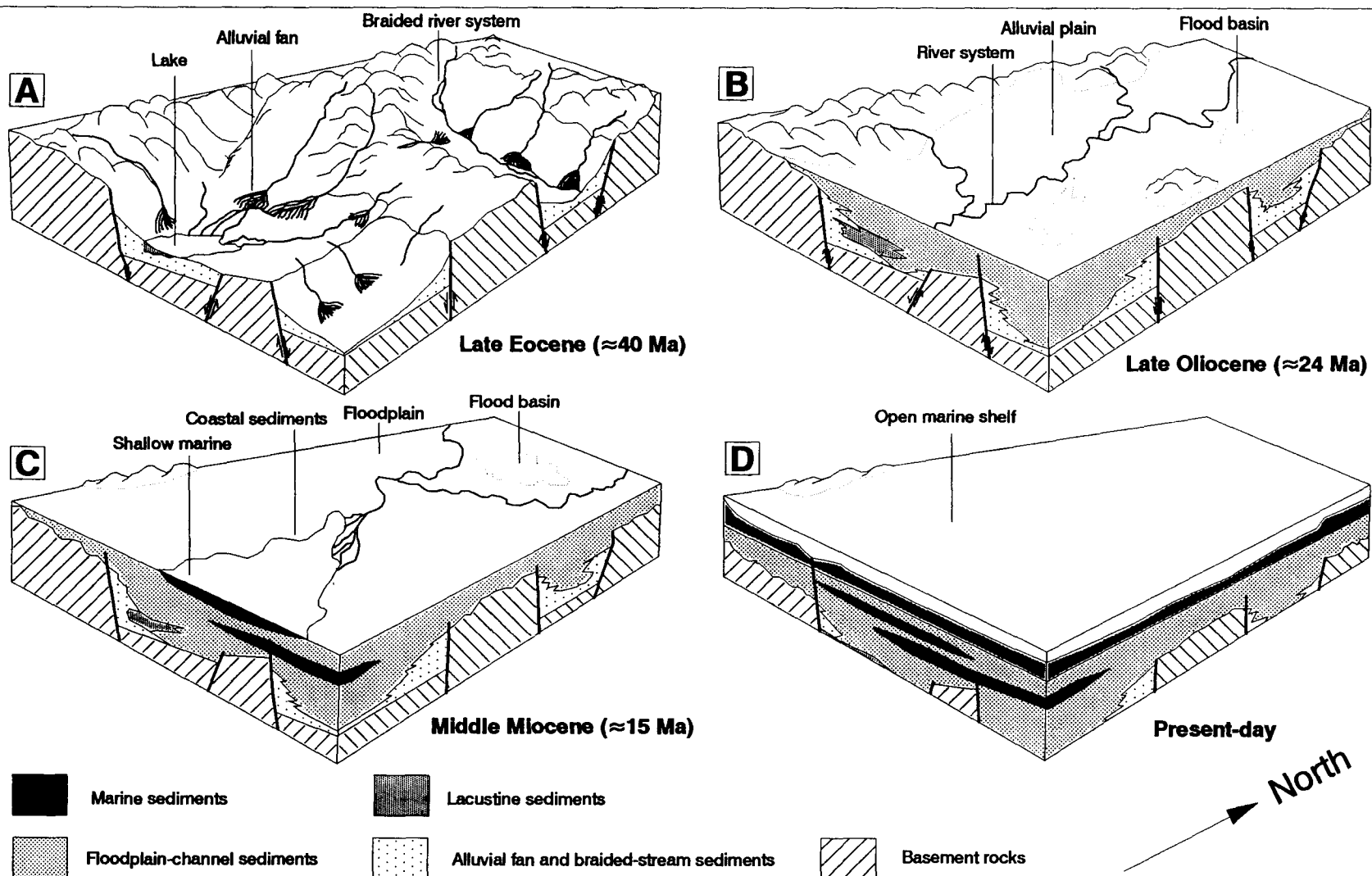


Figure 3.35: Schematic evolution of sedimentary environments of the Pattani Basin. (A) Late Eocene: after the formation of basin by extension. Alluvial fan and braided stream sedimentation is dominant. (B) Late Oligocene: most basement highs were eroded, extensive floodplain develop. (C) Middle Miocene: extensive low- gradient floodplain passed southward to shallow marine during transgression. (D) Present-day condition: establishment of shallow marine condition which may have started in the Late Miocene.

c. Late Miocene to Pleistocene (12-0 Ma)

After the Middle Miocene, the Pattani Basin was subjected to slow subsidence and sedimentation (Figure 3.34). Slow subsidence, decreasing sediment influx together with eustatic sea-level rise (Haq et al., 1988) caused a slow rise in relative sea-level and hence transgression (Figure 3.35D). A broad transgressive succession (unit 1) is characterized by basal nonmarine, distributary channel deposits overlain by fine-grained, brackish water, interdistributary bay deposits and marsh and swamp complexes which, in turn, are overlain by fine-grained, prodelta to shallow marine deposits. The shoreline advanced westward and northward to the present-day location (Figure 3.35D).

3.6 SUMMARY AND CONCLUSIONS

Rifting, as well as other tectonic processes, plays a major role in controlling the rate and amount of subsidence and the amount of sediment supply into a sedimentary basin. The rate and amount of basin subsidence, together with the amount of sediment influx generally dictated the sedimentary record developed in the study area, especially during the rifting phase and early part of the post-rift phase. Fluctuation in eustatic sea-level played a major role in controlling the sedimentary record in the latter part of the post-rift phase, during which subsidence and sediment supply rates were reduced significantly. The sedimentary history in the Pattani Basin, and the Gulf of Thailand in general, is a response to rifting which began in Late Eocene. The sedimentary succession in the Pattani Basin can be divided, based on the rifting process, into synrift and post-rift sequences. Three factors controlling the sedimentary records are evident in the Pattani Basin stratigraphy: (1) basin subsidence, (2) sediment supply and (3) sea-level fluctuation.

The effect of basin subsidence and sediment supply were probably greatest during the rifting phase and the early part of post-rift phase, characterized by block faulting and high topographic relief. In contrast, sea-level fluctuation probably played a more important role in the later part of post-rift phase, characterized by relatively slow and continuous subsidence.

The synrift stratigraphy comprises three stratigraphic units (units 6, 5, and 4). The basal unit (unit 6) represents Late Eocene to Early Oligocene (40-30 Ma) nonmarine sediments of alluvial fan, braided stream environments in the lower part and flood-plain deposits in the upper part. Lacustrine deposits were probably deposited in the vicinity of the basin center throughout this interval. The overlying unit (unit 5) represents Late Oligocene to Early Miocene (30-24 Ma) nonmarine floodplain-channel sediments in the lower part and coarse-grained channel deposits in the upper part. The uppermost succession of the synrift sequences (unit 4) represents an Early Miocene (24-20 Ma) broad regressive sedimentary package in which the basal prodelta to shallow marine sediments were overlain by distributary-mouth bar deposits and beach-ridge complexes. In turn, these were overlain by nonmarine floodplain and meandering channel deposits at the top. The deposition of the synrift sequence corresponded to the rifting and extension of the continental Southeast Asia which induced episodic block faulting and rapid subsidence. The sedimentary record of synrift sequences is the response to high subsidence rate and high sediment influx which were a direct result of rifting. The first marine transgression in the Pattani Basin in the Early Miocene might have been the result of rapid subsidence due to the episode of block faulting and the rise in eustatic sea-level. The following broad regressive succession in unit 4 resulted when the rate of deposition exceeded the rate of relative sea-level rise.

The post-rift stratigraphy comprises stratigraphic units 3, 2, and 1. The first post-rift unit (unit 3) represents an Early to Middle Miocene regressive sedimentary package, in which the basal prodelta and shallow marine sediments were overlain by distributary mouth bar deposits and beach complexes. These, in turn, are overlain by nonmarine floodplain and meandering channel deposits. The post-rift phase marks a slower subsidence rate, hence the amount of sediment influx and eustatic sea-level fluctuation played an important role in the resulting sedimentary record. Late Early Miocene transgression, which was probably the result of rapid eustatic sea-level rise, created a short period of nondeposition during which the rate of relative sea-level rise exceeded the rate of deposition. As the rate of deposition slowly exceeded the rate of relative sea-level rise, a broad regressive sedimentary succession resulted. The transgressive succession of unit 2 (Middle Miocene, 15-12 Ma) was the result of the slow rise of relative sea-level and progressive decreasing sediment supply, probably from a lowering of source areas toward the end of this time interval. The rapid fall of relative sea-level, resulting in subaerial exposure, intense oxidation, and possible erosion of the Middle Miocene sediments, was probably the effect of the global eustatic sea-level fall at the end of Middle Miocene. The uppermost transgressive succession of unit 1 (Late Miocene to Holocene, 12-0.01 Ma) was the result of a slow rise in relative sea-level, probably a result of a slow rise in eustatic sea-level, slow subsidence, and decreasing sediment supply. The present-day shallow marine condition in the Pattani Basin and throughout the Gulf of Thailand is the continuation of the latest transgressive phase.

4. TECTONIC EVOLUTION AND BASIN MODELLING OF THE PATTANI BASIN, THE GULF OF THAILAND

4.1 ABSTRACT

Subsidence and thermal histories of the Pattani Basin have been investigated using a nonuniform lithospheric stretching model. The predicted heat flow history is used to calculate the degree of organic maturation, in this case: vitrinite reflectance. The validity of the model is verified by comparing the calculated vitrinite reflectance with the measured values.

The opening of the Pattani Basin is related to a northward collision of Indian subcontinent with Eurasia in the Eocene. The penetration of India into Eurasia caused clockwise rotation of Southeast Asia, resulting in an increasingly oblique subduction of the Indian Ocean plate beneath the western edge of Southeast Asia. The oblique subduction changed the stress field in Southeast Asia from one of convergence to one with a strike-slip component which led to right-lateral movement on NW-SE fault systems and left-lateral movement on NE-SW conjugate fault systems. The E-W extension associated with the right-lateral fault systems caused crustal thinning and lithospheric stretching in Thailand. This, in turn, induced the formation of N-S trending sedimentary basins along an old Triassic-Jurassic suture zone and the similar NNW-SSE tectonic trends which are the weak zones in the lithosphere.

The nonuniform lithospheric stretching model is generally consistent with the observed geological constraints in the Pattani Basin. The amount of lithospheric stretching and surface heat flow generally increase from the basin margin to the

basin center. The crustal lithospheric stretching factor (β) ranges from 1.3-1.4 at the basin margin to 2.6-2.8 in the center. The subcrustal stretching factor (δ) varies from 1.3 at the basin margin to 3.0 in the basin center. Generally, the amount of subcrustal stretching is greater than that of crustal stretching, except in areas with a great thicknesses of synrift sediments, where the amount of crustal stretching is greater than that of subcrustal stretching. Such areas might have been affected by the pre-existing basement topography prior to rifting.

The lithospheric stretching in the Pattani Basin may have extended the basement as much as 45 to 60 km and have caused the passive upwelling of the hot aesthenosphere, resulting in high surface heat flow (1.9-2.5 HFU) and high geothermal gradient (45-60°C/km).

4.2 INTRODUCTION

Recent advances in understanding the mechanisms of basin formation have made possible quantitative basin modelling, based on known physical principles. Two processes believed to create sedimentary basins are flexure of the lithosphere in response to surface loading by overthrusts (Beaumont, 1981; Jordan, 1981) and thinning of the lithosphere by stretching (McKenzie, 1978). Tertiary basins in the Gulf of Thailand, having a series of normal faults, horsts, grabens, and half graben structures, are thought to have been initiated by continental rifting and lithospheric stretching (Bunopas and Vella, 1983; Hellinger and Sclater, 1983). This chapter applies the modified McKenzie's kinematic lithospheric stretching model (McKenzie, 1978; Hellinger and Sclater, 1983; Allen and Allen, 1990) to predict subsidence and thermal histories of the Pattani Basin (Figure 4.1). The predicted heat flow history is used to calculate the degree of organic maturation and the

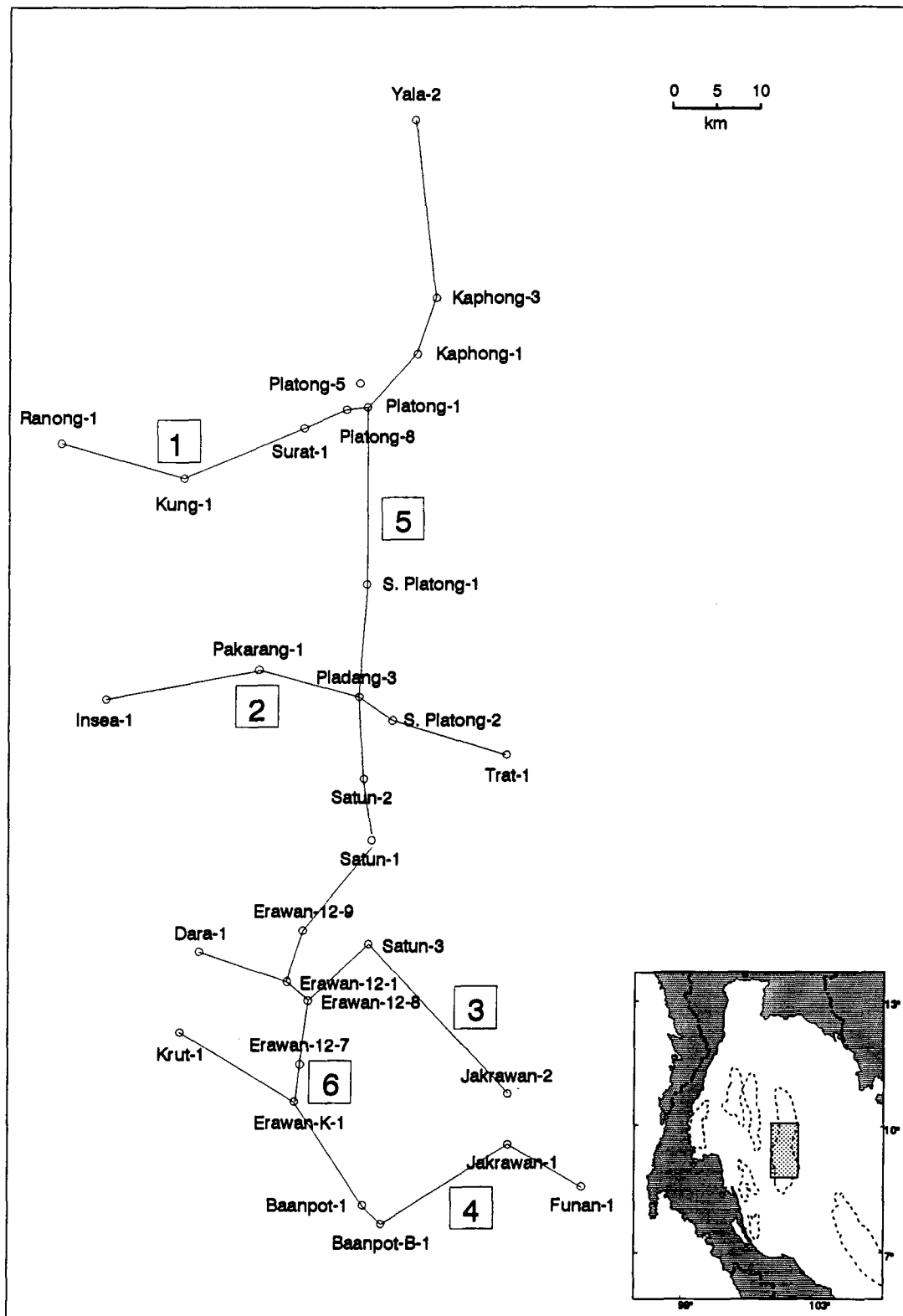


Figure 4.1: Location of well data used in this study. Numbers in the box indicate the cross sections shown in Figures 4.2 through 4.7

timing and location of hydrocarbon generation (Turcote and McAdoo, 1970; Royden et al., 1980; Issler and Beaumont, 1987). The validity of the model is then assessed by comparing the calculated thermal maturation index, in this study: vitrinite reflectance, with the measured values.

4.3 METHODS OF STUDY

4.3.1 Geohistory Analysis

The total amount of subsidence in sedimentary basins is the sum of the true tectonic subsidence and the subsidence due to sediment loading. The total subsidence history of a sedimentary basin can be analyzed from outcrop sections, well data, and seismic sections using the technique referred to as "Geohistory analysis" by Van Hinte (1978).

Geohistory provides a true picture of subsidence and sediment accumulation rates through time by making three corrections to the present (observed) stratigraphic thickness. The three corrections are decompaction, paleobathymetry, and eustatic sea-level fluctuations. Decompaction is applied to the observed stratigraphic thickness in order to remove the progressive effects of rock volume changes with time due to the progressive loss of porosity with depth. Paleobathymetry, the water depth at the time of deposition, is used to determine the position of a stratigraphic layer relative to a datum such as present-day sea-level. Eustatic sea-level fluctuation data is used to remove the effect of changes in paleosea-level relative to a datum such as today's sea-level.

True tectonic subsidence is obtained only after the removal, from the total subsidence, of the subsidence due to the sediment load and after corrections for variations in water depth and eustatic sea-level fluctuations. The common approach for removing the effect of sediment loading is by assuming a simple Airy's local isostatic model in which the sedimentary units can be removed (backstripped), and the basin is allowed to isostatically rebound (Steckler and Watts, 1978; Angevine et al., 1990). The true tectonic subsidence obtained from backstripping can be used in interpreting the mechanisms of basin formation.

The following sections describe the methods of decompaction, backstripping, and corrections for paleowater depth and eustatic sea-level changes used in this study in order to obtain the total subsidence and the true tectonic subsidence, respectively.

a. Decompaction

The purpose of decompaction is to remove progressive effects of rock volume change with time and depth due to the progressive loss of porosity during burial. Assuming, for clastic sediments, no significant chemical diagenesis, volume of grains does not change during burial (Van Hinte, 1978). Volume of pore space, however, decreases with time and depth of burial. The original thickness (T_o) is related to the present-day thickness (T_n) as follows (Van Hinte, 1978; Sclater and Christie, 1980):

$$T_o = \frac{(1 - \phi_n) T_n}{1 - \phi_o} \quad (4.1)$$

Where ϕ_o is the original porosity at time of deposition. T_n and ϕ_n are present-day (observed) thickness and porosity of the stratigraphic unit, respectively. Several porosity-depth functions for various lithologies have been proposed (Sclater and Christie, 1980; Baldwin and Butler, 1985). For normally compacted sediments the porosity-depth function can be either exponential or linear (Ruby and Hubbert, 1960; Sclater and Christie, 1980; Friedinger, 1988) according to the following equations:

$$\phi_{(z)} = \phi_o \exp(-cz) \quad (\text{exponential}) \quad (4.2)$$

or

$$\phi_{(z)} = \phi_o - cz \quad (\text{linear}) \quad (4.3)$$

Where $\phi_{(z)}$ is the porosity at depth z . Variables ϕ_o and c are surface porosity and compaction coefficient, respectively, and are controlled by lithological properties of the sediment layer.

The thickness of a sediment layer at any time in the past can be calculated by moving the layer up along an appropriate porosity-depth curve. This exercise is equivalent to sequentially removing overlying sediment layers and allowing the sediment layer of interest and underlying layers to decompact. If a sediment layer between depth z_1 (top) and z_2 (bottom) moves up to the surface, z_1' (new top) becomes zero and the new bottom depth z_2' can be calculated using (Sclater and Christie, 1980; Friedinger, 1988):

$$\begin{aligned}
& z_2' - z_2 + z_1 - z_1' + \frac{\phi_o}{c} \exp(-cz_2') \\
& + \frac{\phi_o}{c} [\exp(-cz_1) - \exp(-cz_2') - \exp(-cz_1')] = 0
\end{aligned} \tag{4.4}$$

or in case of a linear-depth porosity function:

$$z_2'^2 + \frac{2}{c}(1 - \phi_o)z_2' - \frac{2}{c} \left[k + z_1'(1 - \phi_o + \frac{c}{2}z_1') \right] = 0 \tag{4.5}$$

where

$$k = (z_2 - z_1) \left[1 - \phi_o + \frac{c}{2}(z_2 + z_1) \right]$$

The depth z_2' then becomes the new top (z_1') for the underlying layer. When this procedure is applied successively from top to bottom of the sedimentary column, the decompacted subsidence history of each sediment layer in a stratigraphic column can be determined.

The rate of sediment-fill, R_f , for the topmost layer, after each backstripping exercise, of thickness z_2' (where $z_1' = 0$) can be calculated using the equation:

$$R_f = \frac{z_2'}{\Delta_t} \quad \text{where } \Delta_t = t_2 - t_1 \tag{4.6}$$

Where t_1 and t_2 are the ages of top and base boundaries of the layer, respectively.

The rate R_f thus calculated, however, still does not fully represent the sedimentation process. Thicker units, due to their heavier loads, are subject to more compaction and have lower initial porosity than thinner units (Van Hinte, 1978). A true rate of sediment-mass accumulation, R_a , for each top layer corrected for self-compaction of the sediments is, therefore, calculated by:

$$R_a \Delta_t (1 - \phi_o) + \frac{\phi_o}{c} [1 - \exp(-c R_a \Delta_t)] - z_2' = 0 \quad (\text{exponential}) \quad (4.7)$$

or

$$R_a^2 - \frac{2}{c \Delta_t} R_a + \frac{2 z_2'}{c \Delta_t} = 0 \quad (\text{linear}) \quad (4.8)$$

The new mean porosity of each decompacted sediment layer, ϕ_i , is calculated using:

$$\phi_i = \frac{\phi_o}{c} \frac{\exp(-c z_1') - \exp(-c z_2')}{z_2' - z_1'} \quad (\text{exponential}) \quad (4.9)$$

or

$$\phi_i = \phi_o - \frac{c}{2} (z_2' + z_1') \quad (\text{linear}) \quad (4.10)$$

The new mean density of each decompacted sediment layer, ρ_i , is calculated using:

$$\rho_i = \phi_i \rho_w + (1 - \phi_i) \rho_s \quad (4.11)$$

Where ρ_w and ρ_g are the densities of water and the sediment grains, respectively.

The new mean density of the total sediment column, ρ_s , is:

$$\rho_s = \sum_{i=1}^n \left[\frac{\phi_i \rho_w + (1 - \phi_i) \rho_g}{S} z_i' \right] \quad (4.12)$$

Where ϕ_i and z_i' are the mean porosity and decompacted thickness, respectively, of the i^{th} sediment layer, and S is the total decompacted thickness of individual sediment column at the time of interest.

b. Backstripping

The total subsidence calculated from decompaction described in the previous section includes the contribution of all factors that affect the subsidence of the basin: tectonics, sediment load, sea-level changes, and paleowater depth. In a study oriented toward interpreting tectonic processes responsible for the basin formation, the effect of subsidence caused by loading during deposition needs to be removed (Allen and Allen, 1990; Angevine et al., 1990).

The backstripping technique (Steckler and Watts, 1978) is used to remove the effect of sediment loading on the total subsidence by assuming a simple Airy's local isostatic model in which the sedimentary units are removed and replaced by water, and the basin is allowed to isostatically rebound.

The tectonic subsidence of the basement, Y , is given by (Steckler and Watt, 1978):

$$Y = S \left(\frac{\rho_m - \rho_s}{\rho_m - \rho_w} \right) + W_d \quad (4.13)$$

Where S is the decompacted thickness of a sediment column, W_d the water depth at time of sediment deposition, ρ_m the mean density of mantle, ρ_w the mean density of water, and ρ_s the mean density of a sediment column.

c. Eustatic correction

Equation 4.13 is used for cases in which the eustatic sea-level fluctuation is not considered. If the magnitude of sea-level change is known, then equation 4.13 can be rewritten to give a more accurate true tectonic subsidence of the basin as:

$$Y = S \left(\frac{\rho_m - \rho_c}{\rho_m - \rho_w} \right) + W_d - \Delta SL \left(\frac{\rho_w}{\rho_m - \rho_w} \right) \quad (4.14)$$

Where ΔSL is the eustatic sea-level change relative to the present-day sea-level. ΔSL is positive for a sea-level rise and negative for a sea-level fall.

4.3.2 Basin Forming Modelling

The true tectonic subsidence obtained from backstripping analysis is very important in characterizing structural style and determining the mechanism causing the occurrence and development of the sedimentary basins. Intracratonic rift basins and Atlantic-type continental margins are extensional basins believed to have been initiated by lithospheric stretching. The lithospheric stretching model, first

quantified by McKenzie (1978), can be used to predict subsidence of such basins (Royden and Keen, 1980; Sclater and Christie, 1980; Wood, 1982; and Hellinger and Sclater, 1983).

McKenzie (1978) proposed the uniform lithospheric stretching model in which the extension of crustal and subcrustal continental lithosphere are identical. In the model, a rapid extension of continental lithosphere causes lithospheric thinning and passive upwelling of hot asthenosphere to maintain isostatic balance. This rifting stage is associated with block faulting and initial subsidence or uplift. Following rifting, the attenuated region slowly subsides over a period of time due to thermal contraction and thickening of the lithosphere as it cools. The overall tectonic subsidence is amplified by sediment and water loading. McKenzie's model assumes that rifting is an instantaneous event and that the amount of lithospheric extension, β , is uniform with depth in the lithosphere, but β varies laterally.

Royden and Keen (1980) proposed the dike-intrusion model in which fracturing of lithosphere and intrusion of dense ultramafic mantle materials into the crust are assumed. Addition of dense ultramafic material to light crustal rocks results in initial subsidence associated with block faulting. The relatively slow post-rift subsidence is controlled by a decreasing thermal anomaly. Hellinger and Sclater (1983) modified McKenzie's model by proposing the non-uniform lithospheric extension model in which the amount of thinning of the crust is different from that of the subcrustal lithosphere. The amount of crustal lithospheric stretching is β whereas that of subcrustal lithospheric stretching is δ . Friedinger (1988) combined the three models outlined above and provided a modelling technique for calculating subsidence and heat flow history of the sedimentary column formed by rapid extension of the lithosphere.

Initial or synrift, fault-controlled, subsidence or uplift (S_i) caused by instantaneous lithospheric stretching is the difference between subsidence due to isostatic compensation of denser mantle material (E) and the thermal expansion of lithosphere (T , Friedinger, 1988):

$$S_i = \frac{E - T}{\rho_m(1 - \alpha T_m) - \rho_w} \quad (4.15)$$

Where

$$E = (\rho_m - \rho_c)t_c \left(1 - \frac{1}{\beta}\right) \left(1 - \frac{T_m \alpha t_c}{2a}\right)$$

$$T = \frac{T_m \alpha a \rho_m}{2} \left[\left(1 - \frac{1}{\delta}\right) + \left(\frac{t_c^2}{a^2} - \frac{2t_c}{a}\right) \left(\frac{1}{\beta} - \frac{1}{\delta}\right) \right]$$

Where β and δ are crustal and subcrustal lithospheric stretching factors, respectively. ρ_w , ρ_m , and ρ_c are densities of water, mantle and lithospheric crust, respectively. T_c is the pre-rift thickness of the crust. α and a are thermal expansion coefficient and thickness of lithosphere. T_m is the temperature of upper mantle. The surface of the crust is assumed to lie at sea-level before extension, to subside below sea-level after extension ($S_i > 0$) and then to be water-loaded. In the case where the surface rises above sea-level after extension ($S_i < 0$), ρ_w should be replaced by zero (air density).

As time elapses ($t \rightarrow \infty$) the thermal perturbation within the lithosphere gradually decays; thermal contraction due to the cooling of the lithosphere induces post-rift or thermal subsidence. In order to predict the cooling of the lithosphere after rifting, the heat flow variation through time must be known. To simplify the calculation, it is assumed that lateral temperature gradients are much smaller than vertical temperature gradients; that is, heat is conducted upwards in a vertical direction only. If a is the lithosphere's thickness, z is the elevation above the final equilibrium depth and $T_{(z)}$ is the temperature at depth z , the boundary conditions are:

$$T_{(z)} = 0 \quad \text{at} \quad z = 0$$

$$T_{(z)} = T_m \quad \text{at} \quad z = a$$

The one-dimensional unsteady state heat flow is:

$$\frac{\delta T}{\delta t} = k \frac{\delta^2 T}{\delta z^2} \quad (4.16)$$

Where k is the diffusivity of both crustal and subcrustal materials. The second derivative gives the curvature of the geotherm as it relaxes to its pre-stretching gradients.

The temperature at any depth and time, $T_{(z,t)}$ is made up of a steady-state component, $s_{(z)}$, and an unsteady-state component, $u_{(z,t)}$ (Allen and Allen, 1990):

$$T_{(z,t)} = s_{(z)} + u_{(z,t)} \quad (4.17)$$

Where

$$s_{(z)} = T_m \left(1 - \frac{z}{a} \right)$$

$$u_{(z,t)} = \sum_{n=0}^{\infty} X_n \exp \left(-n^2 \frac{t}{\tau} \right)$$

with

$$\tau = \frac{a^2}{\pi^2 k}$$

$$X_n = \left[(\beta - \delta) \sin \left\{ n\pi \left(1 - \frac{t_c}{a\beta} \right) \right\} + \delta \sin \left\{ n\pi \left[\left(1 - \frac{t_c}{a\beta} \right) - \frac{\left(1 - \frac{t_c}{a} \right)}{\delta} \right] \right\} \right] \times \frac{(-1)^{n+1}}{n\pi}$$

Where n is an integer which expresses the order of the harmonic of the Fourier transform; τ and k are the thermal-time constant and thermal diffusivity of the lithosphere.

The surface heat flux (Q) at time t after the end of rifting is given by Fourier's law:

$$Q_{(t)} = Q_e \left\{ 1 + 2 \sum_{n=1}^{\infty} \left[X_n \exp \left(-n^2 t / \tau \right) \right] \right\} \quad (4.18)$$

Where Q_e is the equilibrium heat flux:

$$Q_e = \frac{T_m K}{a} + Q_r \quad (4.19)$$

where K is the mean thermal conductivity of the lithosphere and Q_r is the internal heat created by radioactive decay within the lithosphere.

The elevation, $z_{(t)}$, above the final equilibrium depth to which the upper surface of the lithosphere subsides at time t is (Friedinger, 1988):

$$z_{(t)} = \frac{4a\alpha\rho_m T_m}{(\rho_m - \rho_w)\pi^2} \sum_{m=0}^{\infty} \times \left\{ \frac{x_{(2m+1)}}{(2m+1)^2} \exp\left[-(2m+1)^2 t / \tau\right] \right\} \quad (4.20)$$

The water-loaded thermal subsidence, $S_{(t)}$, is obtained:

$$S_{(t)} = z_{(0)} - z_{(t)} \quad (4.21)$$

The total tectonic subsidence is the sum of initial (synrift) and thermal (post-rift) subsidences. The total lithospheric extension (ϵ), including both crustal (β) and subcrustal (δ) extension is:

$$\epsilon = \frac{a}{\frac{t_c}{\beta} + \frac{(a - t_c)}{\delta}} \quad (4.22)$$

Assuming that heat flux is independent of depth within the sediment column and neglecting deep water circulation of pore water, the temperature, $T_{(z)}$, at depth z is given by (Andrews-Speed et al., 1984):

$$T_{(z)} = T_o + \frac{Q}{K} z \quad (4.23)$$

Where $T_{(o)}$ is the temperature at the sediment surface, Q is the heat flux conducted vertically upwards through the sediment column, K is the mean thermal conductivity of sediments which is (Woodside and Messmer, 1961):

$$K = K_b^\phi K_g^{(1-\phi)} \quad (4.24)$$

Where ϕ is the porosity of the sediment column, K_b and K_g are the thermal conductivities of pore water and sediment grains, respectively.

The temperature, $T_{(z)}$, at a given depth z within the n^{th} layer from the surface of the sediment column is (Friedinger, 1988):

$$T_{(z)} = T_o + Q \left[\frac{1}{K_n} \left(Z - \sum_{i=1}^{n-1} d_i \right) + \sum_{i=1}^{n-1} \frac{d_i}{K_i} \right] \quad (4.25)$$

Where d_i and K_i are the thickness and thermal conductivity of each individual layer from top to bottom. K_n is the mean thermal conductivity of the sediment column.

A basin modelling program using the concepts described above is included in a computer disk at the end of this thesis. This program is used to calculate decompacted total and tectonic subsidences and predict thermal history of a sedimentary basin formed by non-uniform lithospheric stretching. Appendix A describes how to run the program.

4.4 BASIN FORMING MECHANISM IN THE PATTANI BASIN

The extensional nature of the Tertiary basins in the Gulf of Thailand has been documented (Bunopas and Vella, 1983; Hellinger and Sclater, 1983; and many others) but the controlling tectonic regime responsible for the origin of these basins has been a subject of discussion. Tapponnier et al. (1982), Pelzer and Tapponnier (1988), and Ohnstad (1990) related this extension to the extrusion of a portion of Indochina away from India as the Indian plate collided with the Eurasian plate. Bunopas and Vella (1983) related the Tertiary extension and rifting in the Gulf of Thailand and onshore Thailand to back-arc spreading accompanying the subduction of the Indian plate beneath Continental Southeast Asia along the Java Trench and Andaman-Nicobar Island chain. Polachan and Sattayarak (1989) considered Tertiary basins in Thailand as transtensional basins whose development is related to right-lateral simple shear along the NW-SE fault system.

4.5 TIMING OF BASIN FORMATION

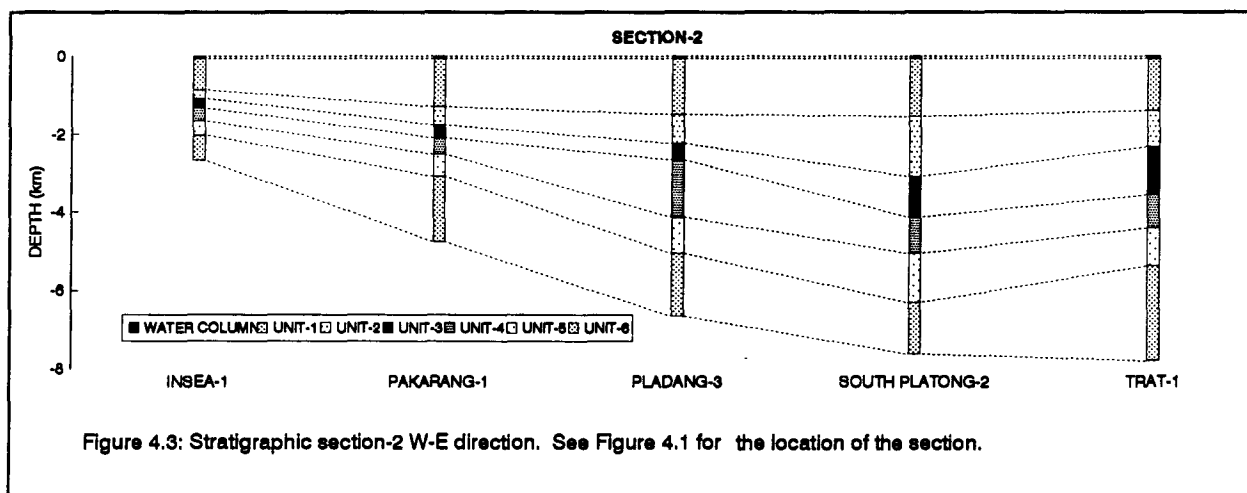
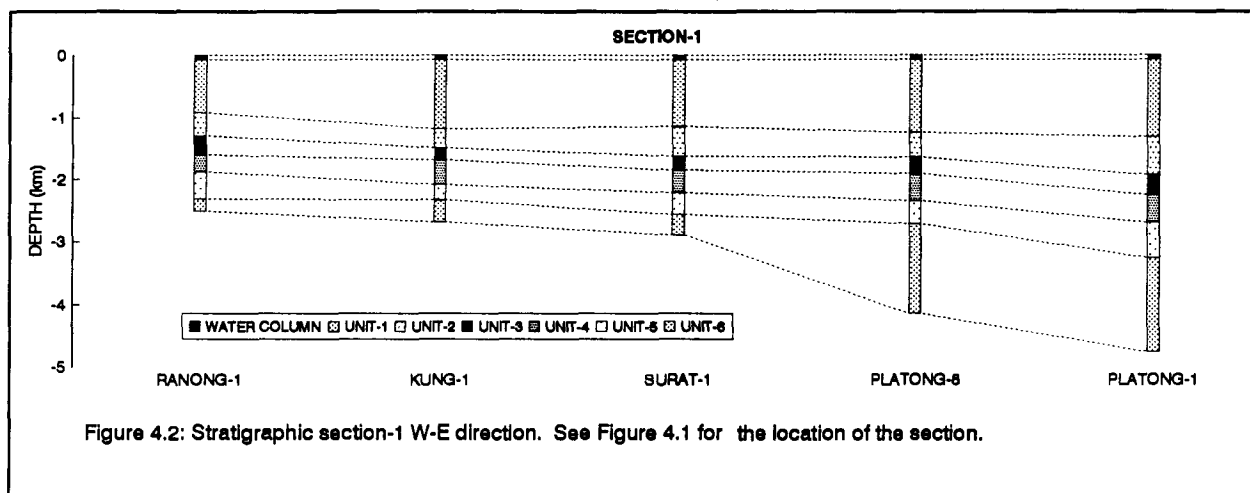
The proposed initiation of Tertiary basins, including the Pattani Basin, took place from as early as Late Cretaceous to as late as Early Tertiary. Woollands and Haw (1976) pointed out that deposition of Tertiary sediments and facies distribution in the restricted basins were tectonically controlled, and suggested that the

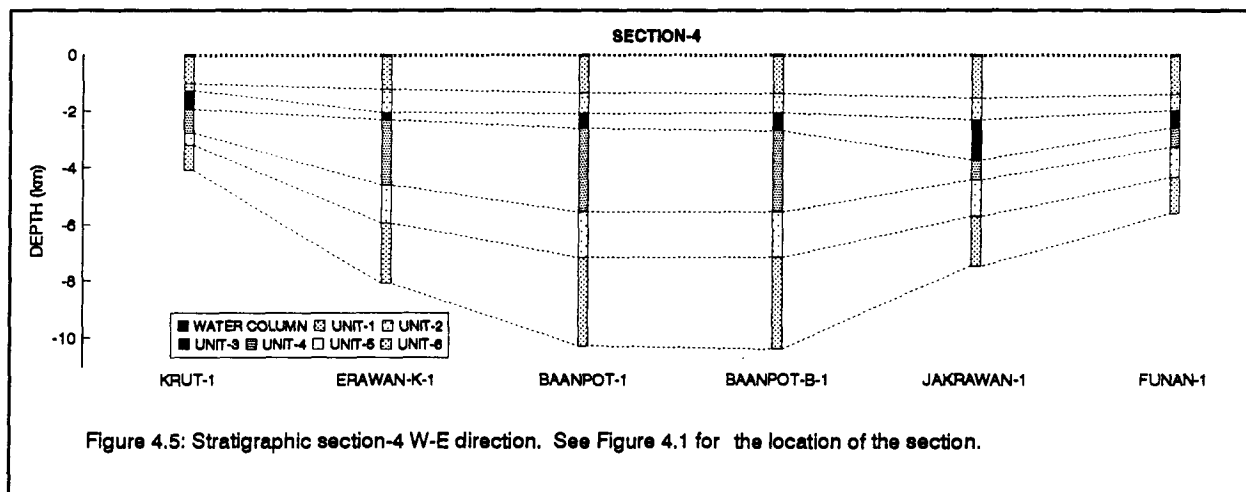
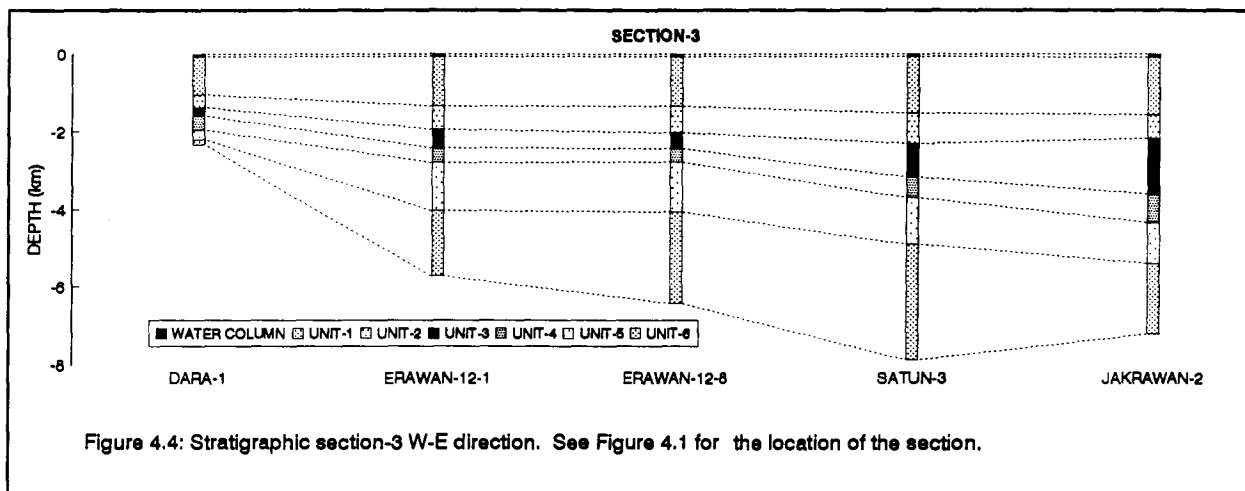
intracratonic basins in the Gulf of Thailand were formed during Late Mesozoic to Early Tertiary by block faulting which occurred along earlier N-S and NNE-SSW tectonic trends of a Triassic-Jurassic suture zone. Tapponnier et al. (1982), Knox and Wakefield (1983), and Bunopas and Vella (1983) suggested Early Tertiary as the time of basin formation. Ohnstad (1990) suggested that the basins were formed in Early Tertiary time, no later than Oligocene.

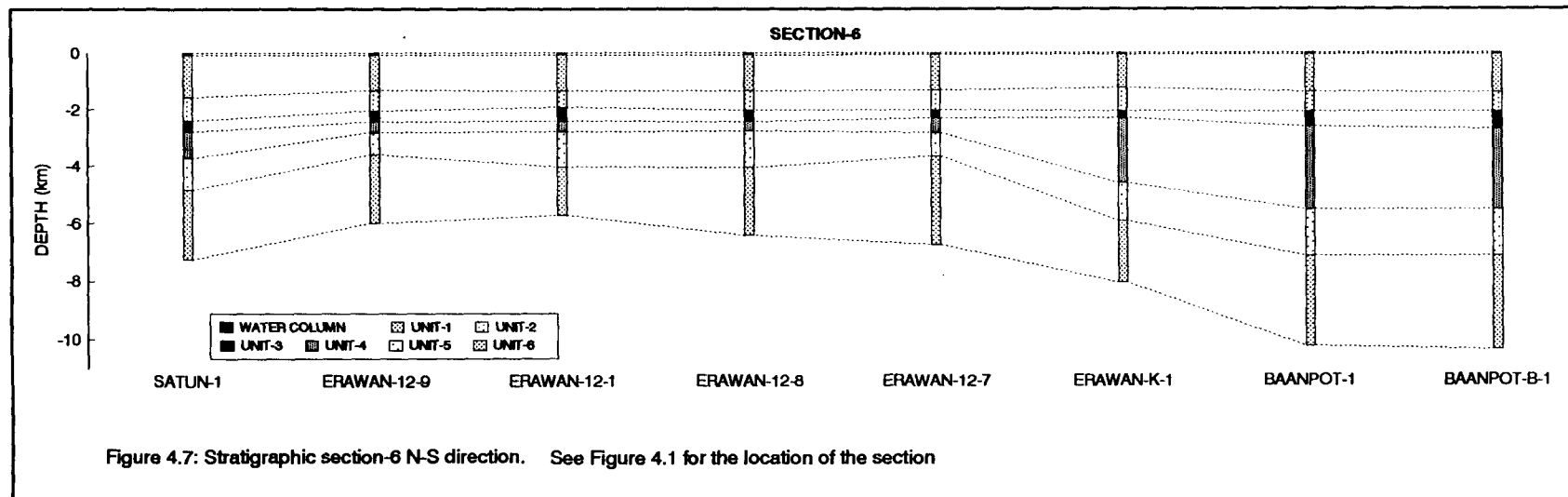
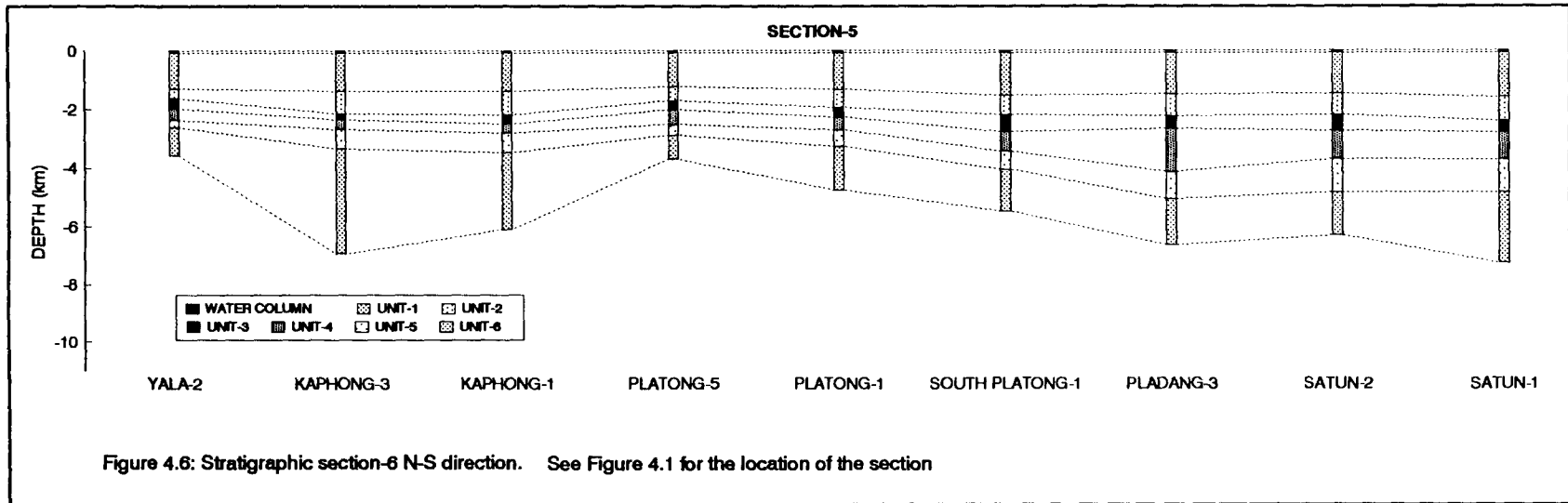
Tertiary stratigraphy in the Pattani Basin is summarized in Figure 4.2 through Figure 4.7. Stratigraphic analysis of sedimentary successions in the Pattani Basin (chapter 3) suggests that the onset of rifting of the Pattani Basin coincided with deposition of the oldest synrift sediments (Late Eocene to Early Oligocene, approximately 40 Ma) penetrated by drilling. These strata (units 6, 5 and 4) unconformably overlie a basement comprising Mesozoic sedimentary rocks and granite. Rifting associated with extensive normal faults lasted approximately 20 million years (Chinbunchorn et al., 1989). After the middle of the Early Miocene (the base of unit 3) major tectonic activity ceased and the area gradually subsided. The base of unit 3 marks the break between the highly faulted synrift sedimentary successions (units 6, 5 and 4) and the post-rift sedimentary successions (units 3, 2 and 1).

4.6 SUBSIDENCE HISTORY

In order to determine the history of subsidence of the Pattani Basin, the sediment columns from thirty wells were decompacted and backstripped using the basin modelling concept described in the previous section. Tectonic subsidence thus obtained was then used to determine the crustal and subcrustal lithospheric stretching factors, β and δ , respectively. The lithospheric stretching factors were







further employed to determine the history of heat flow and temperature and present-day geothermal gradients.

The validity of the lithospheric stretching model used in this study can be tested by comparing the level of organic maturation predicted by the model and that observed in the field. Because the chemical composition and reflectivity of vitrinite change with time and temperature, the vitrinite reflectance provides an important boundary condition to constrain the predicted time-temperature history of any stratigraphic unit. Verification of the lithospheric stretching model used in this study is, therefore, carried out by comparing predicted and measured vitrinite reflectance, an organic maturity indicator, at various depths and locations.

4.6.1 Total Subsidence and Burial History

Data from wells located in the Pattani Basin (Figure 4.1) are used to study subsidence. Ages, present-day depths, and lithological data of each stratigraphic layer needed for decompaction and backstripping are obtained from well data (Figure 4.2 through Figure 4.7). The depths to basement and the depths to deeper stratigraphic unit boundaries where they were not penetrated by wells were determined from seismic cross sections.

Physical parameters such as surface porosity, compaction coefficient, porosity-depth function, grain density, and thermal conductivity for each lithology are listed in Table 4.1 (from Sclater and Christie, 1980). Lithologies of different stratigraphic units are obtained from well log data. Physical and thermal parameters of the lithosphere and other parameters necessary for modelling were

Table 4.1: A list of Thermo-physical parameters used in the lithospheric stretching model (After Sclater & Christie, 1980; Issler & Beaumont, 1987)

1. Water layer

Density of sea water	1.03 g/cm ³
----------------------	------------------------

2. Sedimentary layer

Lithology	Sandstone	Shale	Shaly sandstone
Surface porosity (%)	49	63	56
Compaction constant (x10 ⁻⁵ cm ⁻¹)	0.27	0.51	0.39
Matrix density (g cm ⁻³)	2.65	2.72	2.68
Matrix thermal conductivity (mcal cm ⁻¹ sec ⁻¹ °C)	9.6	5.5	7.5

3. Lithosphere and mantle

Pre-rift thickness of crust	35 km
Thickness of lithosphere	125 km
Thermal expansion coefficient of lithosphere	3.3 x10 ⁻⁵ /°C
Thermal conductivity of lithosphere	7.5 mcal/cm sec °C
Thermal-time constant of lithosphere	62.8 m.y.
Density of lithosphere	2.8 g/cm ³
Density of mantle	3.3 g/cm ³
Temperature of mantle	1350 °C

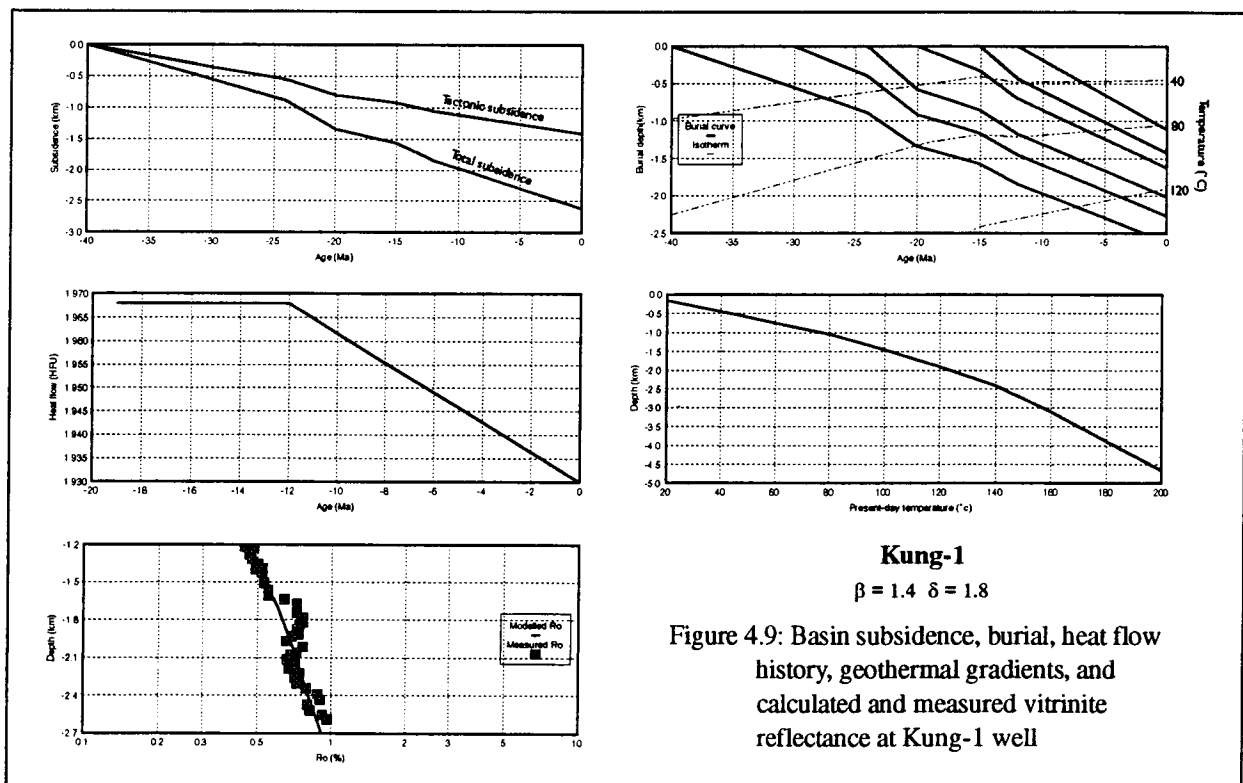
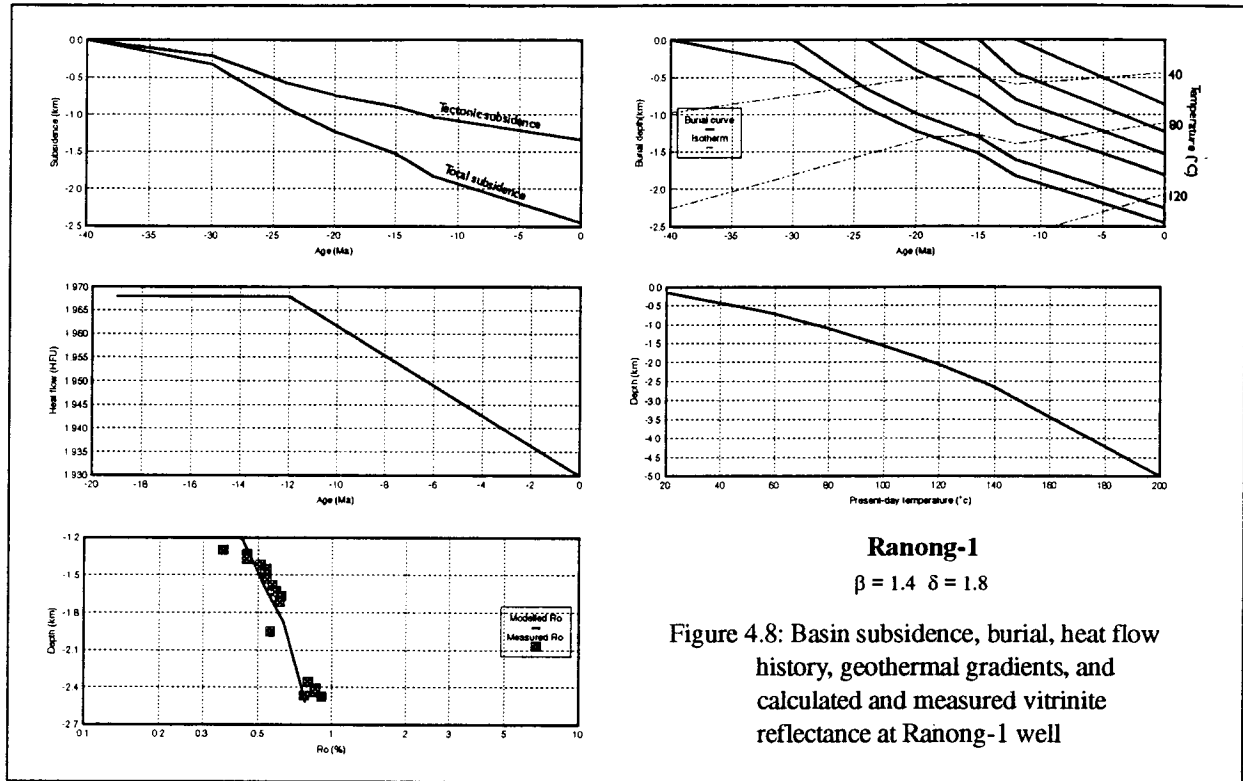
obtained from the studies of Parsons and Sclater (1977), Issler and Beaumont (1987), and Friedinger (1988).

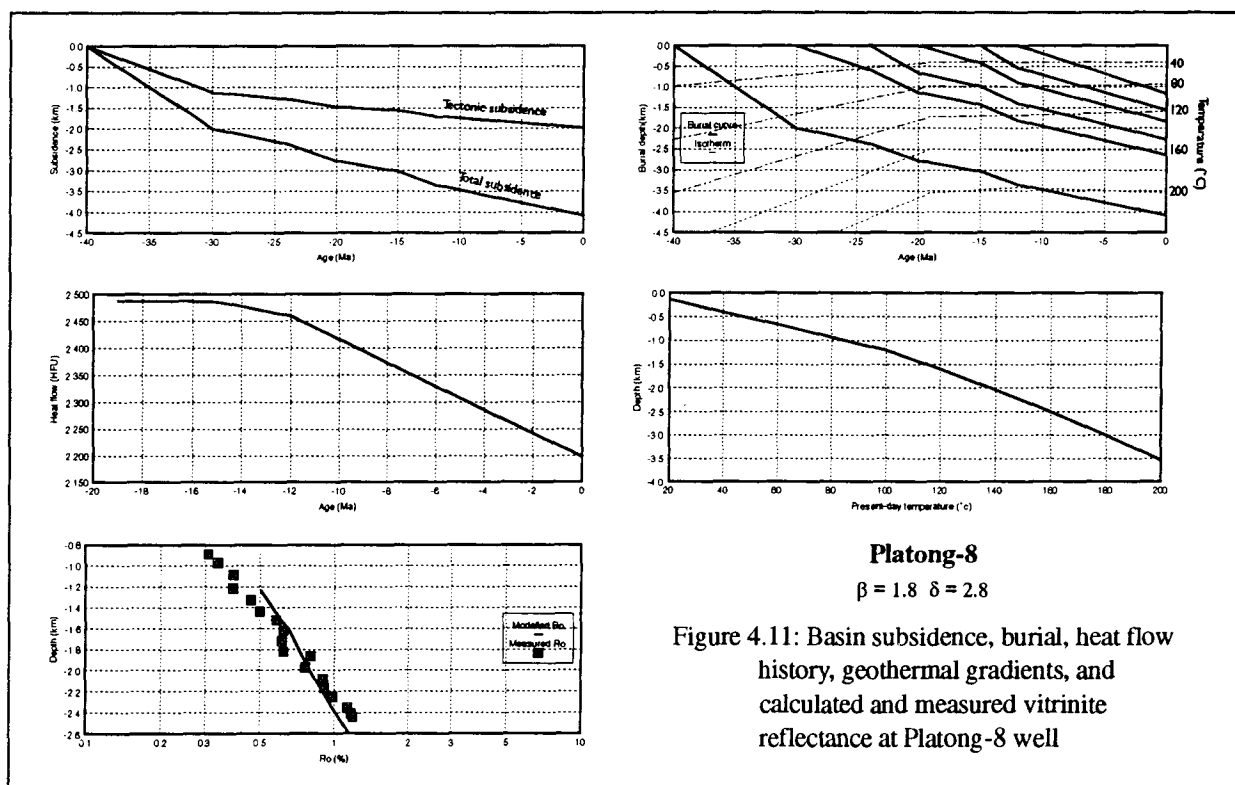
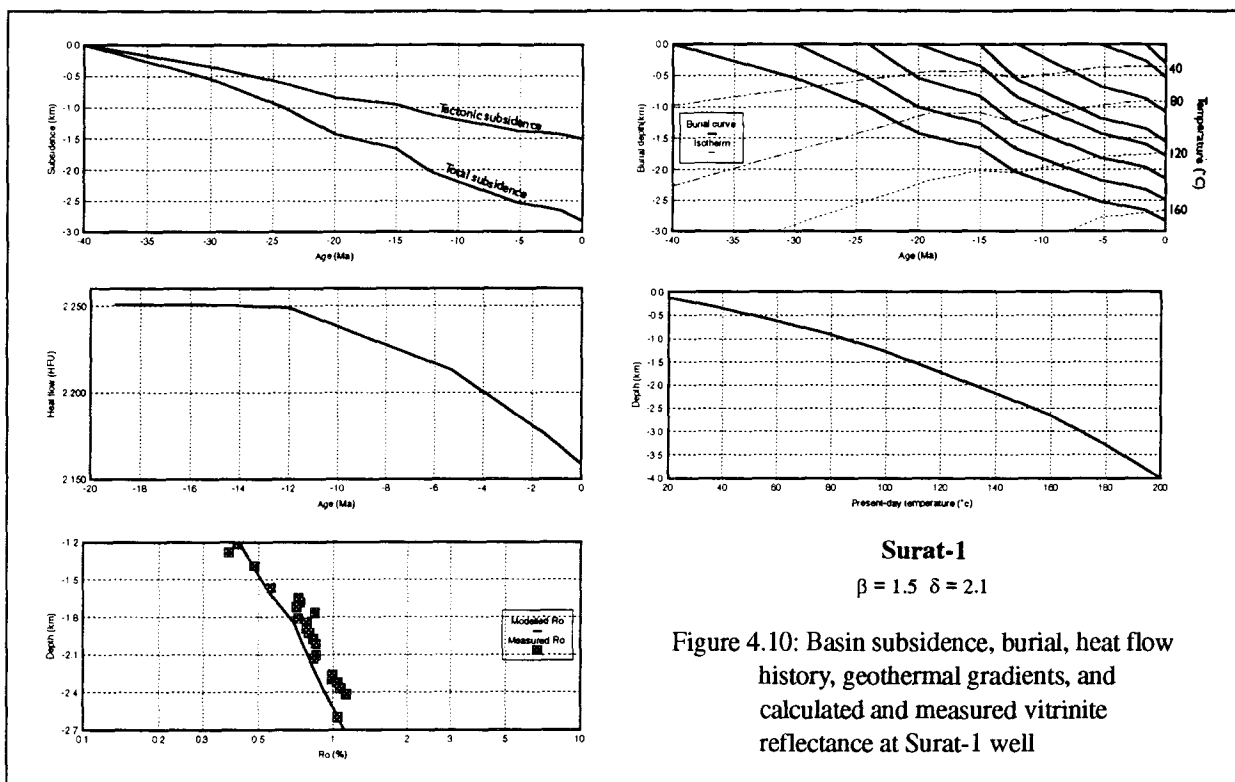
Total subsidence and decompacted burial histories of the basement rocks and all other stratigraphic layers at well locations are displayed in Figures 4.8 through 4.37.

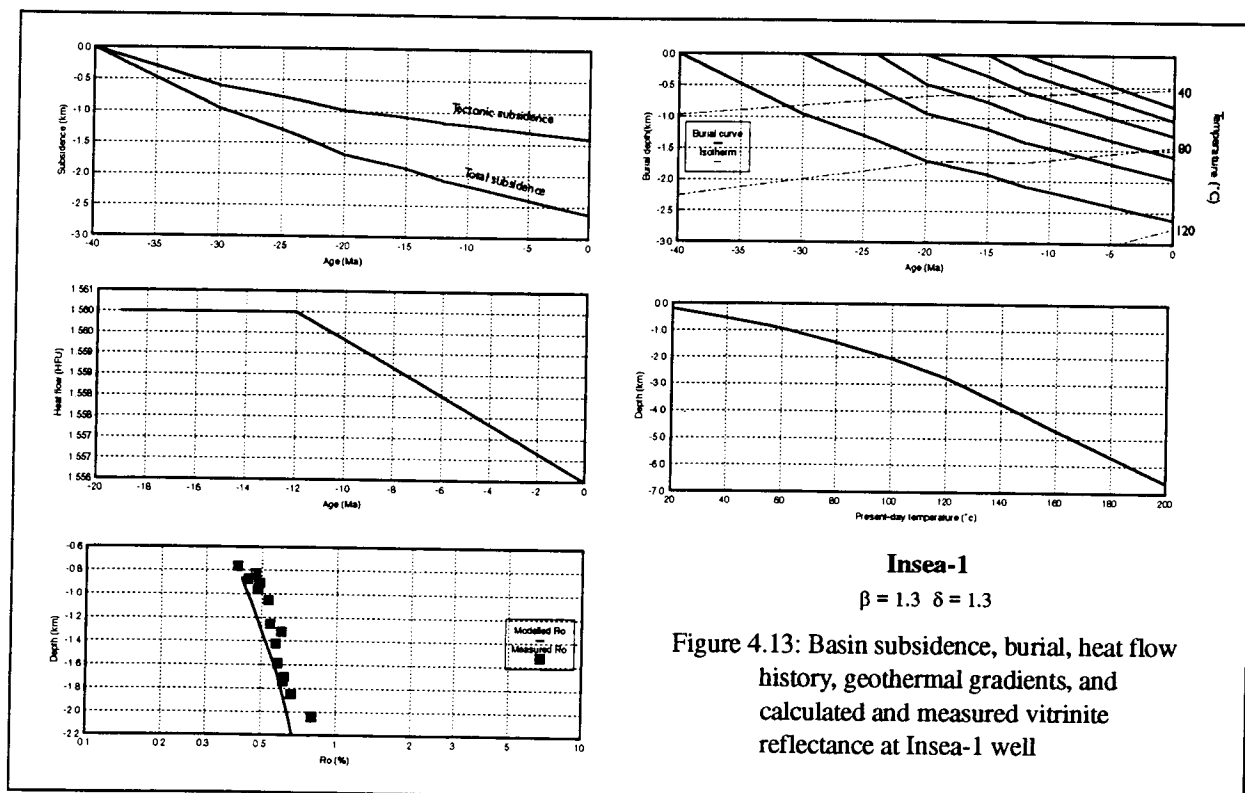
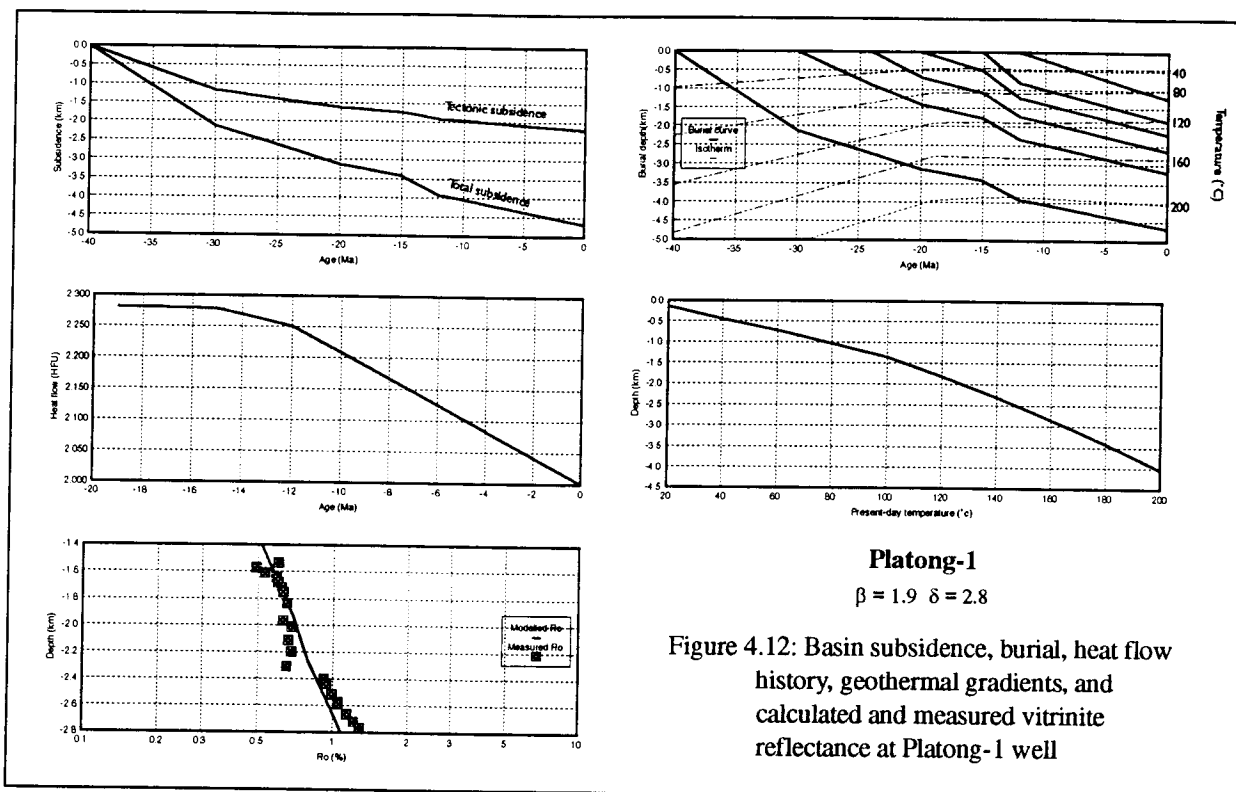
4.6.2 Tectonic Subsidence

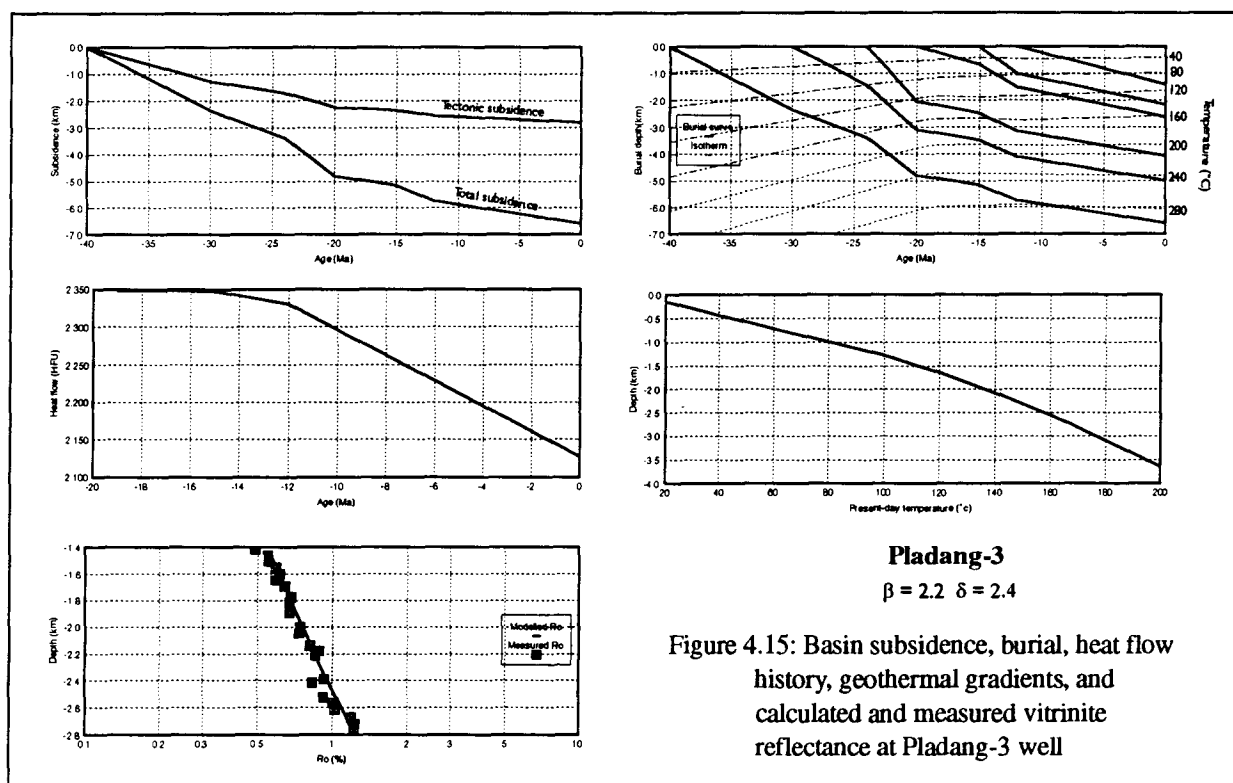
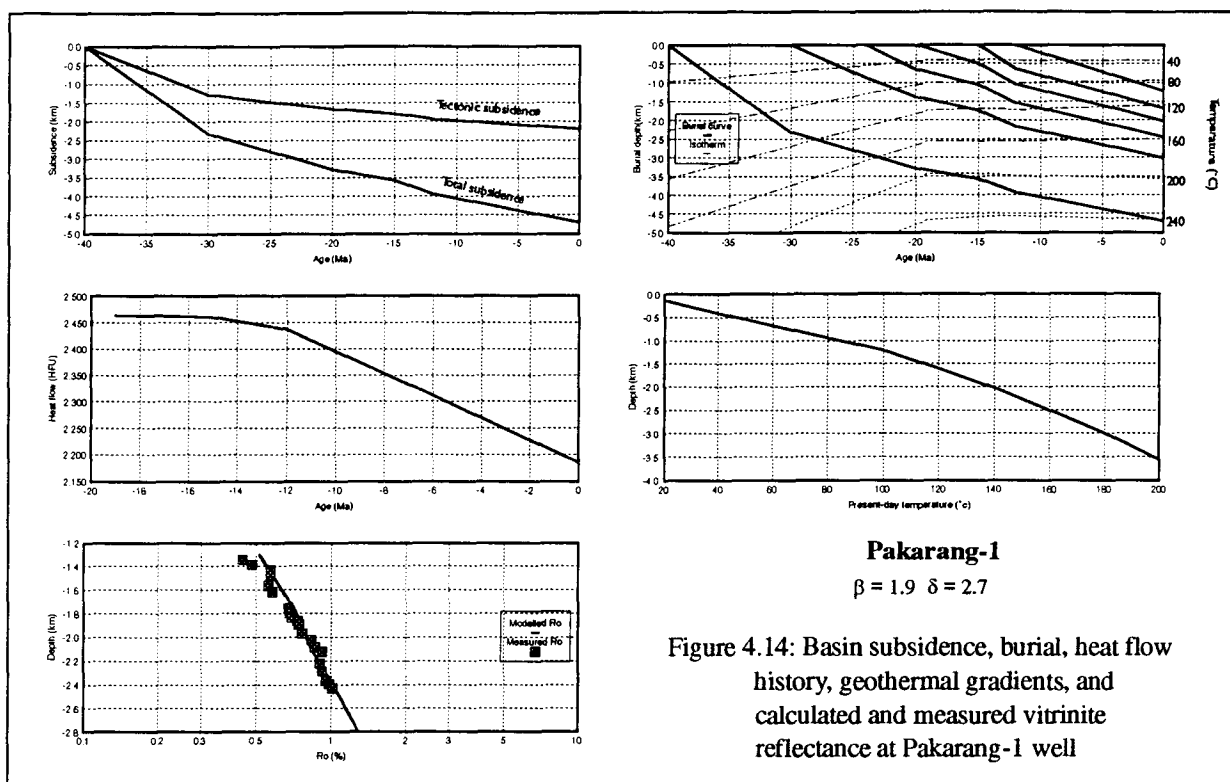
By subtracting the sediment loading effect from the total subsidence, the tectonic subsidence of basement through time at each well location is acquired. Because the entire Tertiary sediment column in the Pattani Basin was deposited in fluvio-deltaic to shallow marine environments, it is assumed that sedimentation of all strata took place at sea-level and thus eustatic sea-level fluctuation was not considered. It is further assumed that there was no basement topography prior to rifting. The tectonic subsidence histories at each well location are displayed in Figure 4.8 through Figure 4.37.

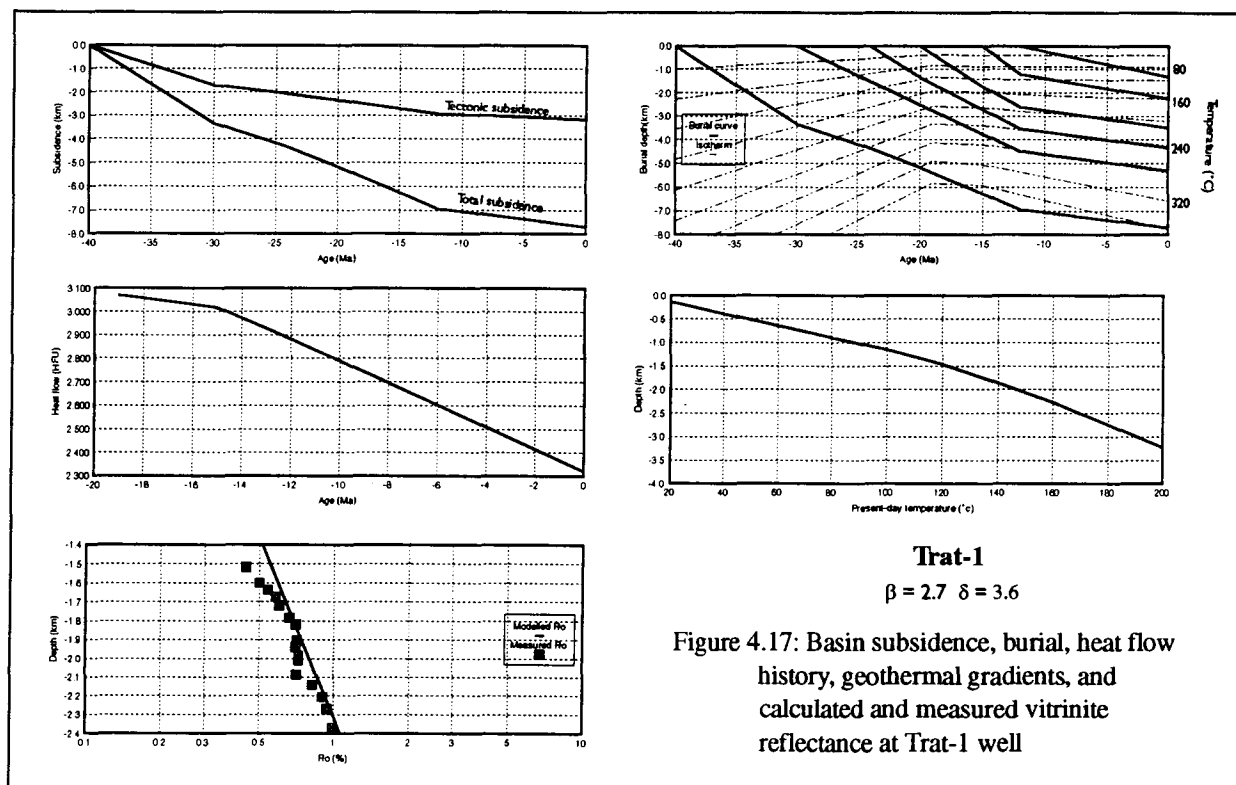
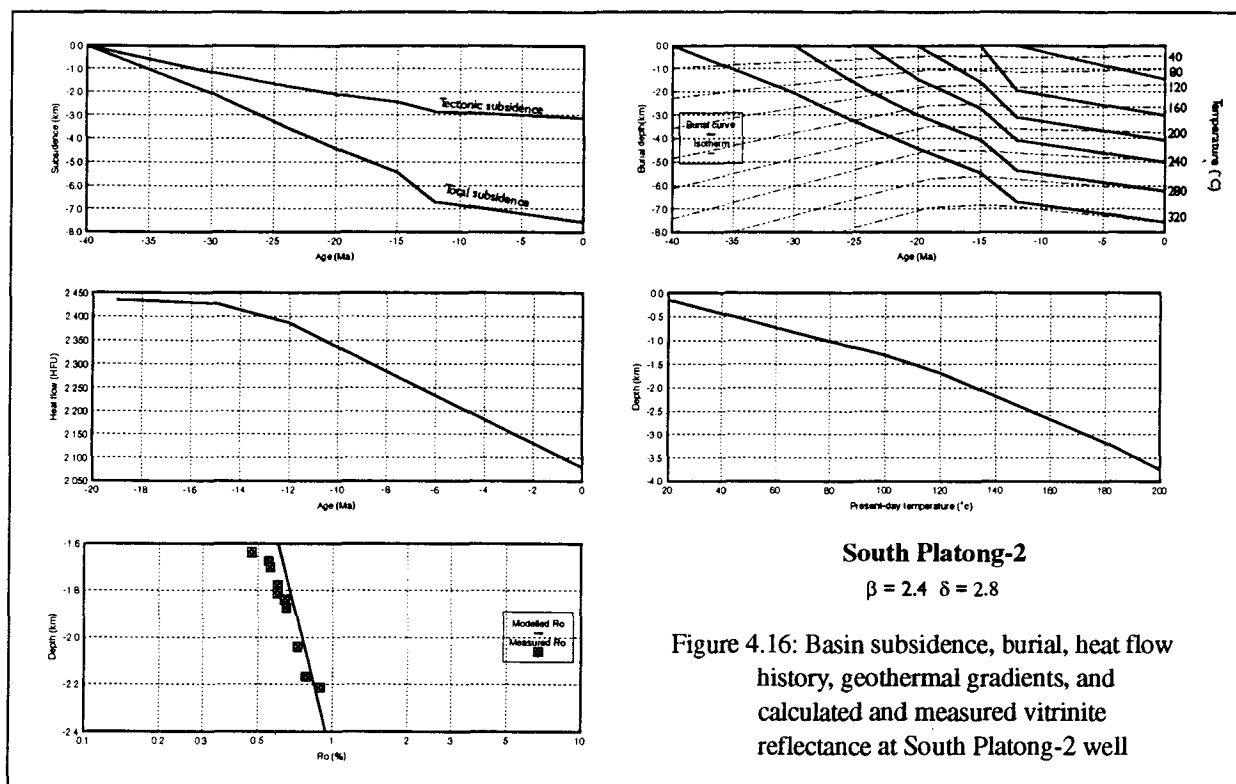
The comparison of total and tectonic subsidence curves at well locations (Figure 4.8 through Figure 4.37) indicates that the effect of sediment loading accounted for up to 50% of the total subsidence. The tectonic subsidence curves also indicate that, in general, most of the subsidence took place from 40 Ma to 20 Ma. Subsidence which occurred after 20 Ma was considerably smaller and more gradual.

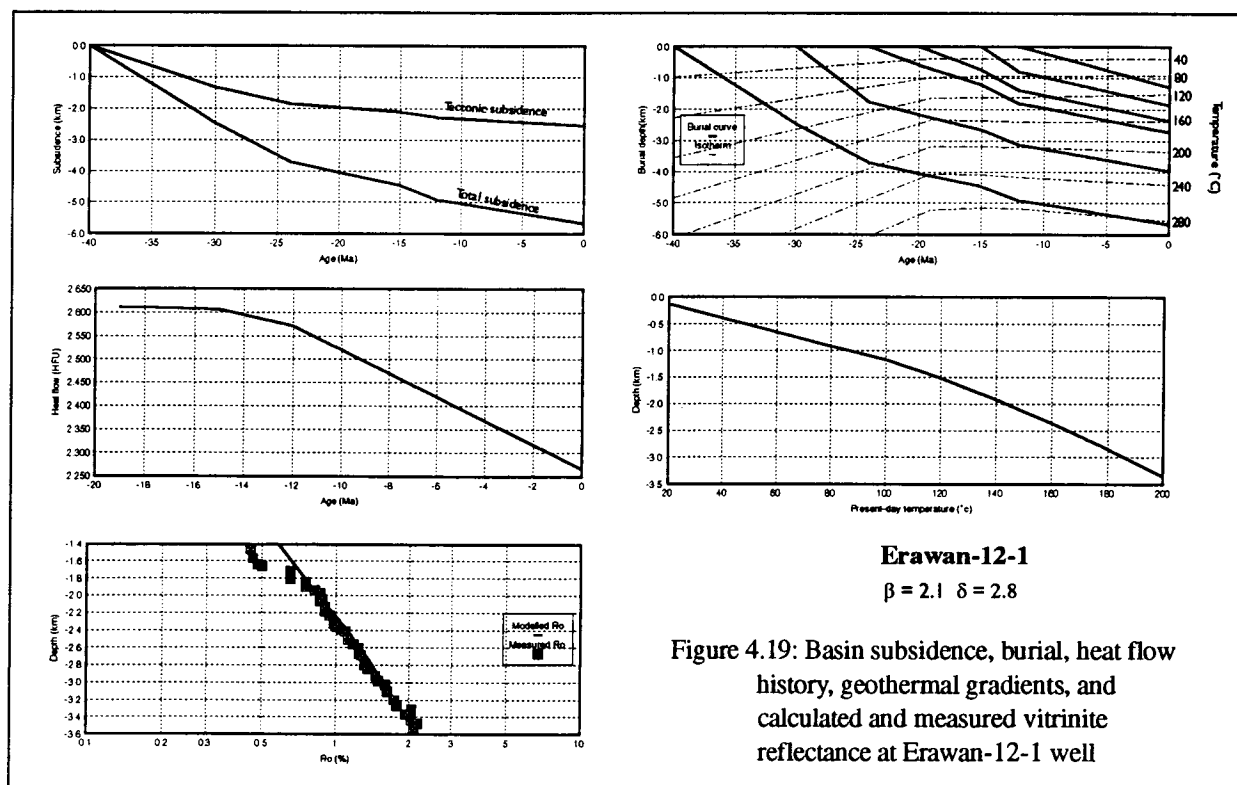
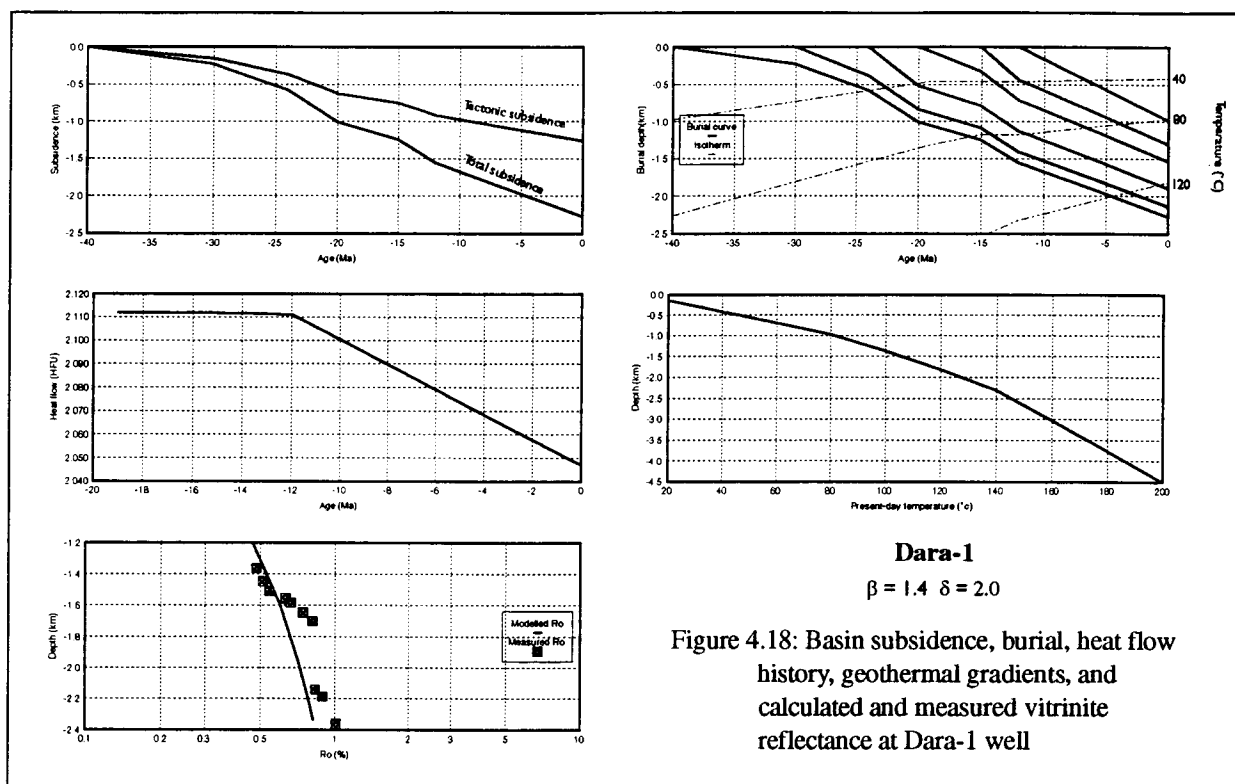


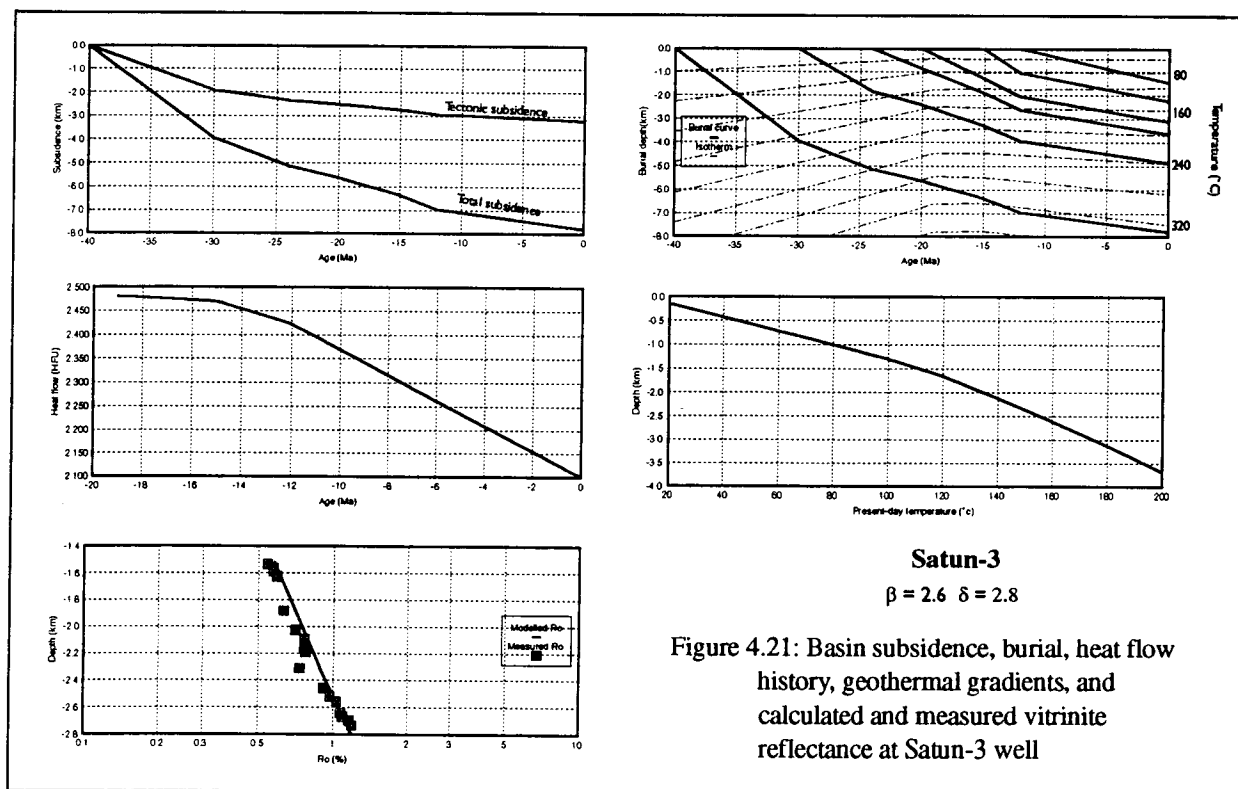
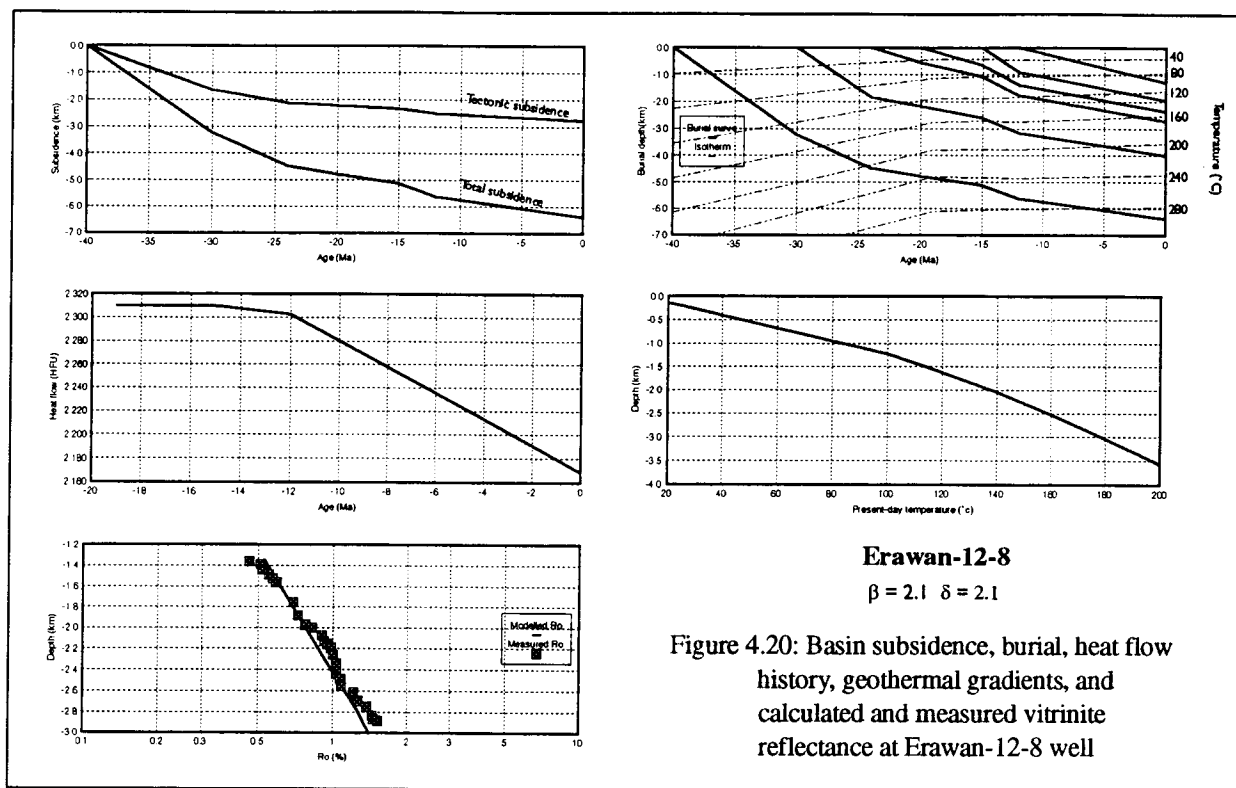


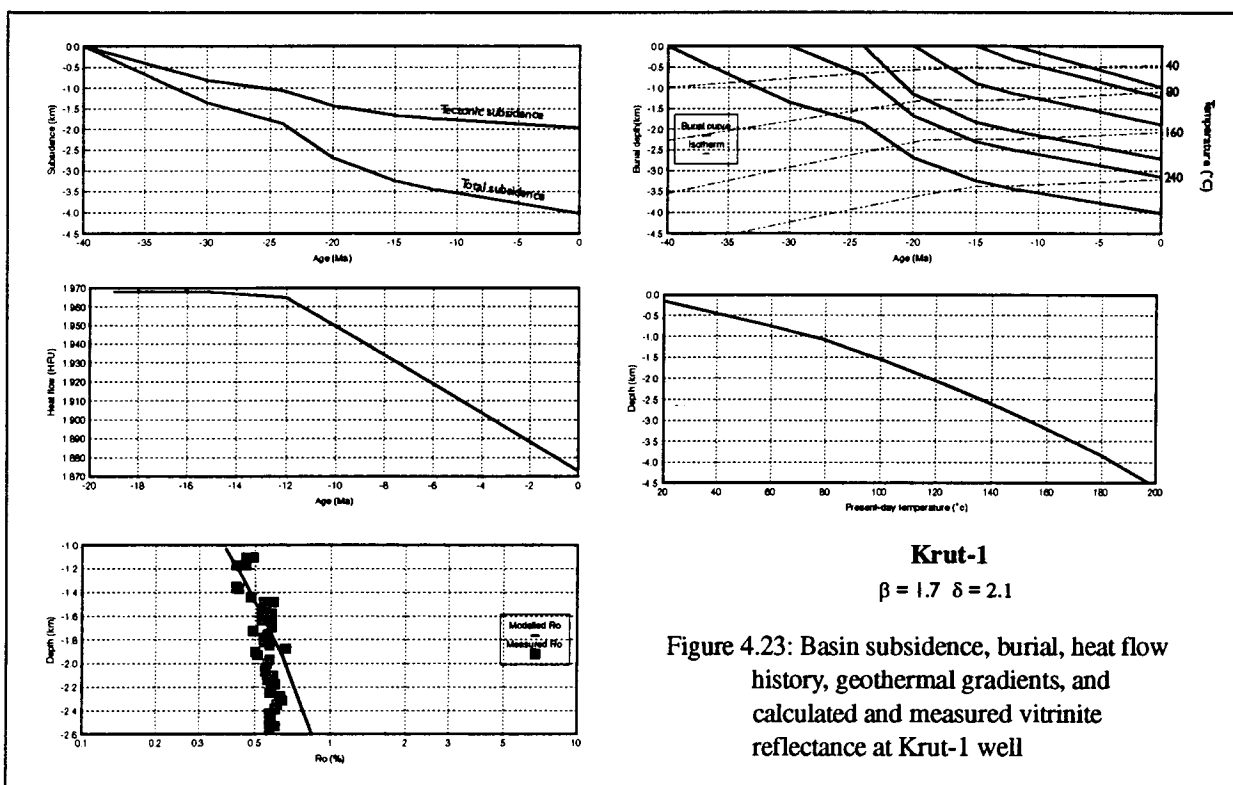
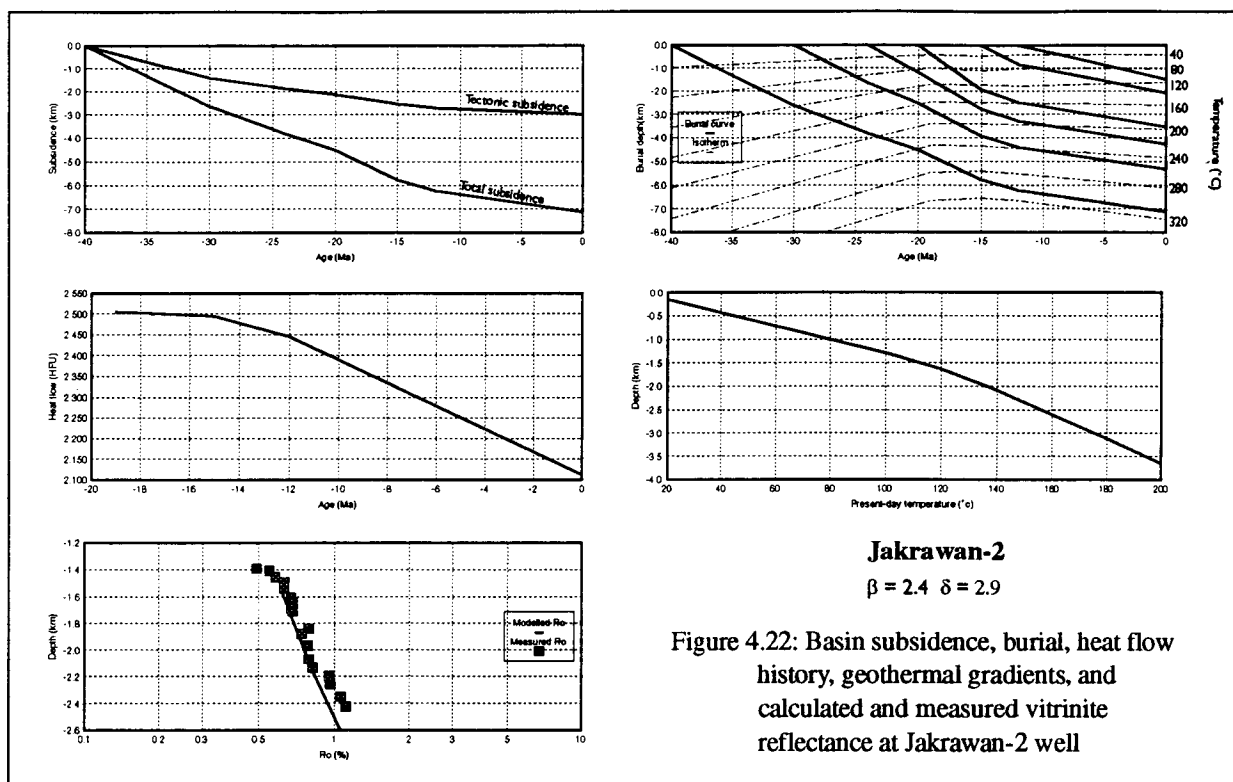


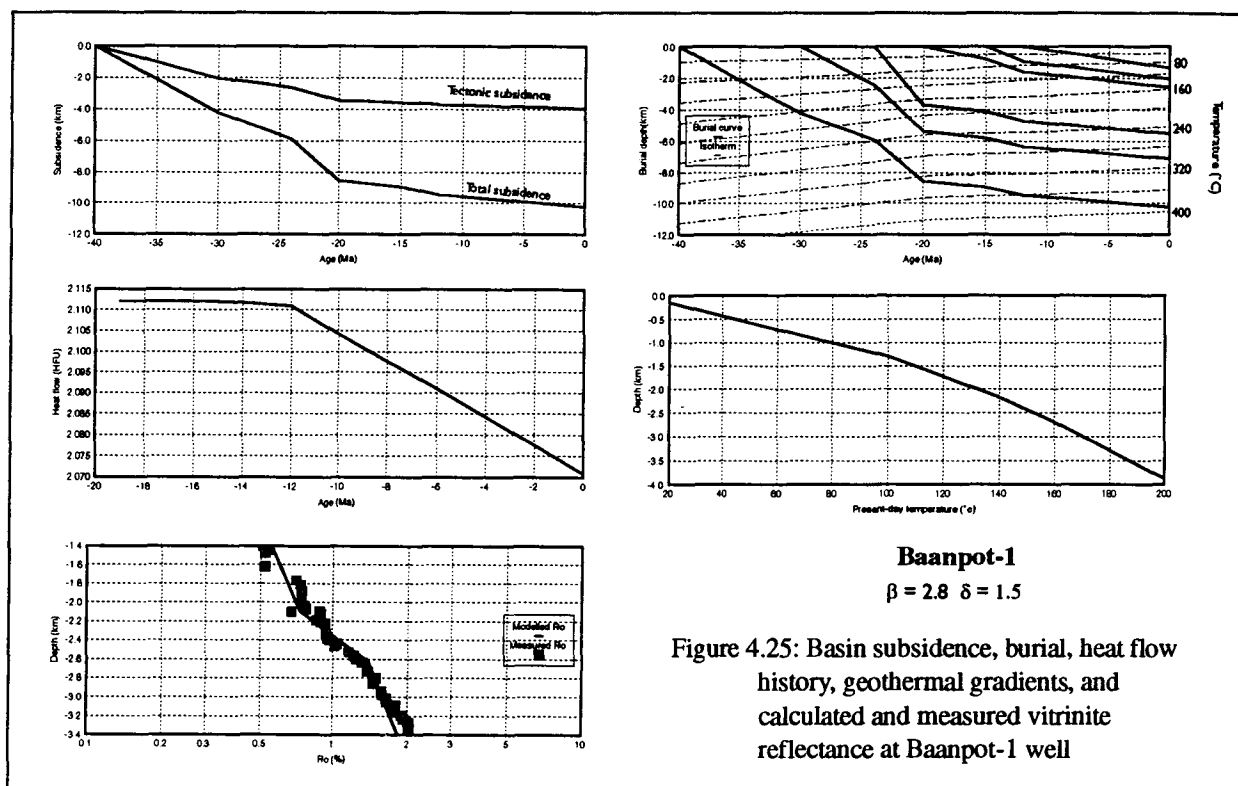
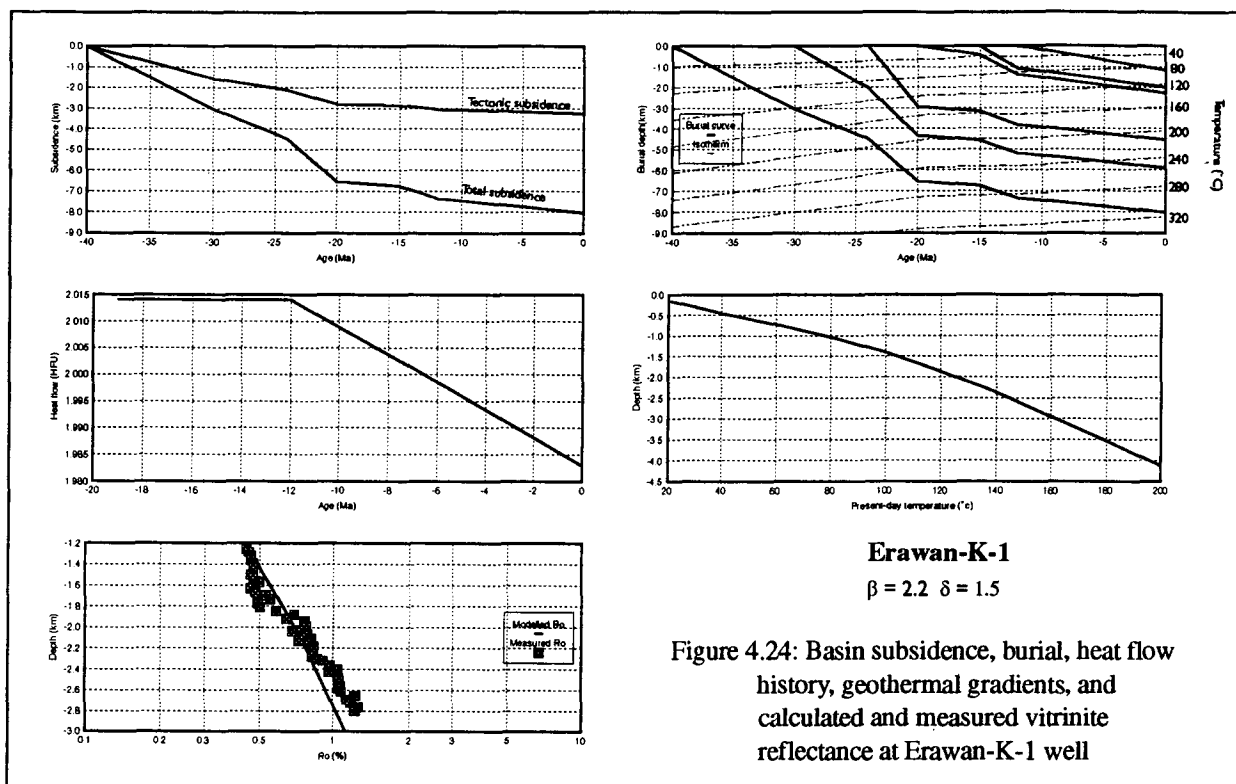


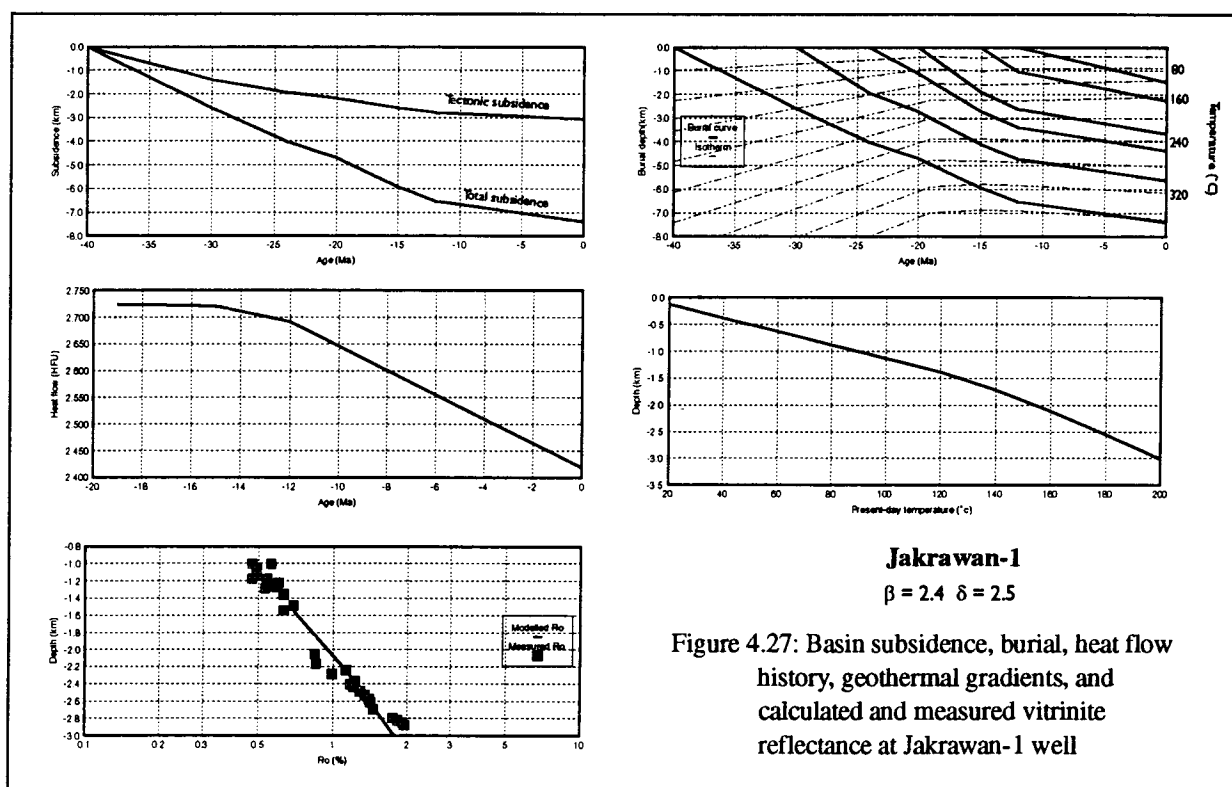
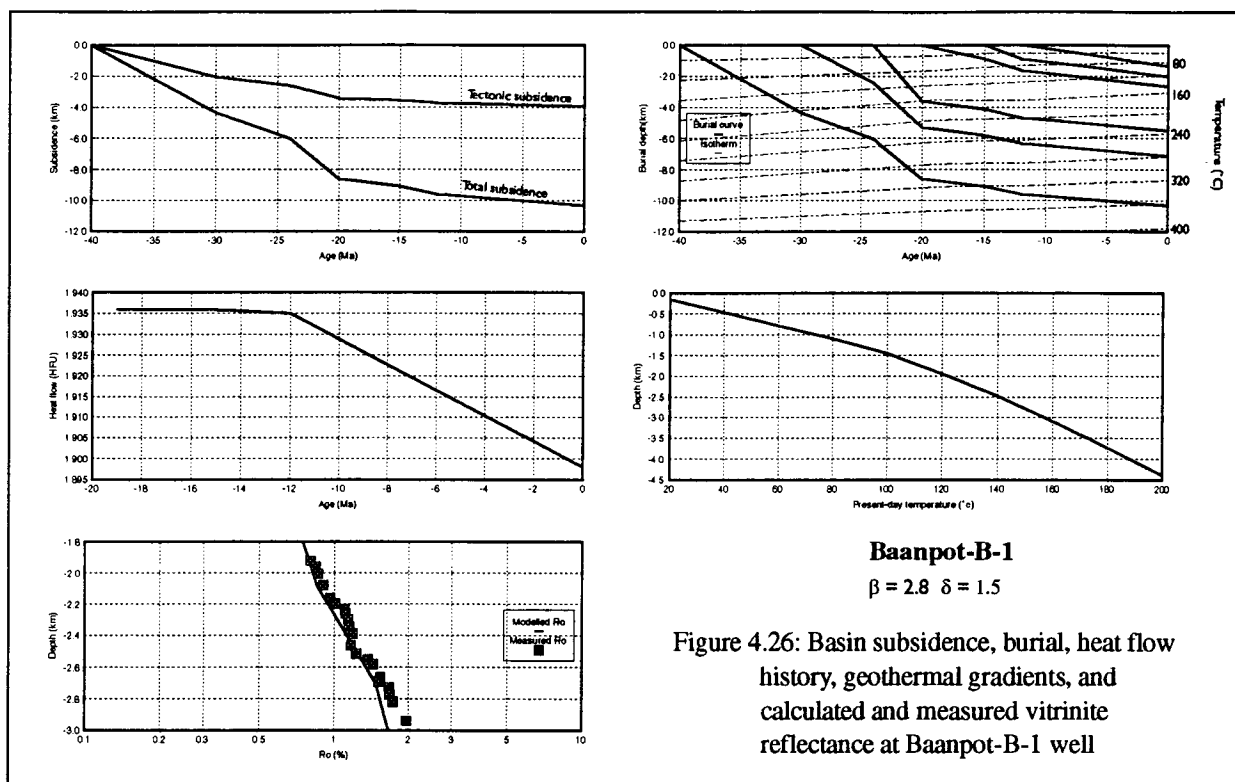


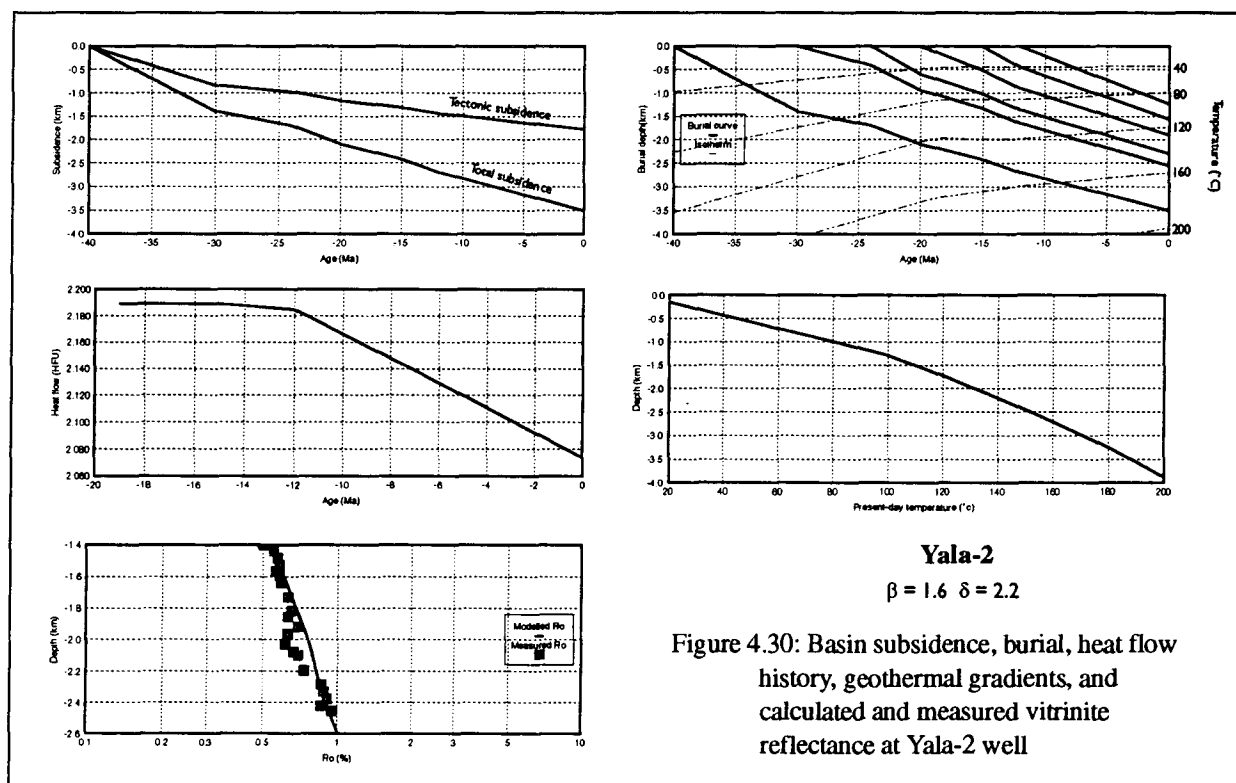
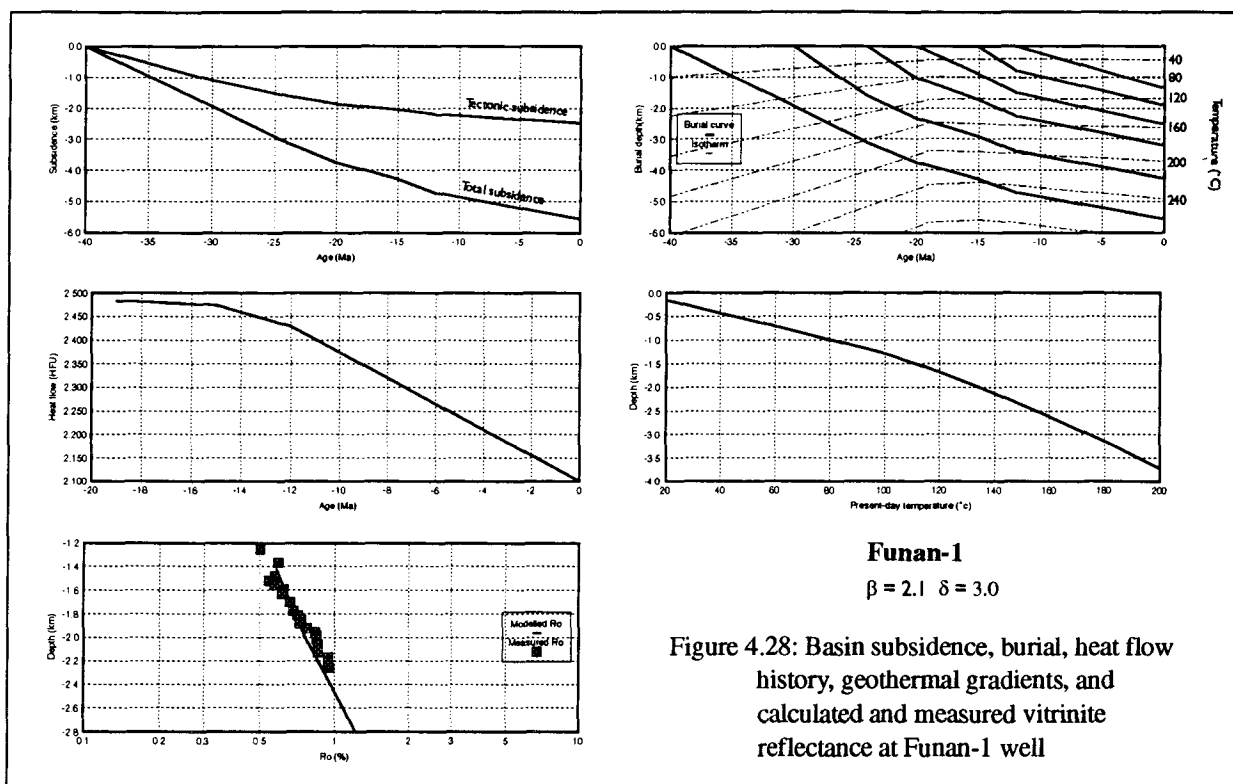


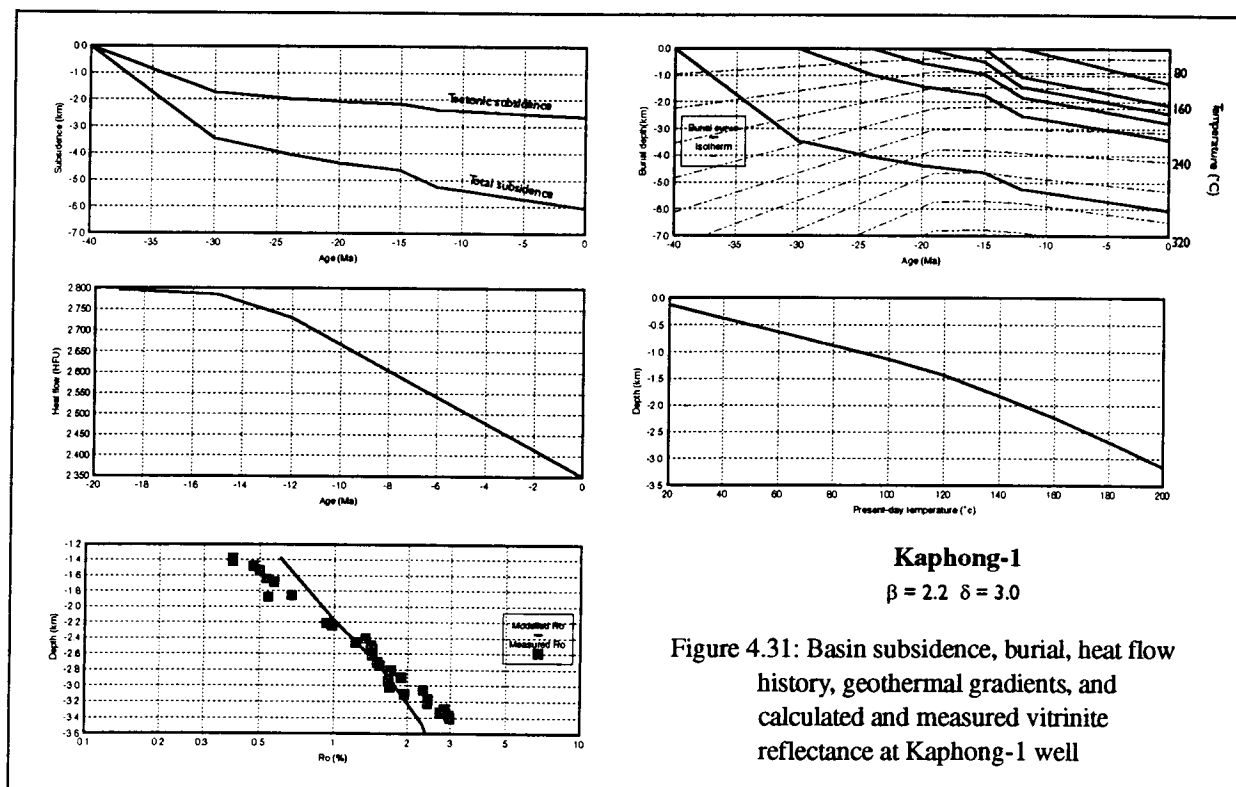
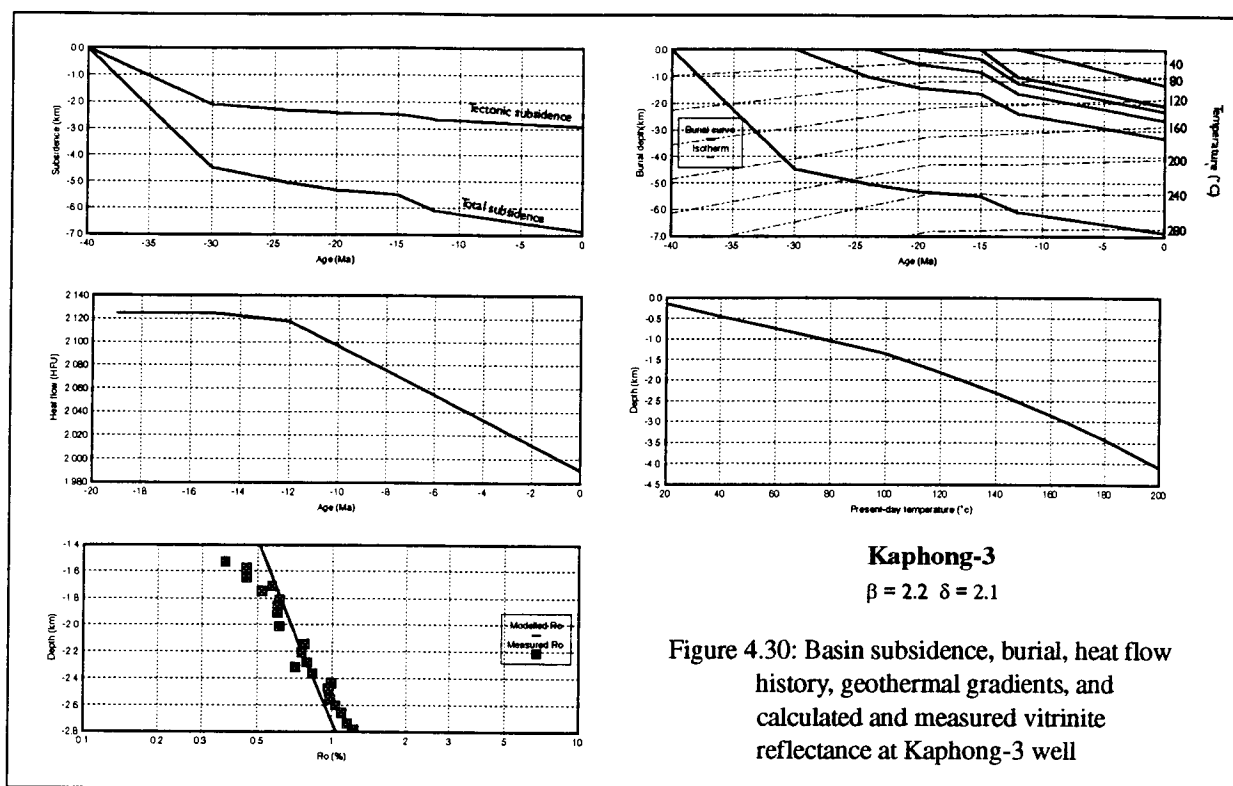


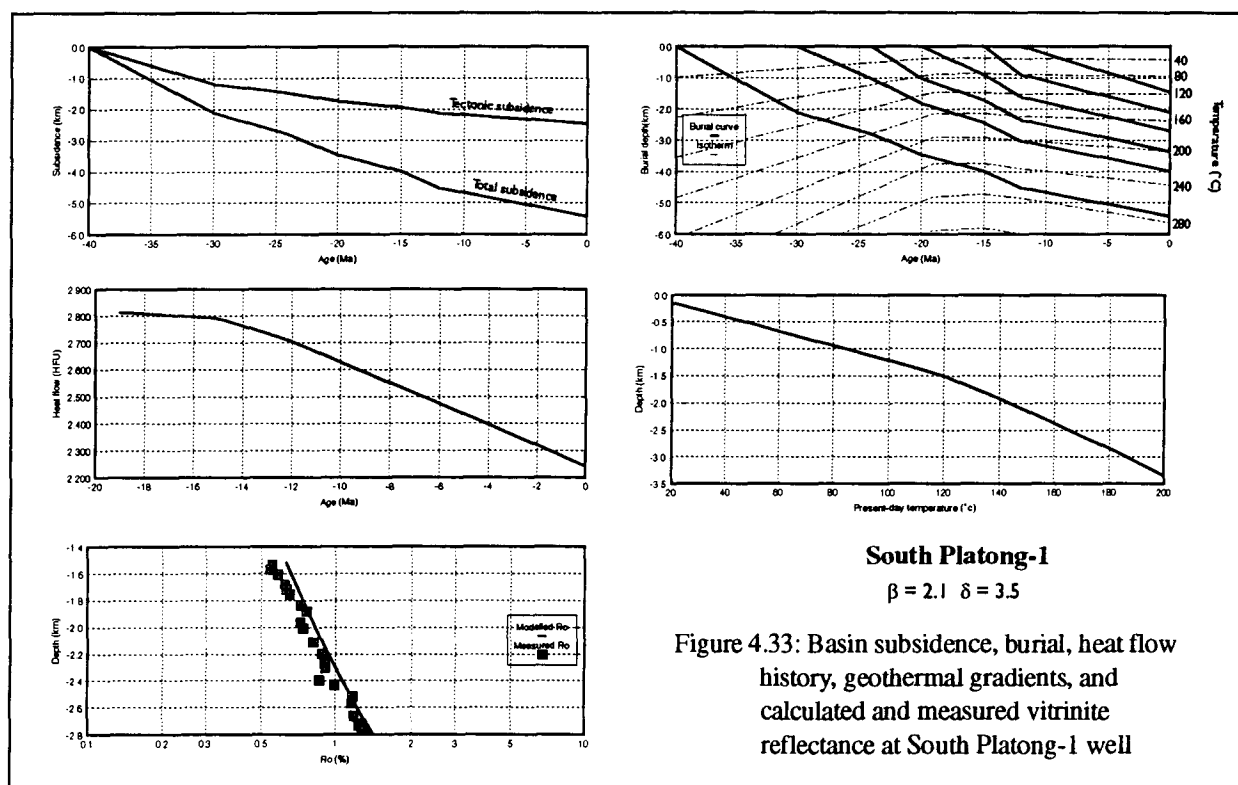
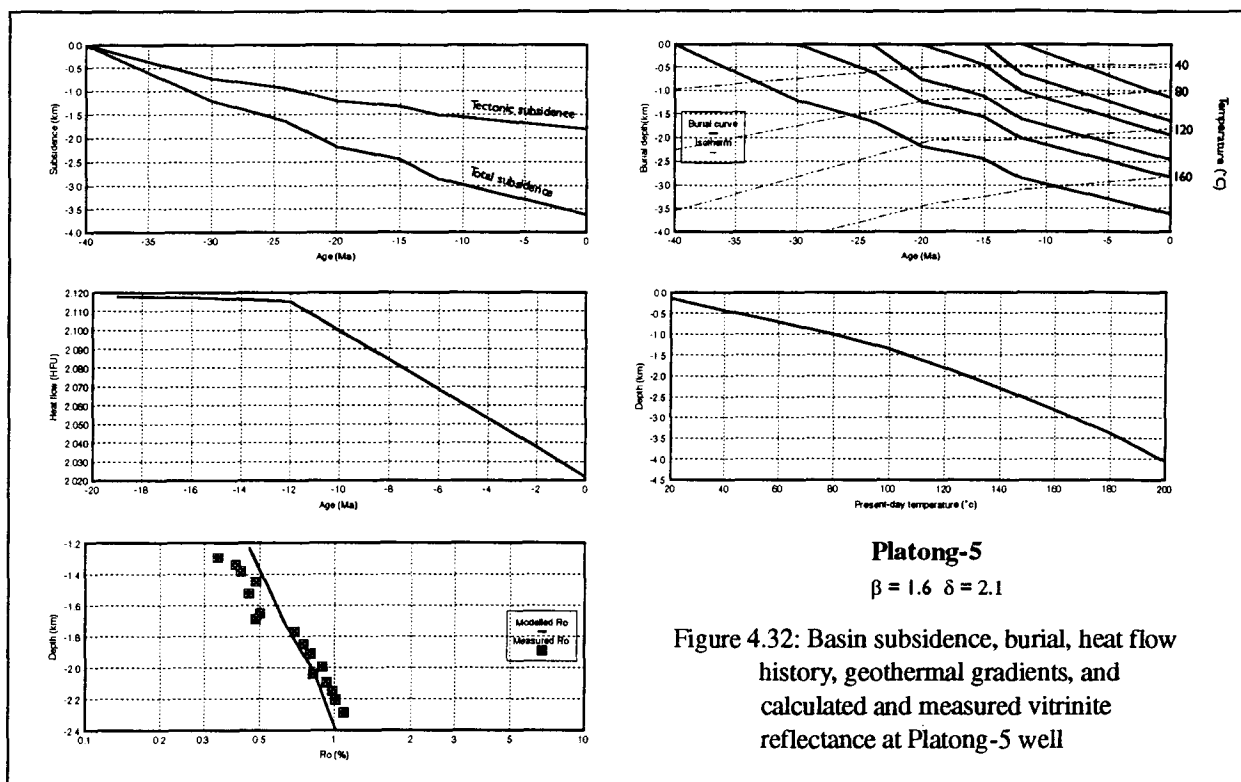


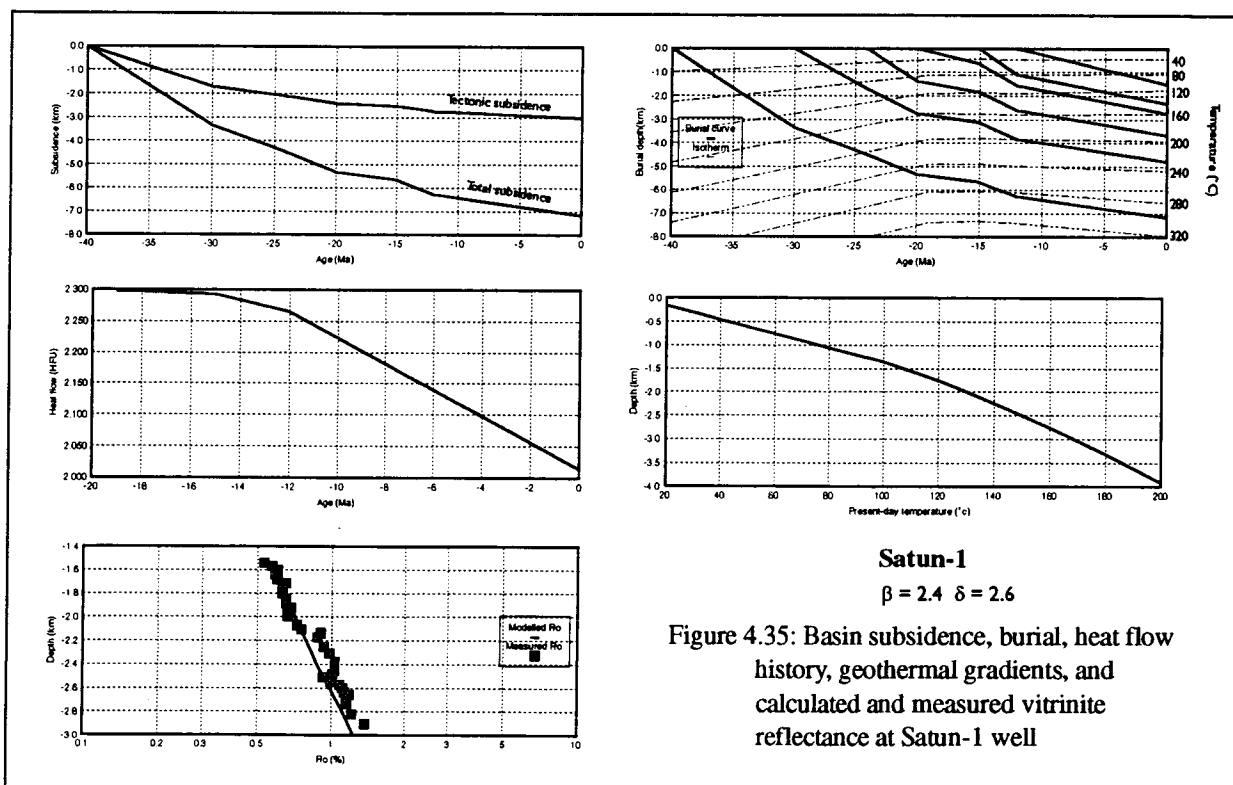
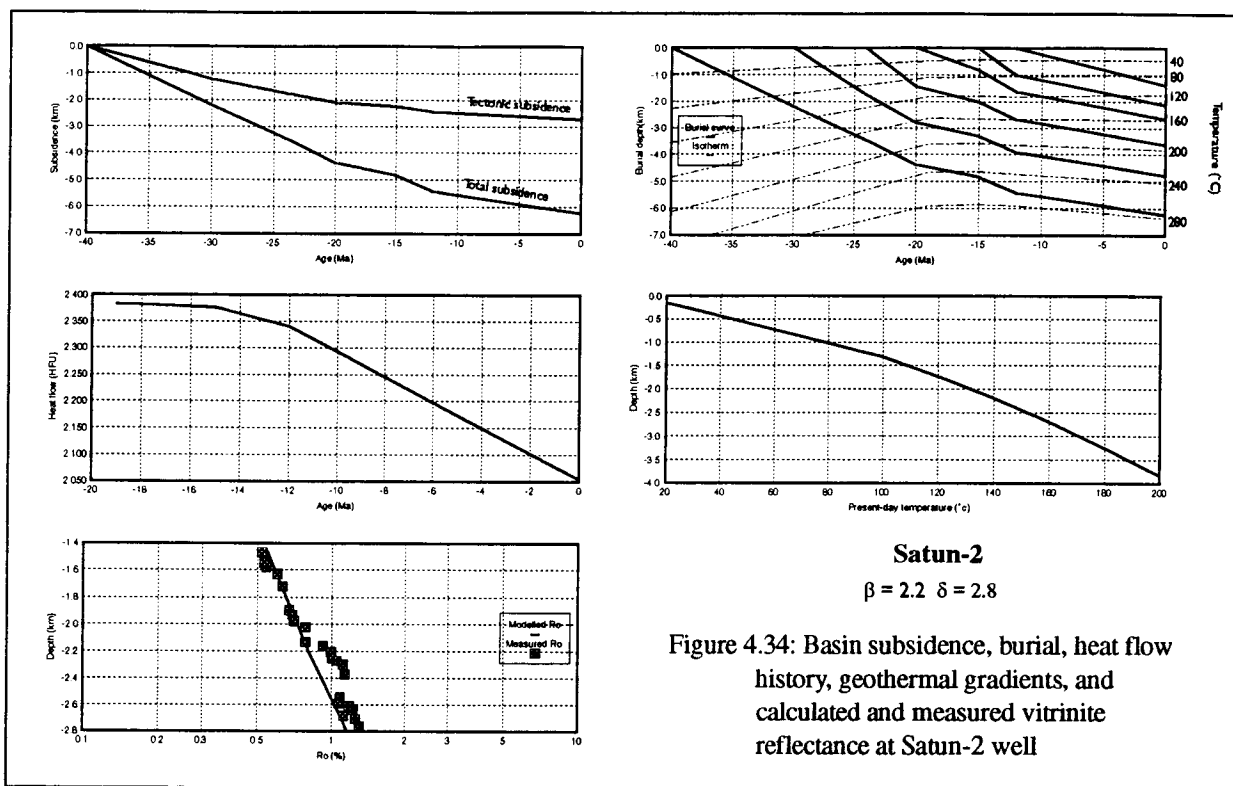


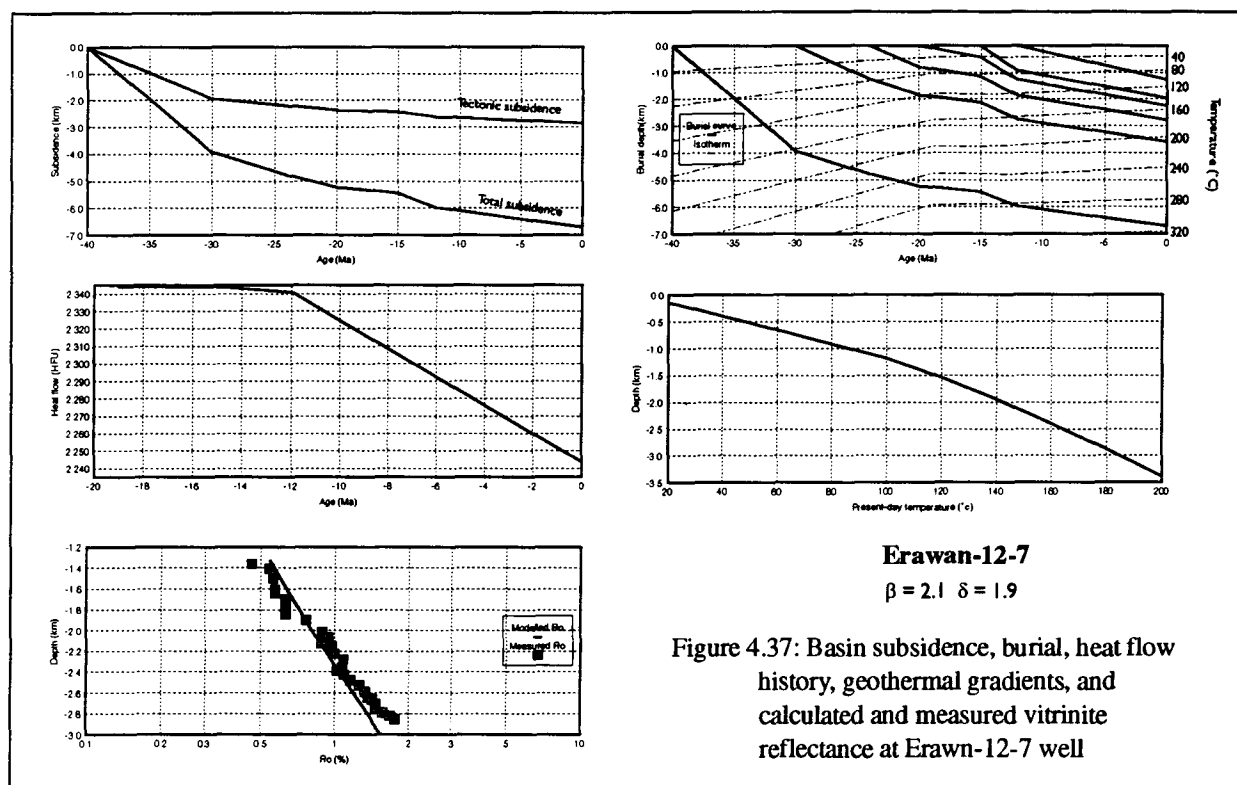
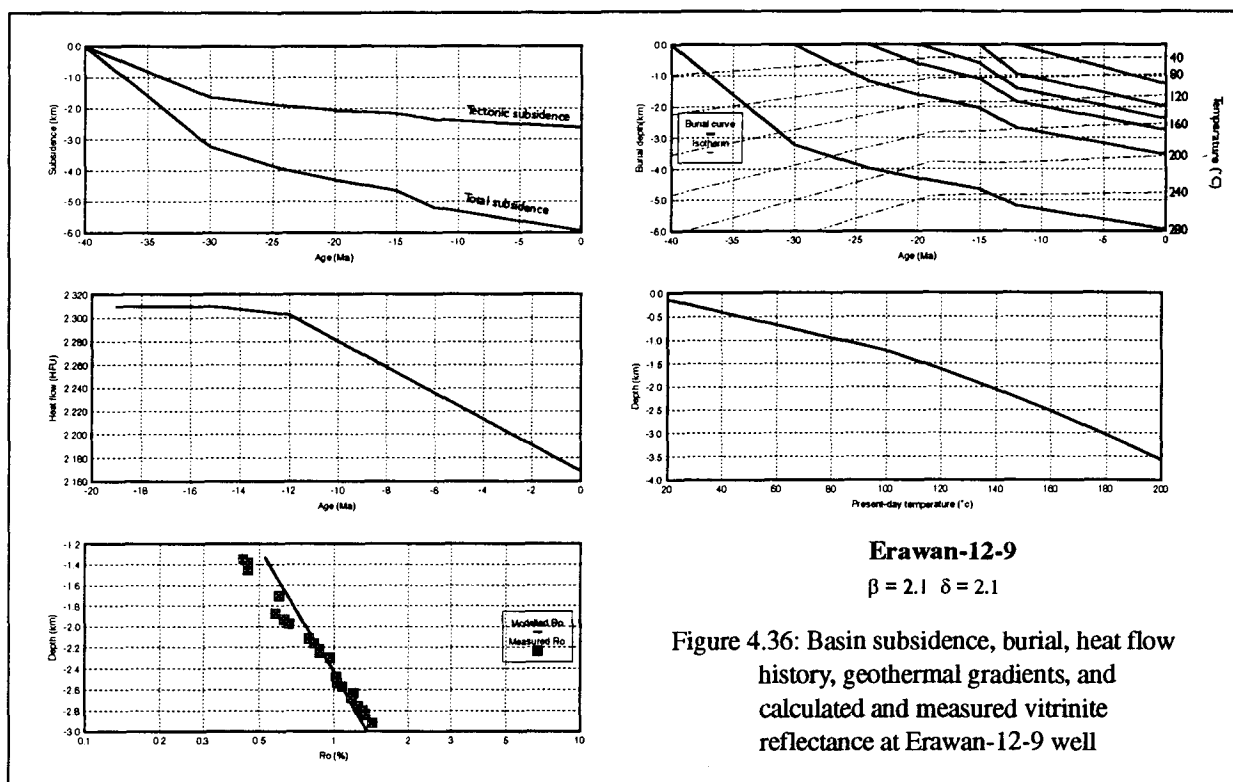












4.6.3 Lithospheric Stretching Factors

Crustal and subcrustal stretching factors (β and δ , respectively) at well locations can be determined by best-fitting the observed basement's tectonic subsidence with the total (initial and thermal) tectonic subsidence predicted from nonuniform lithospheric stretching model.

For the purpose of computation, rifting in the Pattani Basin is assumed to have started approximately 40 Ma (Late Eocene) and lasted until about 20 Ma (middle Early Miocene) and thermal subsidence took place afterward. Thus the extensional or rifting phase lasted about 20 million years. This was probably long enough to cause some heat loss during rifting. Jarvis and McKenzie (1980), however, found that as long as rifting times were not more than 20 million years in duration, the lithospheric stretching model, assuming instantaneous rifting, was a reasonable approximation. The basement underlying unit 6 comprises Paleozoic and Mesozoic metamorphosed sedimentary rocks and Mesozoic plutonic rocks. Any compaction that occurred in these Paleozoic and Mesozoic rocks is assumed to have terminated prior to the Late Eocene rifting phase. The surface of these rocks is therefore taken as a reference surface for calculating the basement subsidence.

The values of crustal and subcrustal stretching factors (β and δ) and the corresponding correlation coefficients at well locations are shown in Figure 4.8 through Figure 4.37 and are summarized in Table 4.2. The lateral distributions of crustal and subcrustal stretching factors (β and δ) and the total lithospheric attenuation (ϵ) in the Pattani Basin are shown in a series of maps in Figure 4.38, Figure 4.39, and Figure 4.40, respectively.

Table 4.2: Summary of crustal and subcrustal stretching factors, geothermal gradients, organic maturation gradients, and present-day heat flow at well locations in the Pattani Basin

WELL	β	δ	ϵ	GEO THERM. GRADIENT (°C/km)	Ro. GRADIENT (log %/km)	HEAT FLOW (HFU)
Ranong-1	1.4	1.8	1.67	36	0.23	1.93
Kung-1	1.4	1.8	1.67	39	0.20	1.93
Surat-1	1.5	2.1	1.89	46	0.29	2.16
Platong-8	1.8	2.8	2.42	52	0.37	2.20
Platong-1	1.9	2.8	2.47	46	0.28	2.00
Insea-1	1.3	1.3	1.30	28	0.17	1.56
Pakarang-1	1.9	2.7	2.42	52	0.28	2.19
Pladang-3	2.2	2.4	2.34	51	0.26	2.13
S.Platong-2	2.4	2.8	2.68	50	0.38	2.08
Trat-1	2.7	3.6	3.29	58	0.37	2.32
Dara-1	1.4	2.0	1.79	40	0.28	2.05
E-12-1	2.1	2.8	2.56	56	0.31	2.27
E-12-8	2.1	2.1	2.10	52	0.31	2.17
Satun-3	2.6	2.8	2.74	51	0.27	2.10
Jakrawan-2	2.4	2.9	2.74	51	0.28	2.11
Krut-1	1.7	2.1	1.97	40	0.07	1.87
E-K-1	2.2	1.5	1.65	44	0.33	1.98
Baanpot-1	2.8	1.5	1.72	48	0.32	2.07
Baanpot-B-1	2.8	1.5	1.72	42	0.37	1.90
Jakrawan-1	2.4	2.5	2.47	63	0.31	2.42
Funan-1	2.1	3.0	2.68	50	0.30	2.10
Yala-2	1.6	2.2	1.99	49	0.24	2.07
Kaphong-3	2.2	2.1	2.13	45	0.36	1.99
Kaphong-1	2.2	3.0	2.72	59	0.43	2.35
Platong-5	1.6	2.1	1.93	46	0.49	2.02
S.Platong-1	2.1	3.5	2.95	56	0.38	2.24
Satun-2	2.2	2.8	2.60	49	0.31	2.06
Satun-1	2.4	2.6	2.54	48	0.29	2.01
E-12-9	2.1	2.1	2.10	52	0.34	2.17
E-12-7	2.1	1.9	1.95	55	0.36	2.24

* β is a crustal lithospheric stretching factor

δ is a subcrustal lithospheric stretching factor

ϵ is a total attenuation of lithosphere

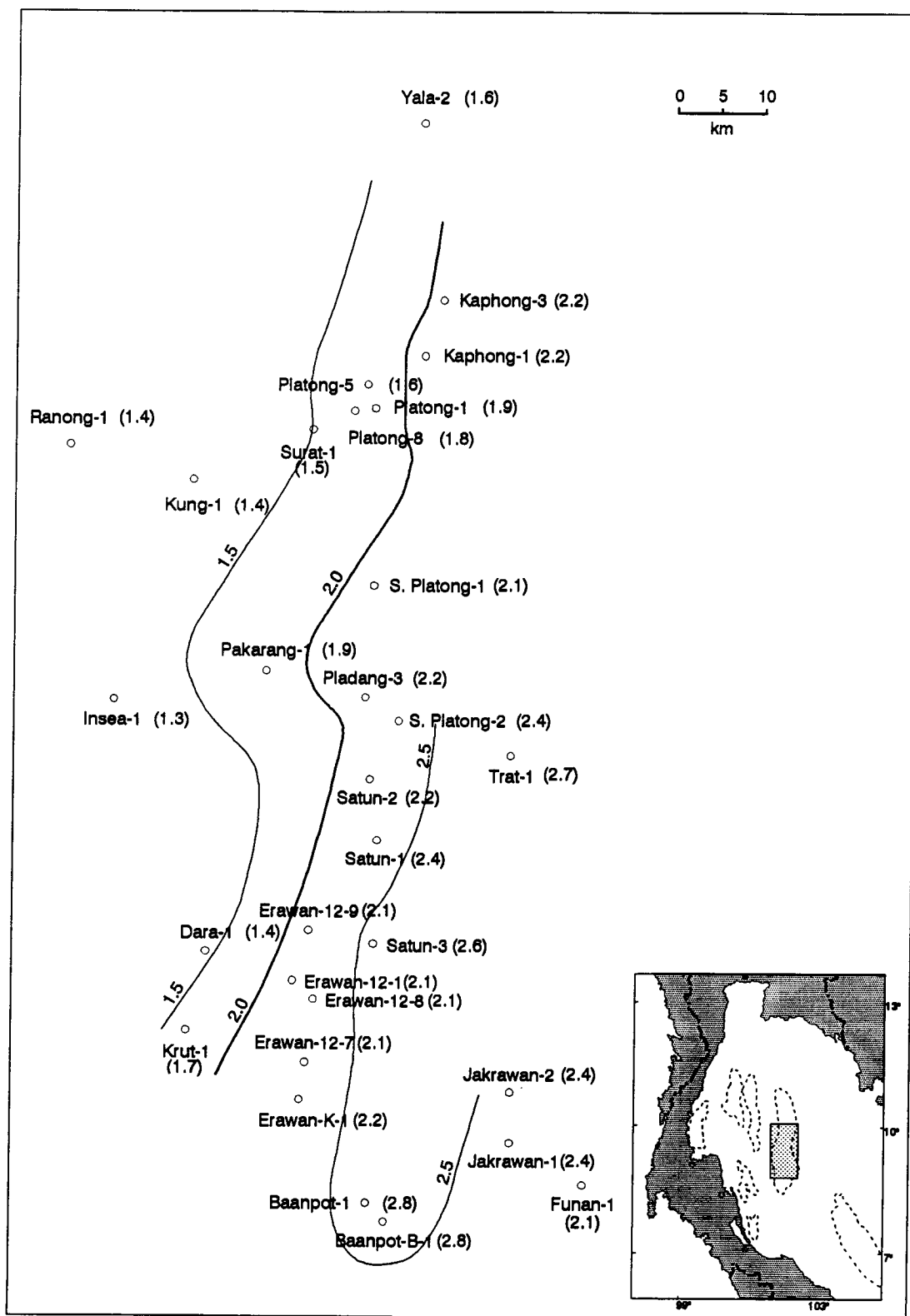


Figure 4.38: Lateral variation of crustal lithospheric stretching (beta)

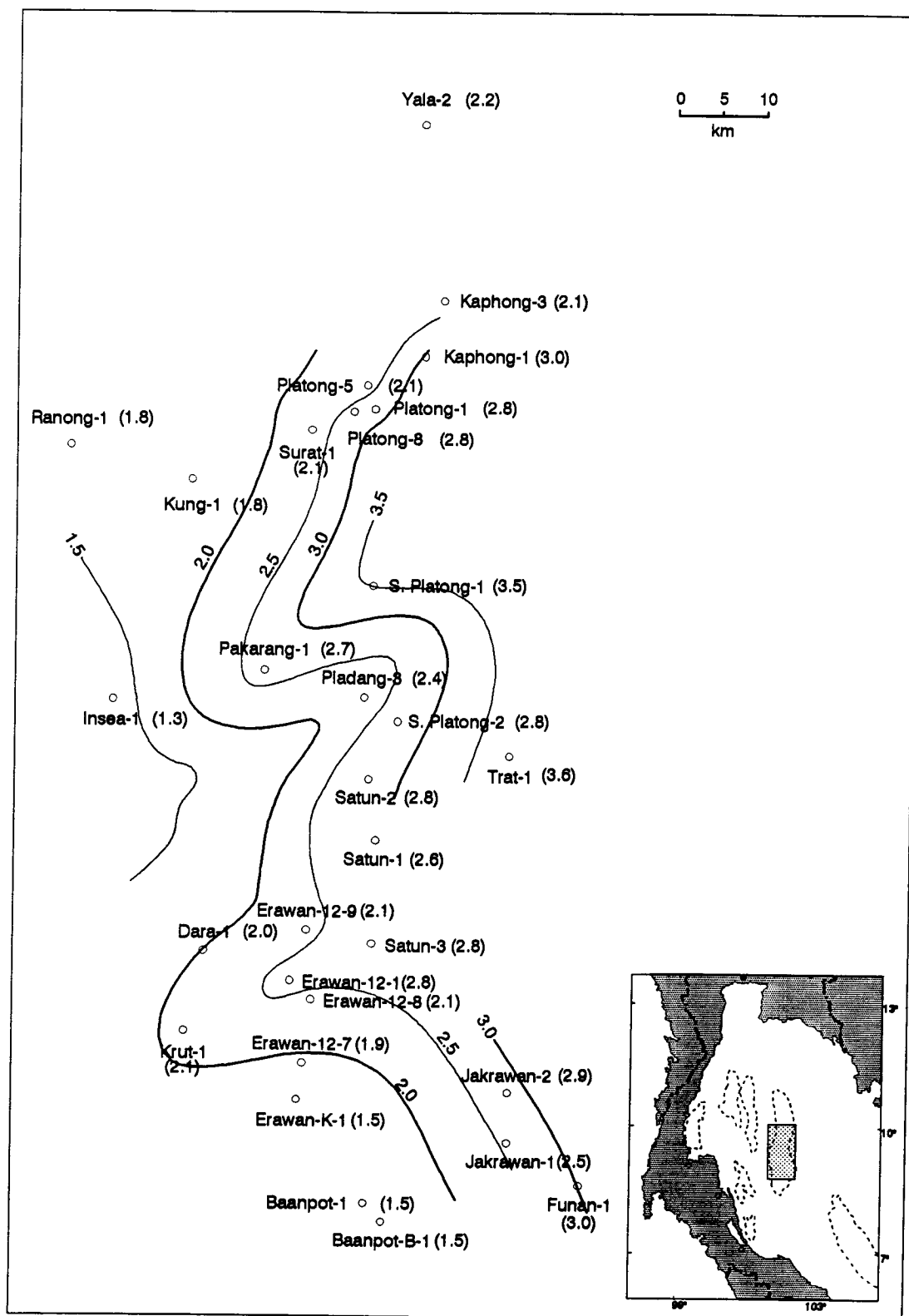


Figure 4.39: Lateral variation of subcrustal lithospheric stretching (δ)

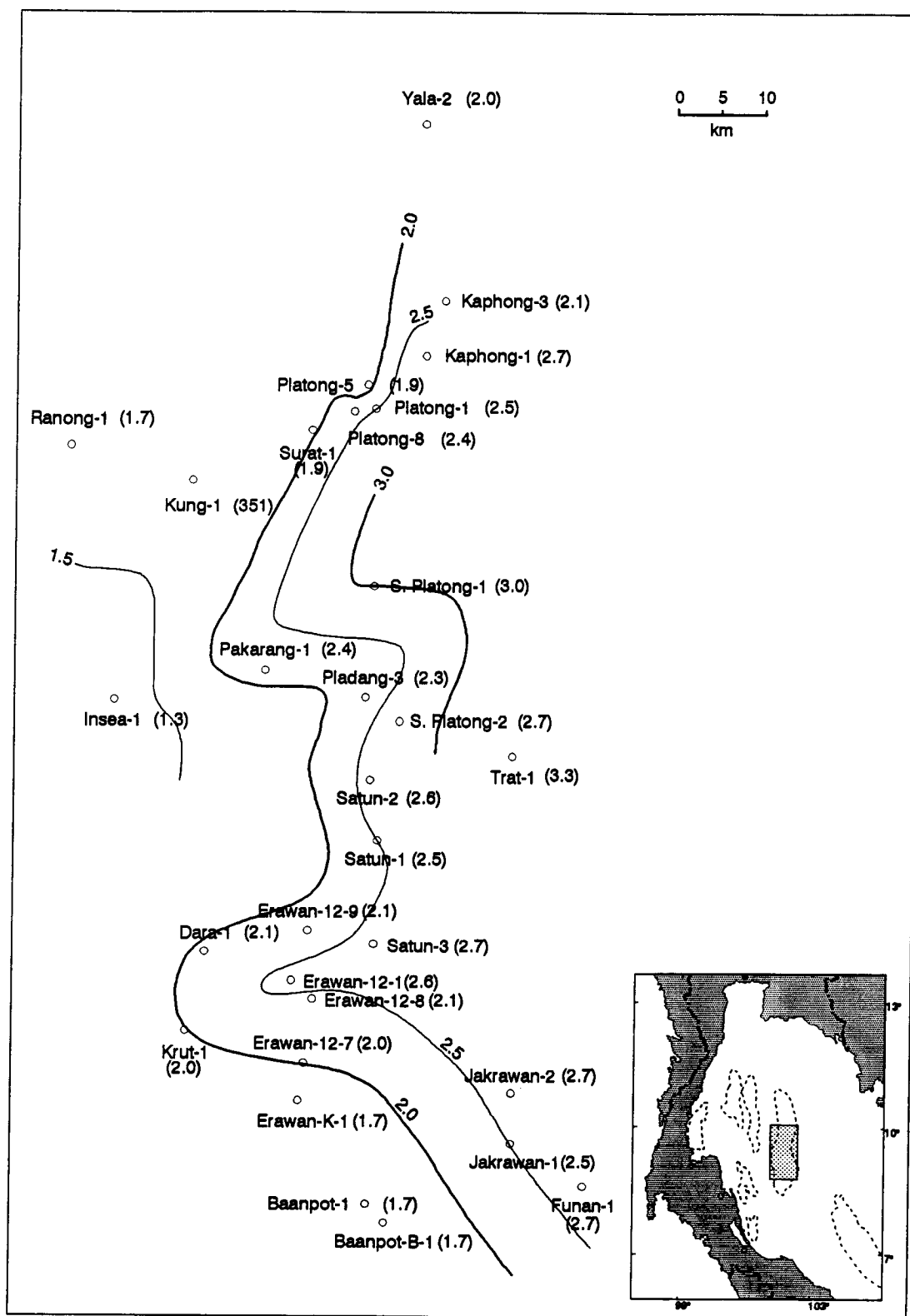


Figure 4.40: Lateral variation of total lithospheric stretching factor (epsilon)

The distribution of total lithospheric stretching, ϵ , (Figure 4.40) indicates that lithospheric stretching generally increases from the basin margin (e.g. Ranong-1, Kung-1, and Insea-1 wells) toward the basin center (e.g. South Platong-1, Trat-1, Satun-3, and Jakrawan-2 wells). In general, subcrustal lithospheric stretching is greater than crustal lithospheric stretching. In some locations in the basin center, however, crustal lithospheric stretching is greater than subcrustal stretching. These wells include Erawan-K-1, Baanpot-1, Baanpot-B-1, Kaphong-3, and Erawan-12-7. This can be rationalized because these wells contain very thick synrift sediment columns. Thick synrift sediments indicate that synrift subsidence is large because crustal thinning or stretching has a much greater effect on initial subsidence than subcrustal stretching. A greater amount of crustal thinning is, therefore, required to accommodate such thick synrift sediments.

4.7 THERMAL HISTORY

4.7.1 Heat flow History

Utilizing the lithospheric stretching factors summarized in section 4.6.3, it is possible to predict heat flow history of the Pattani Basin. Before making any prediction of the heat flow history, however, some assumptions must be made in regard to the background heat flux prior to extension and the heat generated by radioactive decay within the earth's crust. Following McKenzie (1978) and Hellinger and Sclater (1983), an original background heat flux of 0.8 HFU ($\mu\text{cal}/\text{cm}^2 \text{ sec}$) is assumed for the Pattani Basin. It is further assumed that radioactivity in the study area contributed about 0.2-0.4 HFU ($\mu\text{cal}/\text{cm}^2 \text{ sec}$) to the surface heat flow and that this value should be divided by the factor β to give the

post-extensional contribution. Thermo-physical properties of sediments and those of lithosphere and mantle are listed in Table 4.1.

Figure 4.8 through 4.37 show that surface heat flow histories at each well location generally decreased with time since the end of rifting. The present-day surface heat flows calculated from the model described in section 4.6.3 at different well locations are shown in Figure 4.41. The predicted present-day surface heat flow varies approximately from 1.6 to 2.4 HFU. These values generally agree with the measured present-day values reported by Matsubayashi and Uyeda (1979) and Rutherford and Qureshi (1980) which range approximately from 1.9 to 2.5 HFU.

The surface heat flow in the study area is high compared to the earth's average heat flow of 1.4 to 1.6 HFU because the Pattani Basin is a rifted intracratonic basin, less than 25 Ma old. Rifting and consequent upwelling of hot aesthenosphere material elevated the heat flow, which subsequently decreased exponentially with time (McKenzie, 1978). In a "standard" lithosphere, the heat flow reaches approximately $1/e$ of its originally elevated value after 62.8 million years (the thermal-time constant of the lithosphere, τ ; McKenzie, 1978; Hellinger and Sclater, 1983; Allen and Allen, 1990). At this time (62.8 million years after the cessation of rifting), the dependency of heat flow on the stretching factors is insignificant, and surface heat flow of the area returns to a normal value which is about 1.4 to 1.6 HFU.

4.7.2 Temperature History and Present-day

Geothermal Gradients

If the thermal conductivity of the sediments is known as a function of time,

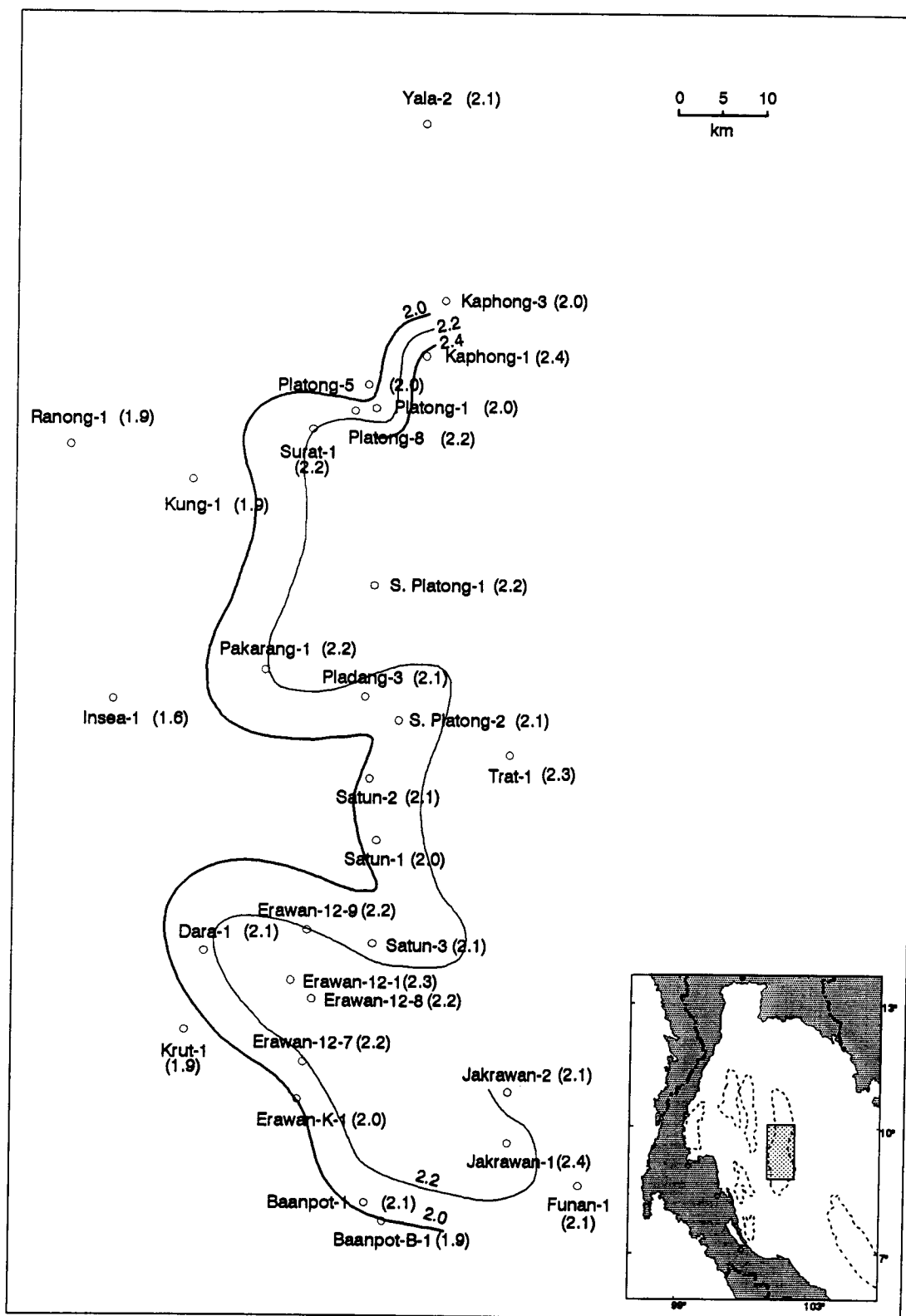


Figure 4.41: Present-day surface heat flow (contour interval = 0.2 HFU)

temperatures at any given depth and time since deposition can be calculated from the heat flow history. Relevant thermo-physical properties of sediments such as thermal conductivity of grains and porosity are listed in Table 4.1. The thermal conductivity of pore water is assumed to be 1.43 mcal/cm sec °C (Friedinger, 1988). For the purpose of computation and lack of reliable measurement, surface temperature during deposition of all stratigraphic layers is assumed to be 10 °C.

Temperature histories at well locations displayed as isotherm lines and present-day geothermal gradients, based on the above consideration, are shown in Figure 4.8 through Figure 4.37. The lateral distribution of the calculated present-day geothermal gradients is shown in a map in Figure 4.42. In general, the geothermal gradients increase from 36 to 40 °C/km in the basin margin to 58 to 60 °C/km at the basin center. The lowest calculated geothermal gradient is in Insea-1 well location which has the lowest lithospheric stretching factors ($\beta = \delta = 1.3$). The calculated geothermal gradients agree well with the measured present-day geothermal gradients in this area which range from 45 to 60 °C/km (Rutherford and Qureshi, 1981).

4.7.3 Vitrinite Reflectance

Given burial history and temperature history, the degree of thermal maturation of any individual stratigraphic layer can be predicted. Because it is an indicator of organic thermal maturity, vitrinite reflectance is widely used in an integrated basin analysis and the exploration for oil and gas (Hunt, 1979; Tissot and Welte, 1984; Waples, 1985; and many others).

Various models that simulate vitrinite maturation fall into four categories (Sweeney and Burnham, 1990): (1) models that describe vitrinite maturation solely as a function of temperature (Price, 1983; Barker and Pawlewicz, 1986); (2) models that incorporate time as a rule of thumb (Hood et al., 1975; Bostick et al., 1978); (3) models that describe vitrinite reflectance as an Arrhenius first-order chemical reaction with a single activation energy (Middleton, 1982; Antia, 1986; Wood, 1988); and (4) models that describe vitrinite reflectance as an Arrhenius first-order chemical reaction with a single activation energy, but with the activation energy itself as a function of temperature (Lerche et al., 1984; Armagnac et al., 1989). The limitation of these models, as pointed out by Sweeney and Burnham (1990), is that they are all empirical.

Larter (1988) described vitrinite maturation with parallel Arrhenius first-order reactions with a Gaussian distribution of activation energies. Larter's model uses a Gaussian distribution of activation energies, with a mean value of 44.5 kcal/mole and a standard deviation of 7 per cent to calculate the decrease of phenol yield with maturity during pyrolysis. Phenol yield, in turn, correlates linearly with vitrinite reflectance. The limitation of Larter's model is that correlation can be made only over the range of phenol reaction which is equivalent to the vitrinite reflectance of 0.45 to 1.6 %Ro.

Burnham and Sweeney (1989), and later Sweeney and Burnham (1990), proposed a vitrinite maturation model that integrates chemical kinetic equations over time and temperature to account for the elimination of water, carbon dioxide, methane, and higher hydrocarbons from vitrinite. The resulting composition of vitrinite is, then, used to calculate vitrinite reflectance via correlation between elemental composition

and reflectance. The model uses a single pre-exponential factor with the activation energy distribution. Table 4.3 lists the activation energies, stoichiometric factors, and a pre-exponential factor used to model vitrinite maturation. The model can be used to calculate vitrinite reflectance ranging from 0.3 to 4.7 %Ro.

The vitrinite maturation model proposed by Burnham and Sweeney (1989) was used in this study to calculate vitrinite reflectance at the boundaries of all stratigraphic units. The modeled vitrinite reflectances were then compared with the measured values obtained from well cutting samples to verify the validity of the lithospheric stretching model used to predict heat flow history of the basin. The plots of calculated and measured vitrinite reflectances at well locations are shown in Figure 4.8 through Figure 4.37. The lateral distribution of the Ro-gradients (%Ro/km) is plotted in the map shown in Figure 4.43.

In general, the measured and modeled vitrinite reflectance values agree reasonably well, considering the uncertainties involved in both modelling and measuring the vitrinite reflectance, as well as uncertainties in geological parameters. The poorest agreement between modeled and measured vitrinite reflectance occurs in Krut-1 well (Figure 4.23) where the measured vitrinite reflectances are more or less constant (about 0.6 %Ro) with depth. This might be due to variation in organic facies rather than abnormal thermal history. Jones (1987) showed that a constantly low vitrinite reflectance profile (about 0.6 %Ro) to the depth of nearly 2500 m was due to the dominance of fine-grained, oxidized detrital vitrinite that had a reflectance of 0.6 %Ro when deposited and matured very slowly. Such a situation might also be the case for the erratic vitrinite profile encountered in Krut-1 well where most of the sediments are substantially oxidized. The computed vitrinite reflectances seem to be too low in Insea-1 well (Figure 4.13) and slightly too high

Table 4.3: A list of pre-exponential factor, activation energies, and stoichiometric (influential) factors used to model vitrinite maturation (After Sweeney and Burnham, 1990)

Pre-exponential factor (A) = 1.00E+13 /sec

Stoichiometric Factor	Activation Energy (kcal/mol)
00.0300	34.00
00.0300	36.00
00.0400	38.00
00.0400	40.00
00.0500	42.00
00.0500	44.00
00.0600	46.00
00.0400	48.00
00.0400	50.00
00.0700	52.00
00.0600	54.00
00.0600	56.00
00.0600	58.00
00.0500	60.00
00.0500	62.00
00.0400	64.00
00.0300	66.00
00.0200	68.00
00.0200	70.00
00.0100	72.00

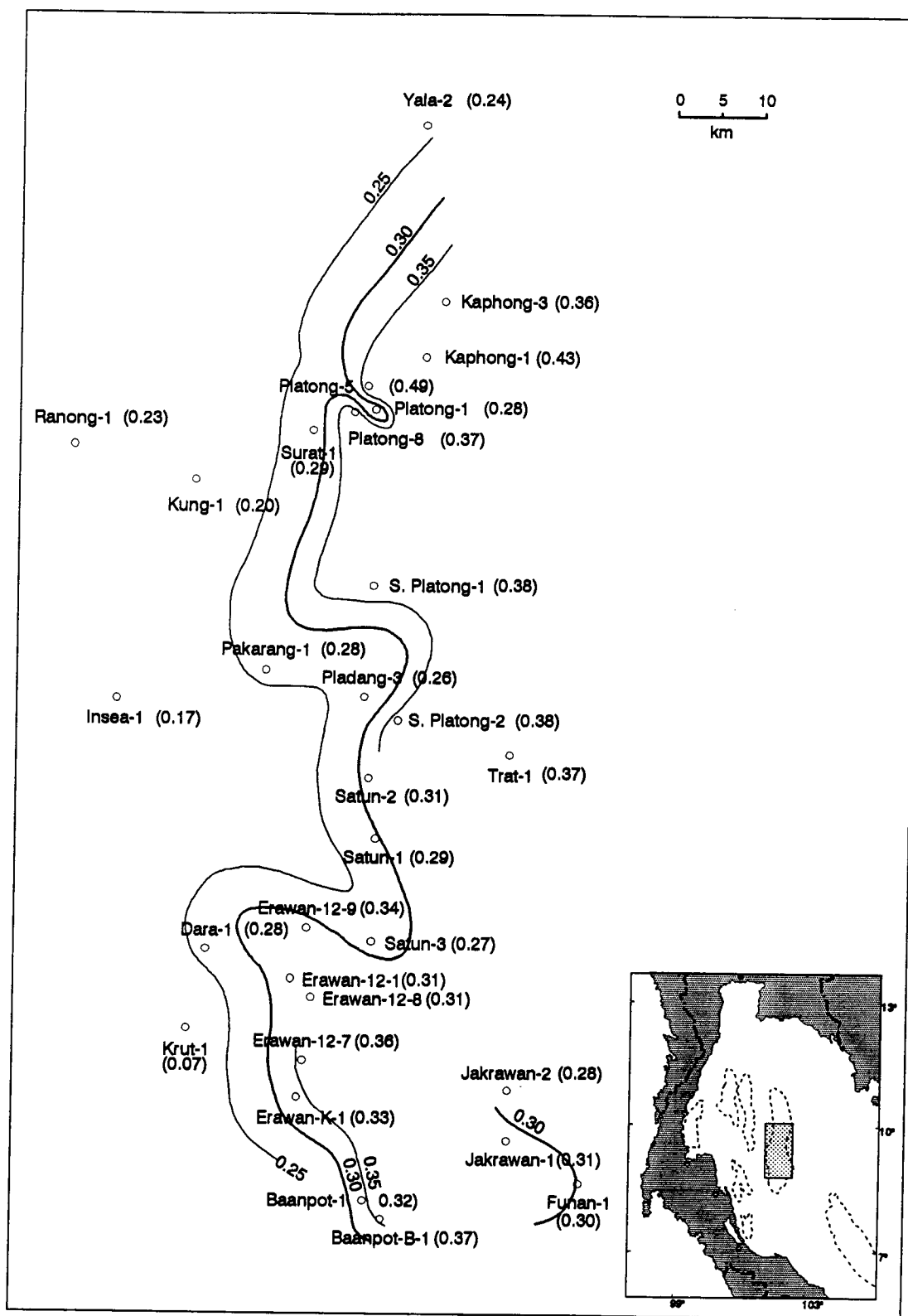


Figure 4.43: Observed present-day organic maturity gradients (contour interval = 0.05 %Ro/km)

in Trat-1 well (Figure 4.17). These variations may be caused by the difference between assumed and true heat flows within the earth's crust. The thermal history of the basin is controlled by radiogenic heat generation as well as by the upwelling of the hot aesthenosphere. Heat generated by the upwelling of the aesthenosphere can be modeled as described earlier, whereas heat from radioactive decay was assumed. Errors in the assumed values could lead to the discrepancies between predicted and measured heat flow histories and the local erratic vitrinite reflectance profiles.

4.8 DISCUSSION

The tectonic regime responsible for the origin of the Tertiary basins in Thailand has been a subject of discussion. Bunopas and Vella (1983) related extension and rifting in the Gulf of Thailand and onshore Thailand to back-arc spreading behind the subduction of the Indian plate beneath Southeast Asia along the Java Trench and Andaman-Nicobar Island chain. However, most back-arc basins develop a few hundred kilometres behind the subduction zone (Karig, 1971; Taylor and Karner, 1983) whereas Tertiary basins in Thailand are located approximately 1000 to 1500 km behind the subduction zone mentioned above. It is also unclear whether subduction even occurs along the Andaman-Nicobar Island chain. Subduction along the Java Trench may become strike-slip motion along the Andaman-Nicobar Island chain (Ohnstad, 1989; Polachan and Sattayarak, 1989). These arguments make the back-arc tectonic regime less likely to be the responsible mechanism for the formation of Tertiary basins in Thailand.

Molnar and Tapponnier (1975), Tapponnier et al. (1982), and Ohnstad (1989) suggested that development of Tertiary basins in Thailand is related to the

northward progressive collision of India with Eurasia since 40-50 Ma. This resulted in the eastward and southward extrusion of Indochina and portions of eastern China along left-lateral, strike-slip faults such as the Red-River and Altyn-Tagh faults (Figure 4.44). The left-lateral motion of the fault systems in Southeast Asia interpreted from this model do not correspond with the present-day right-lateral motions (Allen et al., 1984; Le Dain et al., 1984; Tapponnier et al., 1986), although the India-Eurasia collision zone continues. The contrasting evidence suggests that this geologic model may not be valid for the development of the Tertiary basins in Thailand.

Polachan and Sattayarak (1989) related the development of Tertiary basins in Thailand to the progressive northward collision of India with Eurasia since the Eocene. Penetration of India into Eurasia caused clockwise rotation of Southeast Asia, resulting in increasingly oblique subduction of the Indian Ocean plate beneath the western edge of Southeast Asia. This led to the right-lateral movement on major NW-SE faults such as Red River, Mae Ping, Three Pagodas and Sumatra faults (Figure 4.44). Polachan (1988) and Polachan and Sattayarak (1989) related the fault distribution to the strain ellipsoid during right-lateral motion in the Gulf of Thailand (Figure 4.45), and suggested that E-W extension could develop during right-lateral movement on the NW-SE Three Pagodas faults, and left-lateral movement on the conjugate NE-SW Ranong and Klong Marui faults. This model is supported by paleomagnetic analyses of Cenozoic rocks in Thailand, indicating a nearly 25° clockwise rotation of Western Thailand from Indochina (McCabe et al., 1988); the right-lateral movement of major fault systems in Southeast Asia; and the N-S trending extensional basins in Thailand. The origin and tectonic setting of the Pattani Basin and other Tertiary basins in Thailand are, in general, comparable to that of Late Tertiary basins along the western margin of the Basin and Range

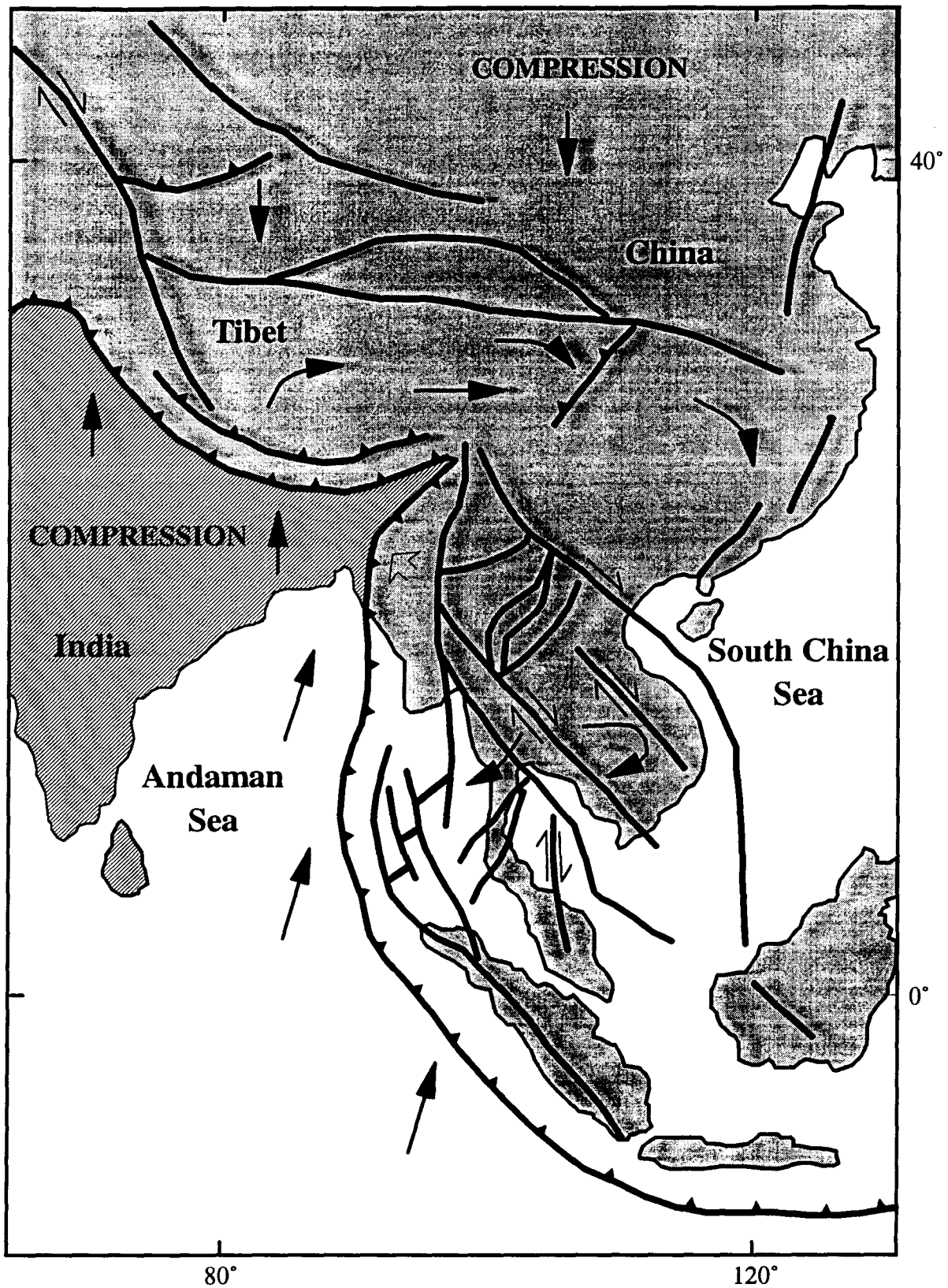


Figure 4.44 Tectonic map of S.E. Asia and South China Sea showing the main fault patterns and the relative movement of crustal blocks in response to the collision of India with Eurasia

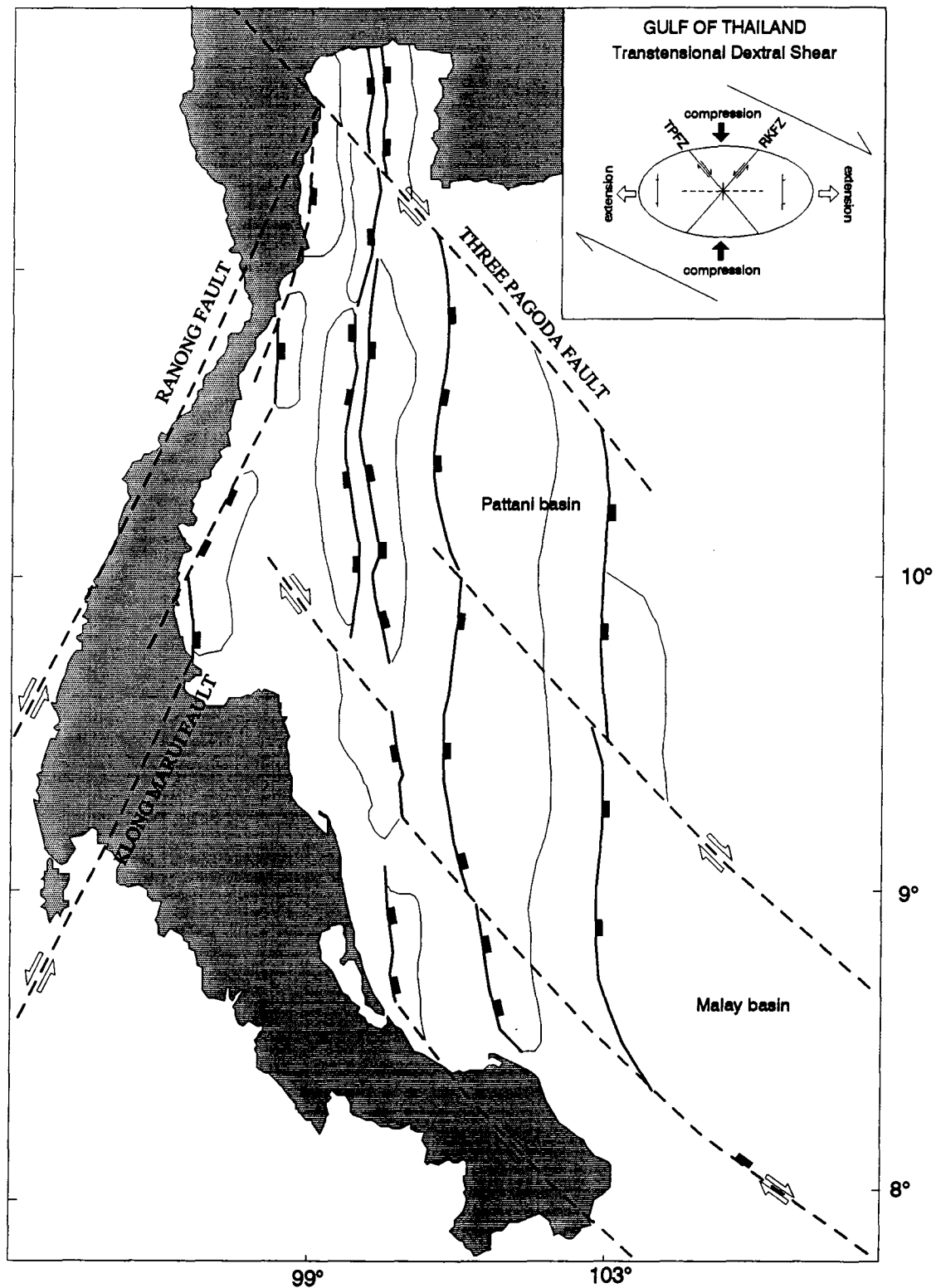


Figure 4.45: Structural map of the Gulf of Thailand. Showing relationship between strike-slip faults and the development of N-S trending (After Polachan & Sattayarak, 1989).

Province in western Nevada. The N-S trending extensional basins in western Nevada are characterized by a series of N-S trending normal faults associated with a NW-SE strike-slip fault system (Link et al., 1985). High heat flow in Tertiary basins in Thailand and volcanism in the western margin of the Basin and Range Province are closely related to mechanical thinning of the lithosphere and consequent upwelling of the hot asthenosphere.

The E-W extension, which was the result of the oblique subduction of the Indian Ocean plate beneath the western edge of Southeast Asia, caused the lithospheric stretching and crustal thinning, which led to the passive upwelling of the hot asthenosphere in Central Thailand and the Gulf of Thailand. Ohnstad (1989) modeled the Bouguer gravity anomaly and suggested an elevated lithosphere-asthenosphere boundary in the Tertiary basins in the Gulf of Thailand. High heat flow in the Tertiary basins in Thailand also supports the crustal thinning model.

Geohistory analysis of well data from the Pattani Basin has shown that the observed synrift and post-rift subsidences can generally be accounted for by simple E-W extension causing crustal and subcrustal lithospheric thinning. The present study also verifies the validity of nonuniform stretching model as a mechanism for modelling the formation of the Pattani Basin. Values predicted by the model for the maturity index, vitrinite reflectance, compared well with the observed values. From these observations and from the stratigraphic analysis carried out in chapter 3, the Tertiary tectonic and stratigraphic evolution of the Pattani Basin is interpreted below.

At the beginning of the Tertiary, most of the Gulf of Thailand probably was elevated above sea-level (Achalabhuti and Oudom-Ugsorn, 1978). Extension in

Continental Southeast Asia was initiated during Late Eocene both along an old Triassic-Jurassic suture zone between the Indochina plate in the east and the Burmese-Thai plate in the west, and along other similar N-S and NW-SE trending weak zones (Burri, 1989; Chinbunchorn et al., 1989). During this primary period of extension, which lasted about 20 m.y., faulting and graben formation were common and probably episodic. A series of N-S and NW-SE trending, fault-controlled, half grabens and grabens developed in the proto-Gulf of Thailand. These faults may have extended the underlying basement by as much as 90 km. The crust underwent brittle failure, producing isostatic fault-controlled subsidence within the graben area. The main extensional area might have been in the south-central part of the study area where the Late Eocene and Early Oligocene depocenters are located (Figure 3.11 and Figure 3.12). Following the rifting phase, the post-rift thermal subsidence was characterized by a slower rate of subsidence and the absence of major fault movement.

The result of the stratigraphic analysis described in detail in chapter 3 suggests that the Tertiary sedimentary succession in the Pattani Basin is generally consistent with the tectonic evolution predicted by the lithospheric stretching model. The synrift basins were dominated by coarse-grained alluvial fan and braided stream deposits along syndepositional faults at the basin margins and by fine-grained lacustrine deposits further from the faults in the basin center (stratigraphic unit 6). These sediments unconformably overlie the Paleozoic and Mesozoic basement. As the extension abated, the area subsided more slowly, and sediments gradually changed upward into nonmarine floodplain and channel deposits (stratigraphic unit 5). A brief and rapid transgression during the Early Miocene (at the base of stratigraphic unit 4) might have been the result of an episode of normal faulting and graben formation leading to rapid subsidence of the basin. After faulting, the rate of

subsidence declined, leading to a decrease in the rate of relative sea-level rise and, as a consequence, the occurrence of a regressive sedimentary succession of the stratigraphic unit 4.

Fault movement decreased toward the end of the rifting phase in Early Miocene (about 20 Ma), after which a post-rift thermal subsidence took place more slowly until the present-day.

The post-rift sediments comprise a regressive sequence in the lower part of the succession (stratigraphic unit 3) and two transgressive cycles in the upper part (stratigraphic units 2 and 1). Because of the relatively slow post-rift subsidence, the regressive and transgressive cycles in the post-rift sedimentary succession are attributed to variations in sediment supply and eustatic sea-level change during this time interval.

In general, the amount of total lithospheric stretching increases from the basin margin to the basin center (Figure 4.40). The crustal lithospheric stretching factors (β) range from 1.3-1.4 at the basin margin to 2.6-2.8 in the basin center (Figure 4.38). These values are, however, affected by basement topography and probably reflect local changes in crustal thickness which are difficult to constrain during modelling. The crustal stretching factors (β) obtained from the model should, therefore, be considered as approximations. The subcrustal lithospheric stretching factors (δ) range from 1.3 at the basin margin to more than 3.0 in the basin center (Figure 4.32). The total (crustal and subcrustal) lithospheric stretching factors (ϵ) range from 1.3-1.6 at the basin margin to more than 2.5 in the basin center (Figure 4.33). Generally, the subcrustal lithospheric stretching factors are greater than the crustal lithospheric stretching factors. In areas with great thickness of synrift

sediments such as those containing the Erawan-K-1, Baanpot-1, and Baanpot-B-1 wells, however, crustal stretching is greater than subcrustal stretching. These areas might have been affected by basement topography prior to rifting.

The amount of lithospheric stretching may have extended the underlying basement as much as 90 km. This amount of extension agrees reasonably well with the 85 km basement extension in the Gulf of Thailand calculated from the modelling of the Bouguer gravity anomalies by Ohnstad (1989).

High geothermal gradients (45-60°C/km) and high surface heat flow (1.9-2.5 HFU) observed in the study area and in other Tertiary basins in Thailand can generally be accounted for by the lithospheric stretching model. The geothermal gradients and present-day surface heat flow predicted from a non-uniform lithospheric stretching model range from 36°C/km to 63°C/km and from 1.6 HFU to 2.5 HFU, respectively. High geothermal gradients and high heat flow can be attributed to the upwelling of hot asthenosphere. This is evident from the modelling of Bouguer gravity anomalies by Ohnstad (1989) which suggested that the lithosphere-asthenosphere boundary in the Gulf of Thailand is shallow. High geothermal gradients still exist in the Gulf of Thailand probably because the area is relatively young and still in thermal disequilibrium, in which thermal decay due to the elevated asthenosphere has not been complete.

4.9 SUMMARY AND CONCLUSIONS

The collision of India with Eurasia which has been continuing since Eocene time has caused clockwise rotation of Southeast Asia, resulting in increasingly oblique subduction of the Indian Ocean plate beneath the western edge of the Continental

Southeast Asia. This led to the right-lateral movement on the major NW-SE fault system and left-lateral movement on the conjugate NE-SW faults in Thailand, which together induced the E-W extensional tectonic regime in the Gulf of Thailand and adjacent areas. Such a tectonic regime is comparable to that of Late Tertiary, NW-SE strike-slip related basins in the western margin of the Basin and Range Province in western Nevada.

The resulting E-W extension caused continental rifting and crustal thinning resulting in the development of a series of N-S trending Tertiary basins in the Gulf of Thailand and onshore Thailand.

Due to the large amount of subsidence during the rifting phase, the sedimentary signature of the synrift deposits in the Pattani Basin was controlled mainly by its tectonic subsidence. Because of the relatively slow and small amount of subsidence during the post-rift phase, the transgressive and regressive cycles in the post-rift, sedimentary succession in the study area might have been the result of variations in sedimentary supply and eustatic sea-level fluctuation.

The amount of lithospheric stretching as well as the surface heat flow in the Pattani Basin generally increased from the basin margin to the basin center.

Subcrustal stretching was generally greater than crustal stretching, except in the areas with a great thickness of synrift sediments where crustal stretching is greater than subcrustal stretching.

The lithospheric stretching in the Pattani Basin may have extended the basement rocks by as much as 45 to 90 km, and may have promoted the upwelling of hot aesthenosphere resulting in high surface heat flow.

The high present-day surface heat flow and geothermal gradients suggest that the Pattani Basin and other Tertiary basins in the Gulf of Thailand are still in the elevated and disequilibrium thermal condition. Apparently, thermal decay from the upwelling of the aesthenosphere has not yet been completed.

5. ORGANIC CHARACTERISTICS AND PETROLEUM SOURCE ROCK POTENTIAL OF TERTIARY STRATA IN THE PATTANI BASIN, THE GULF OF THAILAND

5.1 ABSTRACT

Rock-Eval pyrolysis and organic petrography have been used to evaluate the organic characteristics and petroleum source rock potential of Tertiary strata in the Pattani Basin. Average total organic carbon (TOC) contents are generally low to moderate (0.2 to 1.4%). Dispersed organic matter in the Pattani Basin consists mainly of Type III and Type IV kerogen with minor amount of Type II kerogen. It is composed chiefly of the macerals vitrinite, with minor inertinite and liptinite. Geochemical and petrological studies indicate a predominantly terrestrial and detrital source of organic matter throughout the Tertiary strata.

The variation in abundance and character of organic matter occurs both within and across the stratigraphic units. Within each stratigraphic unit, the lowest TOC and HI (hydrogen index) occur in high energy deposits such as alluvial fan and braided stream deposits; higher TOC and HI generally occur in low energy deposits. Across the stratigraphic units, TOC and HI generally increase in progressively younger strata. The abundance of organic matter within sediments is the combined result of organic input into sediments and degree of organic preservation. Low TOC and HI values in high energy nonmarine deposits reflect both low amount of organic input, and of a low state of preservation. Higher TOC and HI in low energy floodplain and interdistributary bay deposits, on the other hand, may reflect both proximity to marsh complexes, which could be sources of organic matter, and also a high degree of organic preservation which is common in fine-grained

sediments. The variation in abundance and character of organic matter in sediments both within and across the stratigraphic units is, therefore, controlled mainly by the depositional environments within which organic matter was deposited. The effect of sedimentation rate on the abundance of organic matter in the study area is apparent only in the relatively high TOC units (0.6-2.2%, unit 1). In units with low TOC (less than 0.5%), indigenous variation of TOC within the sediments has greater effect than sedimentation rate. A strong negative correlation between TOC and sedimentation rate in organic-rich unit 1 indicates the effect of clastic dilution on organic input with increased rate of sedimentation. A weak correlation between TOC and degree of organic maturation may also reflect the original variation of TOC from place to place within the stratigraphic unit and across the units rather than a true relationship between TOC and degree of organic maturation.

Source rocks of Tertiary strata in the Pattani Basin have very low hydrocarbon potential as defined by pyrolysis. The presence of a number of commercial gas fields suggests that either the source rocks here, despite very low genetic potential, are very effective in producing, migrating, and accumulating hydrocarbons, or the presence of higher quality source rocks within the basin which have not been reached by drilling, or a combination of both factors.

5.2 INTRODUCTION

Recent studies of modern and ancient sediments have revealed that allochthonous organic matter derived from terrestrial sources also comprises a major source of oil and gas, especially in nonmarine and deltaic settings (Compaz and de Matharel, 1978; Snowdon, 1980; Thomas, 1982; Bustin, 1988). The origin, distribution, and character of allochthonous organic matter have an important influence on the

volume and character of hydrocarbon generated. In the Pattani Basin (Figure 5.1), natural gas and condensate are produced from nonmarine and marginal marine Tertiary strata. Subsurface exploration and development provide geochemical and geological data to evaluate the factors controlling the distribution and deposition of source rocks in nonmarine and deltaic settings.

In this chapter, abundance and types of organic matter in Tertiary strata in the Pattani Basin are described, the factors controlling such abundance and characteristics are interpreted, possible petroleum source rocks are identified, and their regional extents are outlined. In particular, this chapter documents the variation in the abundance of organic matter with depositional environments, ages, sedimentation rates, and degree of organic maturation.

5.3 METHODS OF STUDY

The petroleum source rock characteristics of more than four thousand well cutting samples were determined by Rock-Eval pyrolysis (Espitalie et al., 1975). Cutting samples were sieved and the <2 mm (-10 mesh) portion was washed to remove water-soluble drilling mud contaminants. Shale fragments in the samples were hand-picked by the help of binocular microscope and were crushed and pulverized with a centrifugal grinding mill to approximately 170 μ m (80 mesh) particles. Sample sizes used for Rock-Eval pyrolyses were 100 mg for samples containing less than 3% total organic carbon (TOC), and 5 to 50 mg for samples containing more than about 3% TOC. Organic-rich shale or coal fragments in cutting samples were also hand-picked for vitrinite reflectance measurements and organic petrography.

Interpretation of Rock-Eval pyrolysis data in this study is based on parameters and their experimental limits documented by Espitalie et al. (1985) and Peters (1986). Table 5.1 summarizes the measured and calculated parameters derived from Rock-Eval/TOC analysis. The measured S_1 value represents the amount of hydrocarbons pre-existing in the rock since deposition plus those already generated in the subsurface. The S_2 value represents the amount of hydrocarbons being generated during pyrolytic degradation of the kerogen. The S_3 value represents the amount of carbon dioxide being generated during pyrolysis. It is a measure of the oxygen content in the kerogen. The TOC value is used to indicate organic richness of the sediments being analyzed. The S_1+S_2 value indicates the hydrocarbon (HC) potential (Genetic Potential; Tissot and Welte, 1984). The $(S_1+S_2)/\text{TOC}$ ratio expresses the relative quality of organic matter (QOM). The S_2/S_3 ratio is used to indicate the types of product (oil or gas) that will be generated from source rocks at the oil window (a degree of organic maturation (DOM) equivalent to 0.6 %Ro, Peters, 1986). The QOM is a measure of the type of OM and thermal maturity; high ratios indicate immature to mature hydrogen-rich strata. A significant spread in the QOM, which cannot be related to variations in the DOM or type of organic matter (OM), is considered to reflect the effects of migration of hydrocarbons into or out of the strata (Espitalie et al., 1985). Depletion of S_1 and S_2 values is common in oxidized OM (Peters, 1986). Thus, the QOM of some samples does not closely reflect the regional variation in petroleum potential of a particular horizon.

The hydrogen index (peak S_2 normalized for TOC content, HI) and oxygen index (peak S_3 normalized for TOC content, OI), when interpreted in concert with maturation data can be used to define the type of organic matters (Espitalie et al., 1985). Type I OM refers to kerogen with an HI value >600 mg HC/g TOC,

Table 5.1: Measured and calculated parameters derived from Rock-Eval/TOC analysis

1. Measured parameters:

S ₁	Hydrocarbons generated at less than 300°C
S ₂	Hydrocarbons generated during Rock-Eval pyrolysis, from 300-600°C
S ₃	Organic CO ₂ generated during Rock-Eval pyrolysis
Tmax	Temperature of maximum rate of hydrocarbon evolution during pyrolysis
TOC	Total Organic Carbon = (S ₁ + S ₂) plus organic CO ₂ generated from combustion of OM at 600°C after pyrolysis

2. Calculated parameters:

S ₁ + S ₂	Hydrocarbon potential or Genetic potential
S ₁ / (S ₁ + S ₂)	Production Index (PI) or Transformation ratio; maturity index
S ₂ / S ₃	Organic typing parameter; high value means hydrogen-rich OM
HI	Hydrogen Index = (S ₂ * 100) / TOC; organic typing parameter
OI	Oxygen Index = (S ₃ * 100) / TOC; organic typing parameter
QOM	Quality of Organic matter = (S ₁ + S ₂) / TOC; organic typing and maturity indicator, subject to migration

whereas Type II kerogen is defined by HI values ranging from 300 to 600 mg HC/g TOC, assuming a DOM equivalent to 0.6 %Ro (Espitalie et al., 1985). Relatively low HI values (<300 mg HC/g TOC) define Type III kerogen. (Espitalie et al., 1985). Type I and Type II OM comprise oil and gas prone kerogen, whereas Type III kerogen is mostly gas prone (Tissot and Welte, 1984). Some recent studies suggest that Type III OM can contain 10 to 20% liptinite or resinite in a vitrinite matrix and thus may act as effective oil prone source rocks (Snowdon, 1980; Powell and Snowdon, 1983; Snowdon, 1987). Other studies (Lewan and Williams, 1987; Link, 1988) argue that resinite or liptinite in a vitrinite matrix contribute only minor components to conventionally sourced crude oil and are not likely sources of commercial oil deposits.

The DOM can be approximated from the production index, defined as $S_1/(S_1 + S_2)$ ratio, (PI or Transformation Ratio, Tissot and Welte, 1984) and the temperature of maximum HC evolution during pyrolysis (Tmax). In general, PI and Tmax values of <0.1 and 435°C, respectively, indicate immature OM (Peters, 1986). The oil zone starts at 435°C for both Type II and Type III OM, whereas the wet gas zone starts at about 450°C for the type II OM but not until 465°C for Type III OM (Espitalie et al., 1985). Overmature OM is defined by Tmax values of >465°C for Type III OM, and >450° to 455°C for Type II OM. Tmax of Type I OM is, for the most part, independent of the DOM, and generally ranges from 460° to 470°C (Link, 1988).

For all types of OM, PI values between approximately 0.1 and 0.4 define the oil zone and the PI value increases to 1.0 when the HC generation capacity of the kerogen is exhausted (Peters, 1986). The PI value best illustrates the DOM by plotting PI versus depth (Espitalie et al., 1977; 1985). Anomalously high PI values

may indicate HC accumulation whereas anomalously low values may indicate depletion (Espitalie et al., 1985). In general, Tmax values cannot be determined as accurately if S₂ yields are less than 0.2 mg HC/g rock (Espitalie et al., 1985).

In order to assess the potential of petroleum source rocks, the regional distribution of organic richness, type, facies and maturity have to be examined. Organic richness is best determined as the average TOC content across the thickness of a potential source horizon rather than considering organic richness as a measure of OM concentrated in a discrete sample. Tertiary stratigraphic succession in the Pattani Basin is subdivided into units and subunits based on the lithological association and palynological assemblages. Average TOC content, HC potential (S₁+S₂) and QOM [(S₁+S₂)/TOC] have been calculated across the thickness of each unit and subunit at different well locations. Variations within the units and subunits, where detectable, are also described. In this way, regional evaluation of each unit and subunit can be discussed by considering how parameters differ and their combined effects on potential hydrocarbon source rocks.

Also described in this chapter is the relationship between the characteristics of dispersed organic matter and depositional environment, stratigraphic age, and degree of organic maturation. The organic characteristics of sediments are described in terms of kerogen type (Espitalie et al., 1985) and organic facies proposed by Jones and Demaison (1982) and Jones (1987) which defined an organic facies as "a mappable subdivision of a designated stratigraphic unit, distinguished from the adjacent subdivisions on the basis of the character of its organic constituents, without regard to the inorganic aspects of the sediments". Jones (1987) stressed that the definition of the term "facies", in organic facies, described a specific body of rock with lateral and vertical extent and not the organic

constituents present in the rock itself. The distribution of organic facies is determined by the origin of organic remains, the time spent in an oxidizing environment prior to deposition, and the redox potential prevailing near the sediment surface in early diagenetic environments (Jones, 1987).

Jones (1987) classified sedimentary organic facies into seven facies namely, A, AB, B, BC, C, CD, and D. The primary basis of the classification is the generating capacity for petroleum per unit of TOC at a vitrinite reflectance of about 0.5 %Ro. Therefore, the H/C ratio as well as HI and OI ratio of the kerogen are the primary discriminants between different facies (Durand, 1980; Hutton et al., 1980; Jones, 1987). Although based on certain combinations of factors that often occur together, the boundaries between different facies are arbitrary. Table 5.2 illustrates some generalized geochemical and microscopic characteristics of the seven organic facies recognized by Jones (1987).

5.4 SUMMARY OF TERTIARY STRATIGRAPHY IN THE PATTANI BASIN

Tertiary strata in the Pattani Basin are subdivided into 6 stratigraphic units (Figure 5.2 through Figure 5.7), based on lithological association and palynomorph assemblages. The stratigraphy and sedimentology of the strata, which have been described in detail in chapter 3, are summarized in this section (Table 5.3).

The stratigraphic and structural evolution of the Pattani Basin reflects the rifting of Continental Southeast Asia during the Tertiary. The geodynamic model for the formation of the Pattani Basin involves stretching of the continental lithosphere and crustal thinning, with an initial phase of rapid, fault-controlled subsidence, followed

Table 5.2: Generalized characteristics of organic facies A-D (After Jones, 1987)

Organic facies	H/C at $R_o=0.5\%$	Hydrogen Index	Oxygen Index	Dominant organic matter
A	> 1.45	> 850	10-30	Algal; amorphous
AB	1.35-1.45	650-850	20-50	Amorphous; minor terrestrial
B	1.15-1.35	400-650	30-80	Amorphous; common terrestrial
BC	0.95-1.15	250-400	40-80	Mixed; some oxidation
C	0.75-0.95	125-250	50-150	Terrestrial; some oxidation
CD	0.60-0.75	50-125	> 150	Oxidized; reworked
D	< 0.60	< 50	> 200	Highly oxidized; reworked

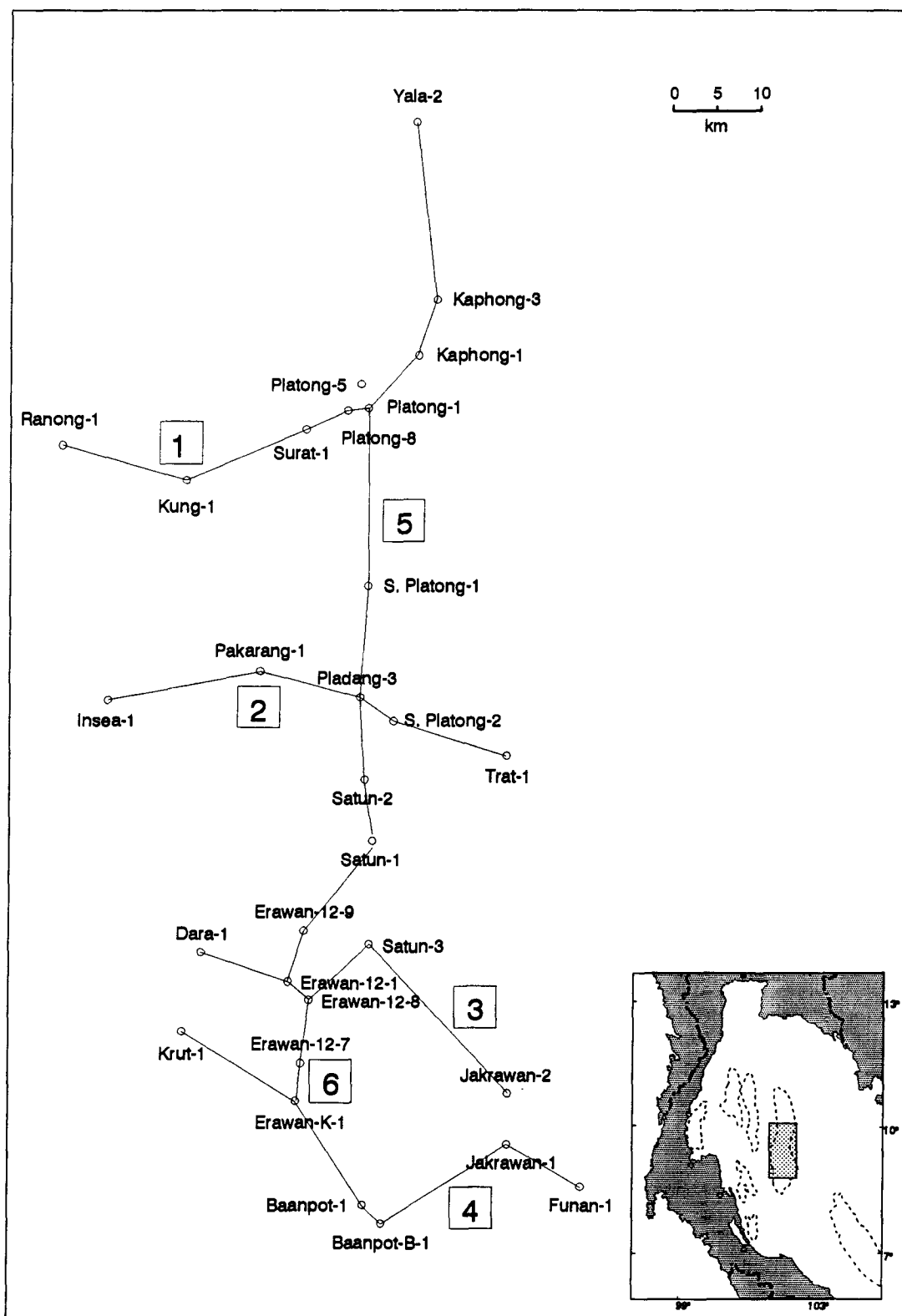
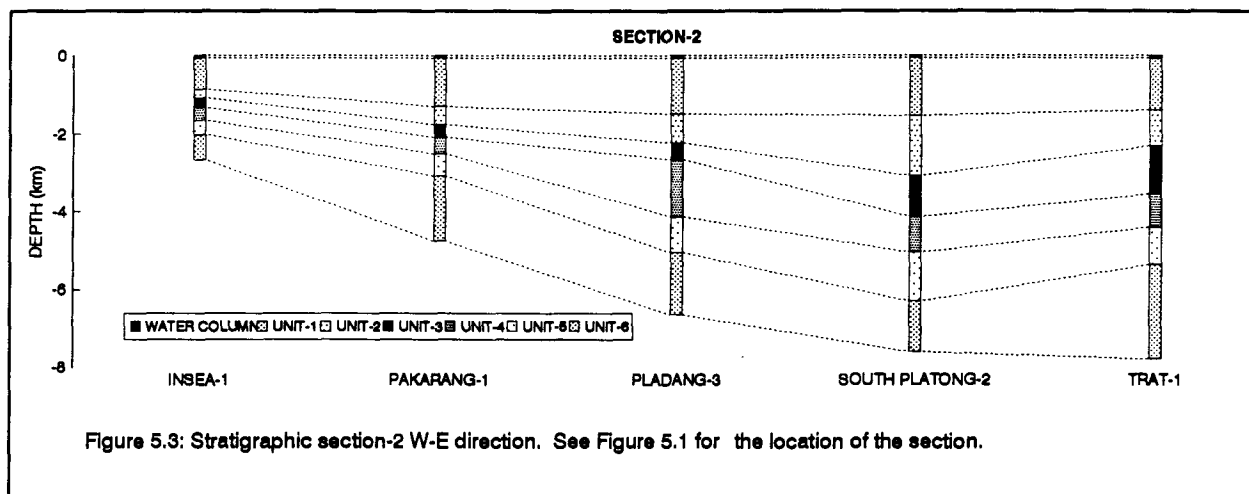
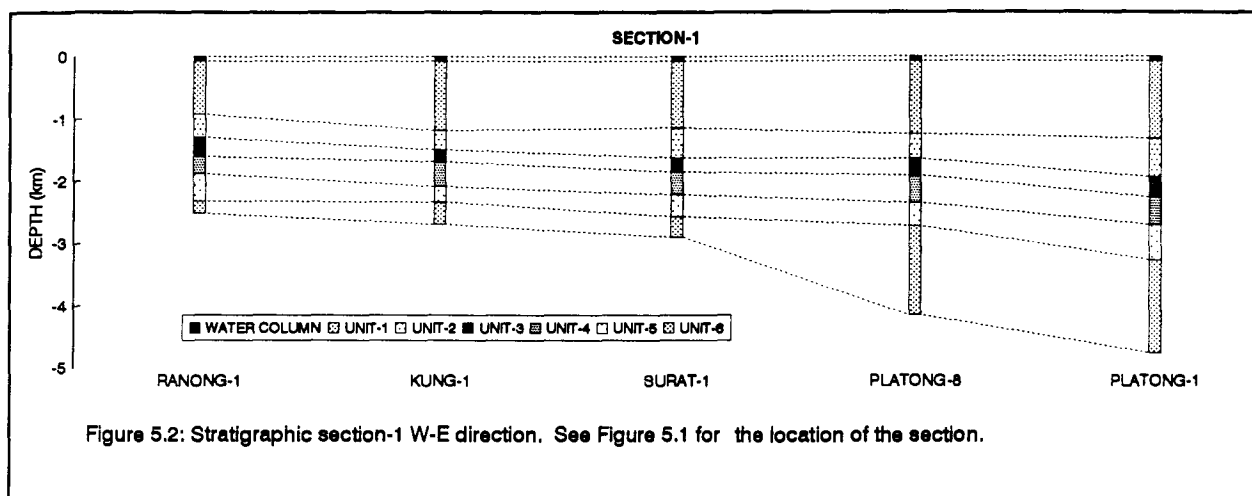
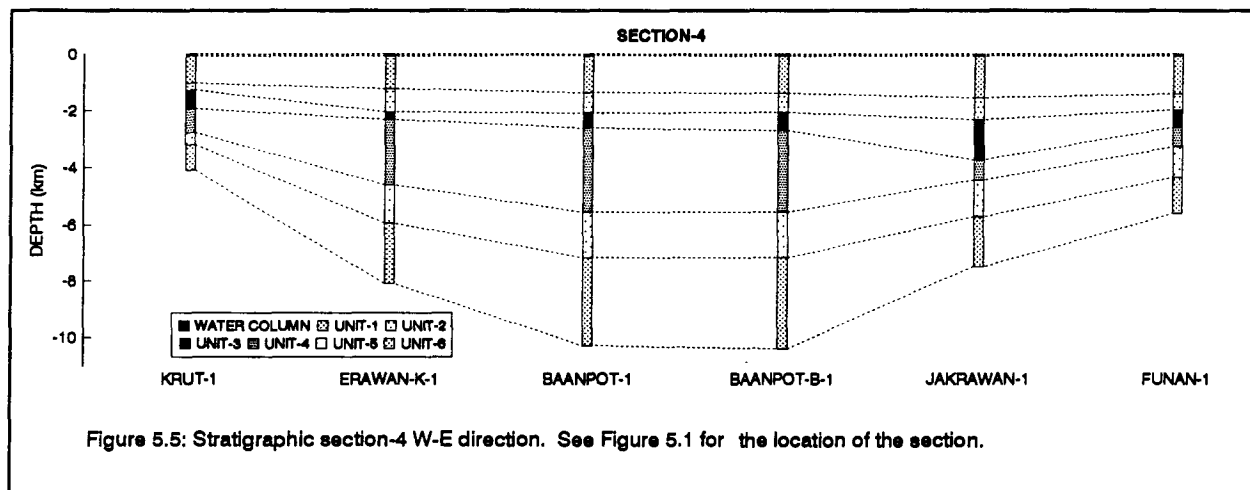
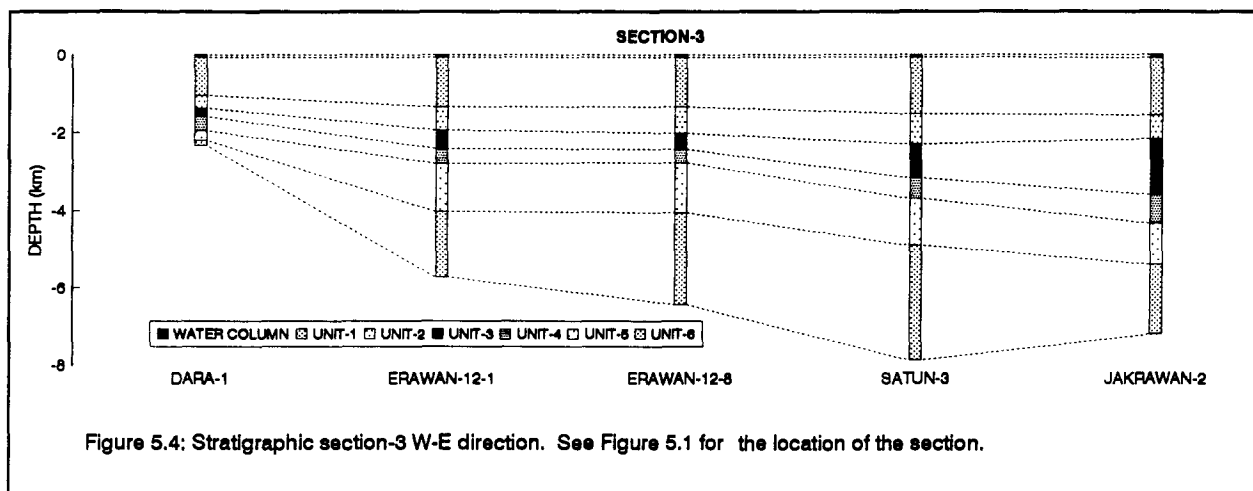


Figure 5.1: Location of well data used in this study. Numbers in the box indicate the cross sections shown in Figures 5.2 through 5.7





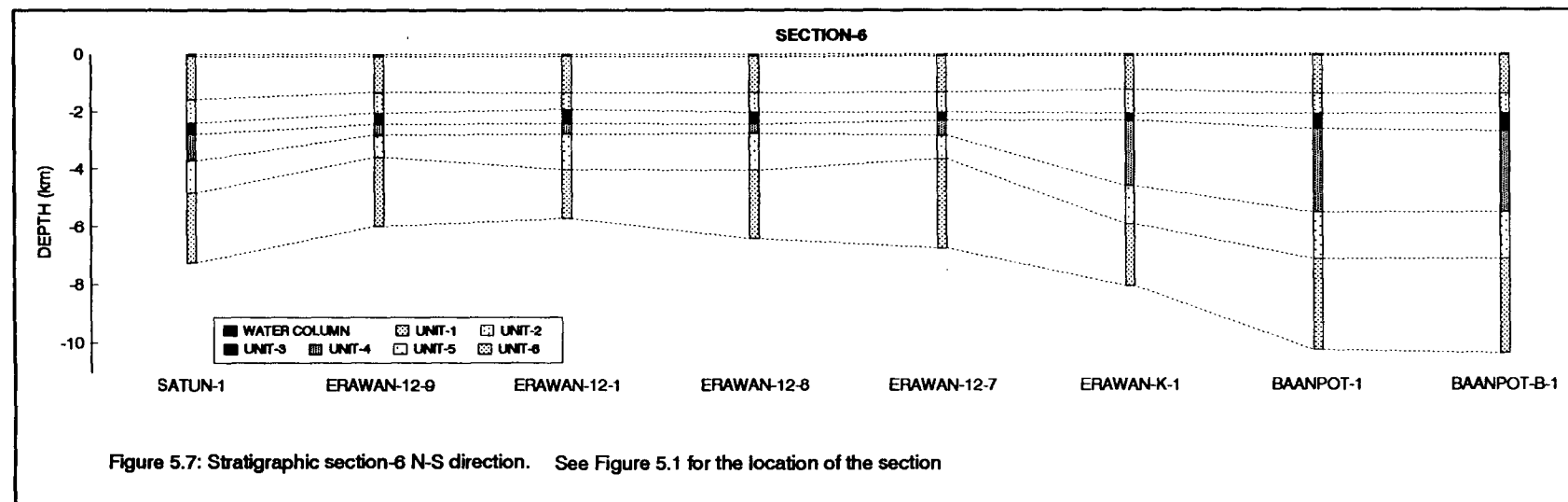
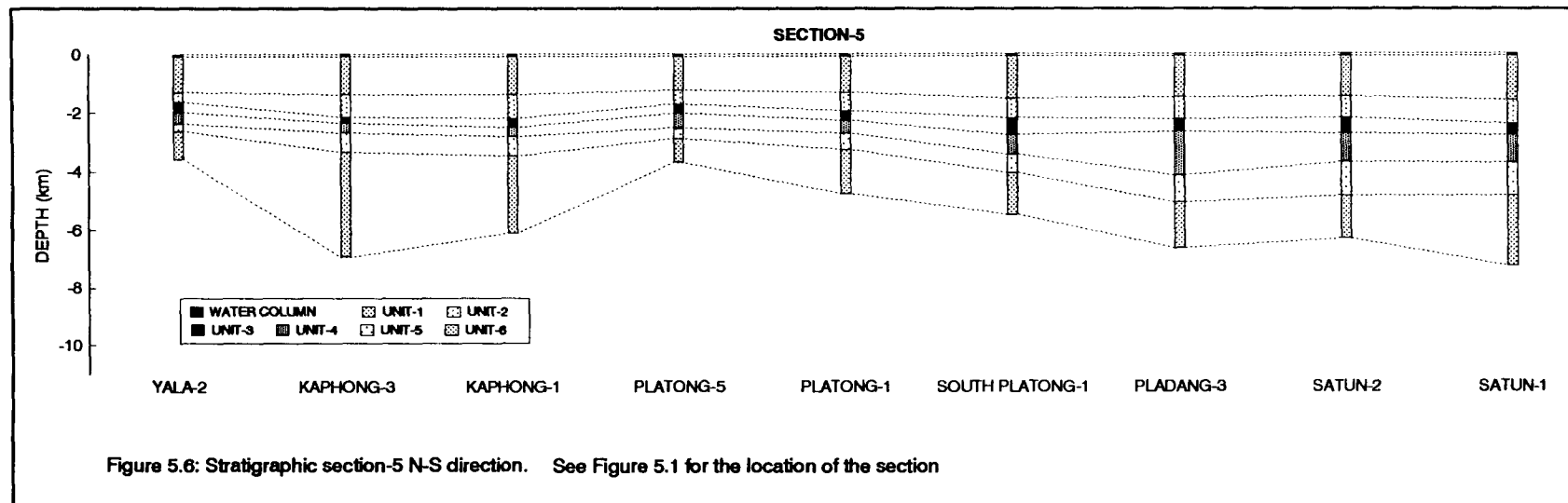


Table 5.3: Stratigraphy and depositional environments of Tertiary strata in the Pattani basin

UNIT	SUBUNIT	DEPOSITION ENVIRONMENTS	SEDIMENTARY STRUCTURES	LITHOLOGY
1	Upper	Shallow marine	Fine-grained	Not available
	Middle	Interdistributary bay and/or crevasse channel	Generally fine-grained	Dark grey claystone
	Lower	Distributary channel in a coastal plain	Fining-upward sequences	Reddish brown claystone and sandstone
2	Upper	Brackish swamp and marginal marine	Generally fine-grained with some fining-upward sequences	Brownish grey claystone and sandstone
	Lower	Distributary channels and floodplain	Fining-upward sequences and fine-grained	Sandstone and claystone
3	Upper	Nonmarine meandering channel	Fining-upward sequences and fine-grained	Sandstone and minor claystone
	Middle	Distributary mouth bar and beach ridge complex	Coarsening-upward sequences	Sandstone and claystone
	Lower	Prodelta and shallow marine	Generally fine-grained	Claystone and minor sandstone

Table 5.3 (Continued): Stratigraphy and depositional environments of Tertiary strata in the Pattani basin

UNIT	SUBUNIT	DEPOSITION ENVIRONMENTS	SEDIMENTARY STRUCTURES	LITHOLOGY
4	Upper	Upper delta plain and floodplain	Generally fine-grained with fining-upward sequences	claystone and sandstone
	Middle	Distributary mouth bar and beach ridge complex	Coarsening-upward sequences	White sandstone and minor claystone
	Lower	Prodelta and shallow marine	Generally fine-grained	brownish claystone with coal partings
5	Upper	Nonmarine meandering channel	Fining-upward sequences	brownish sandstone
	Lower	Meandering channel and floodplain	Generally fine-grained and fining-upward sequences	Red claystone and sandstone
6	Upper	Floodplain and channel	Fine-grained and fining-upward sequences	Sandstone and greyish brown claystone
	Lower	Alluvial fan and braided stream	Coarse-grained and poorly sorted	Conglomerate and coarse-sand

by a subsequent phase of slow, post-rift, thermal subsidence. The rifting phase which lasted about 20 m.y. (from Late Eocene to Early Miocene) was recorded in synrift sediments which comprise two nonmarine sedimentary successions (stratigraphic units 6 and 5) and one regressive package (stratigraphic unit 4). The following post-rift phase comprises one regressive sedimentary package (unit 3) and two transgressive successions (unit 2 and unit 1).

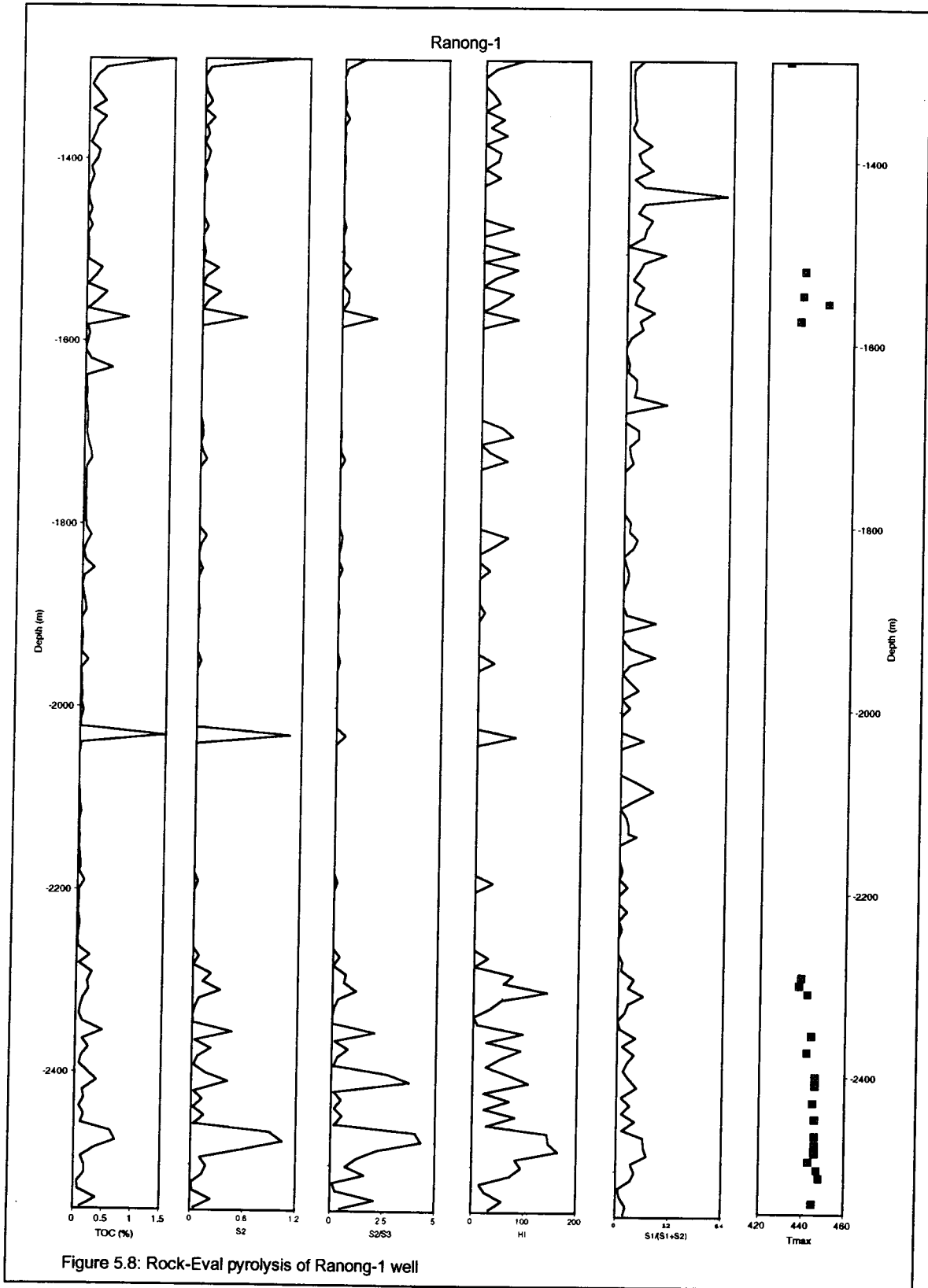
The stratigraphic unit 6, Late Eocene to Early Oligocene age, is characterized by coarse-grained, alluvial fan and braided stream sediments in the lower subunit and fine-grained, floodplain-channel deposits in the upper subunit. Unit 5, Late Oligocene to Early Miocene age, is characterized by fine-grained, floodplain deposits in the lower subunit and somewhat coarser-grained, meandering channel deposits in the upper subunit. A brief transgression which occurred at the end of unit 5 deposition (early part of Early Miocene) caused a short period of nondeposition which marked the boundary between unit 5 and unit 4. The succeeding sedimentary succession (unit 4, Early Miocene age) represents a coarsening-upward regressive sequence which is characterized by fine-grained, prodelta to shallow marine deposits in the lower subunit; coarse-grained, distributary mouth bar deposits and beach complexes in the middle subunit; and coarse- to fine-grained, nonmarine floodplain-meandering channel deposits in the upper subunit.

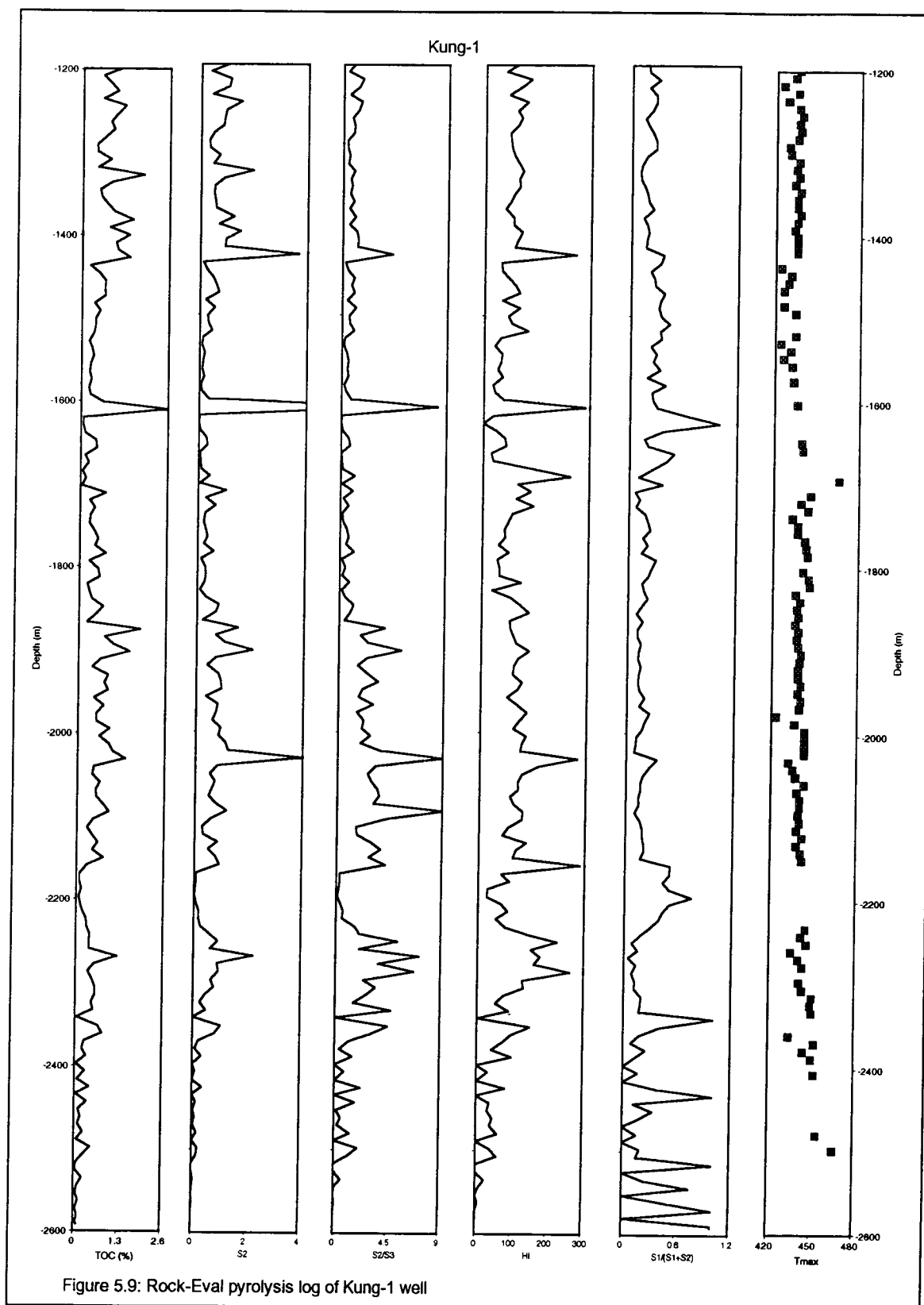
By the end of sedimentation of unit 4 (Early Miocene, about 20 Ma), the Pattani Basin became tectonically quiescent, its post-rift thermal subsidence was slow. The sedimentation was controlled mainly by the amount of sediment influx and eustatic sea level fluctuation. The post-rift sediments comprise one regressive sedimentary package (unit 3) and two transgressive packages (units 2 and 1). A brief and rapid

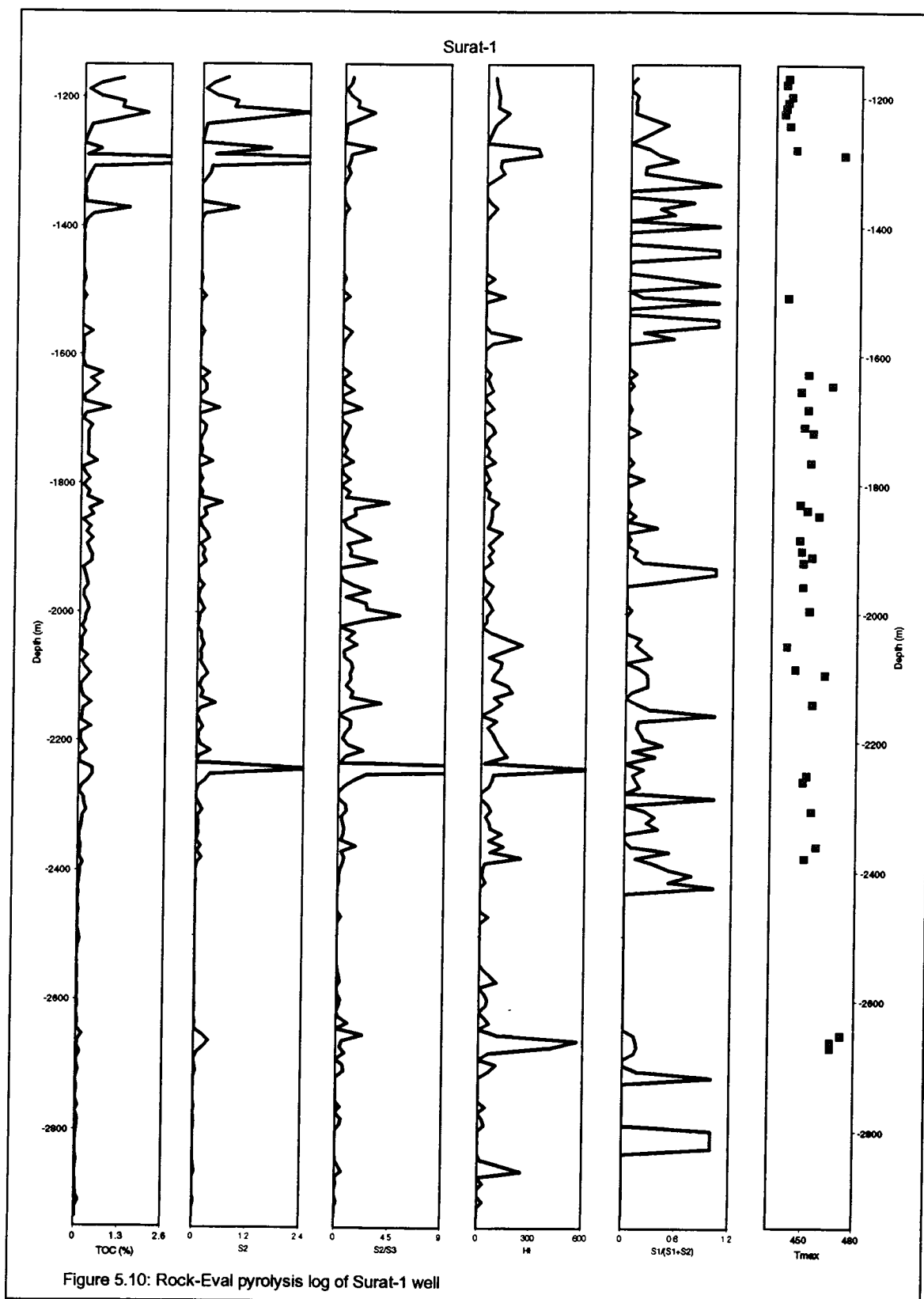
transgression occurred again at the base of unit 3 (Early Miocene, about 20 Ma) and caused a brief period of nondeposition which marked the boundary between unit 4 and unit 3. A coarsening-upward regressive succession of unit 3 (Early to Middle Miocene age), which followed a brief transgression, is characterized by fine-grained, prodelta to shallow marine-shelf deposits in the lower subunit; coarse-grained, distributary mouth bar deposits and beach complexes in the middle subunit; and coarse- to fine-grained, nonmarine floodplain-meandering channel deposits of the upper subunit. Unit 2 (Middle Miocene age) represents a broad transgressive succession which is characterized by coarse-grained, nonmarine meandering channel and floodplain deposits in the lower subunit and fine-grained interdistributary bay complexes and marginal marine deposits in the upper subunit. At the end of Middle Miocene, a rapid regression occurred in the Pattani Basin, probably as a result of rapid eustatic sea level fall, causing subaerial exposure, oxidation, and probable minor erosion of unit 2 sediments. Unit 1 (Late Miocene to Pleistocene age) records the latest transgressive succession and is characterized by the basal coarse-grained, nonmarine, distributary channel deposits of the lower subunit; fine-grained, brackish water, interdistributary bay deposits and marsh and swamp complexes of the middle subunit; and fine-grained, prodelta to shallow marine deposits of the upper subunit.

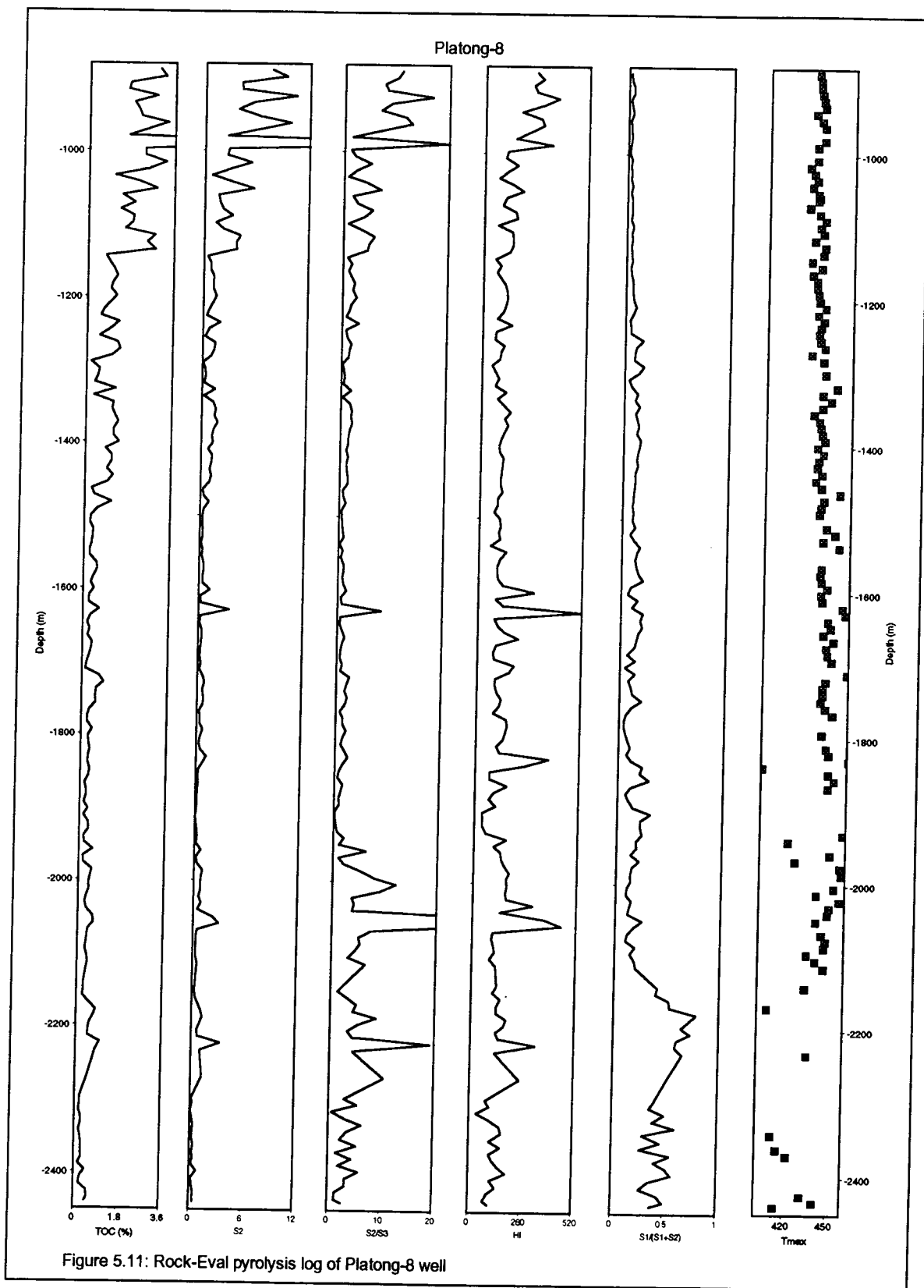
5.5 GENERAL CHARACTERISTICS OF ORGANIC MATTER

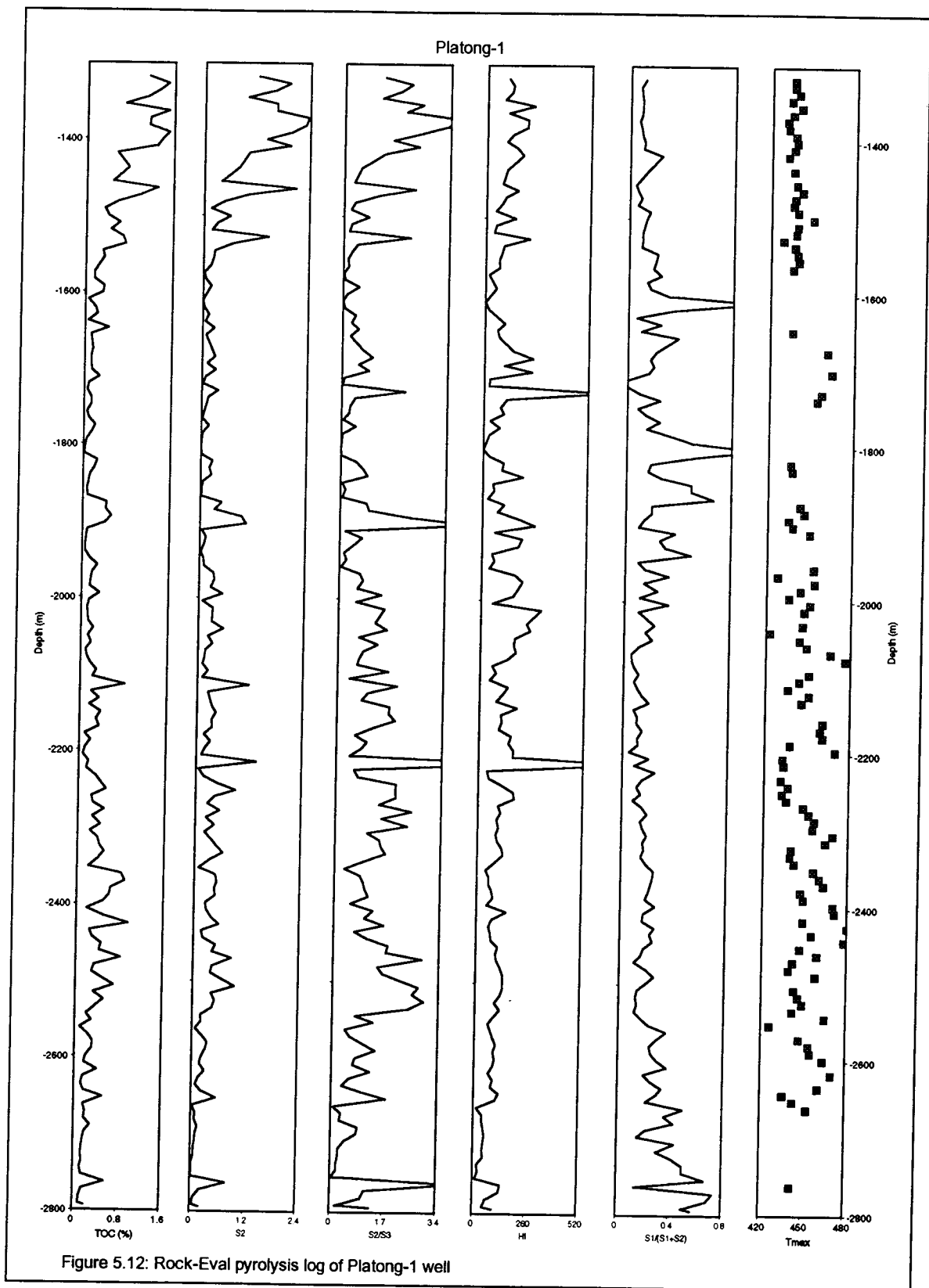
The abundance and type of organic matter in different stratigraphic units and subunits are described in this section. Classification of organic facies and organic matter types are based on the concepts of Tissot and Welte (1984) and Jones (1987), respectively. Rock-Eval log diagrams of well samples are shown in Figure 5.8 to Figure 5.37. The modified Van Krevelen diagrams (HI versus OI plots) of

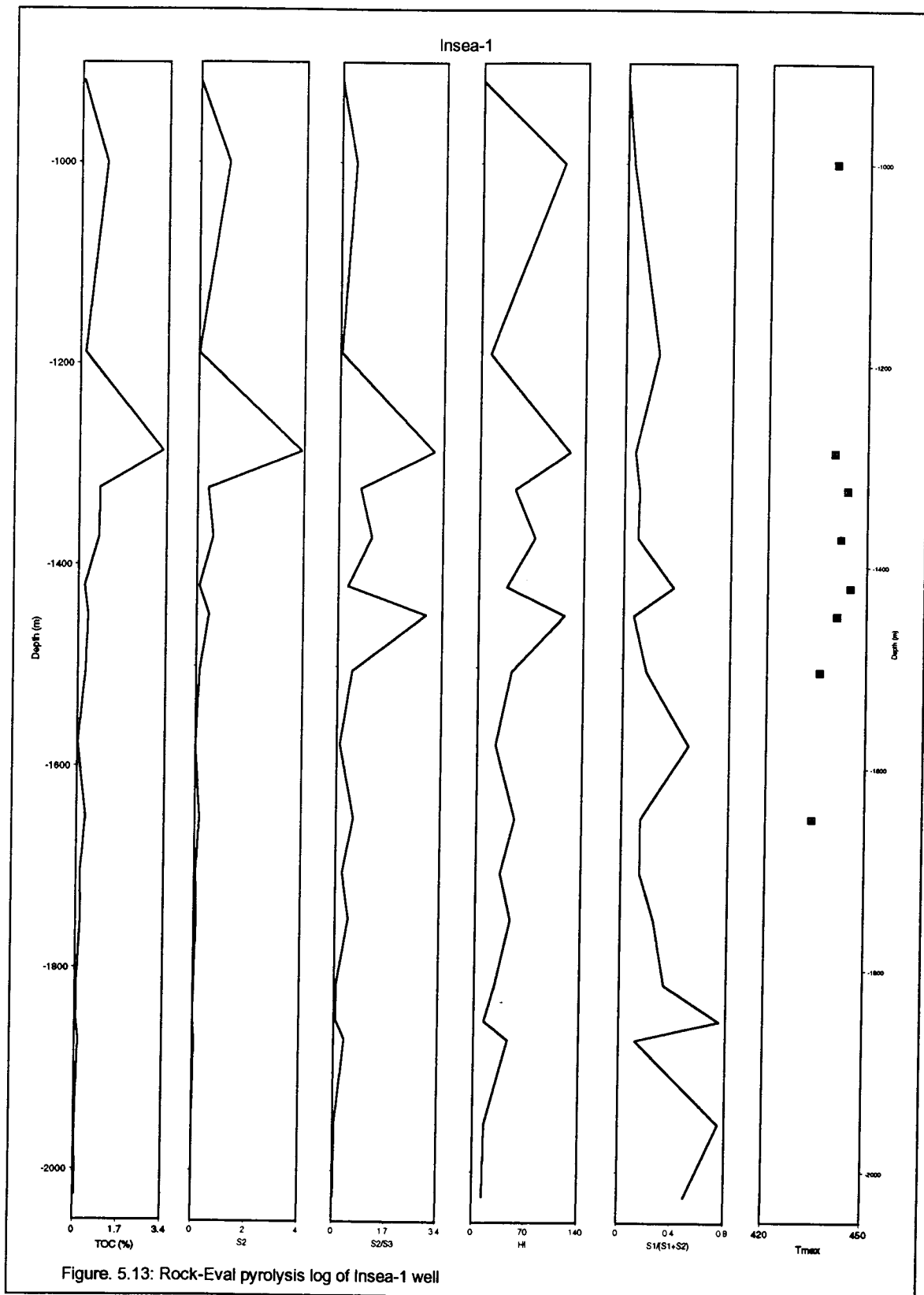


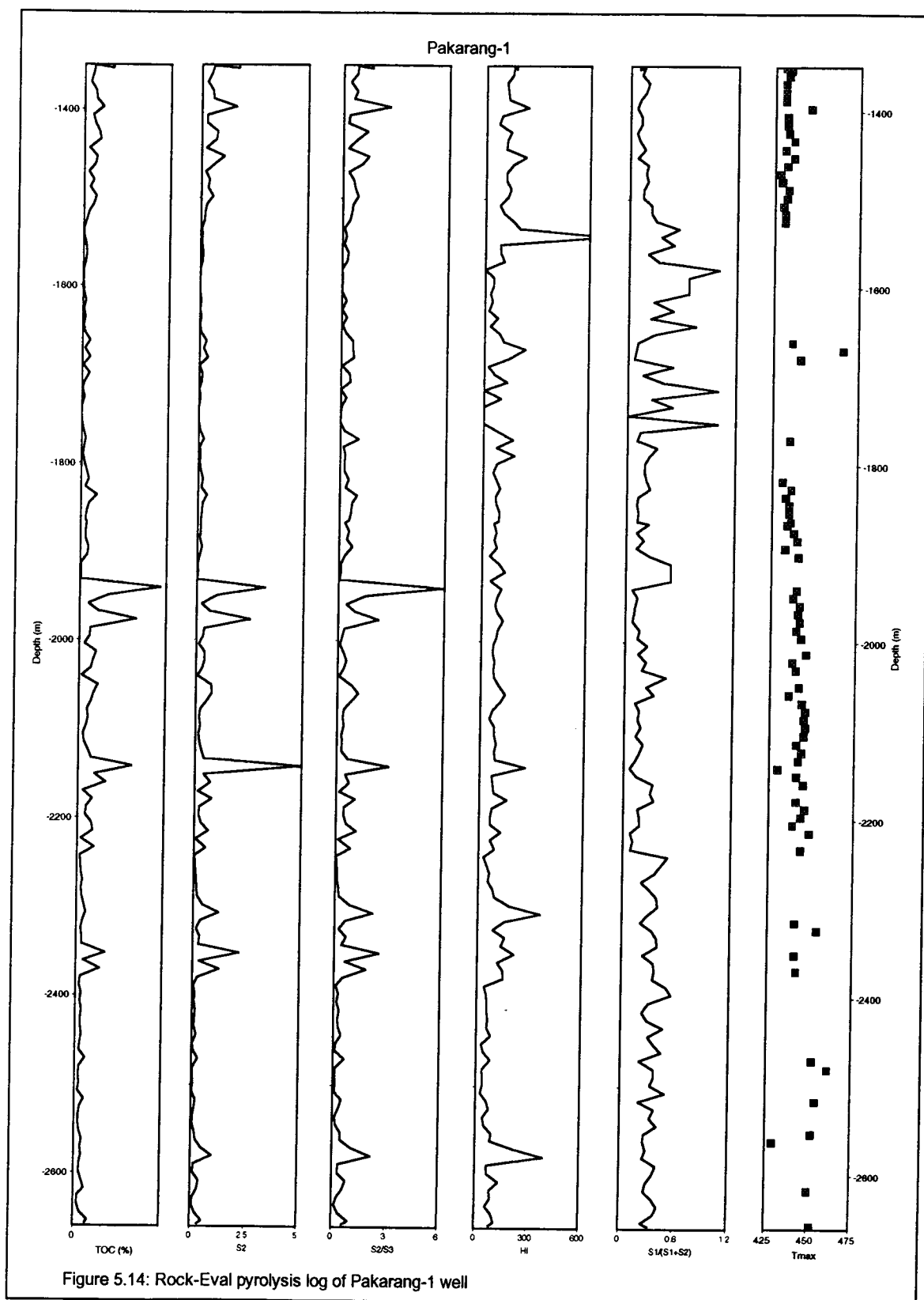


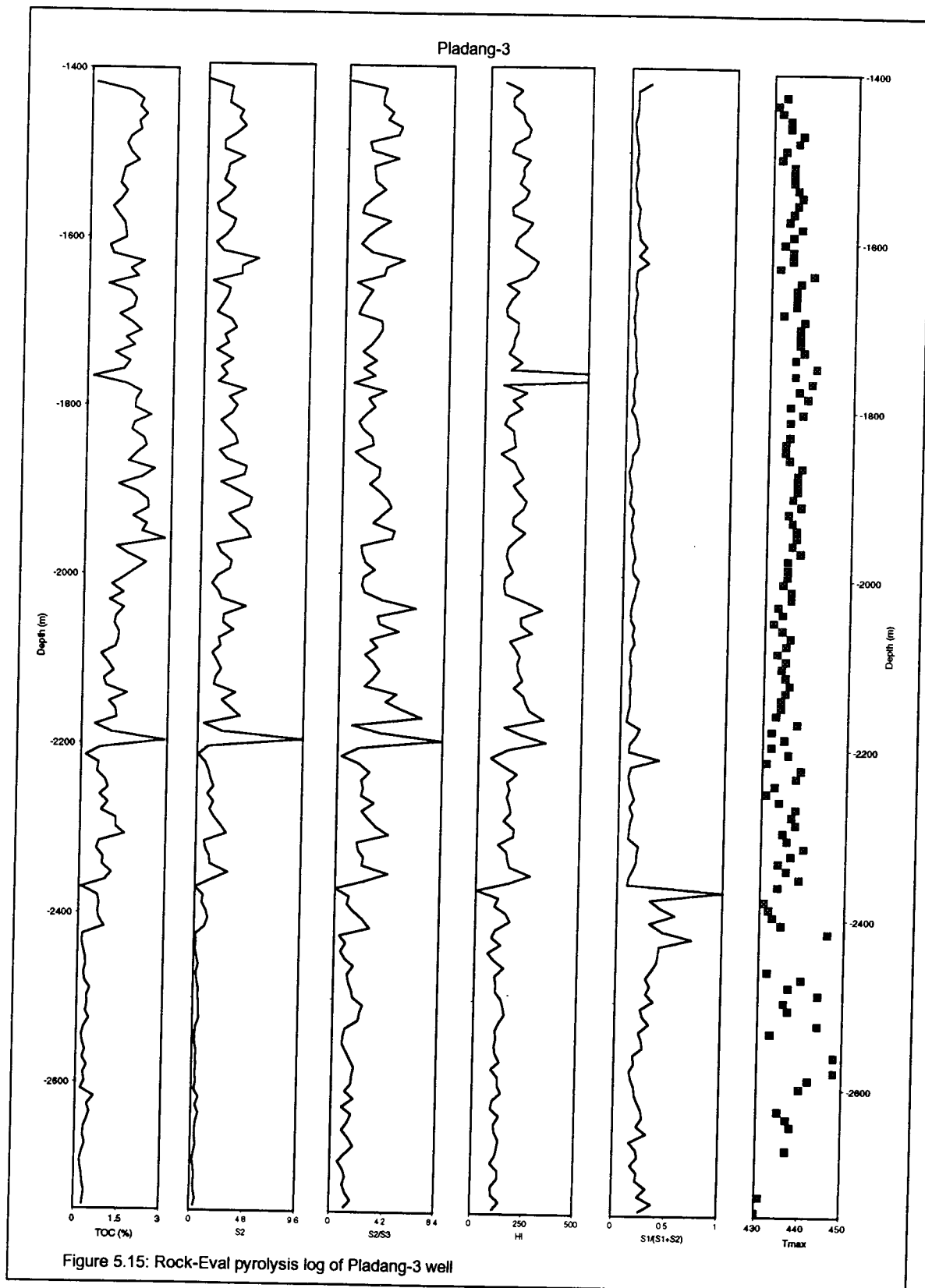


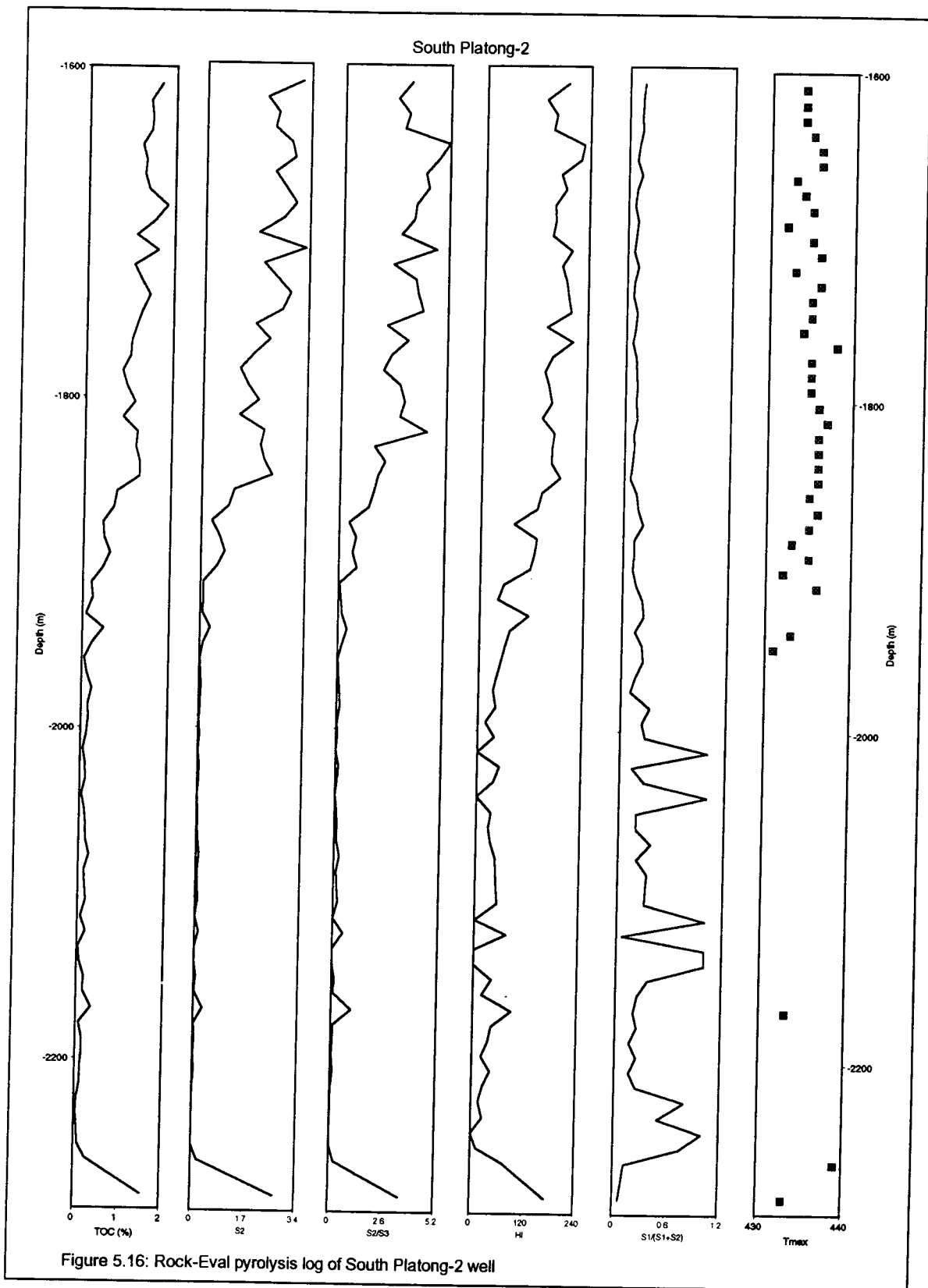


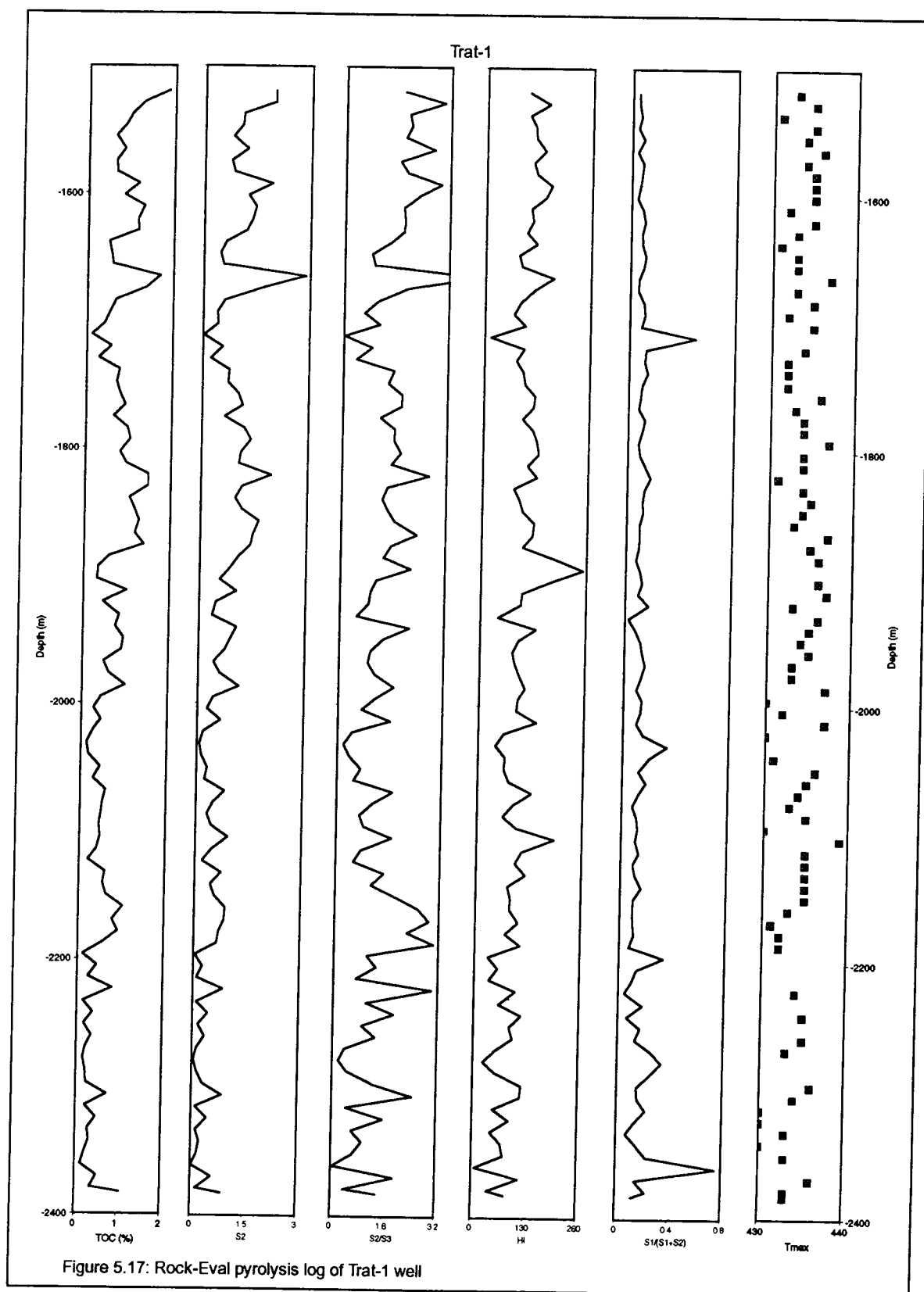


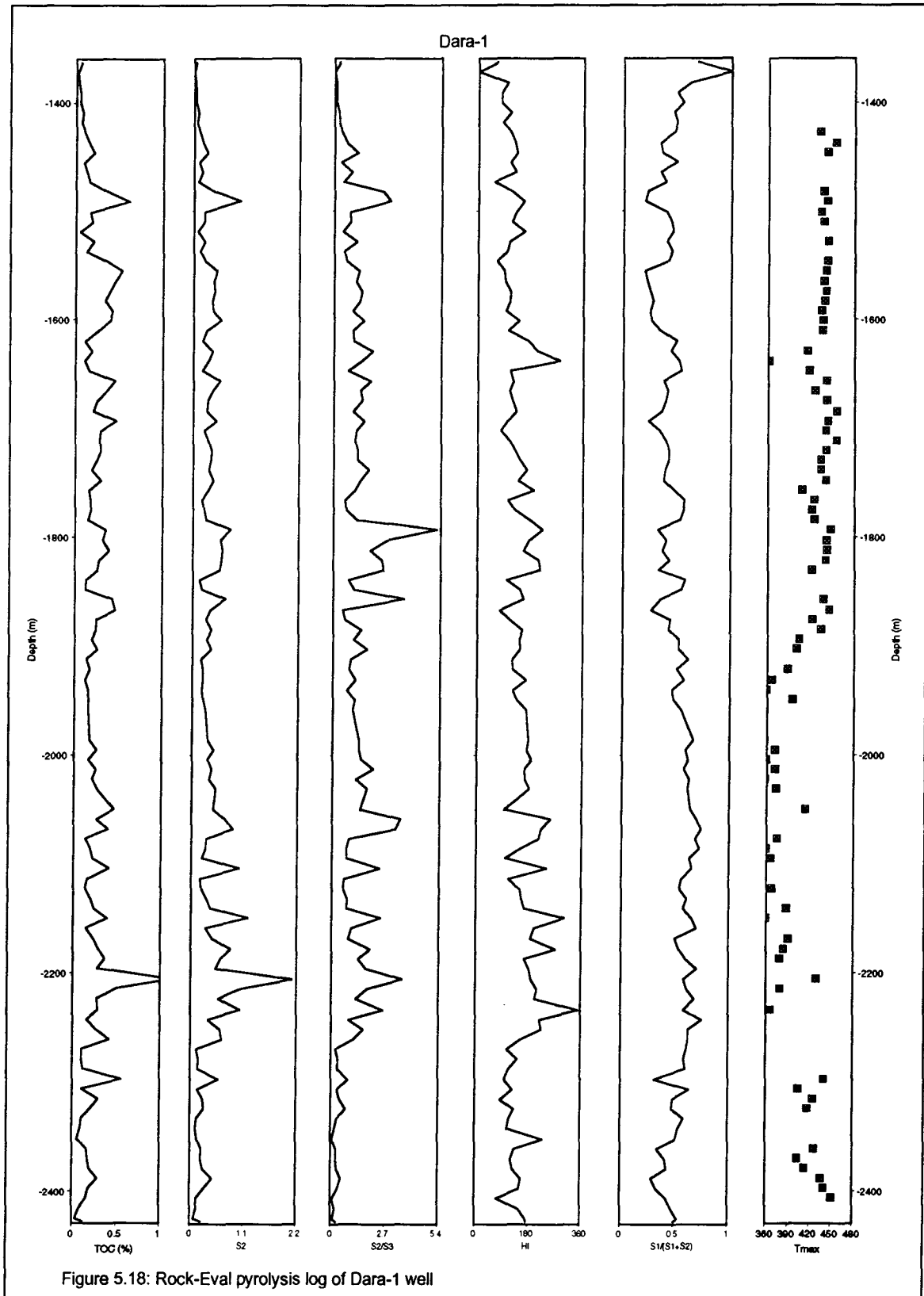


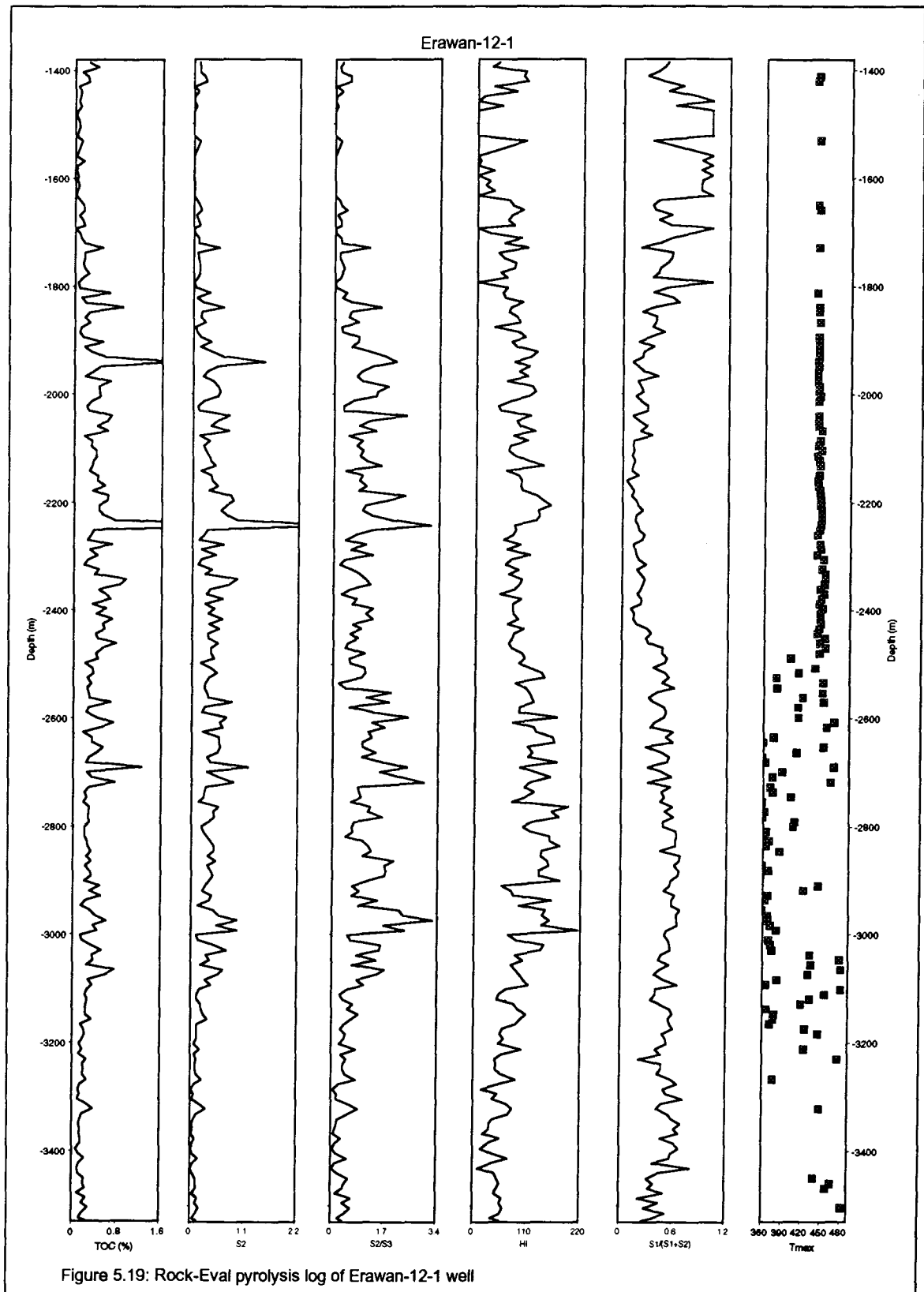


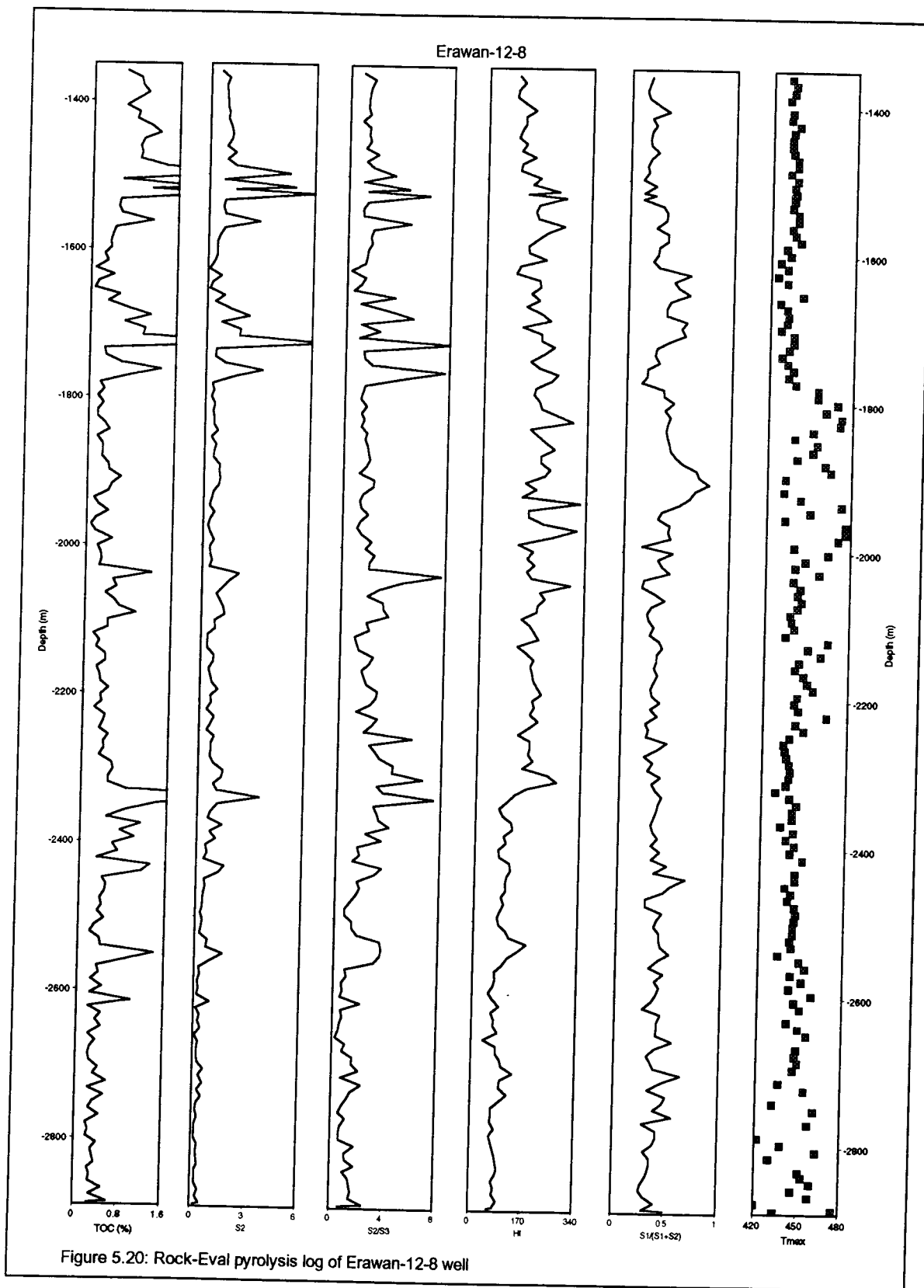


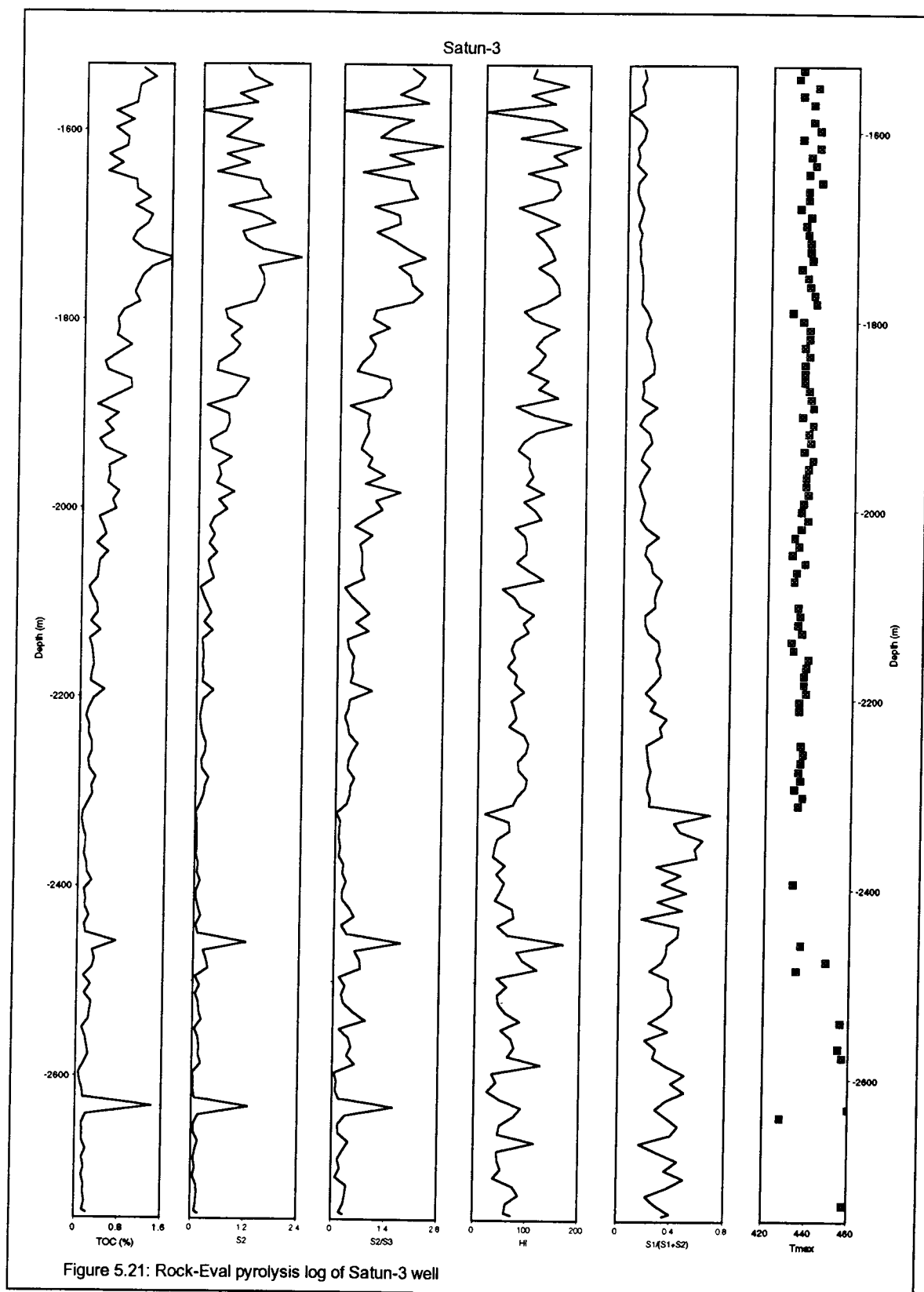


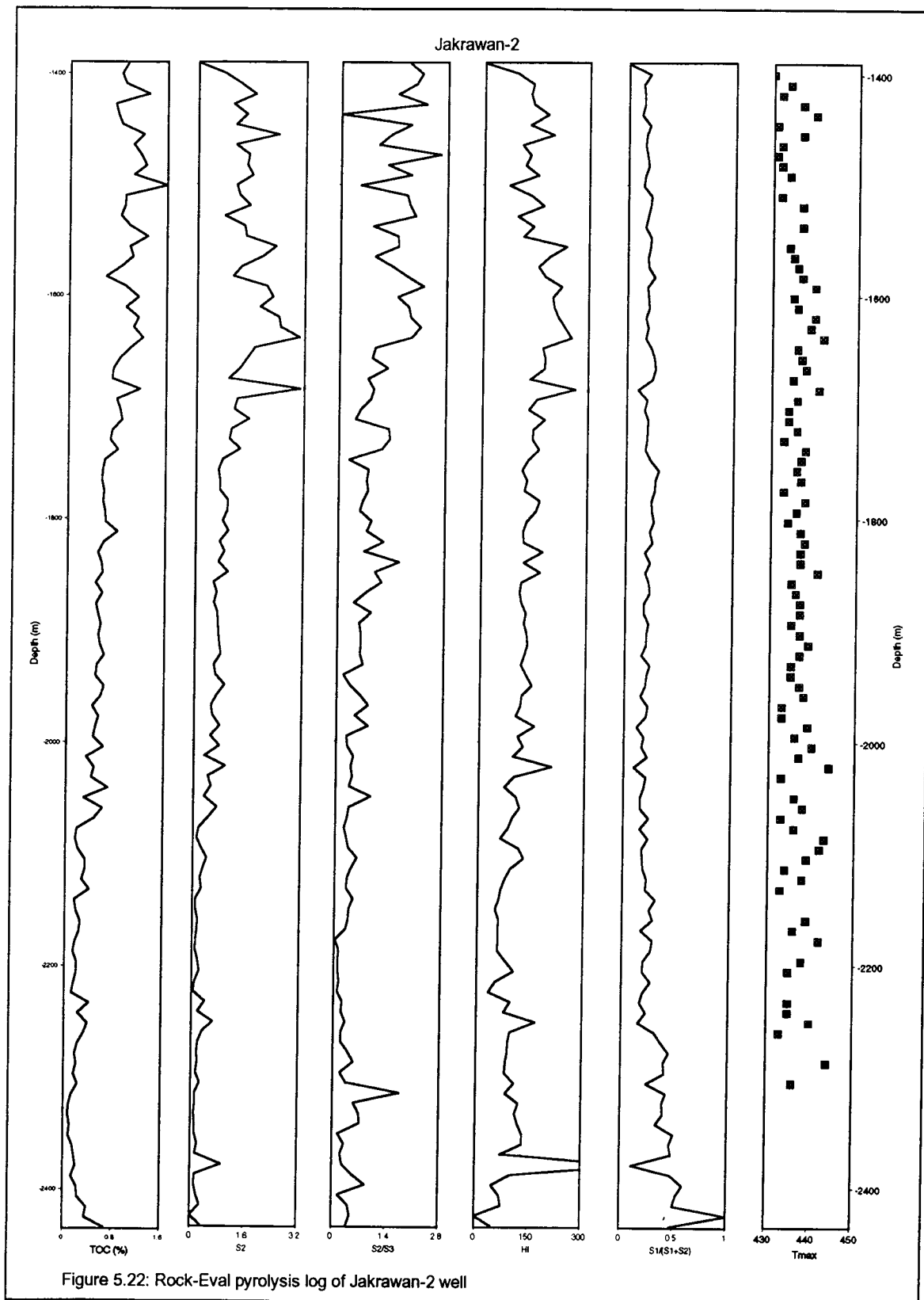


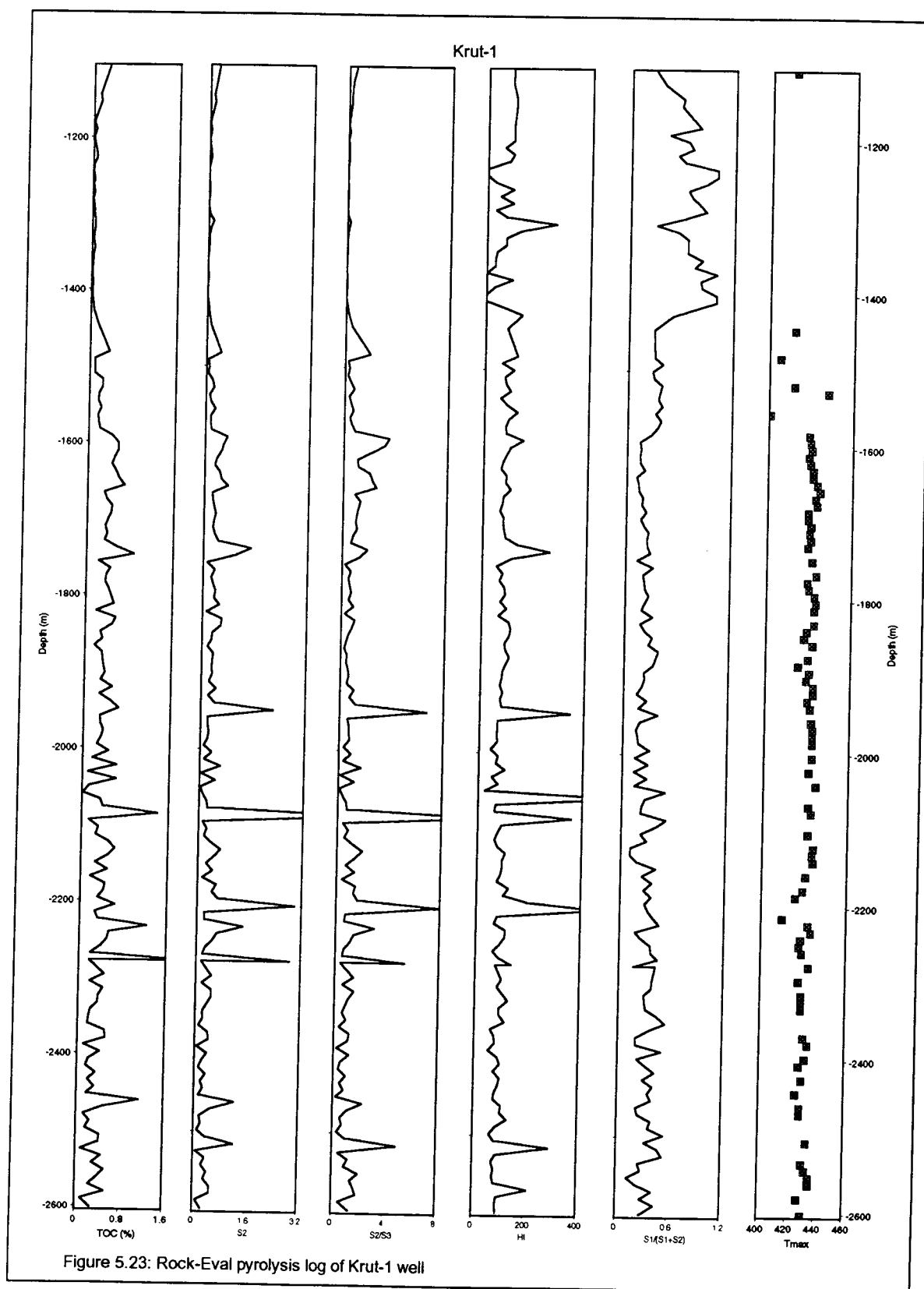


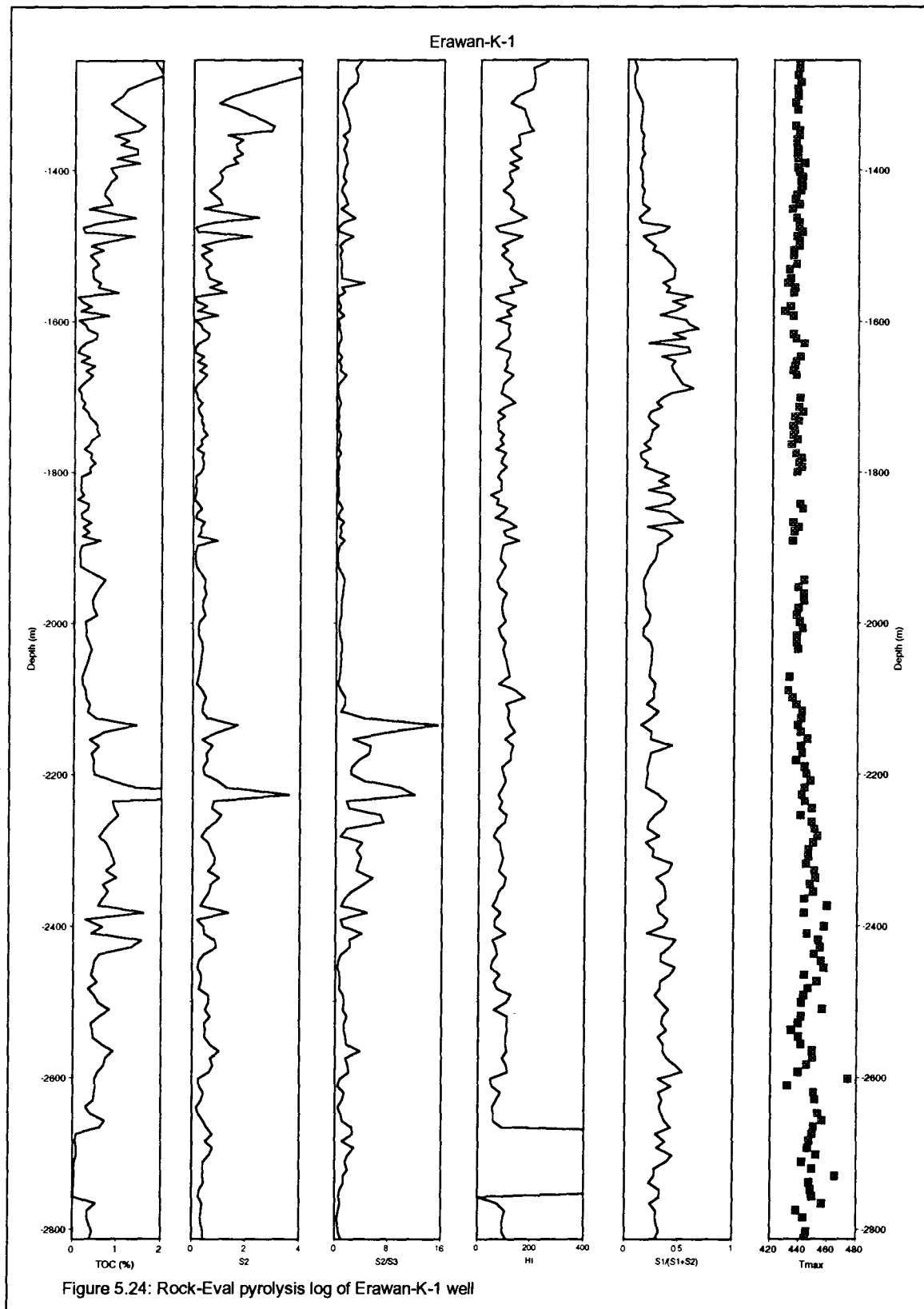


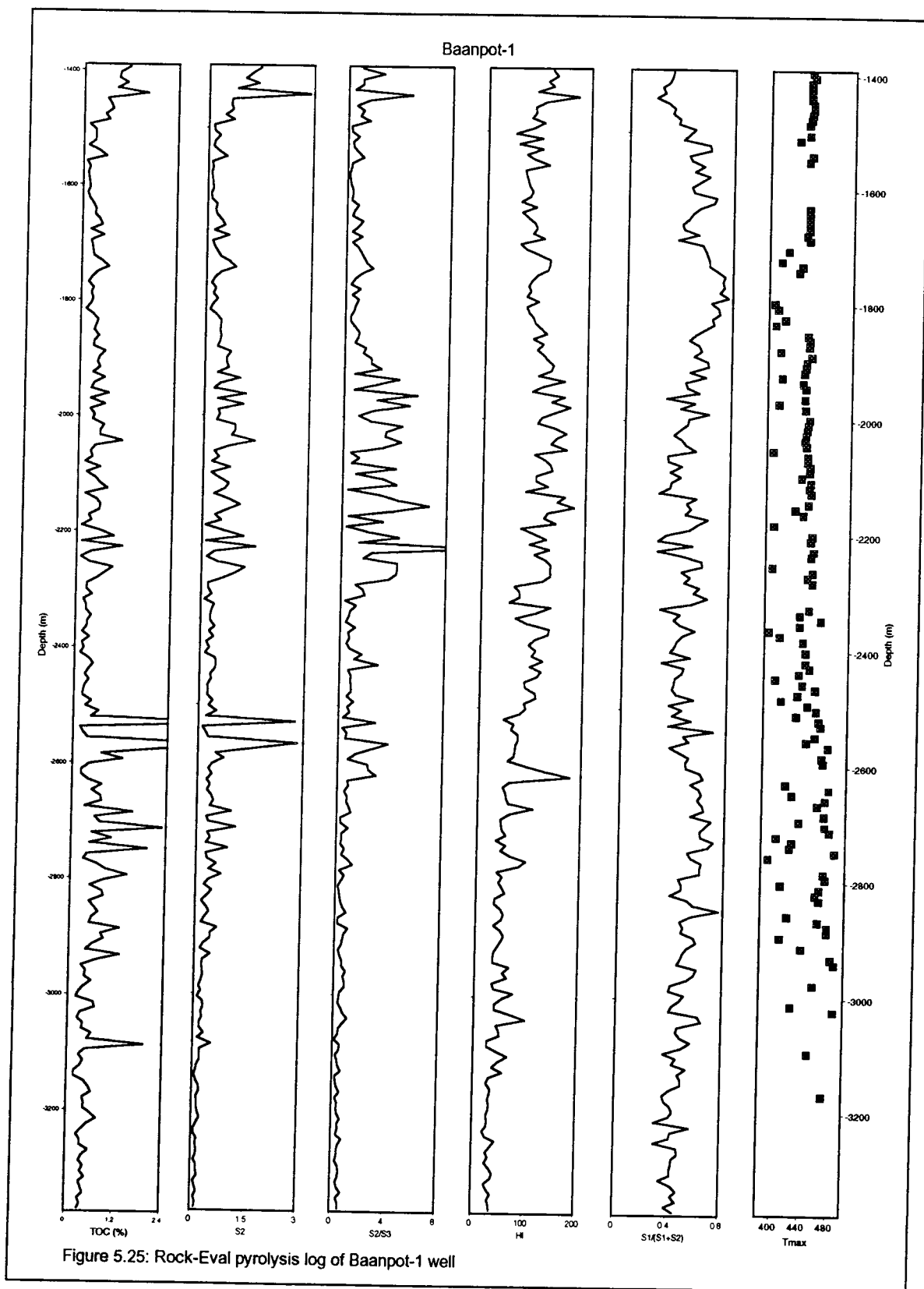


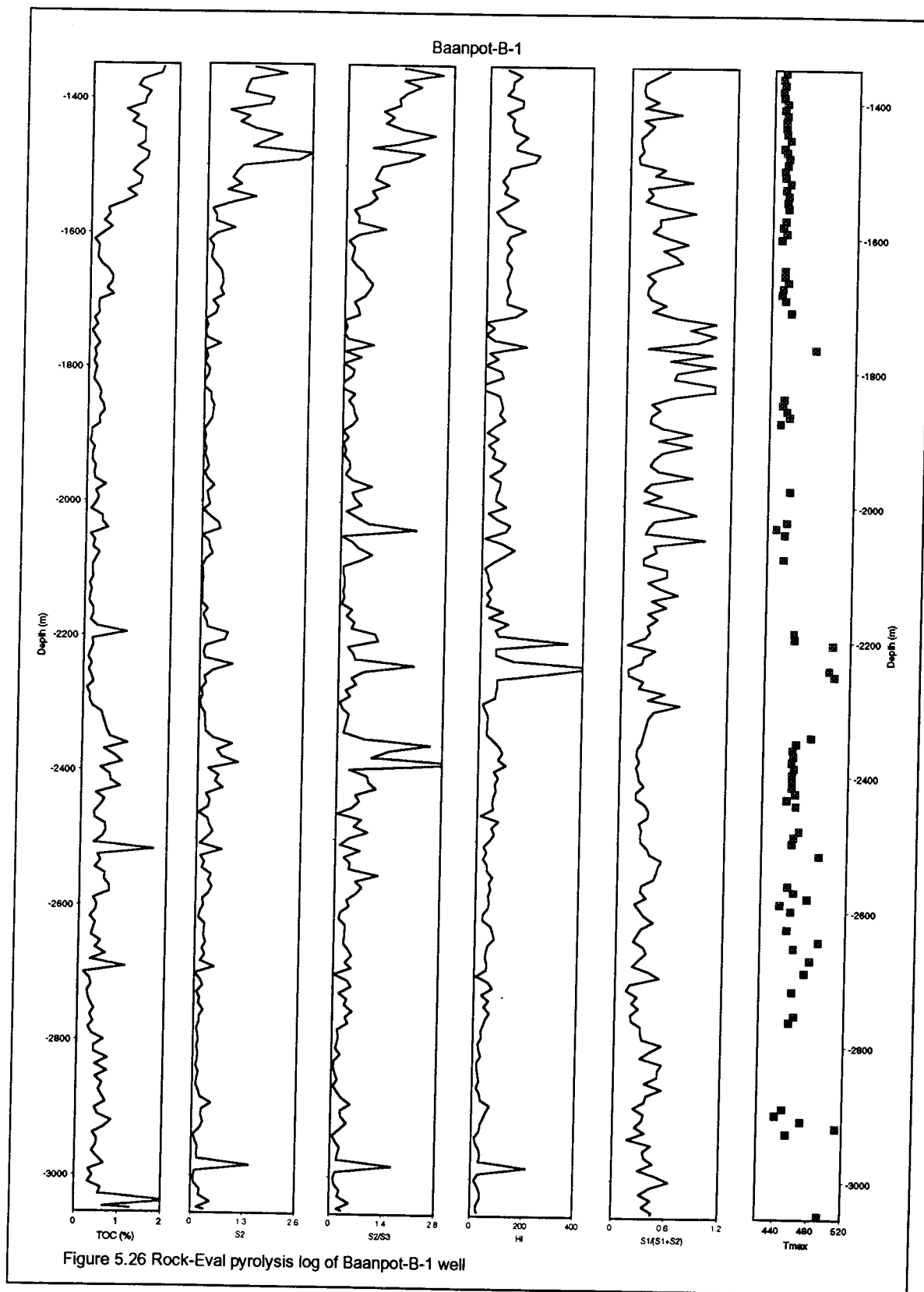


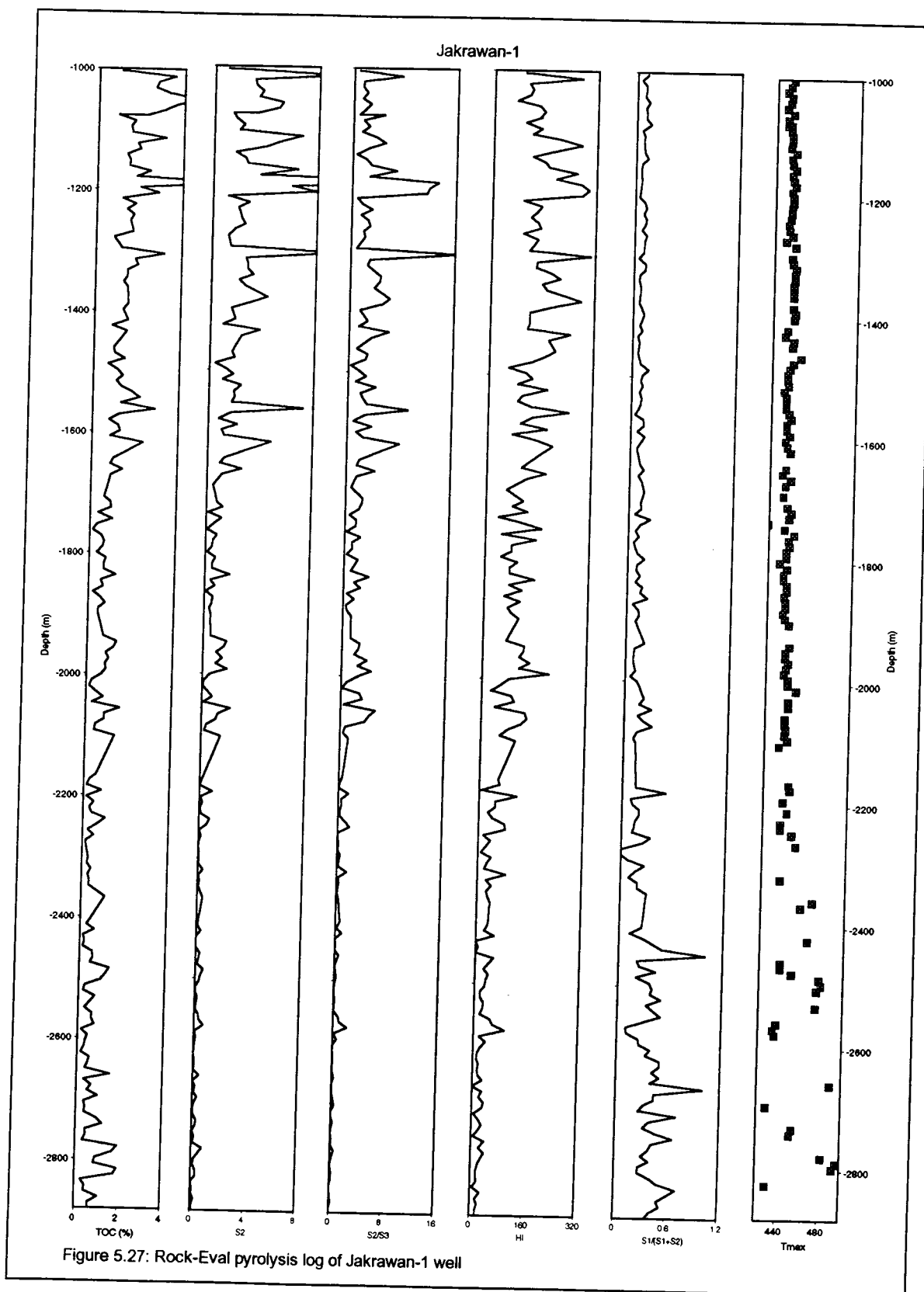


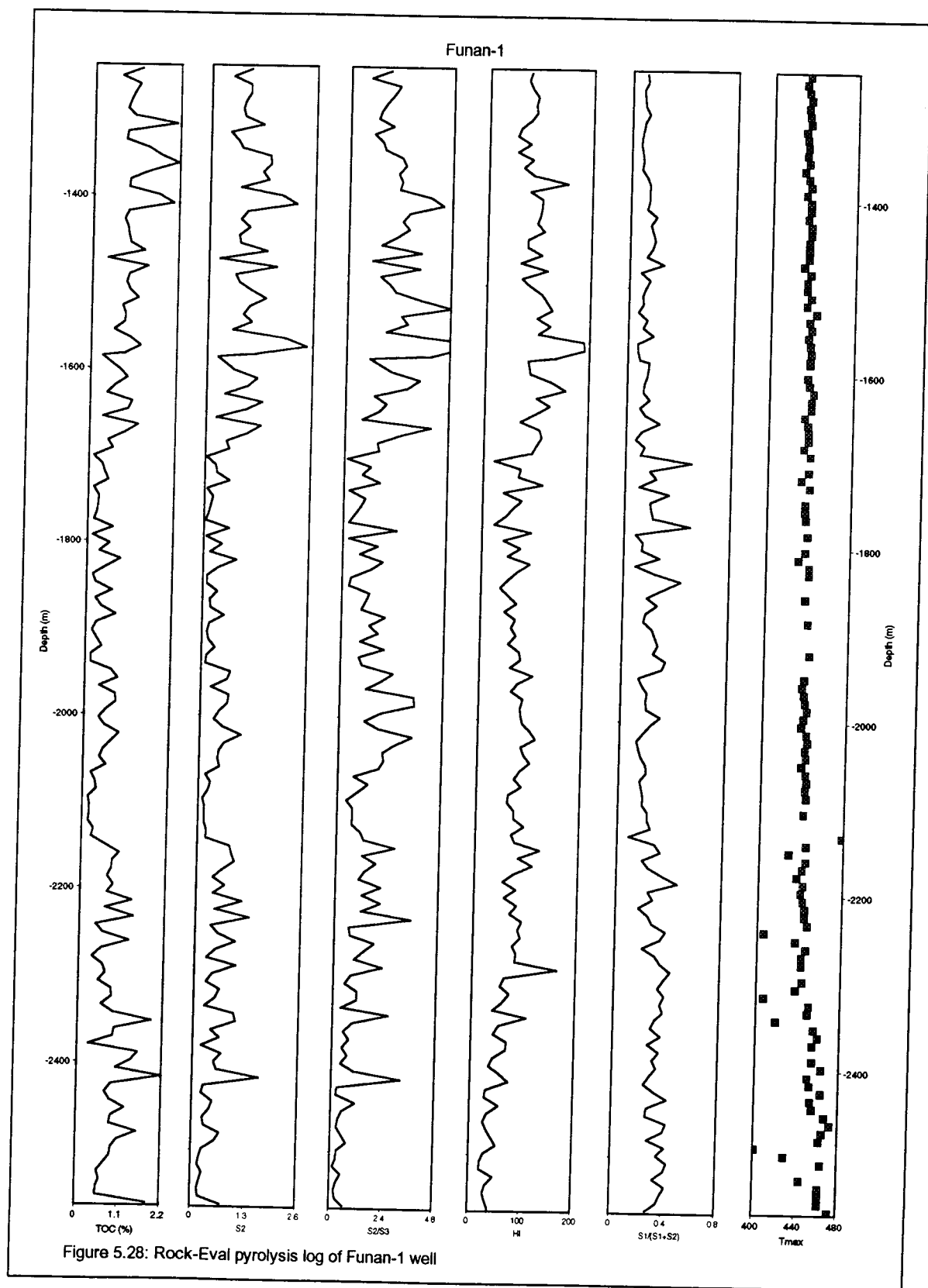


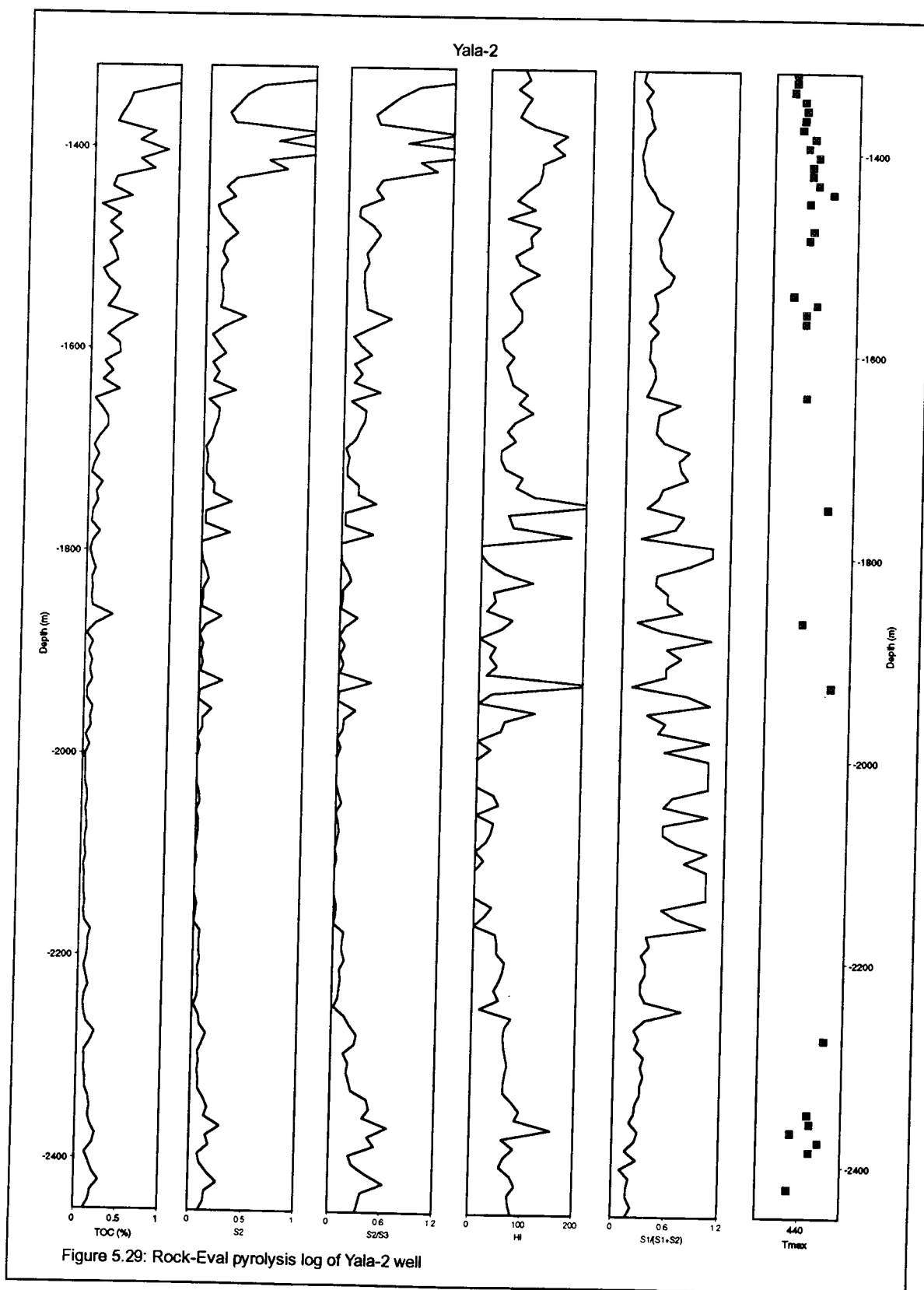


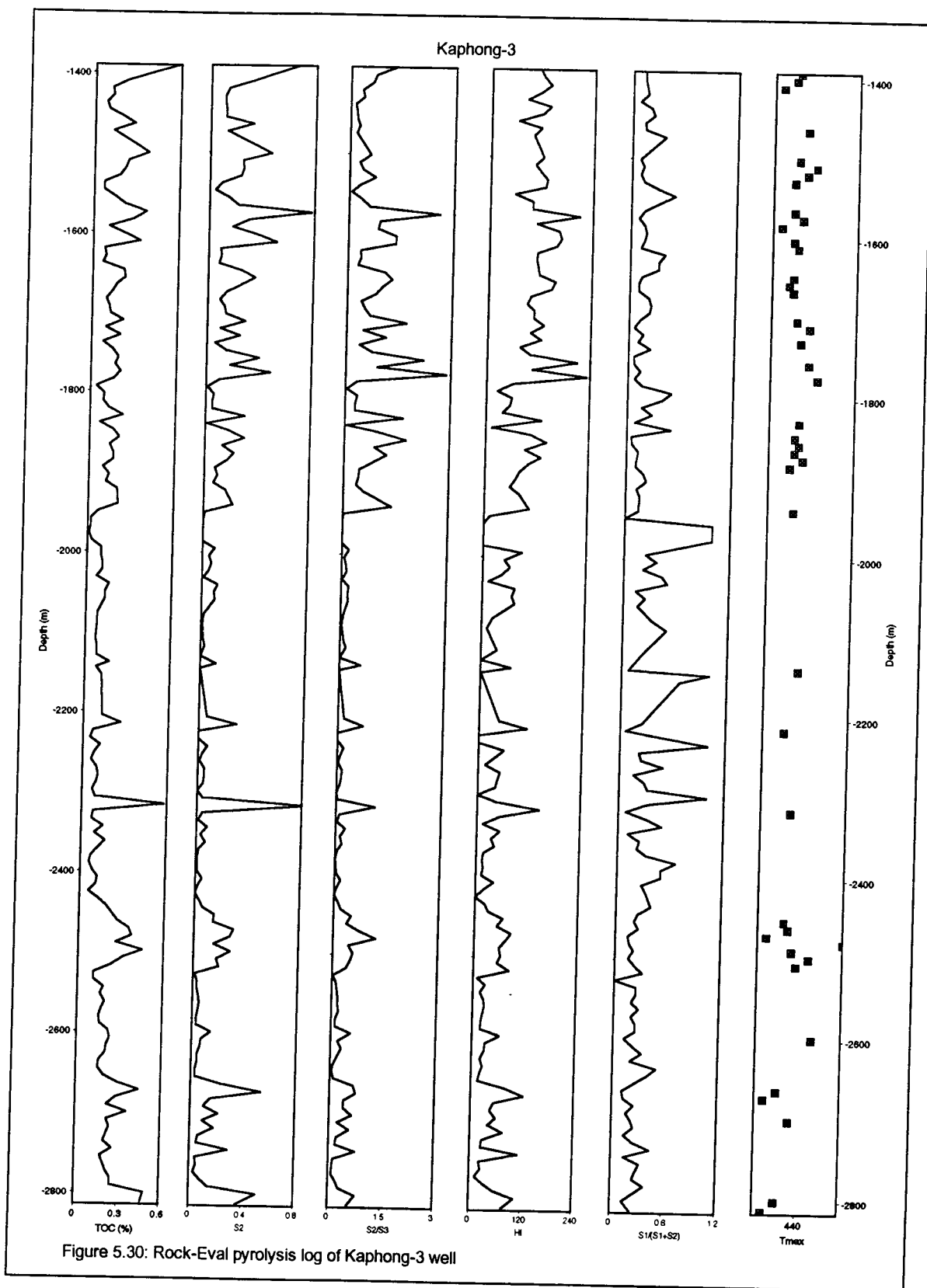


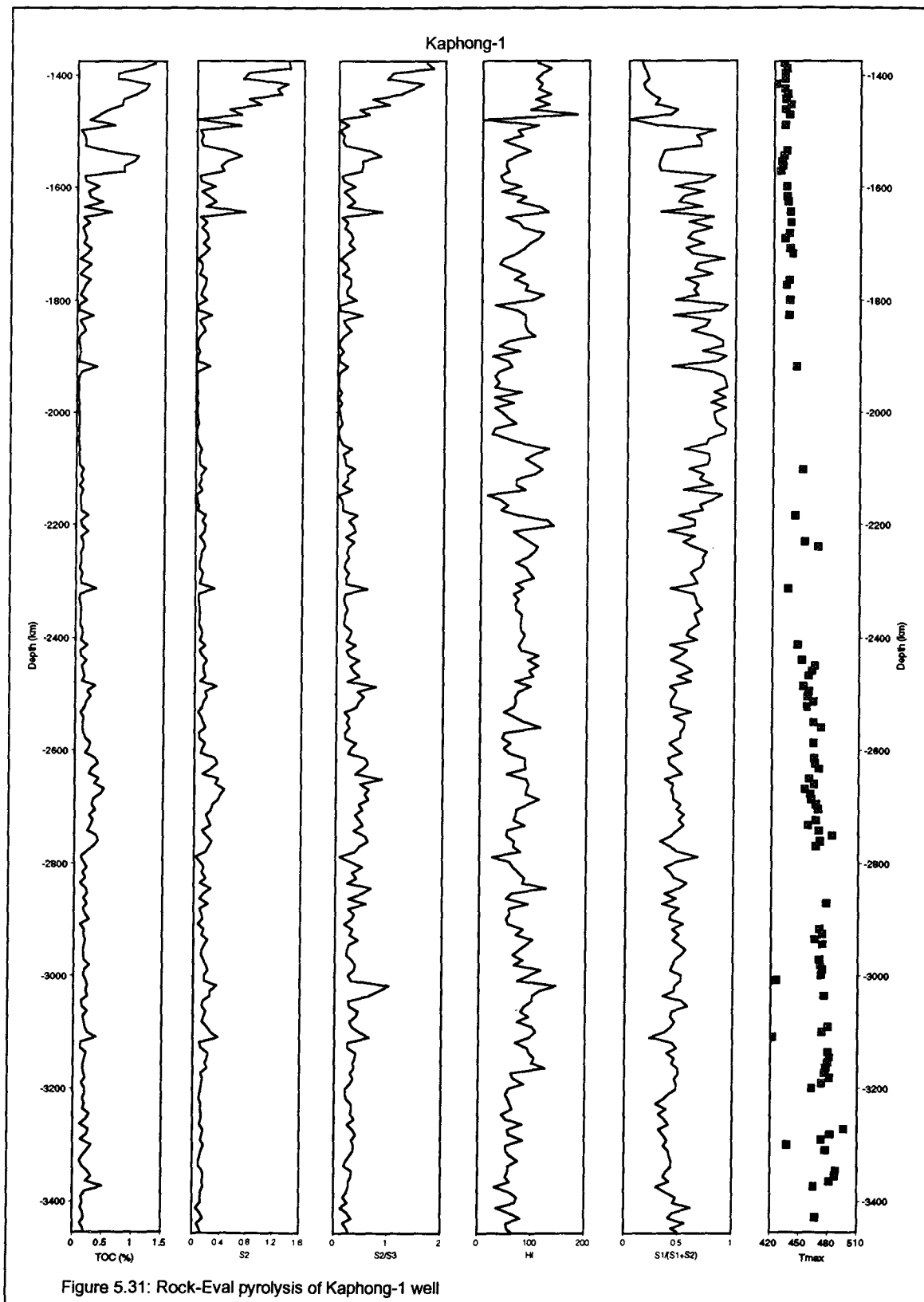


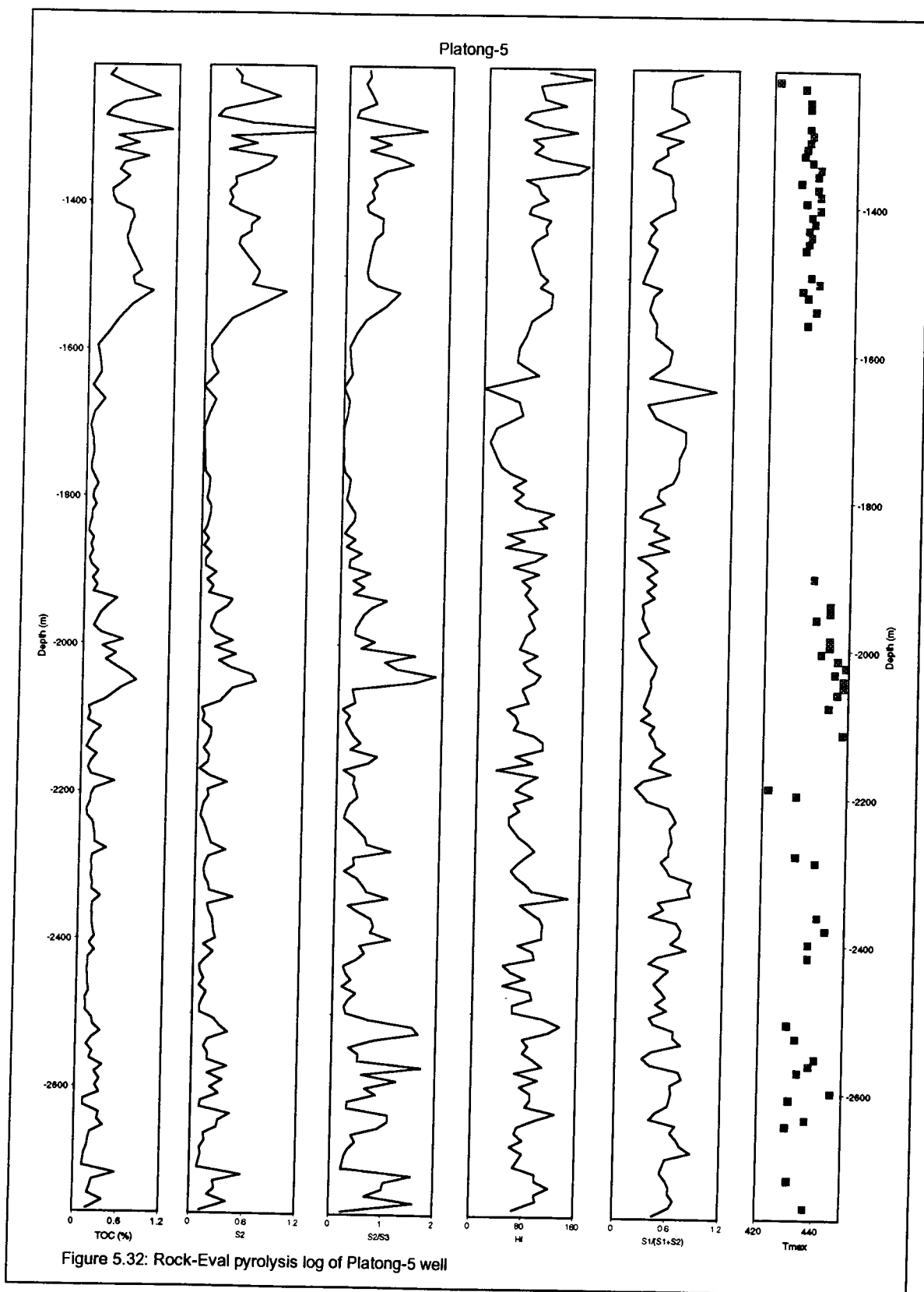


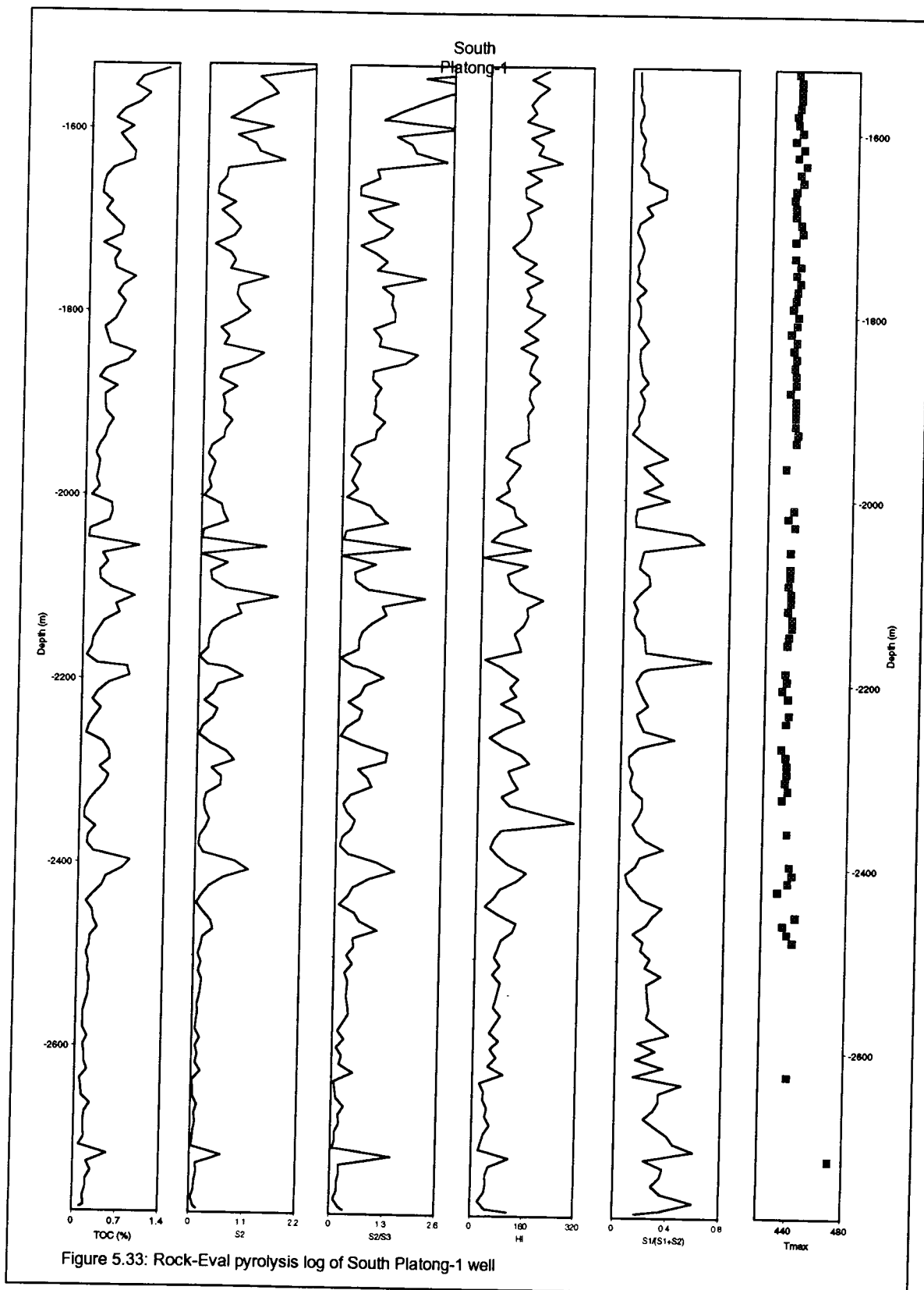


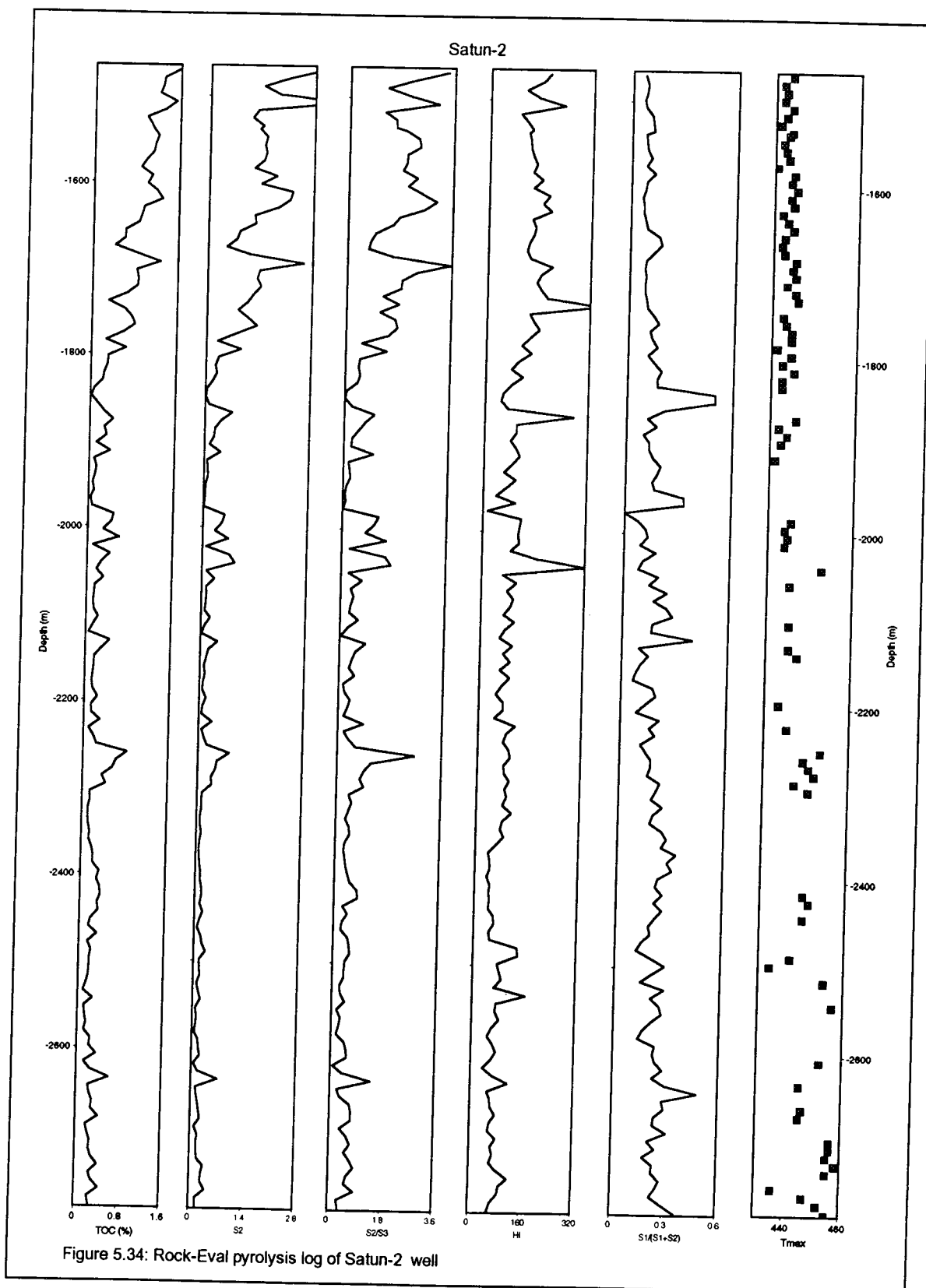


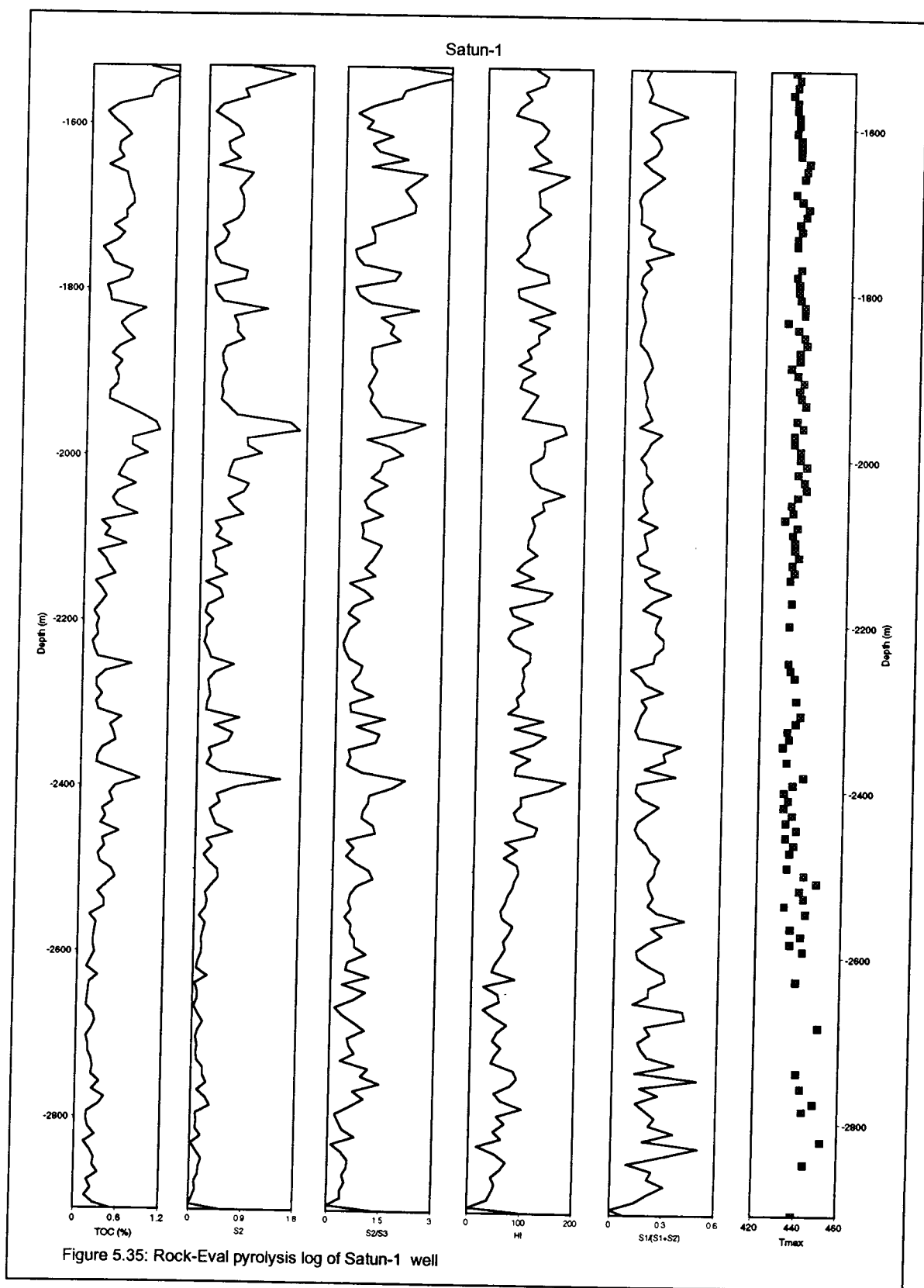


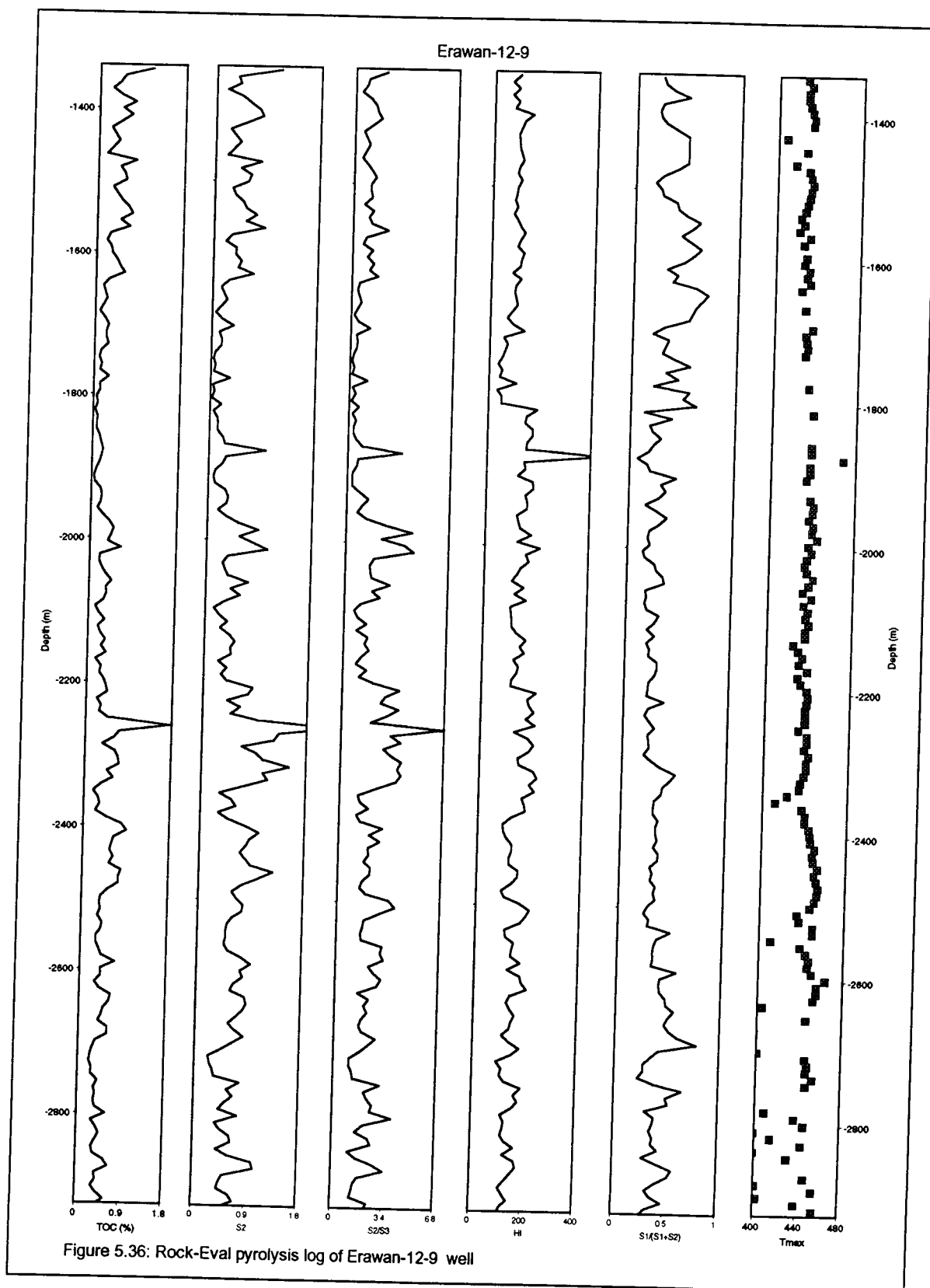


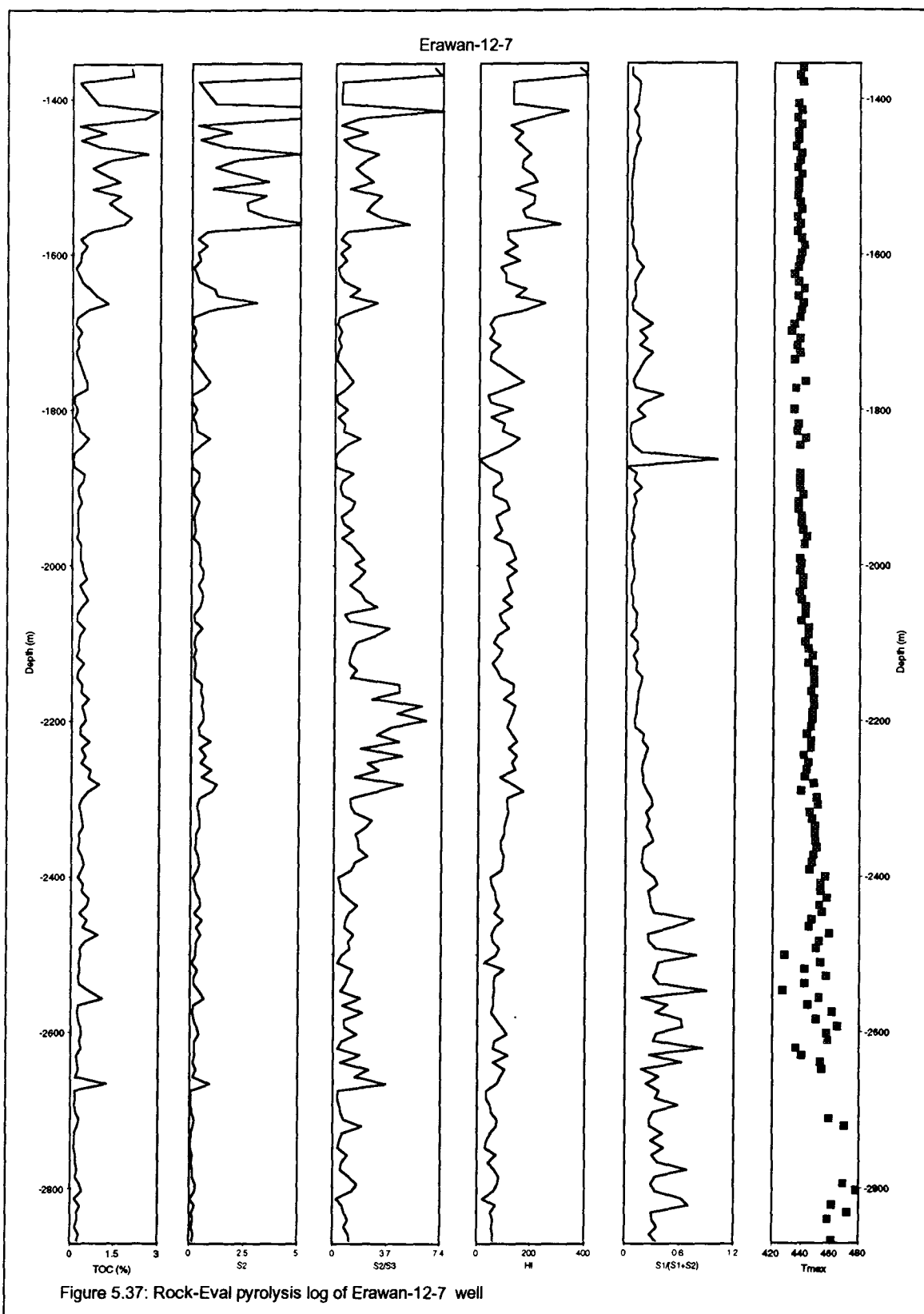












different subunits are shown in Figure 5.38 through Figure 5.51. Table 5.4 and Table 5.5 summarize the classification of specific stratigraphic units and subunits, respectively. The lateral variation of organic richness (TOC) for specific stratigraphic units and subunits are shown in Figure 5.52 through Figure 5.65. The lateral variation of the relative quality of organic matter (QOM, $[S_1 + S_2]/\text{TOC}$) is shown in Figure 5.66 through Figure 5.79.

5.5.1 Unit 6

Only a few samples from four wells located in the western part of the basin margin were available for study. Because of limited data, maps showing lateral variations of organic matter in unit 6 were not constructed. This unit is organically lean. The overall average TOC content of unit 6 is 0.20% with the HI value of 80 mg HC/g TOC, the OI of 204 mg CO₂/g TOC, and the QOM of 1.6 mg HC/g rock (Table 5.4). Organic characteristics of lower and upper subunits are described below.

The lower subunit, which is characterized by alluvial fan and braided stream deposits, is very lean in organic matter. It contains about 0.07 %TOC with HI value of 9 mg HC/g TOC, OI value of 247 mg CO₂/g TOC and QOM value of 0.13 mg HC/g rock (Table 5.5). The organic matter of this subunit comprises organic facies D (Type IV OM, Figure 5.38). The maceral composition of this subunit is dominated by vitrinite.

The upper subunit, which is characterized by a series of channel and floodplain deposits, contains approximately 0.22 %TOC with HI value of 87 mg HC/g TOC, OI value of 199 CO₂/g TOC and QOM value of 1.82 mg HC/g rock (Table 5.5). This organic matter consists mainly of organic facies CD and D (Type III-IV and

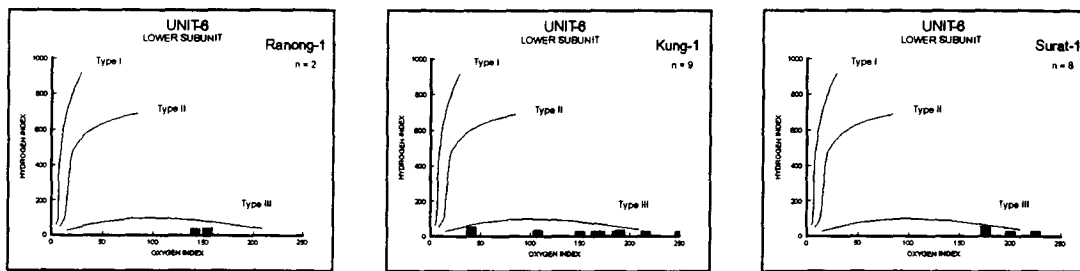


Figure 5.38: Hydrogen index vs. oxygen index for samples from unit 6's lower subunit.

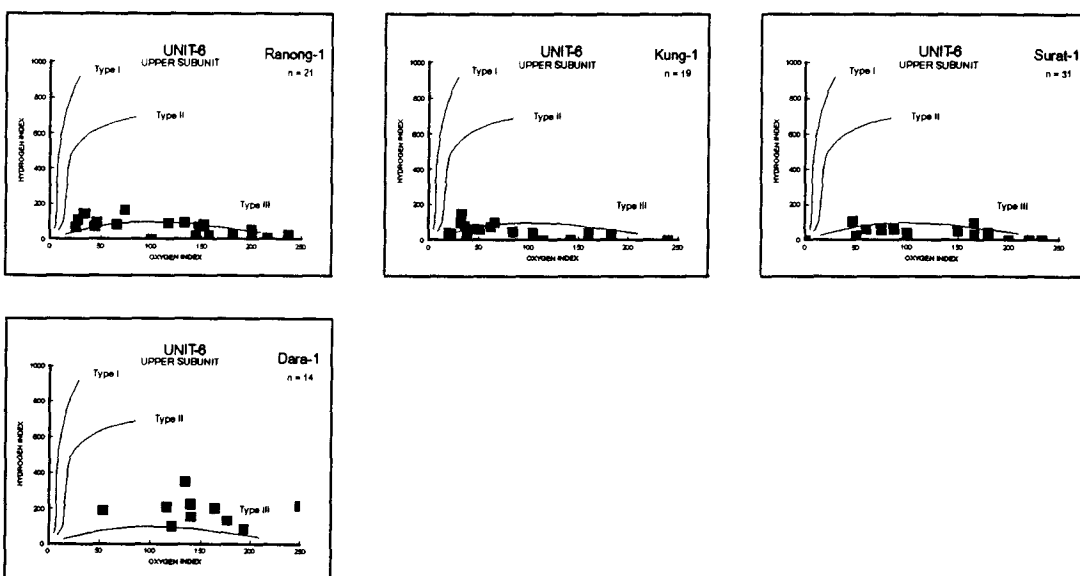


Figure 5.39: Hydrogen index vs. oxygen index for samples from unit 6's upper subunit.

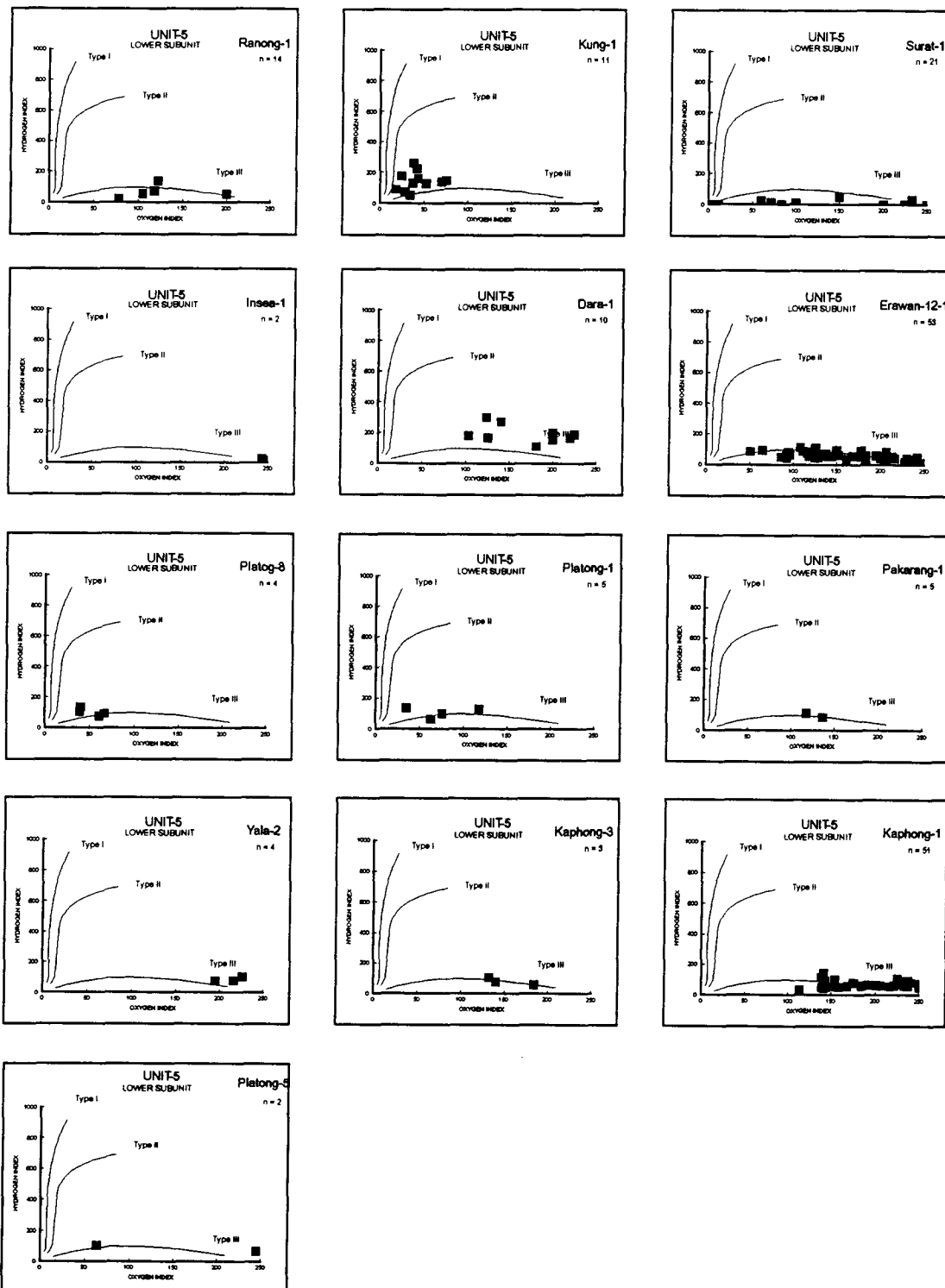


Figure 5.40: Hydrogen index vs. oxygen index for samples from unit 5's lower subunit.

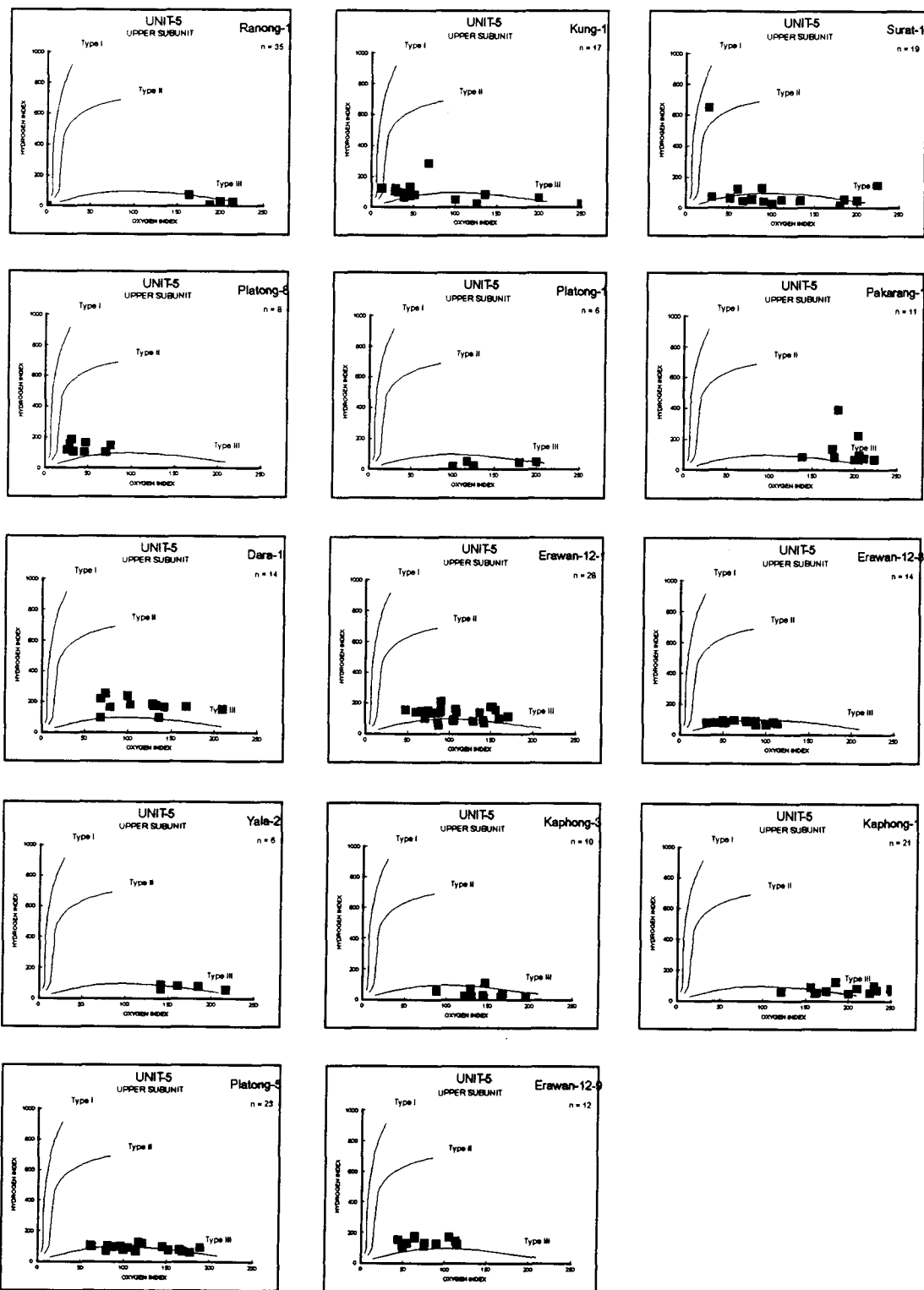


Figure 5.41: Hydrogen index vs. oxygen index for samples from unit 5's upper subunit.

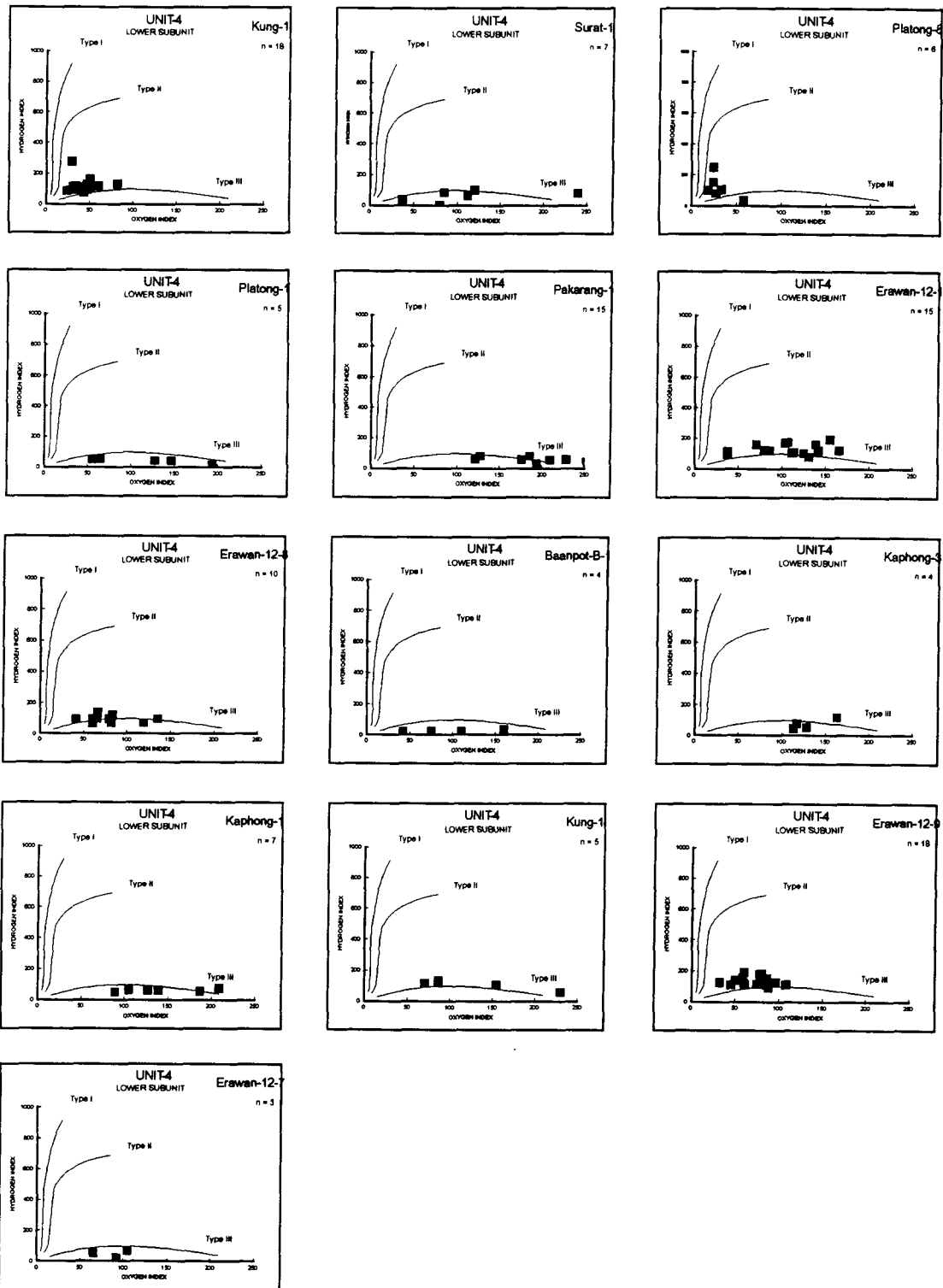


Figure 5.42: Hydrogen index vs. oxygen index for samples from unit 4's lower subunit.

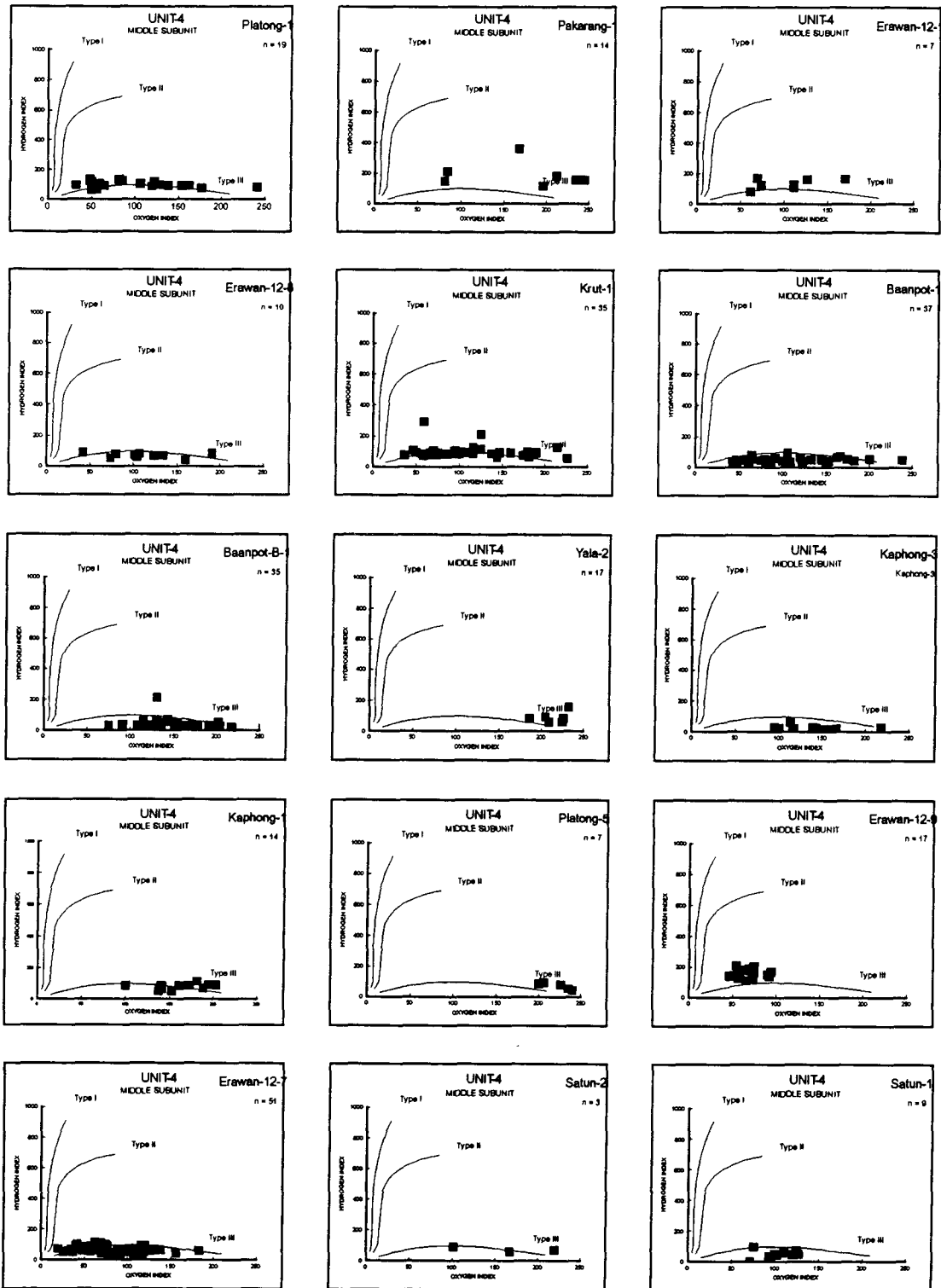


Figure 5.43: Hydrogen index vs. oxygen index for samples from unit 4's middle subunit.

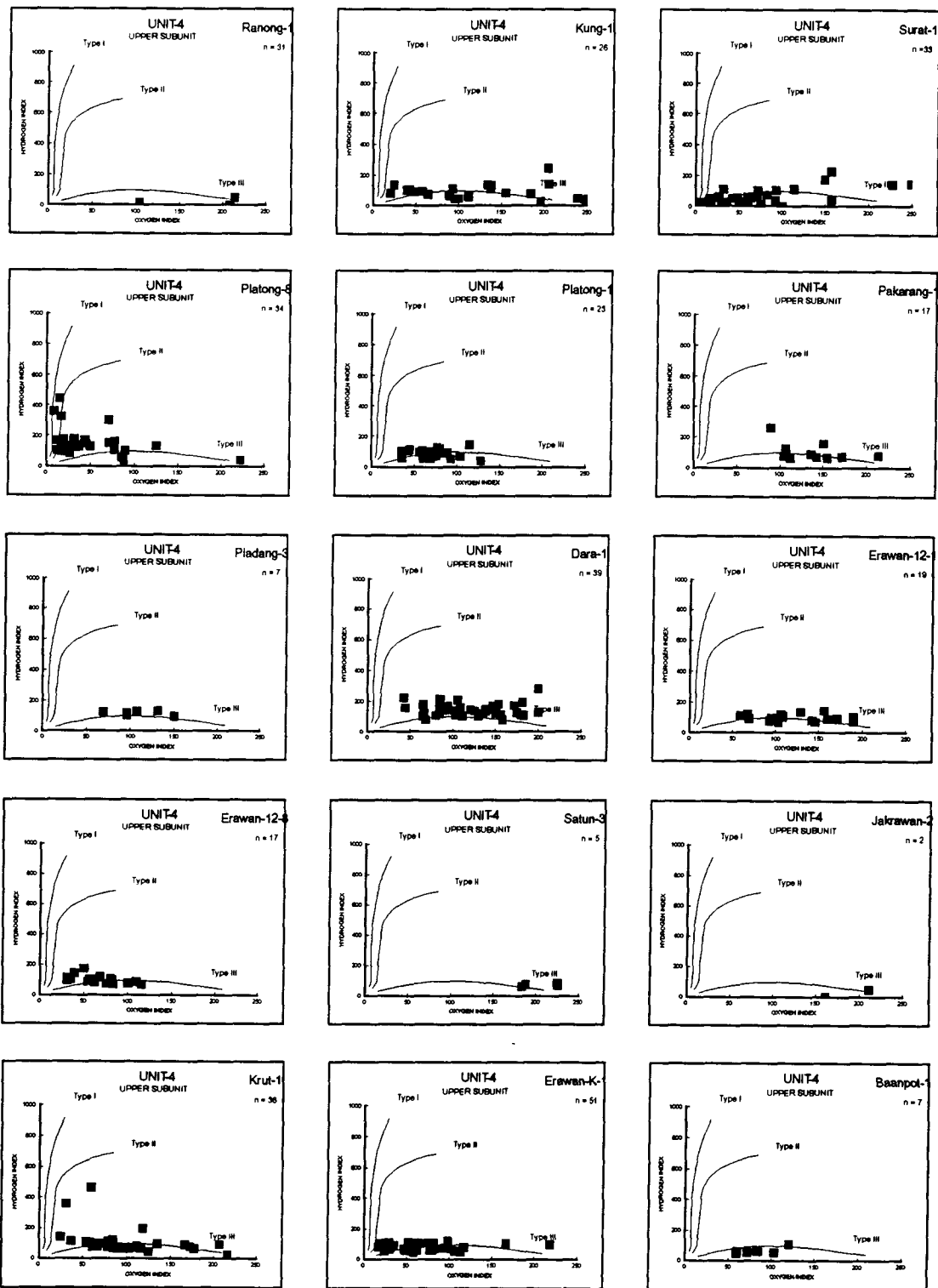


Figure 5.44: Hydrogen index vs. oxygen index for samples from unit 4's upper subunit.

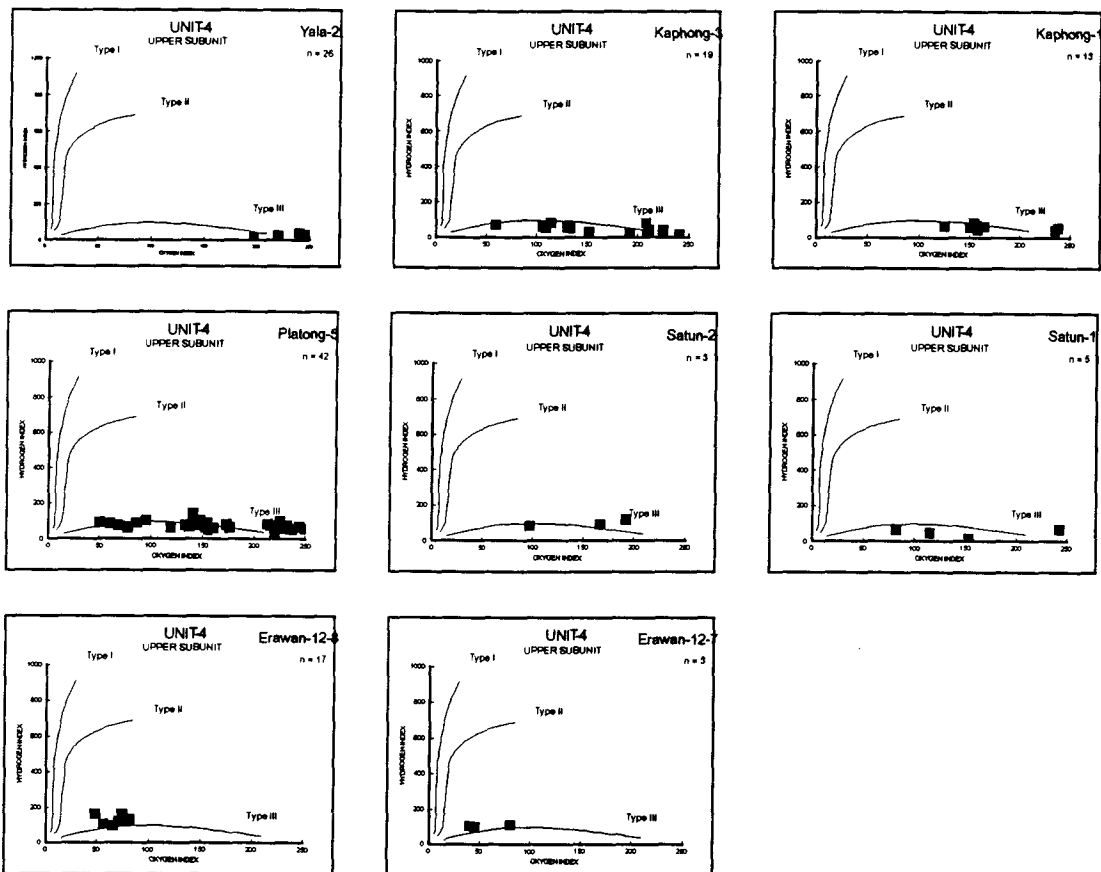


Figure 5.44 (cont.): Hydrogen index vs. oxygen index for samples from unit 4's upper subunit.

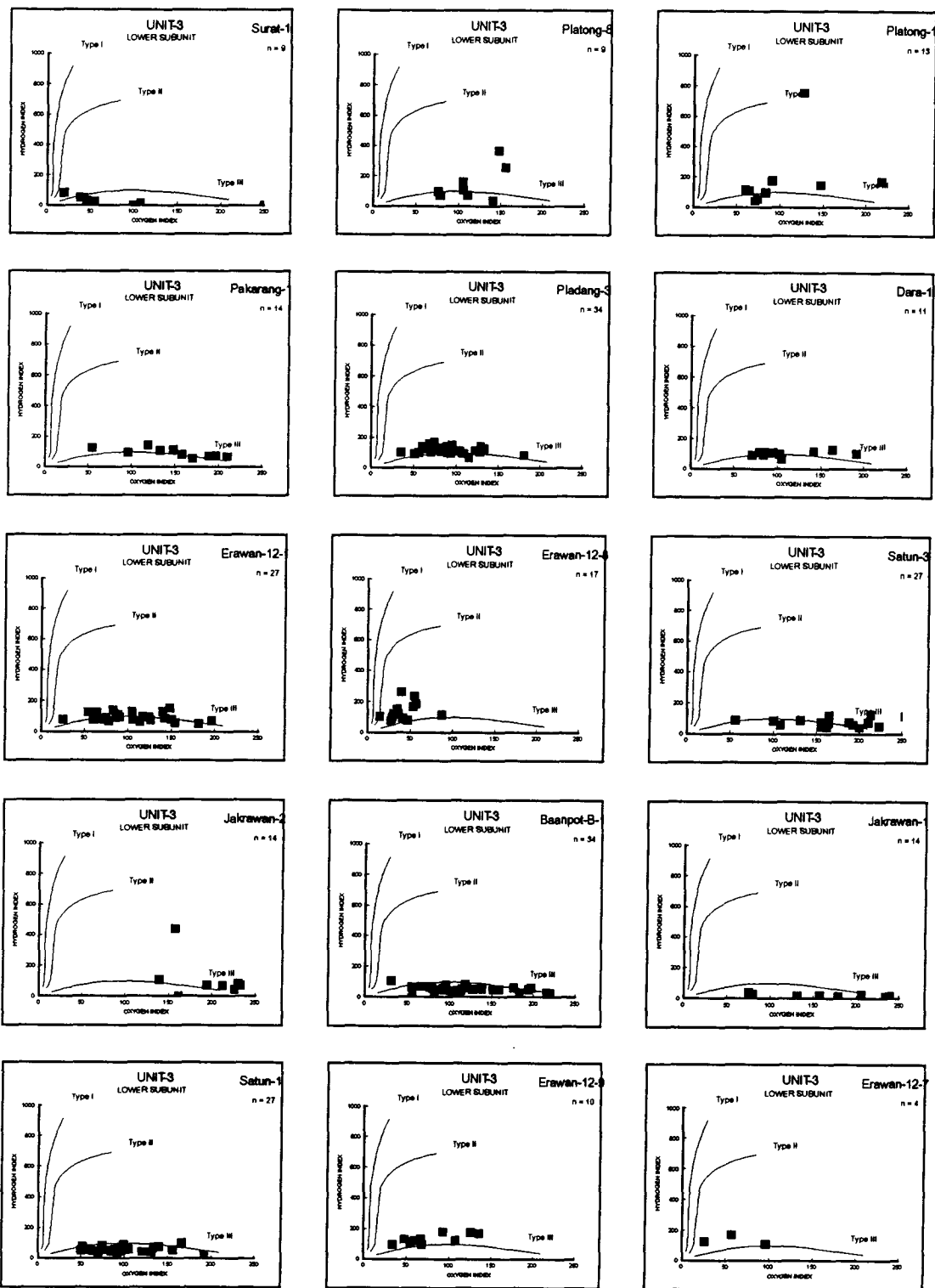


Figure 5.45: Hydrogen index vs. oxygen index for samples from unit 3's lower subunit.

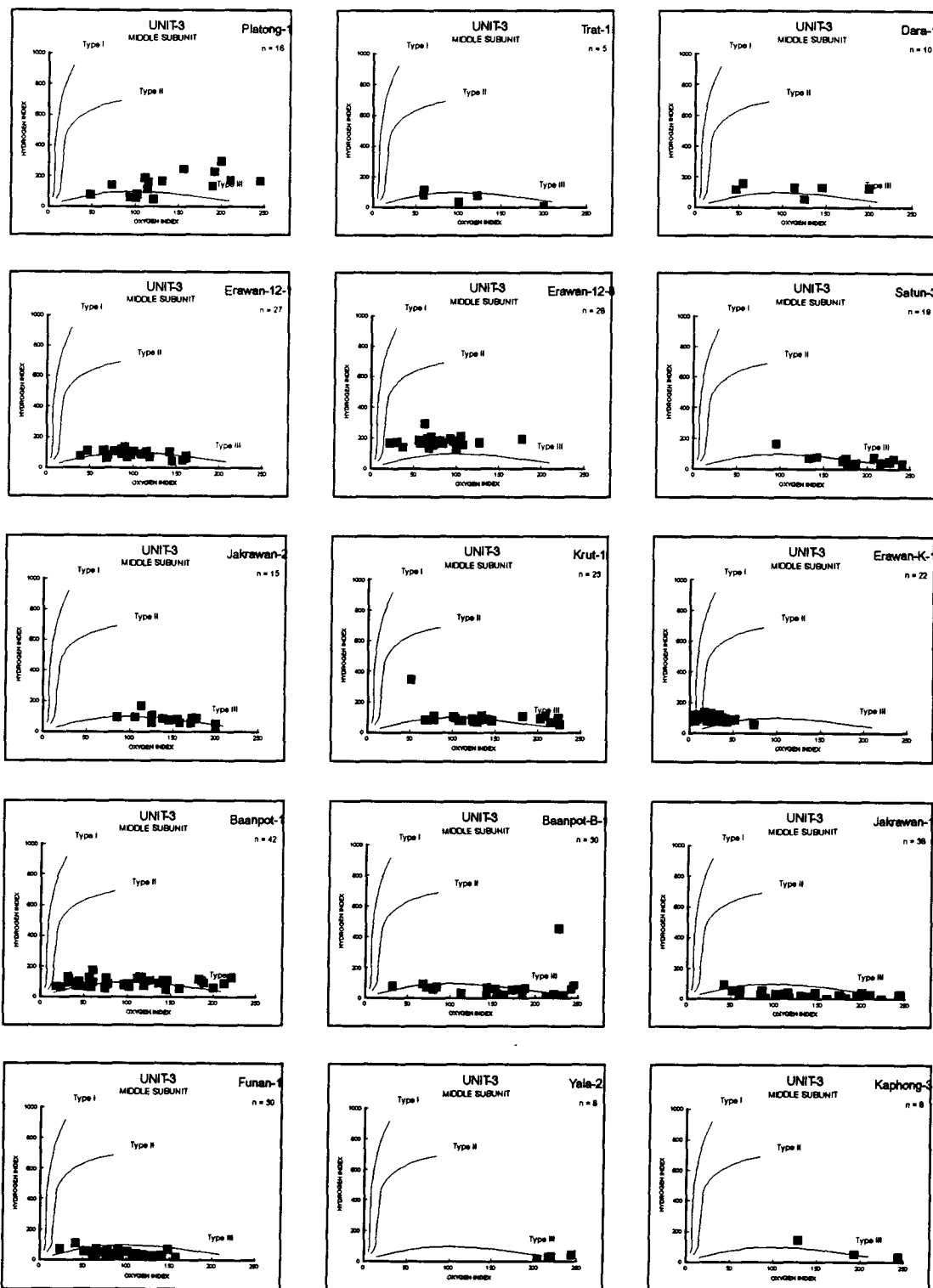


Figure 5.46: Hydrogen index vs. oxygen index for samples from unit 3's middle subunit.

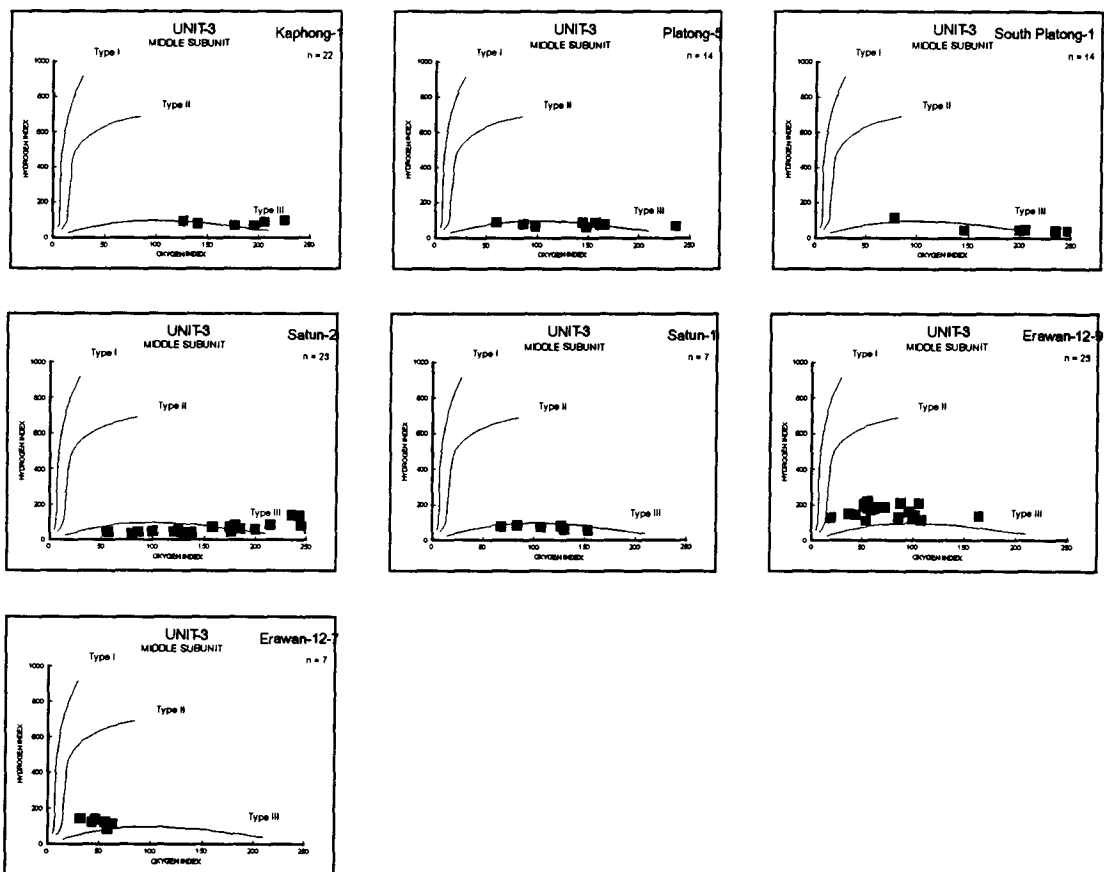


Figure 5.46 (cont.): Hydrogen index vs. oxygen index for samples from unit 3's middle subunit.

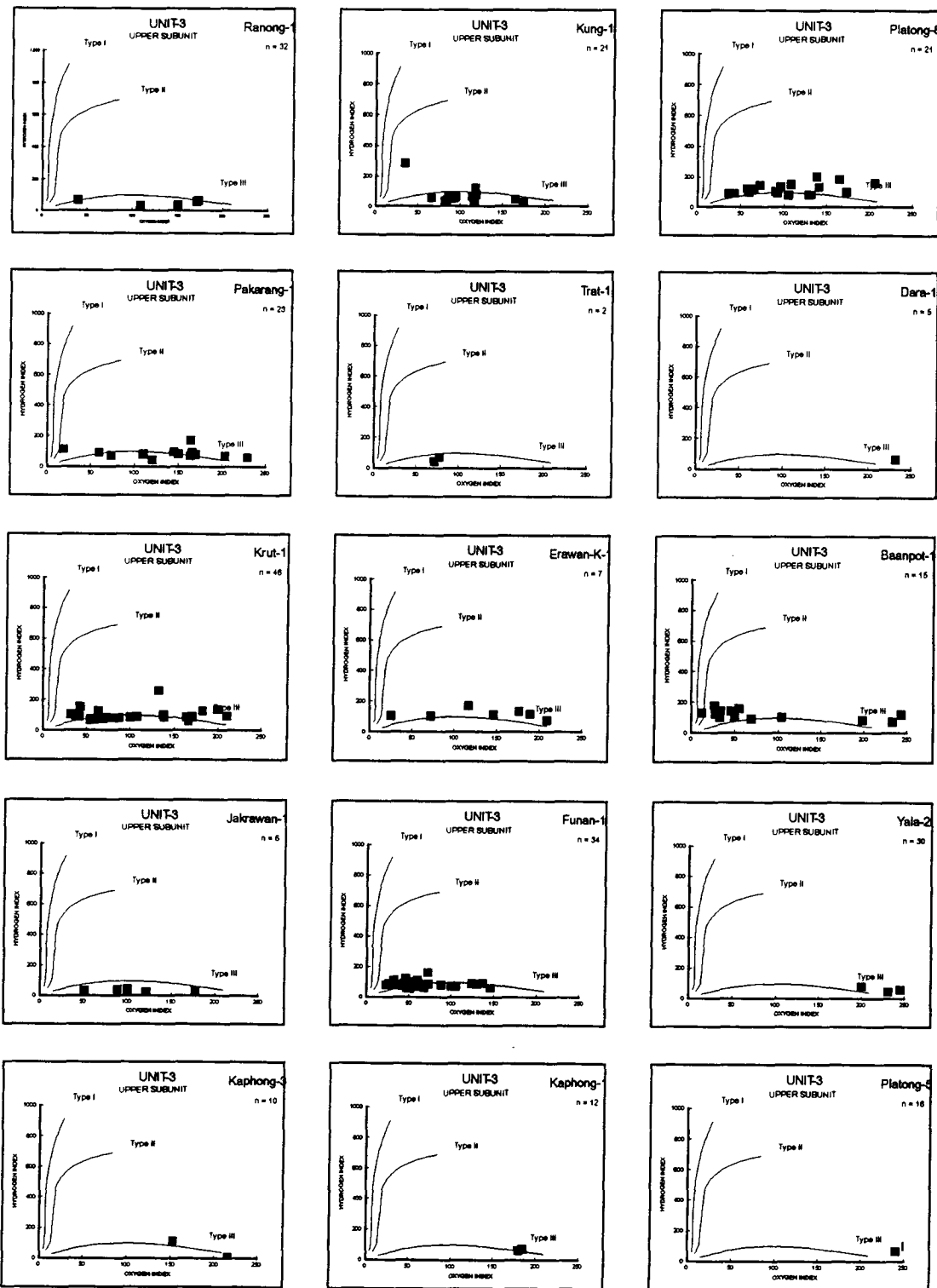


Figure 5.47: Hydrogen index vs. oxygen index for samples from unit 3's upper subunit.

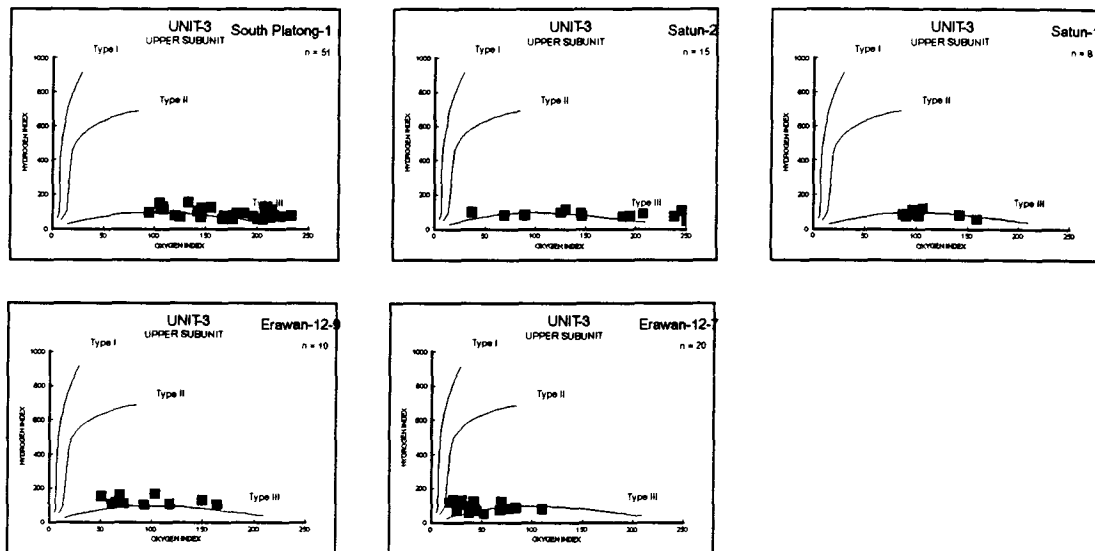


Figure 5.47 (cont.): Hydrogen index vs. oxygen index for samples from unit 3's upper subunit.

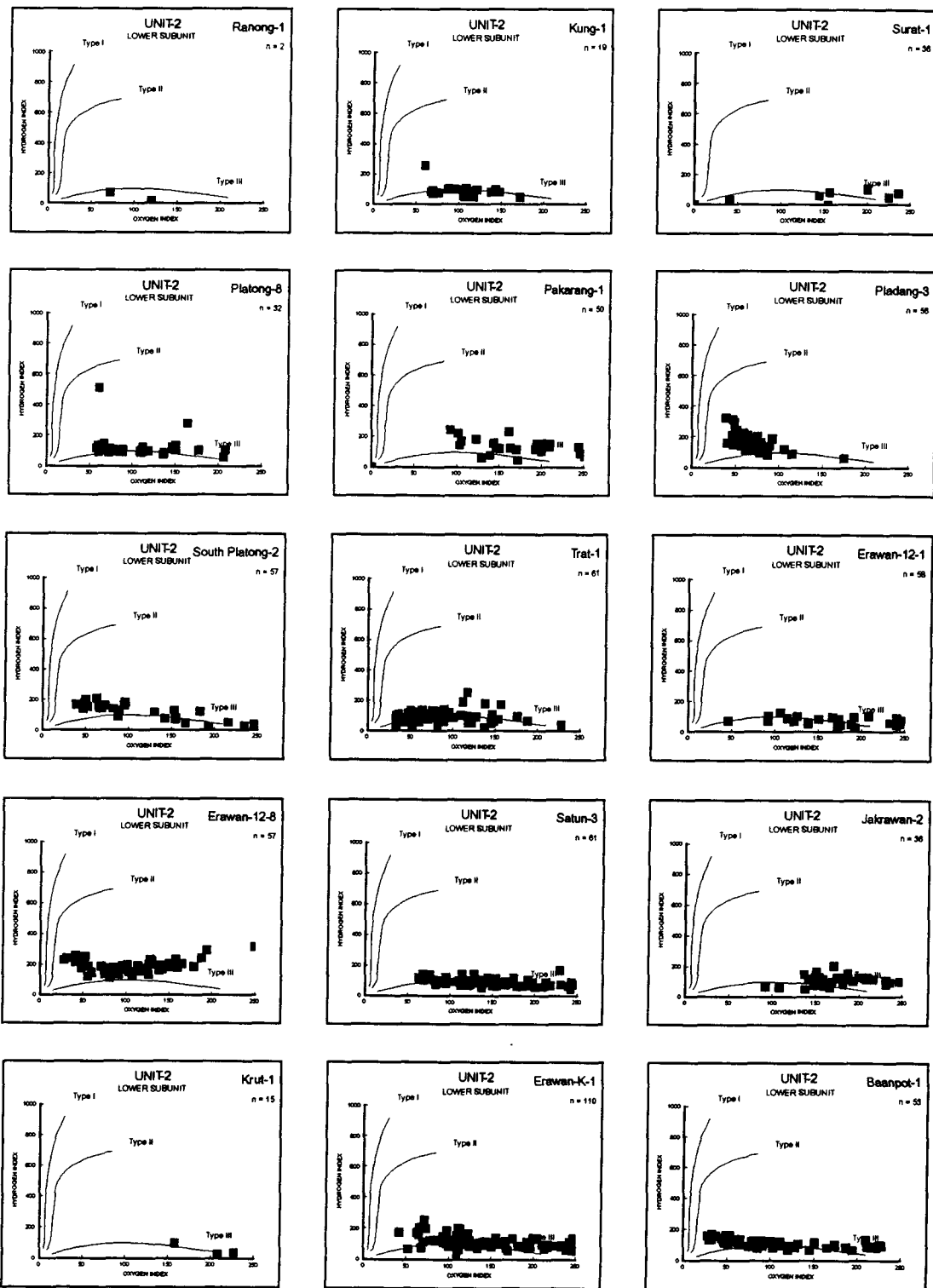


Figure 5.48: Hydrogen index vs. oxygen index for samples from unit 2's lower subunit.

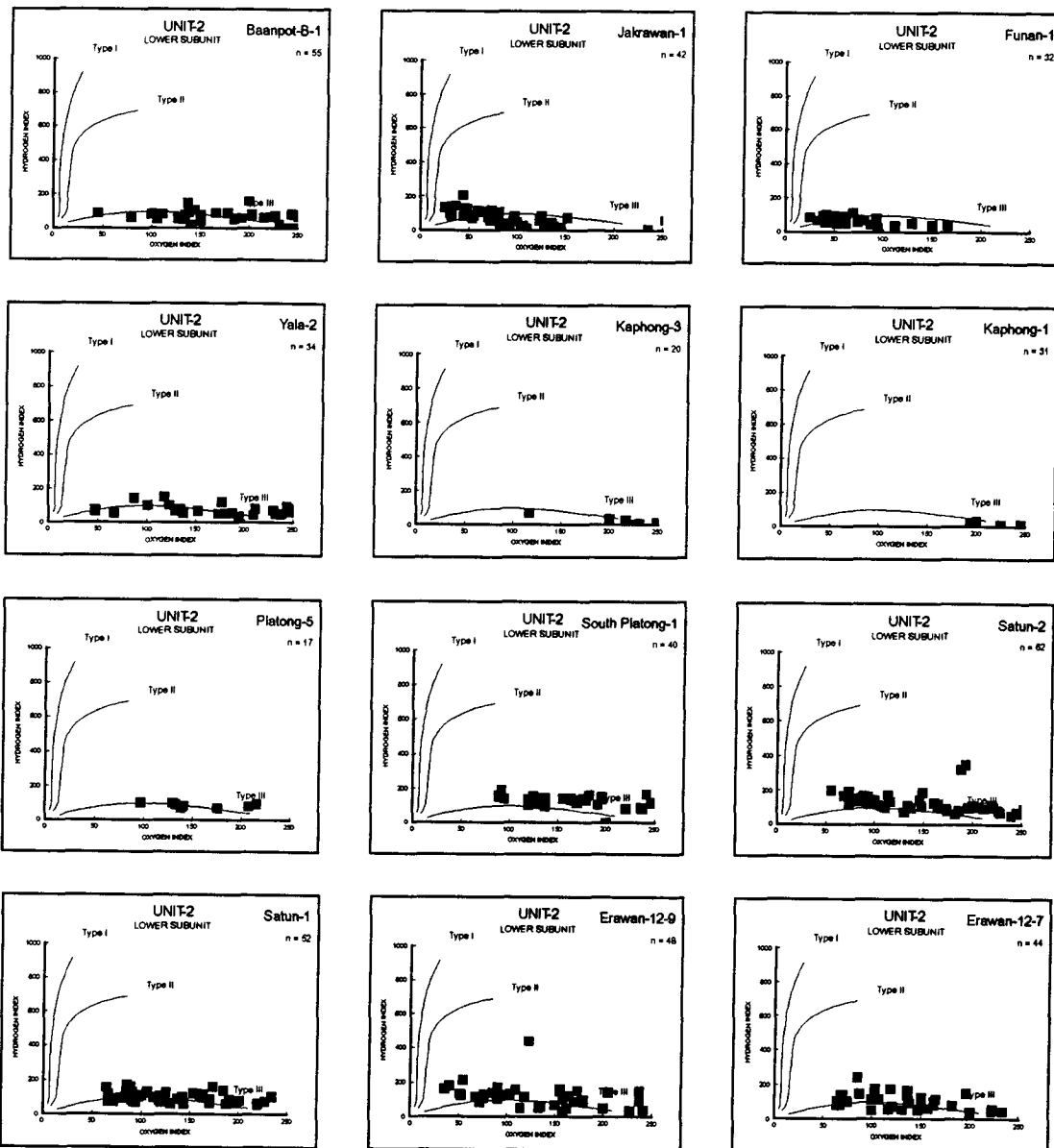


Figure 5.48 (cont.): Hydrogen index vs. oxygen index for samples from unit 2's lower subunit.

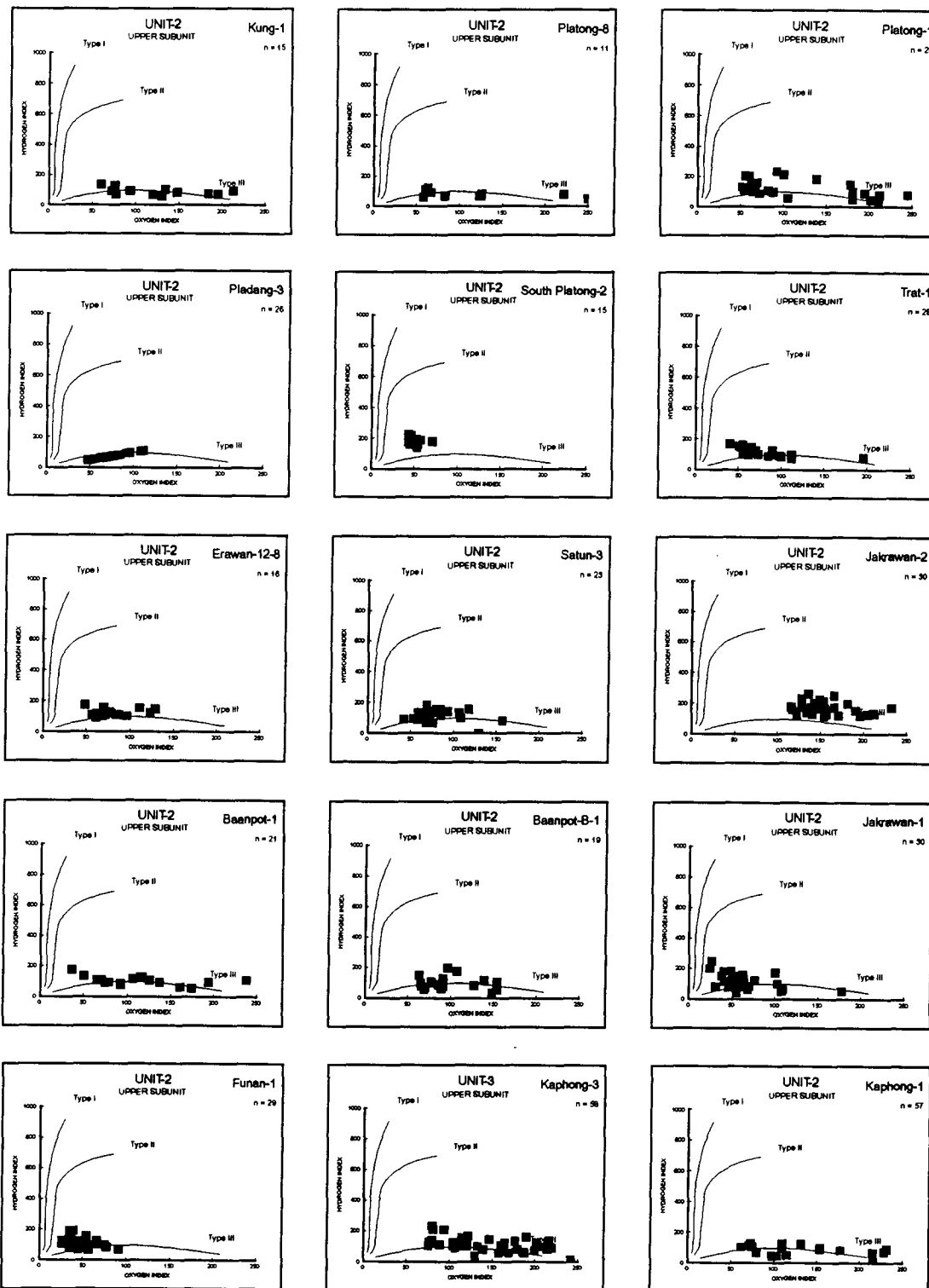


Figure 5.49: Hydrogen index vs. oxygen index for samples from unit 2's upper subunit.

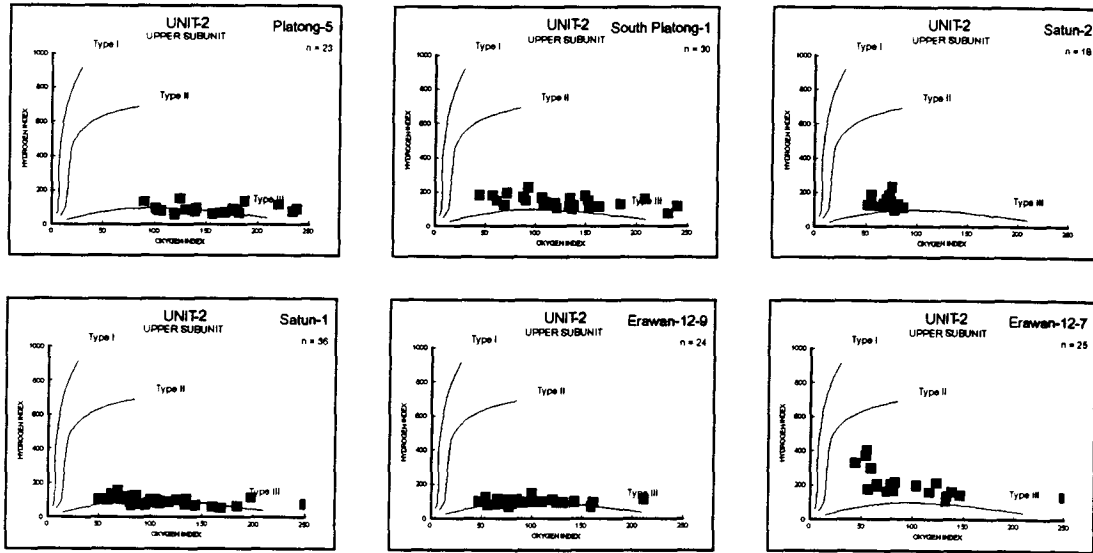


Figure 5.49 (cont.): Hydrogen index vs. oxygen index for samples from unit 2's upper subunit.

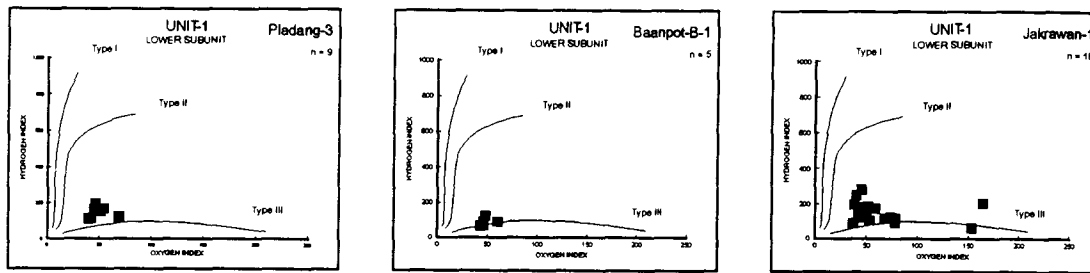


Figure 5.50: Hydrogen index vs. oxygen index for samples from unit 1's lower subunit.

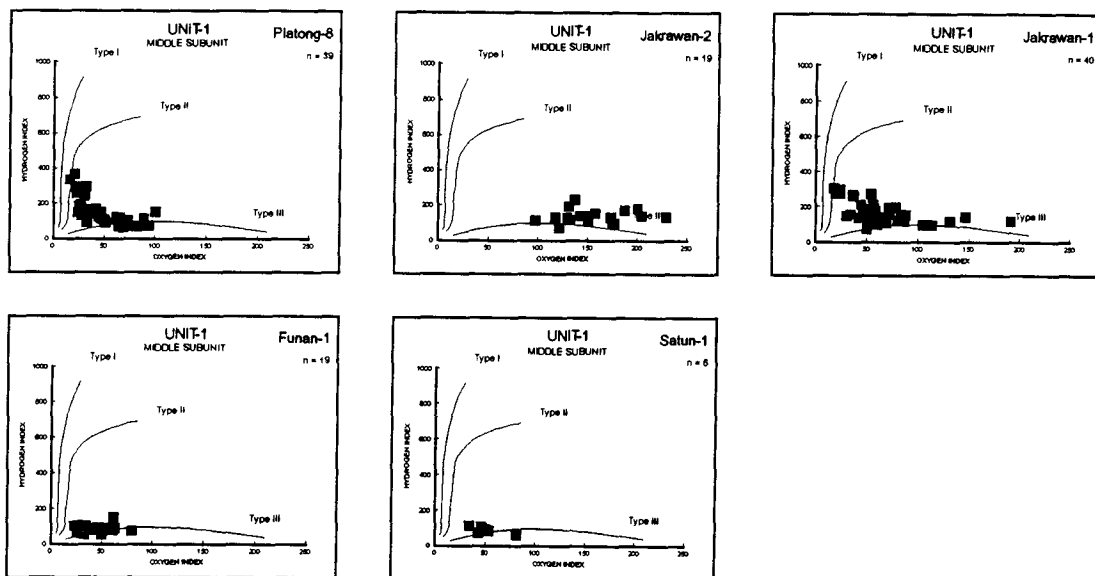


Figure 5.51: Hydrogen index vs. oxygen index for samples from unit 1's middle subunit.

Table 5.4: Summary of organic geochemical characteristics of Tertiary stratigraphic units in the Pattani basin

UNIT	TOC	HI	OI	HC-P	QOM	S ₁	S ₂	S ₃
1	1.41	122	71	2.20	1.39	0.22	1.98	0.84
2	0.54	99	274	0.83	1.44	0.16	0.66	0.61
3	0.36	85	232	0.46	1.30	0.13	0.33	0.40
4	0.33	87	187	0.50	1.44	0.19	0.31	0.36
5	0.24	83	181	0.45	1.60	0.20	0.25	0.28
6	0.20	80	204	0.48	1.61	0.24	0.24	0.24

*TOC is the total organic carbon (%)

HI is the hydrogen index

OI is the oxygen index

HC-P is the hydrocarbon potential = $S_1 + S_2$

QOM is the quality of organic matter = $(S_1 + S_2)/TOC$

Table 5.5: Summary of organic geochemical characteristics of Tertiary stratigraphic subunits in the Patani basin

UNIT	SUBUNIT	TOC	HI	OI	HC-P	QOM	S ₁	S ₂	S ₃
1	Middle	1.47	127	73	2.42	1.64	0.21	2.21	0.92
	Lower	1.37	127	65	2.05	1.49	0.26	1.80	0.73
2	Upper	0.81	120	131	1.31	1.57	0.20	1.11	0.72
	Lower	0.43	91	312	0.64	1.49	0.15	0.50	0.54
3	Upper	0.29	80	316	0.37	1.28	0.10	0.27	0.39
	Middle	0.39	88	191	0.49	1.31	0.14	0.35	0.41
	Lower	0.44	98	137	0.57	1.34	0.16	0.41	0.44
4	Upper	0.36	89	204	0.55	1.39	0.20	0.34	0.41
	Middle	0.35	82	155	0.49	1.37	0.20	0.29	0.42
	Lower	0.32	82	112	0.52	1.56	0.22	0.30	0.28
5	Upper	0.25	94	191	0.52	1.93	0.25	0.27	0.29
	Lower	0.24	75	190	0.40	1.46	0.17	0.23	0.32
6	Upper	0.22	87	199	0.50	1.82	0.25	0.26	0.24
	Lower	0.07	9	223	0.01	0.13	0.00	0.01	0.11

*TOC is the total organic carbon (%)

HI is the hydrogen index

OI is the oxygen index

HC-P is the hydrocarbon potential = $S_1 + S_2$

QOM is the quality of organic matter = $(S_1 + S_2)/TOC$

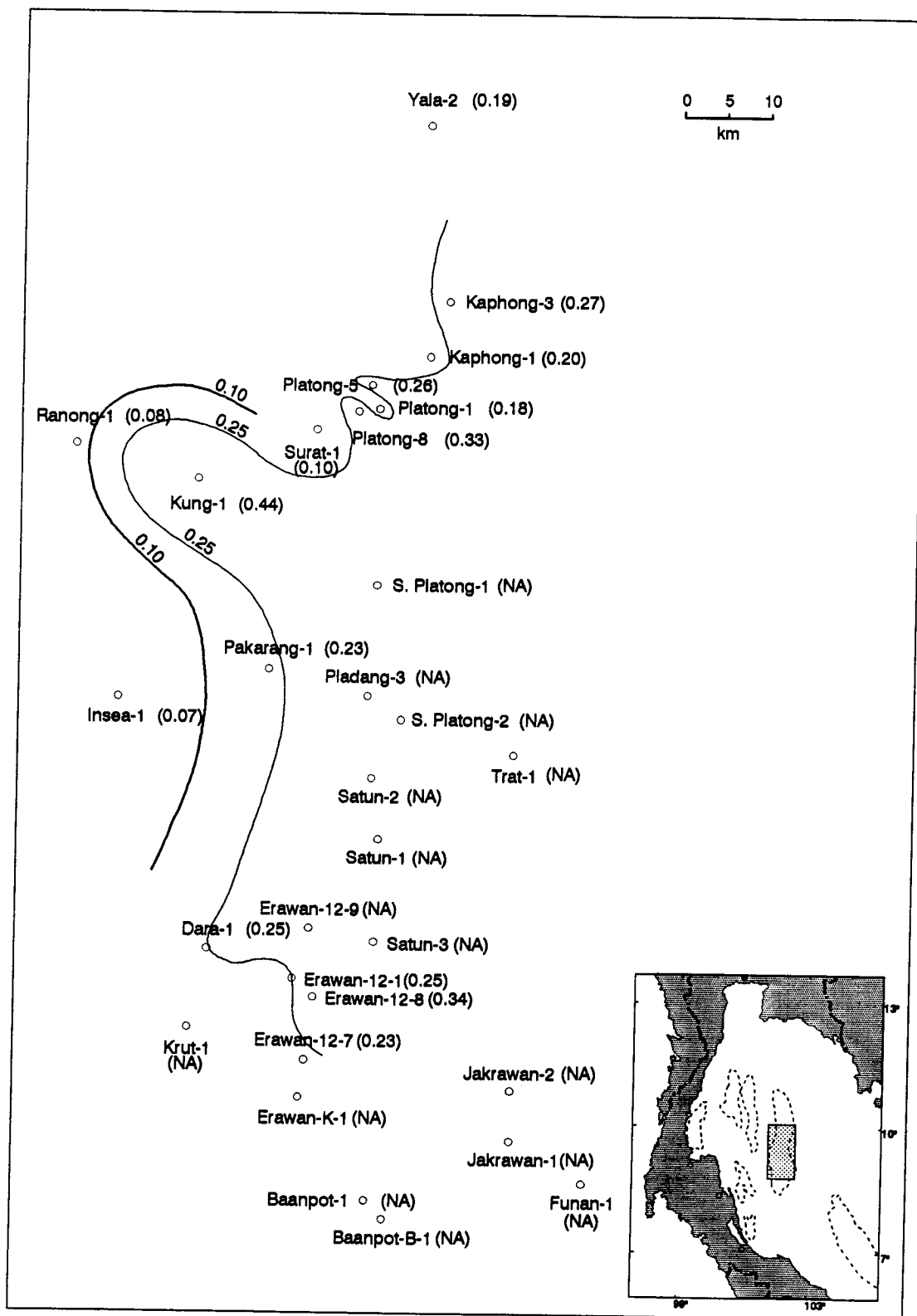


Figure 5.52: Lateral distribution of TOC (%) of unit 5

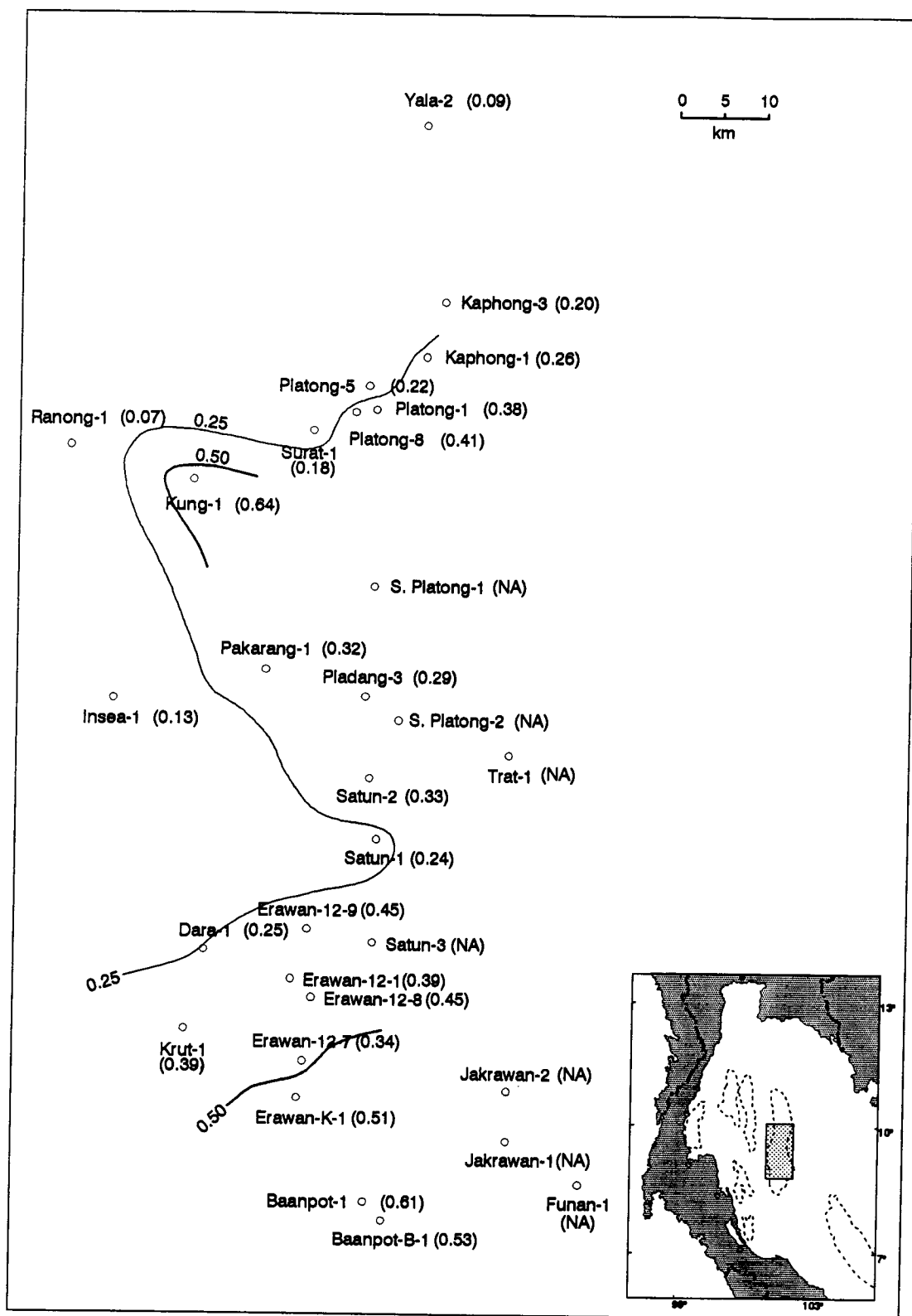


Figure 5.53: Lateral distribution of TOC (%) of unit 4

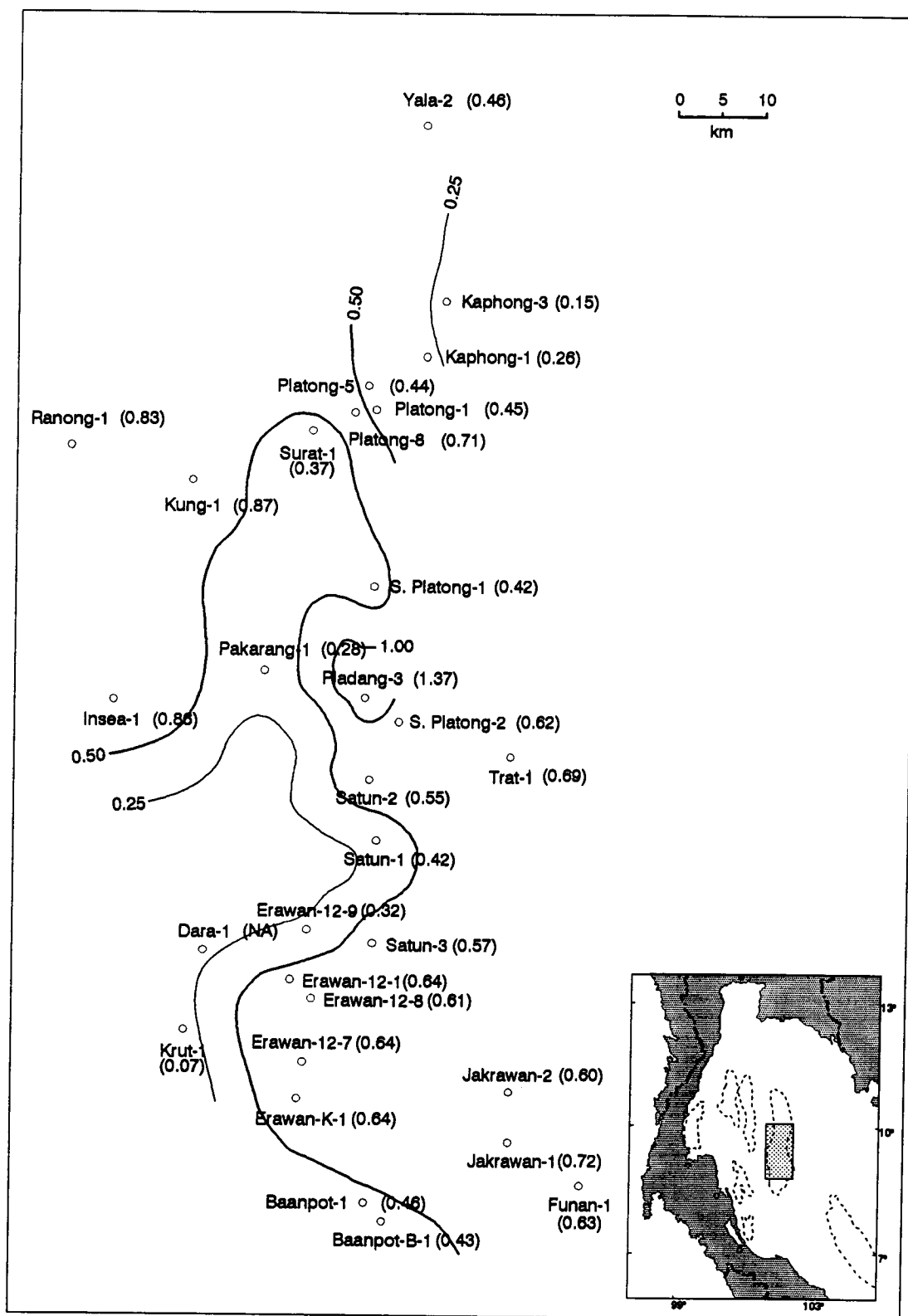


Figure 5.55: Lateral distribution of TOC (%) of unit 2

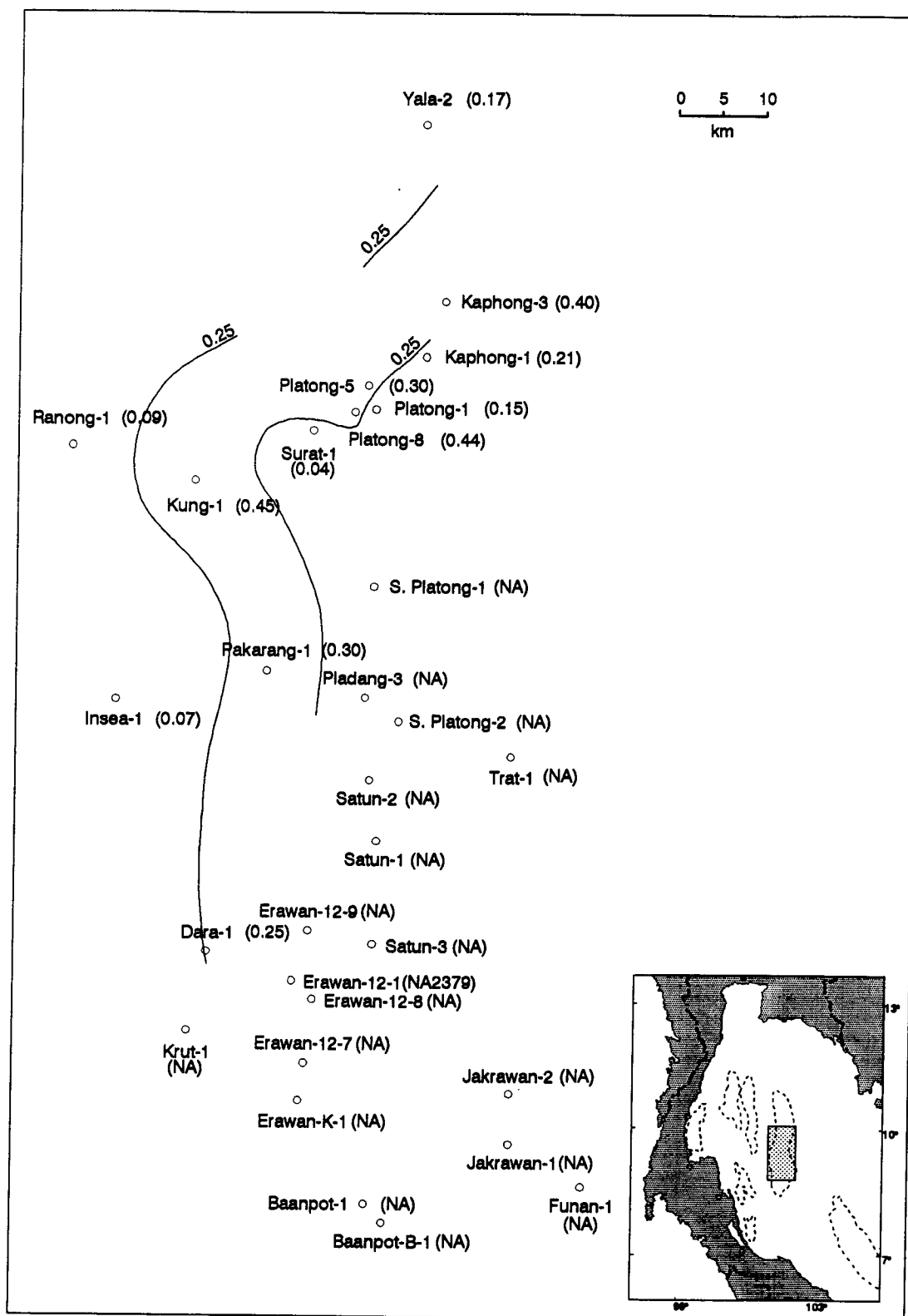


Figure 5.56: Lateral distribution of TOC (%) of unit 5's lower subunit

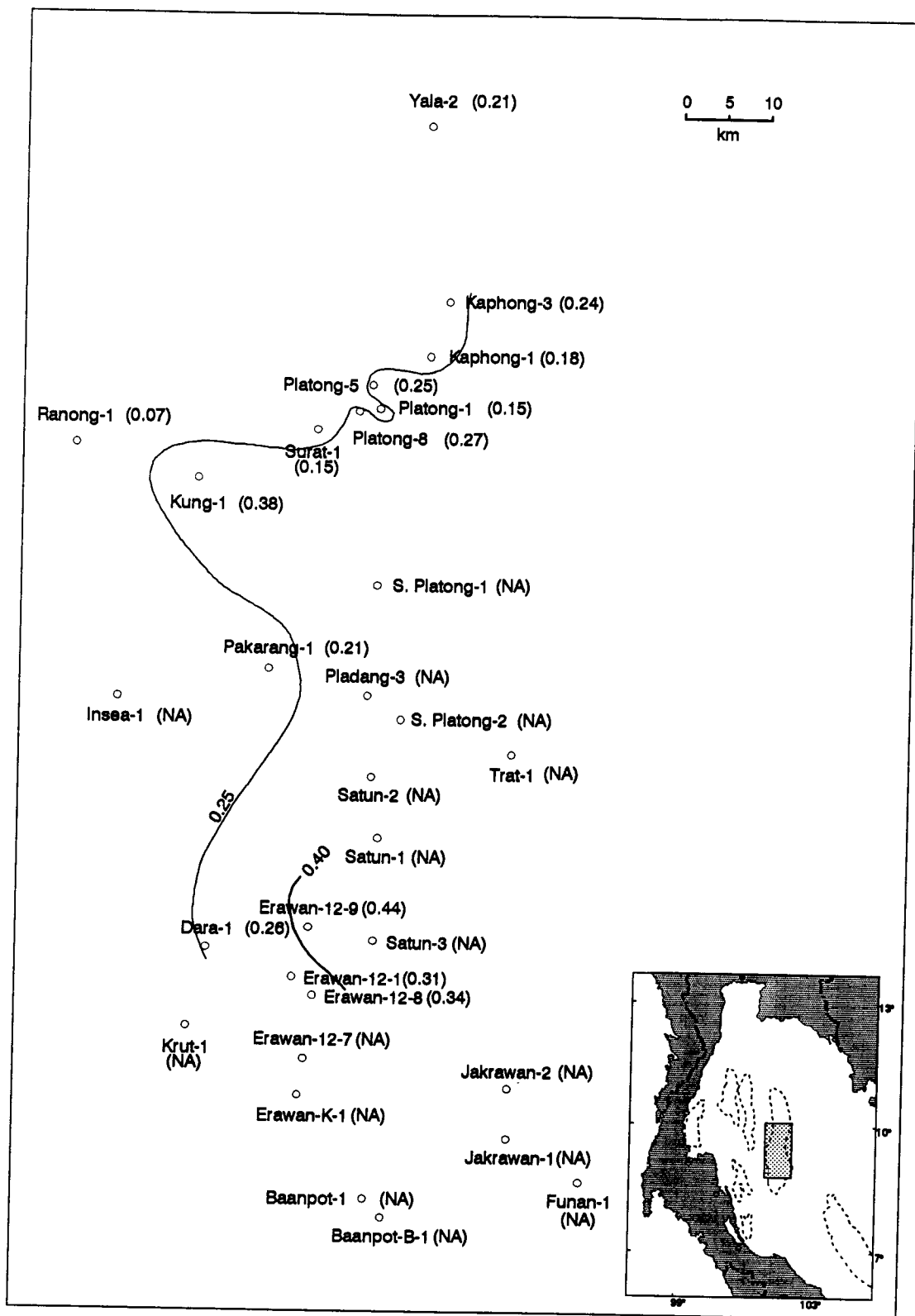


Figure 5.57: Lateral distribution of TOC (%) of unit 5's upper subunit

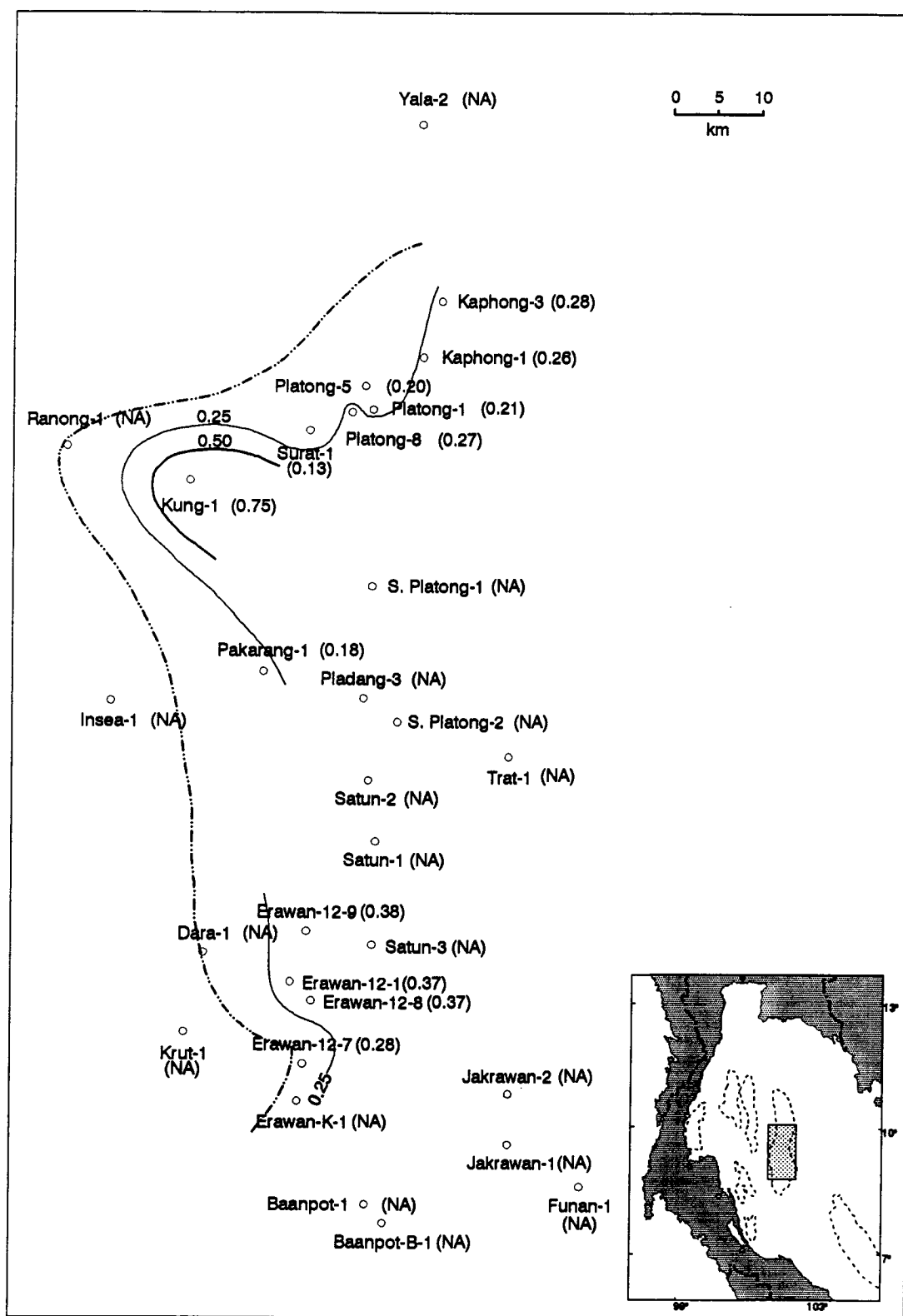


Figure 5.58: Lateral distribution of TOC (%) of unit 4's lower subunit

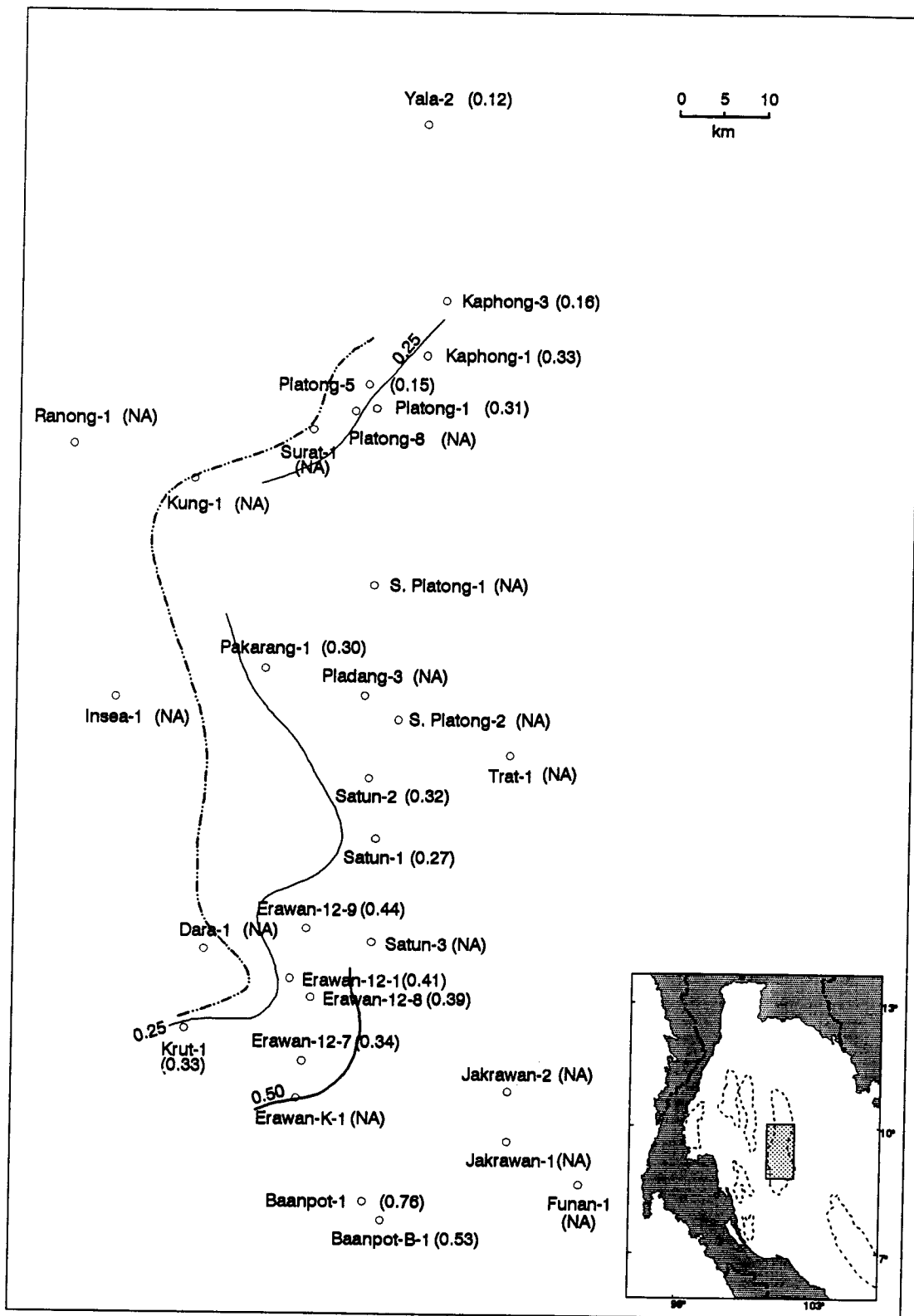


Figure 5.59: Lateral distribution of TOC (%) of unit 4's middle subunit

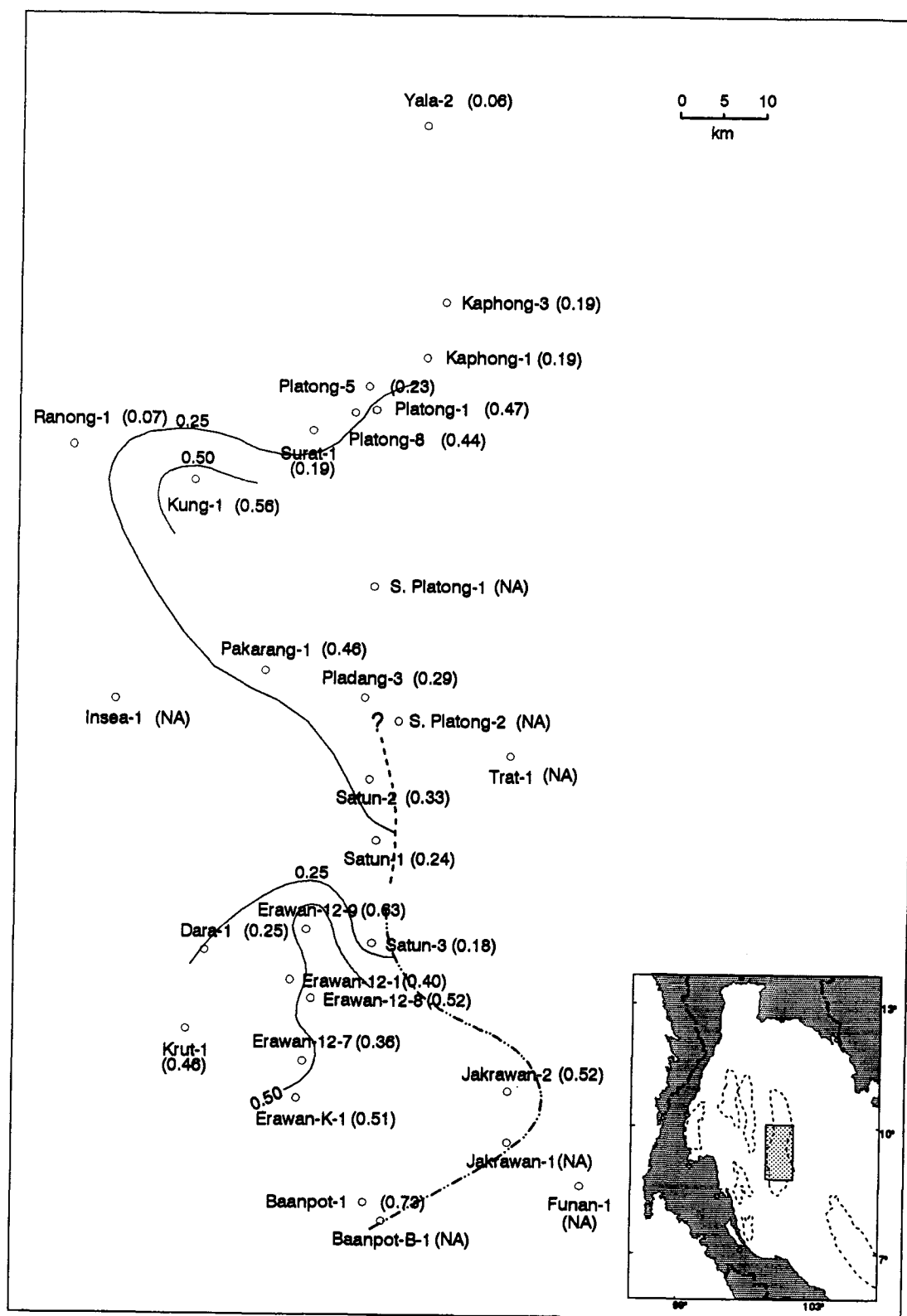


Figure 5.60: Lateral distribution of TOC (%) of unit 4's upper subunit

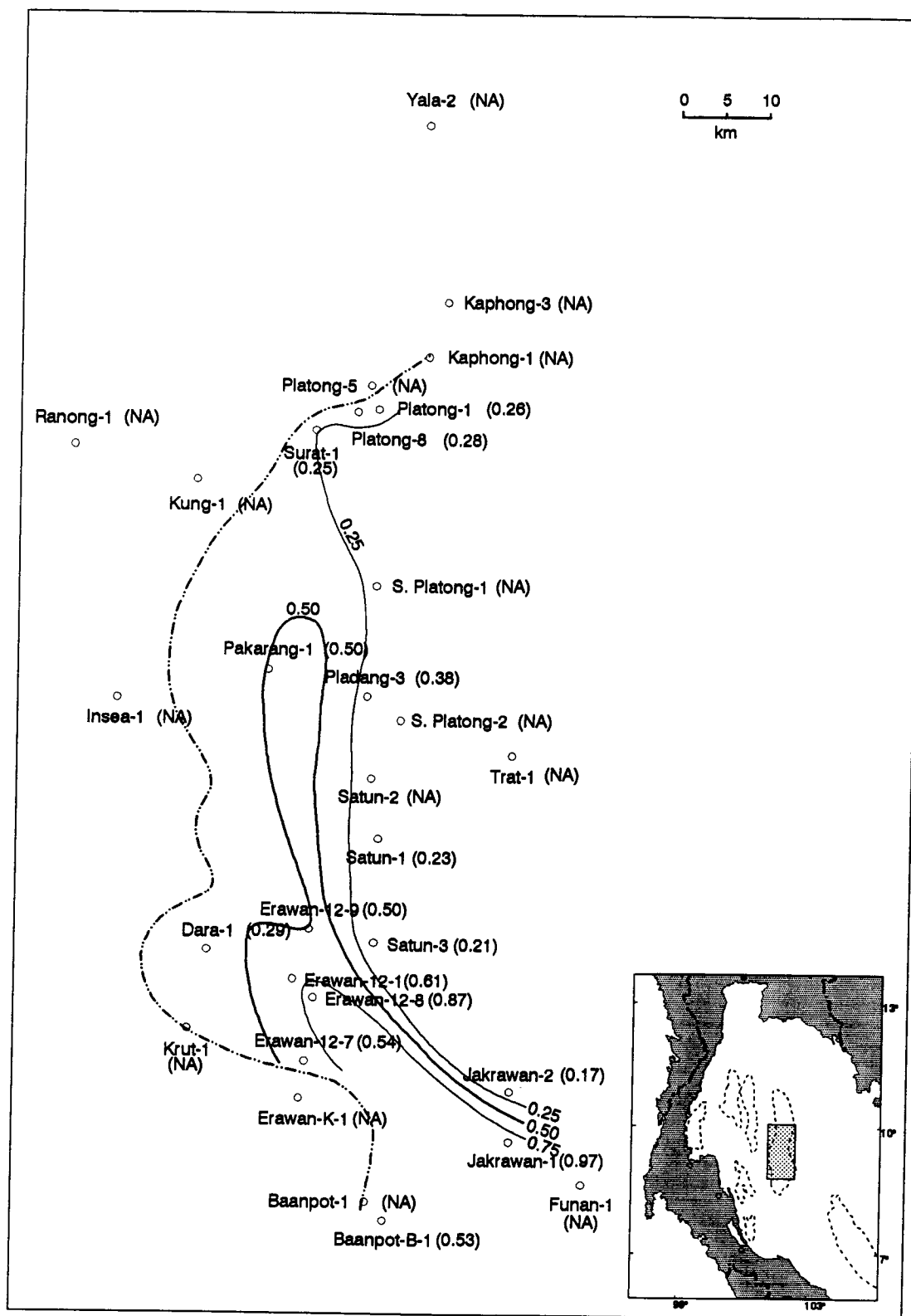


Figure 5.61: Lateral distribution of TOC (%) of unit 3's lower subunit

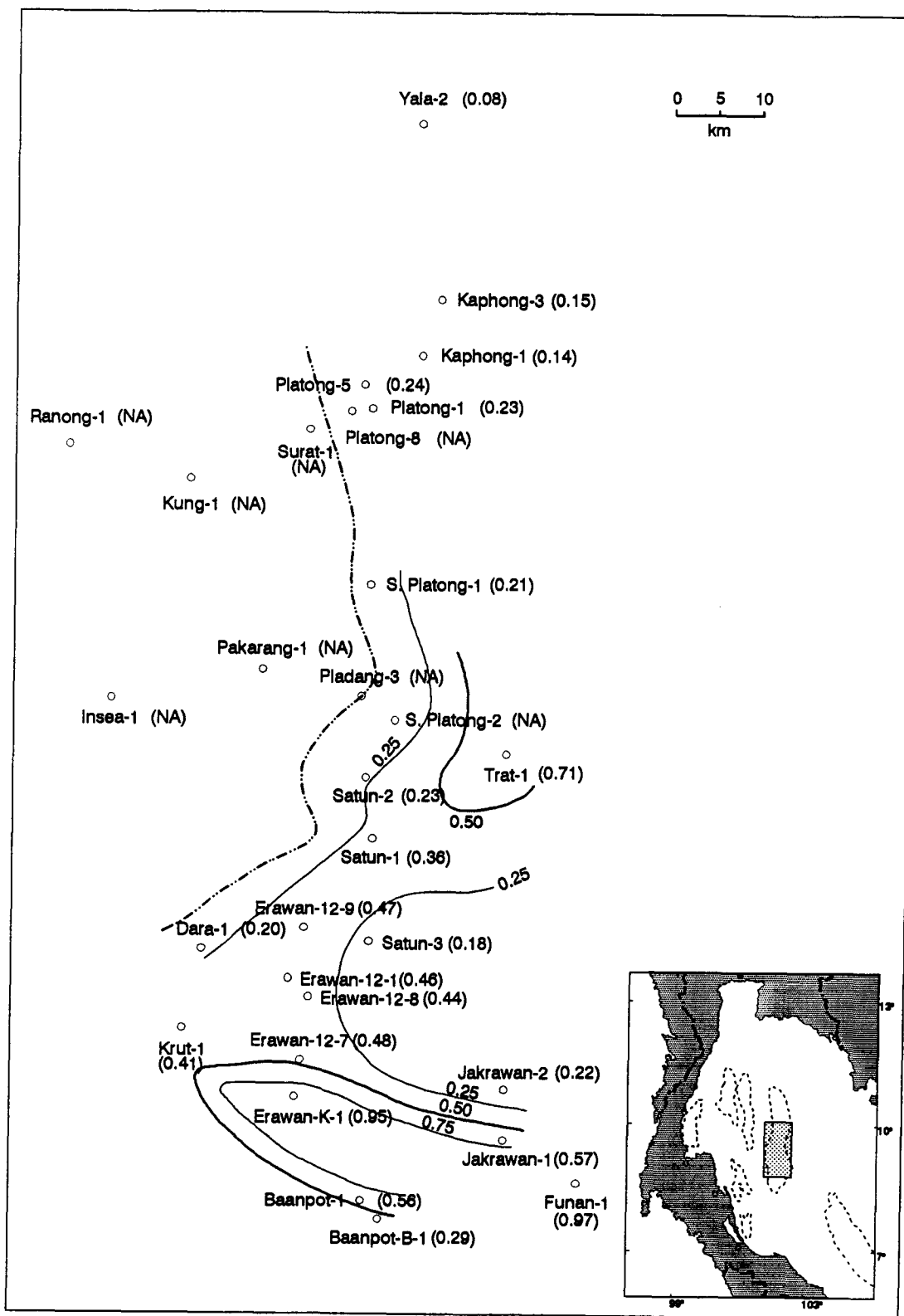


Figure 5.62: Lateral distribution of TOC (%) of unit 3's middle subunit

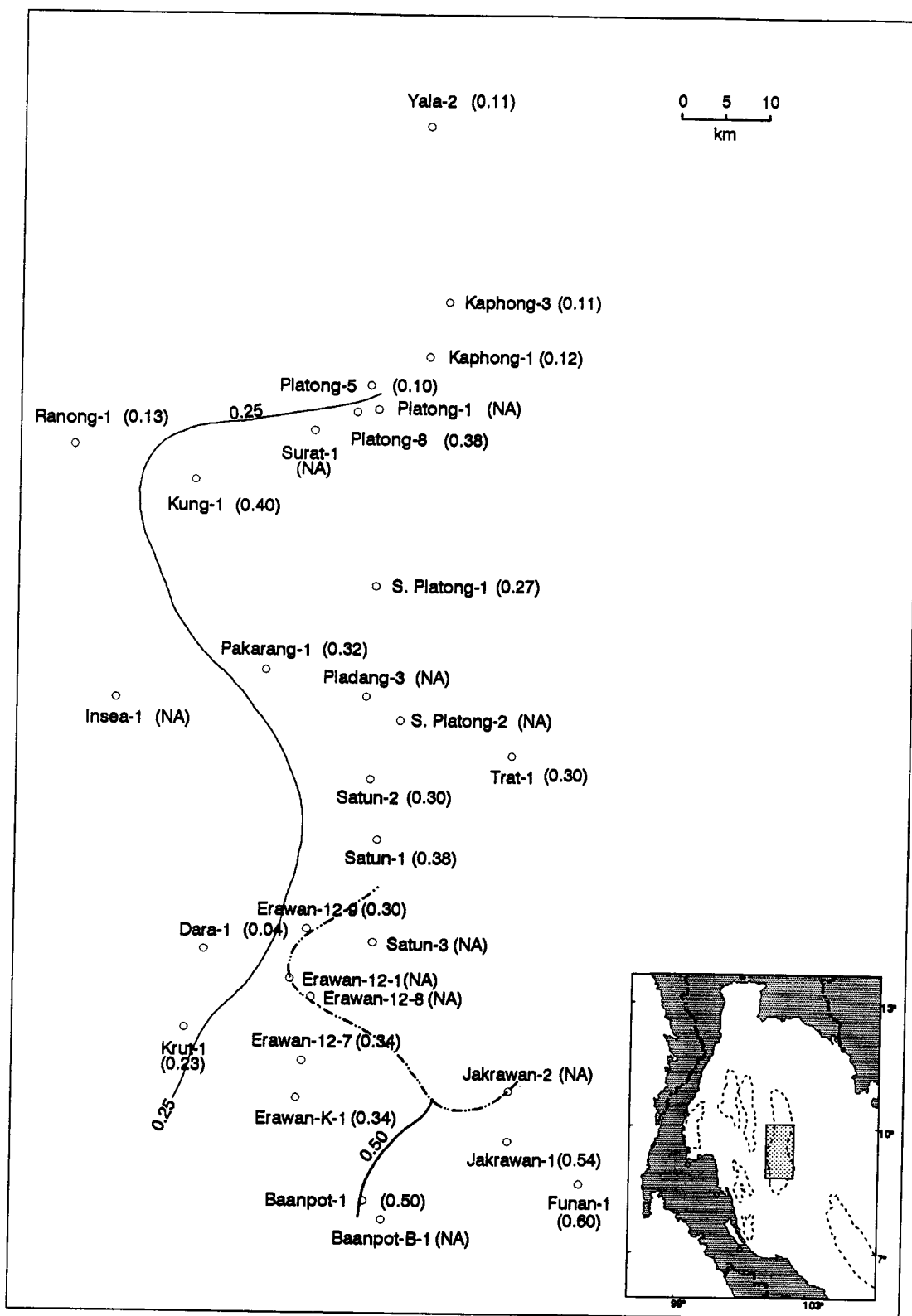


Figure 5.63: Lateral distribution of TOC (%) of unit 3's upper subunit

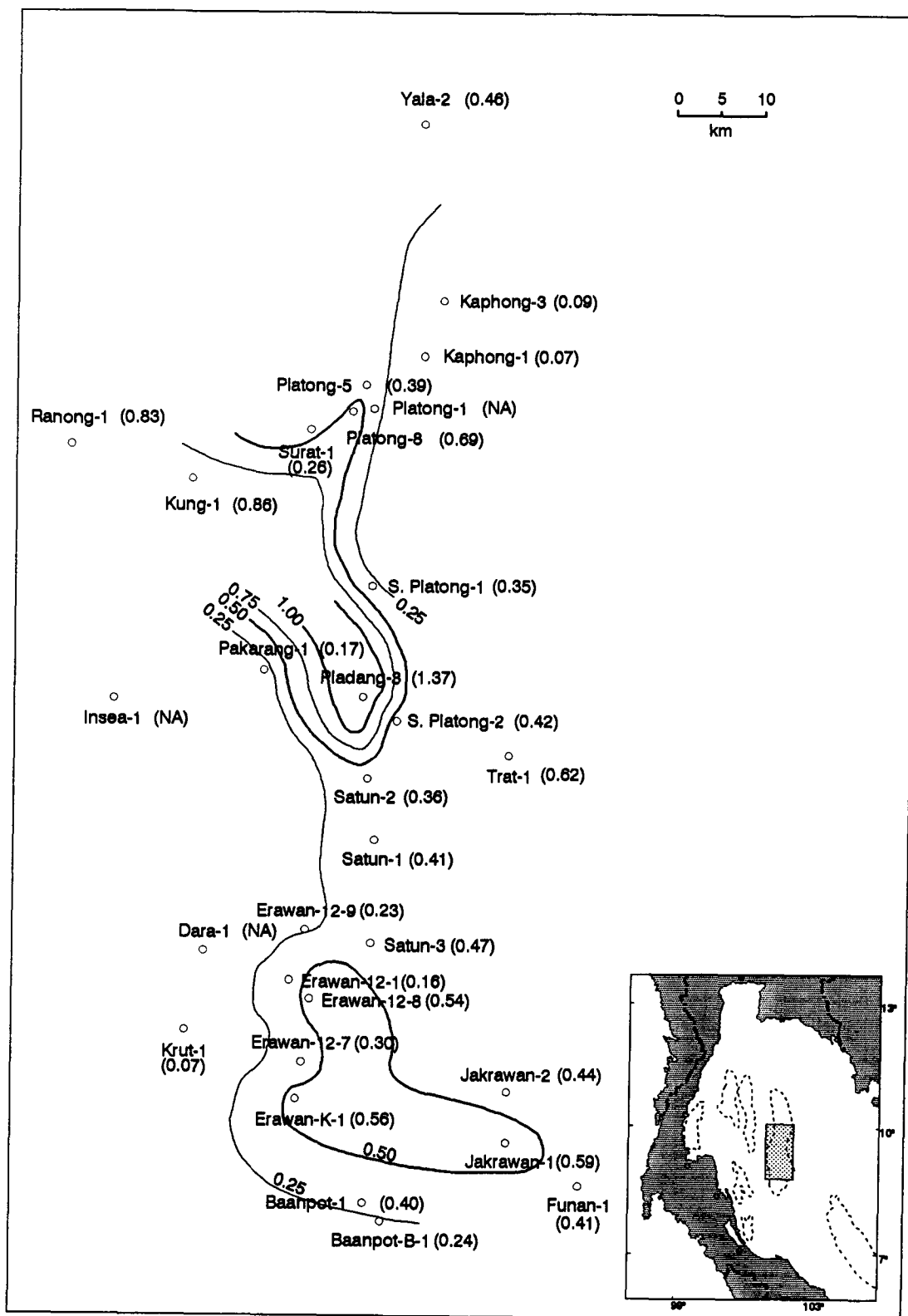


Figure 5.64: Lateral distribution of TOC (%) of unit 2's lower subunit

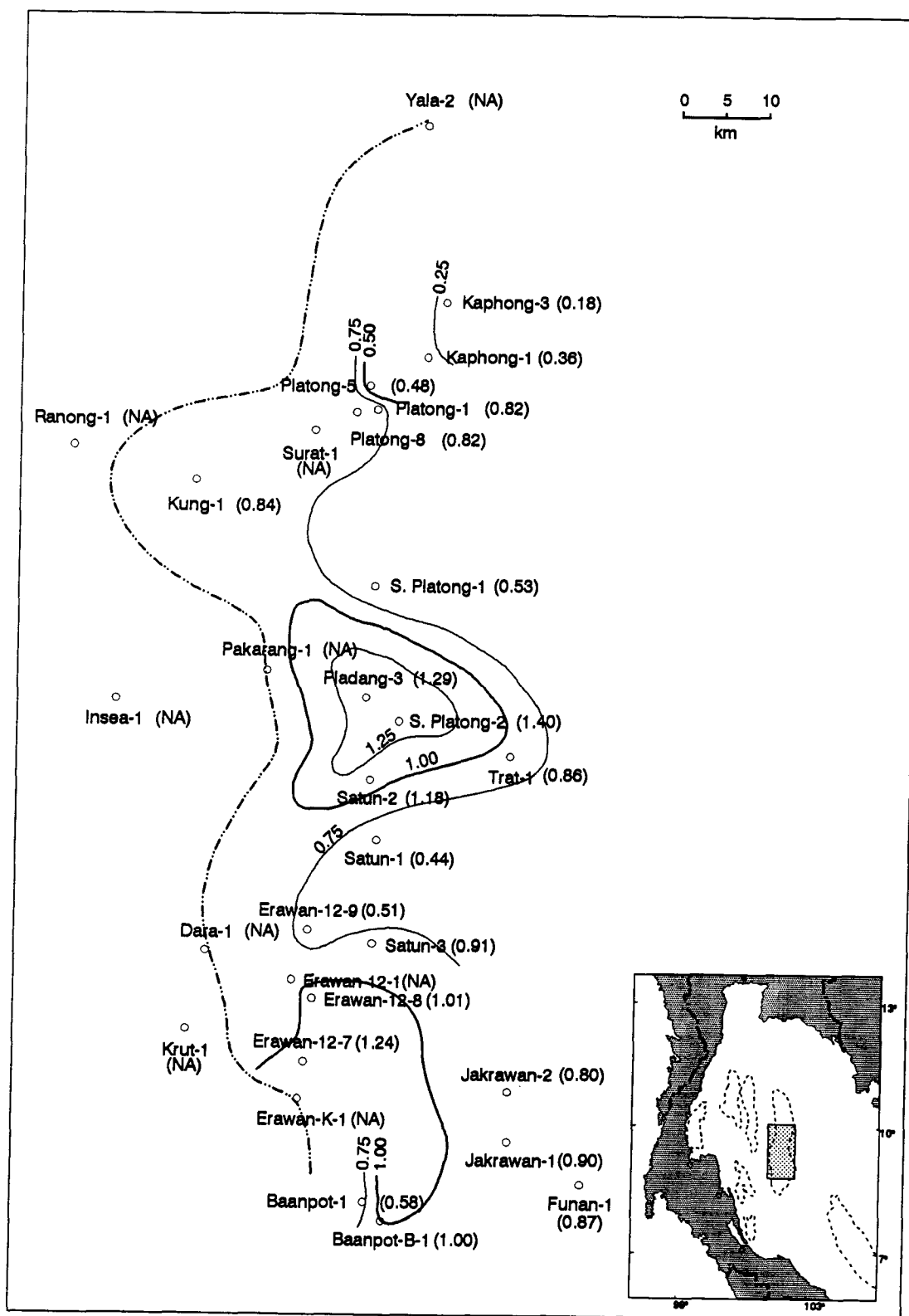


Figure 5.65: Lateral distribution of TOC (%) of unit 2's upper subunit

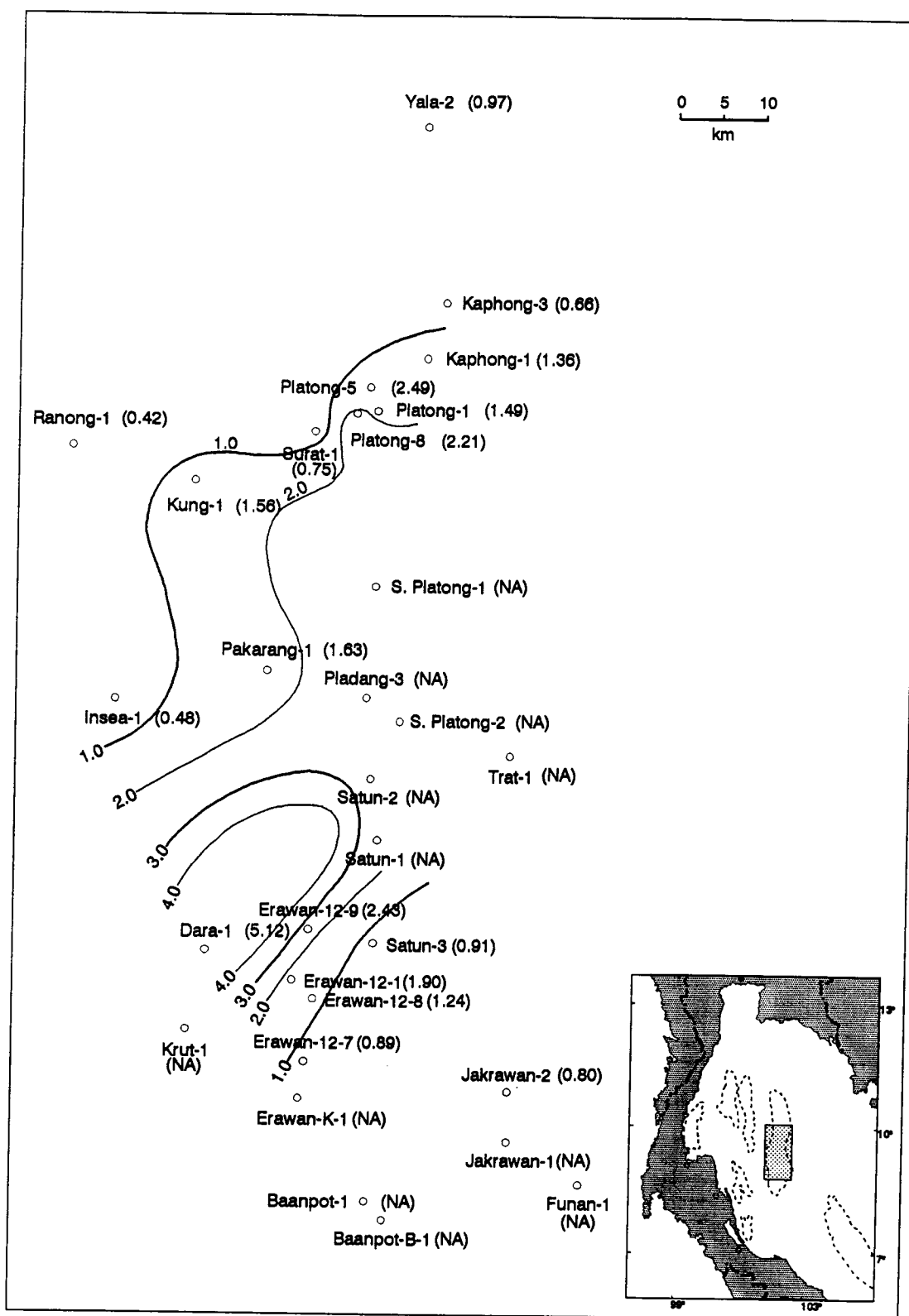


Figure 5.66: Lateral distribution of QOM (mg HC/g rock) of unit 5

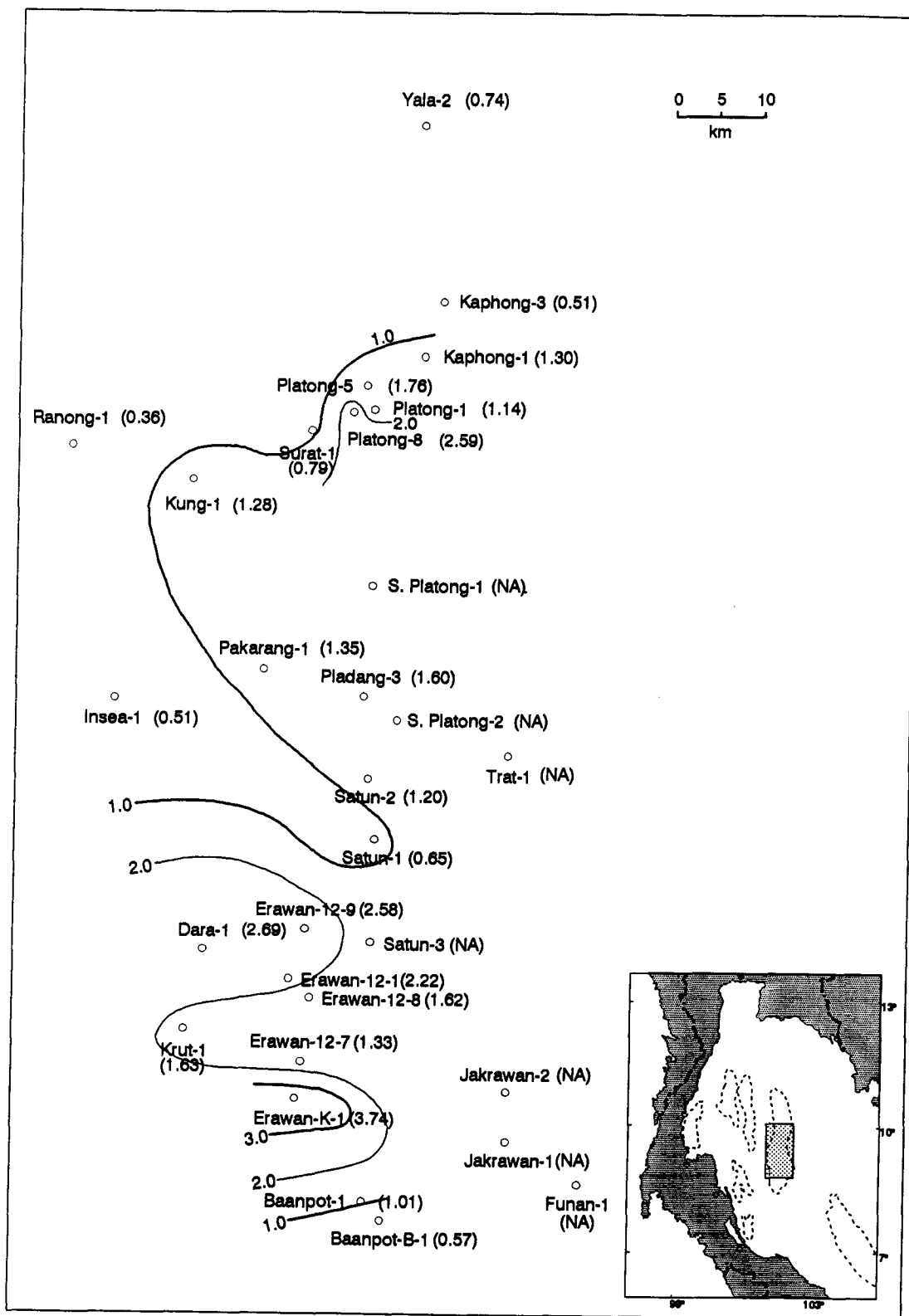


Figure 5.67: Lateral distribution of QOM (mg HC/g rock) of unit 4

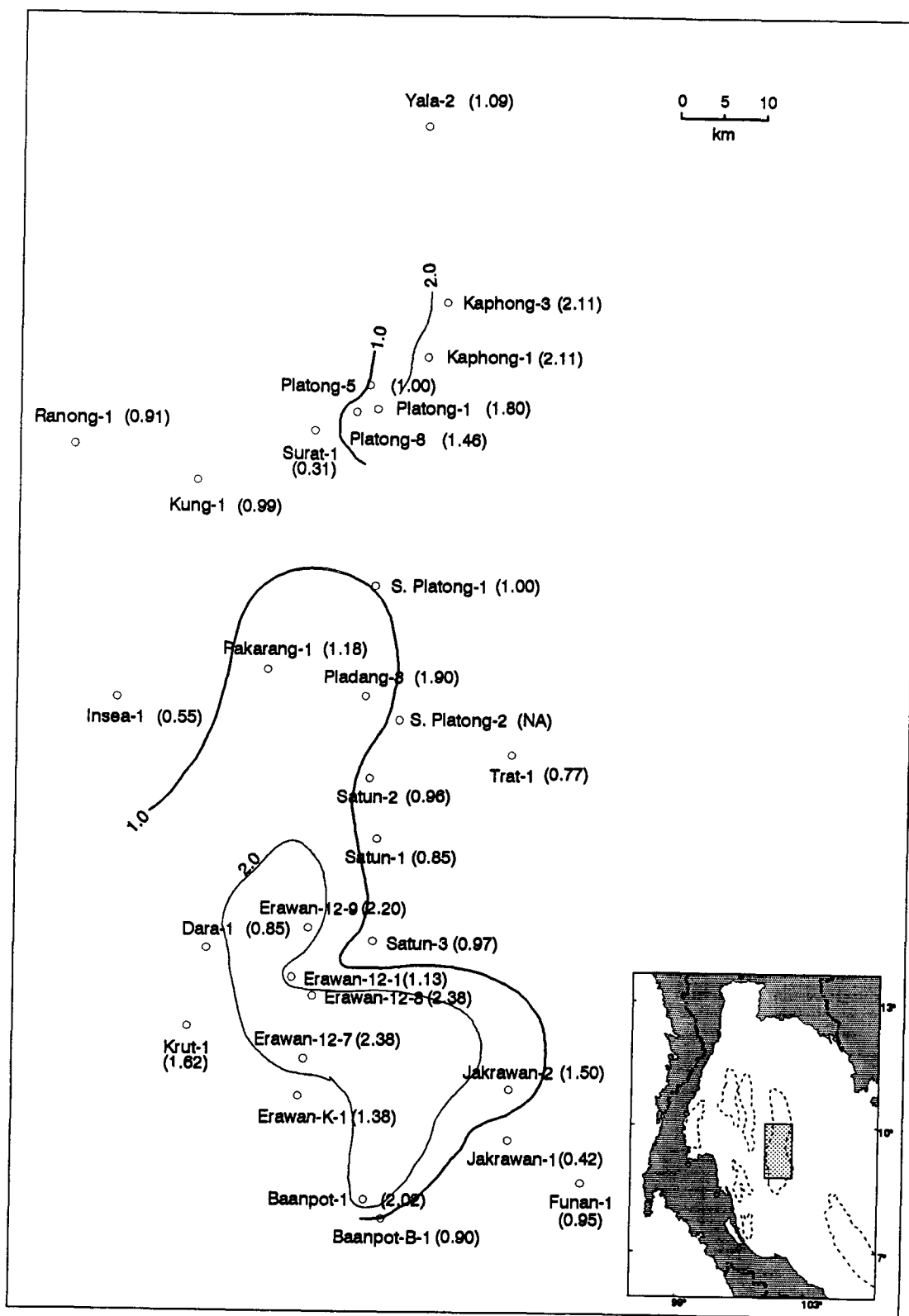


Figure 5.68: Lateral distribution of QOM (mg HC/g rock) of unit 3

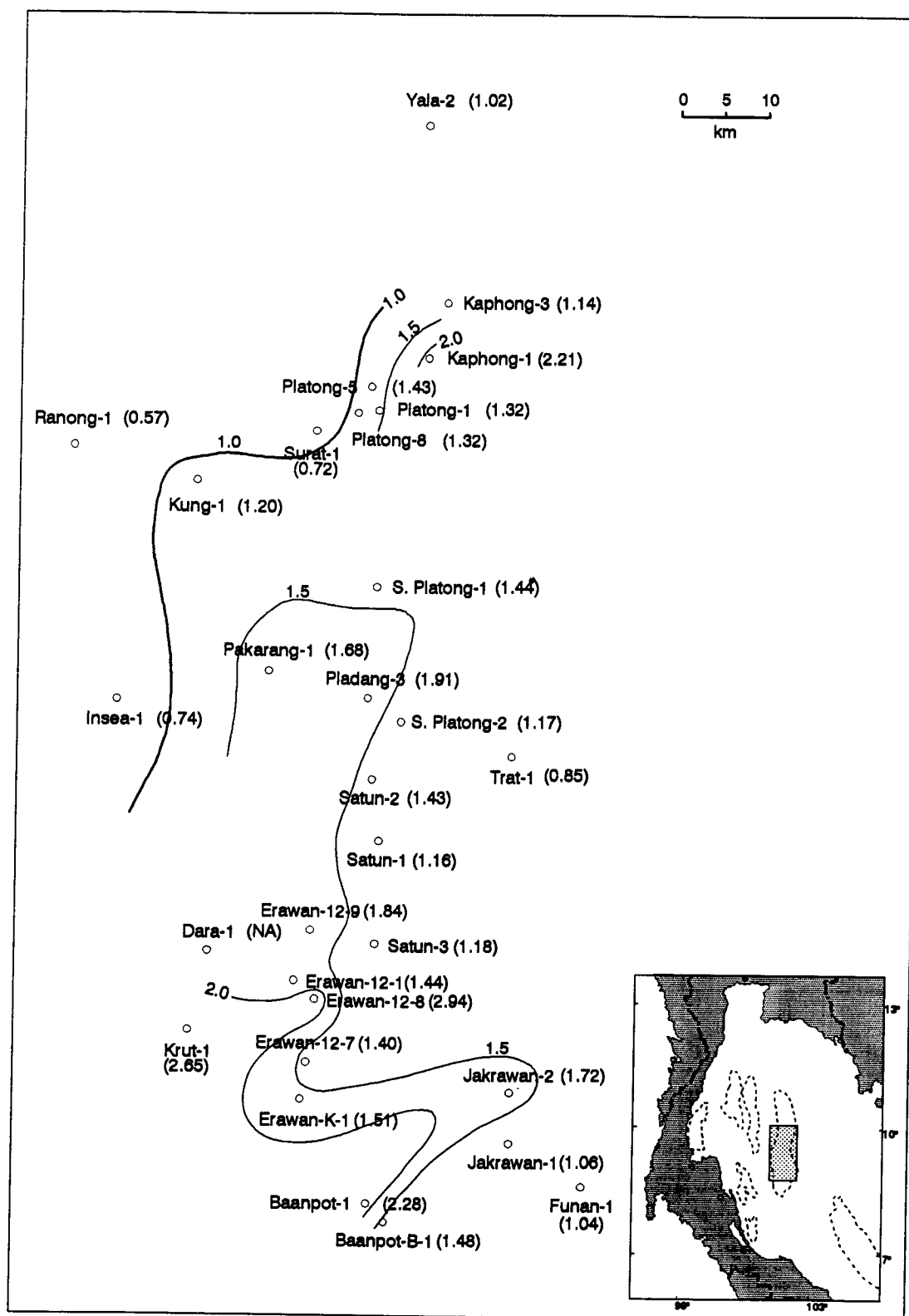


Figure 5.69: Lateral distribution of QOM (mg HC/g rock) of unit 2

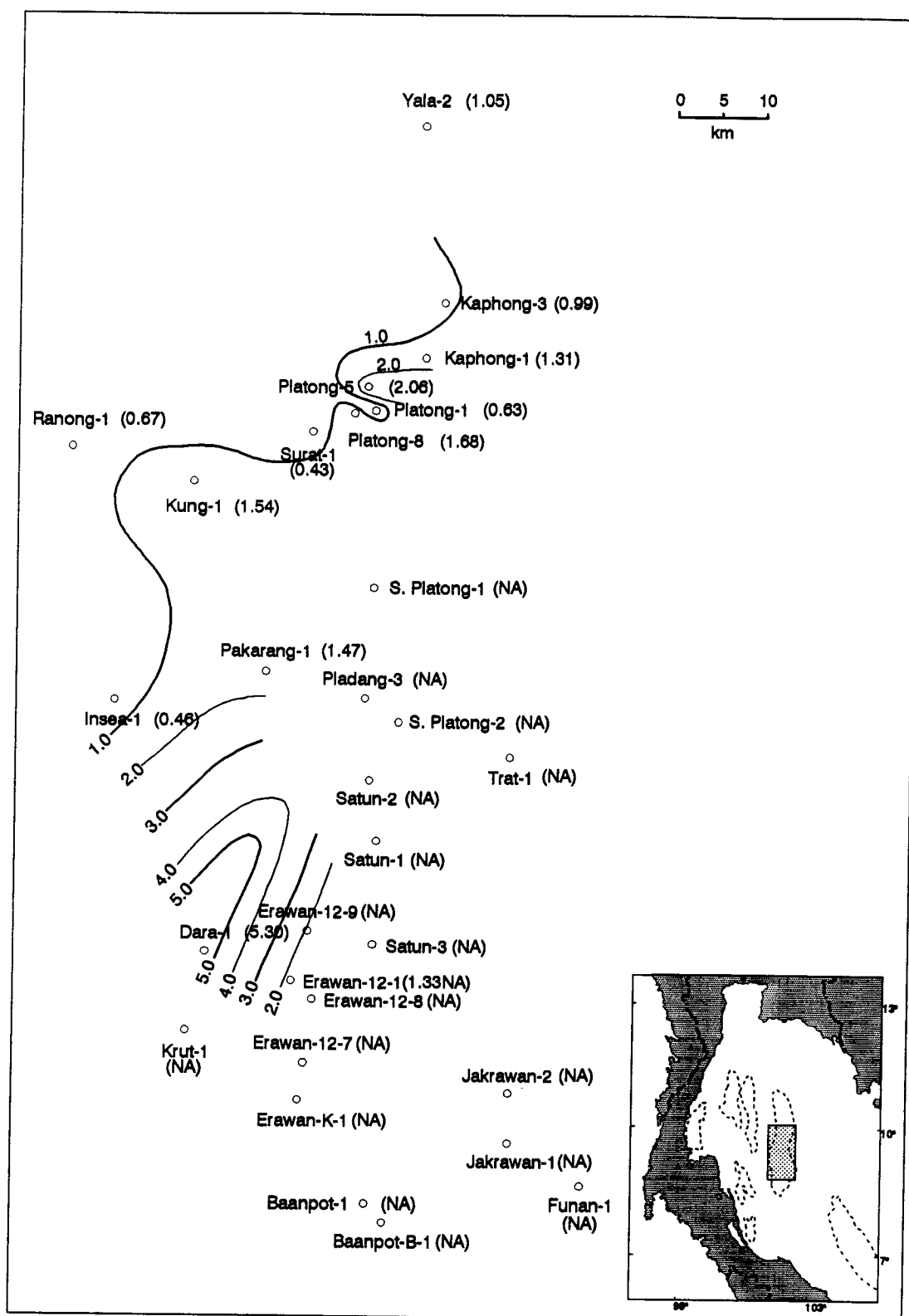


Figure 5.70: Lateral variation of QOM (mg HC/g rock) of unit 5's lower subunit

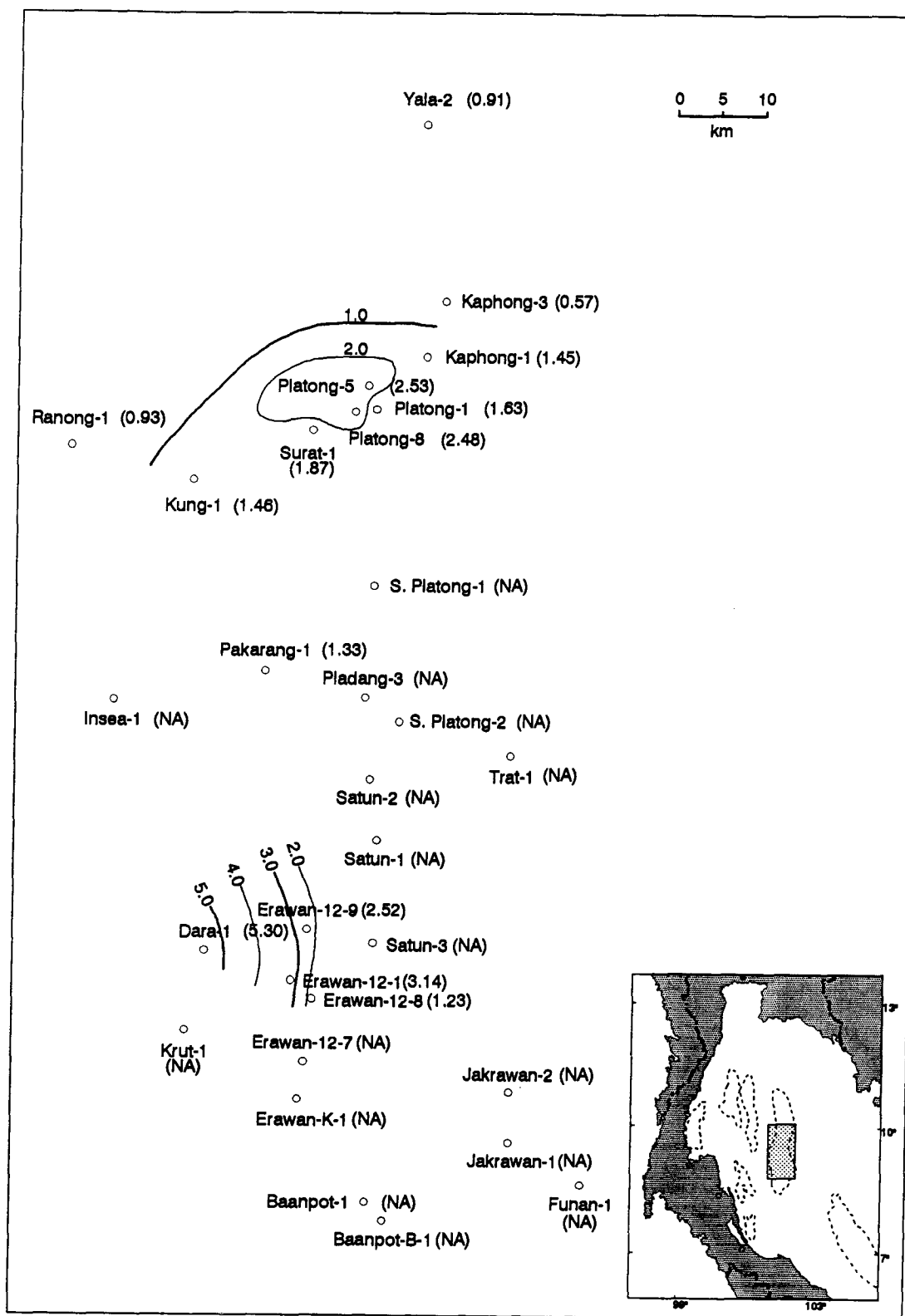


Figure 5.71: Lateral variation of QOM (mg HC/g rock) of unit 5's upper subunit

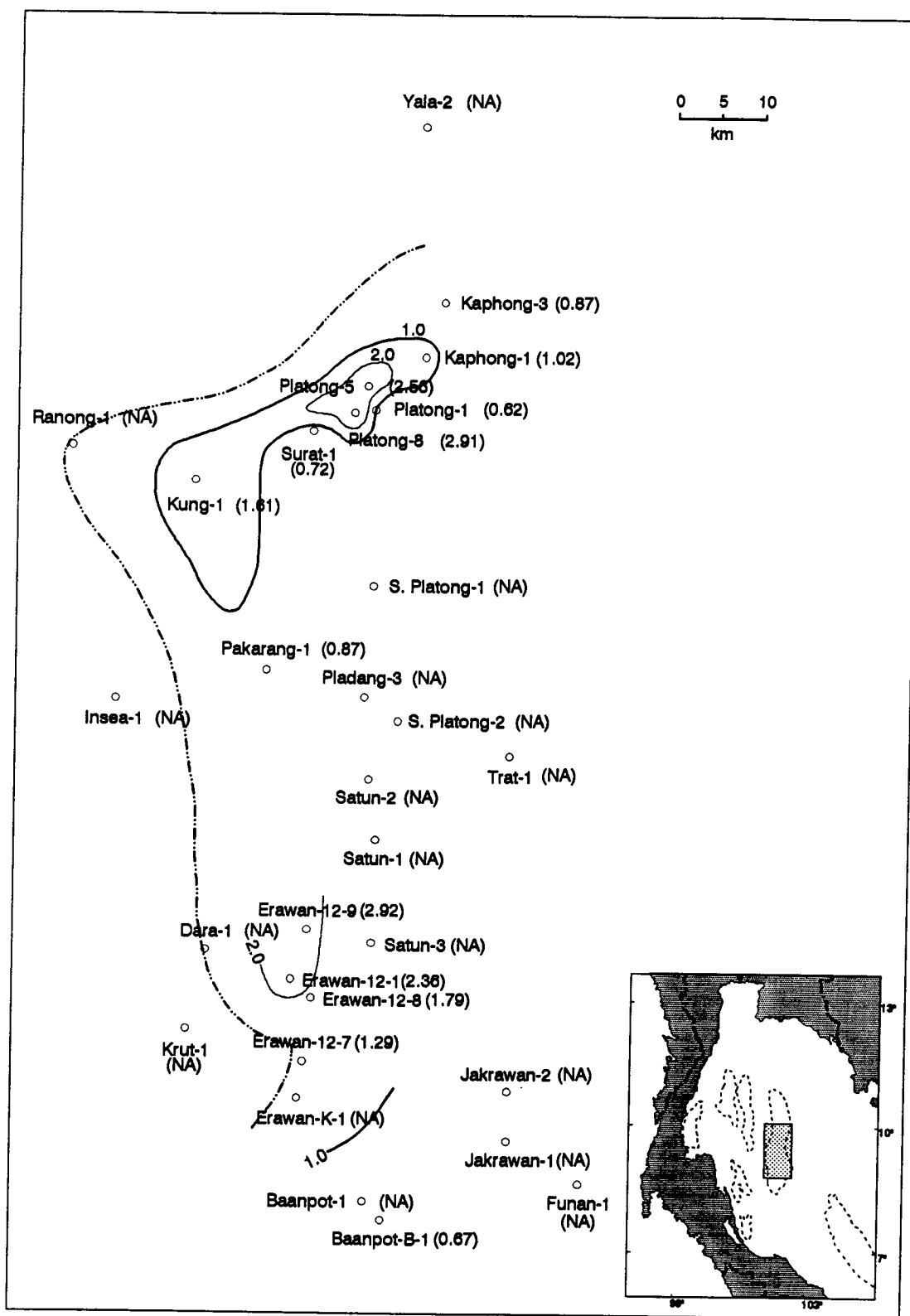


Figure 5.72: Lateral variation of QOM (mg HC/g rock) of unit 4's lower subunit

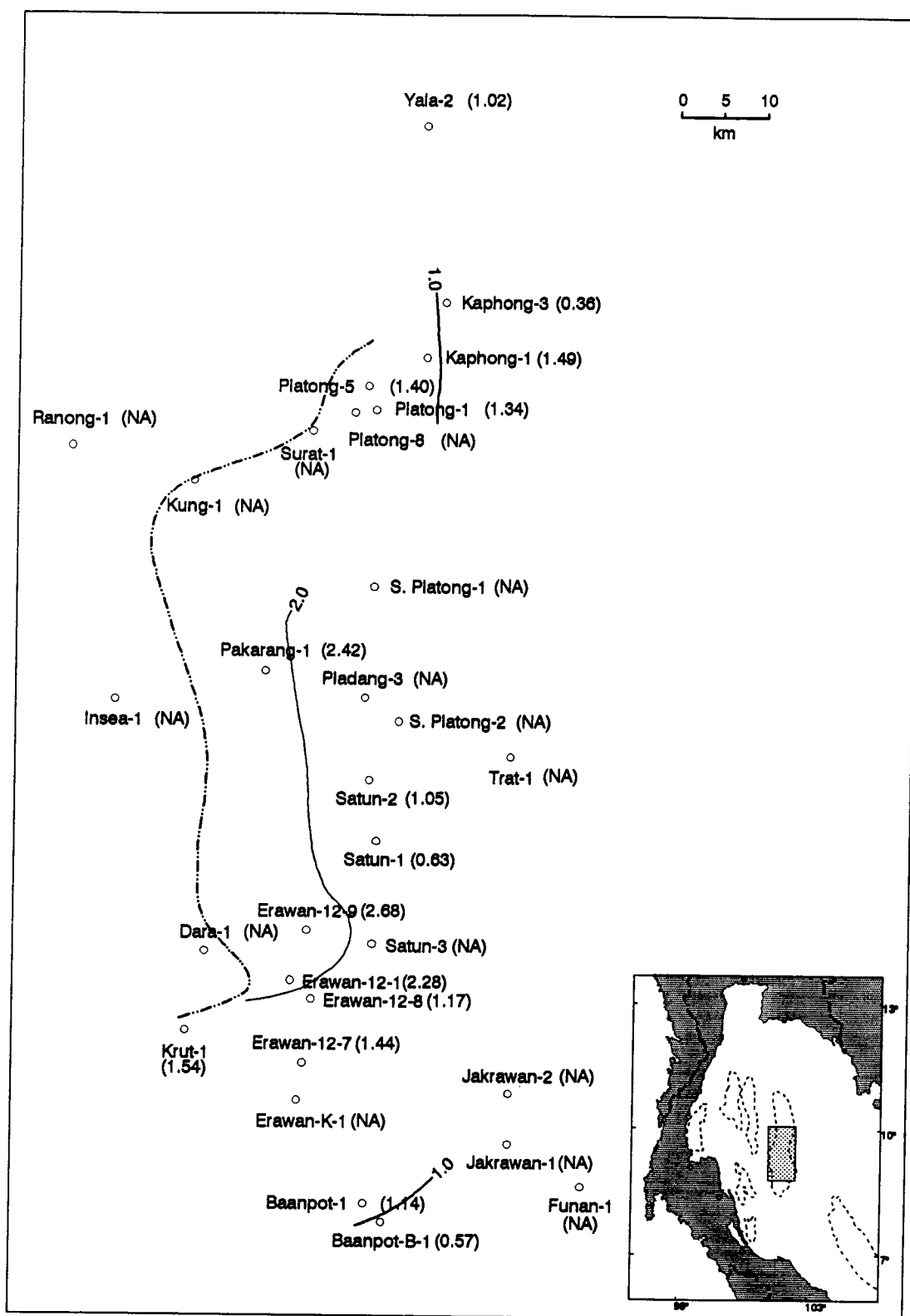


Figure 5.73: Lateral variation of QOM (mg HC/g rock) of unit 4's middle subunit

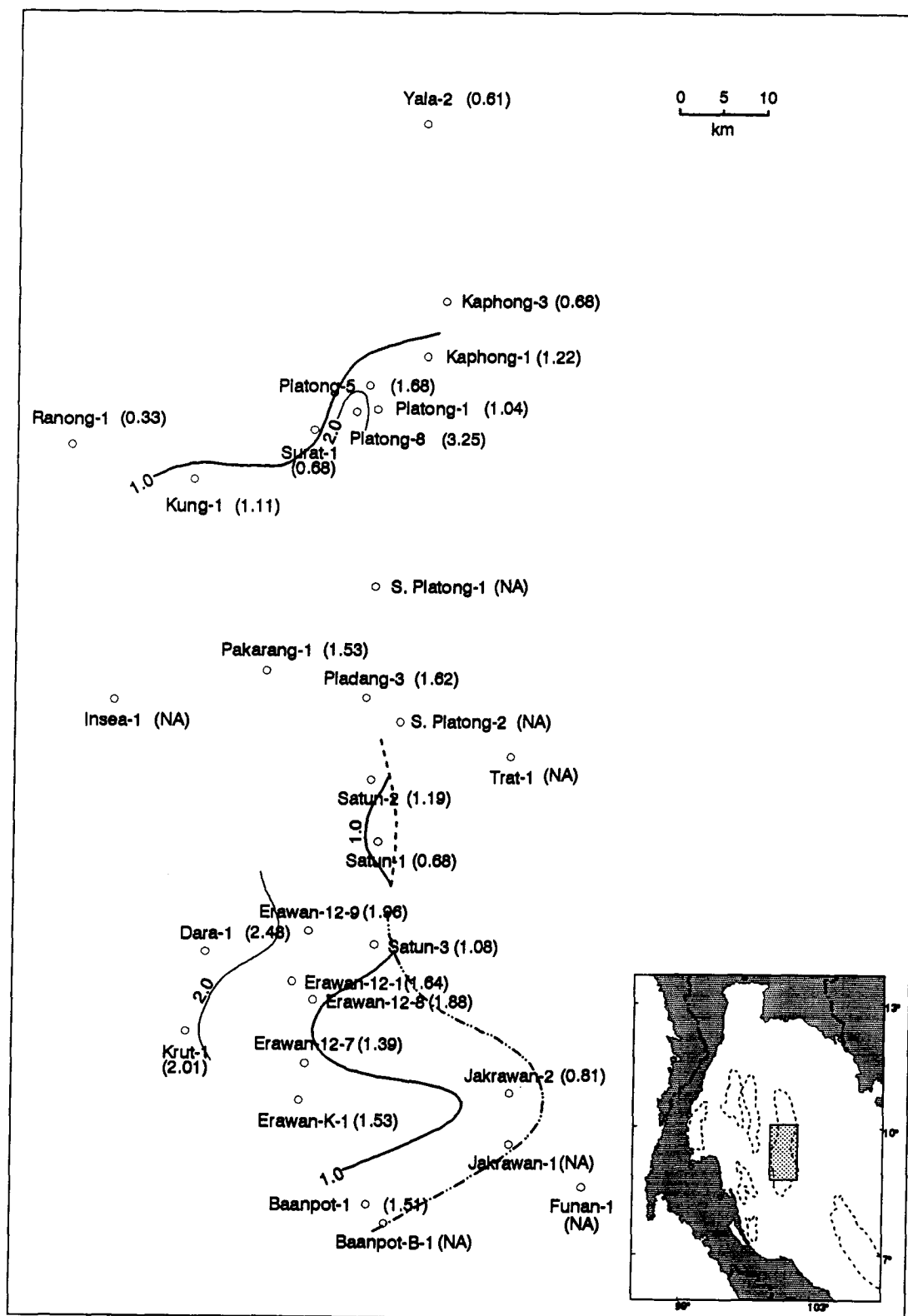


Figure 5.74: Lateral variation of QOM (mg HC/g rock) of unit 4's upper subunit

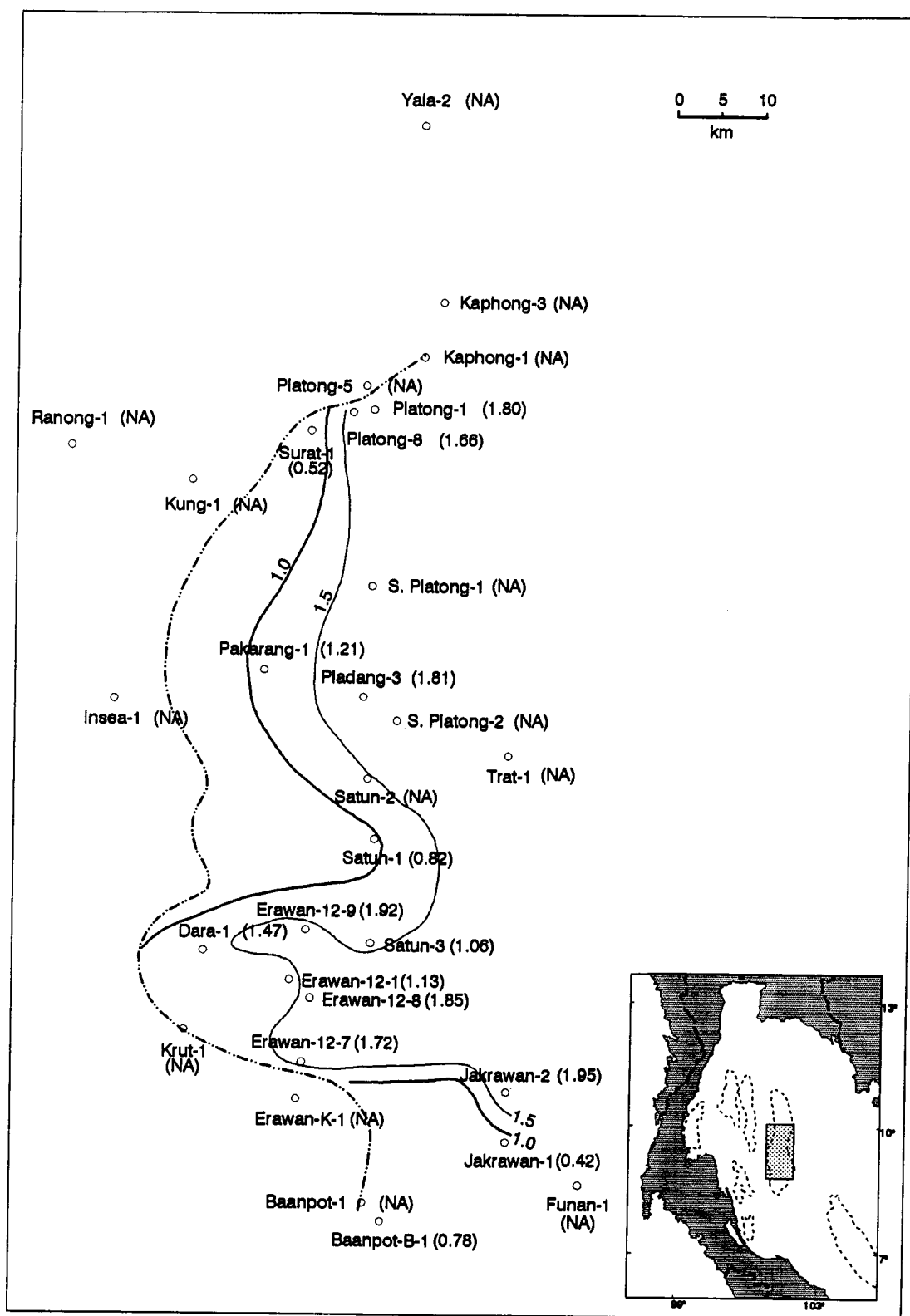


Figure 5.75: Lateral variation of QOM (mg HC/g rock) of unit 3's lower subunit

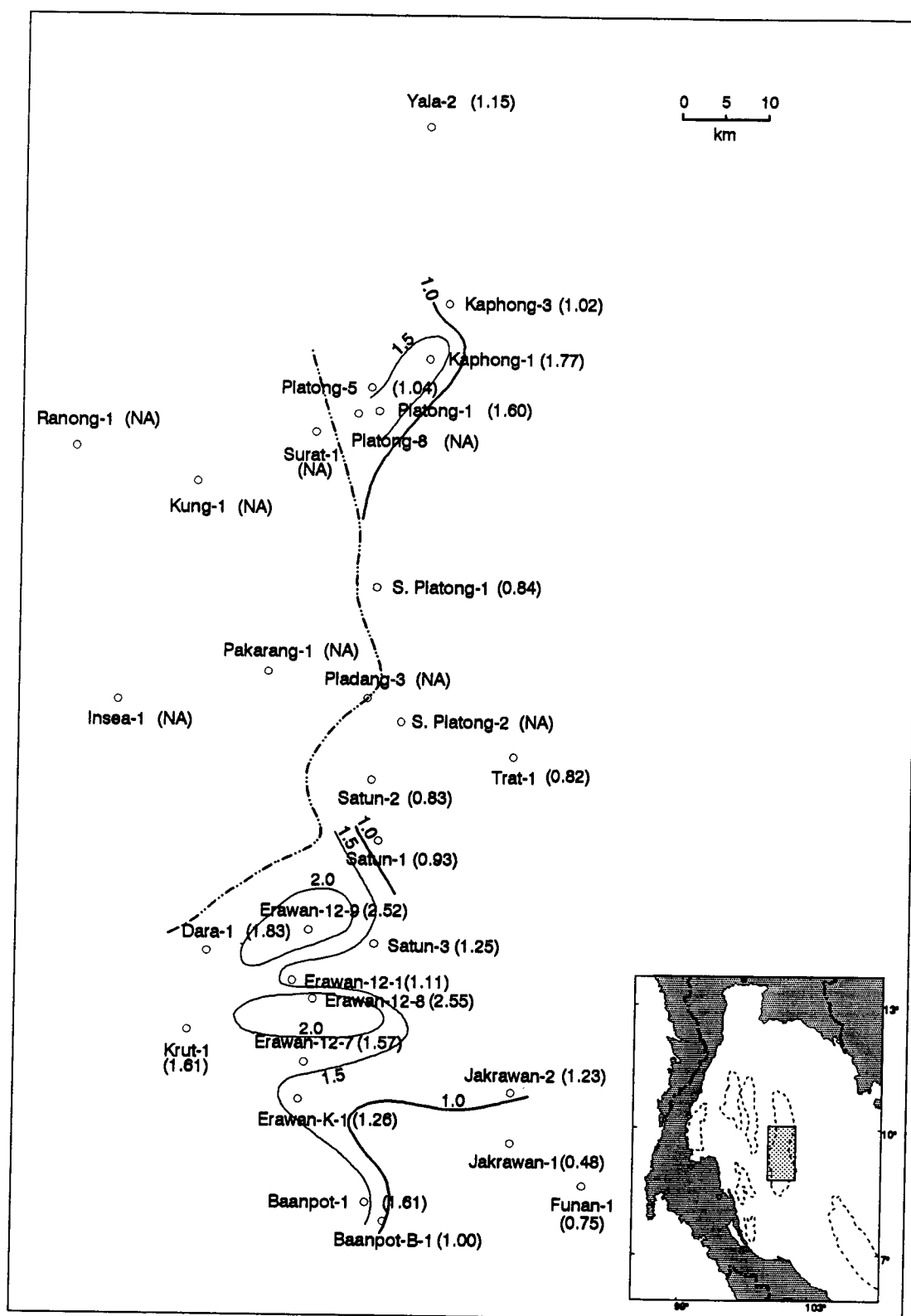


Figure 5.76: Lateral variation of QOM (mg HC/g rock) of unit 3's middle subunit

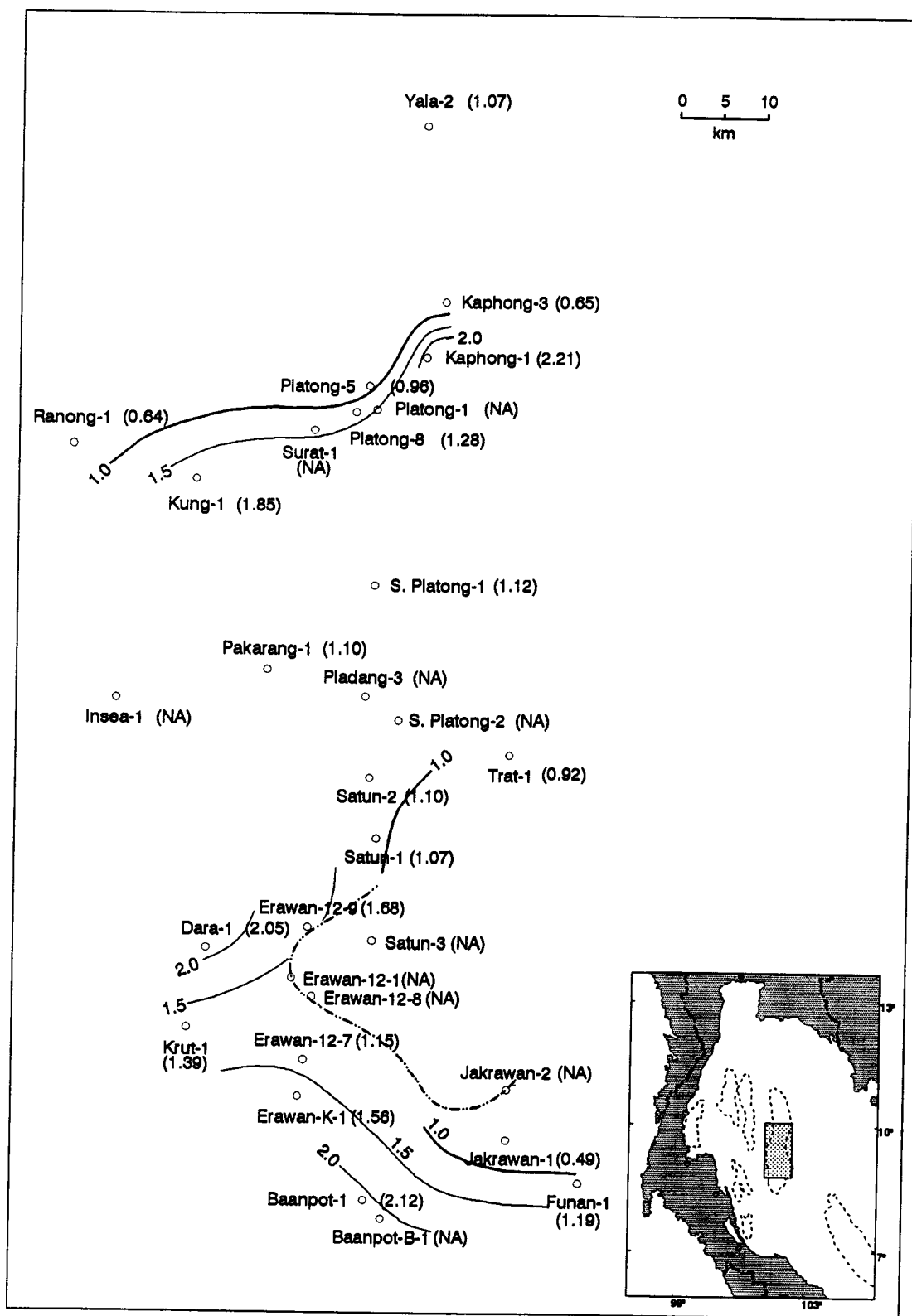


Figure 5.77: Lateral variation of QOM (mg HC/g rock) of unit 3's upper subunit

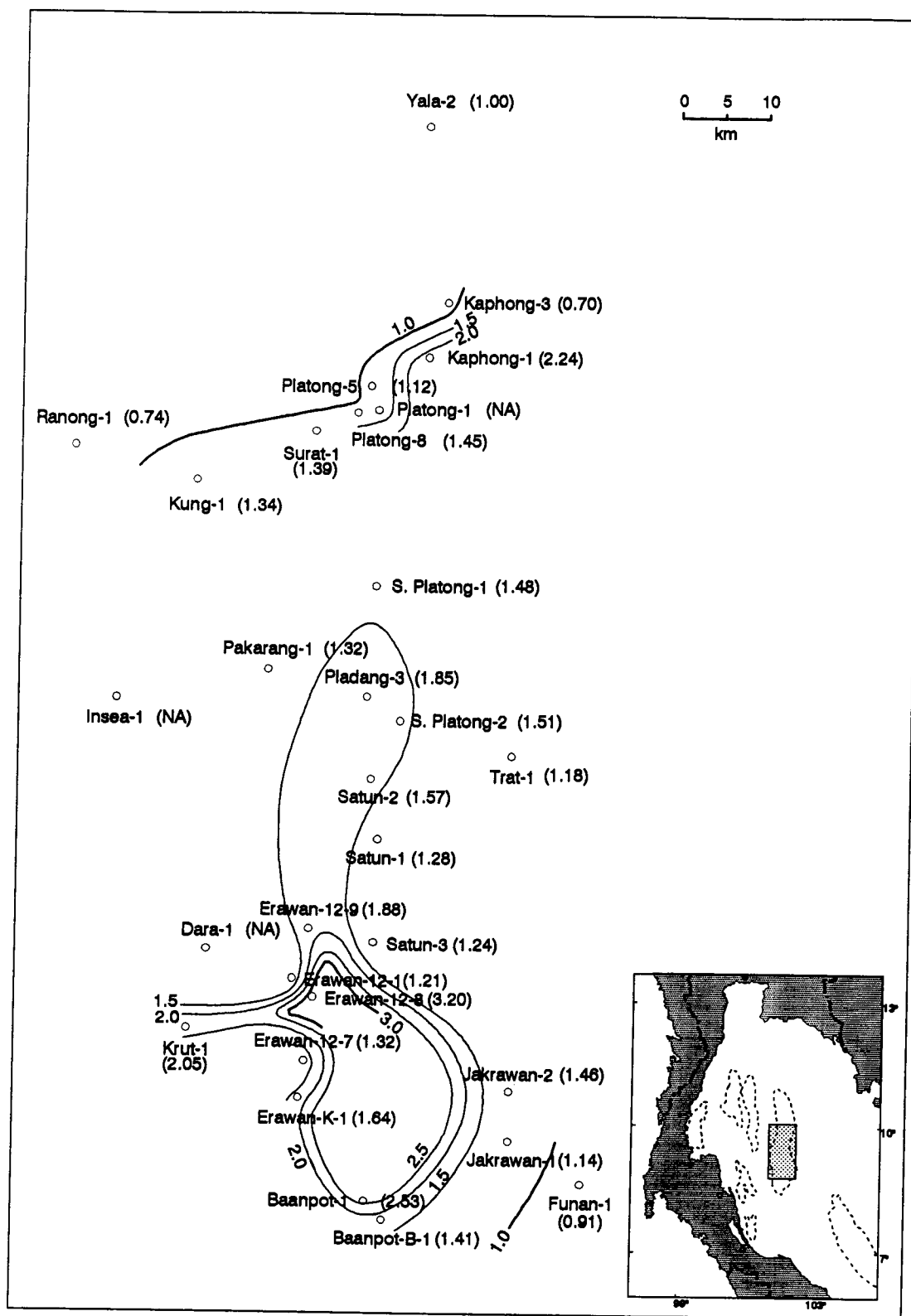


Figure 5.78: Lateral variation of QOM (mg HC/g rock) of unit 2's lower subunit

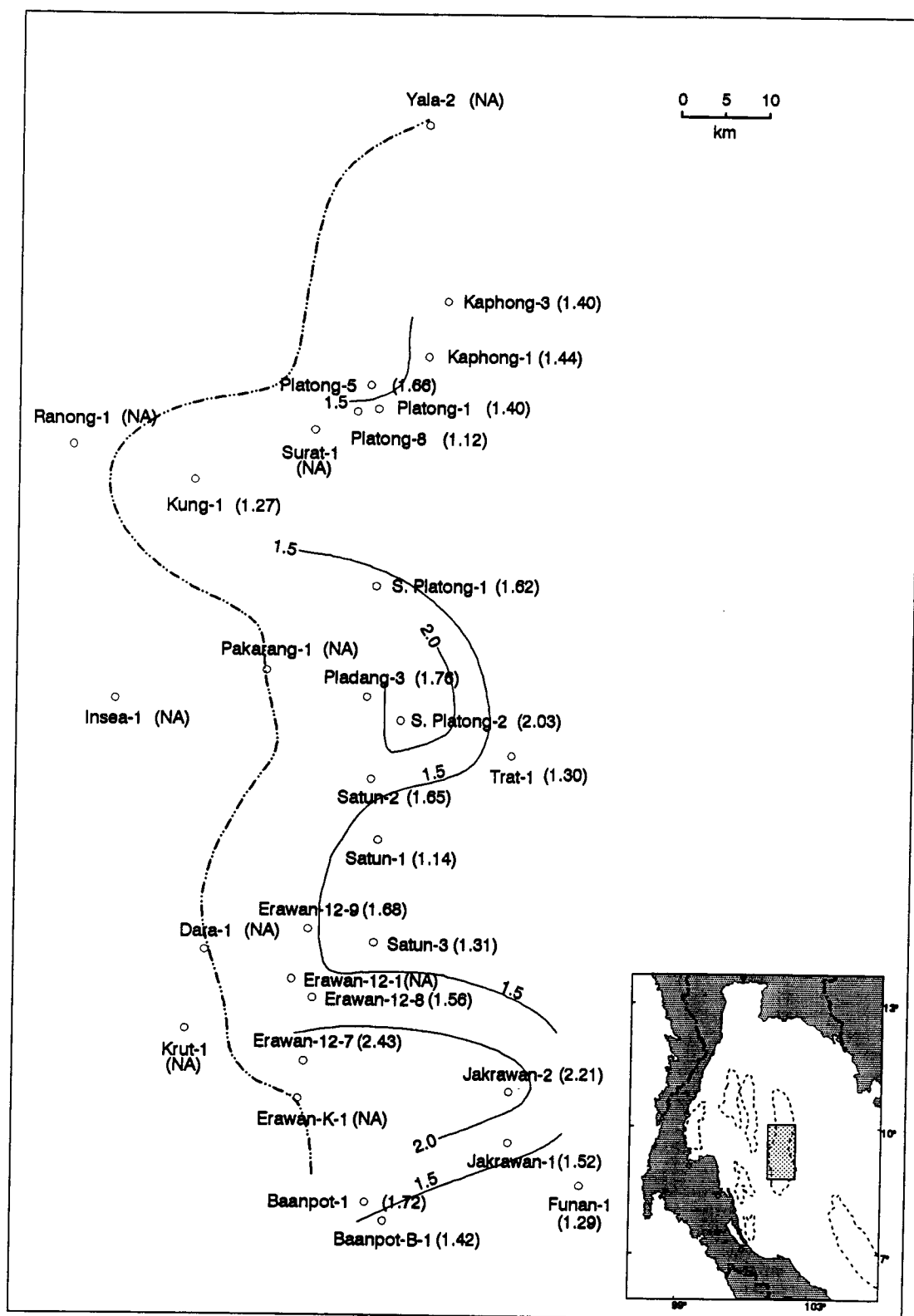


Figure 5.79: Lateral variation of QOM (mg HC/g rock) of unit 2's upper subunit

IV OM, Figure 5.39). This subunit contains mainly vitrinite and minor amounts of liptinite and inertinite. The vitrinite includes eu-ulminite, telocollinite and vitrodetrinite. The liptinite includes liptodetrinite and sporinite; the inertinite group includes semifusinite.

5.5.2 Unit 5

The TOC content of unit 5 ranges from less than 0.10% to about 0.44% (Figure 5.52) with an average value of 0.24% (Table 5.4). In general, the TOC content of this unit increases from the basin margin toward the basin center (Figure 5.52). The QOM of this unit varies from less than 0.5 mg HC/g rock to more than 5.1 mg HC/g rock (Figure 5.66) with an average value of 1.60 mg HC/g rock (Table 5.4). The organic characteristics of lower and upper subunits are described below.

The lower subunit of unit 5 is characterized by generally fine-grained claystone and minor interbeds of sandstone of the nonmarine floodplain deposits. The sediments in this subunit are partly oxidized due to their aerial exposure during and after deposition. The TOC content of this subunit varies from less than 0.1% to about 0.45% (Figure 5.56) with an average TOC of 0.24% (Table 5.5). The QOM of this subunit varies from 0.46 to 5.3 mg HC/g rock (Figure 5.70) with an average QOM of 1.46 mg HC/g rock (Table 5.5). This subunit contains mainly organic facies CD and D (Type III and Type IV OM, Figure 5.40). A mixture of organic facies BC and C (Type II-III OM) occurs in Kung-1 well. The maceral composition of this subunit is mainly vitrinite (including telinite, collinite, eu-ulminite, and corpohuminite) and minor liptinite (including cutinite and resinite).

The upper subunit of unit 5 is characterized by a series of fining-upward sequences of highly oxidized, nonmarine channel-fill and point bar deposits. Its TOC content ranges from less than 0.1% to about 0.44% (Figure 5.57) with an average TOC of 0.25% (Table 5.5). The TOC content generally increases toward the basin center (Figure 5.57). The QOM varies from 0.9 to about 5.3 mg HC/g rock (Figure 5.72) with an average QOM of 1.93 mg HC/g rock (Table 5.5). This subunit contains mainly organic facies C, CD, and D (Type III and Type IV OM, Figure 5.41). A single sample in Surat-1 well with a very high HI value (> 600 mg HC/g TOC) may be from drilling mud contamination. The maceral composition of this subunit is mainly vitrinite (attrinite, collinite, and telocollinite).

5.5.3 Unit 4

The TOC content of unit 4 ranges from less than 0.1% at the western margin of the basin to more than 0.5% at the basin center in the south-central part of the study area (Figure 5.53). The QOM varies from 0.36 mg HC/g rock to about 3.7 mg HC/g rock (Figure 5.67) with an average value of 1.44 mg HC/g rock (Table. 5.4). The organic characteristics of each subunit are described below.

The lower subunit of unit 4 is characterized by generally fine-grained claystone and siltstone interbedded with thin sandstone of the prodelta to shallow marine deposits. Its TOC content varies from less than 0.20% at the basin margin to about 0.3 to 0.5% toward the basin center (Figure 5.58) with an average TOC content of 0.32% (Table 5.5). The QOM increases from less than 0.5 mg HC/g rock to more than 2.0 mg HC/g rock (Figure 5.72) with an average QOM of 1.56 mg HC/g rock (Table 5.5). This subunit contains mainly organic facies CD and D (Type III and Type IV OM, Figure 5.42). Vitrinite (collinite) is the main maceral of this subunit.

The middle subunit of unit 4 is characterized by a series of coarsening-upward sequences representing distributary mouth bar deposits and beach ridge complexes. The TOC content of this subunit increases from less than 0.15% in the northern and western parts of the study area to about 0.7% in the southern part (Figure 5.59) with an average TOC of 0.35% (Table 5.5). The QOM, in contrast, increases from about 0.6 mg HC/g rock in the south to more than 2.4 mg HC/g rock in the western part of the study area (Figure 5.73). The main organic constituents of this subunit are facies D and CD (Type IV and Type III OM, Figure 5.43). Vitrinites, including collinite and eu-ulminite, are the main macerals in this subunit.

The upper subunit of unit 4 is characterized by a series of fining-upward sequences and interbedded claystones of nonmarine channel and floodplain deposits. The TOC content generally increases from less than 0.2% in the northern and western parts of the study area to about 0.7% in the southern and central parts with an average value of 0.36% (Figure 5.60). The highest QOM value in the northern part occurs in Platong-8 well location (3.2 mg HC/g rock) and decreases northwestward to less than 0.3 mg HC/g rock and eastward to about 1.0 mg HC/g rock (Figure 5.74). In the south, the QOM generally increases from less than 0.9 mg HC/g rock in the basin center to more than 2.4 mg HC/g rock to the west (Figure 5.74). The main organic constituents of this subunit are facies D and CD (Type IV and Type III OM, Figure 5.44). A mixture of organic facies BC and C (Type II OM) is found in Platong-8 and Krut-1 wells. Microscopic analysis of kerogen shows abundant vitrinite (collinite and telocollinite) and inertinite (fusinite), with minor amounts of sporinite.

5.5.4 Unit 3

The TOC content of unit 3 varies from about 0.5% to 0.8% in the west central part of the basin to less than 0.25% toward the west and east (Figure 5.54) with an average value of 0.44% (Table 5.5). Its QOM value shows a similar trend to TOC; it is highest (about 2.0 mg HC/g rock) in the south central part of the study area and decreases to less than 1.0 mg HC/g rock northwestward and to about 0.9 mg HC/g rock eastward (Figure 5.68) with an average value of 1.34 mg HC/g rock (Table 5.5). Organic characteristics of each subunit are described below.

The lower subunit of unit 3 is characterized generally by fine-grained, calcareous sediments interbedded with thin, coarse-grained shallow marine deposits. The TOC content of this subunit shows a NNW-SSE trend from relatively higher TOC values (about 0.9%) in the west-central part of the study area to lower values both westward and eastward to less than 0.2% (Figure 5.61), with an average TOC content of 0.44% (Table 5.5). The QOM value of this subunit generally increases from about 0.5 mg HC/g rock in the west to more than 1.8 mg HC/g rock in the central part of the study area (Figure 5.75), with an average value of 1.34 mg HC/g rock (Table 5.5). The main organic constituents of this subunit are facies CD and D (Type III and Type IV OM, Figure 5.45). The organic facies C and CD (Type II-III OM) also occur in Erawan-12-8 well location. The kerogen type is dominated by vitrinites (desmocollinite, eu-ulminite, and collinite) and inertinite (semifusinite), with minor amounts of liptinite (cutinite).

The middle subunit of unit 3 is characterized by a series of coarsening-upward sequences representing distributary mouth bar deposits and beach ridge complexes.

The TOC content is very low (about 0.2%) in the north, and higher (more than 0.5%) in the central part of the basin (Figure 5.62). A NW-SE trend of relatively high TOC (0.4 to 0.7%) occurs in the south (Figure 5.62). Overall, the average TOC content of this subunit is 0.39% (Table 5.5). This unit shows a complex QOM trend especially in the southern part of the study area (Figure 5.76). In general, however, the QOM values of this subunit range from 0.8 to 2.5 mg HC/g rock with an average QOM of 1.31 mg HC/g rock (Table 5.5). The main organic constituents of this subunit are facies D and CD (Type IV and Type III OM, Figure 5.46). A mixture of organic facies C and CD (Type II-III OM) occurs in Erawan-12-8 and Erawan-12-9 well locations. The kerogen types are mainly vitrinites (telinite and collinite) and subordinate liptinites (resinite and cutinite).

The upper subunit of unit 3 is characterized by a series of fining-upward sequences and fine-grained sediments of nonmarine meandering channel and floodplain deposits. The TOC content of this subunit generally increases toward the east from about 0.1% in the northern and western parts of the study area to about 0.6% in the southeastern part (Figure 5.63), with an average TOC content of 0.29% (Table 5.5). The QOM varies from less than 0.5 mg HC/g rock to about 2.1 mg HC/g rock (Figure 5.77), with an average QOM of 1.28 mg HC/g rock (Table 5.5). This subunit consists mainly of organic facies D and CD (Type IV and Type III OM, Figure 5.47). Vitrinites (telocollinite and eu-ulminite) are the main maceral components of this subunit.

5.5.5 Unit 2

Unit 2 is characterized by two relatively high TOC areas (about 0.8% in the northwest and about 0.6% in the east), separated by a NNE-SSW trending low

TOC region (Figure 5.55), with an average TOC of 0.54% (Table 5.4). The QOM values range from less than 0.7 mg HC/g rock to more than 2.0 mg HC/g rock (Figure 5.69), with an average QOM of 1.44 mg HC/g rock (Table 5.4). The organic characteristics of each subunit are described below.

The lower subunit of unit 2 is characterized by a well developed, equally-spaced series of fining-upward sequences of highly-oxidized, nonmarine meandering channel-floodplain deposits. In the northern part of the study area, the lower subunit is characterized by a NW-SE trending high TOC region (about 0.8 to 1.3 %TOC) flanked by low TOC areas (less than 0.3%) in the northeast and southwest (Figure 5.64). Further south, this subunit is characterized by an area of relatively high TOC (0.4-0.5%), flanked by lower TOC areas in the northeast and southwest (Figure 5.64). The average TOC content of the lower subunit is 0.43% (Table 5.5). The QOM in the northern part of the study area generally increases from less than 1.0 mg HC/g rock in the northwestern basin margin to about 2.2 mg HC/g rock in the basin center (Figure 5.78). Further south, a high QOM region (about 1.8-3.2 mg HC/g rock) is flanked by low QOM areas (approximately 1.2-1.3 mg HC/g rock) in the east and west Figure 5.78). The average QOM value of this lower subunit of unit 2 is 1.49 mg HC/g rock (Table 5.5). The subunit contains mainly organic facies C, CD, and D (Type II-III, Type III OM, and Type IV OM, Figure 5.48). Vitrinite (collinite) is the main maceral component.

The upper subunit of unit 2 is characterized by generally fine-grained sediments of marsh complexes to marginal marine deposits. The TOC content of this subunit generally decreases from more than 0.8% in the west to less than 0.5% toward the basin center (Figure 5.65) with an average TOC content of 0.81% (Table 5.5). The QOM, similar to that of TOC, generally decreases basinward from about 2.0

mg HC/g rock to less than 1.5 mg HC/g rock (Figure 5.79), with the average QOM of 1.57 mg HC/g rock (Table 5.5). This subunit contains mainly organic facies CD (Type III OM) and a mixture of organic facies C and CD (Type II-III OM, Figure 5.49). Microscopic analysis of organic matter shows abundant vitrinites (textinite and collinite) with minor liptinites (sporinite and cutinite).

5.5.6 Unit 1

Due to limited information from this unit, maps showing lateral variation of organic matter of this unit were not made. The average TOC content of this unit is 1.41% and an average QOM value is 1.39 mg HC/g rock (Table 5.4). The organic characteristics of each subunit are described below.

The lower subunit of unit 1 is characterized by a series of fining-upward sequences and fine-grained sediments of nonmarine to brackish water, coastal plain deposits. The TOC content ranges from 1.33 to 1.45% with an average TOC of 1.37% (Table 5.5). QOM values vary from 1.20 to 1.66 mg HC/g rock with an average QOM of 1.49 mg HC/g rock. The main organic constituents of this subunit are a mixture of organic facies C and CD (Type II-III OM, Figure 5.50). The dominant maceral is vitrinites (textinite and collinite), with lesser amounts of liptinite (cutinite) and inertinite (sclerotinite).

The middle subunit of unit 1 is characterized generally by fine-grained sediments interbedded with coal stringers representing brackish water interdistributary bay deposition. The TOC of the middle subunit ranges from 0.85 to 2.08%, average 1.47% (Table 5.5). The QOM of this subunit varies from 0.96 to 2.04 mg HC/g rock with an average QOM of 1.64 mg HC/g rock. This subunit contains mainly

organic facies BC, C and CD (Type II and Type III OM, Figure 5.51). The main maceral composition determined from reflected white light examination is dominated by vitrinite (textinite and collinite) with minor amounts of liptinite (cutinite).

The upper subunit of unit 1 is characterized by fine-grained sediments of shallow marine deposition. No samples from this interval are available.

5.6 DISCUSSION

5.6.1 Origin of Variation in Organic Matter

Factors that control the abundance of organic matter in sediments include organic inputs, sedimentation rates, degree of preservation of organic matter after deposition, and degree of organic maturation. Depending on the combination of these factors, the organic carbon content and characteristics in sediments will vary significantly. It is very important to note that using any one of the factors may not exclusively explain the variation in organic characteristics in the sediments because as one factor changes, other factors might also change. This section documents the source, character, and factors affecting the distribution of organic matter. In order to examine the influence of geology on the variation of organic characteristics of the Tertiary strata in the Pattani Basin, various diagrams of organic properties versus geological factors such as depositional environments, sedimentation rates, and age were prepared.

a. Origin of Organic Matter:

The dispersed organic matter in the Tertiary sediments in the Pattani Basin is composed mainly of Type III (organic facies C and CD) and Type IV (organic facies D) kerogen with minor mixtures of Type II and Type III kerogen. The organic matter is characterized by relatively low HI and high OI values. The maceral composition of the organic matter is consistent in all units with vascular plant sources. The dominant maceral component of all studied samples is vitrinite (collinite, eu-ulminite, and textinite) with minor amounts of inertinite (semifusinite and sclerotinite) and liptinite (sporinite and cutinite).

Because most of the Tertiary stratigraphic units in the Pattani Basin were deposited in nonmarine to marginal marine environments, the dispersed organic matter in the sediments was probably of detrital, and continental in origin. The detrital and continental origin of the sedimentary organic matter is supported by the predominant occurrence of Type III-Type IV kerogen, combined with the presence of vitrinite, liptinite, and especially sporinite and cutinite, which were derived from vascular plants, accompanied by relatively low HI and high OI values of the kerogen (Tissot and Welte, 1984; Bustin, 1988). The detrital organic matter was supplied to the depositional sites mainly by the river systems that also fed clastic sediments to the areas and hence was mainly allochthonous. Autochthonous and hypautochthonous origins are also evident from the presence of interbedded coals and carbonaceous partings in many stratigraphic units.

b. Organic Characteristics and Depositional Environments

Variations of TOC and HI in different stratigraphic units with respect to depositional environments are shown in Figure 5.80.

For almost all stratigraphic units, both the TOC and HI increase from high energy nonmarine environments to lower energy marginal marine or shallow marine environments (Figure 5.80), although the mean TOC contents and HI values differ for different stratigraphic units. The lowest TOC and HI (0.07% and 9 mg HC/g TOC, respectively) occur in high energy, alluvial fan and braided stream deposits of the lower subunit of unit 6. The highest TOC (1.47%) occurs in fine-grained shallow marine deposits of the middle subunit of unit 1. The highest HI (120-127 mg HC/g rock) occurs floodplain deposits in the lower subunit of unit 1 and prodelta to shallow marine deposits of the upper subunit of unit 2 and the middle subunit of unit 1.

The very low TOC of alluvial fan and braided stream sediments of the lower subunit of unit 6 can be explained by the fact that the subunit consists of coarse-grained sediments deposited in a high energy environment. Under such aerobic promoting conditions, low quantities of organic input and low degrees of preservation resulted. A low organic supply reflects less vegetation hence a minimal source of organic matter for the subunit. Free circulation of water containing dissolved oxygen would be common in such an aerobic environment, resulting in intense destruction of organic matter by oxidation.

Higher TOC and HI in floodplain deposits may reflect the proximity to swamp complexes, hence, sources of organic matter. Fine-grained sediments in floodplain

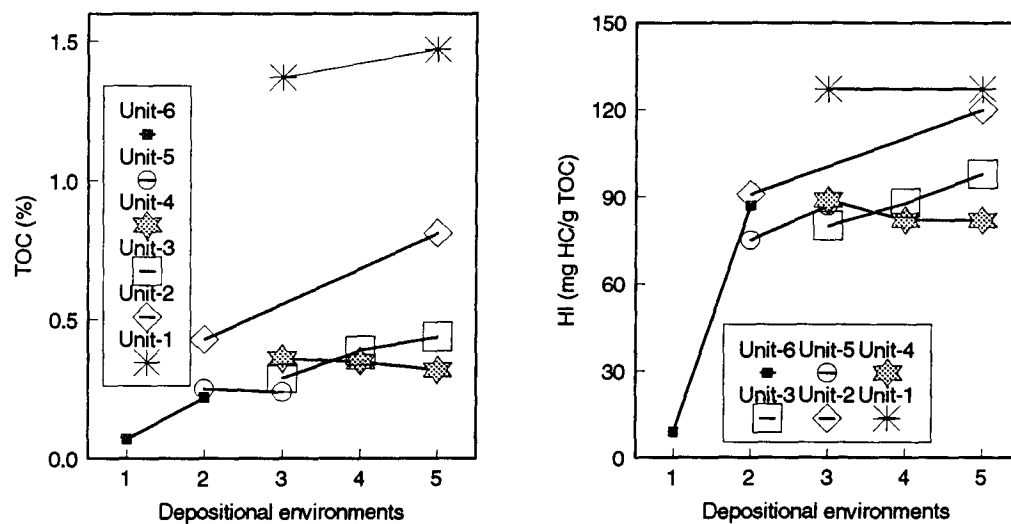


Figure 5.80: Variation of TOC (%) and HI (mg HC/g TOC) v.s. depositional environment of different stratigraphic units. 1. Alluvial fan and braided stream sediments; 2. Channel deposits; 3. Floodplain deposits; 4. Distributary mouth bars; 5. shallow marine deposits. (n = 4500).

deposits would further enhance the degree of organic preservation because the fine-grained sediments would quickly form a closed environment. In such confinement, there would be no replenishment of oxygen, anaerobic conditions would be rapidly established, and hence the rate of destruction of organic matter was reduced (Tissot and Welte, 1984).

TOC content in river mouth bar deposits and beach complexes in this study is as high as that in floodplain deposits. Such a similarity may reflect a balance between the degree of organic preservation and the effect of dilution of mainly allochthonous organic matter by rapid sedimentation.

The highest TOC and HI in this study occur in interdistributary bay and shallow marine deposits, especially in units 2 and 1. This may be the result of both high organic input and high degree of organic preservation. High organic input may reflect the proximity to sources of organic matter such as marsh and peat swamp environments. A high degree of organic preservation may be the result of the fine-grained nature of the sediments and the transgressive nature of the stratigraphic units. This would prevent easy circulation of free oxygen, and thus reducing oxidation of organic matter.

c. Organic Characteristics and Maturation

The relations of organic maturation with both the abundance and characteristics of organic matter in sediments can be assessed by comparing maps of TOC distribution (Figure 5.52 through Figure 5.55) with maps of organic maturation, in this case, the extent of hydrocarbon generation (Figure 6.41 through Figure 6.44). They can also be noted by plots of TOC and HI versus maturity indices, as

expressed by the extent of hydrocarbon generation and vitrinite reflectance (Figure 5.81).

The TOC values of most strata do not conform with the isomaturity lines. In general, there is a weak positive correlation between degree of organic maturation and TOC and HI. Such a weak correlation might be fortuitous, and simply be the result of natural variations in TOC from place to place within the same stratigraphic unit and variations across the unit. A weak positive correlation between HI and degree of organic maturation also indicates that the sediments in the deeper, thus more mature, part of the basin are richer in organic content and pyrolysis yield than those in the shallow part.

d. Organic Abundance and Sedimentation Rate

The variation in TOC with sedimentation rate is shown in Figure 5.82. Sedimentation rates, corrected for sediment compaction, were calculated using geohistory analysis described in chapter 4. Relationships between sedimentation rate and organic abundance on the scale of the unit were made because the age constraint available did not permit the relation to be lowered to the subunit scale. Except for unit 6 and unit 1, the correlation coefficient between sedimentation rate and TOC is very poor ($r^2 < 0.10$, Figure 5.82). In units 6 and 1, TOC generally decreases as sedimentation rate increases (Figure 5.82). In general, the TOC versus sedimentation rate relationship is poor (Figure 5.82). The sedimentation rate in the study area is very high compared to that of marine sedimentation, with the decompacted sedimentation rate ranging from about 0.02 km/m.y. to more than 0.9 km/m.y. (Figure 5.82). High sedimentation rates such as these are a common characteristic of sediments deposited in deltaic environments such as the Tertiary

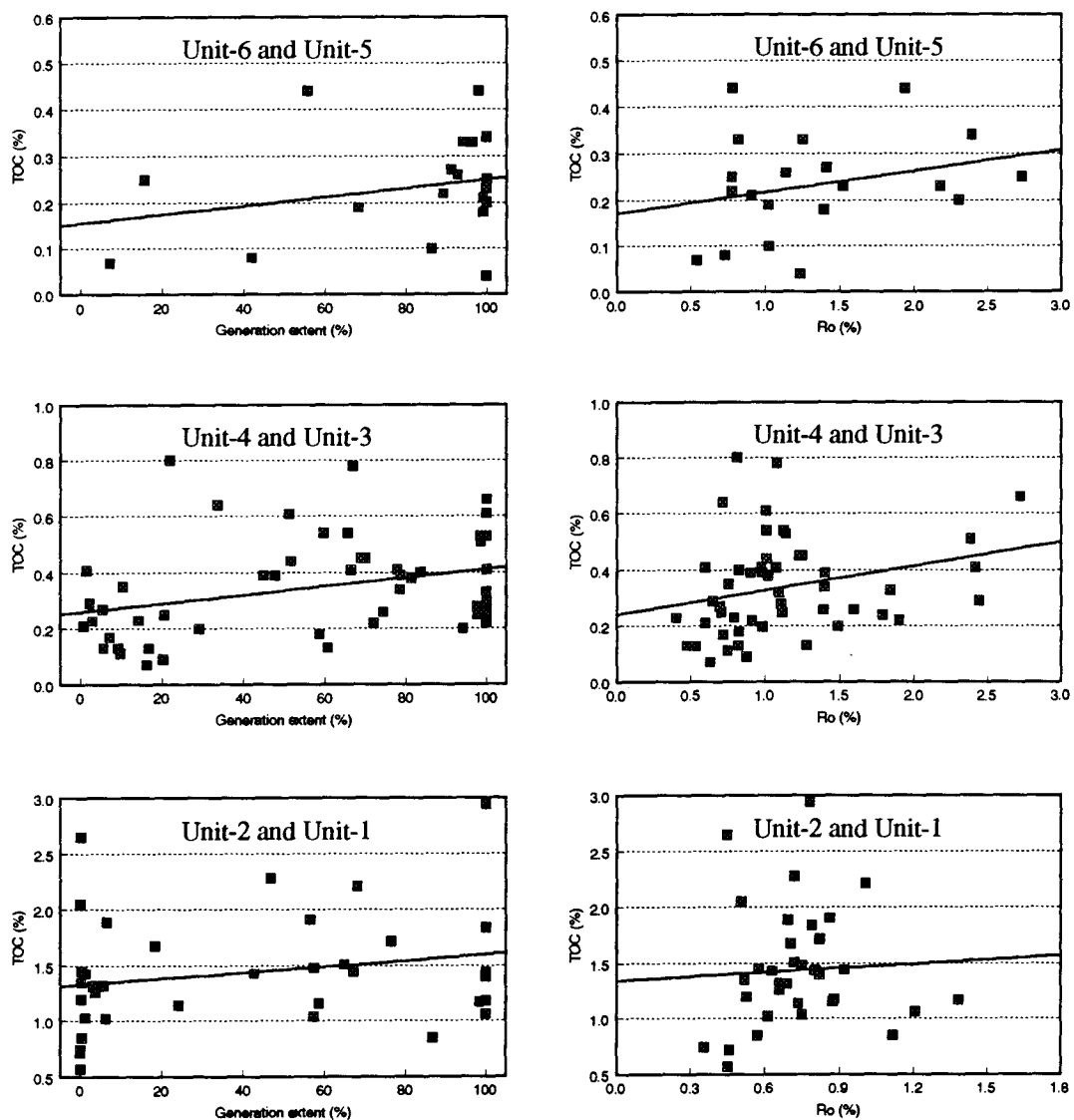


Figure 5.81: Variation of TOC v.s. degree of organic maturation of different stratigraphic units

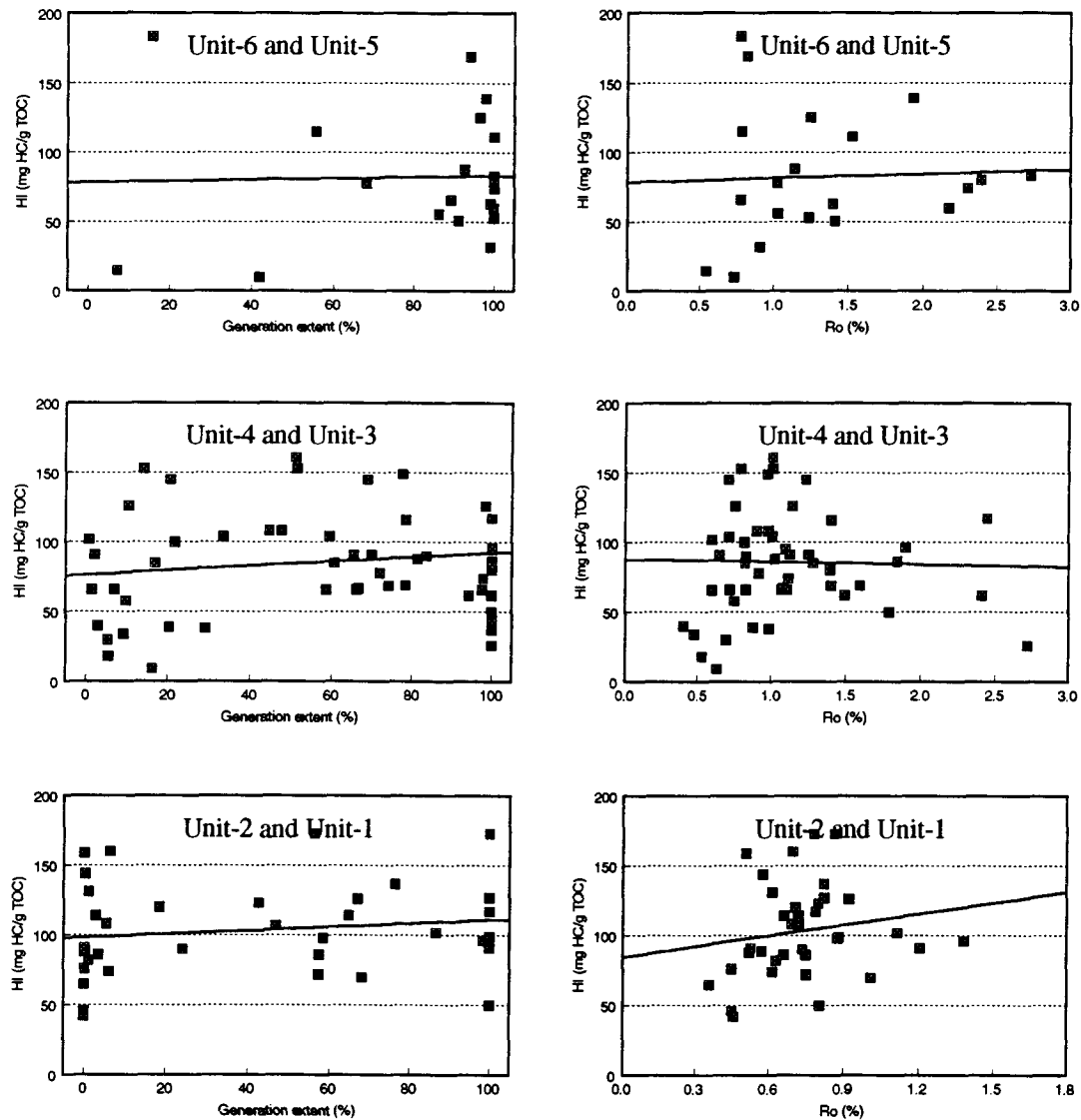


Figure 5.81 (Continued): Variation of HI v.s. degree of organic maturation of different stratigraphic units

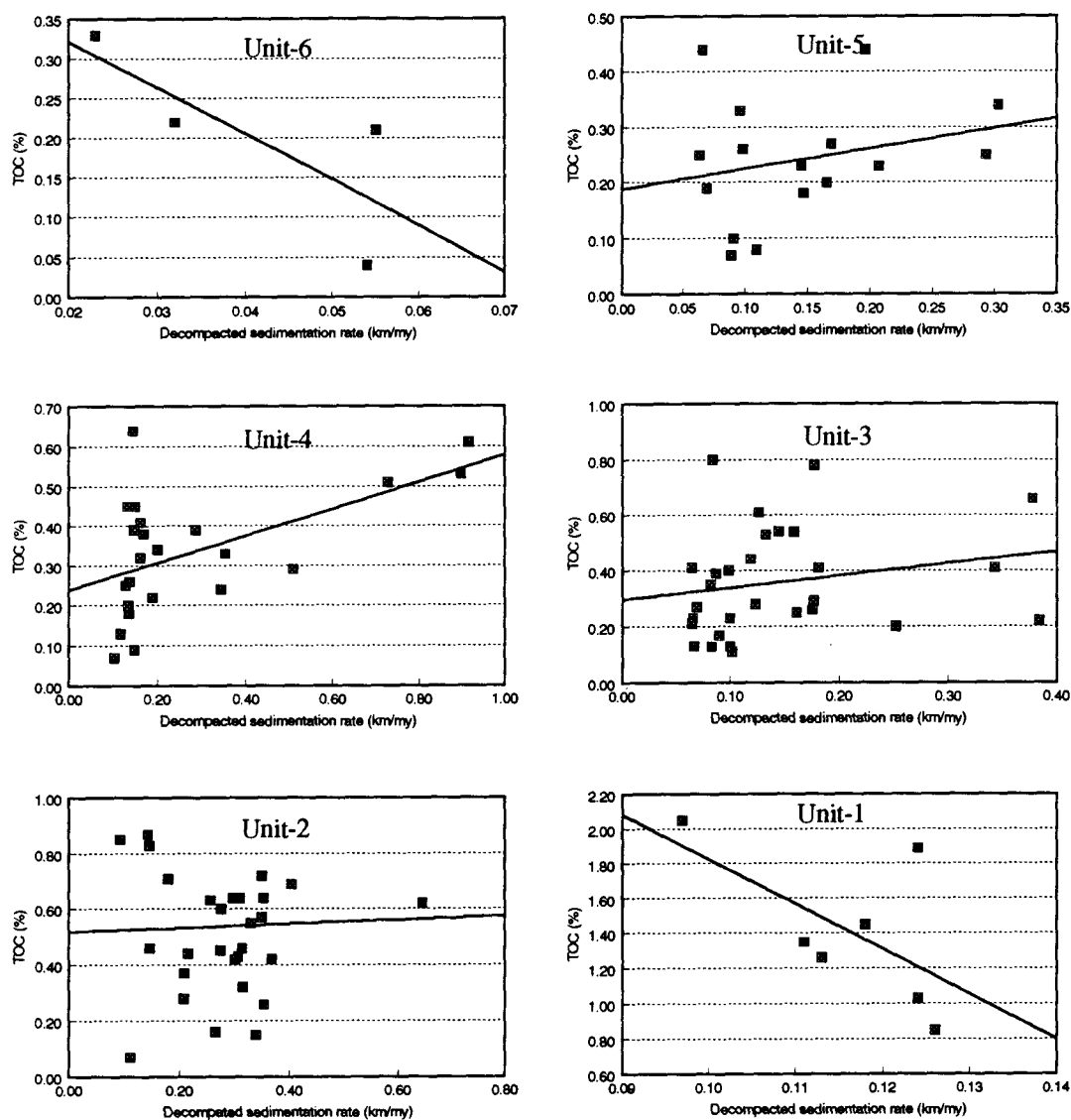


Figure 5.82: Variation of TOC (%) v.s. sedimentation rate (km/my) of different stratigraphic units

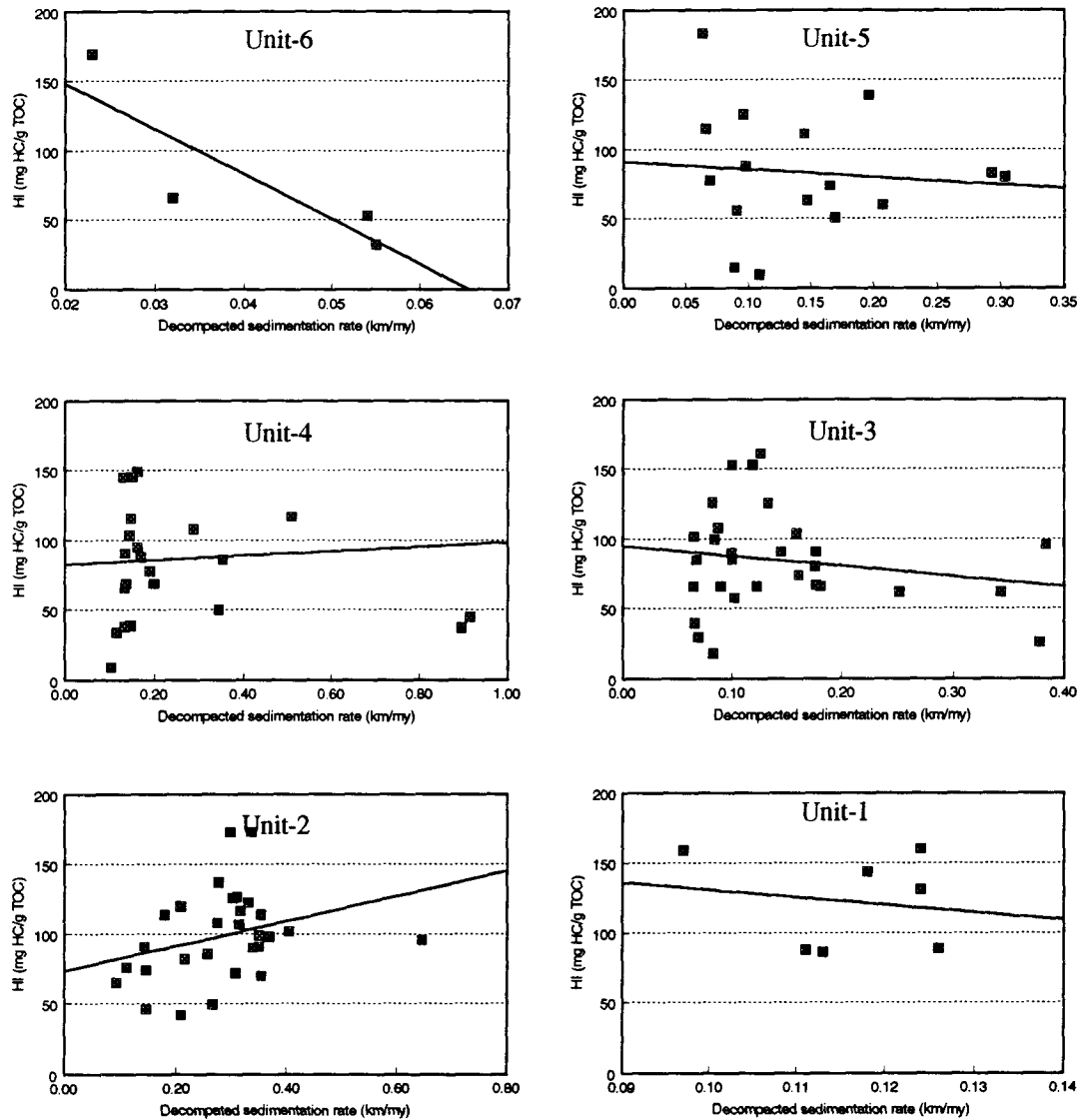


Figure 5.82 (Continued): Variation of HI (mg HC/g TOC) v.s. sedimentation rate (km/my) of different stratigraphic units

Niger Delta, where the undecomposed sedimentation rate ranges between 0.07-0.70 km/m.y. (Bustin, 1988).

The relationship between sedimentation rates and TOC has been studied by various authors. Toth and Lerman (1977) and Muller and Suess (1979) suggested that in areas of mainly primary autochthonous production, organic matter content generally increases with sedimentation rate due to rapid burial. Ibach (1982) carried out the study on DSDP cores of ancient marine sediments, and suggested that at slow sedimentation rates, TOC content increases with sedimentation rate due to greater preservation of organic matter with more rapid burial which prevents oxidation. Above a critical sedimentation rate (0.021 km/m.y. for siliceous sediments and 0.041 km/m.y. for black shale), the TOC content decreases with increasing sedimentation rate due to dilution by mineral matter. The relationship between allochthonous organic matter and sedimentation rate was documented, though indirectly, by both Meybeck (1982) and Bustin (1988). Meybeck (1982) studied the total organic carbon transport in rivers, and pointed out that, although the total particulate organic carbon content increases with river discharge, total suspended matter concentration increases more rapidly with increasing discharge. This results in an absolute increase in TOC, but a decrease in TOC content relative to the volume of sediment transported. Bustin (1988), based on his study on the dispersed organic matter in the Niger Delta, suggested, in the semi-quantitative terms, that TOC content decreases with increasing sedimentation rate due to increased dilution by mineral matter.

Compared to the study of other ancient marine sediments, the sedimentation rate of Tertiary sediments in the Pattani Basin is much higher than the critical sedimentation rates proposed by Ibach (1982). The TOC of Tertiary sediments in

the Pattani basin, except for unit 1, is very low (less than 1.0%, Figure 5.82). For those units with low TOC, there is no correlation between sedimentation rate and TOC. Such results indicate that in the units with low TOC, indigenous variation of TOC within the sediments has greater effect on TOC than the sedimentation rate. By contrast, in the unit with high TOC (more than 0.6-2.2%, unit 1), there is a strong negative correlation between TOC and sedimentation rate. Such a result suggests that in organic-rich sediments, sedimentation rate has greater control on TOC. A decrease in TOC with increasing sedimentation rate in unit 1 may be the result of clastic dilution of the organic input.

e. Organic Abundance and Age

The variation in abundance and characteristics of organic matter in the Pattani Basin is closely correlated with the age of strata. Younger strata have higher TOC and generally higher HI (Figure 5.83) and the increases occur in almost all sedimentary facies (Figure 5.80). The variation of TOC and HI with age is greater than the variation within strata of the same age but among different sedimentary facies (Figure 5.80). The strong correlation between the age of strata and TOC and HI must be an indication of: (1) factors controlling either the relative availability of organic matter, such as organic supply, or the preservation of organic matter, such as sedimentation rate, organic maturation or both such as depositional environment; (2) changes in main plant types; and (3) changes in paleoclimate.

The fact that there is no significant correlation between organic maturation and the abundance of organic matter in sediments suggests that an increase in TOC content in younger strata cannot be accounted for by the decreasing degree of organic maturation of younger strata. Figure 5.84 shows the variation in mean

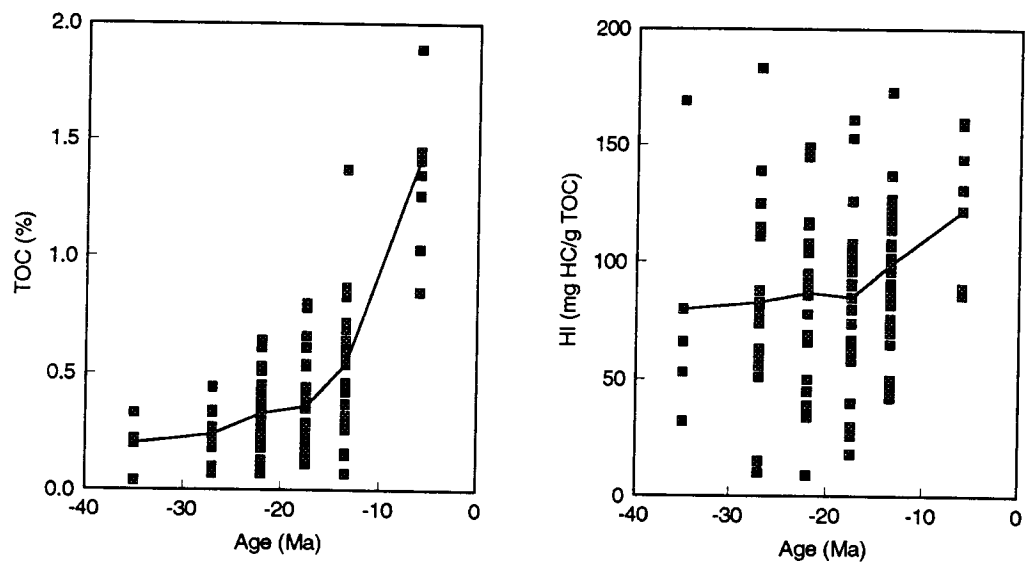


Figure 5.83: Variation of TOC (%) and HI (mg HC/g TOC) v.s. age (n = 4500)

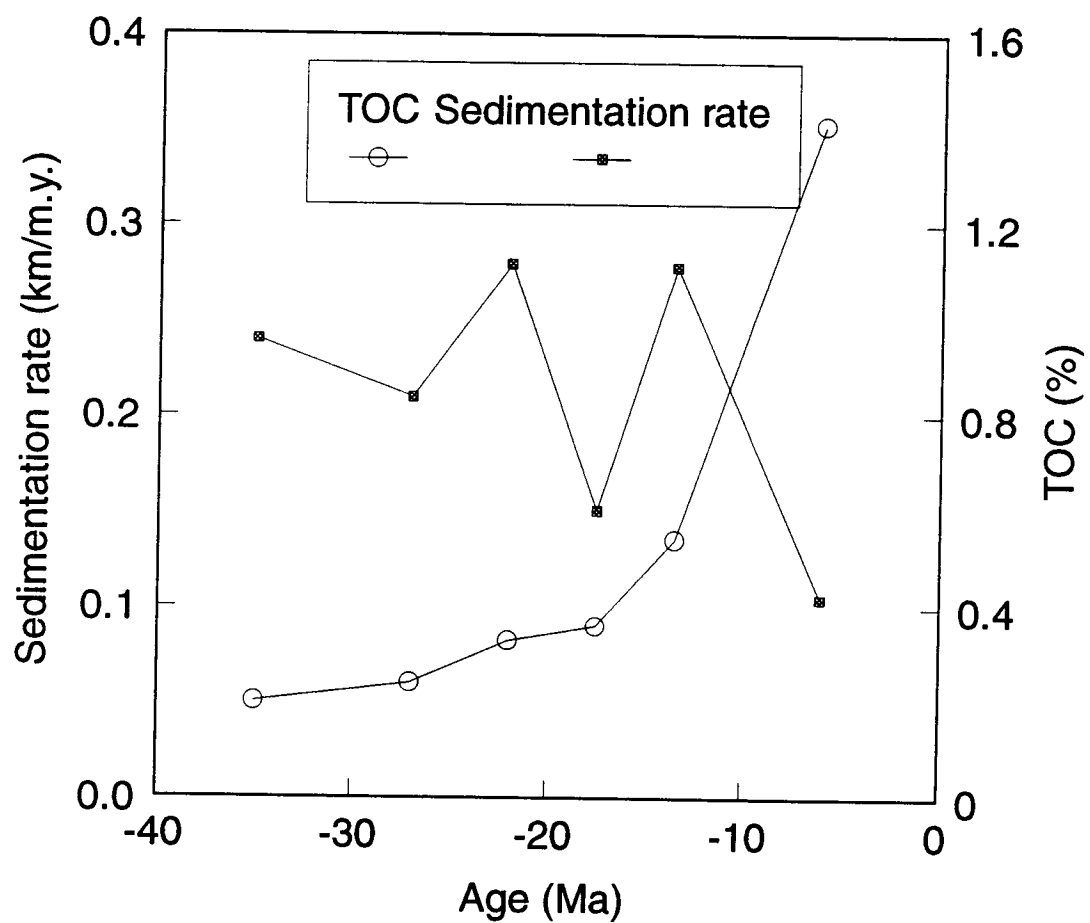


Figure 5.82: Variation of sedimentation rate and TOC with age

sedimentation rates and mean TOC for strata of different ages. It can be seen that although the mean TOC contents increase in younger strata, the sedimentation rate varies considerably with age. This relationship suggests that, for nonmarine and deltaic deposits in general, sedimentation rate cannot be used exclusively to predict organic abundance in sediments.

The increase in TOC and HI contents in younger strata may, in part, be related to organic preservation. The sedimentary environment in the study area has evolved from totally nonmarine (units 6 and 5) to regressive sequences (units 4 and 3) and finally to transgressive sequences (unit 2 and 1). If the production of organic matter remained constant throughout the Tertiary, the TOC in sediments would depend upon the ability of a depositional site to preserve it. In nonmarine conditions, organic matter is unstable and quickly oxidized and decomposed because of aerial exposure. Low TOC values found in units 6 and 5 are the result of such a highly oxidizing condition. In the case of regressive units 4 and 3, of all the organic matter deposited, only that in the prodelta and shallow marine sediments in the lower subunits was relatively better preserved. These were least aurally exposed, thus subjected to less oxidation and less destruction. In contrast, the organic matter mainly deposited in nonmarine sediments in the higher subunits, was mainly oxidized from aerial exposure. The highest TOC's were found in transgressive sequences (units 2 and 1), probably reflecting higher degrees of preservation, resulting from the fine-grained nature of sediments, and the subsequent transgression which prohibited, or at least reduced, oxidation. The other important aspect of depositional environments on the abundance of organic matter in sediments is the relative distance from sources. Greater proximity to a source of organic matter such as marsh and peat swamp complexes of the middle and upper subunits of units 2 and 1 may have resulted in higher autochthonous

organic input into these two youngest strata, thereby contributing to the higher TOC contents.

The increase in TOC and HI in younger strata in the Pattani Basin may, therefore, suggest that younger strata have more favorable depositional environments for organic input and preservation.

Other contributors to the progressive change in TOC with time include variations in the paleoclimate and changes in plant types. During the Tertiary, the flora evolved and the availability and type of organic matter probably changed. The progressive evolution of mangrove flora is marked by the disappearance of the *Pinus* sp. and the appearance of *Rhizophora* sp. during the Early Miocene, and the appearance of *Nypa* sp. in the Late Miocene. Significant climate changes in Thailand during the Tertiary have not been documented, however, the appearance of *Nypa*-type pollen has been considered the result of more seasonal climate and increasing temperatures (Germeraad et al., 1968). The consequence of factors such as the evolution of mangrove flora and minor paleoclimate fluctuations that may have occurred remains largely unknown. Such factors probably did not play an important role in determining TOC content independent of depositional environment and/or sedimentation rate.

f. Discussion

Of all the parameters influencing the abundance and types of the organic matter in the study area, the most prominent parameter is depositional environment. Hence, changes in organic characteristics both within and across the stratigraphic units are mainly the result of changes in depositional environments. Within the stratigraphic

units, the abundance of organic matter generally increases from high energy nonmarine to low energy marine subunits. Across the stratigraphic units, an increase in TOC and HI values in progressively younger strata also reflects the shift from high energy nonmarine environment to low energy marine environments. Effects of sedimentation rate and the degree of organic maturation on organic characteristics in the study area is not distinct. Such an ambiguous result, especially in the units with low TOC, may be the result of original variation of TOC within the sediments rather than the effect of sedimentation rate or the degree of organic maturation.

5.6.2 Source Rock Considerations

The general evaluation of hydrocarbon potential in the Tertiary strata in the Pattani Basin, in terms of maturation history, tectonic history, and possible trap formation, is discussed in chapters 4 and 6. This section will focus on the hydrocarbon source quality of the sediments available for analysis.

Lateral distributions of QOM of different stratigraphic units and subunits are shown in Figure 5.66 through Figure 5.79. Figure 5.85 shows the variations of hydrocarbon potential (or Genetic Potential, $S_1 + S_2$) and QOM (quality of organic matter, $S_1 + S_2 / \text{TOC}$) for different strata of different ages. The variations of genetic potential values in the stratigraphic units 6, 5, 4, and 3 are very similar to each other, varying from less than 0.1 to 1.5 mg HC/g rock with an average value of approximately 0.5 mg HC/g rock. Unit 2 shows higher genetic potential which ranges from 0.1 to 2.8 mg HC/g rock with an average value of 0.8 mg HC/g rock. The highest genetic potential value in the study area occurs in stratigraphic unit 1,

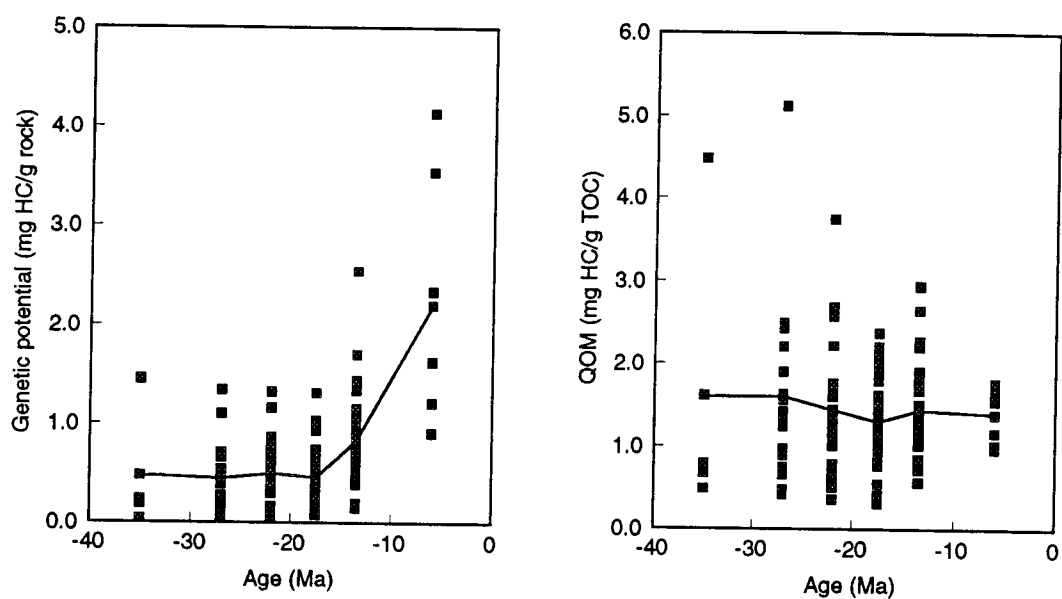


Figure 5.85: Variation of Genetic potential (mg HC/g rock) and QOM (mg HC/g TOC) v.s. age (n = 4500)

ranging from 0.8 to 4.3 mg HC/g rock with an average value of 2.2 mg HC/g rock.

While the genetic potential of the Tertiary strata in the Pattani Basin increases in younger strata, the QOM variation shows a minor decreasing trend toward younger rocks, from 1.6 mg HC/g rock in unit 6 to 1.4 mg HC/g rock in unit 1 (Figure 5.85).

It is evident that all stratigraphic units, except unit 1, which is immature with respect to the oil generation window, have very low hydrocarbon source potentials as measured by pyrolysis. Synrift sediments (units 6, 5, and 4) and early post-rift sediments (unit 3) contain very low TOC (less than 0.4%), very low HI (between 80-90 mg HC/g TOC), very low genetic potential (less than 0.5 mg HC/g rock), and low QOM (between 1.3 to 1.6 mg HC/g rock). Based on a conventional definition of hydrocarbon source rocks (Tissot and Welte, 1984; Waples, 1985), these sediments cannot be considered as source rocks at all. Although Unit 2 has TOC of 0.5% and HI of 100 mg HC/g TOC, it also has very low genetic potential (about 0.8 mg HC/g rock) and low QOM (1.4 mg HC/g rock). Unit 1, on the other hand, has the highest hydrocarbon source potential with TOC content of 1.4%, HI value of 122 mg HC/g TOC, genetic potential of 2.2 mg HC/g rock, and QOM of 1.4 mg HC/g rock. This unit is immature relative to the oil generation window. The variation in HI, genetic potential, and QOM values of all samples in the study area may represent variations in source rock quality, but may also be due to the mineral matrix absorption effect (Espitalie et al., 1985). The mineral matrix absorption effect results in the suppression of the pyrolysis yield, particularly in samples with low TOC (less than 2-3%) and high clay content. Such a condition is generally the case for Tertiary sediments in the study area.

The fact that the Pattani Basin is a producing basin suggests that: either source rocks have been very effective at an overall lower organic matter quality than generally considered necessary; or higher quality source rocks, possibly at depths, and have not been reached by drilling, are present in the basin; or a combination of both factors. The potential source rocks in the Pattani Basin, despite their very low oil generating potential, may represent an enormous volume of low quality source beds, which together with interbedded sandstones throughout the succession, would function as highly effective carrier beds during migration. In addition, the rapid subsidence rate and high heat flow, resulting in rapid hydrocarbon generation, may also have facilitated creating commercial hydrocarbon accumulations. Such conditions are not unique. Bustin (1988) studied the source rock characteristics of the Niger Delta sediments and suggested that despite very low oil generating potential of the source rocks, a combination of favorable intercalation of source beds and carrier beds which provides excellent drainage for hydrocarbon migration, together with the rapid rate of maturation, may have helped in creating commercial oil accumulations. The synrift and possibly post-rift lacustrine deposits, which widely occur in other Tertiary basins in Thailand, are believed to occur in the center of the Pattani Basin as well (Gibling, 1988; Burri, 1989; Chinbunchorn et al., 1989). These lacustrine sediments may possibly be the source rocks contributing a major part of hydrocarbons to the commercial gas fields.

5.7 SUMMARY AND CONCLUSIONS

The dispersed organic matter in Tertiary strata in the Pattani Basin is composed mainly of Type III (organic facies CD) and Type IV (organic facies D) kerogen with minor amounts of mixed Type II and Type III (organic facies C and CD)

kerogen. Because of the nonmarine and marginal marine nature of the sediments, the presence of low HI and high OI values, and the types of organic matter (primarily vitrinite), the organic matter found in these sediments is interpreted to be predominantly of detrital and continental origin.

The variation of organic characteristics of the sediments occurs both within and across the stratigraphic units. Within each stratigraphic unit, the lowest TOC and HI values occur in the high energy nonmarine deposits such as alluvial fan and braided stream deposits in unit 6, whereas low energy deposits such as floodplain deposits of unit 6 normally contain higher TOC and HI values. The increase in TOC content and HI value in the sediments also occurs from nonmarine floodplain deposits to shallow marine and interdistributary bay deposits. Across the stratigraphic units, TOC and HI generally increase in progressively younger strata. The abundance of organic matter within the sediments is the combined result of organic input into the sediments plus the degree of organic preservation. Higher TOC and HI values in floodplain deposits, for example, may reflect proximity to swamp complexes, thus, sources of organic matter. Fine-grained sediments further enhance the degree of organic preservation by the rapid development of an anaerobic condition within the sediment column which reduces oxidation, hence destruction, of organic matter. The variation of abundance and characteristics of organic matter in the sediments both across and within the stratigraphic units is, therefore, controlled, in large part, by the depositional environments within which the organic matter was deposited.

A weak positive correlation between TOC and HI and degree of organic maturation in the study area may reflect the natural variation in TOC from place to place

within the same stratigraphic unit and across the units rather than a true relationship between TOC and HI and maturation.

The general increase in TOC in progressively younger strata may reflect more favorable sedimentary facies for organic matter of younger strata. No significant correlation occurs between maturity parameters, such as the extent of hydrocarbon generation and vitrinite reflectance, nor the abundance and type of organic matter.

The sedimentation rate, corrected for compaction, of the Tertiary strata in the Pattani Basin varies from 0.02 km/m.y. to more than 0.9 km/m.y. Such a high sedimentation rate is quite common in the Tertiary deltaic deposits such as the Niger Delta (Bustin, 1988), and it is considerably higher than the sedimentation rate of ancient marine sediments (Ibach, 1982). A very weak correlation between TOC and sedimentation rate in all units, except unit 1, is the result of variable TOC within and across the units. A negative correlation between TOC and sedimentation rate in unit 1 may be the result of clastic dilution of the organic input. It is, however, important to point out that to use the sedimentation rate alone to predict the organic abundance might be misleading. Other factors, such as the types of plant and/or animal organic; the proximity to sources of organic matter; and the depositional environments can also have influence on the organic input and preservation, hence, the abundance of organic matter in the sediments.

Source rocks of the Tertiary strata in the Pattani Basin represent an end member in terms of source rock composition and properties. The source rocks contains mainly Type III, Type IV and a relatively small amount of Type II kerogens, and have very low hydrocarbon potential as defined by pyrolysis (Tissot and Welte, 1984). The presence of numbers of commercial gas fields suggests that either the source

rocks here, despite very low genetic potential, have been very effective in producing, migrating, and accumulating the hydrocarbon or the presence of higher quality source rocks within the basin which have not been reached by drilling, or a combination of both factors.

6. ORGANIC MATURATION AND HYDROCARBON GENERATION

6.1 ABSTRACT

The kinetic parameters of potential source rocks and the extent and timing of hydrocarbon generation in Tertiary strata in the Pattani Basin have been investigated. Kinetic parameters of source rocks were determined from Rock-Eval analyses of whole rock samples or kerogens at multiple heating rates using a linear regression technique based on the assumption of a Gaussian distribution of activation energies with some mean value (E_0) and standard deviation (σ_E). The extent and timing of hydrocarbon generation were predicted using a chemical kinetic model proposed by Sweeney and Burnham (1990), based on known burial and thermal histories, and kinetic properties of the stratigraphic units.

The mean activation energies of the source rocks in the Pattani Basin, ranging from 46 to 61 kcal/mol, coincide generally well with the activation energies required to break down carbon-oxygen and carbon-carbon bonds (40 to 70 kcal/mol). The dispersion of activation energies ranges from 0.26 to 9.30% of the mean value (E_0). The kinetic parameters derived from kerogen samples are not much different from those derived from whole rock samples of the same sediments. Such results suggest that, at least for sediments with high TOC, either whole rock samples or kerogens can be used to determine the kinetic parameters of the source rocks. For organically lean sediments, whole rock samples should be used to model hydrocarbon generation because the effect of matrix adsorption may become significant. Notable variation of activation energies within the same type of kerogen in all samples may reflect the variability of chemical composition of

kerogen. It, therefore, cannot be assumed that activation energies depend only on kerogen type.

Depositional environments seem to have no influence on the value of mean activation energies (E_0) but show a weak influence on their dispersion (σ_E). Large dispersions of activation energies (σ_E) correspond to high energy sediments, whereas low dispersions (σ_E) correspond to low energy sediments. Such results suggest that depositional environment may have an effect, at least in part, on a redistribution and the oxidation of organic matter and the variation of its activation energy dispersion (σ_E) within sediments. A weak correlation occurs between kinetic parameters (mean activation energies and their dispersion) and the degree of thermal maturation. This correlation may reflect the original variation of kinetic properties of organic matter rather than the effect of maturation. By using a distribution of activation energies, kinetic parameters of organic matter are independent of degree of organic maturation.

Most of the stratigraphic units in the Pattani Basin, except that of the youngest unit (unit 1), are either mature or overmature with respect to the oil window. The main phase of hydrocarbon generation began at about 33-35 Ma and has continued to the present. A relatively early generation (about 5-7 m.y. after deposition) is attributed to the area's high geothermal gradients and rapid sedimentation-hence high heating rate for the sediments. Low mean activation energy in some stratigraphic units also enhanced early generation.

The presence of good, although laterally discontinuous, reservoir rocks, the adjacent occurrences of source and reservoir rocks, and the structural and

stratigraphic traps in the study area are the key factors that made the Pattani Basin a prolific hydrocarbon basin.

6.2 INTRODUCTION

Knowledge of the degree and timing of maturation of organic matter is important in hydrocarbon exploration. In particular, modelling of organic maturation history provides details on the timing of hydrocarbon generation relative to the tectonic evolution of a sedimentary succession. In the Pattani Basin, Gulf of Thailand (Figure 6.1), a thick succession of Tertiary strata is preserved (Figure 6.2 through Figure 6.7). The succession was penetrated and studied by exploration wells and by geophysical surveys. No equivalent sequences crop out onshore. Although the area has been active in terms of hydrocarbon exploration and production since 1970's, there is very limited documentation in terms of the degree of organic maturation or timing of hydrocarbon generation (Lian and Bradley, 1986; Achalabhuti and Oudom-Ugsorn, 1978; Chinbunchorn et al., 1989). The present investigation is one of the first attempts to determine the extent and history of organic maturation as well as hydrocarbon generation in this area.

In this study, a chemical kinetic model is used to predict the degree of organic maturation and the extent and timing of hydrocarbon generation. The input information needed for the model includes burial and thermal histories of the sedimentary successions, and the chemical kinetic properties of the included organic matter. Burial history of any stratigraphic layer within a sedimentary basin, corrected for compaction, can be acquired by backstripping analysis of the well data. Because thermal history and paleotemperatures are controlled by the basal heat flow history, which in turn reflects the lithospheric mechanics and heat

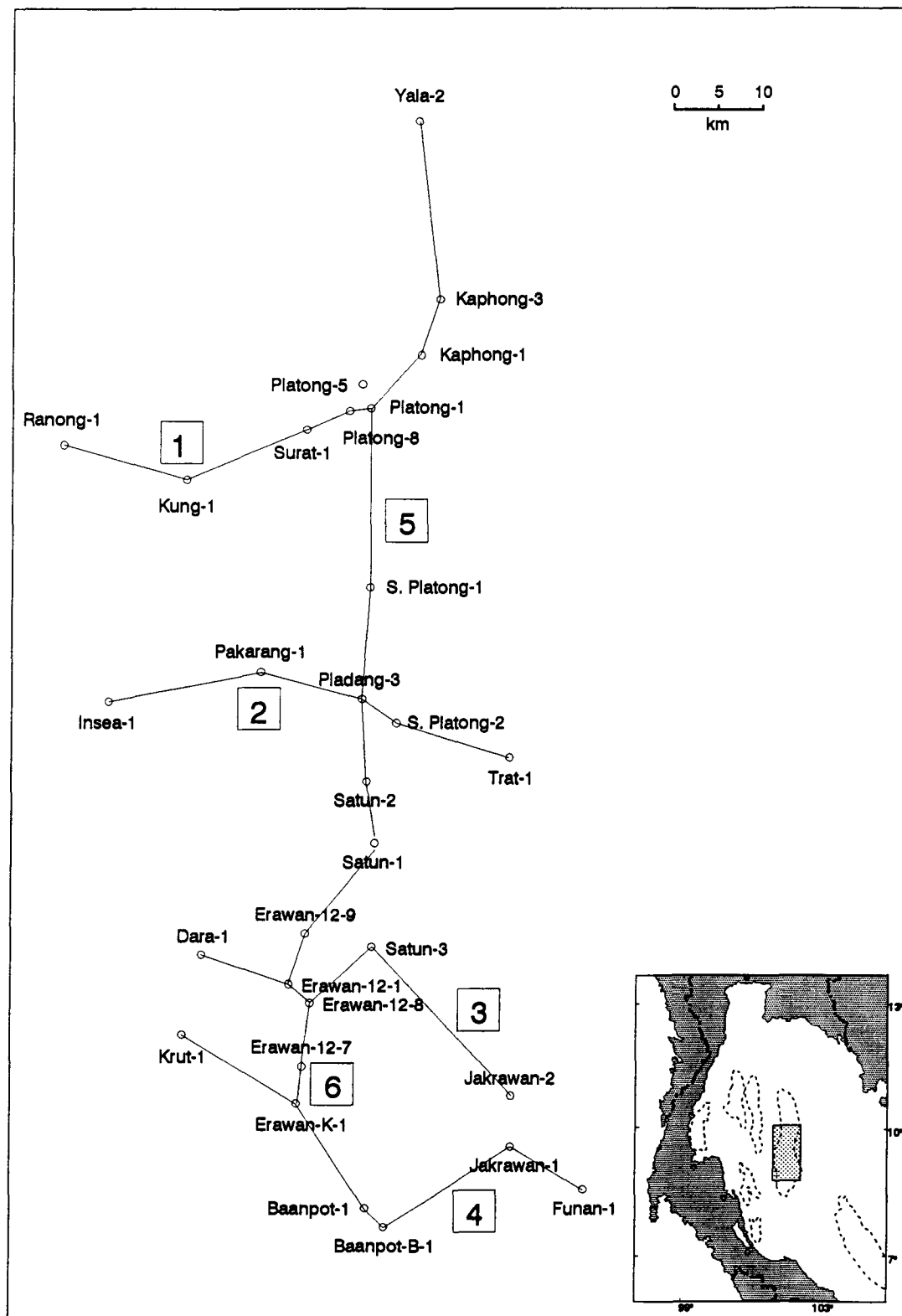
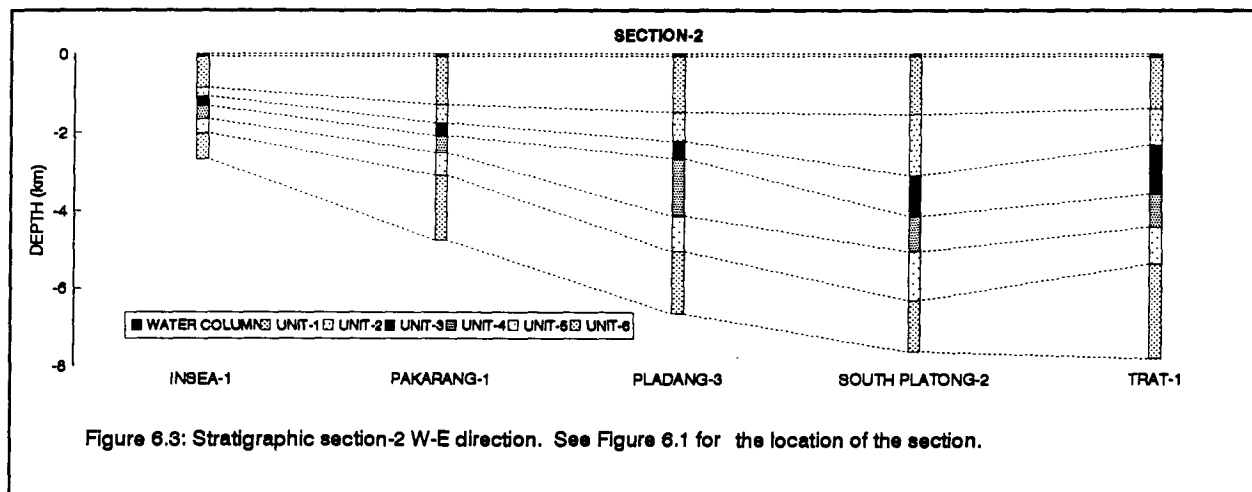
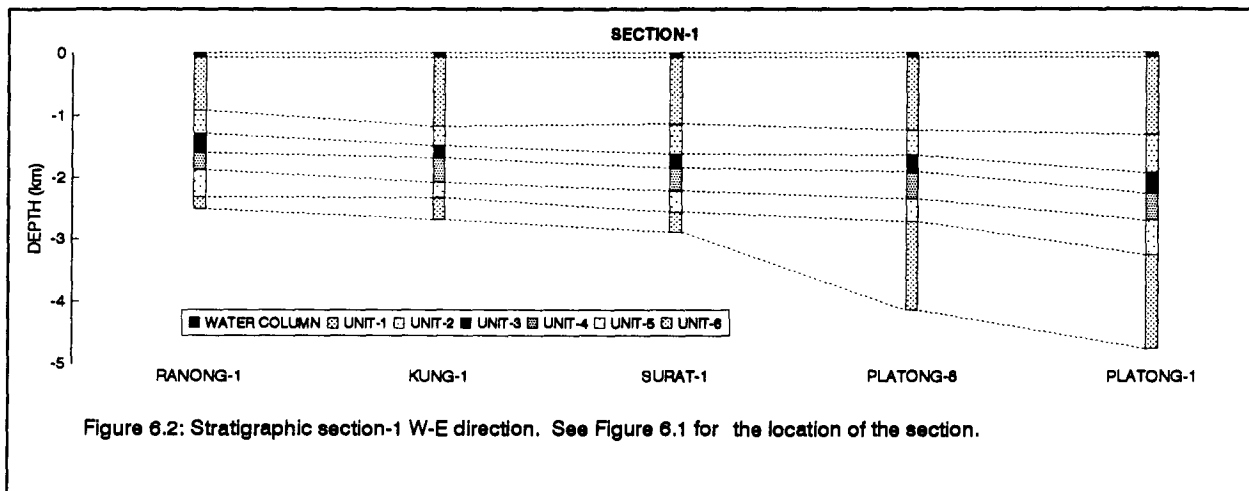
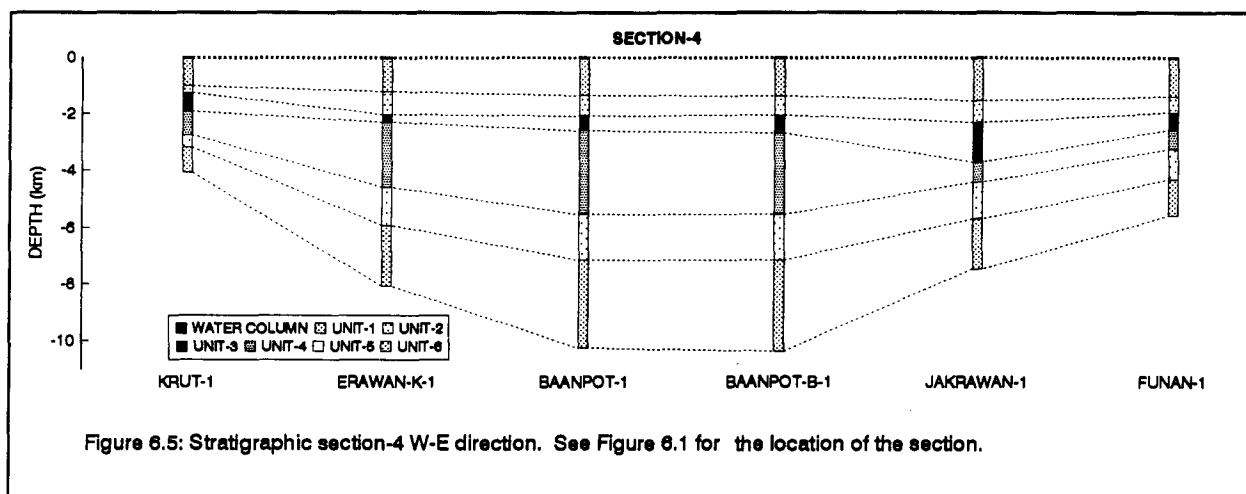
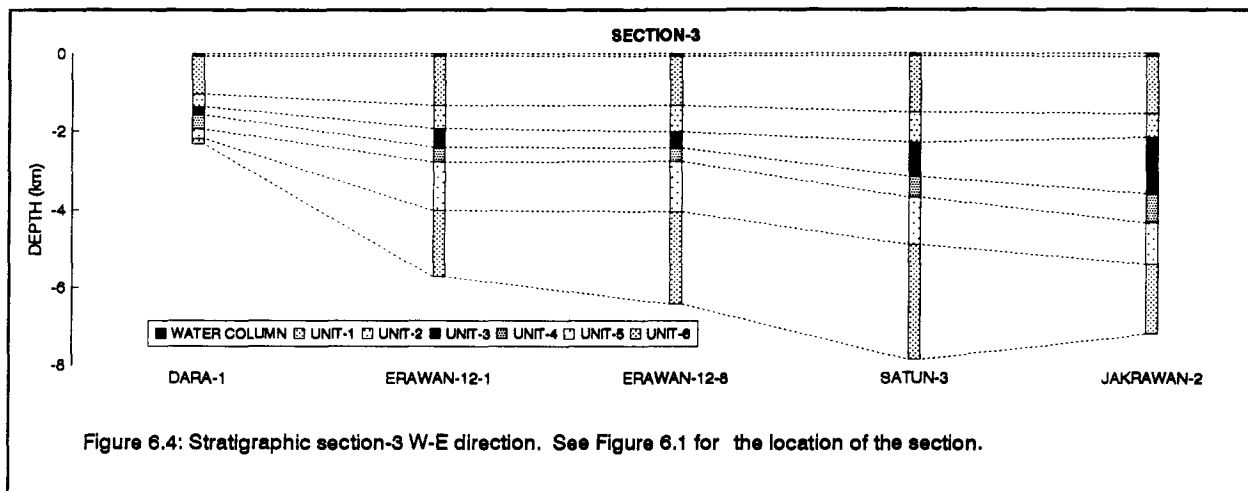
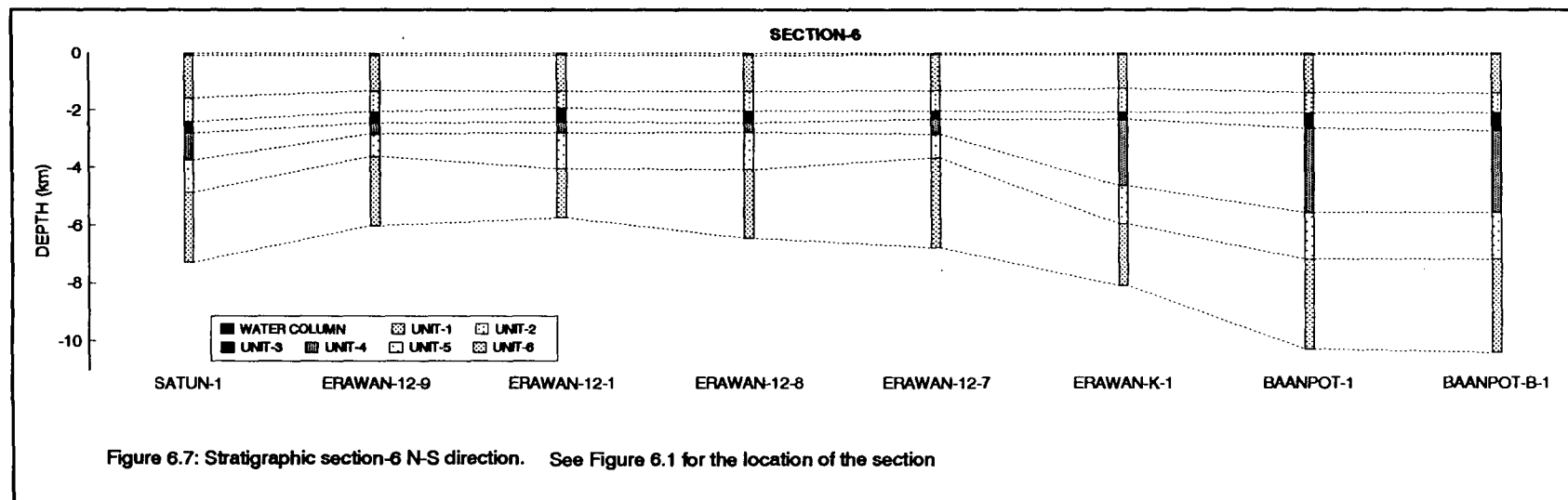
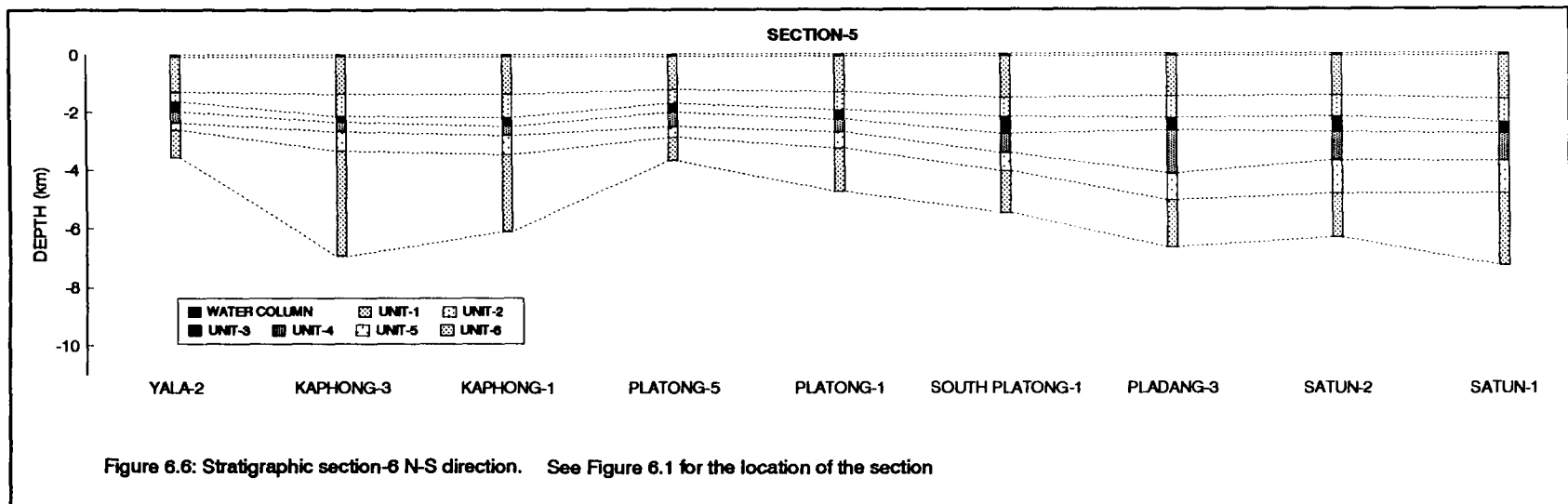


Figure 6.1: Location of well data used in this study. Numbers in the box indicate the cross sections shown in Figures 6.2 through 6.7







generation from radioactive sources within the earth's crust (McKenzie, 1978; Allen and Allen, 1990), thermal history of a rifted intracratonic basin formed by lithospheric stretching can be estimated from the amount of crustal and subcrustal lithospheric stretching (β and δ factors respectively; Hellinger and Sclater, 1983). Thermal history of the Tertiary strata in the Pattani Basin is estimated using a nonuniform lithospheric stretching model described in chapter 4.

6.3 METHODS OF STUDY

6.3.1 Kinetics and Organic Maturation Modelling

Hydrocarbon generation, organic maturation as well as other chemical reactions of natural materials are rate-controlled, thermocatalytic processes. These processes are essentially controlled by a time-temperature relationship. The simplest form of the chemical kinetics is a first order reaction, where the instantaneous rate of conversion of component x to component y is proportional to the amount of the reactant x as follows (Lerche, 1990; Sweeney, 1990):

$$-\frac{dx}{dt} = \frac{dy}{dt} = k_{(T)}x \quad (6.1)$$

The dependence of chemical reaction rates upon temperature, $k_{(T)}$, is commonly expressed by the Arrhenius equation (Waples, 1985; Allen and Allen, 1990):

$$k = Ae^{-E_a/RT} \quad (6.2)$$

Where k is the reaction rate, A is a pre-exponential factor (it is the maximum value that can be reached by k when given an infinite temperature, sec^{-1}), E_a is the activation energy of the reaction (it is the energy barrier over which molecules must pass before a chemical reaction can occur, kcal/mol), R is the universal gas constant ($1.987 \text{ cal/mol K}^{-1}$), and T is the absolute temperature (K).

Once the kinetic parameters and thermal history of a sedimentary succession have been determined, the extent of reaction is determined by integrating equation (6.1) over the temperature range expressed by thermal history. Lopatin (1971) and Waples (1980) proposed the rule-of-thumb estimate for hydrocarbon maturity using the time-temperature index (TTI) based on the assumption that the reaction rate of kerogen maturation doubles with every 10°C increase.

A single first order reaction described in equation 6.2 is sufficient for the chemical reaction involving a single component. Kerogen is, however, a mixture of complex organic and inorganic components. The evolution of kerogen during maturation includes a complex set of chemical reactions such as progressive elimination of functional groups and of the linkages between nuclei. A wide range of compounds is formed during the thermal evolution of organic matter, including water, carbon dioxide, medium to low molecular weight hydrocarbons, etc. Hence a single first order reaction is insufficient to describe the variety of complex chemical processes occurring over a wide range of temperatures during organic maturation. Juntgen and Klein (1975), Burnham and Sweeney (1989), and Sweeney (1990) have pointed out that hydrocarbon generation involves the simultaneous occurrences of many distinct chemical reactions, and that the overall rate of hydrocarbon generation should depend upon the sum of the rates of all simultaneous reactions that produce hydrocarbon molecules. Braun and Burnham (1987), Sweeney et al. (1987), and

Burnham et al. (1987) proposed that the hydrocarbon generation reaction kinetics can be better described in terms of a distributed activation energies model, in which there is an infinite number of channels for hydrocarbon production, but with an energy weighting per channel. For the i^{th} component of the reaction with a time-dependent temperature $T_{(t)}$, the extent of the reaction can be calculated as (Sweeney and Burnham, 1990):

$$\frac{dx_i}{dt} = -x_i A \exp\left[-E_i / RT_{(t)}\right] \quad (6.3)$$

and

$$\frac{dx}{dt} = \sum_i \frac{dx_i}{dt} \quad (6.4)$$

The amount of unconverted organic matter remaining in the i^{th} reaction is described by:

$$x_i = x_{0_i} - \int_0^t \left[\frac{dx_i}{dt} \right] dt \quad (6.5)$$

and the fraction of reactant converted (oil generated, if oil generation kinetics are used) is (Sweeney, 1990):

$$F = 1 - \frac{x}{x_0} = 1 - \sum_i f_i \left[\frac{x_i}{x_0} \right] \quad (6.6)$$

Where x_{0_i} is the initial concentration of component i , x_0 is the initial concentration of the total reactant, and f_i values are the stoichiometric, or weighting, coefficients for the simultaneous reaction components.

The amount of reactant converted (F) can be calculated by dividing the time-temperature history into a series of constant heating rate segments (Braun and Burnham, 1987; Sweeney, 1990; Sweeney and Burnham, 1990). H_j is a heating rate between times j and $j-1$ as:

$$H_j = \frac{(T_j - T_{j-1})}{(t_j - t_{j-1})} \quad (6.7)$$

The extent of reaction of the i^{th} component at time j is:

$$\frac{x_i}{x_{0_i}} = 1 - \exp(-\Delta I_{ij}) \quad (6.8)$$

Where

$$\Delta I_{ij} = \frac{(I_{ij} - I_{i,j-1})}{H_{ij}} \quad (6.9)$$

and

$$I_{ij} = T_j A \exp\left(\frac{E_i}{RT_j}\right) \left[1 - \frac{\left(\frac{E_i}{RT_j}\right)^2 + a_1 \left(\frac{E_i}{RT_j}\right) + a_2}{\left(\frac{E_i}{RT_j}\right)^2 + b_1 \left(\frac{E_i}{RT_j}\right) + b_2} \right] \quad (6.10)$$

Where $a_1 = 2.334733$, $a_2 = 0.250621$, $b_1 = 3.330657$, and $b_2 = 1.681534$ (Braun and Burnham, 1987; Sweeney, 1990; Sweeney and Burnham, 1990).

Provided that the activation energy distributions are known, the technique described above can be used to calculate the extent of reaction of any chemical transformation. An organic maturation program used to predict the extent of hydrocarbon generation and vitrinite reflectance of a sedimentary layer is included in a computer disk at the end of this thesis. Appendix B describes how to run the program.

6.3.2 Determination of Kinetic Parameters

Although the concept that petroleum generation as a kinetic process is well established (Juntgen and Klein, 1975; Tissot and Welte, 1984), determining kinetic parameters for quantitative prediction has been elusive because of the complexity of both the maturation processes and organic matter precursors. It is often found that fitting a single first order reaction to experimental data gives an activation energy much smaller than can be attributed to a chemical reaction (Connan, 1974; Waples, 1985). Braun and Burnham (1987) have shown that the presence of a distribution of activation energies caused the effective activation energy, or Waples' (1985)

"pseudo-activation energy", determined by simple kinetic analysis to be much lower than the true average value, and that ignoring even a small distribution would cause problems in extrapolating the reaction rate obtained from the laboratory environment to the geologic temperatures.

The actual distributed activation energy parameters can be determined by using nonlinear regression to decouple the effects of time and temperature over the whole extent of the reaction. Because of the large amount of computation power required to determine the distributed activation energy parameters using multiple nonlinear regression, Braun and Burnham (1987) proposed a simpler technique using linear regression based on the assumption of a simple Gaussian distribution of the activation energies with some mean value (E_0) and a standard deviation (σ_E). Braun and Burnham (1987) further showed that a very good agreement occurred between the kinetic parameters determined by multiple nonlinear regression and those determined by linear approximation.

For a single first order reaction, the kinetic parameters E_0 and A can be determined from a shift in T_{\max} with heating rate (Van Heek et al., 1968). T_{\max} is the temperature at which the maximum amount of hydrocarbons is generated during pyrolysis. Thus, from the linear plots of $\ln(H_r / T_{\max}^2)$ versus $1000 / T_{\max}$ in Figure 6.8, E_0 can be obtained from the slope and A from the intercept using equation:

$$\ln\left(\frac{H_r}{T_{\max}^2}\right) = -\frac{E_0}{RT_{\max}} + \ln\left(\frac{AR}{E_0}\right) \quad (6.11)$$

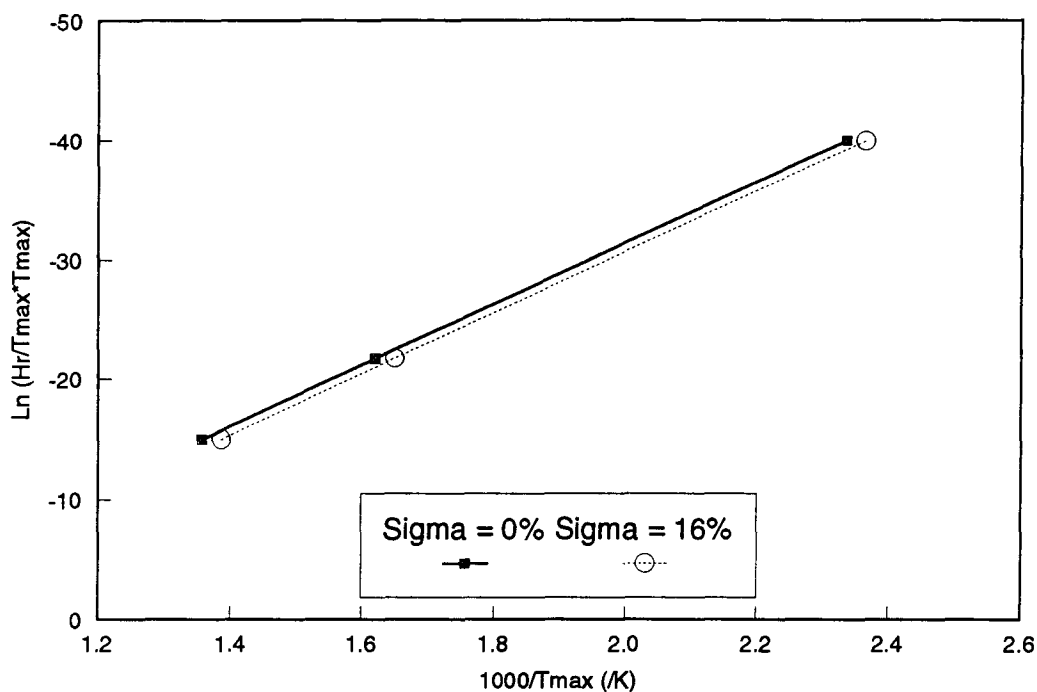


Figure 6.8: Shift of T_{max} with heating rate used to determine values of E_o (from slope) and A (from the intercept) for different values of σ_E (After Braun & Burnham, 1987)

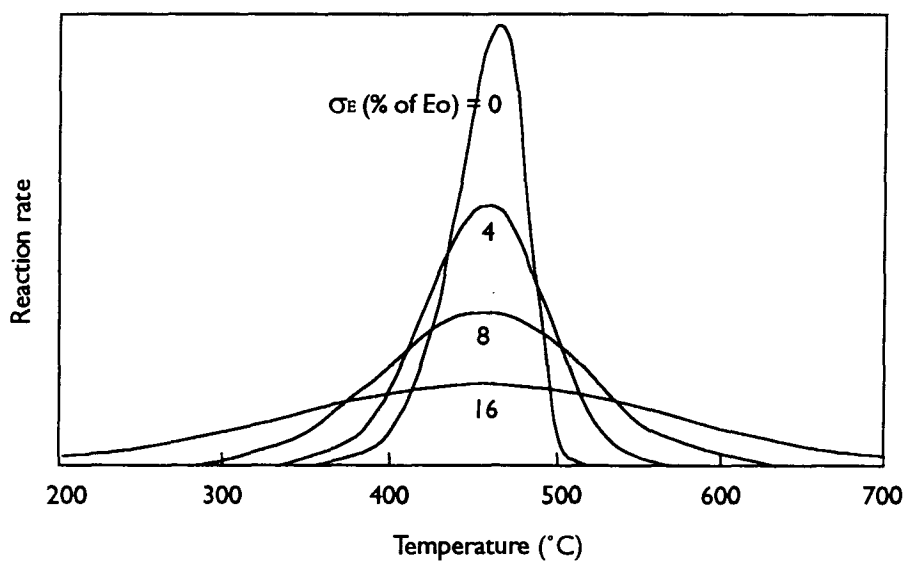


Figure 6.9: Reaction rate profiles generated at a heating rate of $10\text{ }^{\circ}\text{C/Min}$ by using a distribution of activation energies, $E_o = 52.44\text{ kcal/mol}$ and $\sigma_E = 0\text{-}16\%$ of E_o (After Braun & Burnham, 1987)

As shown in Figure 6.8, even for a wide dispersion of activation energies (σ_E), the linear regression technique, assuming a Gaussian distribution of activation energies outlined above, is a good method for determining E_0 and an approximate value of A . This technique is consistent with the fact that the activation energy distribution broadens the reaction profile without substantially shifting T_{\max} (Figure 6.9; Braun and Burnham, 1987). An approximate value of σ_E can be determined from the ratio $\Delta T_\sigma / \Delta T_0$ of the temperature width of the reaction rate profile (ΔT_σ , measured from Rock-Eval analysis pyrogram) to that calculated from the linear regression parameters (ΔT_0). ΔT_σ is directly obtained from the measured reaction rate profile (full width at half-height). The so called "full width at half-height" of the temperature is determined from measuring, from the Rock-Eval pyrolysis rate profile, the difference in temperature at half the maximum rate of hydrocarbon generation during pyrolysis. ΔT_0 can be calculated from the simple kinetic parameters (E_0 and A) determined in the first step. That is, T_{\max} when $\sigma_E = 0$ must first be calculated from:

$$\ln \left[\frac{H, E_0}{A R T_{\max}^2} \right] + \frac{E_0}{R T_{\max}} = 0 \quad (6.12)$$

Then ΔT_0 can be calculated from the approximate rate equation by iterative solution for two values of T on both sides of the T_{\max} in the reaction profile at which

$$\frac{dx}{dt} = 0.5 \left(\frac{dx}{dt} \right)_{T_{\max}} \quad (\text{Braun and Burnham, 1987) where:}$$

$$-\frac{dx}{dt} \approx A \exp\left[\frac{-E_0}{RT} - \exp\left(\frac{-E_0}{RT}\right) \frac{ART^2}{H_r E_0}\right] \quad (6.13)$$

Then the value of σ_E can be calculated from (Braun and Burnham, 1987):

$$\sigma_E = -\frac{1.1}{\rho^3} - \frac{0.66}{\rho^{30}} + 2.88\rho - 1.12 \quad (6.14)$$

Where

$$\rho = \left(\frac{52.4}{E_0}\right)^{\frac{1}{2}} \left(\frac{\Delta T_\sigma}{\Delta T_0}\right) \quad (6.15)$$

The accurate value of A corrected for the effect of dispersion (σ_E) can be calculated from the equation:

$$A = A_{\text{approx}} \left\{ 1 - 0.4 \left[1 - \exp\left(\frac{-\sigma_E}{2.5}\right) \right] \right\} \quad (6.16)$$

The relationship of $\Delta T_\sigma / \Delta T_0$ and σ_E depends on heating rate, but the dependence is relatively small over the range of most laboratory experiments (Braun and Burnham, 1987). A Lotus 1-2-3 template file, Eo.wk1, using a linear regression/correlation approach delineated above to determine the kinetic parameters (E_0 , A , and σ_E) from Rock-Eval analyses of a potential source rock is included in a computer disk at the end of this thesis. Appendix C describes how to run the program.

6.4 SUMMARY OF TERTIARY STRATIGRAPHY AND ORGANIC CHARACTERISTICS IN THE PATTANI BASIN

This section comprises a review of stratigraphy and organic characteristics of the Tertiary sediments in the Pattani Basin. Detailed descriptions of the stratigraphy and organic characteristics of these sediments are given in chapters 3 and 5, respectively.

The stratigraphic and structural evolution of the Pattani Basin reflects the rifting of the Continental Southeast Asia during Tertiary. The geodynamic model for the formation of the Pattani Basin involves stretching of the continental lithosphere and crustal thinning, with an initial phase of rapid, fault-controlled subsidence, followed by a subsequent phase of slow, post-rift, thermal subsidence. The rifting phase, which lasted about 20 m.y. (from Late Eocene to Early Miocene), was recorded in the synrift sediments which comprise two nonmarine sedimentary successions (stratigraphic units 6 and 5) and one regressive package (stratigraphic unit 4). The following post-rift phase comprises one regressive sedimentary package (unit 3) and two transgressive successions (unit 2 and unit 1).

Stratigraphic unit 6, of Late Eocene to Early Oligocene age, is characterized by coarse-grained, alluvial fan and braided stream sediments in the lower subunit and fine-grained, floodplain-channel deposits in the upper subunit. The lower subunit is practically barren of organic matter; its TOC content ranges from 0.03% to 0.1% with an average value of 0.07 %. Its QOM value ranges from 0.08 to 0.14 mg HC/g TOC, with an average value of 0.13 mg HC/g TOC. The kerogens which occur in this unit are mainly Type IV kerogen (or organic facies D, based on Jones'

(1987) classification of sedimentary organic matter). The TOC content of the upper subunit of unit 6 ranges from 0.04 to 0.33%, with an average value of approximately 0.22%. Its QOM ranges from 0.9 to 0.33 mg HC/g TOC, with an average value of 1.82 mgHC/g TOC. This upper subunit contains mainly of Type III-IV OM (organic facies CD and D).

Stratigraphic unit 5, of Late Oligocene to Early Miocene age, is characterized by fine-grained, floodplain deposits in the lower subunit and somewhat coarser-grained, meandering channel deposits in the upper subunit. The TOC content of the lower subunit ranges from less than 0.1% to 0.45%, with an average TOC content of 0.24%. Its QOM value ranges from 0.46 to 5.3 mg HC/g TOC, with an average QOM value of 1.46 mg HC/g TOC. The kerogens which occur in this subunit are mainly Type III and Type IV OM with minor amounts of mixed Type II-III OM. The TOC content of the upper subunit of unit 5 varies from 0.1% to 0.44%, with an average value of 0.25%. The QOM value of this subunit varies from 0.9 to 5.3 mg HC/g TOC, with an average value of 1.93 mg HC/g TOC. The kerogens which occur in this subunit are Type II-III OM (organic facies C).

A brief transgression occurred at the end of unit 5 deposition (early part of Early Miocene) and caused a brief period of nondeposition marking the boundary between stratigraphic units 5 and 4. The following sedimentary succession (unit 4-Early Miocene age) represents a broad regressive cycle characterized by fine-grained, prodelta to shallow marine deposits in the lower subunit; coarse-grained, distributary mouth bar deposits and beach complexes in the middle subunit; and coarse- to fine-grained nonmarine, floodplain-meandering channel deposits in the upper subunit. The TOC content of the lower subunit varies from about 0.2% to 0.5%, with an average value of 0.32%. The QOM value of this subunit varies

from 0.5 to 2.0 mg HC/g TOC, with an average value of 1.56 mg HC/g TOC. The organic constituents of the lower subunit are mainly Type III (facies CD) and Type IV (facies D) OM. The TOC content of the middle subunit varies from 0.15% to 0.7%, with an average value of 0.35%. The QOM value of this subunit varies from 0.6 to 2.4 mg HC/g TOC, with an average QOM value of 1.37 mg HC/g TOC. The main organic constituents of the middle subunit are Type IV and Type III (facies D and CD) OM. The TOC content of the upper subunit of unit 4 varies from 0.2% to 0.7%, with an average value of 0.36%. The QOM value of this subunit varies from 0.3 to 2.4 mg HC/g TOC, with an average value of 1.39 mg HC/g TOC. The main organic constituents are Type III-IV OM (facies CD and D) and Type II OM (facies BC and C).

Following deposition of unit 4 (Early Miocene-about 20 Ma), sedimentation in the Pattani Basin was in response to tectonic quiescence; subsidence was relatively slow. The sedimentary signatures were controlled mainly by the amount of sediment influx and the eustatic sea level fluctuation. Post-rift sediments comprise one regressive sedimentary package (unit 3) and two transgressive packages (units 2 and 1). A brief and rapid transgression occurred again at the base of unit 3 (Early Miocene-about 20 Ma) and caused a short period of nondeposition marking the boundary between unit 4 and unit 3. The regressive succession of unit 3 (Early to Middle Miocene), that followed the brief transgression, is characterized by fine-grained, prodelta to shallow marine-shelf deposits in the lower subunit; coarse-grained, distributary mouth bar deposits and beach complexes in the middle subunit; and coarse- to fine-grained, nonmarine, floodplain-meandering channel deposits of the upper subunit. The TOC content of the lower subunit of unit 3 varies from 0.2% to 0.9%, with an average TOC content of 0.44%. The QOM value of this subunit varies from 0.5 to 1.8 mg HC/g TOC, with an average QOM

value of 1.34 mg HC/g TOC. The organic constituents of this subunit are Type III and Type IV OM (organic facies CD and D respectively) with minor amounts of Type II-III OM. The TOC content of the middle subunit varies from 0.2% to 0.9%, with an average TOC content of 0.39%. The QOM value of this subunit varies from 0.8 to 2.5 mg HC/g TOC, with an average QOM value of 1.31 mg HC/g TOC. The organic constituents of this subunit are Type III and Type IV OM (organic facies CD and D respectively) with minor amount of Type II-III OM. The TOC content of the upper subunit of unit 3 varies from 0.1% to 0.6%, with an average TOC value of 0.29%. The QOM of this subunit ranges from 1.0 to 2.0 mg HC/g TOC, with an average QOM of 1.28 mg HC/g TOC. This subunit contains mainly Type IV and Type III OM (organic facies D and CD).

Stratigraphic unit 2 (Middle Miocene) represents a transgressive succession characterized by coarse-grained, nonmarine, meandering channel deposits in the lower subunit, and fine-grained interdistributary bay complexes and marginal marine deposits in the upper subunit. The TOC content of the lower subunit of unit 2 varies from 0.2% to 1.3%, with an average TOC content of 0.43%. Its QOM value ranges from 1.0 to 3.2 mg HC/g TOC, with an average QOM of 1.49 mg HC/g TOC. This subunit consists mainly of Type II-III, Type III, and Type IV OM (organic facies C, CD, and D). The TOC content of the upper subunit ranges from 0.2% to 1.4%, with an average TOC content of 0.81%. The QOM value of this subunit varies from 1.3 to 2.4 mg HC/g TOC, with an average value of 1.57 mg HC/g TOC. This subunit consists mainly of Type III OM (facies CD) and a mixture of Type II-III OM (organic facies C and CD).

At the end of the Middle Miocene, a rapid regression occurred in the Pattani Basin, probably as a result of a rapid eustatic sea level fall, causing subaerial exposure,

oxidation, and probably minor erosion of stratigraphic unit 2. Following this brief regression is a transgressive sedimentary package of unit 1 (Late Miocene to Pleistocene age). Unit 1 is characterized by basal coarse-grained, nonmarine, distributary channel deposits of the lower subunit; fine-grained, brackish water, interdistributary bay deposits and marsh and swamp complexes of the middle subunit; and fine-grained, prodelta to shallow marine deposits of the upper subunit. The TOC content of the lower subunit of unit 1 varies from 1.33% to 1.45%, with an average value of 1.37%. The QOM value of this subunit varies from 1.20 to 1.66 mg HC/g TOC, with an average value of 1.49 mg HC/g TOC. The main organic constituents of this subunit are a mixture of Type II-III OM (organic facies C and CD). The TOC content of the middle subunit varies from 0.85% to 2.08%, with an average TOC content of 1.47%. The QOM value of this subunit ranges from 0.96 to 2.04 mg HC/g TOC, with an average QOM value of 1.64 mg HC/g TOC. This subunit consists mainly of Type II and Type III OM (organic facies BC, C and CD). The organic characteristics of the upper subunit of unit 1 are not described here because the samples are not available.

6.5 KINETIC PARAMETERS OF THE POTENTIAL SOURCE ROCKS

The potential hydrocarbon source rocks (high HC potential and high TOC content) of each stratigraphic unit in the Tertiary strata in the Pattani Basin, Gulf of Thailand, were identified from Rock-Eval analysis. Rock-Eval pyrolyses were conducted on whole rock samples at a series of heating rates equal to 5, 25, and 50 °C/min (cycle 4, 1, and 2 of Rock-Eval II instrument respectively). The values of T_{max} and the corresponding heating rates, together with the temperature width of the Rock-Eval reaction rate profile (full width at half-height), were used as input to the

Lotus 1-2-3 program, Eo.WK1, to determine the kinetic parameters (A , E_o , and σ_E) following procedures outlined earlier. The output of the Eo.WK1 program is a pre-exponential factor (sec^{-1}) and a series of activation energies (cal/mol) and their corresponding stoichiometric, or weighting factors. This output file can be used directly as an input file for the organic maturation modelling program described in section 6.2.1 to calculate hydrocarbon generation and organic maturation histories of the sedimentary strata of interest.

Table 6.1 and Figure 6.10 list the kinetic parameters (A , E_o , and σ_E) for the potential hydrocarbon source rocks of the subunits of each stratigraphic unit at different locations.

6.5.1 Unit 6

The lower subunit of stratigraphic unit 6 is practically non-organic. The kinetic parameters of the fine-grained, floodplain deposits of the upper subunit of unit 6 were represented by samples from Ranong-1 well. The main organic matter occurring in this subunit is Type III-IV kerogens. The kinetic parameters of the upper subunit is characterized by a pre-exponential factor (A) of $1.97 \times 10^{12} \text{ sec}^{-1}$, a mean activation energy (E_o) of 46.7 kcal/mol , and a dispersion (σ_E) of 3.67% of E_o .

6.5.2 Unit 5

Nonmarine channel and floodplain deposits of the lower subunit of unit 5, which comprise mainly Type III-IV kerogens and a mixture of Type II-III kerogens, are characterized by a variation of kinetic parameters. Its pre-exponential factors range

Table 6.1: Kinetic parameters for potential source rocks of Tertiary stratigraphic units in the Pattani basin

UNIT	SUBUNIT	WELL	A (/sec)	E_o (kcal/mol)	σ_E (% E_o)
1	Lower	Funan-1	2.08E+16	58.19	3.54
		Pladang-3	1.08E+16	58.45	3.45
2	Upper	Kaphong-1	1.76E+13	48.89	2.60
		Platong-5	3.05E+14	52.65	1.75
		Pladang-3	2.64E+16	59.15	3.68
		E-12-1	3.73E+13	49.63	0.26
		Funan-1	1.80E+14	52.11	1.44
	Lower	Kaphong-1	2.82E+13	52.20	5.05
		Platong-5	2.49E+15	55.77	2.62
		Pladang-3	1.79E+15	55.12	4.10
		Funan-1	7.34E+13	50.88	3.74
		Kaphong-1	1.26E+13	51.28	3.78
3	Upper	E-12-1	1.01E+15	54.53	2.24
		Funan-1	1.55E+14	52.22	4.32
		Kaphong-1	1.13E+16	59.83	5.63
	Middle	Funan-1	4.27E+14	55.10	4.64
		E-12-1	7.55E+15	58.08	4.07
	Lower	Pladang-3	3.15E+12	47.29	5.52
		Platong-5	3.84E+13	51.07	3.72
		Pladang-3	2.45E+12	46.11	3.52
4	Upper	E-12-1	2.15E+14	54.87	7.66
		Kaphong-1	1.39E+16	60.63	6.22
		Platong-5	1.15E+14	51.94	9.30
	Middle	E-12-1	3.36E+15	50.81	6.47
		Kaphong-1	1.01E+13	51.25	6.12
		Platong-5	1.73E+14	52.15	5.06
	Lower	E-12-1	2.77E+14	55.87	5.10
		Ranong-1	1.97E+12	46.70	3.67

*A is the pre-exponential factor

E_o is the mean activation energy

σ_E is the standard distribution of activation energies

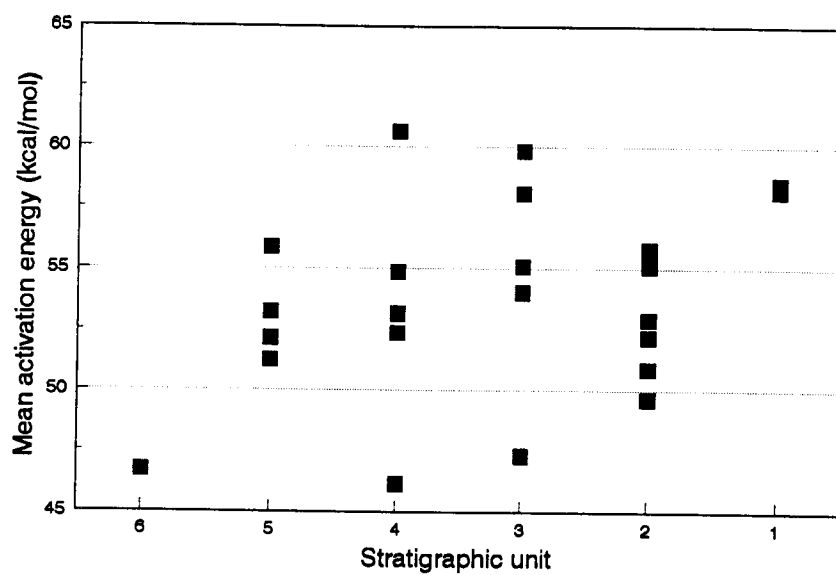


Figure 6.10: Mean activation energy of each stratigraphic unit

from 1.01×10^{13} to $2.77 \times 10^{14} \text{ sec}^{-1}$, its mean activation energies vary from 51.2 to 55.9 kcal/mol, and its dispersions vary from 5.06 to 6.12% of E_0 . The fine-grained, floodplain deposits of the upper subunit of stratigraphic unit 5, containing mainly Type II-III OM, are kinetically characterized by pre-exponential factors ranging from 9.41×10^{14} to $3.36 \times 10^{15} \text{ sec}^{-1}$, mean activation energies varying from 50.8 to 57.4 kcal/mol, and dispersions ranging from 5.70 to 9.30% of E_0 .

6.5.3 Unit 4

Floodplain deposits of the lower subunit of unit 4, containing Type III and Type IV kerogens, are kinetically characterized by a pre-exponential factor of $1.39 \times 10^{16} \text{ sec}^{-1}$, a mean activation energy of 53.4 kcal/mol, and a dispersion of 6.22% of E_0 . The marginal marine, beach and distributary mouth bar deposits of the middle subunit, containing mainly Type IV and Type III kerogens, are characterized by pre-exponential factors ranging from 2.45×10^{12} to $2.15 \times 10^{14} \text{ sec}^{-1}$, mean activation energies ranging from 46.1 to 54.9 kcal/mol, and dispersions varying from 3.52 to 7.66% of E_0 . A pre-exponential factor of the shallow marine deposits of the upper subunit of unit 4, containing mainly Type III-IV OM and Type II OM, is $3.84 \times 10^{13} \text{ sec}^{-1}$, with a mean activation energy of 51.1 kcal/mol, and a dispersion of 3.72% of E_0 .

6.5.4 Unit 3

Nonmarine floodplain deposits of the lower subunit of unit 3, containing mainly Type III OM and Type IV OM with minor amount of Type II-III OM, are kinetically characterized by pre-exponential factors ranging from 3.15×10^{12} to $7.55 \times 10^{15} \text{ sec}^{-1}$, mean activation energies varying from 47.3 to 58.1 kcal/mol, and

dispersions ranging from 4.07 to 5.52% of E_0 . The marginal marine, beach and distributary mouth bar deposits of the middle subunit of unit 3, containing mainly Type III-IV OM and minor Type II-III OM, are marked by pre-exponential factors varying from 4.27×10^{14} to $4.27 \times 10^{16} \text{ sec}^{-1}$, mean activation energies varying from 55.1 to 59.8 kcal/mol, and dispersions ranging from 4.64 to 5.63% of E_0 . The shallow marine deposits of the upper subunit of unit 3 contain mainly Type IV and Type III OM, and are marked by pre-exponential factors ranging from 1.26×10^{13} to $1.01 \times 10^{15} \text{ sec}^{-1}$, mean activation energies varying from 51.3 to 54.5 kcal/mol, and dispersions ranging from 2.24 to 4.32% of E_0 .

6.5.5 Unit 2

Nonmarine channel and floodplain deposits of the lower subunit of stratigraphic unit 2 contain a mixture of Type II-III, Type III and Type IV OM, and are kinetically characterized by pre-exponential factors ranging from 2.82×10^{13} to $2.49 \times 10^{15} \text{ sec}^{-1}$, mean activation energies varying from 52.2 to 55.8 kcal/mol, and dispersions ranging from 2.62 to 5.05% of E_0 . The shallow marine deposits of the upper subunit of unit 2, which contain mainly a mixture of Type III and Type II-III OM, are marked by pre-exponential parameters varying from 1.76×10^{13} to $2.64 \times 10^{16} \text{ sec}^{-1}$, mean activation energies ranging from 48.9 to 59.6 kcal/mol, and dispersions ranging from 0.26 to 3.68% of E_0 .

6.5.6 Unit 1

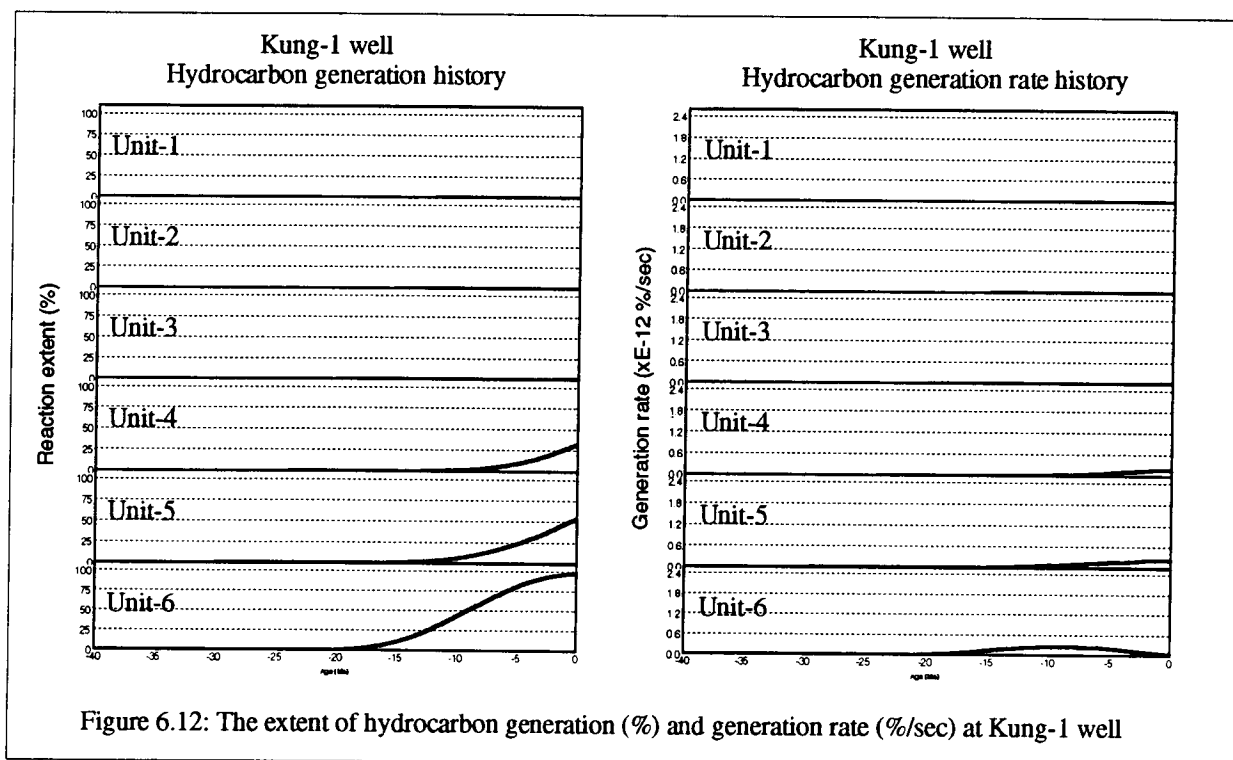
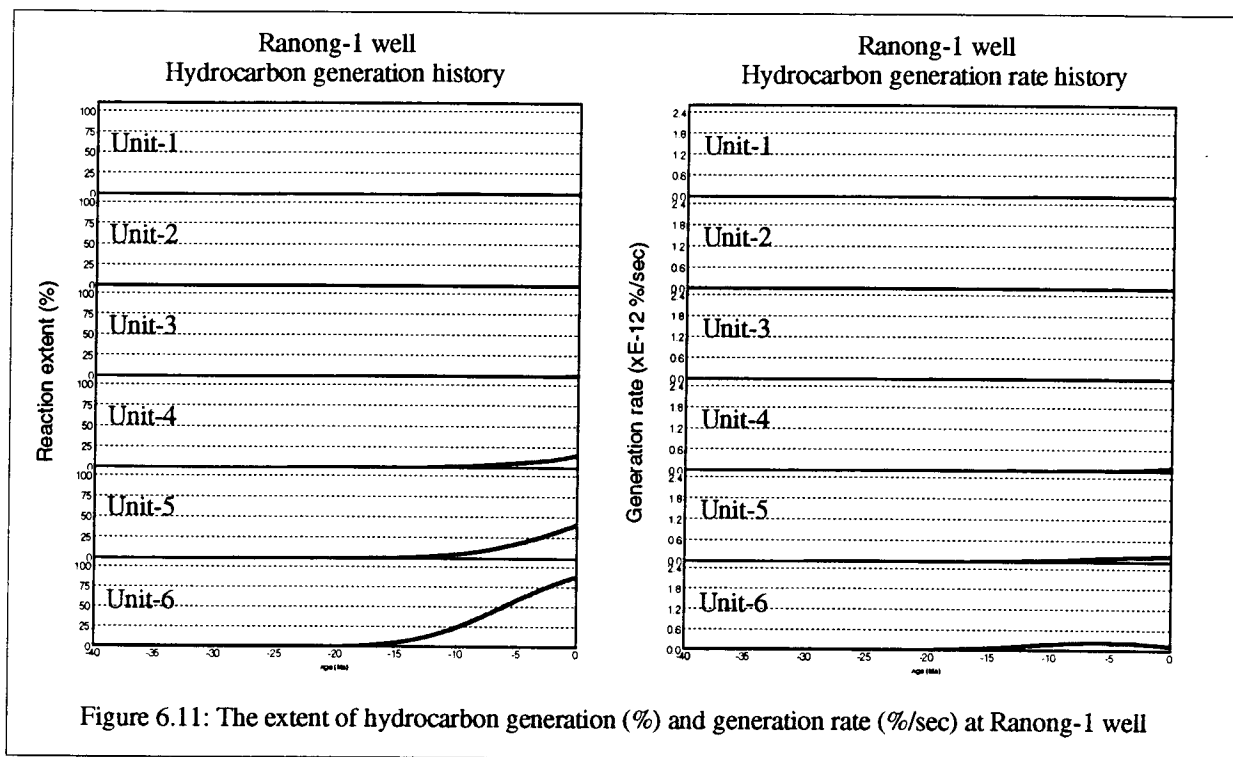
No samples were available from the upper and middle subunits of stratigraphic unit 1. Hence, only nonmarine, floodplain deposits of the lower subunit containing a mixture of type II-III OM were used to determine the kinetic parameters. Pre-

exponential factors of the lower subunit vary from 1.82×10^{16} to 2.08×10^{16} sec⁻¹, mean activation energies range from 58.2 to 58.4 kcal/mol, and dispersions range from 3.45 to 3.54% of E_0 .

6.6 HYDROCARBON GENERATION MODELLING

The extent and rate of hydrocarbon generation through time since deposition of each stratigraphic unit at different well locations are predicted using an organic maturation model outlined in section 6.3.1. The inputs needed for this maturation model are thermal and burial histories and the kinetic parameters of the stratigraphic unit of interest. The burial and thermal histories of each stratigraphic unit are obtained by the backstripping analysis and lithospheric stretching modelling described in chapter 4. The kinetic parameters for the potential hydrocarbon source rocks used here were derived from the kinetic modelling described in section 6.2.2 and are shown in Table 6.1. The kinetic parameters for calculating vitrinite reflectance are shown in Table 4.3 (Sweeney and Burnham, 1990). Because there is no age constraint within the stratigraphic units, the maturation history modelling of the stratigraphic units was carried out at the basal boundaries of the units. This practice results in the earliest possible time of thermal maturation of each unit because the base of the unit is buried longer and to a greater depth, and hence experienced higher temperatures than the top of the unit.

The extents and the rates of hydrocarbon generation at different well locations are shown in Figure 6.11 through Figure 6.40. Figure 6.41 through Figure 6.45 are a series of maps of the present-day extents of hydrocarbon generation in each stratigraphic unit. Figure 6.46 through Figure 6.50 are a series of maps showing timing of main hydrocarbon generation phase (reaction extent = 40%) of each



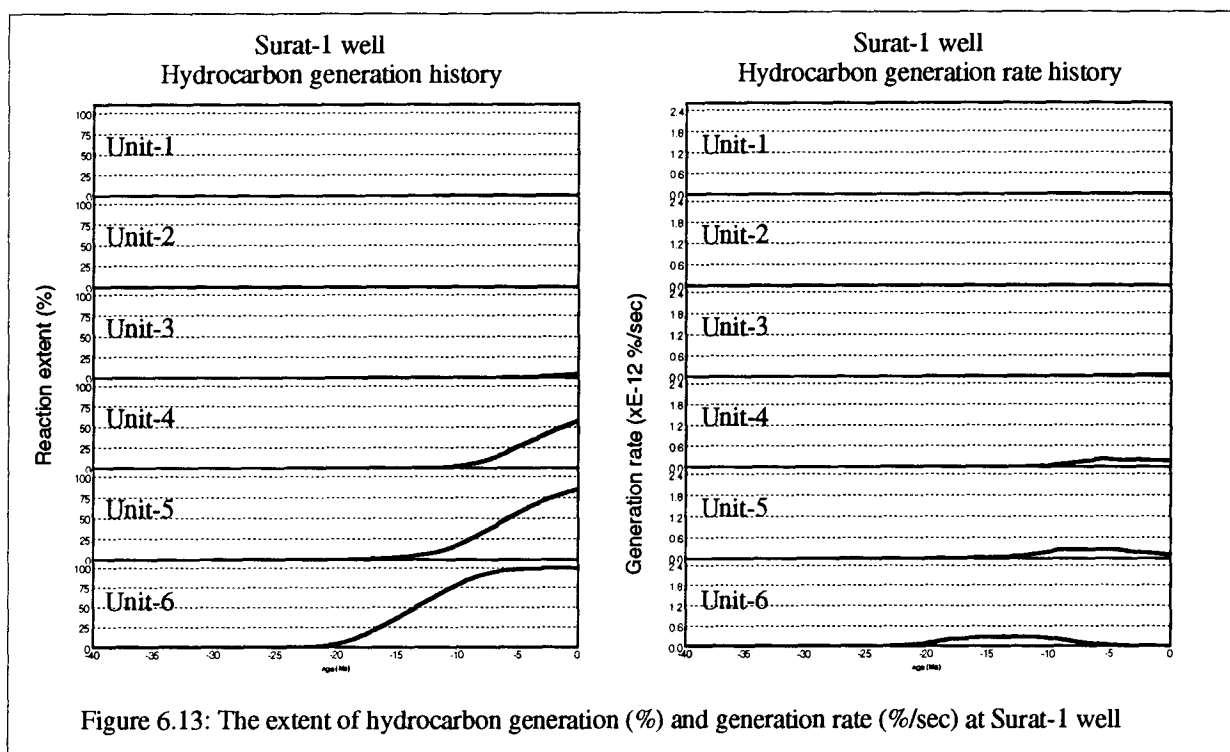


Figure 6.13: The extent of hydrocarbon generation (%) and generation rate (%/sec) at Surat-1 well

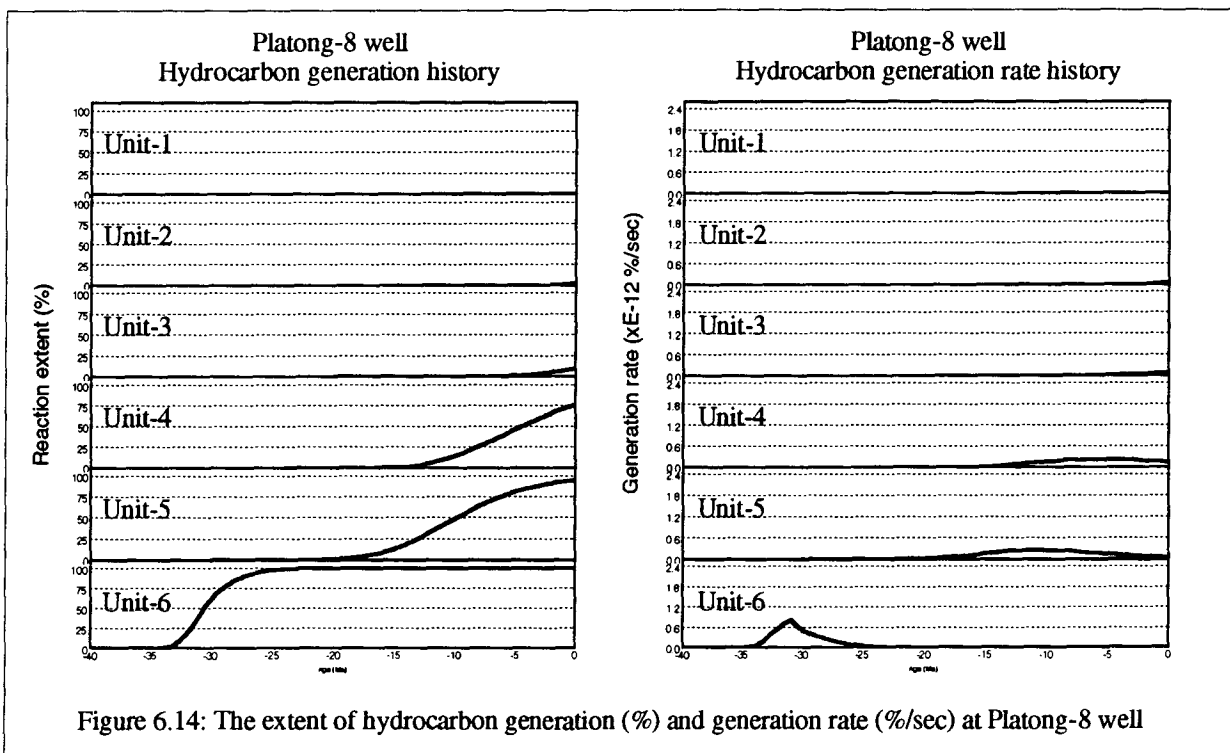


Figure 6.14: The extent of hydrocarbon generation (%) and generation rate (%/sec) at Platong-8 well

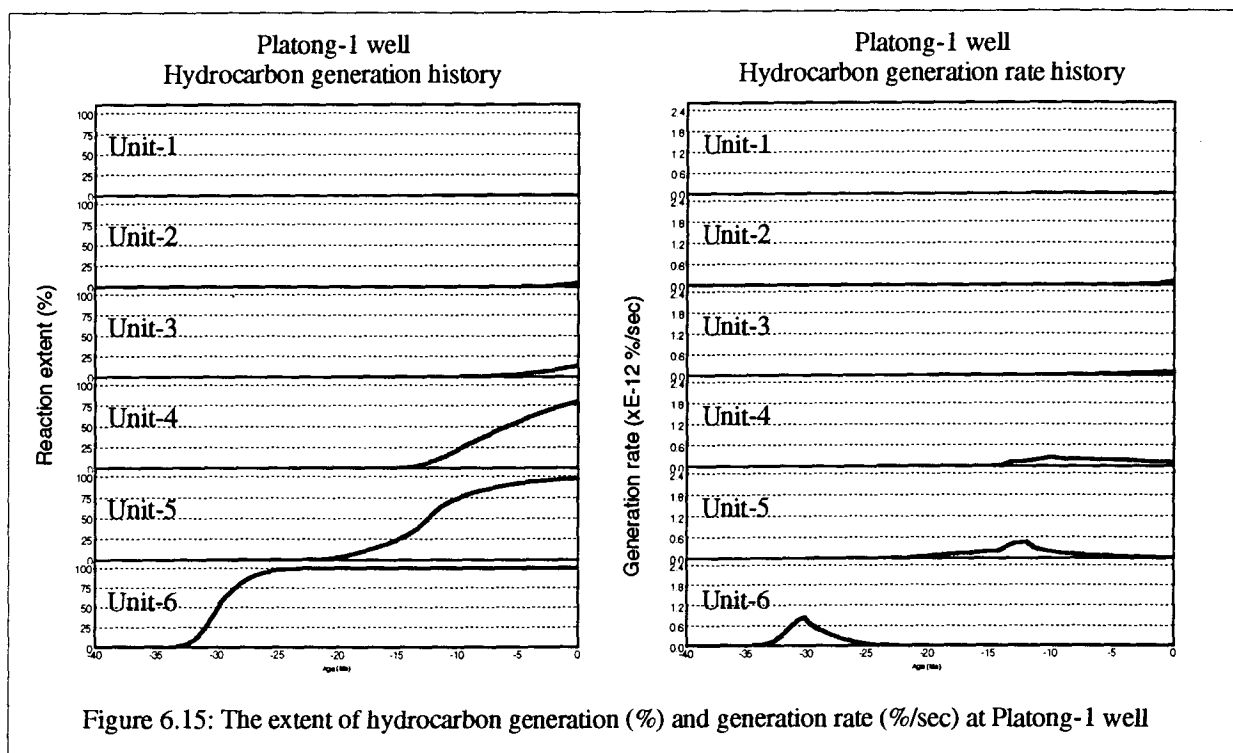


Figure 6.15: The extent of hydrocarbon generation (%) and generation rate (%/sec) at Platong-1 well

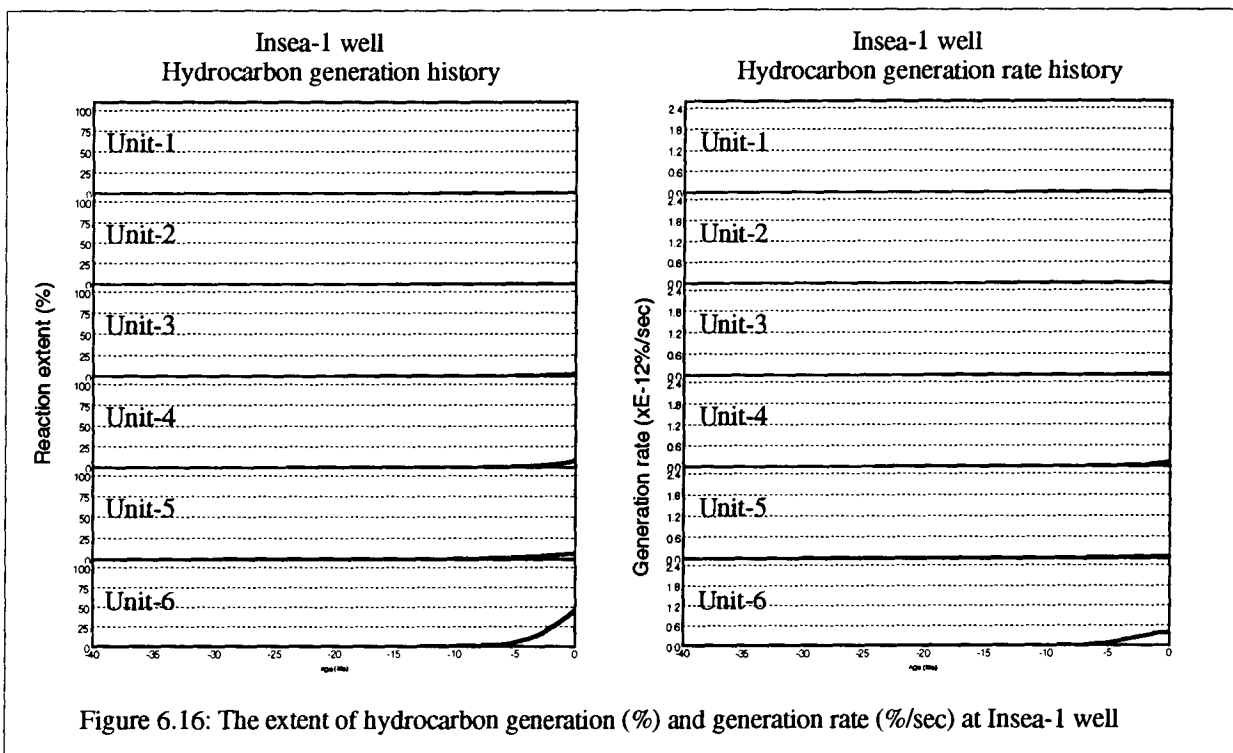
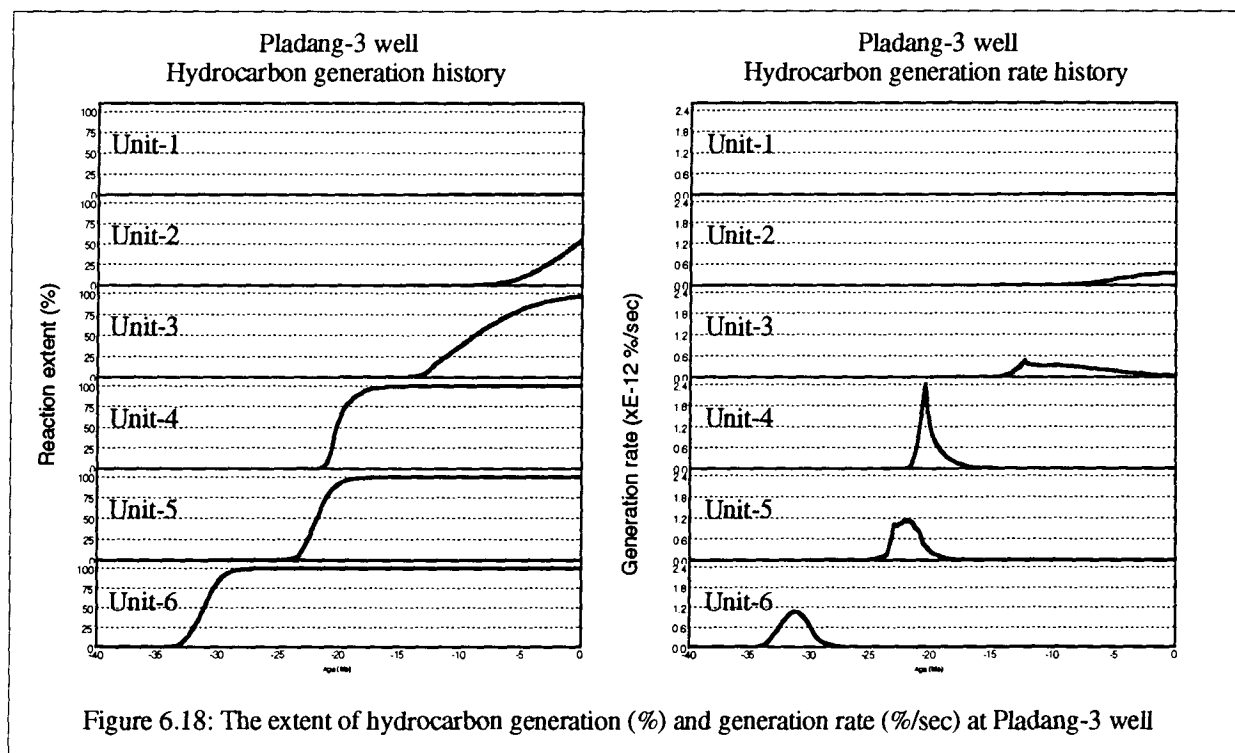
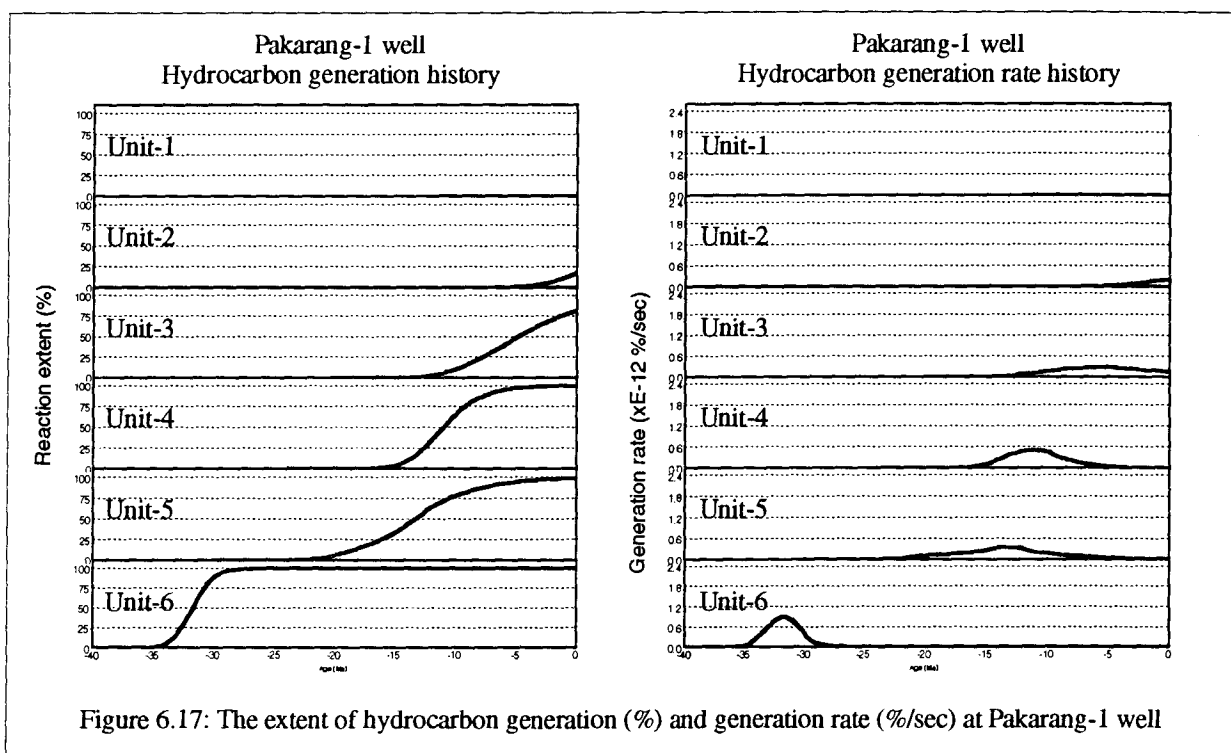
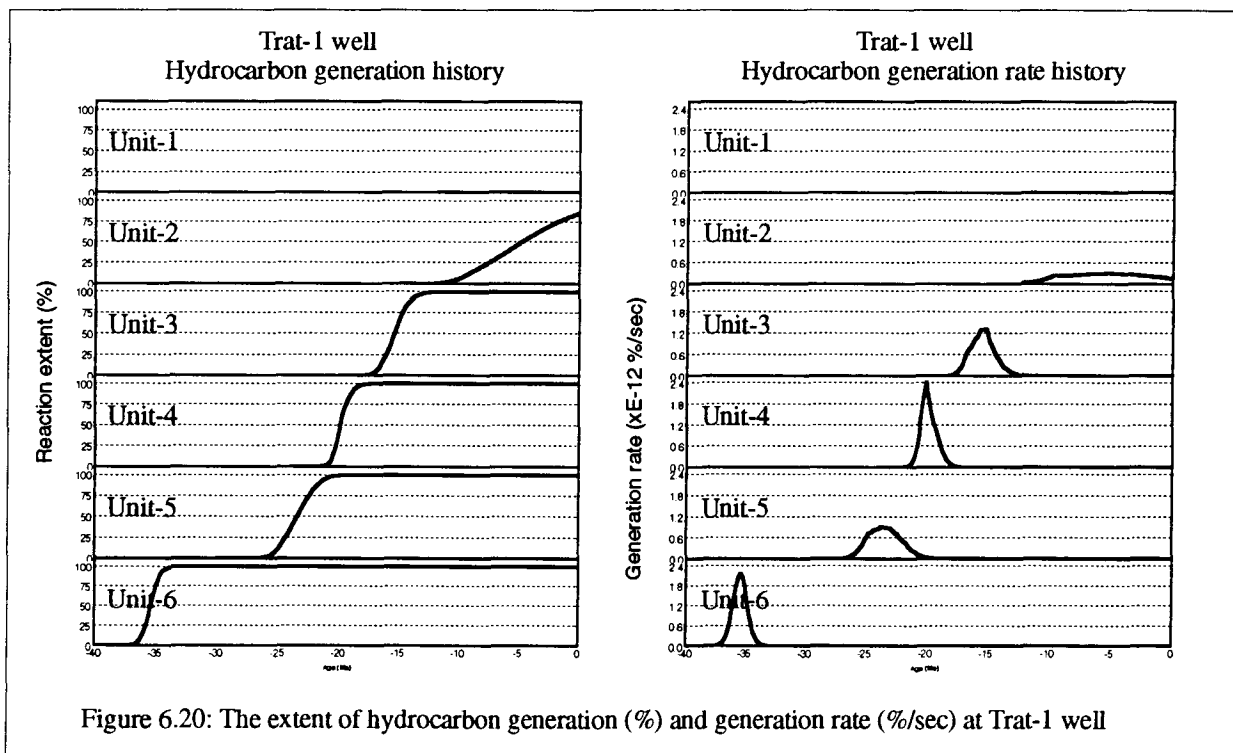
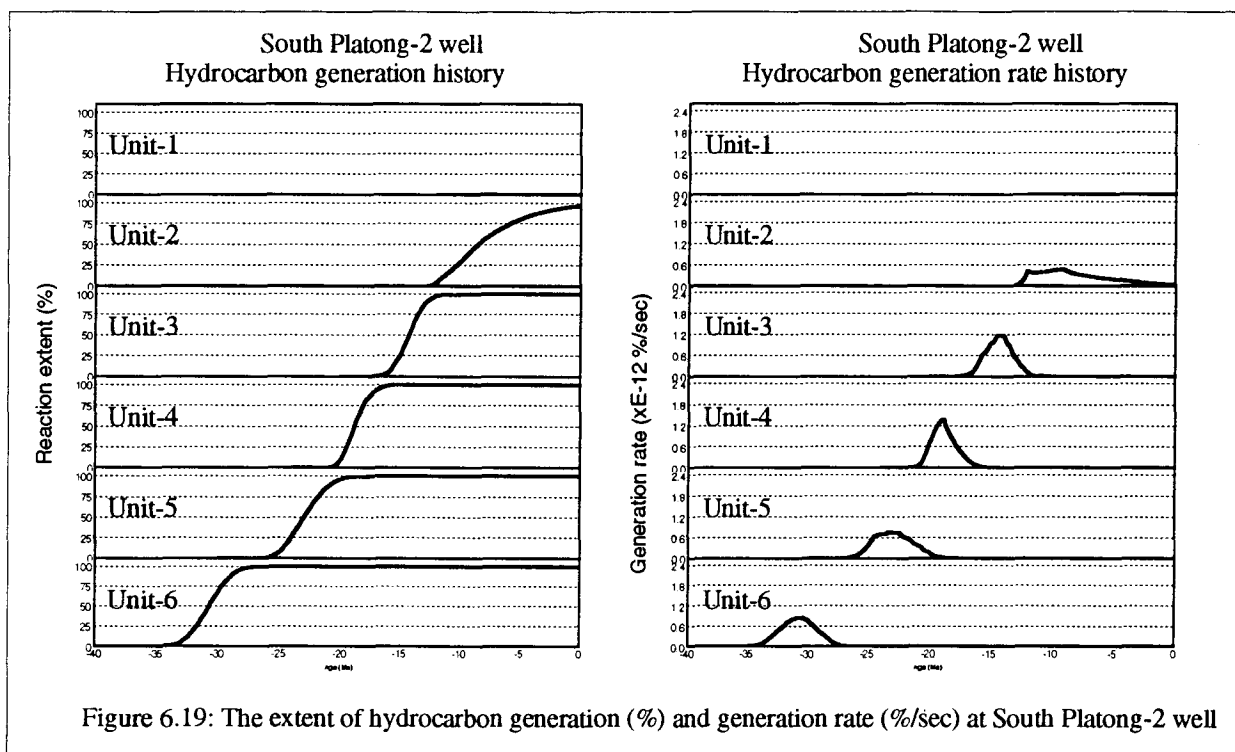
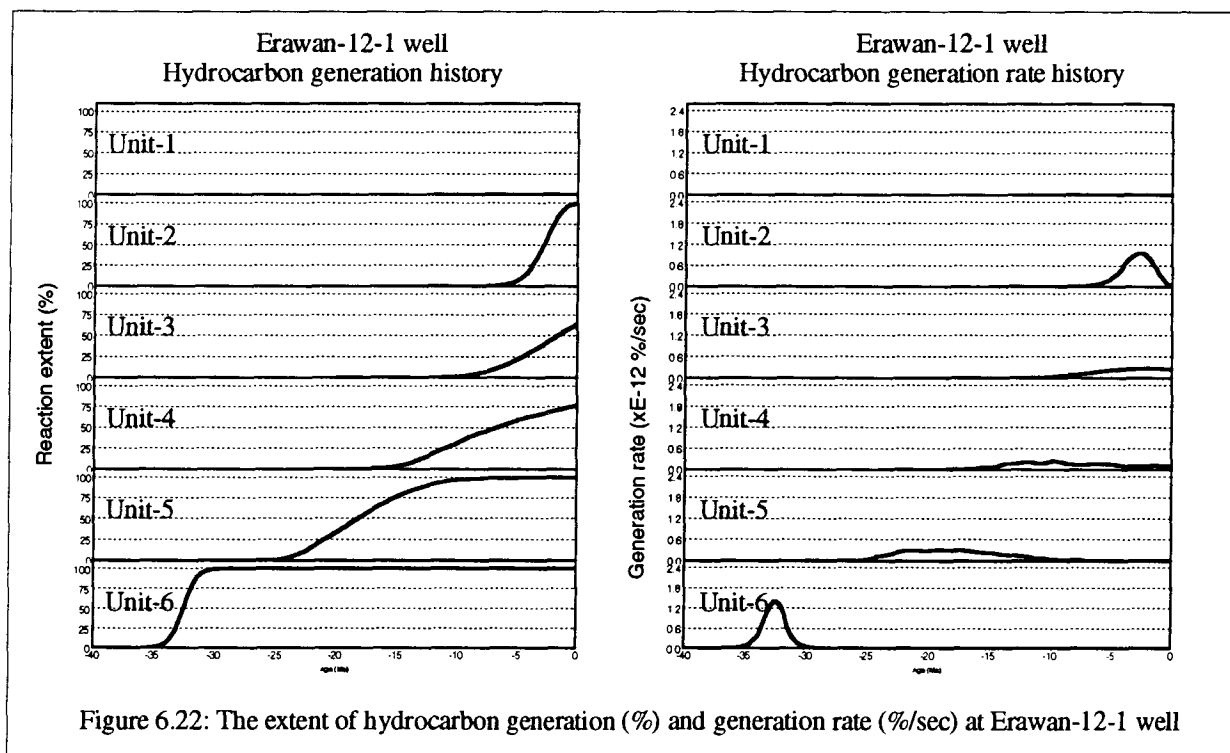
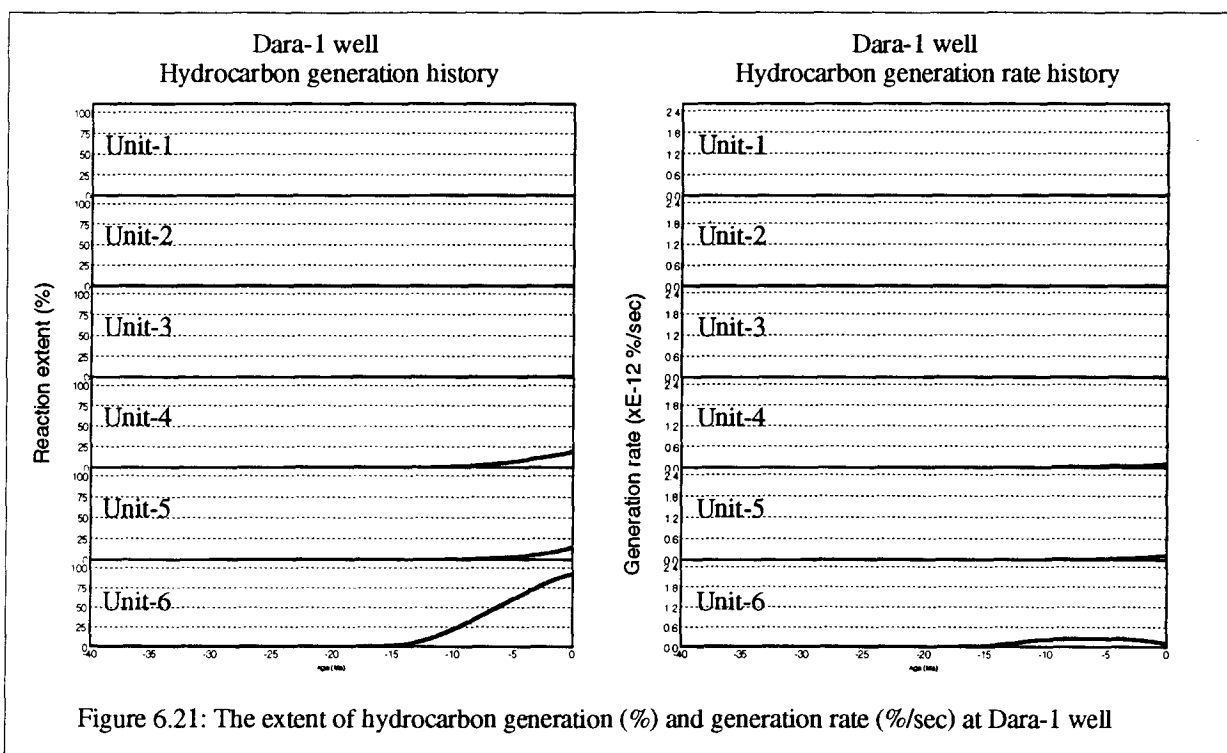
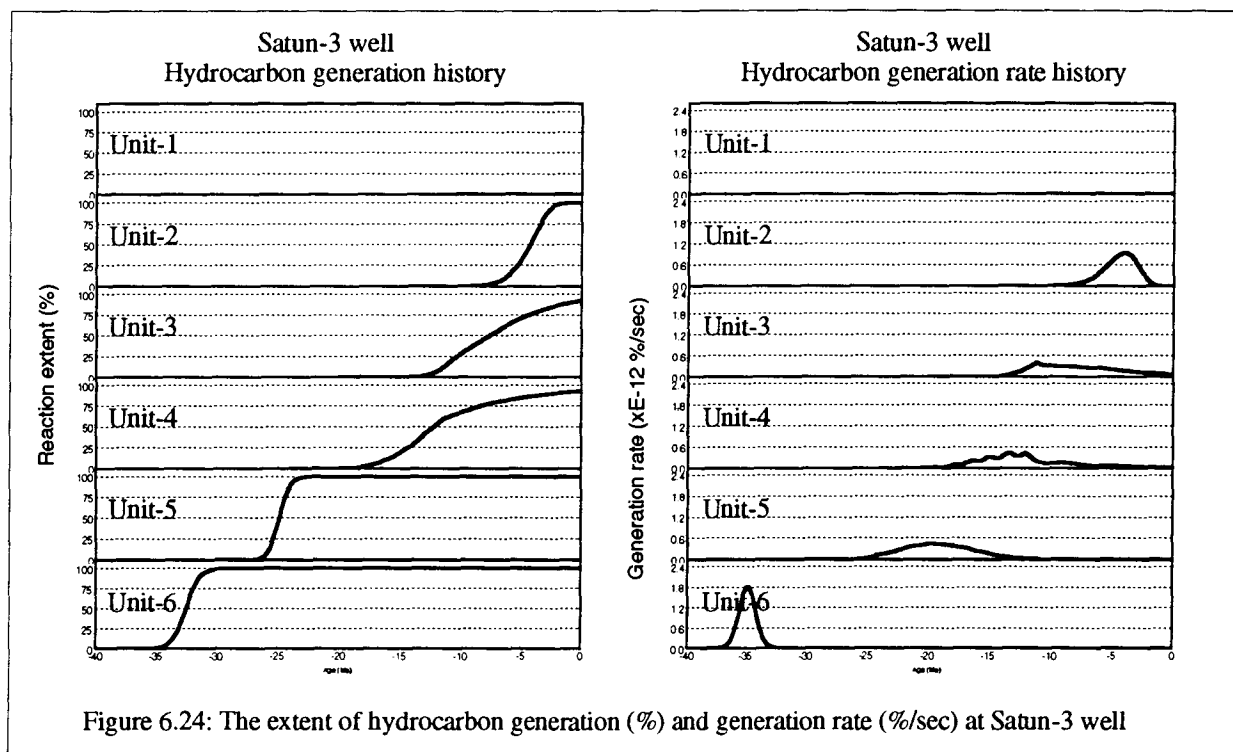
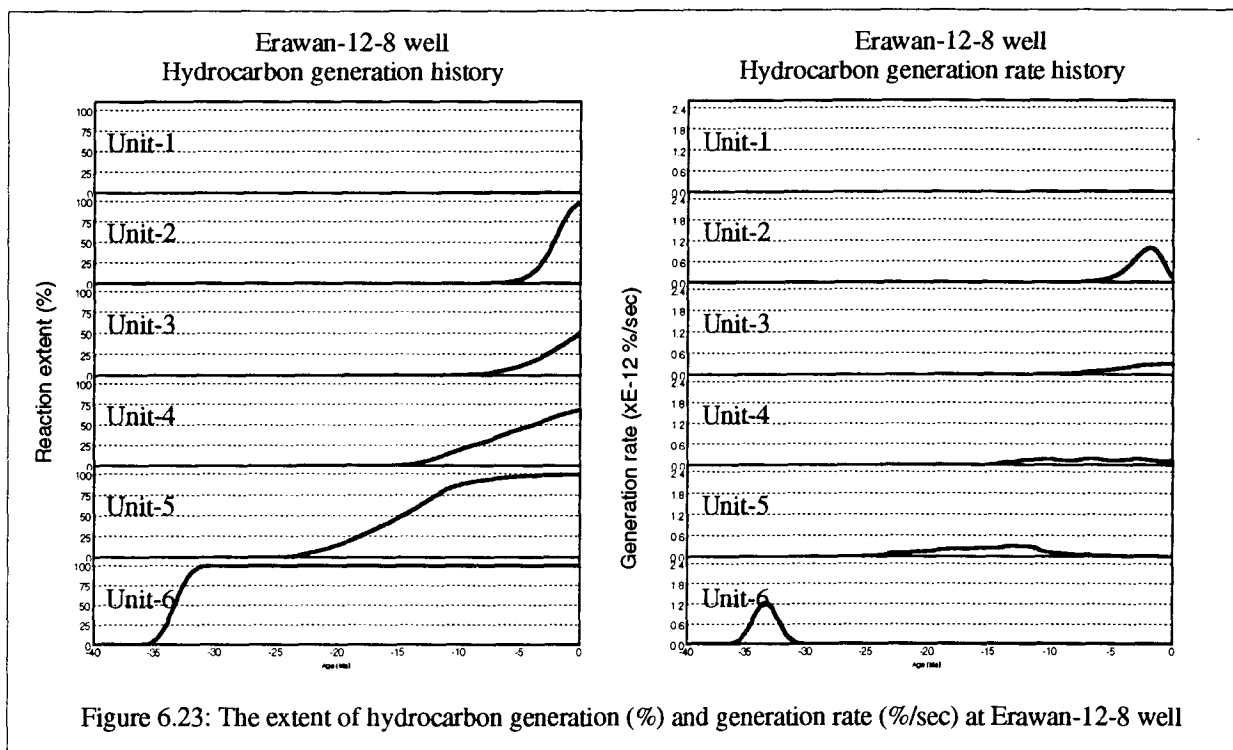


Figure 6.16: The extent of hydrocarbon generation (%) and generation rate (%/sec) at Insea-1 well









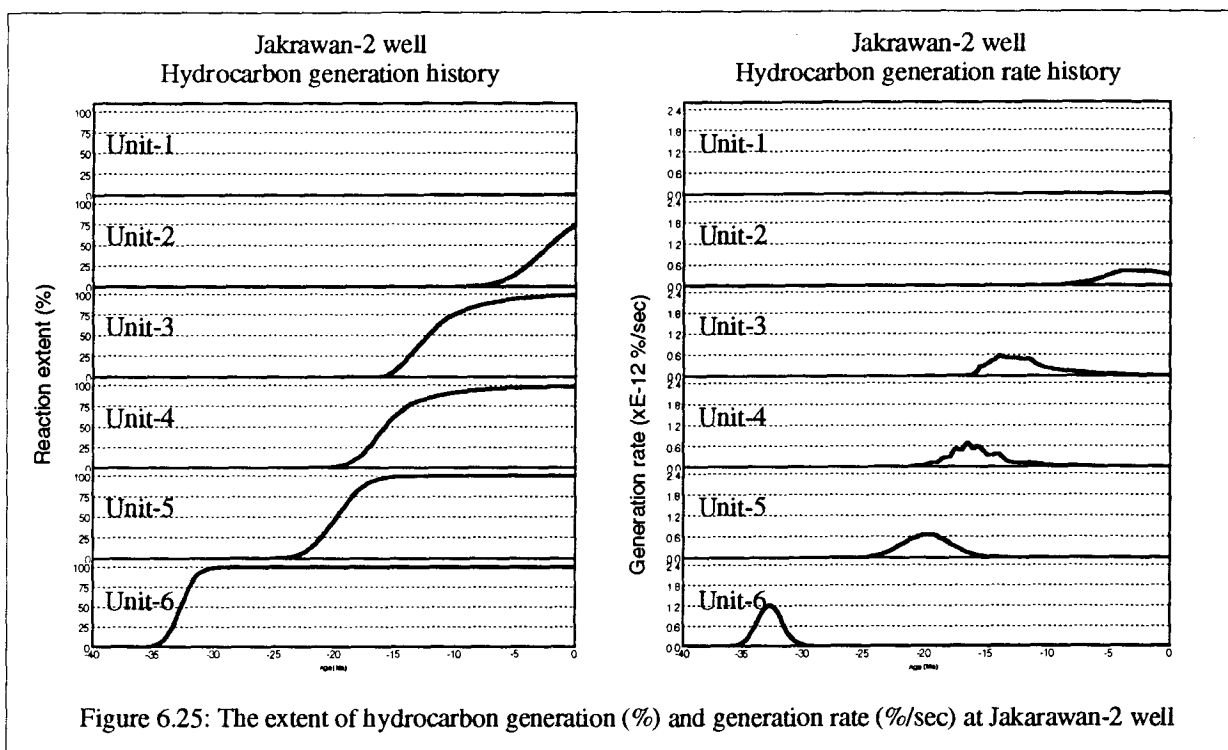


Figure 6.25: The extent of hydrocarbon generation (%) and generation rate (%/sec) at Jakrawan-2 well

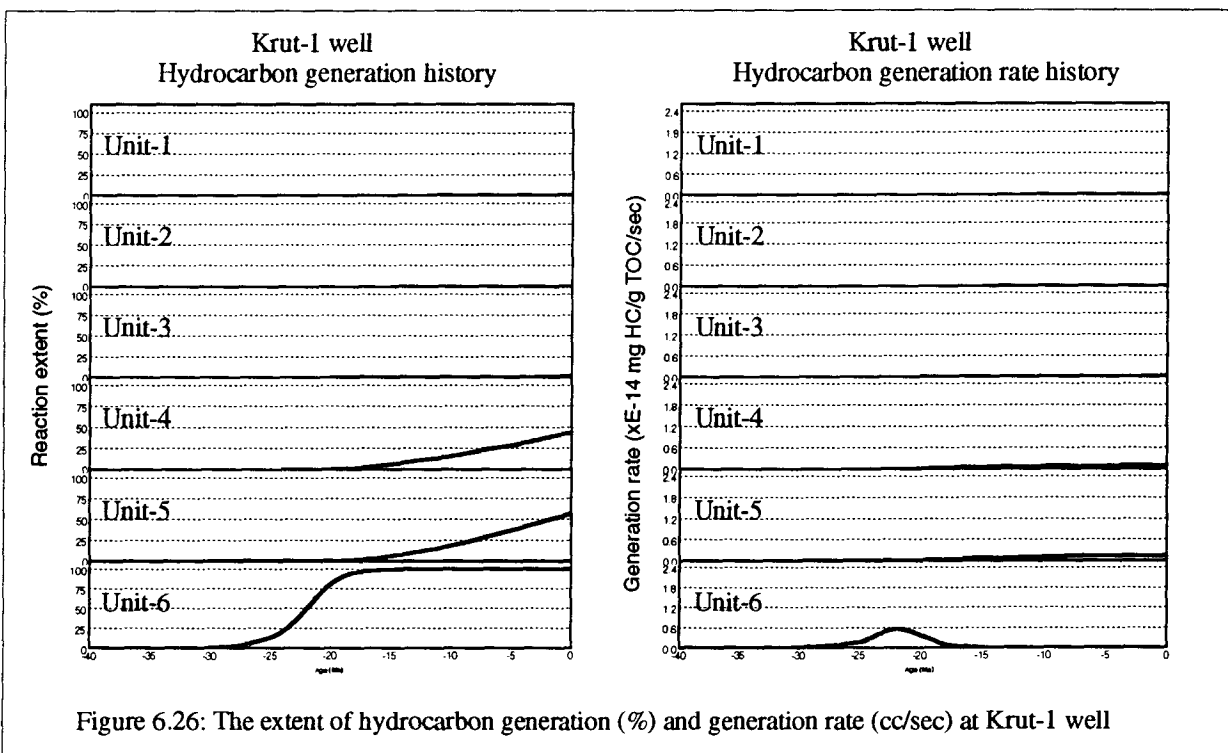


Figure 6.26: The extent of hydrocarbon generation (%) and generation rate (cc/sec) at Krut-1 well

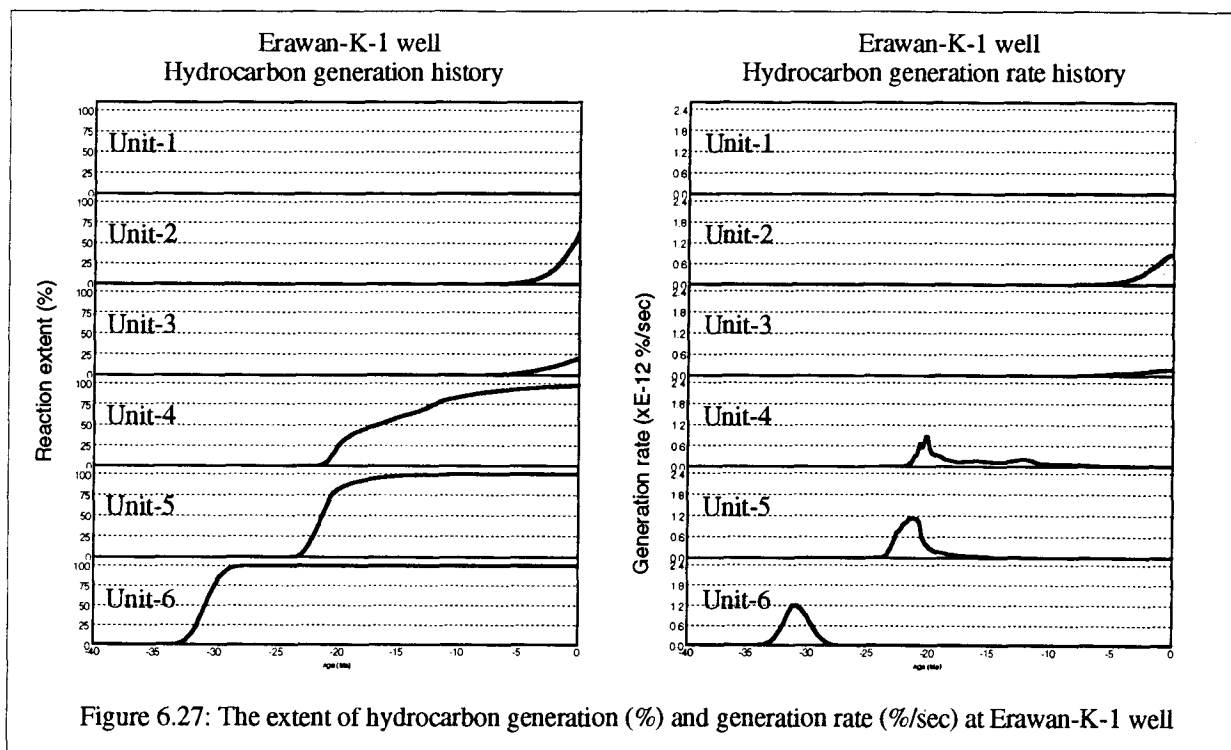


Figure 6.27: The extent of hydrocarbon generation (%) and generation rate (%/sec) at Erawan-K-1 well

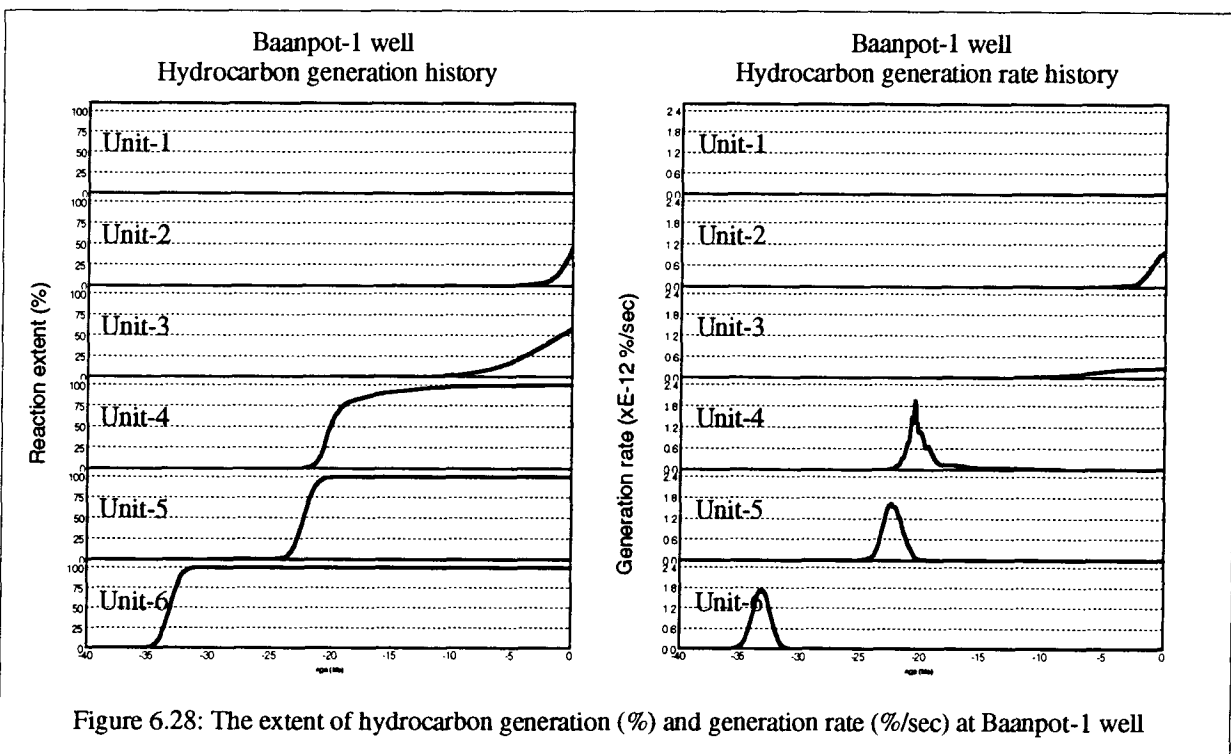
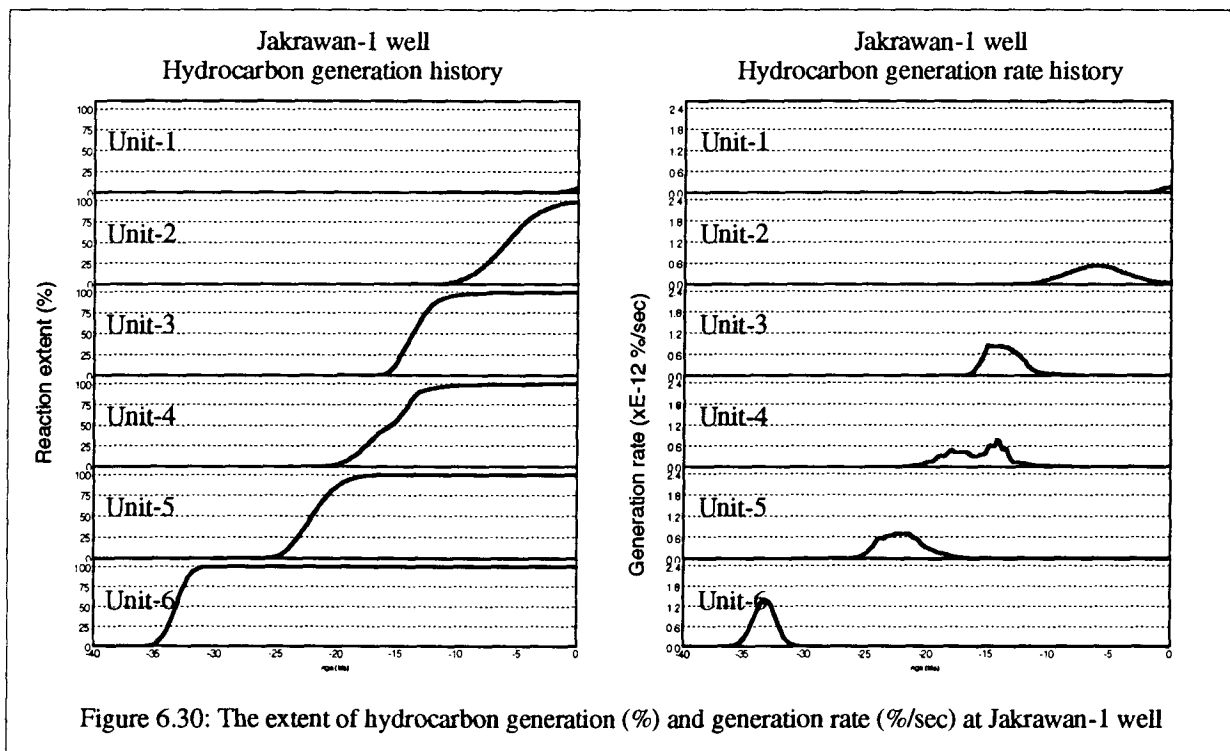
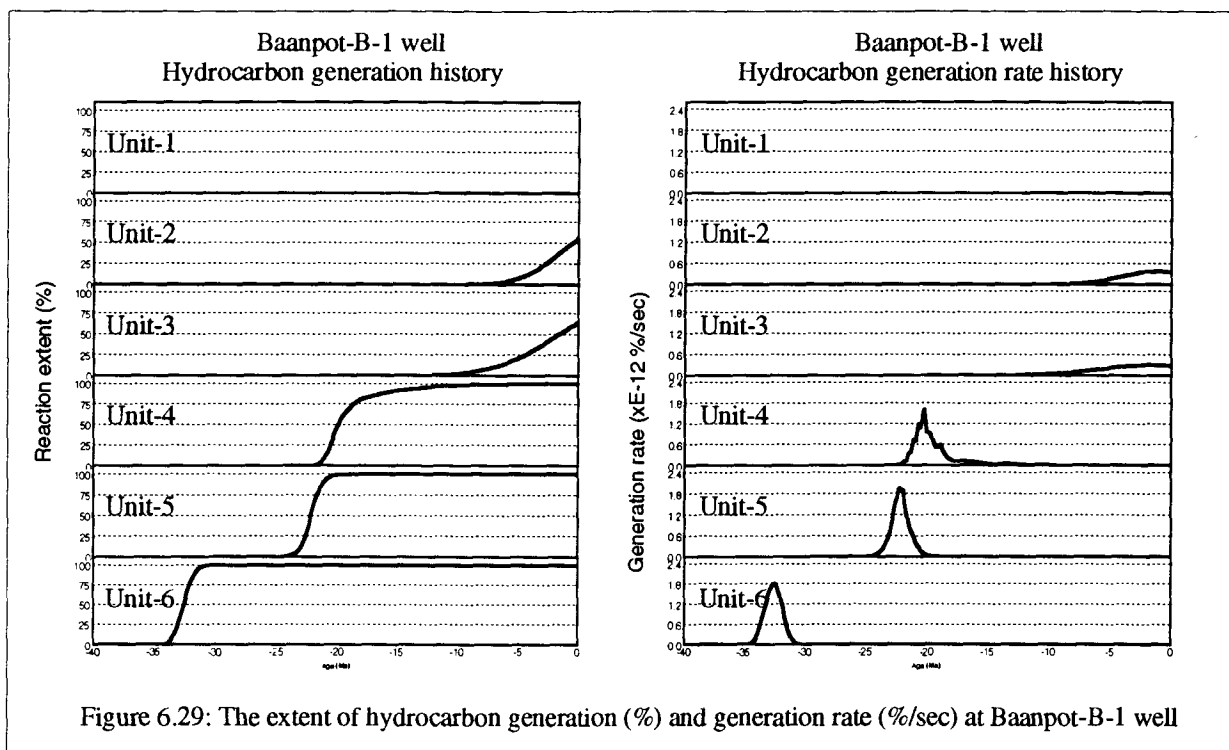
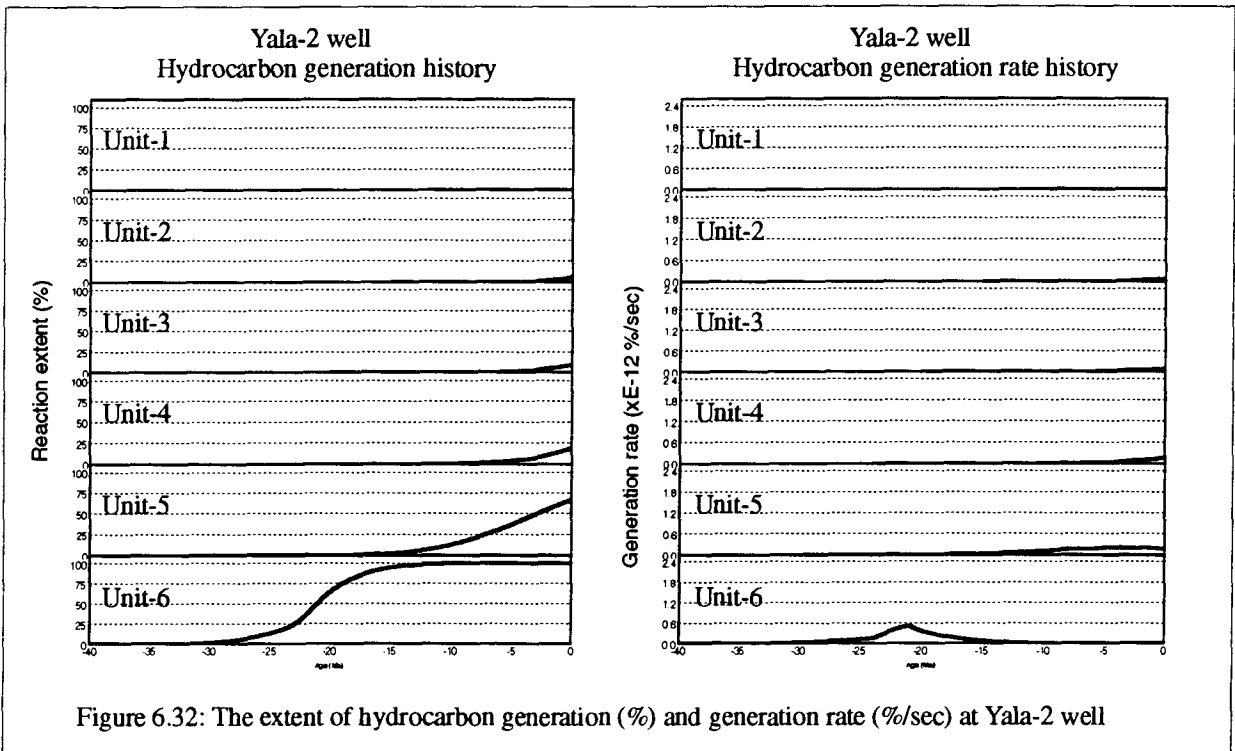
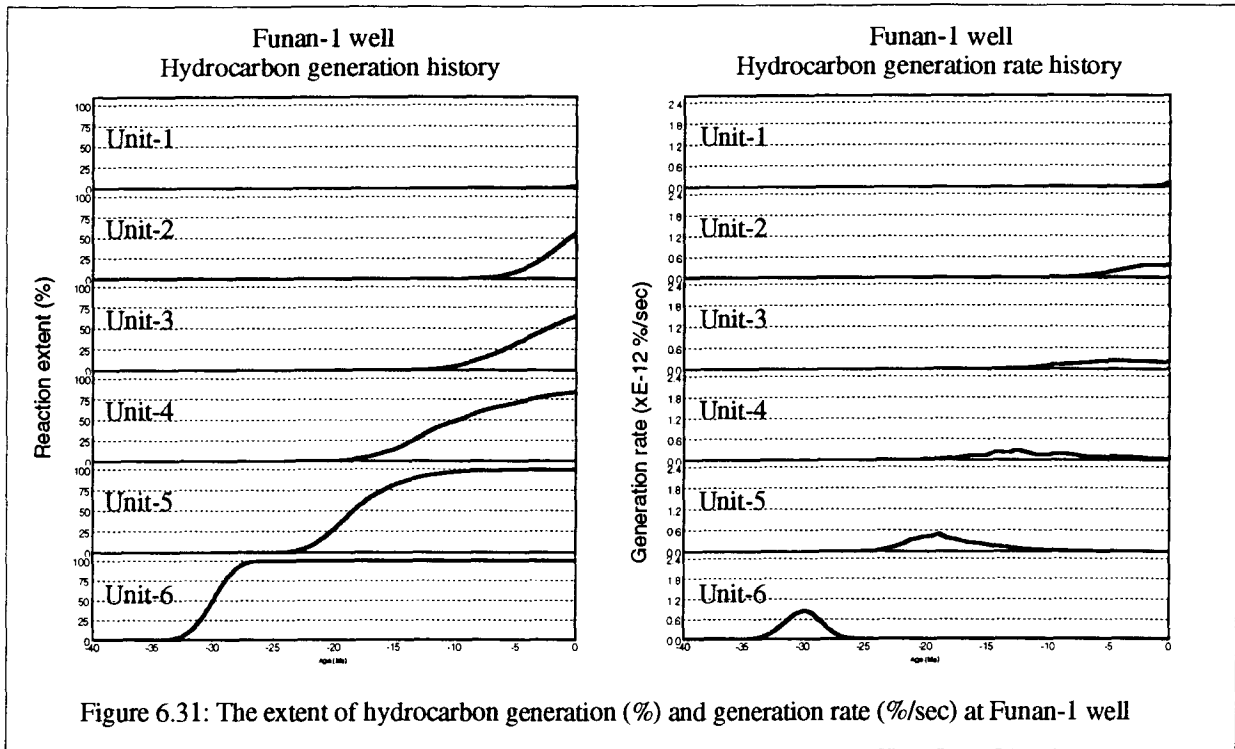
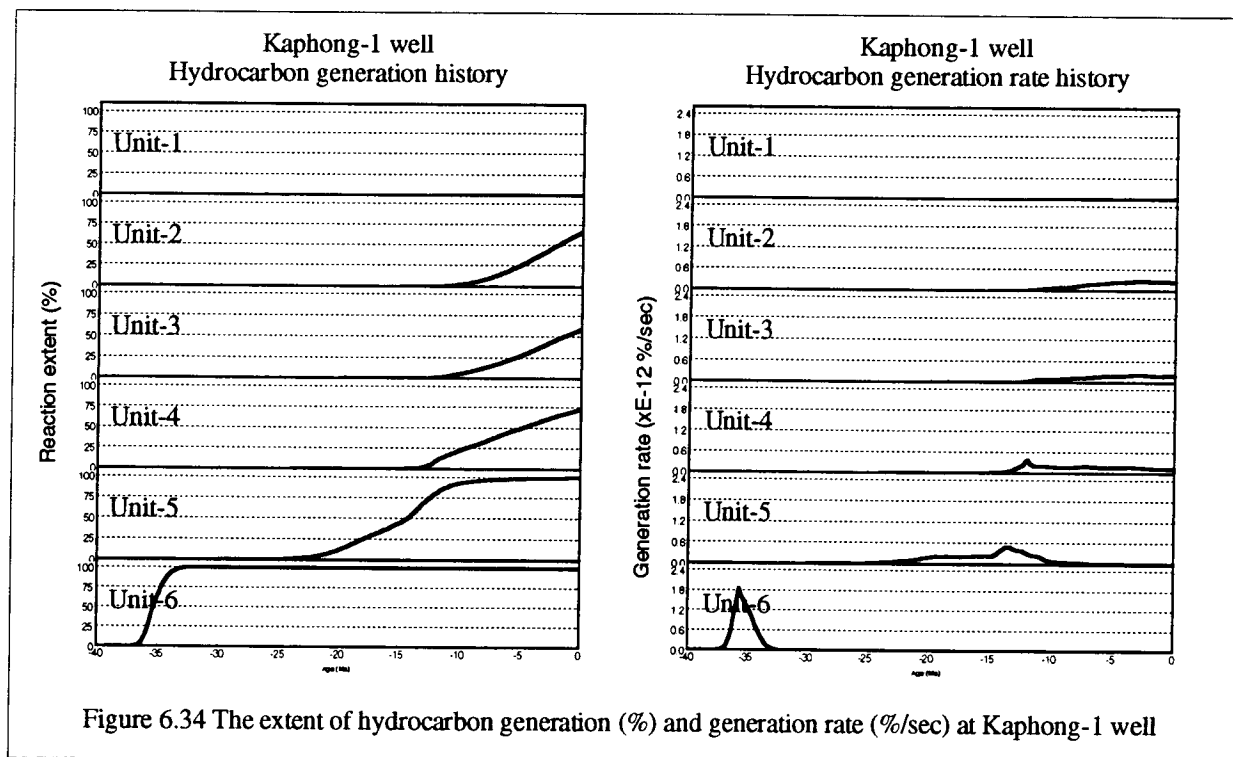
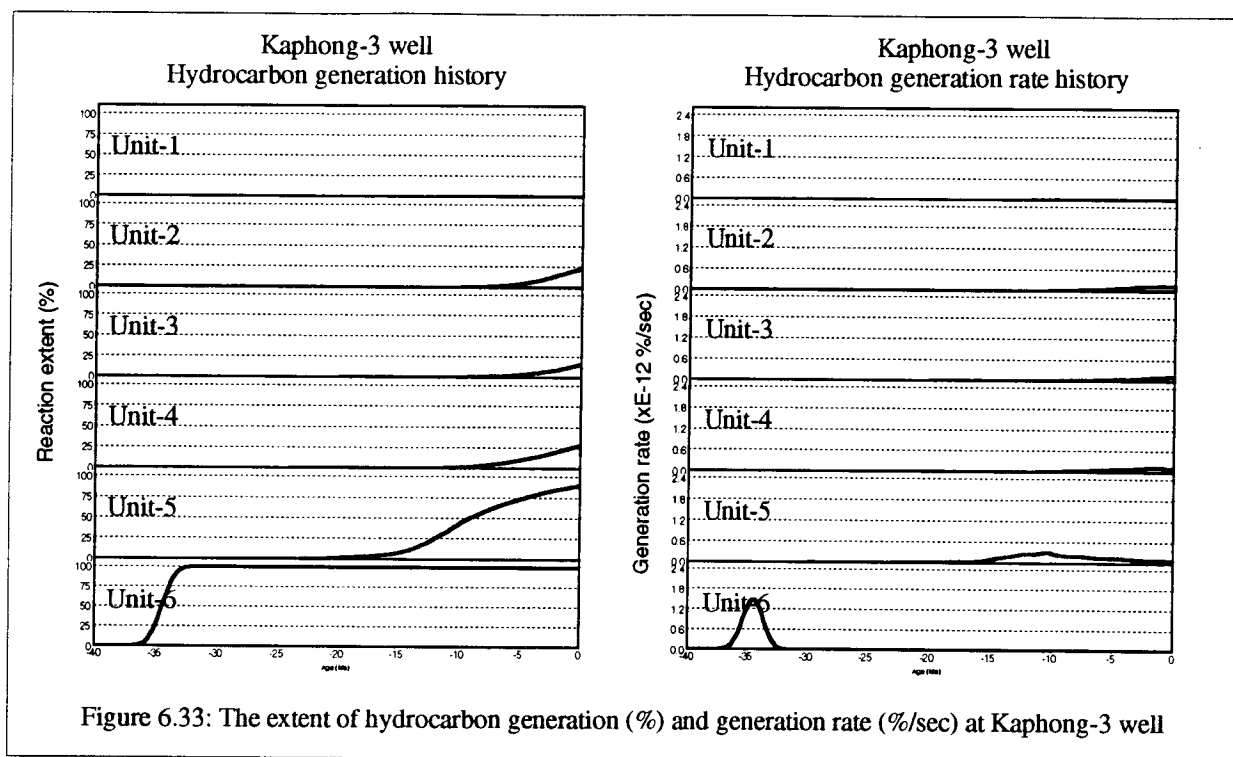


Figure 6.28: The extent of hydrocarbon generation (%) and generation rate (%/sec) at Baanpot-1 well







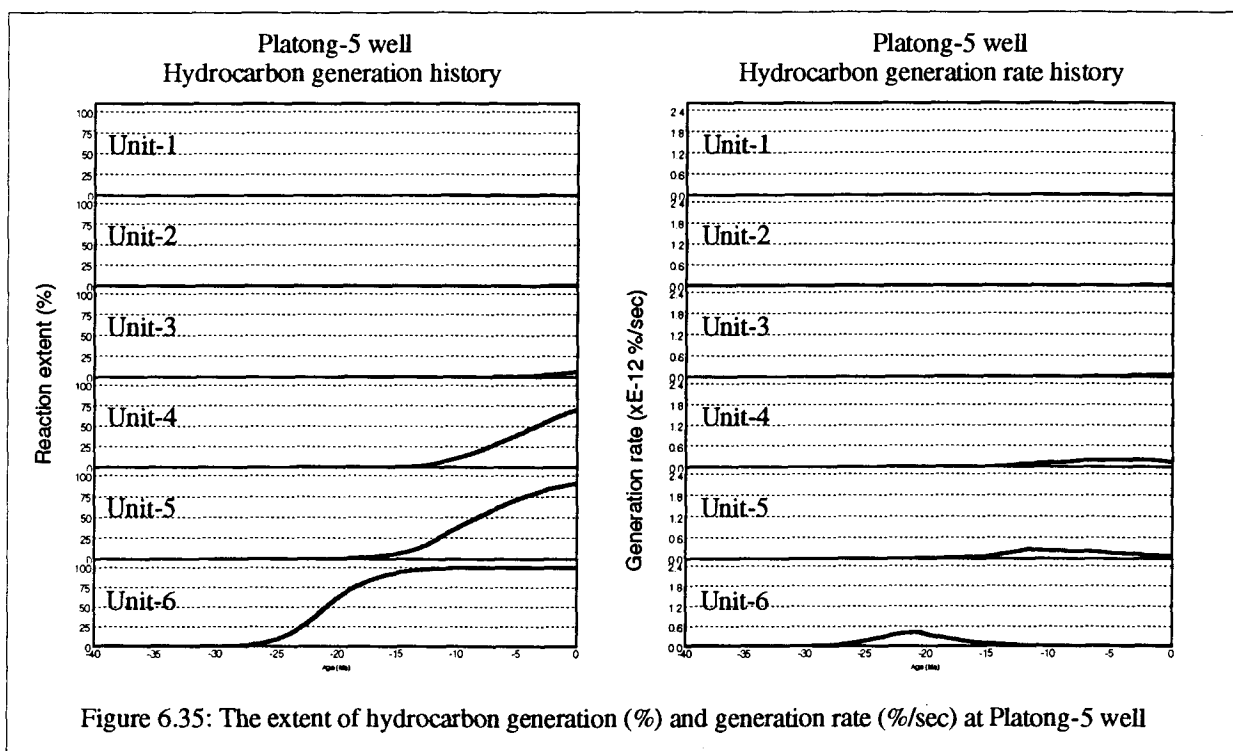


Figure 6.35: The extent of hydrocarbon generation (%) and generation rate (%/sec) at Platong-5 well

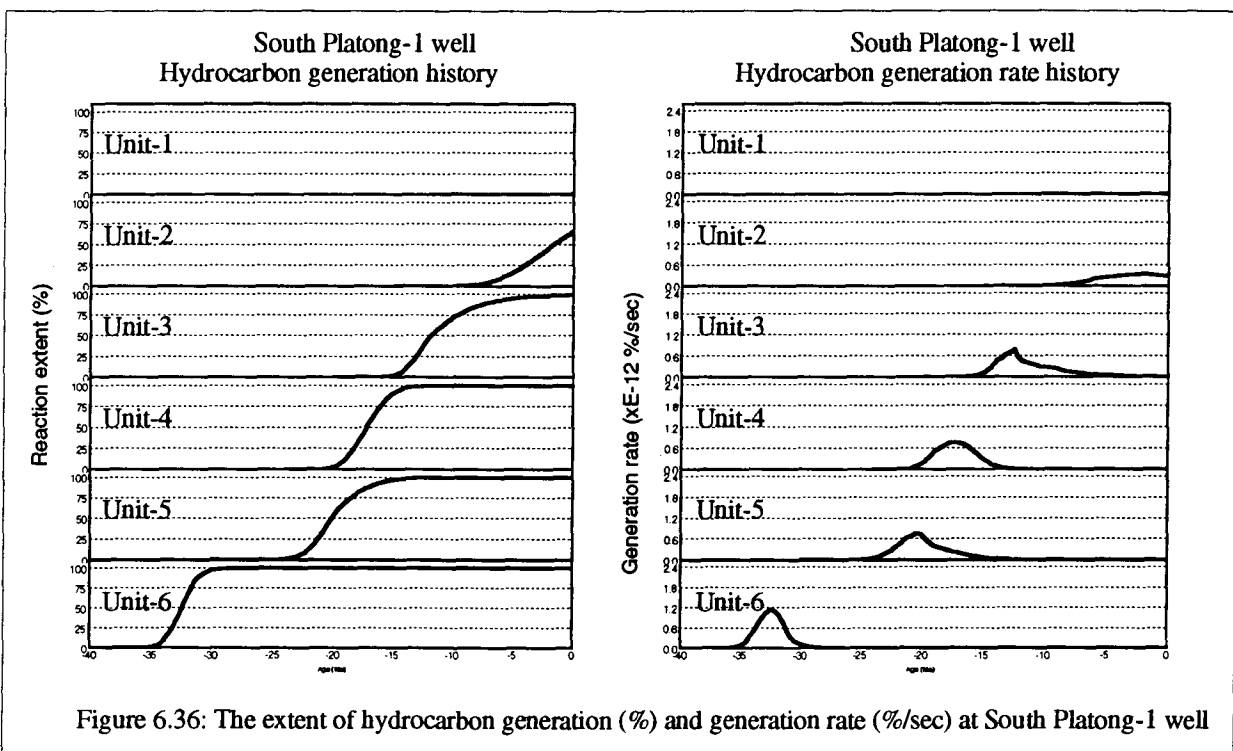
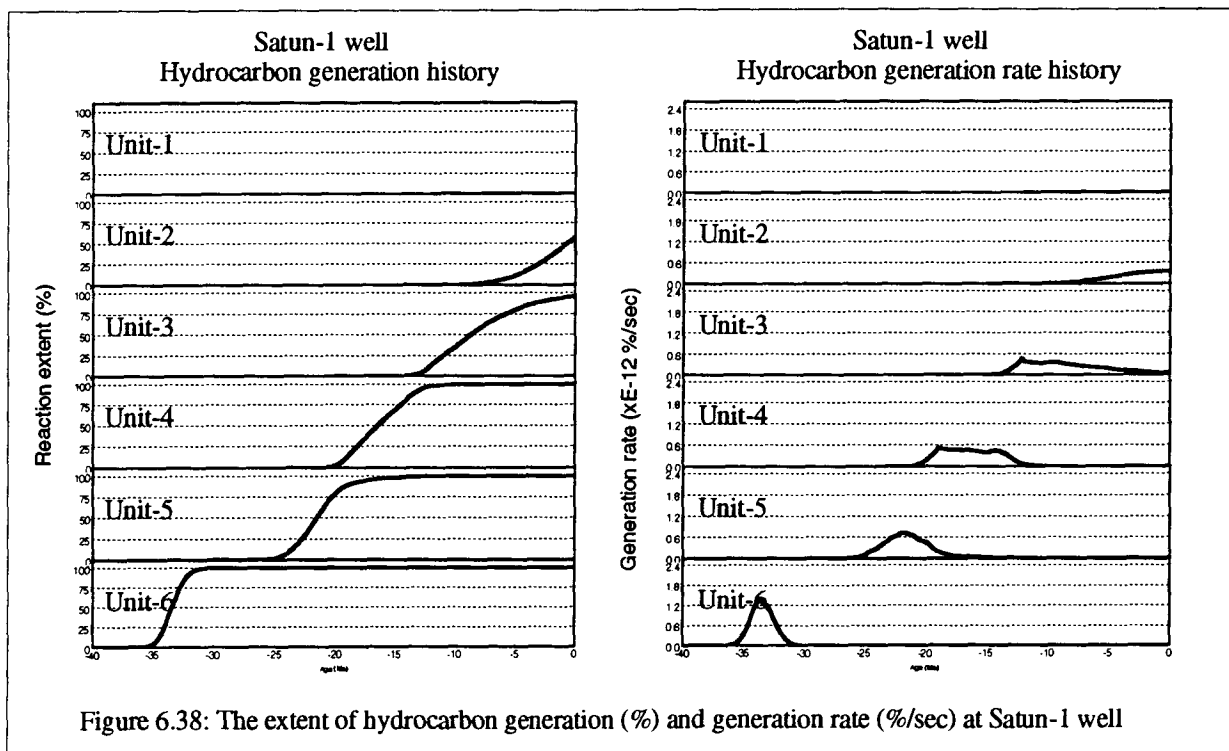
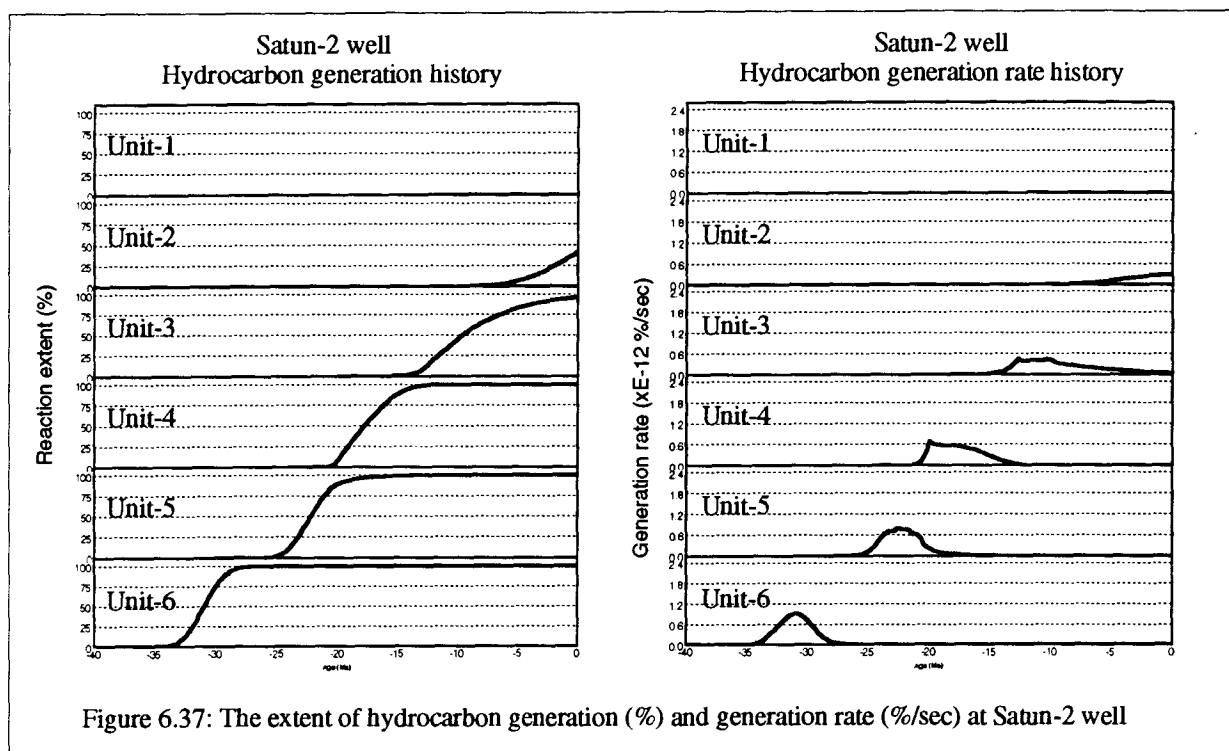
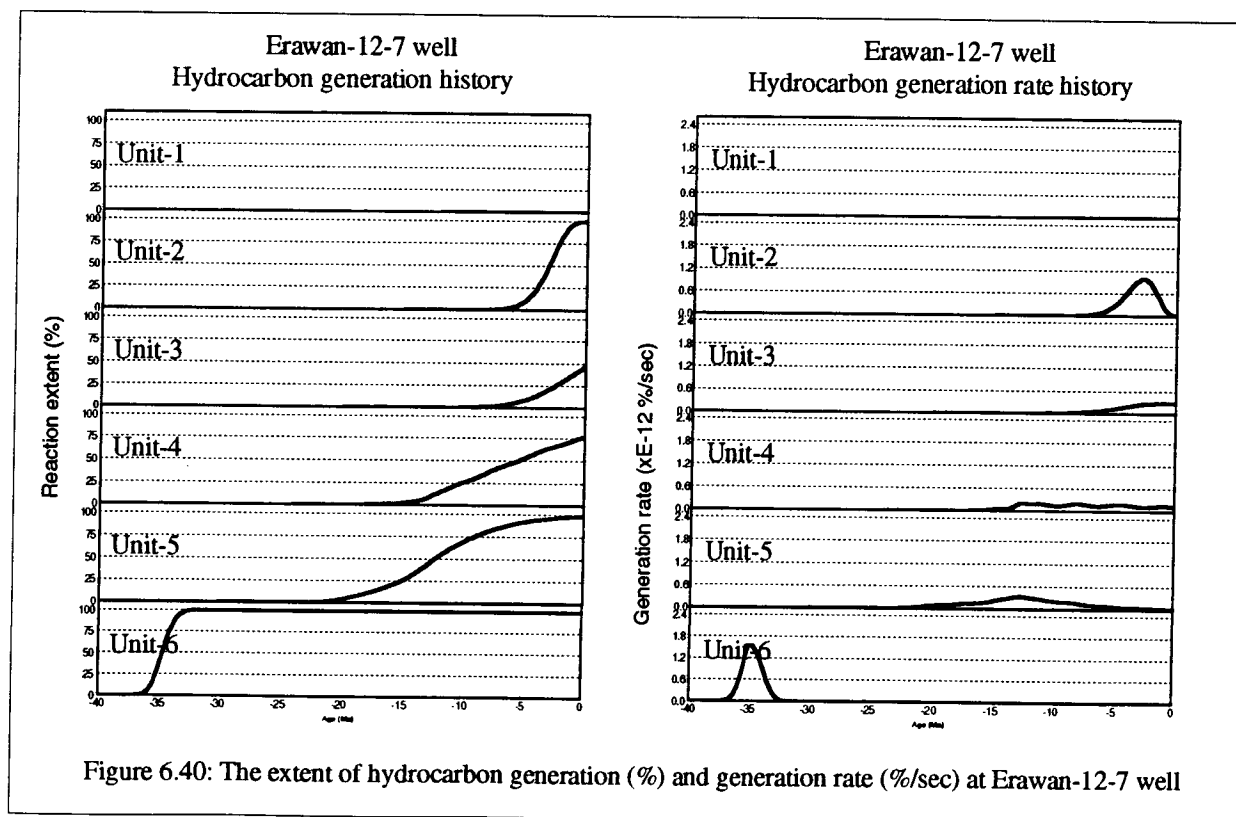
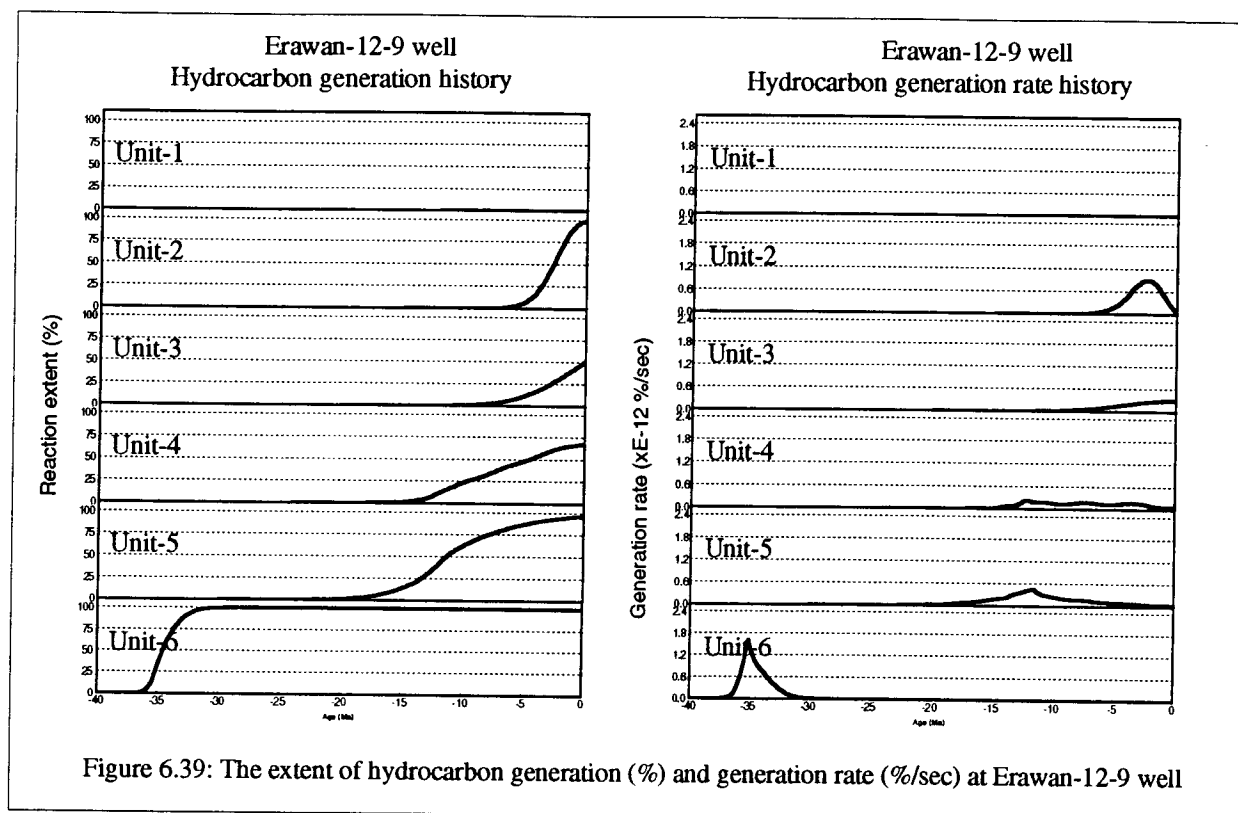


Figure 6.36: The extent of hydrocarbon generation (%) and generation rate (%/sec) at South Platong-1 well





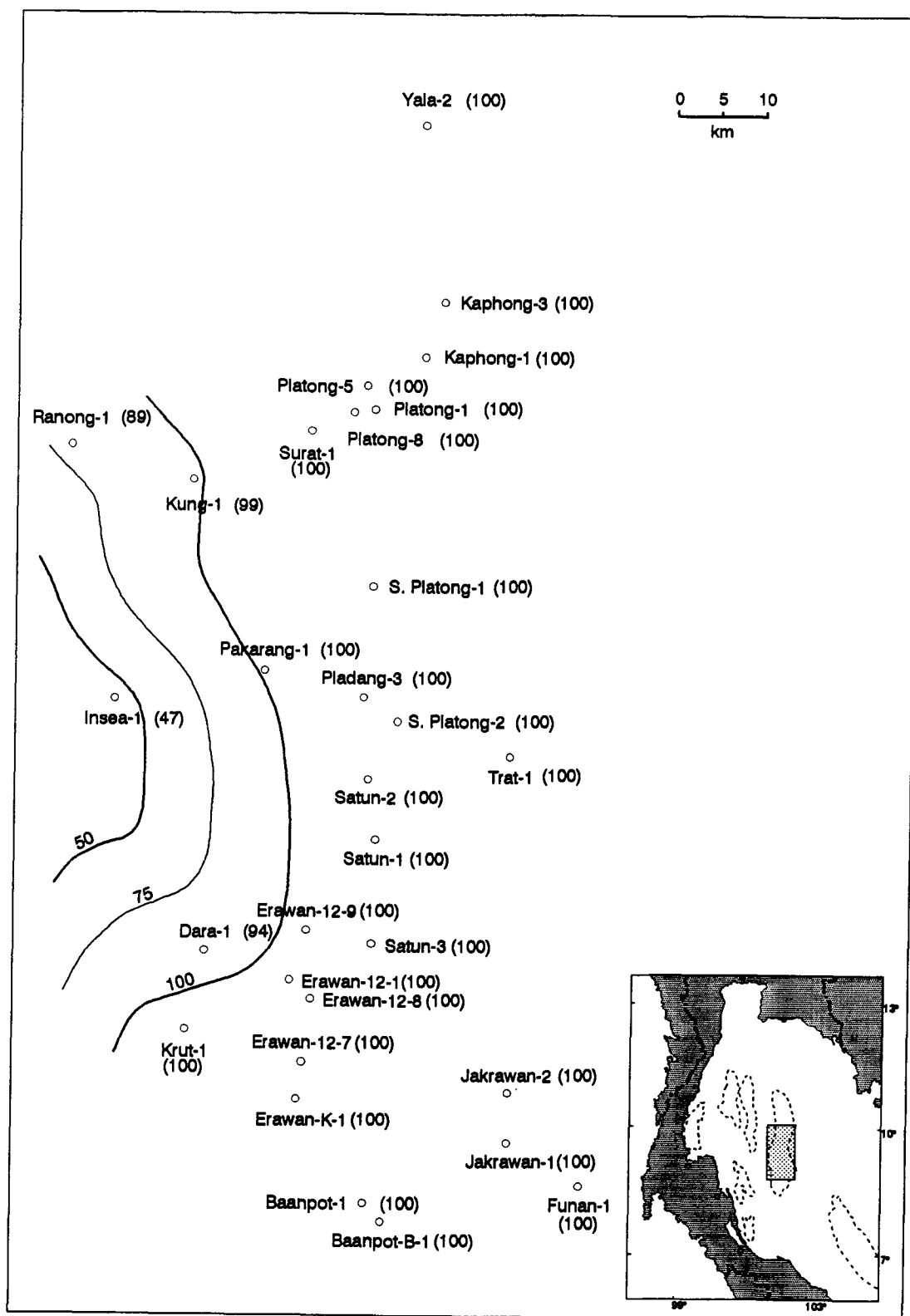


Figure 6.41: Calculated present-day reaction extent of unit 6's hydrocarbon generation (%)

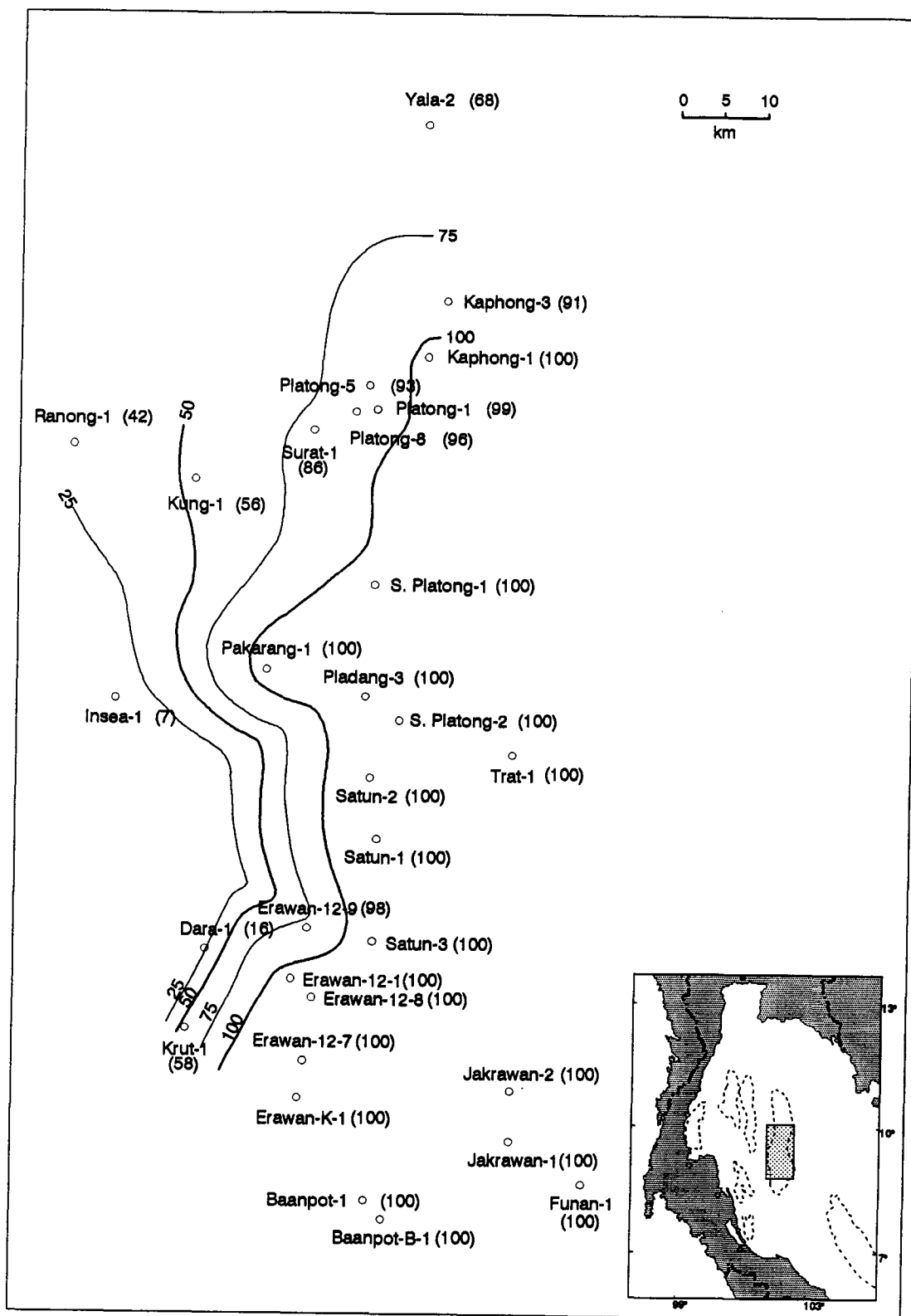


Figure 6.42: Calculated present-day reaction extent of unit 5's hydrocarbon generation (%)

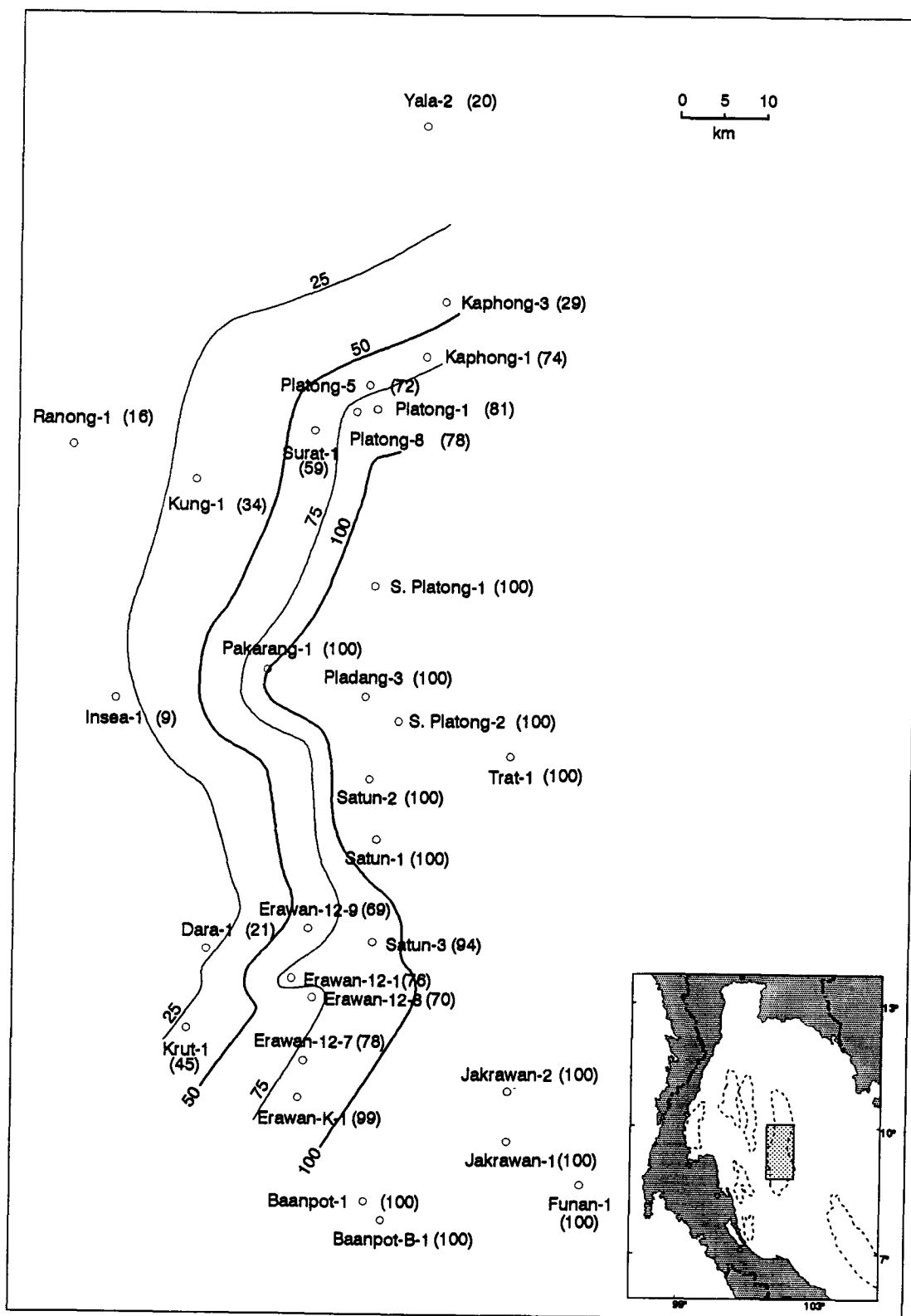


Figure 6.43: Calculated present-day reaction extent of unit 4's hydrocarbon generation (%)

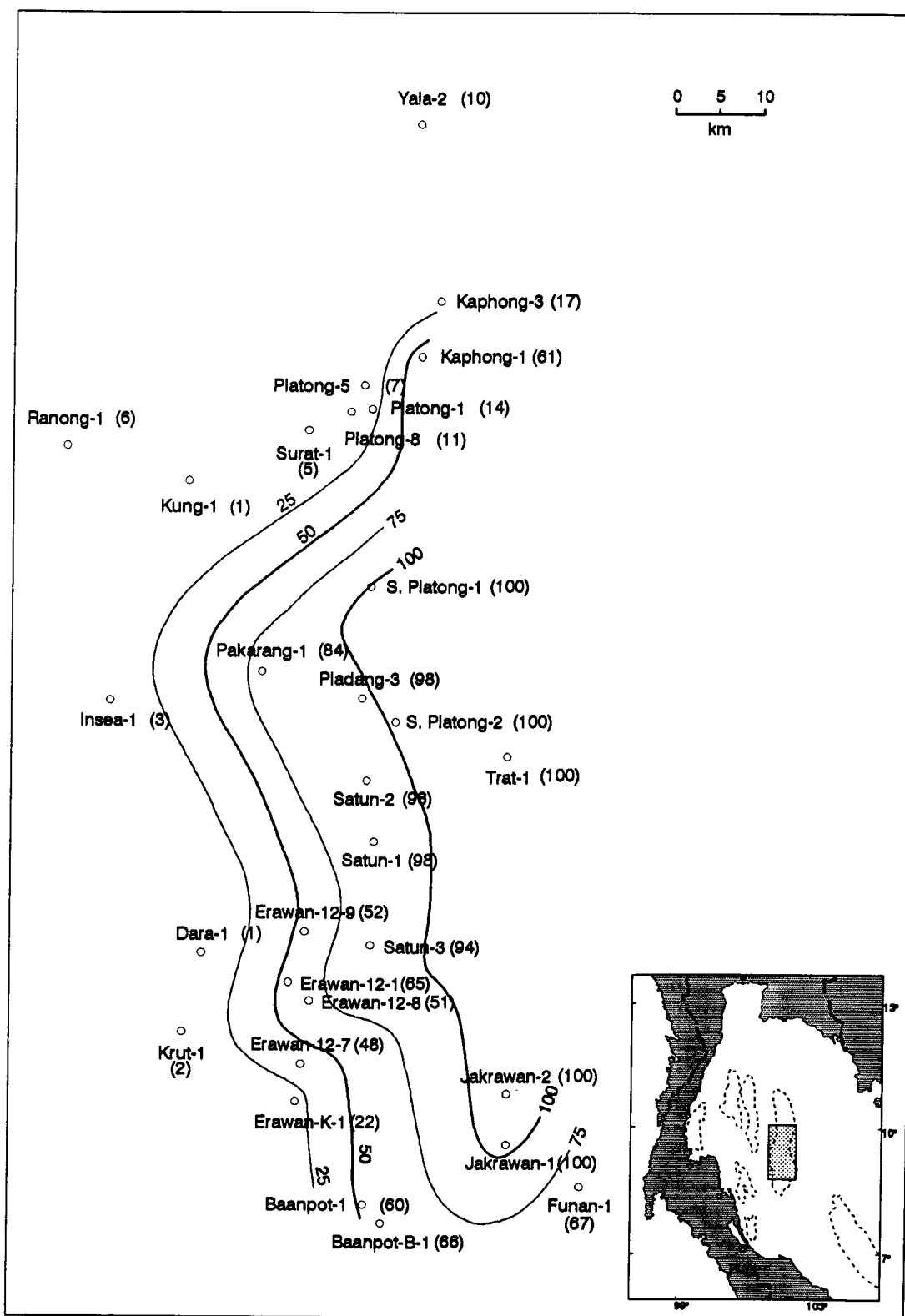


Figure 6.44: Calculated present-day reaction extent of unit 3's hydrocarbon generation (%)

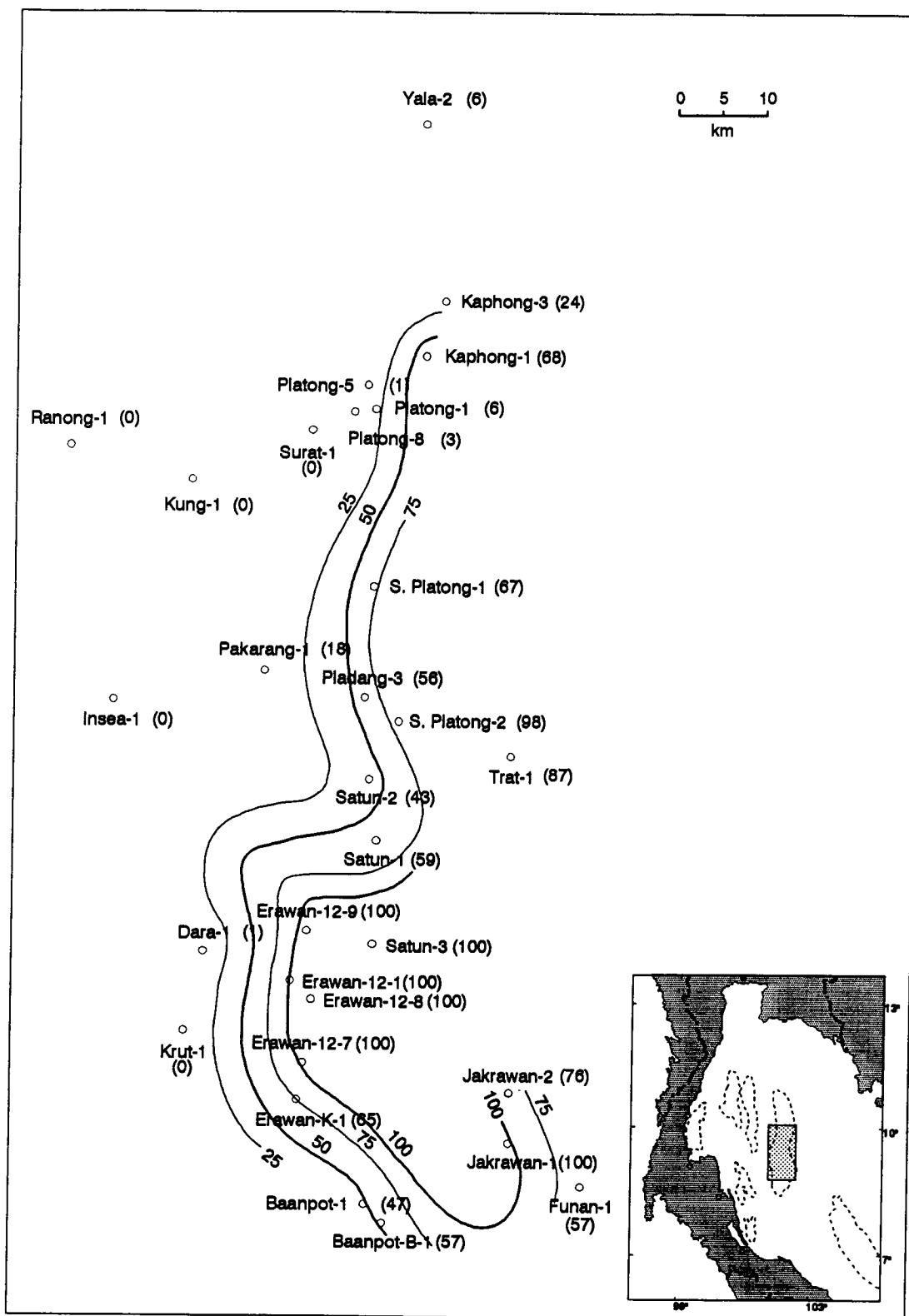


Figure 6.45: Calculated present-day reaction extent of unit 2's hydrocarbon generation (%)

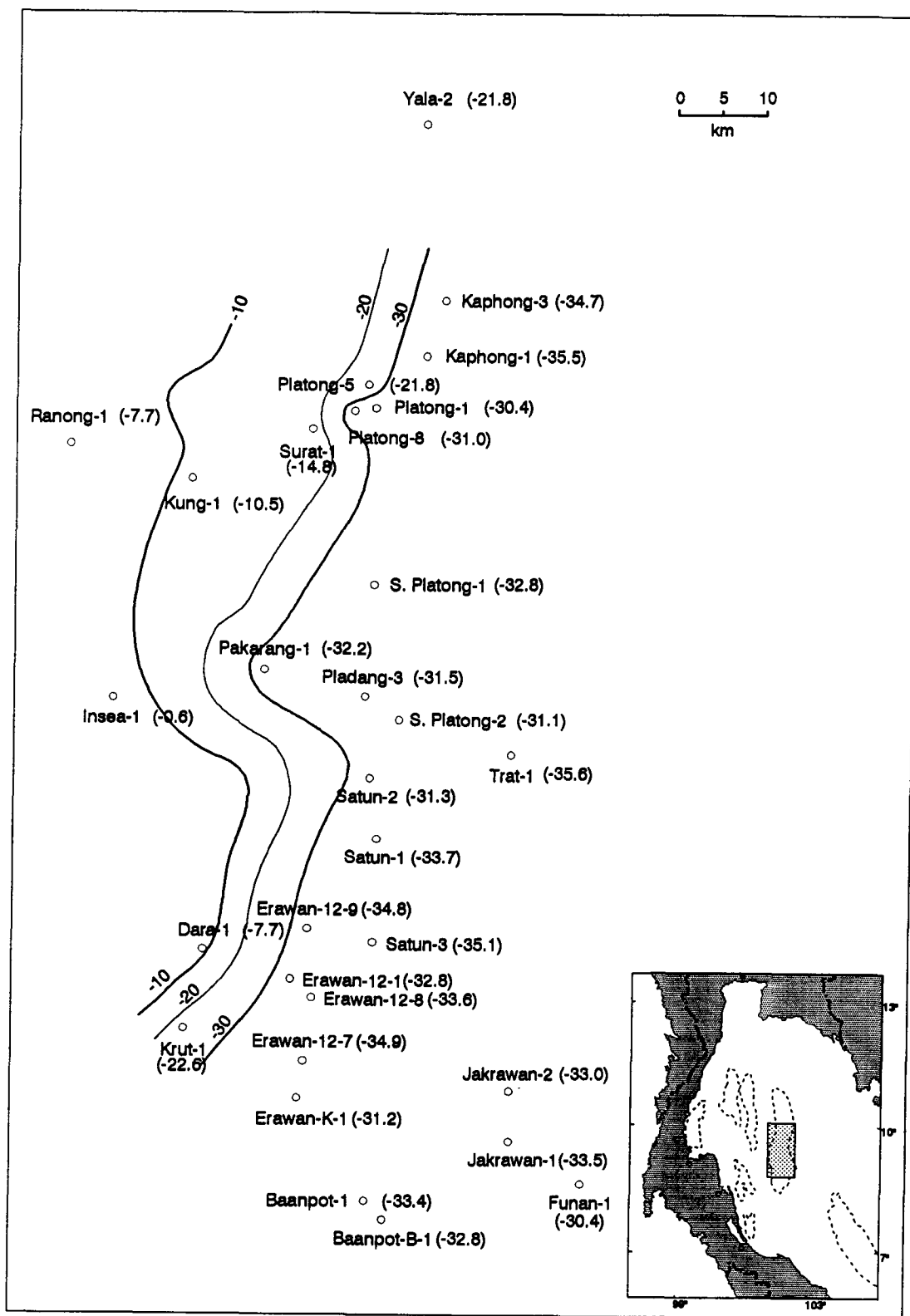


Figure 6.46: Timing of main hydrocarbon generation phase (reaction extent=40%) of unit 6 (Ma)

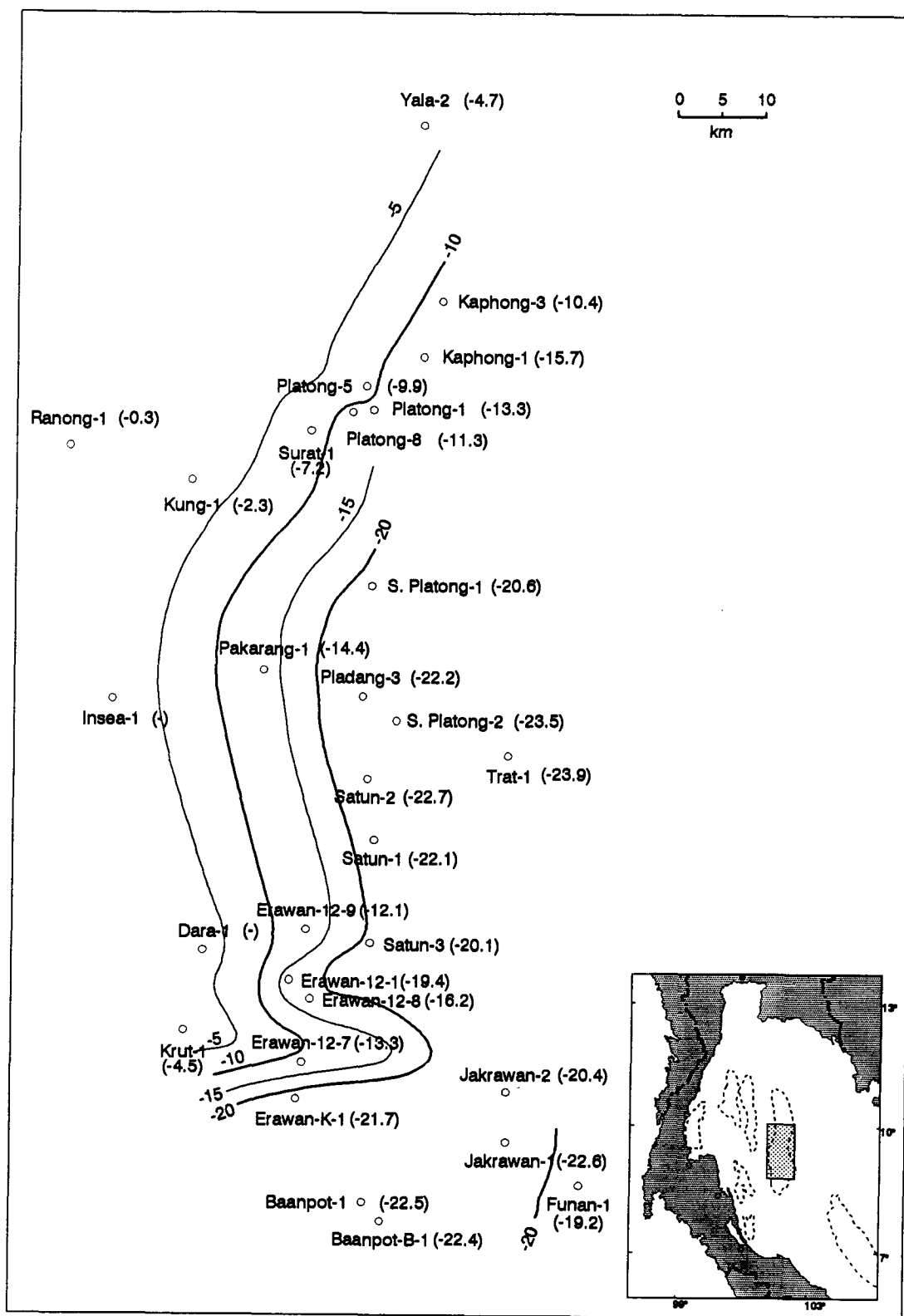


Figure 6.47: Timing of main hydrocarbon generation phase (reaction extent=40%) of unit 5 (Ma)

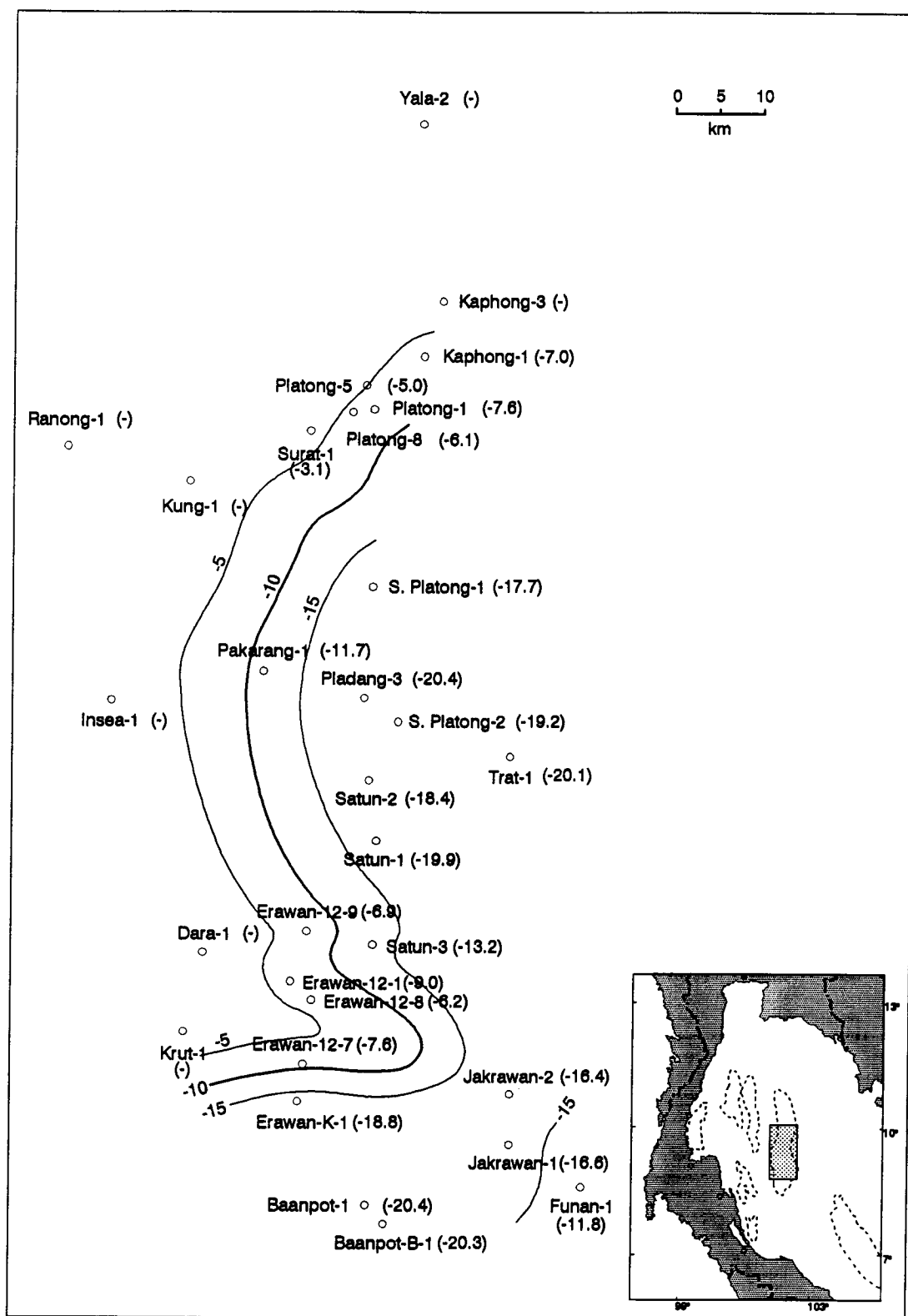


Figure 6.48: Timing of main hydrocarbon generation phase (reaction extent=40%) of unit 4 (Ma)

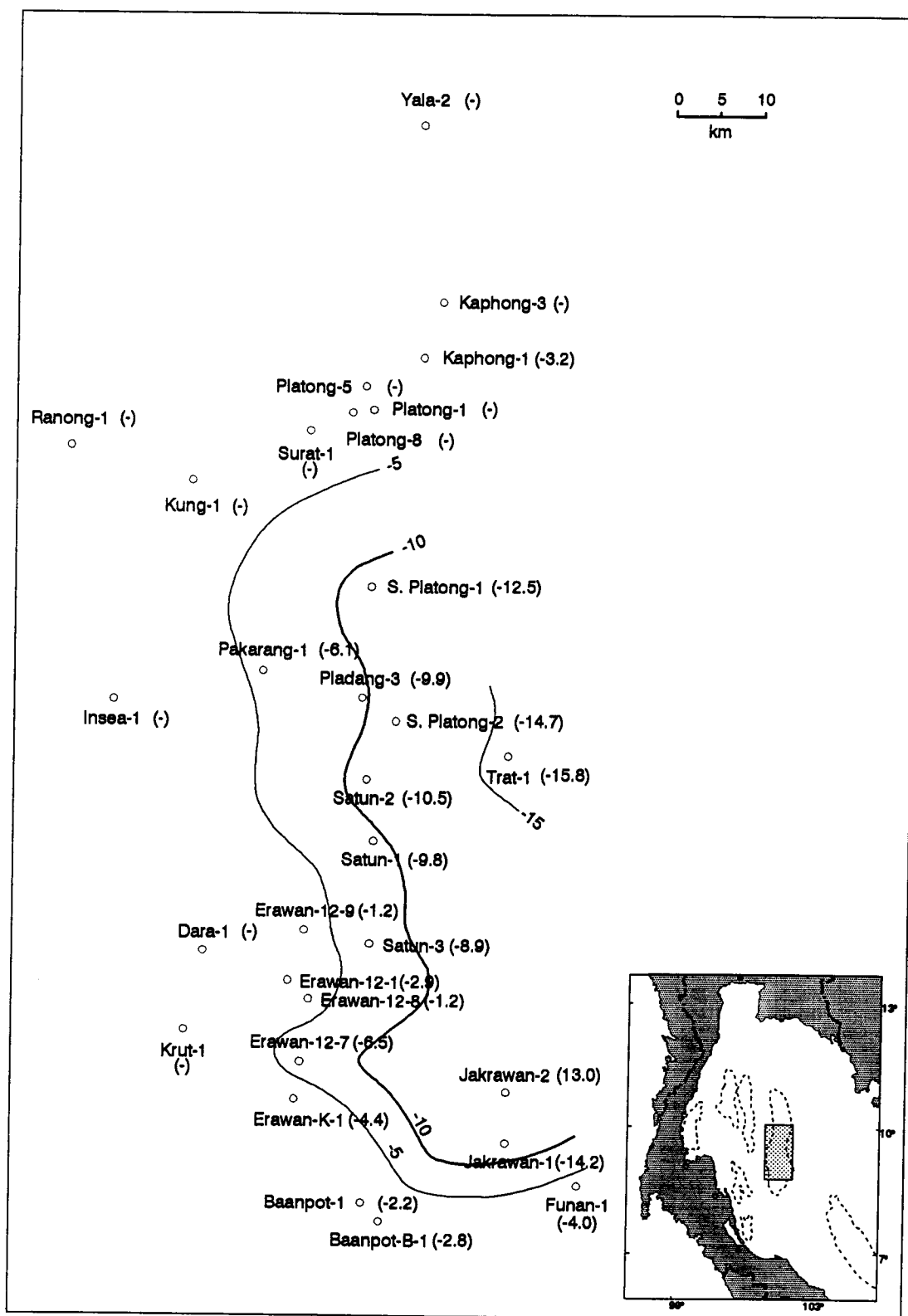


Figure 6.49: Timing of main hydrocarbon generation phase (reaction extent=40%) of unit 3 (Ma)

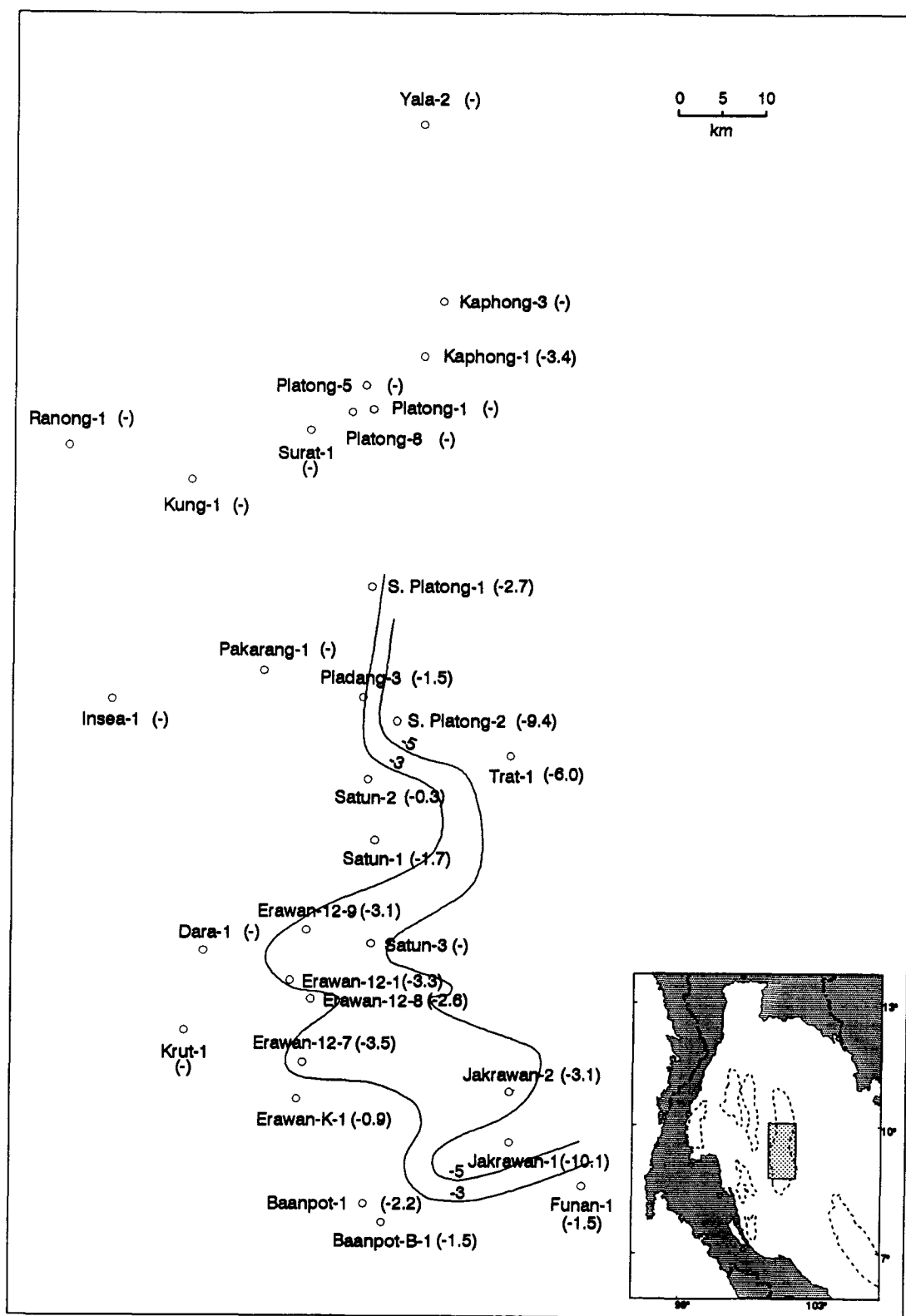


Figure 6.50: Timing of main hydrocarbon generation phase (reaction extent=40%) of unit 2 (Ma)

stratigraphic unit. The maps of stratigraphic unit 1 are not shown here because the unit is immature with respect to the main hydrocarbon generation phase at all well locations in the study area.

The present-day maturation level of the stratigraphic unit 6 (Figure 6.41) indicates that in most parts of the basin, this unit is overmature (reaction extent = 100%) with respect to the oil window, except in the western part of the basin where the unit is still in the oil window. The main hydrocarbon generation phase (= 40% hydrocarbon generation extent) of this unit started from as early as 35 to 36 Ma in the basin center to as late as less than 1 Ma at the basin margin (Figure 6.46). The peak hydrocarbon generation rates occurred from about 35 Ma in the basin center to the present-day at the basin margin (Figure 6.11 through Figure 6.40).

The present-day maturation level of stratigraphic unit 5 (Figure 6.42) indicates that this unit is overmature (reaction extent = 100%) in the south and central part of the basin. In the northern and western part of the basin, this unit is still within the oil window. In the western-most area, immediately west of the Insea-1 and Dara-1 wells, unit 5 is still immature (reaction extent < 25%). The main phase of hydrocarbon generation (= 40% hydrocarbon generation extent) started from about 24 to 22 Ma in the basin center to as late as 3 Ma at the western margin (Figure 6.47). The peak hydrocarbon generation rates of this unit occurred from 22 Ma in the basin center to the present-day at the basin margin (Figure 6.11 through Figure 6.40).

The present-day maturation level of the stratigraphic unit 4 (Figure 6.43) suggests that this unit is overmature (reaction extent = 100%) with respect to the oil window in the central and south central parts of the basin. The degree of maturation of this

unit decreases westward and northwestward toward the basin margin. This unit is still within the oil generation window in the northern and western parts of the basin. It is immature in the western-most margin of the basin. The main phase of hydrocarbon generation began from 20 Ma in the basin center to 2-3 Ma at the basin margin (Figure 6.48). The peak generation rates of unit 4 started from about 19 Ma in the basin center to the present-day at the margin.

The present-day level of maturation of the stratigraphic unit 3 (Figure 6.44) indicates that this unit is overmature (reaction extent = 100%) with respect to the oil window in the central part of the basin. It is within the oil window in the west central, north central, and southeastern parts of the basin. It is immature in the western and northern parts of the basin (Figure 6.44). The main phase of hydrocarbon generation started from 16 Ma in Trat-1 well in the basin center to the present-day in the area more to the west (Figure 6.49).

The present-day level of maturation of the stratigraphic unit 2 (Figure 6.45) suggests that this unit is overmature with respect to the oil window in a small area in the south central part of the basin. From this area, the degree of maturation decreases outward in every direction. This unit is still within the oil generation window in a narrow band extending from the north central to the south central and southeastern parts of the basin. It is still immature in much of the western part of the basin. The main hydrocarbon generation phase started from 6 to 9 Ma in the central part of the basin to about 1 Ma in the mature zone in the west central area. In many locations the generation rates have not yet reached the peak level.

Stratigraphic unit 1 is immature with respect to the oil generation window in all locations in the study area. The present-day maturation level of this unit suggests that less than 3% of kerogen has been converted to hydrocarbons.

6.7 DISCUSSION

6.7.1 Variation of Kinetic Parameters

The characteristics of the kinetic parameters of each stratigraphic unit and the possible influence of sample preparation, kerogen types, and depositional environments on the kinetic parameters of the sediments are examined in this section.

a. Sample preparation vs. kinetic determinations

The effect of sample preparation, i.e. whole rock sample vs. kerogen, in determining kinetic parameters using Rock-Eval pyrolysis has been a subject of discussion. Espitalie et al. (1980) reported that organically lean, gas prone, clastic sediments were most likely to be affected by the mineral matrix during pyrolysis. Burnham and Sweeney (1989) suggested that kinetic differences between whole rock and kerogen samples of an organically rich sediment were negligible because the mineral matrix interferences were minimal. In order to test the effect of sample type on kinetic parameters, both the whole rock sample and the kerogen of sediments containing 1.0-1.5% TOC were analyzed. Mean activation energies (E_0) of kerogens are slightly higher than those of the whole rock samples, whereas there is no significant difference in their dispersions (σ_E , Figure 6.51). The slight

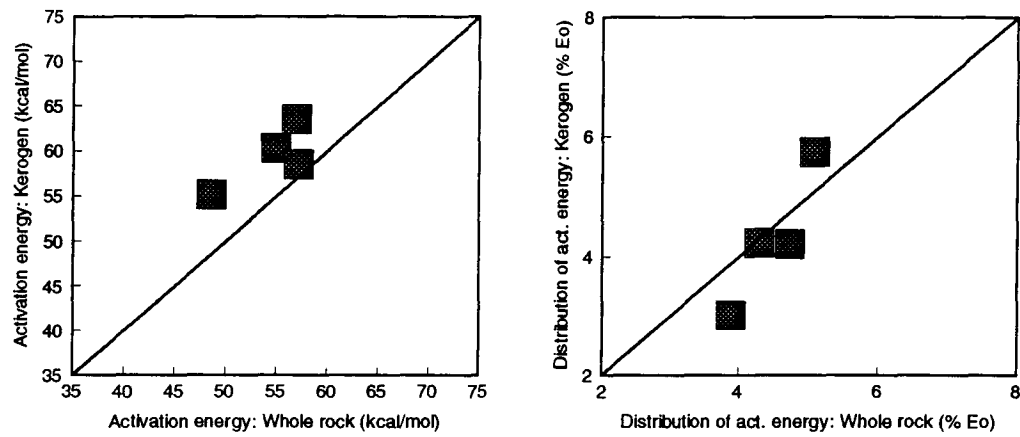


Figure 6.51: The effect of sample preparation (whole rock v.s. kerogen) on kinetic parameters

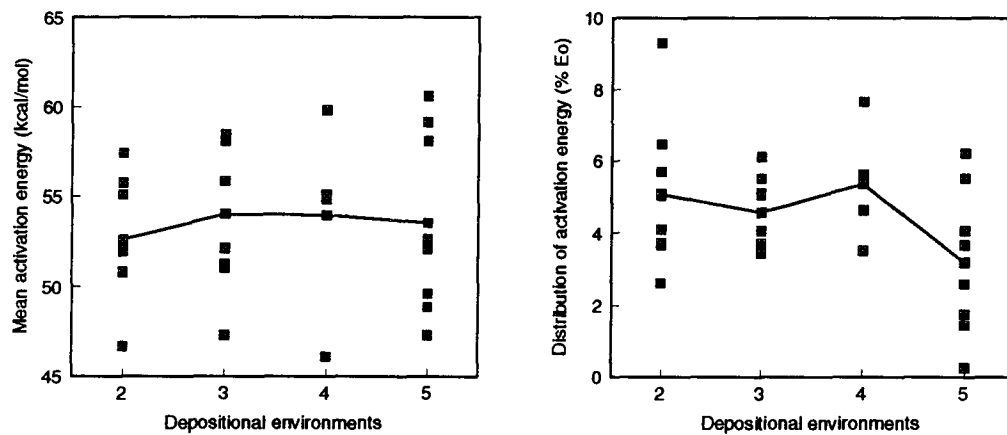


Figure 6.52: Variation of kinetic parameters v.s. depositional environment. 2. Channel deposits; 3. Floodplain deposits; 4. Distributary mouth bars; 5. Shallow marine deposits.

difference in kinetic parameters of whole rock samples and kerogens may be the result of mineral matrix interference as suggested by Espitalie et al. (1980). Espitalie et al. (1980) indicated that, during pyrolysis some minerals, such as illite, retain heavy hydrocarbons ($>C_{15}$) generated from kerogen. The trapped heavy hydrocarbons ($>C_{15}$) may be subsequently cracked at higher temperatures. Such a phenomenon may increase the value of T_{max} , hence affecting the value of mean activation energy and its dispersion. Such a result suggests that, for a sediment with high TOC, either a whole rock sample or kerogen can be used for modelling hydrocarbon generation. For organically lean sediments, whole rock samples should be used for hydrocarbon generation modelling because the effect of mineral matrix interference may become significant.

b. Type of organic matter vs. kinetic variation

Mean activation energies of the Tertiary strata in the Pattani Basin, Gulf of Thailand, which mainly contain Type III OM and a mixture of Type II-III OM, generally range from 46.1 to 60.6 kcal/mol (Table 6.1; Figure 6.10). This range of values coincides reasonably well with the activation energies required to break down carbon-oxygen and carbon-carbon bonds (40 to 70 kcal/mol; Tissot and Welte, 1984; Waples, 1985). Because organic matter in the Pattani Basin is mainly Type III OM and a mixture of Type II and Type III OM, it is impossible to compare the kinetic parameters between different types of organic matter in the study area. It is, however, possible to compare the results from this study with those of others such as Tissot and Welte (1984) and Burnham et al. (1987). The mean activation energy of the Tertiary strata in the study area is comparable with that of Type II and Type III source rocks in Paris Basin, France and Duoala Basin, Cameroon respectively (about 50-60 kcal/mol; Tissot and Welte, 1984), although

the dispersions of activation energies are different because this study assumes a Gaussian distribution of activation energies, whereas Tissot and Welte's (1984) study employed a discrete distribution. The kinetic parameters of Tertiary strata in the study area compare reasonably well with those of whole rock samples and extracted kerogen containing Type I and Type II OM studied by Burnham et al. (1987). This study and the study of Burnham et al. (1987) show that mean activation energies of kerogen and source rocks, regardless of the type of OM, are sufficiently variable that one cannot assume that activation energies depend only on kerogen type. Such a variation may reflect the difference in chemical composition of kerogen.

c. Depositional environment vs. kinetic variation

Mean activation energies (E_0) of organic matter deposited in different depositional environments in the study area extend over almost the same interval (45-60 kcal/mol, Fig 6.52). There is no correlation between depositional environment and mean activation energies. The dispersion of activation energies (σ_E) is, however, slightly higher in nonmarine and coarse-grained beach and distributary mouth bar deposits than in fine-grained shallow marine and interdistributary bay deposits (Figure 6.52). This relationship may relate to grain-size distribution of sediments which, in turn, relate to the energy regime during deposition. Interdistributary bay and shallow marine sediments were deposited under uniform and low energy environments, resulting in uniform organic matter distribution and thus lower variation in activation energies and lower σ_E values. Nonmarine channel, floodplain and coarse-grained beach and distributary mouth bar sediments, on the other hand, were deposited under high energy and often laterally discontinuous

environments, resulting in highly variable sediments and organic matter, which in turn resulted in a higher variation of activation energies and higher σ_E values.

d. Degree of thermal maturation vs. kinetic variation

A weak negative correlation occurs between degree of organic maturation and mean activation energies (E_0) of organic matter in the study area (Figure 6.53). The dispersion of activation energies (σ_E), on the other hand, shows a positive correlation against degree of organic maturation (Figure 6.53). Such correlations may indicate the original variation of kinetic properties of organic matter, due to the difference in kerogen composition, rather than the effect of maturation. This is because kinetic parameters (A , E_0 , and σ_E) of the hydrocarbon generation process are independent of the degree of thermal maturation, and represent a wide range of simultaneous reactions occurring during maturation (Braun and Burnham, 1987). The effective activation energy, which is actually the activation energy of the remaining material, however, increases with the degree of pre-reaction (maturity) as can be seen from the increasing T_{\max} with thermal maturation. This phenomenon can be explained by the fact that at low maturity, only reactions with low activation energies occur, and as the maturity increases, those reactions with low activation energies gradually continue to completion, yielding reactions with higher activation energies. The effective activation energy of the reaction, which is an average of those high activation energies, is, therefore, relatively higher in more mature samples.

6.7.2 Hydrocarbon Generation History

As noted earlier that hydrocarbon generation modelling of all stratigraphic units was

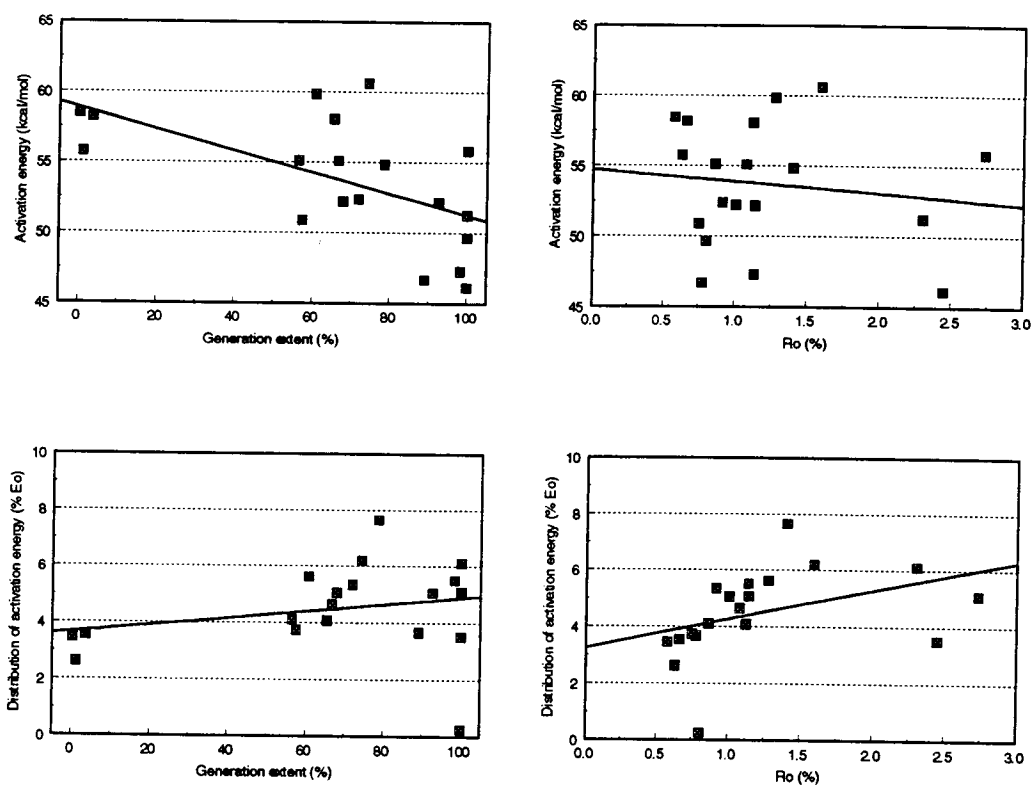


Figure 6.53: Variation of kinetic parameters v.s. degree of organic maturation

carried out at their basal boundaries; hence, the timings of generation obtained from this study reflect the earliest possible times of generation for these units. Compared to most other basins, hydrocarbon generation in the Pattani Basin is relatively early. The relatively early hydrocarbon generation in most stratigraphic units (generally 5-7 m.y. after deposition or 35-33 Ma in the basin center) is attributed mainly to high geothermal gradients and rapid deposition of sediments, especially in the basin center. Rapid sedimentation and rapid burial combined with high geothermal gradients resulted in rapid temperature increase and consequently rapid and early hydrocarbon generation of a stratigraphic unit. This rapid hydrocarbon generation is characterized by a narrow and high reaction rate profile (Figure 6.11 through Figure 6.40). Relatively later and slower hydrocarbon generation occurring in the basin margin, on the other hand, was caused by lower geothermal gradients, relatively slow sedimentation and burial-hence slow temperature increase and slow generation rate. This slow generation rate is characterized by a broad and low reaction rate profile (Figure 6.11 through Figure 6.40). The other cause of rapid hydrocarbon generation especially in unit 6 is its low activation energy (46.7 kcal/mol). Such a low activation energy indicates that unit 6 would generate hydrocarbon at lower temperatures and hence earlier than units with higher activation energy.

6.7.3 Hydrocarbon Potential Considerations

The present-day maturation levels of all the Tertiary stratigraphic successions in the Pattani Basin suggest that most of the stratigraphic units except unit 1 are either mature or overmature with respect to the oil window. Hydrocarbon generation started as early as 33-35 Ma and lasted until the present-day. There is no doubt that any potential source rocks in this area would have generated or still are generating

hydrocarbons. The quality of the source rocks is, however, questionable. All the samples available for this study show very low TOC contents (in average, less than 0.4% in units 6, 5, 4, and 3, and about 0.5% in unit 2) and low genetic potentials (less than 1.0 mg HC/g rock). Almost all samples have genetic potentials less than generally considered necessary for accumulation of commercial hydrocarbon deposits (Tissot and Welte, 1984). The fact that the Pattani Basin is one of the producing basins suggests either the source rocks here, despite very low genetic potential, are very effective in producing, migrating, and accumulating hydrocarbons. Alternatively, it indicates the presence of higher quality source rocks within the basin that have not been reached by drilling, or a combination of both factors.

6.7.4 Other Considerations

In the Pattani Basin, hydrocarbons are currently produced from reservoir packages of channel, beach, and distributary mouth bar sandstones of middle and upper synrift sequences (Lian and Bradley, 1986; Chinbunchorn et al., 1989). The porosity of these sandstones ranges from 15 to 30% at depths above 2700 m (Lian and Bradley, 1986). Below this depth, sandstones are generally too tight to be reservoirs. Reservoir rocks of good quality are also likely present in coarse-grained alluvial fan and braided channel sediments on the flanks of the basin as well as channel sandstones of the post-rift sequences. All reservoirs encountered in the Pattani Basin are, however, generally small, with rapid horizontal and vertical changes in qualities such as thickness, facies and porosity (Lian and Bradley, 1986). The reservoirs here are also highly compartmentalized due to high fault density.

The potential seals in the Pattani Basin are fine-grained claystones and shales of floodplain, interdistributary bay and shallow marine deposits. Floodplain claystones may be laterally discontinuous, and hence may not be good seals. In contrast, interdistributary bay and shallow marine shales are likely to be more laterally extensive, hence make better seals. Clay smear-controlled fault-seals are also one of the main sealing mechanisms in the study area (Burri, 1989).

In an extensional rift basin such as the Pattani, structural traps are the major trapping mechanism. The traps include tilting fault blocks, faulted and rollover anticlines. However, stratigraphic traps such as pinch-out sandstone bodies are also believed to play an important role in the accumulation of commercial hydrocarbon deposits in the Pattani as well as other Tertiary basins in Thailand. Timing of trap formation relative to petroleum generation and migration is very important in the formation of commercial hydrocarbon deposits. If traps predate migration, the area will be productive. High sedimentation rates in the study area might have created early seals, which together with block faulting during rifting, might have resulted in the occurrence of traps predating hydrocarbon migration.

6.8 SUMMARY AND CONCLUSIONS

By using a simple linear regression/correlation technique, kinetic parameters of a kerogen such as a pre-exponential factor (A), the mean activation energies (E_0), and the dispersions of the activation energies (σ_E) can be determined from the Rock-Eval analyses of kerogen at multiple heating rates.

Mean activation energies (E_0) of the potential Tertiary source rocks in the Pattani Basin range from 46.1 to 60.6 kcal/mol, which coincide reasonably well with the

activation energies required to break down carbon-oxygen and carbon-carbon bonds (40 to 70 kcal/mol). The dispersions of the activation energies (σ_E) range from 0.26 to 9.30% of the mean values.

Kerogen type, as defined by Rock-Eval pyrolysis, includes a wide range of activation energies. A wide range of activation energies may reflect differences in the chemical composition of kerogen. The depositional environments of the sediments have no influence on the values of mean activation energies, but show a weak influence on the dispersion of the activation energies. In general, high activation energy dispersions (σ_E) correspond to sediments deposited under a high energy regime, whereas low activation energy dispersions (σ_E) correspond to sediments deposited under a low energy regime. Such results indicate that the energy regime hence the depositional environment may have an effect on a redistribution of organic matter and the variation of its activation energy dispersion (σ_E) within sediments.

In the study area, the degree of organic maturation shows a weak negative correlation with mean activation energies (E_0) but a positive correlation with the dispersion of activation energies (σ_E). Such correlations may reflect the original variation of kinetic parameters of organic matter, due to difference in the kerogen composition, rather than the effect of degree of organic maturation. The kinetic parameters of organic matter in sediments are independent of the degree of organic maturation. The effective activation energy of a sample, which is actually the average activation energy of the remaining material, increases with the degree of thermal maturation because at high maturity levels, reactions with lower activation energies are already complete; the effective activation energy of the remaining

material, therefore, represents only those reactions with high activation energies. The result is a higher effective activation energy in a more mature sample.

Compared to other basins, hydrocarbon generation in the Pattani Basin is relatively early, about 5-7 m.y. after deposition. This early generation is attributed to the area's high geothermal gradients and rapid sedimentation, and hence high heating rates for the stratigraphic successions. In some stratigraphic units (unit 6), low mean activation energy also enhanced early generation. Most of the stratigraphic units in the Pattani Basin, except the youngest unit (unit 1), are either mature or overmature with respect to the oil window. The main phase of hydrocarbon generation began at about 33-35 Ma and will continue into the future.

Although most samples available for this study are very lean in TOC content and have low genetic potentials, the fact that the area is a producing one suggests that either the poor hydrocarbon potential of the sediments is offset by the great volume of low-yield source rocks, good migration and drainage enhanced by interbedded sandstones, or the presence of unsampled good quality source rocks in the basin. The possible source rocks may be the synrift and post-rift lacustrine and marine deposits which are not reached by drilling.

The presence of good, although laterally discontinuous, reservoir rocks, the juxtaposition of source and reservoir rocks, and structural and stratigraphic traps in the study area are the key factors that made the Pattani Basin a prolific hydrocarbon basin.

7. SUMMARY AND CONCLUSIONS

The Pattani Basin, the Gulf of Thailand, is filled with Tertiary and Quaternary sediments. The basin formed during the Early Tertiary as a result of extensional rifting related to the collision of India with Eurasia. Stratigraphic correlations and sedimentology were carried out based on wireline logs, seismic sections, and biostratigraphic data. Subsidence and thermal histories of the basin were predicted based on the lithospheric stretching model (McKenzie, 1978; Hellinger and Sclater, 1983). Source rock potential and characteristics were made based on Rock-Eval pyrolysis data and organic petrography. Hydrocarbon generation histories of different strata were calculated based on a chemical kinetic model of organic maturation (Sweeney and Burnham, 1990; Sweeney, 1990).

The extensional origin of the Pattani Basin has a major effect on the subsequent geologic and stratigraphic evolution. The opening of Tertiary basins in Continental Southeast Asia, including the Pattani Basin, is related to collision of the northward moving Indian subcontinent with Eurasia in the Eocene. The penetration of India into Eurasia caused clockwise rotation of Southeast Asia, resulting in an increasingly oblique subduction of the Indian Ocean plate beneath the western edge of Southeast Asia. This, in turn, changed the stress field of the region from one of convergence to one with a major component of strike-slip movement. The change in stress field led to right-lateral movement on major NW-SE fault systems, and left-lateral movement on conjugate NE-SW fault systems. The resultant strain ellipsoid indicates the E-W extension associated with right-lateral fault systems. The E-W extensional tectonic regime included lithospheric stretching and crustal and subcrustal thinning in Thailand, which led to the occurrence of N-S trending

sedimentary basins along an old Triassic-Jurassic suture zone, which is the weakest zone in the local lithosphere.

The stretching of the lithosphere caused rifting in the Continental Southeast Asia as well as in the proto-Pattani Basin. Synrift and post-rift subsidence, analyzed using geohistory analysis and basin modelling, can generally be accounted for by simple extension causing a nonuniform, crustal and subcrustal lithospheric thinning. The validity of the nonuniform lithospheric stretching as a mechanism responsible for the formation of the Pattani Basin is confirmed by a reasonably good agreement between the modeled and observed vitrinite reflectance values (one of the maturity indices) at various depths and locations. The amount of lithospheric stretching as well as surface heat flow in the Pattani Basin generally increases from the basin margin to the basin center. The crustal stretching factor (β) ranges from 1.3-1.4 at the basin margin to 2.6-2.8 in the center. The subcrustal stretching factor (δ) varies from 1.3 at the basin margin to more than 3.0 in the basin center. Generally, the amount of subcrustal stretching is greater than that of crustal stretching except in areas with great thicknesses of synrift sediments where the amount of crustal stretching is greater than that of subcrustal stretching. Such areas might have been affected by the pre-existing basement topography prior to rifting.

The stretching of the crust across the Pattani Basin may have been as much as 45 to 90 km ($\beta = 1.3-2.8$), and may have caused passive upwelling of hot asthenosphere, resulting in high surface heat flow. Because the Pattani Basin is relatively young (less than 20 m.y. after rifting), it still has elevated thermal gradients and is in thermal disequilibrium, as is evident from its high present-day surface heat flow (1.9-2.5 HFU) and high geothermal gradient (45-60°C/km).

Rifting has been the major control of the rate and amount of subsidence and the amount of sediment supply into the Pattani Basin. The rate and amount of basin subsidence, the sediment influx, and the fluctuation in the eustatic sea level during deposition has, in turn, dictated the sedimentary signatures recorded in the study area. The sedimentary succession in the Pattani Basin is divided into synrift and post-rift sequences. The synrift sequence comprises three stratigraphic units. The basal unit comprises Late Eocene to Early Oligocene nonmarine, alluvial fan and braided stream deposits in the lower part and floodplain deposits in the upper part. The middle synrift unit comprises Late Oligocene to Early Miocene nonmarine, floodplain-channel deposits in the lower part and coarse-grained channel deposits in the upper part. The upper synrift succession comprises an Early Miocene, regressive sequence, in which basal prodelta to shallow marine sediments are overlain by distributary mouth bar deposits and beach ridge complexes. These, in turn, are overlain by nonmarine floodplain and meandering channel deposits. Deposition of the synrift sequences was synchronous with extension of Continental Southeast Asia, which was accompanied by episodic block faulting and rapid subsidence. The main characteristics of the synrift sequence are a high rate of subsidence and a large influx of sediment supply, both the direct result of rifting. The first marine transgression in the Pattani Basin in the Early Miocene might have been a result of rapid subsidence due to block faulting and/or a eustatic rise in sea level. The following regressive succession in the upper part of the synrift sequence resulted when the rate of deposition exceeded the rate of relative sea level rise. Beyond the reach of drilling, a thick succession of synrift lacustrine deposits are believed to have been deposited in the center of the basin throughout the early parts of the rifting period.

The post-rift succession also comprises three stratigraphic units. The lower post-rift unit is an Early to Middle Miocene regressive sequence in which basal prodelta and shallow marine sediments are overlain by distributary mouth bar and beach ridge complexes which, in turn, are overlain by nonmarine floodplain and channel deposits. The post-rift phase coincided with a slower subsidence rate and a decreasing sediment influx. Hence, eustatic sea level fluctuations had a more important affect on sedimentation. A late Early Miocene transgression, which was probably the result of a rapid eustatic sea level rise, created a brief period of nondeposition during which the rate of relative sea level rise exceeded the rate of deposition. Later, as the rate of deposition slowly exceeded the rate of relative sea level rise, a broad regressive sedimentary succession prograded. The middle post-rift unit represents a Middle Miocene transgressive succession that was probably the result of a slow rise of relative sea level and a decreasing amount of sediment supply due to lowering of source areas. Rapid fall of relative sea level resulted in subaerial exposure, intense oxidation, and possibly erosion of the Middle Miocene strata, and was probably the result of eustatic sea level fall at the end of the Middle Miocene (Haq et al., 1988). The upper post-rift unit is a Late Miocene to Pleistocene transgressive succession indicating a slow rise of relative seal level. This was probably caused by a slow rise in eustatic sea level, slow subsidence, and a decreasing sediment supply. The present-day shallow marine condition in the Pattani Basin is the continuation of the latest transgressive phase.

The dispersed organic matter in Tertiary strata in the Pattani Basin is composed mainly of Type III and Type IV kerogens with minor amounts of mixed Type II-III kerogens. Due to the nonmarine and marginal marine features of the sediments, the presence of low HI and high OI values, and the type of organic matter (mainly vitrinite), the organic matter found in these sediments is interpreted to be

predominantly of detrital and continental origin. Variation of organic characteristics occurs both within and across stratigraphic units. Within each stratigraphic unit, the lowest TOC and HI occur in high energy nonmarine deposits such as alluvial fan and braided stream deposits, whereas higher TOC and HI generally occur in low energy deposits. TOC and HI values also increase from nonmarine deposits to interdistributary bay and shallow marine deposits. TOC and HI generally increase in progressively younger strata. The abundance of organic matter within sediments is the result of the combination of organic input into sediments and degree of organic preservation. Higher TOC and HI values in floodplain and interdistributary bay deposits may reflect the proximity to marsh complexes, a source of organic matter. Fine-grained sediments further enhance the degree of organic preservation by the rapid development after deposition of anaerobic conditions that reduce oxidation and the destruction of organic matter. The variation of abundance and characteristics of organic matter in the basin was, therefore, controlled, in large part, by depositional environments. A general increase in TOC and HI with decrease in age may reflect an increasing degree of preservation and/or increasing proximity to sources of organic matter as the basin aged.

A very weak correlation between TOC and HI and the degree of organic maturation (extent of hydrocarbon generation and vitrinite reflectance) in sediments in the study area can be explained by the original variation in TOC and HI from place to place within the same stratigraphic unit and across the units.

Sedimentation rate, corrected for compaction, of Tertiary strata in the Pattani Basin ranges from 0.023 km/m.y. to more than 1.2 km/m.y. Such high sedimentation rates are common in Tertiary deltaic deposits and are much higher than those of

marine sediments. The effect of sedimentation rate on the abundance of organic matter in nonmarine and deltaic deposits in the study area is apparent only in units containing relatively high TOC (e.g., 0.6-2.2%, unit 1). In the units with low TOC (less than 0.5%), original variation of TOC within the sediments has a greater effect than sedimentation rate. A strong negative correlation between TOC and sedimentation rate in unit 1 indicates the effect of clastic dilution of organic input as sedimentation rate increases.

Source rocks of Tertiary strata in the Pattani Basin represent an end member in terms of composition and properties. The source rocks here contain mainly Type III, Type IV kerogens, and minor amounts of mixed Type II-III kerogen and have very low hydrocarbon potential as defined by pyrolysis (Tissot and Welte, 1984). Numerous commercial gas fields in the basin suggest that either the source rocks here, despite very low genetic potential, are very effective in producing, migrating, and accumulating hydrocarbons, or the presence of higher quality source rocks within the basin which have not been reached by drilling, or a combination of both factors.

Kinetic parameters of source rocks in Tertiary strata in the Pattani Basin in terms of a pre-exponential factor (A), mean activation energies (E_0), and the dispersions of the activation energies (σ_E) were determined from Rock-Eval analyses of whole rock samples at multiple heating rates using a linear regression/correlation technique. The mean activation energies of the potential source rocks vary from 46.1 to 60.6 kcal/mol, and coincide reasonably well with the activation energies required to break down carbon-oxygen and carbon-carbon bonds (40 to 70 kcal/mol). The dispersion of activation energies (σ_E) ranges from 0.26 to 9.30% of the mean value (E_0).

The effects of sample preparation on kinetic determination were studied by comparing kinetic parameters derived from whole rock and kerogen samples of the same sediments. The results suggest that, for sediments with high TOC, either whole rock samples or kerogen can be used for modelling hydrocarbon generation. For organically lean sediments, whole rock samples should be used to model hydrocarbon generation because the effect of matrix adsorption may become significant.

Comparison of activation energies of source rocks in the study area with other areas, indicates that activation energies are sufficiently variable that one cannot safely assume that they depend only on the kerogen type. Such a variation may reflect difference in the chemical composition of kerogen. Depositional environments have no influence on the value of mean activation energies (E_0) but show a weak influence on their dispersions (σ_E). In general, wide dispersions of activation energies (σ_E) correspond to sediments deposited under a high energy regime, whereas narrow activation energy dispersions (σ_E) correspond to sediments deposited under a low energy regime. Such results suggest that the depositional environment may have an effect on redistribution of organic matter and thus on the variation of its activation energy dispersion (σ_E) within sediments. By using a distribution of activation energies, kinetic parameters of the organic matter in sediments are independent of the degree of organic maturation. The effective activation energy, which is the average activation energy of the remaining material, increases with the degree of thermal maturation because at high maturity levels, reactions with low activation energies have already occurred, and the effective activation energy of the remaining material, therefore, is for those reactions with high activation energies. The result is a higher effective activation energy in a

more mature sediment. The apparent correlation between degree of organic maturation and kinetic parameters of organic matter in the study area may reflect the original variation of the kinetic properties of organic matter rather than the effect of degree of maturation.

Most of the stratigraphic units in the study area, except the youngest unit (unit 1), are either mature or overmature with respect to the oil window. The main phase of hydrocarbon generation began about 33-35 Ma and will continue into the future. A relatively early hydrocarbon generation (about 5-7 m.y. after deposition) is attributed to high geothermal gradients and rapid sedimentation and burial, and hence high heating strata. In some units, low mean activation energy has also enhanced early generation.

Good, although laterally discontinuous, reservoir rocks; the proximity of source and reservoir rocks; and structural and stratigraphic traps are the key factors in making the Pattani Basin a prolific hydrocarbon basin.

REFERENCES

- Alchalabhuti, C., and P. Oudom-Ugsorn, 1978, Petroleum potential in the Gulf of Thailand, *Journal of the Geological Society of Thailand*, v. 3, no. 1, p. 1-12.
- Allen, C.R., A.R. Gillespie, Y. Han, K.E. Sieh, B. Zhang, and C. Zhu, 1984, Red River and associated faults, Yunnan Province, China: Quaternary geology, slip rates and seismic hazard, *Geological Society of America Bulletin*, v. 95, p. 686-700.
- Allen, P.A., and J.R. Allen, 1990, *Basin analysis: Principles and applications*, London, Blackwell Scientific Publication, 451 pp.
- Andrews-Speed, C.P., E.R. Oxburgh, and B.A. Cooper, 1984, Temperatures and depth-dependent heat flow in western North Sea, *American Association of Petroleum Geologists Bulletin*, v. 68, no. 11, p. 1764-1781.
- Angevine, C.L., P.L. Heller, and C. Paola, 1990, Quantitative sedimentary basin modeling, *American Association of Petroleum Geologists Short Course Note Series 32*, 133 pp.
- Antia, D.J., 1986, Kinetic method for modeling vitrinite reflectance, *Geology*, v. 14, p. 606-608.
- Armagnac, C., J. Bucci, C.G.St.C. Kendall, and I. Lerche, 1989, Estimating the thickness of sediment removed at an unconformity using vitrinite reflectance data, *in* N.D. Naeser and T.H. McCulloh, eds., *Thermal history of sedimentary basins-methods and case histories*, New York, Springer-Verlag, p. 217-238.
- ASCOPE, 1981, Tertiary sedimentary basins of the Gulf of Thailand and South China Sea: Stratigraphy, structure and hydrocarbon occurrences, ASEAN Council on Petroleum, Jakarta.
- Baldwin, B., and C.O. Butler, 1985, Compaction curves, *American Association of Petroleum Geologists Bulletin*, v. 69, no. 4, p. 622-626.
- Barker, C.W., and M.J. Pawlewicz, 1986, The correlation of vitrinite reflectance with maximum temperature in humic organic matter, *in* G. Buntbarth and L. Stegena, eds., *Paleogeothermics, Lecture Notes in Earth Sciences*, v. 5, p. 79-228.
- Beaumont, C., 1981, Foreland basins, *Geophysical Journal of the Royal Astronomical Society*, v. 65, p. 291-329.

- Bostick, N.H., S.M. Cashman, T.H. McCulloh, and C.T. Well, 1978, Gradients of vitrinite reflectance and present temperature in the Los Angeles and Ventura basins, California, *in* D.F. Oltz, ed., Low temperature metamorphism of kerogen and clay minerals, Pacific Section of Society of Economic Paleontology and Mineralogy Special Symposium, p. 65-96.
- Braun, R.L. and A.K. Burnham, 1987, Distribution of activation energies and simpler models, *Energy and Fuels*, v.1, p. 153-161.
- Bunopas, S. and P. Vella, 1983, Opening of the Gulf of Thailand-rifting of the continental Southeast Asia, and Late Cenozoic tectonics, *Journal of the Geological Society of Thailand*, v. 6, no. 1, p. 1-12.
- Burnham, A.K., R.L. Braun, H.R. Gregg, and A.M. Samoun, 1987, Comparison of methods for measuring kerogen pyrolysis rates and fitting kinetic parameters, *Energy and Fuels*, v.1, p. 452-458.
- Burnham, A.K., and J.J. Sweeney, 1989, A chemical kinetic model of vitrinite maturation and reflectance, *Geochimica et Cosmochimica Acta*, v. 53, p. 2649-2657.
- Burri, P., 1989, Hydrocarbon potential of Tertiary intermontane basins in Thailand, *in* T.T. Pitak, ed., *Proceeding of international symposium on intermantane basins: Geology & Resources*, Chiang Mai, Chiang Mai University, p. 3-12.
- Bustin, R.M., 1988, Sedimentology and characteristics of dispersed organic matter in Tertiary Niger Delta: Origin of source rocks in a delta environment, *American Association of Petroleum Geologists Bulletin*, v. 72, no. 3, p. 277-298.
- Cant, J.D., 1982, Fluvial facies models and their application, *in* P.A. Scholle and D. Spearing, eds., *Sandstone depositional environments*, American Association of Petroleum Geologists, memoir 31, p. 115-137.
- Cant, J.D., 1984, Subsurface facies analysis, *in* R.G. Walker, ed., *Facies Models*, 2nd edition, Geoscience Canada, Reprint Series 1, p. 297-310.
- Chinbunchorn, N., S. Praditjan, and N. Sattayarak, 1989, Petroleum potential of Tertiary intermontane basins in Thailand, *in* T.T. Pitak, ed., *Proceeding of international symposium on intermantane basins: Geology & Resources*, Chiang Mai, Chiang Mai University, p. 29-41.

- Coleman, J.M. and D.B. Prior, 1982, Deltaic environments, *in* P.A. Scholle and D. Spearing, eds., Sandstone depositional environments, American Association of Petroleum Geologists, memoir 31, p. 139-178.
- Combaz, A. and M. de Matharel, 1978, Organic sedimentation and genesis of petroleum in Mahakam delta, Borneo, American Association of Petroleum Geologists Bulletin, v. 62, p. 1684-1695.
- Connan, J., 1974, Time-temperature relation in oil genesis, American Association of Petroleum Geologists Bulletin, v. 58, p. 2516-2521.
- Durand, B., 1980, Sedimentary organic matter and kerogen: Definition and quantitative importance of kerogen, *in* B. Durand., ed., Kerogen, Editions Technip, Paris, p. 13-14.
- Espitalie, R., M. Madec, and B.P. Tissot, 1977, Source rock characterization method for petroleum exploration, 9th Annual Offshore Technology Conference, Houston, Texas, p. 439-444.
- Espitalie, R., G. Daroo, and F. Marquis, 1985, Rock-Eval pyrolysis and its applications, Institut Francais du Petrole, reprint no. 27299, 132 pp.
- Friedinger, P.J.J., 1988, BASTA: Subsidence and paleotemperature modeling of rift basins, Computer & Geosciences, v. 14, no.4, p. 505-526.
- Galloway, W.E., and D.K. Hobday, 1893, Terrigenous clastic depositional systems: Applications to petroleum, coal, and uranium exploration, New York, Springer-Verlag, 423 pp.
- Germeraad, J.H., C.A. Hopping, and J. Muller, 1968, Palynology of Tertiary sediments from tropical areas, Review of Palaeobotany and Palynology, v. 6, p. 189-348.
- Gibling, M.R., 1988, Cenozoic lacustrine basins of South-east Asia, their tectonic setting, depositional environments and hydrocarbon potential, *in* A.J. Fleet and M.R. Talbot, eds., Lacustrine petroleum source rocks, Blackwell Scientific Publications, Boston, p. 341-352.
- Haq, B.U., J. Hardenbol, and P.R. Vail, 1988, Mesozoic and Cenozoic chronostratigraphy and eustatic cycles, *in* C.K. Wigus, B.S. Hastings, C.G. St. C. Kendall, H.W. Posamentier, C.A. Ross, and J.C. Van Wagoner, eds., Sea-level changes: an integrated approach, Society of Economic Paleontologists and Mineralogists, special publication, no. 42, p. 71-108.

- Hellinger, S.J. and J. G. Sclater, 1983, Some comments on two-layer extensional models for the evolution of sedimentary basins, *Journal of Geophysical Research*, v. 88, p. 8251-8269.
- Hood, A., C.M. Gutjahr, and R.L. Peacock, 1975, Organic metamorphism and the generation of petroleum, *American Association of Petroleum Geologists Bulletin*, v. 59, p. 986-996.
- Hunt, J.M., 1979, *Petroleum geochemistry and geology*, San Francisco, W.H. Freeman, 617 pp.
- Hutton, A.C., A.J. Kantsler, A.C. Cook, and D.M. McKirdy, 1980, Organic matter in oil shale, *Journal of Australian Petroleum Exploration Association*, v. 20, p. 44-68.
- Ibach, L.E.J., 1982, Relationship between sedimentation rate and total organic carbon in ancient marine sediments, *American Association of Petroleum Geologists Bulletin*, v. 66, p. 170-188.
- Issler, D.R. and C. Beaumont, 1987, Thermal and subsidence history of the Labrador and West Greenland continental margins, *in* C. Beaumont and A.J. Tankard, eds., *Sedimentary basins and basin-formation mechanisms*, Canadian Society of Petroleum Geologists, memoir 12, p. 45-69.
- Jarvis, G.T. and D.P. McKenzie, 1980, The development of sedimentary basins with finite extension rates, *Earth and Planetary Sciences Letters*, v. 48, p. 42-52.
- Jones, R.W. and G.J. Demaison, 1982, Organic facies-stratigraphic concept and exploration tool, *in* A. Saldivar-Sali, ed., *Proceeding of the second ASCOPE Conference and Exhibition*, Manila, p. 51-68.
- Jones, R.W., 1987, Organic facies, *in* J. Brooks and D. Welte, eds., *Advances in petroleum geochemistry vol.2*, London, Academic Press, p. 1-90.
- Jordan, T.E., 1981, Thrust loads and foreland basin evolution, Cretaceous, western United States, *American Association of Petroleum Geologists Bulletin*, v. 65, p. 2506-2520.
- Juntgen, H. and J. Klein, 1975, Formation of natural gas from coaly sediments, *Erdol und Kohle-Erdgas-Petrochemie*, v. 28, p. 65-73 (in German).
- Karig, D.E., 1971, Origin and development of marginal basins in the western Pacific, *Journal of Geophysical Research*, v. 76, no. 11, p. 2542-3561.

- Knox, G.J., and L.L. Wakefield, 1983, An introduction to the geology of the Pitsanulok basin, Presented at the Conference on Geology and Mineral Resources in Thailand, Bangkok, Department of Mineral Resources, Section A.
- Larter, S.R., 1988, Some pragmatic perspectives in source rocks geochemistry, *Marine and Petroleum Geology*, v. 5, p. 194-204.
- Le Dain, A.Y., P. Tapponnier, and P. Molnar, 1984, Active faulting and tectonics of Burma and surrounding region, *Journal of Geophysical Research*, v. 89, p. 453-472.
- Lerche, I., 1990, *Basin analysis: Quantitative methods*, v. 1, California, Academic Press, 562 pp.
- Lerche, I., R.F. Yarzab, and C.G.St.C. Kendall, 1984, Determination of paleoheat flux from vitrinite reflectance, *American Association of Petroleum Geologists Bulletin*, v. 68, p. 1704-1717.
- Lewan, M.D. and J.A. Williams, 1987, Evolution of petroleum generation from resonites by hydrous pyrolysis, *American Association of Petroleum Geologists Bulletin*, v. 71, p. 207-214.
- Lian, H.M., and K. Bradley, 1986, Exploration and development of natural gas, Pattani basin, Gulf of Thailand, *in* Fourth Circum-Pacific energy and mineral resources conferences, Singapore.
- Link, C.M., 1988, A reconnaissance of organic maturation and petroleum source potential of Phanerozoic strata in northern Yukon and Northwestern district of Mackenzie, Master's thesis, Geology Department, University of British Columbia, 153 pp.
- Link, M.H., M.T. Roberts, and M.S. Newton, 1985, Walker Lake Basin, Nevada: an example of Late Tertiary (?) to Recent sedimentation in a basin adjacent to an active strike-slip fault, *in* K.T. Biddle and N. Christie-Blick, eds., *Strike-slip deformation, basin formation, and sedimentation*, Society of Economic Paleontologists and Mineralogists Special Publication 37, p. 105-126.
- Matsubayashi, O., and S. Uyeda, 1979, Estimation of heat flow in certain exploration wells in offshore areas of Malaysia, *Bulletin of Earthquake Research Institute*, v. 54, p. 31-44.
- McCabe, R., M. Celeya, J. Cole, H.C. Han, T. Ohnstad, V. Pajitpraporn, and V. Thitipawan, 1988, Extension tectonics: The Neogene opening of the N-S

- trending basins of Central Thailand, *Journal of Geophysical Research*, v. 93, p. 11899-11910.
- McKenzie, D.P., 1978, Some remarks on the development of sedimentary basins, *Earth and Planetary Sciences Letters*, v. 40, p. 25-32.
- Meybeck, M., 1982, Carbon, nitrogen, and phosphorus transport by world rivers, *American Journal of Science*, v. 282, p. 401-450.
- Miall, A.D., 1984, Deltas, in R.G. Walker, ed., *Facies Models*, 2nd edition, Geoscience Canada, Reprint Series 1, p. 105-118.
- Middleton, M.F., 1982, Tectonic history from vitrinite reflectance, *Geophysical Journal of the Royal Astronomical Society*, v. 68, p. 121-132.
- Molnar, P. and P. Tapponnier, 1975, Cenozoic tectonics of Asia: effect of a continental collision, *Science*, v. 189, p. 419-426.
- Muller, P.J. and E. Suess, 1979, Productivity, sedimentation rate, and sedimentary organic matter in the ocean-I, Organic carbon preservation, *Deep-Sea Research*, v. 26A, p. 1347-1362.
- Nakanart, A., 1978, Up to 1978: Petroleum exploration in Thailand offshore, *Journal of the Geological Society of Thailand*, v. 3, no. 1, p. 2.1-2.14.
- Nilsen, T.H., 1982, Alluvial fan deposits, in P.A. Scholle and D. Spearing, eds., *Sandstone depositional environments*, American Association of Petroleum Geologists, memoir 31, p. 49-86.
- Ohnstad, T.A., 1989, Evidence of Cenozoic rifting in Thailand from gravity modeling, Master's thesis, Texas, Texas A&M University, 92 pp.
- Parsons, B. and J.G. Sclater, 1977, An analysis of the variation of ocean floor bathymetry and heat flow with age, *Journal of Geophysical Research*, v. 82, p. 803-827.
- Patriat, P. and J. Achache, 1984, India-Eurasia collision chronology has implications for crustal shortening and driving mechanism of plates, *Nature*, v. 311, p. 615-621.
- Peltzer, G., and P. Tapponnier, 1988, Formation and evolution of strike-slip faults, rifts, and basins during the India-Asia collision: An experimental approach, *Journal of Geophysical Research*, v. 93, p. 15085-15117.

- Peters. K.E., 1986, Guidelines for evaluating petroleum source rocks using programmed pyrolysis, American Association of Petroleum Geologists Bulletin, v. 70, no. 3, p. 318-329.
- Polachan, S., and N. Sattayarak, 1989, Strike-slip tectonics and the development of Tertiary basins in Thailand, *in* T.T. Pitak, ed., Proceeding of international symposium on intermontane basins: Geology & Resources, Chiang Mai, Chiang Mai University, p.243-253.
- Powell, T.G., and L.R. Snowdon, 1983, A composite hydrocarbon generation model: implication for evaluation of basins of oil and gas, Erdol and Kohle Erdgas, Petrochemie, v. 36, p. 163-170.
- Price, L.C., 1983, Geologic time as a parameter in organic metamorphism and vitrinite reflectance as an absolute paleogeothermometer, Journal of Petroleum Geology, v. 6, p. 5-38.
- Ratanasthien, B., 1988, Correlation of Neogene tectonic events in Thailand by means of radiometric dating and biostratigraphy (including palynology), Presented at the Conference on Pacific Neogene Continental and Marine Events, Nanjing, China.
- Royden, L., and C.E. Keen, 1980, Rifting process and thermal evolution of the continental margin of eastern Canada determined from subsidence curves, Earth and Planetary Science Letters, v. 51, p. 343-361.
- Ruby, W.W., and M.K. Hubbert, 1960, Role of fluid pressure in mechanics of overthrust faulting, II, Overthrust belt in geosynclinal area of western Wyoming in light of fluid-pressure hypothesis, Geological Society of America Bulletin v. 60, p. 167-205.
- Rutherford, K.J., and M.K. Qureshi, 1981, Geothermal gradient map of Southeast Asia - 2nd edition, Southeast Asia Petroleum Exploration society and the Indonesian Petroleum Association.
- Sclater, J.G., and P.A.F. Christie, 1980, Continental stretching: An explanation of the post-mid-Cretaceous subsidence of the central North Sea Basin, Journal of Geophysical Research, v. 85, p. 3711-3739.
- Scrutton, M.E., and G.L. Tidey, 1974, The micropaleontology, playnology and stratigraphy of the Union Oil 13-1 well, The Gulf of Thailand, Union Oil of Thailand Confidential Report, Bangkok, Thailand, 29 pp.
- Selley, R.C., 1979, Ancient sedimentary environments and their subsurface diagnosis, 2nd edition, London, Chapman and Hall, 287 pp.

- Snowdon, L.R., 1980, Resinite-A potential petroleum source in the Upper Cretaceous/Tertiary of Beaufort-Mackenzie basin, *in* A.D. Miall, ed., Facts and principles of world petroleum occurrence, Canadian Society of Petroleum Geologists, Memoir 6, p. 421-446.
- Snowdon, L.R., 1987, Organic properties and source rock potential of two Early Tertiary shales, Beaufort-Mackenzie Basin, Canadian Society of Petroleum Geologists Bulletin, v. 35, p. 212-232.
- Steckler, M.S. and A.B. Watts, 1978, Subsidence of the Atlantic type continental margin off New York, Earth and Planetary Science Letters, v. 42, p. 1-13.
- Sweeney, J.J., Burnham, A.K., and Braun, R.L., 1987, A model of hydrocarbon generation from Type I kerogen: application to Uinta basin, Utah, American Association of Petroleum Geologists Bulletin, v. 71, 368-388.
- Sweeney, J.J., 1990, BASINMAT: Fortran program calculates oil and gas generation using a distribution of discrete activation energies, Geobyte, v. 5, no. 2, p. 37-43.
- Sweeney, J.J., and A.K. Burnham, 1990, Evaluation of a simple model of vitrinite reflectance based on chemical kinetics, American Association of Petroleum Geologists Bulletin, v. 74, no. 10, p. 1559-1570.
- Tapponnier, P., G. Peltzer, A.Y. Le Dain, R. Armijo, and P. Cobbold, 1982, Propagating extrusion tectonics in Asia: new insights from simple experiments with plasticine, Geology, v. 10, p. 611-616.
- Tapponnier, P., G. Peltzer, and R. Armijo, 1986, On the mechanism of the collision between India and Asia, *in* M.P. Coward and A.C. Ries, eds., Collision Tectonics, Geological Society of London Special Publication, v. 19, p. 115-157.
- Taylor, B. and G.D. Karner, 1983, On the evolution of marginal basins, Review of Geophysics and Space Physics, v. 21, no. 8, p. 1727-1741.
- Thomas, B.M., 1982, Land-plant source rocks for oil and their significance in Australian basins, Australian Petroleum Exploration Association Journal, v. 22, p. 164-170.
- Tissot, B.P., and D.H. Welte, 1984, Petroleum formation and occurrence: 2nd edition, New York, Springer-Verlag, 699 pp.

- Toth, D.J. and A. Lerman, 1977, Organic matter reactivity and sedimentation rates in the ocean, *American Journal of Science*, v. 277, p. 465-485.
- Turcotte, D.L. and McAdoo, D.C., 1979, Thermal subsidence and petroleum generation in the southwestern block of the Los Angeles Basin, California, *Journal of Geophysical Research*, v. 84, p. 3460-3464.
- Van Heek, K.H., and H. Juntgen, 1968, Determination of reaction-kinetic parameters from nonisothermal measurement, *Ber. Bunsenges Physics and Chemistry*, v. 72, p. 1223.
- Van Hinte, J.E., 1978, Geohistory analysis-application of micropaleontology in exploration geology, *American Association of Petroleum Geologists Bulletin*, v. 62, p. 201-222.
- Van Wagoner, J.C., 1991, Nonmarine sequence stratigraphy and facies architecture of the updip Desert and Castlegate sandstones in the Book Cliffs of Western Colorado and Eastern Utah, *in* Van Wagoner, J.C., D. Nummedal, C.R. Jones, D.R. Taylor, D.C. Jennette, and G.W. Riley, eds., *Sequence stratigraphy applications to shelf sandstone reservoirs*, American Association of Petroleum Geologists Field Conference Guide Book, p. 3.1-3.6.
- Waples, D.W., 1985, *Geochemistry in petroleum exploration*, Boston, IHRDC, 232 pp.
- Wood, R.J., 1982, Subsidence in the North Sea, Ph.D. thesis, University of Cambridge, Cambridge, England, 94 pp.
- Wood, D.A., 1988, Relationships between thermal maturation indices calculated using Arrhenius and Lopatin methods: implications for petroleum exploration, *American Association of Petroleum Geologists Bulletin*, v. 72, p. 115-134.
- Woodside, W., and J.H. Messmer, 1961, Thermal conductivity of porous media, *Journal of Applied Physics*, v. 32, no. 9, p. 1688-1707.
- Woollands, M.A., and D. Haw, 1976, Tertiary stratigraphy and sedimentation in the Gulf of Thailand, Presented at the Offshore South East Asia Conference, SEAPEX Program, paper 7.

APPENDIX A

BASIN FORMATION MODELLING

The basin formation modelling program used in this study to predict subsidence, the amount of crustal and subcrustal lithospheric stretching, and heat flow of the basin is based on a modified McKenzie's lithospheric stretching model, in which the crust is thinned by different amounts from that of subcrustal lithosphere (Hellinger and Sclater, 1983; See detail in CHAPTER 4). The model first decompacts the observed (present-day) thickness to calculate the subsidence history, then backstrips all the overlying sedimentary layers to calculate tectonic subsidence of the basement of the basin (Van Hinte, 1978; Allen and Allen, 1990). The program subsequently uses a nonuniform lithospheric stretching model to calculate tectonic subsidence history at different amounts of stretching (Hellinger and Sclater, 1983; Friedinger, 1988). The modeled tectonic subsidence is then used to best-fit the tectonic subsidence obtained from backstripping. When the best-fitted model is obtained, the program subsequently uses the crustal and subcrustal stretching factors (β and δ respectively) to calculate surface heat flow and temperature histories of the basin.

This program requires two input files. The first input file contains thermo-physical properties of the lithosphere, crust, and sediments; and the modelling parameters. The second input file contains well information such as depth, lithology, paleobathymetry, and age of the stratigraphic units. The output from the program includes decompacted subsidence of the stratigraphic units, basement subsidence, crustal and subcrustal lithospheric stretching factors (β and δ), surface heat flow and temperature history of the basin. The format of input and output files is shown as follows.

FIRST INPUT FILE: EXAMPLE.IN1

'EXAMPLE-1 EHFU = 1.2 NONUNIFORM STRETCHING'	Line 1
0,1.03,3.33	Line 2
3	Line 3
'SH',0.63,0.51,2.72,5.5,'E'	Line 4
'SD',0.49,0.27,2.65,9.6,'E'	Line 5
'SS',0.56,0.39,2.68,7.5,'E'	Line 6
3.3,1.2,1350.0,125.0,35.0,62.8,2.8,7.5	Line 7
1.3,1.8,0.1,2.0,2.4,0.1,20	Line 8
10	Line 9
40,80,120,160,200,10	Line 10

Line 1: Well name in single quotation marks

Line 2: 1st number is 0 when the datum is sea floor or
1 when the datum is sea level

2nd number is sea water density (g/cm)

3rd number is mantle density (g/cm)

Line 3: Numbers of lithologies present in the study area

Line 4-6: 1st input is the lithology in single quotation marks

2nd input is the surface porosity (decimal point)

3rd input is the compaction constant ($\times 10^{-5} \text{cm}^{-1}$)

4th input is the grain density (g/cm^3)

5th input is the grain's thermal conductivity

(mcal/cm sec °C)

6th input is the type of porosity-depth function
in single quotation marks

E when it is exponential

L when it is linear

Line 7 1st input is thermal expansion coefficient of
 lithosphere ($\times 10^{-5}/^{\circ}\text{C}$)
 2nd input is the equilibrium heat flow (HFU)
 3rd input is temperature of mantle ($^{\circ}\text{C}$)
 4th input is thickness of lithosphere (km)
 5th input is pre-rift thickness of crust (km)
 6th input is thermal-time constant (m.y.)
 7th input is density of mantle (g/cm)
 8th input is thermal conductivity of lithosphere
 (mcal/cm sec $^{\circ}\text{C}$)

Line 8: 1st input is the lower limit of β
 2nd input is the upper limit of β
 3rd input is the increment of β
 4th input is the lower limit of δ
 5th input is the upper limit of δ
 6th input is the increment of δ
 7th input is the time when thermal
 cooling started (m.y.)

Line 9: numbers of isothermperature lines to be calculated
 maximum = 10

Line 10: 1st to 5th input are values of temperature to be
 calculated ($^{\circ}\text{C}$)
 6th input is surface temperature ($^{\circ}\text{C}$)

SECOND INPUT FILE: EXAMPLE.IN2

'EXAMPLE-1 THE GULF'	Line 1
7	Line 2
0.0,0.073,'SH',0.0,0.0	Line 3
12.0,1.143,'SS',0.0,0.0	Line 4
15.0,1.617,'SS',0.0,0.0	Line 5
20.0,1.848,'SS',0.0,0.0	Line 6
24.0,2.211,'SS',0.0,0.0	Line 7
30.0,2.562,'SS',0.0,0.0	Line 8
40.0,2.898,'SS',0.0,0.0	Line 9

Line 1: well name in quotation marks

Line 2: numbers of stratigraphic unit including basement

Line 3-9: 1st input is the age of upper boundary of the
stratigraphic unit (Ma)

2nd input is the present depth below sea level (km)

3rd input is the lithology in quotation marks

4th input is the paleowater depth (km)

5th input is the eustatic sea level change compare to
the present day sea level (km)

OUTPUT FILE: EXAMPLE.OUT

****LITHOSPHERIC STRETCHING BASIN MODELLING****

WELL-NAME: EXAMPLE-1 THE GULF

EXAMPLE-1 THE GULF DECOMPACTED COLUMNS (DEPTHS IN REFERENCE
TO SEA FLOOR):

40.0	30.0	24.0	20.0	15.0	12.0	0.0
0.00	0.00	0.00	0.00	0.00	0.00	0.00
****	0.54	0.55	0.54	0.34	0.63	1.07
	****	1.01	1.01	0.83	0.90	1.54
		****	1.42	1.26	1.33	1.78
			****	1.66	1.72	2.14
				****	2.09	2.49
					****	2.83

EXAMPLE-1 THE GULF

(BASEMENT DEPTH IN REFERENCE TO SEA FLOOR):

1	2	3	4	5	6	7
40.0-30.0	1.847	0.505	0.543	0.054	0.350	0.035
40.0-24.0	1.916	0.463	1.007	0.063	0.619	0.039
40.0-20.0	1.970	0.430	1.419	0.071	0.839	0.042
40.0-15.0	1.999	0.413	1.655	0.066	0.957	0.038
40.0-12.0	2.048	0.383	2.085	0.075	1.163	0.042
40.0-00.0	2.111	0.350	2.825	0.071	1.498	0.038

column 1: Time interval (m.y.)

column 2: Density of sedimentary column

column 3: Porosity of sedimentary column

column 4: depth to basement (km)

column 5: Total subsidence (km)

column 6: Unloaded basement depth (km)

column 7: Subsidence rate (km/m.y.)

EXAMPLE-1 THE GULF

BASEMENT SUBSIDENCE IN REFERENCE TO SEA FLOOR

AND SEDIMENTATION :

1	2	3	4	5	6	7	8	9	10
40.0-30.0	.543	.054	.350	.035	.543	.543	.577	.577	SS
30.0-24.0	.463	.077	.269	.045	.547	.091	.581	.097	SS
24.0-20.0	.412	.103	.220	.055	.542	.136	.575	.144	SS
20.0-15.0	.236	.047	.119	.024	.343	.067	.356	.071	SS
15.0-12.0	.431	.144	.205	.068	.625	.208	.670	.223	SS
12.0-00.0	.740	.062	.335	.028	1.070	.089	1.286	.107	SS

column 1: Time interval (m.y.)

column 2: Basement subsidence (km)

column 3: Subsidence rate (km/m.y.)

column 4: Tectonic subsidence (km)

column 5: Tectonic subsidence rate (km/m.y.)

column 6: Sedimentary layer thickness (km)

column 7: Sediment accumulation rate (km/m.y.)

column 8: Initial layer thickness (km)

column 9: Sediment supply rate (km/m.y.)

column 10: Lithology

EXAMPLE-1 THE GULF

BEST-FITTING MODEL:

DIFFERENCE MODEL/OBSERVATION.....0.05
 CRUSTAL STRETCHING (BETA).....1.500
 SUBCRUSTAL STRETCHING (DELTA).....2.100
 TOTAL LITHOSPHERE ATTENUATION.....1.888
 INITIAL SUBSIDENCE.....0.994
 START OF RIFT-PHASE.....40.000
 START OF THERMAL COOLING.....20.000
 PRESENT-DAY SURFACE HEAT FLOW..... .2.159
 EQUILIBRIUM HEAT FLOW OF
 LITHOSPHERE.....1.200

EXAMPLE-1 THE GULF

BEST-FITTED MODEL:

ISOTHERMS (IN KM) BELOW SEA FLOOR

1	2	3	4	5	6	7	8	9	10
19.0	1.0	0.020	1.01	2.25	0.43	1.10	2.17	3.51	4.84
15.0	5.0	0.099	1.09	2.25	0.43	1.10	2.02	3.35	4.68
12.0	8.0	0.162	1.16	2.25	0.44	1.10	1.89	3.11	4.45
00.0	20.0	0.417	1.41	2.16	0.40	0.93	1.66	2.58	3.88

column 1: Time before present (Ma)

column 2: Elapsed time after the end of rifting (m.y.)

column 3: Thermal subsidence (km)

column 4: Total tectonic subsidence (km)

column 5: Surface heat flow (HFU)

column 6: Depth at which subsurface temperature = 40°C (km)
column 7: Depth at which subsurface temperature = 80°C (km)
column 8: Depth at which subsurface temperature = 120°C(km)
column 9: Depth at which subsurface temperature = 160°C (km)
column 10: Depth at which subsurface temperature = 200°C (km)

TO RUN THIS PROGRAM:

1. Insert a computer disk containing the "BASIN" program in to the computer drive
2. Type "BASIN" then press ENTER
3. Type 1st input file name (Thermo-physical properties and model parameters file) e.g. "EXAMPLE.IN1" then press ENTER
4. Type 2nd input file name (Well information file)
e.g. "EXAMPLE.IN2" then press ENTER
5. Type name of the output file e.g. "EXAMPLE.OUT"
then press ENTER

APPENDIX B

ORGANIC MATURATION MODELLING

The organic maturation modelling program used in this study to predict the extent of hydrocarbon generation through time and the vitrinite reflectance is based on the chemical kinetic model of Braun and Burnham (1987) and Sweeney (1990). This program proposes that chemical reaction kinetics for natural materials such as hydrocarbon generation can be better described by models using a distribution of activation energies (See detail in CHAPTER 6). The program requires two input files. The first file contains time-temperature history of the stratigraphic unit of interest. The second input file contains the unit's kinetic parameters. This program also requires one more input file containing the kinetic parameters for vitrinite, but this input file will be read automatically without the user's input. The output from the program includes the extent and rate of hydrocarbon generation through time, the corresponding vitrinite reflectance value, and the Tmax value if the sample is pyrolyzed. The format of input and output files is shown as follows.

FIRST INPUT FILE: EX.IN

3	Line 1
'Time-Temp Model-1'	Line 2
5	Line 3
0.000 10.000	Line 4
2.000 20.000	Line 5
7.000 40.000	Line 6
10.000 60.000	Line 7
12.000 66.000	Line 8

'Time-Temp Model-2'	Line 9
4	Line 10
0.000 10.000	Line 11
4.000 40.000	Line 12
14.000 80.000	Line 13
26.000 140.000	Line 14
'Time-Temp Model-3'	Line 15
4	Line 16
0.000 10.000	Line 17
9.000 20.000	Line 18
11.000 40.000	Line 19
12.000 54.000	Line 20

Line 1: Number of the time-temperature history
models to be run

Line 2: Name of the 1st model in single quotation marks

Line 3: Number of time-temperature pairs for the model

Line 4-8: 1st input is time after deposition (m.y.)
2nd input is the corresponding temperature (°C)

Line 9: As Line 2

Line 10: As Line 3

Line 11-14: As line 4-8

And -----> So on...

SECOND INPUT FILE: KIN.ARR

17		Line 1
4.2964E+14		Line 2
0.000068	46765.8847	Line 3
0.000441	47536.8015	Line 4
0.002242	48307.7183	Line 5
0.008866	49078.6351	Line 6
0.027310	49849.5519	Line 7
0.065512	50620.4687	Line 8
0.122393	51391.3855	Line 9
0.178081	52162.3023	Line 10
0.201792	52933.2191	Line 11
0.178081	53704.1359	Line 12
0.122393	54475.0527	Line 13
0.065512	55245.9695	Line 14
0.027310	56016.8863	Line 15
0.008866	56787.8031	Line 16
0.002242	57558.7199	Line 17
0.000441	58329.6367	Line 18
0.000068	59100.5535	Line 19

Line 1: Number of influential factor-activation energy pairs

Line 2: Pre-exponential factor (sec^{-1})

Line 3-19: 1st input is the influential or weighing factor

2nd input is the corresponding activation

energy (cal/mol)

OUTPUT FILE: EX.OUT

For Model # 1

For the Time-Temp Model-1

well

Time	Temp	Oilgen	Genrate	%Ro	Conrate
(my)	(°C)				
0.00	10.0	0.00	0.00E+00	0.20	0.00E+00
1.00	15.0	0.00	0.11E-23	0.23	0.34E-15
2.00	20.0	0.00	0.47E-23	0.23	0.32E-15
3.00	24.0	0.00	0.15E-22	0.24	0.38E-15
4.00	28.0	0.00	0.44E-22	0.25	0.25E-15
5.00	32.0	0.00	0.13E-21	0.26	0.21E-15
6.00	36.0	0.00	0.37E-21	0.27	0.35E-15
7.00	40.0	0.00	0.53E-20	0.29	0.37E-15
8.00	46.0	0.00	0.98E-20	0.30	0.42E-15
9.00	53.3	0.00	0.26E-19	0.31	0.48E-15
10.00	60.0	0.00	0.12E-18	0.33	0.67E-15
11.00	63.0	0.00	0.23E-18	0.34	0.30E-15
12.00	66.	0.00	0.45E-18	0.36	0.32E-15

Rock-Eval Tmax = 394.5 °C

For Model # 2

For the Time-Temp Model-2

well

Time	Temp	Oilgen	Genrate	%Ro	Conrate
(my)	(°C)				
0.00	10.0	0.00	0.00E+00	0.20	0.00E+00
1.00	17.5	0.00	0.23E-23	0.23	0.34E-15

2.00	25.0	0.00	0.19E-22	0.24	0.61E-15
3.00	32.5	0.00	0.15E-21	0.26	0.37E-15
4.00	40.0	0.00	0.10E-20	0.27	0.69E-15
5.00	44.0	0.00	0.28E-20	0.29	0.44E-15
6.00	48.0	0.00	0.74E-20	0.30	0.24E-15
7.00	52.0	0.00	0.19E-19	0.31	0.34E-15
8.00	56.0	0.00	0.48E-19	0.32	0.43E-15
9.00	60.0	0.00	0.12E-18	0.34	0.34E-15
10.00	64.0	0.00	0.29E-18	0.35	0.28E-15
11.00	68.0	0.00	0.69E-18	0.36	0.40E-15
12.00	72.0	0.00	0.16E-17	0.38	0.50E-15
13.00	76.0	0.00	0.36E-17	0.40	0.41E-15
14.00	80.0	0.00	0.81E-17	0.42	0.30E-15
15.00	85.0	0.00	0.21E-16	0.44	0.46E-15
16.00	90.0	0.00	0.54E-16	0.46	0.59E-15
17.00	95.0	0.00	0.13E-15	0.49	0.47E-15
18.00	100.0	0.01	0.28E-15	0.52	0.49E-15
19.00	105.0	0.02	0.58E-15	0.56	0.66E-15
20.00	110.0	0.05	0.11E-14	0.60	0.53E-15
21.00	115.0	0.09	0.18E-14	0.63	0.35E-15
22.00	120.0	0.16	0.28E-14	0.66	0.44E-15
23.00	125.0	0.27	0.37E-14	0.69	0.44E-15
24.00	130.0	0.39	0.44E-14	0.72	0.35E-15
25.00	135.0	0.54	0.46E-14	0.75	0.45E-15
26.00	140.0	0.68	0.42E-14	0.80	0.54E-15

Rock-Eval Tmax = 415.0 °C

For Model # 3

For the Time-Temp Model-3

well

Time	Temp	Oilgen	Genrate	%Ro	Conrate
(My)	(°C)				
0.00	10.0	0.00	0.00E+00	0.20	0.00E+00
1.00	11.1	0.00	0.34E-24	0.22	0.35E-15
2.00	12.2	0.00	0.47E-24	0.23	0.10E-15
3.00	13.3	0.00	0.66E-24	0.23	0.87E-16
4.00	14.4	0.00	0.92E-24	0.23	0.98E-16
5.00	15.6	0.00	0.13E-23	0.24	0.11E15
6.00	16.7	0.00	0.18E-23	0.24	0.11E-15
7.00	17.8	0.00	0.25E-23	0.24	0.12E-15
8.00	18.9	0.00	0.34E-23	0.24	0.11E-15
9.00	20.0	0.00	0.47E-23	0.25	0.99E-16
10.00	30.0	0.00	0.75E-22	0.25	0.29E-15
11.0	40.0	0.00	0.10E-20	0.27	0.77E-15
12.00	54.0	0.00	0.30E-19	0.30	0.74E-15

Rock-Eval Tmax = 394.5 °C

TO RUN THE PROGRAM:

1. Insert a computer disk containing "BASINMAT" program in to a computer drive
2. Type "BASINMAT" then press ENTER
3. Type 1st input file name (Time-Temperature file)
e.g. "EX.IN" then press ENTER
4. Type 2nd input file name(source rock's kinetic parameter file) e.g. "KIN.ARR" then press ENTER

5. Type name of the output file e.g. "EX.OUT" then
press ENTER
6. Type time-step increment (m.y.) e.g. "1.0" then press ENTER
this number must be able to divide the time input
in Time-Temp file and result in integer number

APPENDIX C

DETERMINATION OF KINETIC PARAMETERS

A LOTUS 1-2-3 template file, Eo.wk1, used in this study to determine the kinetic parameters such as a pre-exponential factor (A), mean activation energy (E_0), and a standard deviation of the activation energies (σ_E) from the Rock-Eval analyses of a potential source rock is based on a linear regression/correlation technique of Braun and Burnham (1987) which assumed a simple Gaussian distribution of activation energies (See detail in CHAPTER 6). The program requires input data from three Rock-Eval analyses of a sample at different heating rates. The format of input data is shown as follows.

INPUT DATA: For the Eo.wk1 template file

Eo.wk1

Determine a distribution of
activation energies using
Rock-Eval pyrolysis

SAMPLE I.D.: **RE-LAB STANDARD** <=== Cell B7

REMARK: **write any remark here!** <=== Cell B8

INPUT

RUN #	HEATING RATE	T _{max}
	(°C/min)	(°C)

1	Cell B15==>	5	410 <=== Cell C15
2	Cell B16==>	25	441 <=== Cell C16
3	Cell B17==>	50	451 <=== Cell C17

CORRESPONDING	HEATING RATE	ΔT (FWHH)
VALUES OF ==>	($^{\circ}\text{C}/\text{min}$)	($^{\circ}\text{C}$)

Cell B22==>	25	51.2 <=== Cell C22
-------------	----	--------------------

Regression output should be in cell E25 =====>

Cell B7: Sample I.D.

Cell B8: Any remarks on the sample

Cell B15: Heating rate of a first run pyrolysis ($^{\circ}\text{C}/\text{min}$)

Cell C15: A corresponding Tmax obtained from

a first run pyrolysis ($^{\circ}\text{C}$)

Cell B16: Heating rate of a second run pyrolysis ($^{\circ}\text{C}/\text{min}$)

Cell C16: A corresponding Tmax obtained from

a second run pyrolysis ($^{\circ}\text{C}$)

Cell B17: Heating rate of a third run pyrolysis ($^{\circ}\text{C}/\text{min}$)

Cell C17: A corresponding Tmax obtained from

a third run pyrolysis ($^{\circ}\text{C}$)

Cell B22: Heating rate of any run of pyrolysis ($^{\circ}\text{C}/\text{min}$)

Cell C22: A temperature width at half the height of a pyrolysis

profile whose heating rate corresponds to

that used in Cell B22 ($^{\circ}\text{C}$)

OUTPUT: From the Eo.wk1 template file

OUTPUT

FREQUENCY FACTOR (A)	=	7.5316E+13	/sec
ACTIVATION ENERGY (E_0)	=	51200.45	cal/mol
STANDARD DEVIATION (σ_E)	=	3.57	%

APPROXIMATED DISCRETE VALUES
OF ACTIVATION ENERGIES:

STOICHIOMETRIC FACTORS	ACTIVATION ENERGIES (cal/mol)
---------------------------	----------------------------------

0.000068	43881.5697
0.000441	44796.4295
0.002242	45711.2893
0.008866	46626.1490
0.027310	47541.0088
0.065512	48455.8686
0.122393	49370.7283
0.178081	50285.5881
0.201792	51200.4479
0.178081	52115.3077
0.122393	53030.1674

0.065512	53945.0272
0.027310	54859.8870
0.008866	55774.7467
0.002242	56689.6065
0.000441	57604.4663
0.000068	58519.3260

TO RUN THIS TEMPLATE FILE:

1. Call up the LOTUS spread sheet program
2. Retrieve a template file "Eo.WK1" from the disk
3. Type in input data described above e.g.
 - sample I.D. in cell B7
 - remarks in cell B8
 - heating rate and a corresponding Tmax in cells B15 and C15
 - heating rate and a corresponding Tmax in cells B16 and C16
 - heating rate and a corresponding Tmax in cells B17 and C17
 - heating rate and a corresponding FWHH in cell B22 and C22
4. Use the LOTUS menu to execute linear regression with the output of a regression go to cell E25, after which all kinetic parameters are automatically calculated
5. Use the LOTUS menu to print a block of cells P55..Q73 to a text file which will be readily used as an input file (e.g. KIN.ARR in Appendix B) for hydrocarbon generation modelling.